An Investigation into the Behaviour of Fibre Reinforced Natural Gas Powered Vehicle (NGV) Pressure Cylinders under Impact Loading

By
Chun Fai Patric MAK

UNIVERSITY OF
NEWCASTLE UPON TYNE

A Thesis Submitted for the Degree of Doctor of Philosophy

Department of Mechanical, Materials and Manufacturing Engineering
University of Newcastle upon Tyne
England

June, 1998

Abstract

Commonly encountered accidental impact, e.g. due to roadway stone hitting, is detrimental not only because it can produce apparent surface defects, but also because barely visible impact damage (BVID) can be induced inside the material, which is not easy to detect by routine inspection. Reliable prediction of the amount of damage of this type induced under known service conditions is particularly important. Therefore, this type of impact was chosen as the focus of the present investigation.

A combination of experimental techniques and finite element modelling was used to explore the behaviour of a fibre reinforced natural gas powered vehicle (NGV) pressure cylinder subjected to a low energy impact.

In order to identify the modes of failure and understand the structural response, quasi-static indentation tests were carried out on sections of composite pipes and of a composite pressure cylinder. Delamination and matrix cracking were established to be the two major failure modes induced by indentation. Experimental findings were used as a basis for assessing the validity of the modelling approach.

Thick shell and three dimensional finite element models were developed using PAFEC, a general purpose finite element code for dynamic and static analysis. It established that the composite pressure cylinder under this type of impact behaves quasi-statically, i.e. the impact phenomenon predominately excites low frequency response. Repeated impact was considered in order to extend the study to include the impact behaviour of a cylinder with pre-existing damage. It was found that a bulging effect was produced in the pressure cylinder at the impact site, where a weak spot was created due to fibre breakage.

A fully three dimensional finite element model with static analysis was developed to investigate the damage and material degradation during the BVID phenomenon. The contact pressure distribution based on the Hertzian contact relationship was applied. Failure mode identification criteria proposed by Hashin (1980) and Chang and Springer (1986) were used to establish the mode and extent of damage in the composite cylinder under quasi-static loading. The predicted failure modes agreed well with the experimental results.

Finally, the present study sets out the methodology allowing systematic design of structures having optimal impact tolerance. Based on the findings of this project, suggestions for the improvement of impact resistance of NGV cylinders were given in Chapter six.

The LORD is my shepherd; I shall not want.

He maketh me to lie down in green pastures: he leadeth me beside the still waters.

He restoreth my soul: he leadeth me in the paths of righteousness for his name's sake.

Yea, though I walk through the valley of the shadow of death, I will fear no evil: for thou art with me; thy rod and thy staff they comfort me.

Thou preparest a table before me in the presence of mine enemies: thou anointest my head with oil; my cup runneth over.

Surely goodness and mercy shall follow me all the days of my life: and I will dwell in the house of the LORD forever. Amen.

Psalm 23

THE HOLY BIBLE [KJV]

Acknowledgements

I would like to express my wholehearted gratitude to my academic supervisor, Dr Alexander Korsunsky. I consider him one of the greatest teachers I have ever met, not only because of his profound knowledge in mechanics, but also for his warm thoughtfulness and good sense of humour. I shall be forever grateful for his guidance, valuable suggestions and enlightening discussion.

I wish to express my sincere appreciation to Mr J.F.L. Chan for his guidance and advice so that I have had the chance to experience the world of philosophy.

I want to express my sincere gratitude to Professor A.G. Gibson and Dr J.T. Evans for their kindness and generosity to my education at Newcastle.

Special thanks go to Dr C.H. Woodford and Dr George Kotsikos for their technical advice. Thanks are also due to Mr Ken Madden for his technical advice and assistance in the mechanical tests, Mr Bob Stalker for his assistance in the production of photographic illustrations.

Acknowledgement is made to ORS Awards and British Gas Plc for their financial sponsor for this research.

Also, I wish to thank Rev David Holloway, Rev Jonathan Pryke, Pastor Robert Germany, Pastor David Roper, Pastor Desmond Chong, Mr & Mrs K.Y. Leung, Mr & Mrs N. Ng, Mrs Celia Chan, Professor R.I. Lewis, Dr Nelson Yung, Mr Nick Dillon and all the brothers and sisters in Newcastle CCC for their warm supports and encouragement at the final stage of my study.

Most of all, I am grateful to my beloved wife, Fanny, my two lovely sons, Ho-Shing and Ho-Yon, and my wonderful parents-in-law, Mr & Mrs Y.P. Put, from the bottom of my heart. Without their understanding and support and many prayers, I would have never been able to pursue my advanced study.

Finally, I must thank my dearest sister, Mrs Christine Chan, who always kindly and lovingly reminds me that I have a family to raise so that I cannot stay at Newcastle forever.

Table of Contents

Chapter 1 Introduction

1.1 Composite Materials

Fundamentally, a composite can be considered to consist of three constituents : the fibre, the matrix, and an interphase region of finite thickness responsible for assuring good adhesion between the fibre and the matrix. A lamina or ply is created by aligning the reinforcing fibres in an appropriate matrix in one direction. Sheets of unidirectional pre-impregnated laminae are laid-up in a specific sequence to form a fibre reinforced laminate. This lay-up sequence is very much dependent on the load carrying requirement of the laminates. Typical laminates may have between 4 and 40 layers, each layer (or ply) being around 0.125 mm thick if it is a carbon or glass / epoxy lamina. More details of the lay-up and cure processes can be found in Frame (1989). Only once the mechanical behaviour and properties of fibres, matrices, fibre / matrix laminae and various laminates have been understood can engineering designers hope to tailor composites to specific applications.

Filament winding is a process for winding a continuous fibre that is coated with raw resin over a rotating mandrel. A computer controlled winding machine sets the winding pattern and tension at which the fibre is laid on. Successive layers are added at the same or different winding angles until the designated thickness is reached. More details of the filament winding process can be found in the Handbook of Composites [Lubin (ed.), 1969]. The advantages of using filament wound cylindrical structures over conventional metal cylindrical structures are their attractive weight-to-strength ratio, good corrosive resistance and a low thermal expansion coefficient. In the age when computational tools were not available, analytical methods developed for laminates were used to predict the mechanical behaviour of filament wound composites. However, due to the complexity of the structure and the huge amount of variables and material constants involved, these analytical methods can only provide a very limited information for engineering design purposes. With the advancement of information technology, finite element analysis of anisotropic systems become the latest trend used in predicting the behaviour of filament wound structures.

In spite of the distinct advantages of the fibre-reinforced-polymer matrix composite material, it has a relatively serious drawback. It is brittle and has no significant strength in the thickness direction. Therefore, it is susceptible to low velocity, low energy impact in which through-thickness axial and shear stresses are induced, which can cause significant or barely visible impact damage (BVID) such as matrix cracking, delamination and fibre breakage. BVID would be difficult to detect in a routine inspection, but may result in significant reductions in stiffness and strength, especially the in-plane compressive strength which may result in a premature buckling of layers [Cantwell and Morton, 1991].

1.2 Composite NGV Cylinders

The major advantage of using natural gas such as methane as a fuel for vehicles is that it is clean and cheap compared to petrol. Additionally, petrol pricing and production can be unstable compared to natural gas. Moreover, internationally, 'green' legislation is in force (in USA) or expected (in Europe) that will encourage cleaner fuels, so legal as well as political pressure may encourage the use of NGVs [Stephenson (ed.), 1991]. Countries with natural gas resources will obviously see NGVs as attractive, but would need to invest in an extensive and expensive infrastructure of filling stations.

NGV cars typically use a 50 litre high pressure cylinder. Metal cylinders are the most popular, but these are heavy (about 60 kg if made to a British specification - BS5450) and give high axle loads. Also, they have a limited range as they contain only about one third of the energy of a conventional fuel petrol tank, and less power. Therefore, lighter, more efficient cylinders are needed.

More energy density can be achieved by higher pressures, and/or absorbing more gas in the cylinder, e.g. by filling the cylinder with carbon to absorb the natural gas. Increasing the pressure from the current typical levels of 200-240 bar (3000-3500 psi) would pose safety problems, so absorption appears to be the best route. However, both higher pressures and absorption methods mean heavier cylinders. Lighter cylinders can be achieved by the use of fibre reinforcement. The weight-volume (kg/l) ratios of the

current high strength steel cylinders is about 1, whereas cylinders made from epoxy and fibre glass could be as low as 0.3. Cylinders such as steel-lined fibre wrapped reinforcement, aluminium-lined glass / carbon fibre wrapped or all-composite design do offer good weight-to-capacity ratios. However, these composite designs are not well-tried, and are more expensive than the conventional steel design.

Composite cylinders considered in this investigation are made of thin, usually metal, liners, which are completely filament wound with continuous high strength fibres embedded in resins with interspersed helical and hoop patterns (see Fig 1). After overwrapping, a polyurethane coating of the desired colour is applied to the composite cylinder and it is cured in an oven at elevated temperatures [Morris, 1981]. The fibres commonly used have been glass, carbon or Kevlar while the resins are mainly epoxies. The usual liner material is seamless aluminium[1] , but steel and other materials are also utilised. The principal functions of the liner are to prevent leakage, to share a very minor proportion of the pressure load during operation, and to provide a boss for the valve. Comparatively the composite cylinders are safer than all-metal cylinders in term of their leak-before-burst (LBB) failure mode. That is, when a composite cylinder fails during the burst pressure test, it is more likely to remain in one piece, with no fragmentation taking place.

1.3 Problems Associated with Composite NGV Cylinders

Manufacturers, such as SCI, construct high pressure filament wound composite cylinders with a high factor of safety in burst and fatigue[2], and with a thickness adequate to allow for normal abuse and broken/cut/frayed surface fibres [Morris, 1981]. Although these composite cylinders can withstand the severe impact testing with no degradation of burst pressure, however, there still exists the potential threat of these damages, such as fibre breakage, matrix cracking, delamination, and permanent deformation of the cylinder, and

---

[1] According to DOT (Department of Transportation, USA.) exemption document DOT-E-7277 granted to SCI (Structural Composites Industries) for manufacturing commercial filament wound composite cylinder, the liner material should be aluminium alloy and must be seamless [Morris et al, 1977; Morris, 1981].

the possibility of their influence on the post-impact performance. As mentioned above, the thickness chosen for composite cylinders is based on the considerations of load-bearing under burst and fatigue loads. Hence, any damage induced in a composite layer leading to a reduction of the effective load-bearing thickness may result in a degradation of fatigue life even though in the short term, the burst pressure had not been degraded

It was gradually realised that, in practice, while excellent primary load bearing capabilities were obtained, damage, or non-catastrophic microscopical failures, might well develop before the designed failure load has been reached. In this study, damage or microscopical failure refers to the situation when the load-bearing capacity of the basic constituents of material has been lost or impaired. Material damage such as matrix cracking, delamination and fibre breakage may be considered to be secondary failure to a structure. However, this kind of damage is a potential threat to the load carrying capacity of the structure, and is often directly responsible for premature structural failures.

Impact loading is perhaps the most common accidental loading. It is also one of the most detrimental since the damage induced is very often invisible by routine inspection. It occurs in situations such as dropping of tools, runway stone hitting etc. Impact damage is dangerous, and the ability to minimise impact damage of a composite cylinder is a concern. In view of the large factor of safety imposed, manufacturers claim that their composite cylinders possess good impact resistance, since they survive severe impact tests with no evidence of performance degradation as tested by burst testing after impact. Over-winding the cylinder with additional layers of composite in order to gain higher impact resistance does not seem to be an ideal solution, since the pressure vessel efficiency[3] is compromised. However, it is also very difficult to quantify impact damage. Guidelines have been published by Compressed Gas Association, Inc. [CGA C-6.2, 1988] mainly in order to provide sufficient data and details to re-qualify a damaged composite cylinder using an allowable deflection. It highlights the aspects that are

---

[2] In pressure vessel environments, the factor of safety in burst is defined as the ratio of burst pressure to operating pressure, and the factor of safety in fatigue is defined as the ratio of life cycles to operating cycles.

essential to an accurate appraisal of a composite cylinder for compressed gas service. However, due to the complexity of impact damage which may involve the interaction between dynamic matrix crack propagation and delamination growth [Choi et al, 1991a], there is still a lack of standards or established testing techniques for impact on composites. Although, standard tests for isotropic materials, such as Izod impact test and Charpy impact test, are frequently employed to test composites, their tests results often are not sufficiently repeatable and scattered in a wide range. Hence, numerous researchers turned to non-standard tests such as drop weight tests or air guns with point-nose projectiles to perform impact tests on coupons of composite material. Once again, these test results are of limited use, since the structural response is being neglected. A more consistent approach toward better understanding of impact behaviour of composite cylinders remains to be established.

A thin aluminium liner is a crucial component of the composite cylinder, although it shares only a minor portion of internal pressure and provides a barrier to leakage. If the liner fails due to over-strain, excessive stresses, cracking or other causes so as to create a path for leakage, the cylinder can not be used in service. The load-bearing ability of this liner can be used as an indicator for determining the serviceability of the whole cylinder. Whereas under internal pressure, the liner can fail only by bursting under excessive membrane stresses, impact loading exposes both the composite and the aluminium liner to a combination of the out-of-plane and in-plane stresses. This complex impact response of lined cylinders to various kinds of loading under service conditions deserves careful attention.

1.4 Impact Behaviour

In this investigation, impact behaviour is defined as the way in which a composite cylinder responds to impact loading. This impact behaviour can be quantified by various response parameters, such as global elastic deflection and permanent deformation (i.e. structural response), and / or local indentation and internal damage (i.e. material

---

[3] The pressure vessel efficiency is defined as the burst pressure multiplied by the vessel capacity and divided by the vessel weight.

response). However, in order to predict these responses effectively, the nature of influence of the various kinds of impact loading on the composite cylinder must first be examined and classified. For example, the impact velocity has often been used as the parameter used to classify the degree of damage produced in composite structures. Secondly, the impact failure mechanisms of the composite material must be understood. That is to say, the material failure mechanisms that become operational under various kinds of impact loading must be identified, and properly incorporated in the analysis. Thirdly, the impact resistance of a composite cylinder has to be understood and predicted through impact damage analysis and impact damage tolerance examination.

In this study, impact resistance is defined as the capacity of a composite cylinder to endure damage without failure or degradation, ie. so that the load-bearing function of the composite cylinder is maintained to the designed safety margin. Impact tolerance refers to the ability of a composite cylinder to continue performing given a certain amount of impact damage. An approach to impact resistance analysis must be developed by dividing the problems into two stages, ie. the prediction of impact damage (impact damage phase) and post-impact damage tolerance examination (impact damage tolerance phase).

1.5 Scope of Study

A fully fibre reinforced NGV (FRNGV) cylinder manufactured by SCI[4] was the subject of analysis in the present study. The aim was to investigate the impact behaviour of FRNGV cylinders so that both the structural response and material response are examined. An attempt was made to improve the understanding of impact resistance of FRNGV cylinders subjected to various kinds of impact loading. Special attention was devoted to developing a better insight into the BVID phenomenon.

Four kinds of accidental loading were initially selected for consideration in the present investigation, which were a runway stone impact, sledgehammer impact (i.e. dropped tools), a car crash and a bullet shot. These cases encompass a wide range of impact

[4] SCI composite cylinder : Type ALT 576-025, capacity of 35.4 litres, operating pressure 200 bars.

loadings with various combinations of impact velocity, impactor mass and impact energy. The classification of impact loading conditions is given in Table 1. The impacted cylinder may be either empty or filled up to the maximum operating pressure.

Engineering practice has shown that under conditions of low energy impact, even when no damage can be seen on the surface of a composite structure, extensive internal damage may have occurred. BVID may have significant influence on the post-impact performance of the structure, in that the structural integrity may have been impaired. Therefore, an analysis of the exact failure mechanisms dominating each kind of impact loading is needed. Due to the large wall thickness of the composite cylinder (22 mm in total, with 19 mm occupied by the composite layers) it is expected that most of the impact energy will be dissipated locally, with significant amount of damage created. Through this analysis, a more detailed understanding must be achieved of how the impact energy dissipates into the composite cylinder and is absorbed by the composites layer and the liner. The essential parameters governing the impact damage must be identified. Finite element models were constructed to study the BVID phenomenon using thick shell elements for dynamic analysis, and 3D brick elements for more detailed analysis in the quasi-static approximation. In order to confirm the predictions from FE modelling, experimentation was performed in order to investigate the local damage as well as the structural response under quasi-static loading.

Repeated impact was also considered in order to study the effect of pre-existing impact damage on the energy absorbing mechanisms during second and subsequent impact loading. Pre-existing impact damage was modelled by calculating the amount of damage produced, and changing the properties of the failed elements in accordance with the material degradation model.

A cylinder being hit in-service is usually not empty. Therefore, for both single and repeated impact situations, it is important to understand the differences in how the damage is produced in an empty or a fully charged cylinder, and the effect of internal pressure on the propagation of damage. A finite element model of a pre-pressurised

cylinder was used with dynamic analysis. Damage was predicted at the time-step when maximum transverse displacement has been produced.

It is important to understand the impact resistance of composite cylinders under such severe impact loading as produced in a car collision accident. The failure modes produced under this kind of impact are quite different from stone or sledgehammer impact, due to the large contact area between the cylinder and the impacting object. In this case, large global deflection is likely to be the main failure mode.

It is a very rare case for a composite cylinder to be shot by a bullet. However, it is necessary to investigate how the composite cylinder behaves in this situation. Such investigation uncover the mechanisms by which the bullet is arrested by the composite layer, and the minimum velocity for perforating the wall thickness, i.e. ballistic limit or threshold velocity, can be obtained.

The BVID was chosen as the main object of interest in this study, since the damages produced by car crash and bullet shot are usually easily detectable.

The dynamic FE analysis with the use of the thick shell element was performed aimed at finding out the significant of the dynamic effect in the analysed system. Parametric study of impact response was carried out, and kinematic and material response were examined. Repeated impact has also been considered. Failure criteria have been used to identify fibre and matrix failure.

The study was then narrowed down to the study of local damage. A fully three dimensional FE analysis was used to study the local damage and the BVID under quasi-static loading. Failure criteria were employed to examine the stresses obtained from analysis, so as to identify the three major failure modes of material, which are fibre breakage, matrix cracking and delamination. The results were compared with the experimental observations.

A systematic approach towards the problem has been established, which can aid as further investigation of similar problems with different conditions of loading.

The content of the thesis is organised into seven chapters.

Chapter 1 presents the general overview of the subject, and introduces the statement of the problem. Chapter 2 reviews the existing state-of-the-art methodology in experimentation, modelling and applications of NGV cylinders. The fundamentals of the modelling approaches and procedures used in the present investigation are presented in Chapter 3.

Chapter 4 describes the experimental investigation, and contains a discussion of the findings, with a view to comparing them to the model predictions.

The application of the modelling approach to studying impact of NGV cylinders is presented in Chapter 5. Both dynamic and static analyses are used to investigate the impact response of the composite cylinder.

Strength analysis of the composite cylinder under quasi-static loading is presented in Chapter 6. Suggestions for the ways of improvement of impact resistance are put forward.

The aforementioned modelling approaches, applications and results are summarised, and some concluding remarks presented in Chapter 7. Additionally, suggestions for further systematic study of the impact behaviour of composite cylinder are made.

Details of the validation studies of some of the FE modelling methods are given in the Appendices.

Table 1 : Classification of impact loading

Mass of Impactor	**Impact Velocity**			
	10 m/s	***20 m/s***	***40 m/s (90 mph)***	***~500 m/s***
Bullet 80 gm				High Energy 10 kJ
Stone 0.36 kg	Low Energy 18 J	Low Energy 72 J		
Sledgehammer 1 kg	Low Energy 50 J	Mid Energy 200 J		
Car Crash 1000 kg	High Energy 50 kJ	High Energy 200 kJ		

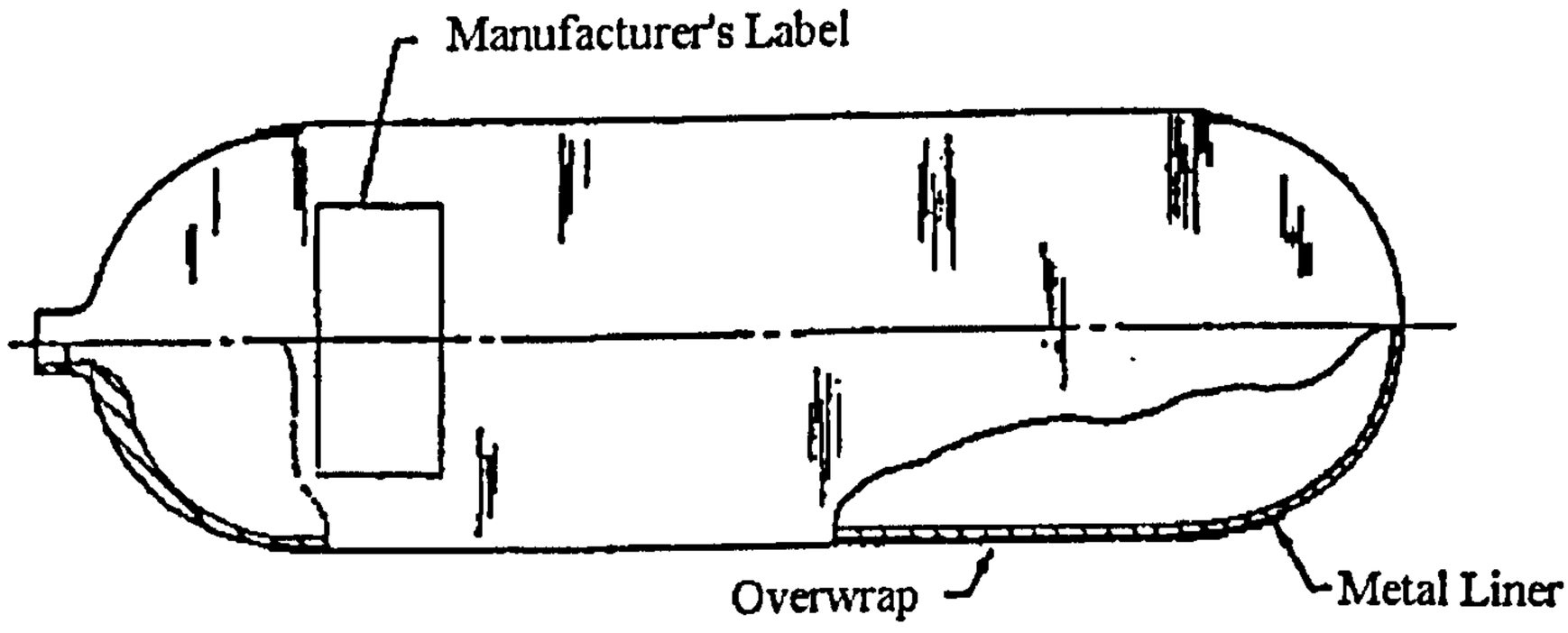

Fig 1 A metal-lined fully-wrapped pressure cylinder

Chapter 2 Literature Review

2.1 Introduction

The aerospace technology of utilising filament-wound metal-lined high pressure vessels has successfully been transferred to commercial applications since 1970's. During that time, the application of high stiffness and strength composites utilised in these filament-wound metal-lined high pressure vessels had been reviewed by several researchers in the Energy Technology Conference in Houston, Texas in 1977, e.g. see Lark (1977), Jones (1977), Morris et al (1977) and Ecord (1977). Their reviews mainly concentrated on the design concept and performance analysis of composite pressure vessels. Since then, these papers have been frequently referred to by numerous researchers working on the further development of various aspects of composite pressure vessels technology.

The role of a liner in a composite cylinder is mainly to provide a barrier against leakage and to contribute a portion of load-sharing. If the liner fails due to over-strain, cracking or other causes, it creates a path for leakage, and the cylinder should not be of use in service. Therefore, many researches have devoted their efforts to the study of the load-sharing behaviour of a liner [Foral, 1979; Babel et al, 1989; Bhuyan, 1992; Lifshitz and Dayan, 1995].

However, to the best knowledge of the author, no substantial work has been published devoted entirely to the investigation of the impact response of the liner and its effect to the impact behaviour of a composite pressure cylinder.

Composite pressure cylinders are claimed by manufacturers to possess good impact resistance as they survived severe impact tests without significant degradation of performance, as evidenced by burst testing after impact.

Tiller et al (1990) have gunfire-tested composite cylinders which were pressurised to service pressure with a 0.3-caliber armour piercing bullet having the velocity of 854 m/s without evidence of fragmentation failure. Morris et al (1977) have conducted a series of similar tests and found that the cylinders survived without subsequent explosion, or

even a cut more than 76 mm long. Morris (1981) drag tested the cylinder by attaching it to a car and dragging it at moderate speeds, and then hitting and bouncing it on a curb. The cylinder showed no performance degradation in burst testing. In the same study, charged pressure cylinders were also repeatedly dropped from 3 to 5 metres height at various orientations onto a rigid steel plate. Still, no performance degradation was found in burst testing. Obviously, these composite pressure cylinders have been over-designed to obtain a very high safety margin. This design approach may have been acceptable in the past, however, the emphasis nowadays is on reducing weight, minimising material usage, utilising new materials, while also preventing product liability lawsuits, which all require a fundamental scientific approach to predicting strength.

2.2 An Overview on Impact

2.2.1 Metal Structures

Impact of metal structures has been thoroughly investigated, and is treated extensively in several classical texts such as Goldsmith (1960 & 1963), Johnson (1972) and Macaulay (1987).

An impact occurs when two or more bodies collide. An important characteristic of impact is the generation of relatively large forces at points of contact for relatively short periods of time. Hence, these relatively large forces cause surface pressure, which in turn generates internal stresses. The complete state of stresses in the structure is the result of the combination of the overall deformation of the structure and local deformations in the contact area due to impact.

The classification of impact is important because the impact phenomenon, and hence the impact behaviour of the structure may change depending on the type of impact. It is commonly defined by the mechanical behaviour of the structure after impact and the failure modes that may be involved. Usually, the velocity and the energy of impact serves as indicators for this classification. However, no rigid boundaries exists for classifying impact velocities. It may depend on by the impact parameters, such as the

target structure geometry, material, and the mass ratio of the impactor to a representative part of the structure.

In general, under the conditions of low velocity, low energy impact, the mechanical behaviour of the impacted structure can be described by elasticity or viscoelasticity, and non-penetration failure modes are involved. In general, under this type of impact, metals absorb energy through plastic deformation. Although it causes some permanent structural deformation, its consequences on the load bearing capacity of the component are usually small [Cantwell and Morton, 1991].

Under high velocity, high energy impact, perforation of a compararively thin target structure may occur. The passage of the impactor will generally result in petalling, cracking and spalling, due to large attendant dissipation of impact energy. This penetration and perforation processes can be analysed by the methods of hydrodynamics involving conservation of mass, momentum, and energy for the system [Goldsmith, 1960 & 1963; Langlie and Cheng, 1989]. Such damage will degrade the load bearing ability of the structure. Its effects can generally be predicted using fracture mechanics principles [Cantwell and Morton, 1991].

2.2.2 Composite Structures

The manner in which composite materials respond to impact loading and dissipate the incident impact energy of the impactor is very different to that of metal. In composites, the ability to undergo plastic deformation is extremely limited, with the result that energy is frequently absorbed in creating large areas of fracture with ensuing reductions in both strength and stiffness. It implies that the load bearing ability of the structure may be significantly degraded due to such damages. Furthermore, the prediction of the post-impact load bearing capability of a damaged composite structure is more difficult than for metals, since the damage zone is generally complex in nature and consequently very difficult to characterise.

Impact Velocity

Robinson and Davies (1992) have undertaken low velocity impact tests, with velocities up to 6 m/s, on fibre reinforced circular laminated panels of 2 and 7 millimetre thickness which were fully clamped around their boundaries. They defined the low velocity as that for which through-thickness stress waves in the specimen play no significant part in the stress distribution at any time during the impact event. By using some simple approximate techniques of Godwin and Davies (1988) for evaluating the transition velocity beyond which stress wave effects dominate, they obtained the result that the transition to stress wave dominated impact mode occurs at the impact velocity of 10 - 20 m/s. The conclusion was obtained by assuming that the stress wave propagates at the speed of sound (approximately 2000 m/s for common epoxy composites), and that the typical failure strains lie between 0.5 and 1.0 percent. Impact velocities up to 6 m/s have consequently been used throughout their experiments. With this definition, the classification of low velocity is solely dependent on the material properties, but disregards details of the structural geometry such as thickness. This approach is often too conservative.

Ainsworth (1990) and Christoforou et al (1987) conducted similar low velocity impact tests on composite pipes. They adopted the definition for the term of low velocity impact as that for which maximum velocity is still low enough to justify static analysis of the response of the structure. The basic idea of this classification is quite similar to that used by Shivakumar et al (1985) in their mathematical models. Christoforos (1987) used less than 5 m/s as impact velocities in all his tests. However, the impact velocities Anisworth (1990) used in her tests were up to 30 m/s, which are not low according to the definition proposed by Robinson and Davies (1992).

The classification adopted by Ainsworth (1990) and Christoforou et al (1987) is quite useful for mathematical modelling and finite element modelling. As long as the impact phenomenon predominately excites only the low frequency structural response, (quasi) static analysis is deemed to be sufficient to describe the behaviour of the system.

Wu and Springer (1988) and Finn and Springer (1993) give a simple definition for low velocity impact. They refer to the situation when the impactor does not penetrate the surface of the composite plate as low velocity impact. For this non-penetrating impact situation, elastic behaviour is the dominant response of the structure.

When the impact velocity reaches to a level when the effect of elastic wave propagation in the material becomes progressively more significant in determining the stress distribution , it is commonly referred to as high velocity impact [Sjoblom et al, 1987]. Under the conditions of high velocity impact, high frequency modes are excited. Stress waves may not travel far in the time available for the impact event, so that the energy is more concentrated in the region of impact [Dorey, 1989]. Hence, it is not uncommon to assume that high velocity impact occurs when the deformation of the structure is localised in a small zone surrounding the contact area [Abrate, 1991]. In this situation, remote boundary conditions often become less important [Cantwell, 1986].

Impact Phenomenon

Under localised impact conditions, for beam / plate structures with moderate effective thickness to length ratio, the incident energy of the impactor is dissipated in a variety of mechanisms. They include the elastic flexure, contact deformation, fracture mechanisms, stress wave propagation, vibrational effects and inertial effects [Cantwell, 1986]. During impact for which the velocity is low enough to justify static analysis, energy is dissipated mainly by the first three mechanisms while the energy losses in dynamic effects are sufficiently small to be negligible.

To summarise, when subjected to low velocity, low energy impact, composite structures respond in bending, allowing the energy to be accommodated in elastic deformations. Although during impact the impactor may not penetrate the structure, internal structural damage may occur, such as extensive sub-surface delamination and cracking [Clark, 1989]. For a given impact velocity, the magnitude of impact force will decrease as the target structure flexibility increases, or its thickness decreases. On the other hand, increase in target structure flexibility will also increase contact duration and the area of contact [Greszczuk, 1982].

Penetration Phenomenon

During penetration impact, fibres are the primary bearer of damage, while the primary function of the matrix is to provide sufficient overall integrity, allowing large deformations without failure or disintegration of the structure [Prevorsek et al, 1993]. This is in contrast to impact of composites without penetration, where damage takes place mainly in the matrix, or at the fibre-matrix interface.

It was established that delamination and plugging are the two major damage modes in the penetration process. Plugging appears to be a localised behaviour, and the experimental data reveal that the load for plug formation is independent of the span of the specimen [Lee, 1992]. From observation of the test panels after impacts, Langlie and Cheng (1989) suggested that the penetration process could be broken down into three sequential stages : 1) plugging; 2) fibre fracture; and 3) delamination. They also found that each stage of the process was characterised by a specific failure mechanism which absorbed a certain proportion of the impact energy and was responsible for the deceleration of the projectile.

Prevorsek et al (1993) established a model for penetration analysis in which three principal modes of deformation have been identified and incorporated in the model. They are the lateral displacement of fibres (related to the matrix and interfacial failures), fracture of fibres in shear or compression (by cutting), and fracture of fibres in tension (see Fig 2.1). The relative importance of these penetration mechanisms in the specific case depends on materials characteristics (fibres and matrix), composite design and the characteristics of penetrator geometry, velocity, mass, hardness etc. It is claimed that by using these penetration mechanisms, a great deal of the experimental results related to the penetration of fibre reinforced composites can be explained.

An interesting design for asymmetric stacked hybrid composites was proposed by Prevorsek et al (1993) in order to enhance the damage tolerance, and at the same time provide maximal penetration resistance. These hybrid composites were formed by joining a structural composite (eg. Carbon or S-2 glass fibre / epoxy) on the side facing the impact, while the backing was made of polyethylene fibre composite possessing good

viscoelastic composites. It was found that such composites provide outstanding flexural and tensile fatigue properties and abrasion resistance.

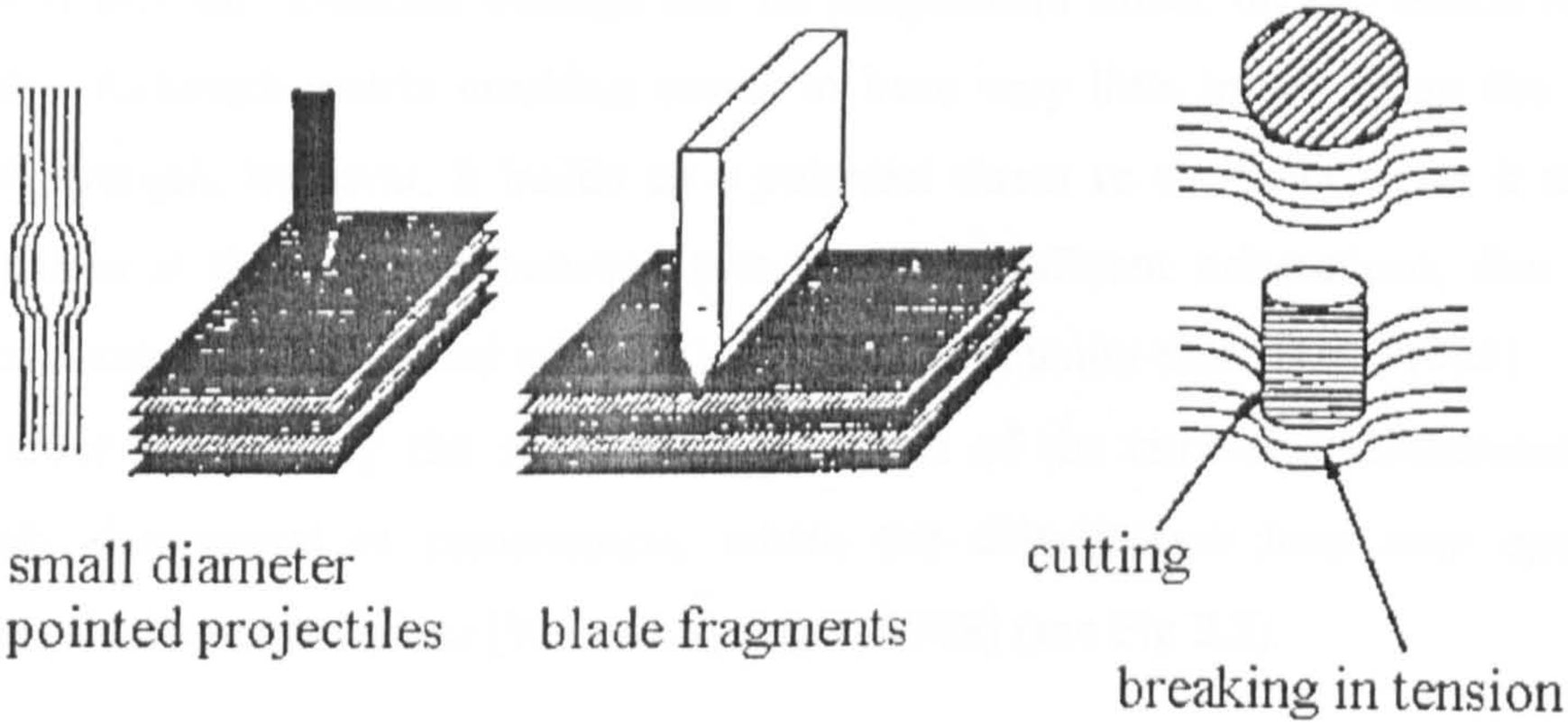

Fig 2.1 Principal mechanisms of failure in penetration

2.3 Impact Mechanics of Composites

2.3.1 Impact Energy Absorbing Mechanisms

Impact of composite materials generates a complex damage envelope consisting of regions of matrix cracking, delamination and transverse fibre fracture, in ascending order of fracture energy. Matrix cracking, the first damage mechanism, propagates in the regions of resin between individual fibres. Two major types of matrix cracks can be identified [Sun and Wang, 1986; Choi et al, 1991]. One is a transverse shear crack which occurs near the impact site due to high transverse shear stresses. The other one is a Mode I opening crack resulting from the bending stresses. According to Cantwell (1986), matrix cracking exhibits a fracture energy similar in magnitude to that of the pure matrix material. The fracture energy associated with matrix cracking is likely to be low, typically several hundreds of J/m^2 for a brittle carbon fibre / epoxy, and several thousand J/m^2 for a thermoplastic-based composite [Cantwell and Morton, 1992]. Therefore, localised matrix cracking is the first damage mechanism actuated during localised impact

loading of composite materials. Cantwell (1986) has conducted low velocity low energy impact tests on eight-ply (+/- 45), sixteen-ply (0,+/- 45) and thirty-two-ply (+/- 45) CFRP composite laminated plates in which matrix cracking was the only type of damage detected. Uniaxial tensile tests examining the residual strength of the laminates suggested that this localised damage had an insignificant effect on the tensile residual strength. Although matrix cracking seems to have very little influence on the tensile residual strength, however, it builds up a potential threat to the laminate as it triggers delamination at the interface between two layers of different orientations, due to the stress concentration associated with the material discontinuity there [Lee, 1988]. It may then reduce significantly the strength and stiffness of the laminate. Delamination is especially detrimental in compression, where the delamination area may open up, rendering the laminate useless [Wu and Springer, 1988] (see Fig 2.2).

The second damage mechanism, delamination, propagates mainly in the resin rich regions at the layer interface as a result of locally large out-of-plane interlaminar shear and tensile stresses [Cantwell, 1986; Wu and Springer, 1988; Sun and Jih, 1990; Kurashige et al, 1995]. Once again, since delamination does not involve the destruction of fibres, it displays a fracture energy comparable to that of the pure matrix system [Cantwell, 1986], and the resin fracture toughness is generally considered to control the delamination fracture [Lee,1988]. Typically, the fracture energy of delamination varies between 100 J/m^2 for epoxy-based composites to 3000 J/m^2 for thermoplastic-based composites [Cantwell and Morton, 1992]. It was observed by Sun and Rechak (1988) that delamination is induced by matrix cracks in the lamina and never seems to appear by itself. Experimental observations on plates indicate that delamination always occurs at interfaces between two layers of different fibre orientations [Cristescu et al, 1975; Abrate, 1991], and its shape is usually oblong or "peanut-shaped" with its major axis oriented in the direction of fibre orientation of the lower layer of the interface [Liu, 1988; Hong and Liu, 1989] (see Fig 2.3). However, experimental observations on cylindrical pipes and pressure cylinders indicate that the shape of delamination is often oval, or close to a fairly regular rectangle [Lloyd and Knight, 1986; Reid et al, 1991]. Considering the area of delamination indicates that this form of interlaminar fracture is a major impact energy absorbing mechanism in laminated composites [Cantwell, 1986]. Findings of several researchers [Dorey et al, 1978; Cantwell et al, 1984; Dorey, 1987; Cantwell,

1986; Reid et al, 1991] indicate that the delamination area increases with impact energy regardless of the target structure geometry. In tension, the presence of delamination around a notch or defect frequently reduces the stress concentrating effect of the defect, leading to a considerably improved tensile strength [Bishop and Morton, 1984]. However, in the case of compression, delamination precipitates a reduction in support around load-bearing fibres which ultimately leads to a premature buckling failure [Cantwell, Curtis and Morton, 1983]. This suggests that, although the presence of delamination in the structure reduces both interlaminar shear and compressive strength, it can be a beneficial in the cases in which the structure is operated purely or mostly in tensile loading (such as pressure cylinders). Moreover, it has been suggested that laminates which encourage the growth of delamination offer superior resistances to localised impact loading [Butcher and Fernback, 1981].

The third damage mechanism, transverse fibre fracture, is generally limited to regions local to the region of impact. It may develop due to high contact stresses, sub-surface local critical bending stresses, and / or stress waves. It exhibits the greatest fracture energy, considerably higher than the other two resin controlled damage modes. The typical transverse fibre fracture energies for treated and untreated CFRP composites were 20 and 60 kJ/m^2 respectively [Cantwell and Morton, 1992]. Therefore, it provides an effective mechanisms for energy absorption. Because fibre fracture frequently involves the destruction of the load-bearing constituents of the composite structure, it can precipitate significant reductions in load carrying capacity, particularly in tension [Cantwell et al, 1984; Lloyd and Knight, 1986]. Many researchers who conducted experiments on flat and cylindrical structures [Cantwell, 1986; Lloyd and Knight, 1986; Wardle and Zahr, 1987] reported that significant reductions in tensile strength were first recorded at the onset of fibre damage. Above this threshold the strength declines rapidly.

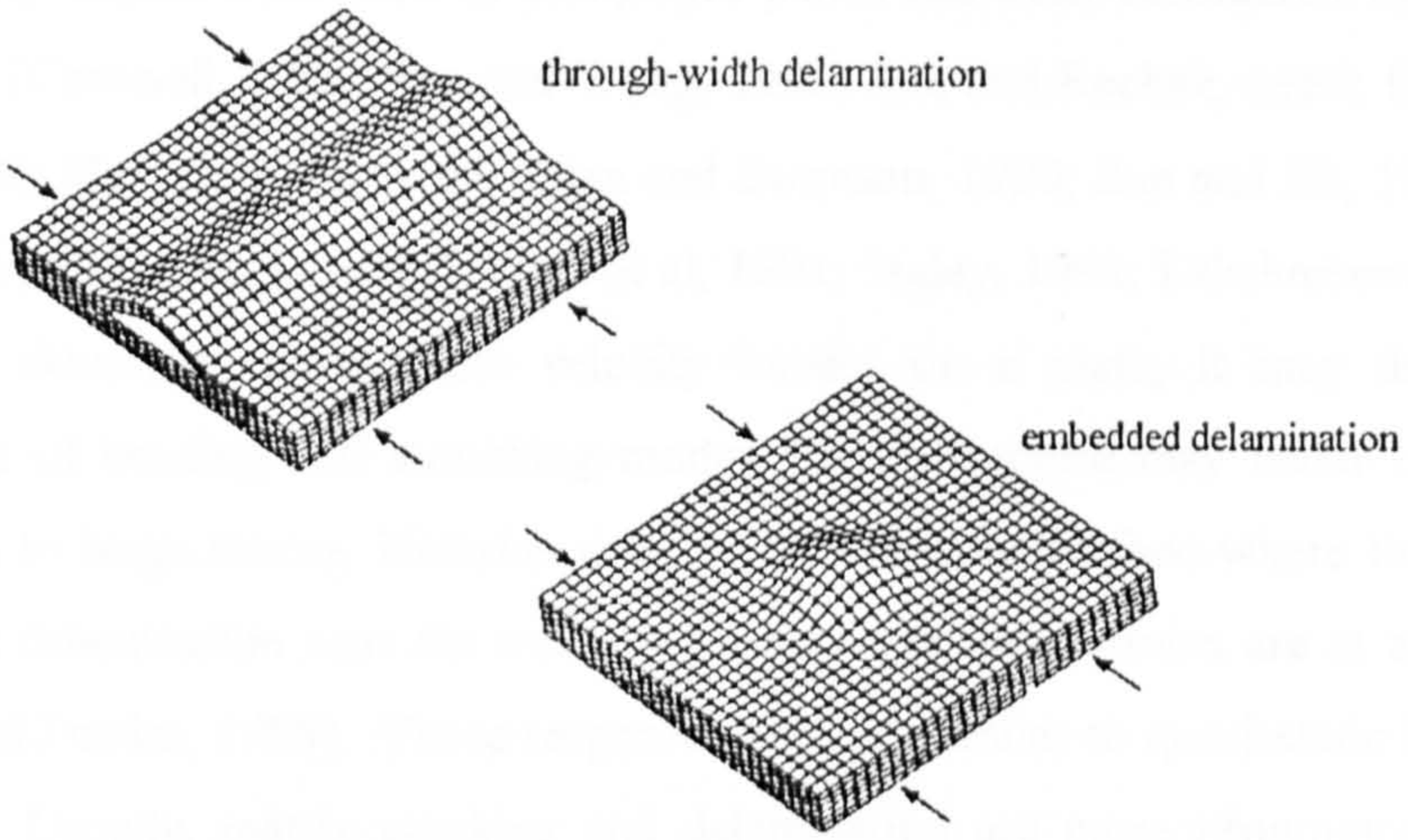

Fig 2.2 Open-up of delamination area under compression

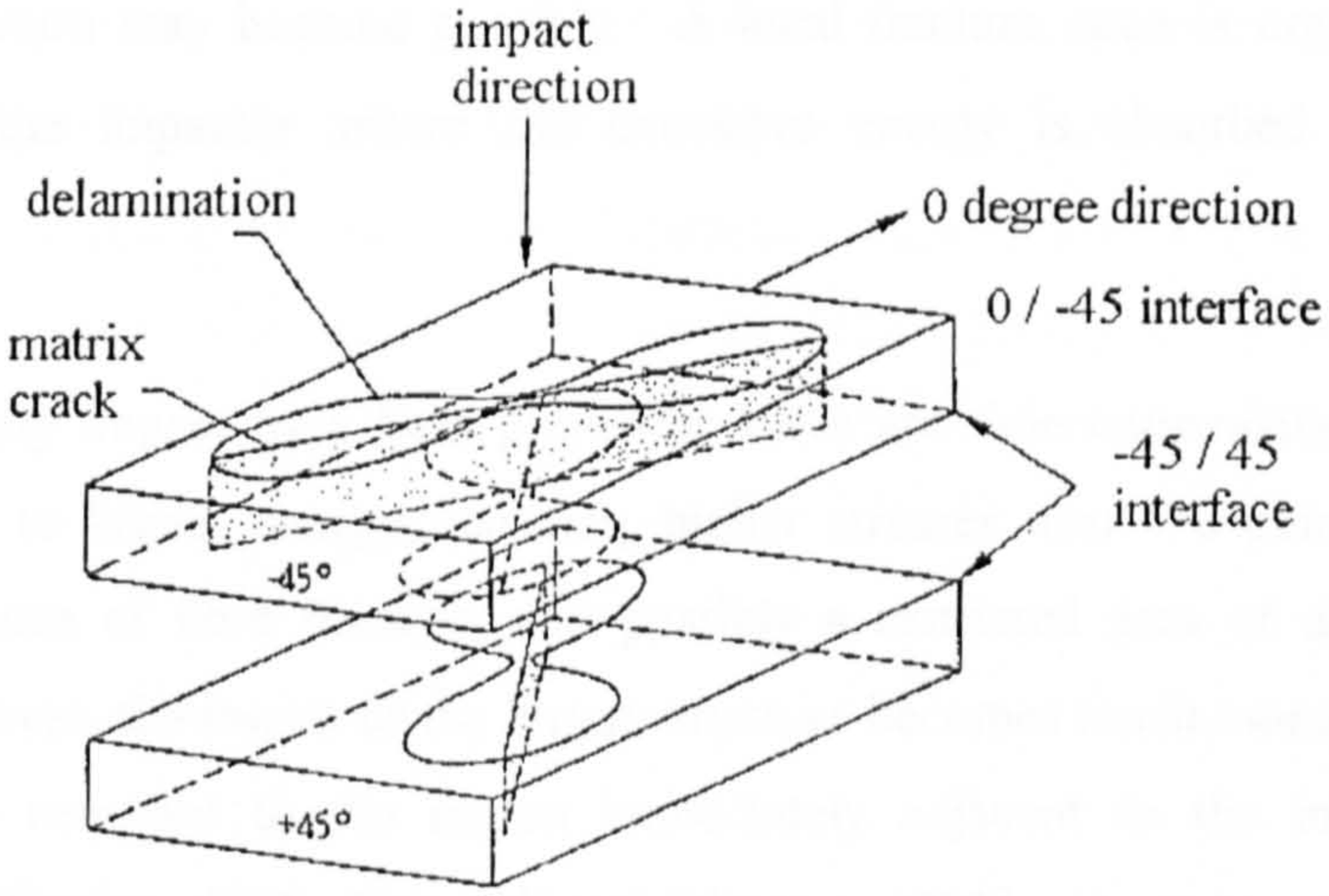

Fig 2.3 Delamination patterns in a laminate $[0/-45/45]_s$ after impact

2.3.2 Composite Plates

Low velocity impact behaviour of composite plates has been considered by numerous researchers [Cantwell, 1986; Sun and Wang, 1986; Sun and Rechak, 1988; Godwin and Davies, 1988; Hong and Liu, 1989; Qian and Swanson, 1990; Sun and Jih, 1990; Lesser and Filippov, 1991; Abrate, 1991; Choi et al, 1991; Jegley, 1992; Lakshminarayana et al, 1994a,b]. Generally, during low velocity impact on a plate, it may deflect in a combination of bending and stretching modes. Fibre fracture may occur on the rear surface due to large strains, Hertzian damage on the front surface where the impactor strikes, and delamination near the mid-plane where the shear strains are at a maximum [Godwin and Davies, 1988]. These responses are very similar to quasi-static indentation of a plate. Usually, matrix cracking and delamination are more pronounced for low velocity impact [Sun and Wang, 1986]. However, the sequence in which failure modes occur for a flat plate is very much dependent on the dimensions and boundary conditions [Robinson and Davies, 1992]. In general, it was found that delamination seems to initiate from matrix cracks [Sun and Rechak, 1988; Sun and Jih, 1990; Choi et al, 1991] As the impact energy is increased further, penetration or even perforation of the impactor into the structure may become possible. A local fracture zone is created under and surrounding the impactor where the excessive energy is absorbed by the failure processes.

At high velocity impact by a light projectile, there are time constraints on the impact event leading to higher energy densities, higher stresses near the point of impact, a greater incidence of fibre fracture, and possibly a restricted area of damage [Dorey, 1989]. Moreover, the inertia of the target structure becomes much more significant and will limit the response to the region immediately adjacent to the impacted region [Godwin and Davies, 1988; Cantwell and Morton, 1991]. A system of compression stress waves is generated around the point of impact. These waves then propagate through the thickness of the composite structure until they encounter a free surface, usually the rear surface of the target. Compressive waves are reflected to form tensile waves, and upon reaching a layer interface these waves generate large through thickness stresses often resulting in the removal of the lower surface fibres [Cantwell, 1986]. Moreover, these stress waves can lead to the detachment of a conical volume of material

with the top at the point of impact [Godwin and Davies, 1988]. If the energy of the projectile is insufficient to cause the complete detachment of this frustum, the detached material may then continue to act in a way similar to the projectile in the low velocity case, causing structure bending and spallation of a region close to the rear surface.

It may be summarised that, if the impact velocity is high enough, the major damage area is likely to be highly localised. Cantwell (1986) examined the effects of specimen geometry on the high velocity impact response, and suggested that under certain conditions, tests on small laboratory test coupons were suitable for assessing the ballistic impact capability of a full scale operational structure. On the other hand, if the impact velocity is low, the damage area of the composite structure will be spread over a large region, and full scale testing of the complete structure may be required.

2.3.3 Composite Cylindrical Structures

The impact response of composite cylindrical structures has a number of features in common with that of flat plates. For instance, the impact load-deflection plots are qualitatively similar to each other in that there are incipient, maximum load, and full penetration points [Wardle and Zahr, 1987]. However, in contrast to the impact on a plate which is influenced by the choice of boundary support, as well as the relative size of the plate, a cylindrical structure provides natural support because of its curvature, so that the boundary conditions imposed in the experiments tend to be less arbitrary [Christoforou et al, 1987].

Cylindrical Pipes

The knowledge of impact response of cylindrical pipes can form a good foundation in investigating the impact behaviour of a composite pressure cylinder. The various published research works on the impact on cylindrical pipes are very helpful when considering the impact behaviour of a composite pressure cylinder [Christoforou et al, 1987; Christoforou and Swanson, 1988; Haanes et al, 1991; Manders et al, 1979; Reid et al, 1991; Swanson and Qian, 1991]. Usually the main differences between cylindrical pipes and pressure cylinders are their geometric dimensions, such as cylindrical diameter

and wall thickness, and the lay-up pattern. Composite pipes may have an inner liner or be without liner, and have no end caps. The impact on a composite pipe generates local displacement and global deformation of the pipe, before perforation of the pipe wall may take place. In the case when perforation of the pipe wall does not occur, impact causes more extensive structural damage of the pipe wall, and significant quantities of energy can be absorbed. At sub-perforation energy levels, the total area of damage (delamination) is seen to be proportional to the applied impact energy [Reid et al , 1991]. As far as the damage mode due to impact is concerned, thin-walled and thick-walled pipes behave in a similar manner [Reid et al, 1991].

The sequence in which the failure modes of GRP pipe occur under low velocity impact at various energy levels was investigated by Reid et al (1991) and Shaw (1992). Resin whitening representing resin cracking at laminae interfaces create an area of delamination. This effect is visible at very low impact energy levels, hence it is an initial failure mode of the laminated composite material. It is closely followed by cracking of the inner liner as the severity of the impact is increased. As the input energy increases, it produces a steady increase in the extent of delamination, with the zone of whitening maintaining a fairly regular oval or rectangular shape. Moreover, two parallel cracks in the direction of fibres in the resin rich top coat appear with increased impact energy. The formation of these cracks is followed by inward collapse of the inner wall. The inner liner then fails by splitting in the circumferential direction. Resin cracking, delamination, and fibre fracture remain even if visibly the pipe restores to its original shape after low level impact. This is the evidence that some of the impact energy is absorbed in damage, and cannot be recovered. The residual strength of the structure is expected to be affected by the existence of material failure. Therefore, commonly, burst test are undertaken to determine its residual performance.

Christoforou et al (1987) have conducted an experimental investigation to study the impact response and evaluate the effects of lateral low velocity impact on the load carrying capacity of pressurised composite pipes. They found that the degree of strength loss is a function of impact energy and the type of internal support during impact (for example, various internal pressure levels). Reid et al (1991) conducted similar experimental tests on GRP pipes. They found that the presence of oil inside the pipe

served somewhat to stiffen the pipe and to localise the damage caused by impact. They concluded, however, that altering the internal pressure of an oil-filled GRP pipe does not significantly alter the response of the pipe to local impact. The presence of the oil was found to be far more important than the level to which it was pressurised.

Both Christoforou et al (1987) and Reid et al (1991) found that delamination of composite pipes is the dominant failure mode. Reid et al (1991) carried out impact tests on composite pipes with inner liner. They found that even when the liner was severely deformed under impact, but contained no fracture, the pipe showed no signs of leakage when subjected to pressure test. Although the pipes could absorb relatively large amounts of energy without perforation, in doing so they suffered considerable structural damage. Reid et al (1991) reported that when the pipes previously subjected to impact were burst-tested they all failed by leakage through the pipe wall at the point of impact.

Composite Pressure Cylinder

Very few research results have been published in the area of impact loading of a composite pressure cylinder. Among the most significant contributions in this area are Lloyd and Knight's work (1986), Wardle and Zahr's work (1987) and Yener and Wolcot's work (1989). However, they investigated mainly the residual strength of pressure cylinders after low velocity impact, and studied the main failure modes leading to performance degradation. The purpose of using composite pressure cylinders in their experiments was to simulate solid rocket motor case. Hence, only a non-load bearing leak prevention liner, such as plastic membrane, was used. For this reason, the liner was not considered in their investigation. The thicknesses of the cylinder wall ranged from 0.762 mm to 4.572 mm, with nominal diameters of 146 mm and 457 mm.

The impact response of a composite pressure cylinder is fairly similar to that of a composite cylindrical pipe. However, Lloyd and Knight (1986), after conducting a large scale low velocity impact experiment on filament-wound composite pressure cylinder, concluded that fibre fracture is the dominant factor that causes degradation in a composite pressure cylinder. They found that delamination of the pressure cylinder, although reducing shear and compressive strength, may not be detrimental to pressure

cylinder strength if no fibre fracture occurs. Wardle and Zahr (1987) have also found out that delamination does not necessarily result in a loss of performance in pressure cylinders, because their performance is controlled by the tensile properties of the fibres. Hence, major losses in burst pressure are unlikely to be seen until the first fibre damage occurs. As fibres are the load-bearing component of the pressure cylinder, the fracture of fibres affects the performance of the cylinder significantly. On the other hand, matrix fracture and delamination, which are the dominant energy-absorbing mechanisms, lead to a moderate reduction of the burst strength in a progressive sense. A much more rapid drop of burst strength can be identified once fibre fracture has occurred [Lloyd and Knight, 1986; Wardle and Zahr, 1987].

As reported by Reid et al (1991), the inner liner plays a significant role in preventing leakage during pressure test, and maintaining the function of the cylindrical pipe. The presence of the liner also can affect the failure mode. Moreover, the liners used in composite pressure cylinders also provide an improvement in mechanical strength [Hardy and Malik, 1990]. Hence, it indicates that the load sharing mechanisms under impact loading and subsequent pressure test may be affected by the presence of the liner.

Roy (1987) and Roy and Tsai (1988) did not include the liner in their analytical model in studying the composite cylinders subjected to internal and external pressure. As load bearing metallic liners always operate in the plastic domain, only the maximum plastic load supported by the liner needs to be added to the predicted failure pressure to get the overall burst pressure. However, in the transverse impact situation, the role of liner may be more important than merely acting as a leakage prevention barrier and load-sharing. When comparing the impact damage of a filament wound pipe without liner with one with a polyethylene liner, Reid et al (1991) reported that the pipe with a plastic liner can withstand impact of higher energy before losing its function. The liner showed no signs of fracture, even though it had been severely deformed inward. The liner may help to improve the impact damage resistance by absorbing significant amounts of energy. During high velocity impact, the inner liner may separate at the composite-metal interface due to the reflected tensile stress wave [Cantwell, 1986; Godwin and Davies, 1988]. Even if the impactor fully penetrate, the composite layer, it may not perforate the liner which kept debonding. This portion of debonded liner becomes more flexible and

can expend more energy than usual for perforation, as more energy would be used in elastic and plastic deformation.

Bhuyan (1992) investigated the effects of an axial defect in the composite layer of hoop-wrapped steel and aluminium NGV cylinders on the stress redistribution as well as on the bulging of the liner. He found that the liner was very effective in taking over the mechanical loading due to internal pressure if the composite layer suffered severe damage. Experimental results of Bhuyan (1992) concern the resultant hoop stress in the liner of aluminium hoop-wrapped cylinders, having an internal diameter of 238 mm and 10.9 mm thick in liner and 3.7 mm thick in composite layer, under the service pressure of 20.6 MPa. The liner stress was found to increase from 55 percent of the material's yield strength (for no defect situation) to 62.5 percent for the cylinder containing an artificial fibre cut 50 mm long, to 69.1 percent for the cylinder with liner only. Even in the worst situation of all composite layer having failed, the liner did not reach its yield strength. This naturally leads to the conclusion that the liner itself may be marginally sufficient to serve as a pressure cylinder. When considering bulging of the liner (i.e. the radial displacement), the cylinder may have already been assumed failed due to the excessive strain in the liner in this situation. However, such approach clearly would not reflect the significant role the liner plays in a composite pressure cylinder.

2.3.4 Influence of Parameters

Considering the response sensitivity to various parameters influence the impact of composite structures under various conditions helps to provide a more complete understanding of the impact behaviour of composite structures.

Lakshminarayana et al (1994a) listed some major parameters which significantly influence the impact response. These include impact velocity / energy, support conditions or boundary conditions, pre-stress state, material system, lay-up, structure geometry, such as its shape, size and thickness, wall construction, such as solid laminate, integrally stiffened, and sandwich, and the initial curvature. These parameters, they can be further classified as cylinder design parameters, or intrinsic parameters, and loading, extrinsic parameters.

2.3.4.1 Intrinsic Parameters

Material

For a composite pressure cylinder, the wall consists of a composite layer backed by a metal liner to form a hybrid composite structure. The metal liner is an isotropic homogenous material for which the material properties are well known and can be found in numerous texts and databases. Moreover, the liner itself is not directly subjected to impact loading, and the impact response of this metal liner material will not be reviewed in this section. The impact resistance of a multi-layered composite is determined by its ability to absorb energy during deformation [Cantwell, 1986]. A composite manufactured from high strength, low stiffness fibres will offer an improved resistance to impact loading. This is because the high strength, low stiffness fibres can offer high strain to failure, which is evidenced by a marked improvement in the post-impact in-plane tensile residual strength [Cantwell, 1986]. Generally, fibres with higher energy absorption property can tolerate higher impact energy before fracture [Wardle and Zahr, 1987]. In constrast, it is generally accepted that the changes in fibre properties do not have a great influence on the compressive residual strength, which is instead more sensitive to the variation in matrix and interface properties [Cantwell, 1986]. Wardle and Zahr (1987) found that soft epoxies give both high burst pressure and better impact performance of a composite pressure cylinder under impact loading than rigid epoxies, especially due to the improvement in the incipient energy required to start damage.

Delamination is known to be a major energy absorbing mechanism under impact conditions; it is primarily a resin controlled failure mode and is influenced by changes in the matrix properties. Williams et al (1982) have considered a range of over twenty different resin systems from low strain to failure epoxy resins to elastomeric resins with strains to failure as high as twenty four percent. They observed that matrix properties are indeed significant in determining the level of damage incurred in a laminated composite. Lloyd and Knight (1986) have impact tested composite cylinders with the same material system cured at two different temperatures (see Fig 2.4). An examination of delamination data indicates a significantly greater delamination for the lower cured system (154°C), 3 to 10 times greater in area. It also was found that in the 154°C cured

system more of the energy was absorbed by matrix fracture than fibre fracture relative to the higher cured system (177°C). Moreover, the cylinders with greater delamination area also had higher strength retention, since little or no fibre fracture had occurred. Therefore, if the material properties of composite structures can be carefully adjusted to encourage more suitable energy absorbing damage mechanisms under impact loading, then the structure can be improved to sustain more impact energy before failure.

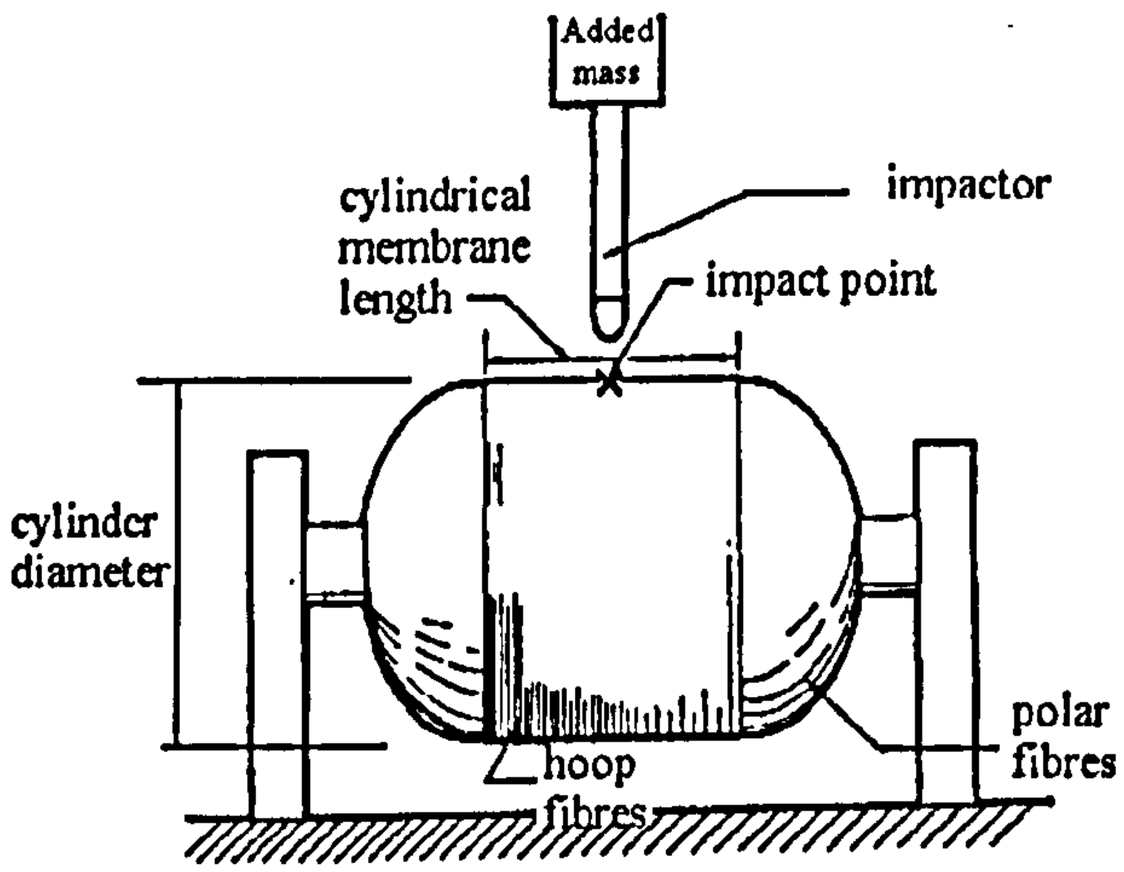

Fig 2.4 Typical impact test set-up [Lloyd and Knight, 1986]

Thickness

Lloyd and Knight (1986) have conducted low velocity impact tests on composite pressure cylinders of various wall thickness with an elastomeric liner which was thin enough to ignore its influence. They found that thin cylinders have the ability to deflect under impact and dissipate the energy without damaging the fibres, and consequently the performance of the cylinder. As the composite thickness increases, the cylinder becomes less flexible resulting in smaller deflections and more surface fibre crushing and / or cutting damage at the point of impact. Haanes et al (1991) examined the performance of GRP pipes under low velocity impact loading. They found that the behaviour of the GRP pipes is very dependent on the pipe wall thickness in that a thicker-walled pipe exhibits better resistance to cracking of the inner liner than a thinner one. Moreover, as

the thicker pipe possesses higher bending stiffness, it attains a higher maximum force and a smaller maximum deflection. As a result, thicker pipes will show a smaller delamination area (Reid et al (1991) reported similar findings). Similar phenomenon can also be found in a laminated plate [Guynn and O'Brian, 1985]. Lloyd and Knight (1988) further observed that there exists a critical combination of stiffness and impact load, for which both surface fibre fracture and fracture due to local bending or stress wave show a significant increase, and result in a large loss (~ 60 percent) in performance. As the composite thickness is increased further a point is reached where only surface damage occurs and local bending fracture is minimised. In this instance, the ratio of damaged surface fibres to total fibres volume decreases, resulting in an increase in residual burst strength.

Lay-up

Two kinds of winding design commonly used for pressure cylinders are external hoop and external polar arrangements which mean that a cylinder is fabricated so that either a hoop-wound layer or a polar-wound layer is applied last. The external polar layer is thought to provide good protection against in-service mechanical damage. The critical hoop fibres should still be able to maintain the performance of the structure, even in the presence of some damage at the surface.

In contrast to composite pipes, the variation of winding angles for pressure cylinders is limited to a small range for polar winding and 90° for hoop winding measured from cylinder axial direction. Under impact loading, an area of delamination will be generated at the interface of two layers with different winding angles due to the transverse stresses [Lee, 1988]. Hence, it appears that the number of interfaces has more effect on the total delamination area than the variation of the winding angle at an interface of two layers.

Cylindrical Diameter

Hannes et al (1991) reported that impact test results on GRP pipes of different diameters and constant wall thickness indicate that the impact energy required to cause cracks in the inner liner increased slightly with increasing pipe diameter. Although the increment of impact energy was mild, it reflected the fact that a larger portion of impact energy is stored as elastic deformation in pipe of larger diameter, since such pipes are more flexible. Lloyd and Knight (1986) found that a 457 mm diameter pressure cylinder was a much more flexible structure and shared greater absolute deflections under impact than a 146 mm diameter cylinder of similar thickness. The experimental findings of both Hannes et al (1991) and Lloyd and Knight (1986) confirm the view that cylinders of larger diameter have higher capacity for deflection without damage of fibre.

Lloyd and Knight (1986) further indicated that on their own the energy and load curves for the cylinders of both sizes, ie. 457 mm and 146 mm diameters, gave no apparent clarification for the difference seen in their performance. This highlights the important of identifying correctly the modes of failure of cylinders with various diameters. For example, elastic deformation may be favoured for larger diameter cylinders, while more localised damage is likely for a smaller diameter cylinder which appears stiffer upon impact.

2.3.4.2 Extrinsic Parameters

Boundary Conditions

Generally, the way in which the structure is restrained can influence the impact response to a large extent. For instance, the impact response for a simply support square plate is very different to that of a plate which is totally clamped at four edges, as their stiffness and response frequencies are different, with the simply supported plate being more flexible [Bachrach and Hansen, 1989]. Cylindrical structures have some natural support due to the initial curvatures, so that the external boundary conditions imposed in experiments tend to be less important [Christoforou and Swanson, 1988]. Details of the external boundary support seem to have less influence on the impact response in this

case. Ainsworth and Evans (1990) have conducted impact tests on pipes with floor support along the pipe length, and simple support in semicircular cradles at the pipe ends. They found that the same failure modes and sequence appeared regardless of the support conditions. Cantwell (1986) found that the boundary conditions have even less influence for high velocity impact situation, as only a very localised region is affected.

Prevorsek et al (1993) considered the case when a rigid carbon fibre composite is impacted without support, as normally done in testing, and then an equivalent sample is impacted while supported by a rigid panel. The impact damage in the second case was either eliminated or greatly reduced compared to the first case. It was concluded that support of any kind can improve the damage tolerance of a composite structure. This conclusion seems to be at a disagreement with what has been reviewed elsewhere in the literature.

Impactor Shape and Mass

Experimental results from Shaw (1992) indicate that impactors with large tip diameter tend to create smaller damage to the pipe, for a larger contact area between the impactor and the pipe surface distributes the load more evenly, and allows a large section of pipe to absorb the impact energy. Similarly, Haanes et al (1991) also suggested that the geometry of the impactor is an important factor for impact response. Their experimental results showed that with the same impact energy a larger contact area between the striking head and the pipe surface will reduce the impact damage. Moreover, various impactor shapes might lead to various levels of intensive shear deformation and fibre fracture, and hence the relationship between impact energy and delamination area may be changed [Reid et al, 1991]

Robinson and Davies (1992) conducted low velocity impact tests with various impactor masses on circular laminated composites of the same dimensions, and concluded that the damage to the specimens only depends the impact energy but not on the impactor mass or velocity separately. However, Christoforou (1988), by considering low velocity impact response of composite pipes, suggested that the response frequency, or the contact duration is independent of the impact velocity, and depends on the mass ratio

and the material and geometrical parameters of the structure. In the case of a heavy impactor (i.e. the mass of impactor is much greater than that of the pipe) the response can be simply obtained in a single degree of freedom analysis. This is commonly termed the quasi-static response. However, as the impactor becomes lighter (i.e. the mass of impactor is comparable or less than that of the pipe), even at low velocities higher response frequencies become important, meaning that dynamic effects must be considered [Christoforou et al, 1987].

Impactor Velocity

The impact response and the associated modes of failure may vary with impact velocity, as has already been reviewed in Section 2.2. The analytical results of Christoforou (1988) demonstrated that in the range of low velocity impact, the velocity affects only the amplitude of the response. Low velocity impact by a large mass tends to excite a global mode of structural response, enabling a high proportion of energy to be accommodated in elastic deformation. In contrast, high velocity light mass impact tends to induce very localised response permitting only a small fraction of the projectile's kinetic energy to be absorbed in elastic deformation. In this case, most of the incident energy has to be dissipated in a small volume of material local to the point of impact, resulting in material damage.

As mentioned before, when considering the impact response of a structure the influence of both the impactor mass and velocity must be taken into account. For example, the same impact energy may be delivered by various combinations of impactor mass and velocity, so that each become a significant parameter influencing the impact response.

Pre-Stress Conditions

Reid et al (1991) have impact tested internally pressurised composite pipes. The delamination area induced was found to be smaller than for an empty pipe. The energy required for perforation was four times less than for an empty pipe with wall thickness of 4.3mm. The damage zone was very highly localised. These observations show that under impact loading, a pressurised composite pipe behaves as if it is stiffer than its

empty counterpart. Christoforou (1987) found that a pipe with stiffer internal support suffered more localised damage with little or no delamination. One must conclude that increase in support, either due to internal pressure or simply by backing up with a block of solid material acts to redistribute the incident energy between various energy absorbing mechanisms, possibly causing the dominant mode of failure to be changed.

Significant results have been reported in the literature on the impact response and damage of laminated plates pre-stressed in tension [Sun and Chattopadhyay, 1975; Sankar and Sun, 1985; Wu and Springer, 1988]. Under transverse impact, tensile initial stresses tend to increase the magnitude of the contact force, but reduce the contact duration and plate deflection. These changes in behaviour reflect the fact that the plate becomes effectively more rigid due to the initial tensile stress. Review of the behaviour of initially pre-stressed plate shows that initial tension redirects impact energy from recoverable elastic deformation into localised fracture processes, and this is detrimental.

Bert and Birman (1988) used a simplified energy-balance approach to study the impact response of prestressed cylindrically curved composite structures subjected to low velocity impact. They concluded that the effect of tensile prestress due to internal pressure is beneficial in reducing impact deflection. Their results indicated that internal pressurisation can improve the low velocity impact resistance of composite panels.

2.4 Impact-Induced Degradation

2.4.1 Failure Criteria

2.4.1.1 Failure of Composite Material

It is commonly accepted that a composite material is regarded as "damaged" when its original design strength or load carrying capacity is reduced by the failure of its constituents, such as matrix cracking, delamination, and fibre fracture. Therefore, a simple criterion which reflects the strength and integrity of the material is preferred for use to characterise the status of the material. However, a composite material has many failure modes, and multiple criteria have been developed to describe these failure modes.

There are two popular approaches for criteria of unidirectional composites, which are the maximum stress and strain criteria, and the quadratic failure criterion [Hoa, 1985]. They are all based on the use of axial stress or strain as the primary variables. Although Hill's classical yield criterion for anisotropic metals was developed within the theory of plasticity, it had been extended to represent a failure criterion for composites, with many further variations of this criterion having been also proposed. Labossiere and Neale (1991) have given a detailed review on the development of these failure criteria. Several commonly used composite strength theories are reviewed here.

2.4.1.2 Failure Theories

I. Maximum Stress Theory

Jenkins (1920) extended the concept of the maximum normal or principal stress theory to predict the strength of planar orthotropic materials such as wood. With this theory, the stresses acting in a material are resolved into the directions of symmetry, i.e. σ_1, σ_2, τ_{12}. It is then postulated that failure will occur when one (or all) of these stresses attains a respective maximum value of its strength, X, Y, S. This criterion states that failure does not occur as long as the following condition prevail,

$$\begin{aligned} -X' < \sigma_1 < X, \\ -Y' < \sigma_2 < Y, \\ -S' < \tau_{12} < S. \end{aligned} \qquad \text{.....(1)}$$

where X, X', Y, Y' and S, S' are the uniaxial tensile and compressive normal and shear strengths, respectively, with respect to the in-plane directions of material symmetry. For the principal material axes, S = S', so that shear strength is independent of the sign of τ_{12}. However, there is absolutely no allowance made for the interaction among different modes of failure with this theory. Rupture may be actually predicted by the least of the three expressions in Equation (1).

II. Tsai-Hill Theory

Tsai-Hill analysis considers the lamina as the basic unit of a laminate. The criterion is not invariant with respect to co-ordinate rotations and is consequently restricted to specially orthotropic materials. This makes this criterion unsuitable for direct application to the whole laminate.

The initiation of failure in each ply is governed by the following Tsai-Hill failure criterion :

$$\left(\frac{\sigma_1}{X}\right)^2 - \frac{\sigma_1\sigma_2}{X^2} + \left(\frac{\sigma_2}{Y}\right)^2 + \left(\frac{\tau_{12}}{S}\right)^2 = 1 \qquad \text{.....(2)}$$

where X and Y are the uniaxial strengths parallel and perpendicular to fibres, and S is the shear strength. The stresses in each lamina σ_{ij} are related through Hook's law to the strains ε_{ij} in each lamina, which in turn can be calculated by from the total laminate strains.

In practice, the loading can be applied to the laminate incrementally until failure is found in one or more of the individual plies according to the above criterion. Each ply failure can then investigated further to determine whether degradation has taken place through resin or fibre failure.

It should be emphasised that the maximum stress theory involves several separate equations and takes no account of the interaction between the stresses or failure modes. In comparison, the Tsai-Hill quadratic criterion does make a provision for interaction between different modes.

III. Tsai-Wu Stress Theory

In order to analyse the experimental results more accurately, Tsai and Wu (1971) proposed a lamina failure criterion with additional stress terms which do not appear in

the Hill analysis (Hill analysis is a generalisation of the Von Mises' formulation which includes anisotropy). They assumed that the failure surface in stress space has the form

$$f(\sigma) = F_i\sigma_i + F_{ij}\sigma_i\sigma_j = 1, \qquad i,j = 1,2,\ldots,6. \qquad \ldots\ldots\ldots(3)$$

Here F_i and F_{ij} are the second and fourth order lamina strength tensors. The linear stress terms account for the possible differences in tensile and compressive strengths. The quadratic stress terms are similar to those in the Tsai-Hill formulation, and describe an ellipsoid in the stress space which is also commonly termed the failure envelope. terms are new. Note that the off-diagonal terms F_{ij} ($i \neq j$) of the strength tensor describe the mived interactions among the stress components. Under plane-stress conditions, this failure criterion becomes

$$F_1\sigma_1 + F_2\sigma_2 + F_6\sigma_6 + F_{11}\sigma_1^2 + F_{22}\sigma_2^2 + 2F_{12}\sigma_1\sigma_2 + F_{66}\sigma_6^2 = 1 \qquad \ldots\ldots(4)$$

where

$$F_1 = \frac{1}{X} - \frac{1}{X'}, \quad F_2 = \frac{1}{Y} - \frac{1}{Y'}, \quad F_6 = \frac{1}{S} - \frac{1}{S'},$$
$$F_{11} = \frac{1}{X\,X'}, \quad F_{22} = \frac{1}{Y\,Y'}, \quad F_{66} = \frac{1}{S\,S'}, \qquad \ldots\ldots(5)$$
$$F_{12} = F_{12}^{*}\sqrt{F_{11}F_{22}} = \frac{F_{12}^{*}}{\sqrt{X\,X'Y\,Y'}}$$

X, Y, S and X', Y', S' are the lamina longitudinal, transverse and shear strengths in tension and compression, respectively. The term F_{12}^{*} is the mixed term and has to be determined from a biaxial test. Performing such a biaxial test on a laminate is not straightforward, and often the value of the coefficient F_{12}^{*} is estimated to be -1/2 without a significant loss in accuracy [Hoa, 1985].

The Tsai-Wu quadratic tensor strength theory has advantages over the Tsai-Hill theory, which include : (1) it transforms according to established tensorial laws, (2) it predicts symmetrical strength properties linked to stiffness and compliance, and (3) it allows for 'mixed' interactions between different stress components.

The Tsai-Wu stress criterion is typically used in conjunction with linear-elastic lamina response in the accompanying lamination theory. The criterion predicts the initiation of the failure but not the active failure mode, such as axial tensile or compressive failure, or transverse shear etc. This theory has gained wide acceptance for plane stress conditions, although estimating the value of the interaction coefficient F_{12}^{*} is still a debated question [Labossiere and Neale, 1991].

IV. The Failure Mode Identification Criterion

Since the Tsai-Wu criterion does not provide any information concerning the failure modes which occur in the material. To remedy this situation, a failure mode identification criterion was proposed by Hashin (1980) and by Chang and Springer (1986). The criteria are :

(1) Fibre breakage

Tensile failure of fibres (for $\sigma_{11} > 0$) :

$$\left[\frac{\sigma_{11}}{S_{1T}}\right]^2 + \left[\frac{\sigma_{12}}{S_{12}}\right]^2 + \left[\frac{\sigma_{13}}{S_{13}}\right]^2 = 1$$

Compressive failure of fibres (for $\sigma_{11} < 0$) :

$$\left[\frac{\sigma_{11}}{S_{1C}}\right]^2 = 1$$

(2) Matrix cracking and delamination

Tensile failure of matrix (for $\sigma_{22} > 0$) :

$$\left[\frac{\sigma_{22}}{S_{2T}}\right]^2 + \left[\frac{\sigma_{23}}{S_{23}}\right]^2 + \left[\frac{\sigma_{12}}{S_{12}}\right]^2 + \left[\frac{\sigma_{13}}{S_{13}}\right]^2 = 1$$

Compressive failure of matrix (for $\sigma_{22} < 0$) :

$$\frac{1}{S_{2C}}\left[\left(\frac{S_{2C}}{2S_{23}}\right)^2 - 1\right]\sigma_{22} + \left[\frac{\sigma_{22}}{2S_{23}}\right]^2 + \left[\frac{\sigma_{23}}{S_{23}}\right]^2 + \left[\frac{\sigma_{12}}{S_{12}}\right]^2 + \left[\frac{\sigma_{13}}{S_{13}}\right]^2 = 1$$

The advantage of this criterion over the other failure theories is that it helps to identify the failure modes occurring to the structure, such as delamination between layers. However, the formulation of this criterion often seems to be too complicated and difficult to apply.

2.4.1.3 The Choice of Failure Theories

There is no single criterion which is universally applicable to the general case of any fibrous composite material subjected to a multiaxial stress system. Moreover, the choice of failure criterion is also related to the type of analysis being undertaken. In other words, it depends on what is expected from the analysis, ie failure detection, failure mode identification, or both. When the behaviour of a pressure cylinder under various impact loading is considered, non-interactive failure criteria such as the maximum stress theory, together with the failure mode identification criteria, can be used to determine the onset of various failure modes, and to rank different energy absorbing mechanisms.

2.4.2 Failure of Structure

In a very broad sense, failure of a structure can be said to have taken place when it ceases to perform its function satisfactorily. Therefore, the definition of failure of the structure could vary from one application to another. For example, in filament-wound pressure vessels with symmetrically laminated walls without a liner and having a single helical angle of winding, the failure of the first ply is usually considered as the total

failure of the vessel [Hoa, 1985; Lifshitz and Dayan, 1995]. However, when the vessel is constructed by filament winding over a metal liner in more than one direction, the wall is no longer symmetric and failure of the first ply cannot be necessarily identified with the total failure of the vessel [Teply and Herbein, 1985; Lifshitz and Dayan, 1995]. Therefore, the choice of a criterion for structural failure plays a significant role in determining the service life of a structure. The choice of failure criterion may also reflect the design concept, ie either conservative or optimistic.

Commonly used failure criteria for composite cylindrical pipes under impact loading include the cracking in the pipe's liner leading to leakage, or the level of impact load to which a pipe can be exposed and still maintain its function [Hannes et al, 1991]. Between these two approaches, the first criterion is optimistic while the second one conservative.

2.4.3 Post-Impact Performance

2.4.3.1 Residual Strength

It has been suggested that strength loss associated with damage induced by impact loading is an important parameter describing response of a structure to impact [Lakshminarayana et al, 1994a]. Impacts may cause both visible and invisible damage. They also can result in a significant reduction in the maximum load-carrying capability. Jegley (1992) found that full penetration of an impactor into a composite panel at a high speed (e.g. 150 m/s) could cause less damage than if an impactor had bounced off the panel. The author concluded that the different amount of damage explains why the panel has a higher post-impact load-carrying capability with a through penetration than without. This may be acceptable for a secondary structure. However, for a primary structure such as a composite pressure cylinder, a fully penetrated hole is not allowed to exist at any part of the cylinder, otherwise, the main function of a pressure cylinder is lost. It has been suggested [Yener and Wolcott, 1989; Wardle and Zahr, 1987; Lloyd and Knight, 1986] that a good measure of damage induced by impact loading is the residual strength of an impact damaged cylinder, as represented by the ratio of the burst pressure of the damaged cylinder, p, to the initial undamaged cylinder burst pressure, p_0.

This performance ratio is often termed the burst pressure ratio p/p_o. Reid et al (1991) conducted residual tests on impact damaged GRP pipes and found that although GRP pipes were capable of absorbing fairly high levels of impact energy through various failure mechanisms without perforation, their designated function may have been lost or reduced to an unacceptable in-service condition due to serious damage so that these GRP pipes had to be replaced. Thus, residual strength can be an indicator of the survivability of a pressure cylinder under impact conditions.

Lloyd and Knight (1986) have undertaken low velocity low energy impact tests on filament-wound pressure cylinders (cylinder diameter, 146 mm; wall thickness, 2 mm). Under the impact energy of 2.7 J, the deflection was 3.81 mm and no performance degradation in terms of the burst pressure ratio was found. By increasing the impact energy to 6.1 J, a 6.35 mm deflection was produced, and the cylinder lost 18 percent in terms of the burst pressure ratio. It was suggested that fibre-fracture by local bending may have happened due to excess deflection generated. This experimental finding could be taken as the evidence that fibre fracture of the cylinder contributes significantly to the loss of residual strength of a pressure cylinder. Wardle and Zahr (1987) have conducted a similar low velocity impact tests on filament-wound pressure cylinders (cylinder diameter, 457 mm; wall thickness, 4.57 mm). Under 15 J impact, the burst pressure ratio p/p_o was nearly unity. A 7.5 % drop of p/p_o was found as the impact energy was further increased to 35 J. However, at 50 J impact, the p/p_o loss was nearly the same as at 35 J impact. It is obvious that more damage would be induced at a higher impact energy. Since no further drop of p/p_o is seen, it can be suggested that the extra energy was absorbed by other energy absorbing mechanisms such as matrix cracking and / or delamination [Bachrach and Hansen, 1989]. As the impact energy was increased to 114 J, a further 5 % drop of p/p_o was found. It indicates that some load bearing fibres were damaged when alternative energy absorbing mechanisms had been saturated. Wardle and Zahr (1987) also suggested that delamination does not necessarily result in a loss of performance in pressures cylinder because the performance of this pressure cylinder is dominated by the tensile properties of the fibres. Therefore, major losses in burst pressure are unlikely to be seen until the first fibre damage occurs. Bachrach and Hansen (1989) investigated the sequential failure in a composite cylinder under low-velocity

impact, and suggested that impact damage may be assumed insignificant if the energy-absorbing phenomenon is dominant. However, once fibre-fracture occurs during an impact event, then catastrophic failure could become possible.

The state of damage induced by impact loading in a composite structure may be complex, with various failure mechanisms co-existing in the structure at the same time. Their interaction under a designated operating load, such as internal pressure for a pressure cylinder, are difficult to predict. Residual strength can be a good experimental measure of how various levels of impact loading influence the ability of the cylinder to maintain its function. This can be seen as a kind of performance test on a cylinder having in-service mechanical damage. Further development of predictive models is required to improve component design.

2.4.3.2 Fatigue Life

Bhuyan (1992) investigated in-service damage to the composite wrapping of an aluminium hoop-wrapped cylinder used in NGV service. He has found that in-service damage not only reduced the residual strength, but also could reduce fatigue life of the cylinders. Connolly and Hudak (1994) also found that damage in composite overwrap transfers an extra portion of load to the liner, thereby reducing the liner life.

Bhuyan (1992) claimed that, by the calculation of a bulging factor for a damaged cylinder, the relative fatigue performance of the cylinders can be assessed without conducting prototype tests.

2.5 Mathematical Models

Kurashige et al (1995) established an analytical approach based on the Ideal Fibre Reinforced Materials (IFRM) theory [Spencer, 1972] in an attempt to evaluate the interlaminar shear stresses developed in a fibre reinforced laminate under a concentrated force (see Fig 2.5). With the use of this analytical model, a remarkable agreement was found in terms of the shape between the contours of interlaminar shear stress in the direction normal to the fibre, and the delamination crack geometries observed

experimentally. This model confirms that delamination may be caused by this interlaminar shear stress.

Many mathematical models and semi-empirical methods have been developed to predict the transient dynamic response, such as force history at the point of impact. The most commonly used models for low velocity impact of composite structures are the spring-mass model with various number of degrees of freedom [Shivakumar et al, 1985; Rotem, 1988; Sjoblom et al, 1988; Abrate, 1991]. These can predict the force history, velocity or displacement throughout the impact. The energy-balance model [Shivakumar et al, 1985; Bert and Birman, 1988] is a first-mode approximation of the spring-mass model and only yields the maximum force. Two commonly used basic methods for predicting the impact force, including the effect of contact deformation of laminated plates and shells, are the Hertz method which includes the contact deformation, and the modified Hertz method which includes both flexural deflection and contact deformation [Greszczuk, 1982; Shivakumar et al, 1985]. These models primarily focus on predicting the contact force of an impactor or the dynamic responses of target structures. Failure mode analysis must be performed subsequently to assess structural damage.

While local deformations in the contact zone are generally not included in the classical structural models for beams, plates, and shells, the above mentioned mathematical models used to predict the contact force and the structural response may adequately represent the global motion of the structure, the dynamics of the impactor, and the local deformation in the contact region.

Due to the complexity of impact loading of a complicated structural shape, it is not possible to establish a reliable mathematical model for analysing impact response. The most commonly adopted numerical method is the finite element analysis [Kubo and Nelson, 1975; Kapania, 1989; Langlie and Cheng, 1989; Reedy et al, 1997].

In recent years, the concept of degenerated shell elements has been introduced to represent composite shells [Kapania, 1989; Lin and Lee, 1990a,b; Doh and Hong, 1995]. The development of this degenerated shell element is an extension of the work by

Ahmad, Irons, and Zienkiewicz (1970). It uses an eight-noded thick shell element consisting of *n* layers of lamina in the thickness direction.

Yener and Wolcott (1989) have illustrated the progressive failure analysis technique by using the finite element method with shell elements to assess damage quantitatively due to any type of loading, including impact. Doh and Hong (1995) have also studied the progressive failure of a filament wound pressure vessel by finite element method with degenerated shell elements. A fairly good agreement was obtained between the analysis and test results.

As suggested by many researchers, for a complicated structure and loading, progressive failure analysis may be even more informative than experimentation. However, an experimental investigation is essential in order to identify initial damage sensitivity parameters [Yener and Wolcott, 1989].

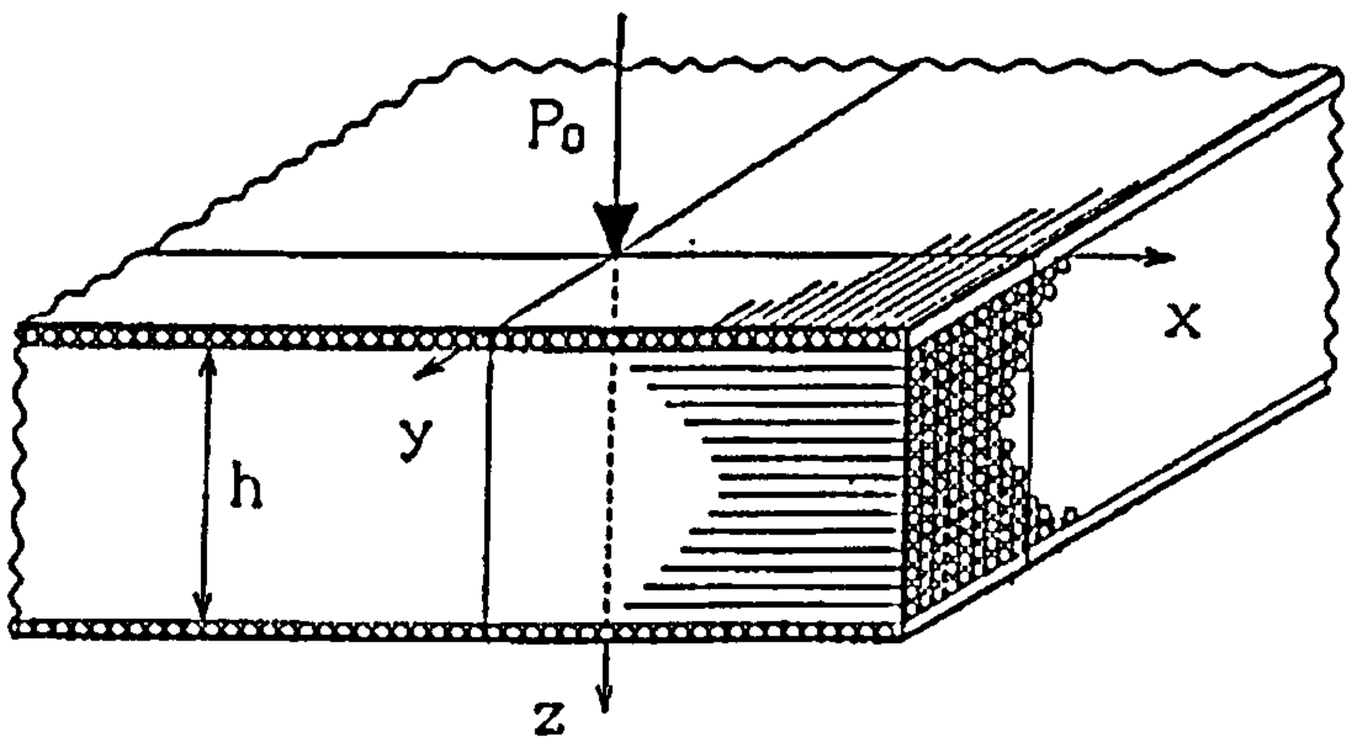

Fig 2.5 Schematic of a 3-layer fibre-reinforced laminate of infinite extent subjected to a concentrated forced P_o (The IFRM Theory) [Kurashige et al, 1995]

Chapter 3 Modelling : Fundamentals

3.1 Analytical Models

3.1.1 The Hertzian Contact Solution

It is obvious that an accurate account of the contact behaviour is one of the most important steps needed to analyse the impact response problems. The classical contact solution between an elastic sphere and an elastic half-space which was first developed by Hertz (1881) has been used by many researchers for the study of impact on homogeneous isotropic materials [Goldsmith, 1960]. Hertz derived the contact solution using a potential function to describe the local stresses and deformations as functions of the geometries of the contacting bodies and their elastic properties. This theory, although both static and elastic in nature, has been widely applied to the impact situation where plastic flow extends only to the vicinity of the contact point and does not permeate throughout the entire cross-section.

In studying impact response of anisotropic materials such as fibre reinforced composite laminates, however, the problem becomes more complicated. As the Hertzian contact law was derived based on homogeneous isotropic materials, it may not be adequate in describing the contact behaviour of composite laminates due to their anisotropic and non-homogeneous properties. Moreover, most of the composite laminates or structures are quite thin and cannot be represented by a half-space [Tan and Sun, 1985]. Therefore, adjustment of stiffness parameters based on the experimental results is needed.

During impact, large local transverse direct stress σ_{33} and strain ε_{33} are expected to be induced in the impacted material by the contact of the impactor. Experimental observations have shown that the material near the contact area is extensively damaged, but the size of the damage zone is not large and is found to be localised around the region near the contact area. Therefore, it seems reasonable to represent the results of the contact deformation by a global equation which relates the average force and the

resulting deformation. In general, for low velocity impact, Hertzian contact law can provide a reasonable agreement with experimental results. Accordingly, an analytical approach has been established based on Hertzian contact law and energy balance equation of plate and impactor system for studying the response of composite materials to low velocity impact. This analytical approach can be summarised into three major steps. First, the impact-induced surface pressure and its distribution are determined based on the Hertzian contact relation. Secondly, the internal triaxial stresses in the composite target caused by this surface pressure can then be determined by using either closed-form solutions or finite element codes. Thirdly, failures and failure modes of the target caused by these internal stresses will be determined by static failure criteria.

The results obtained by Rayleigh (1906) showed that if the contact duration between the impactor and the target is very long in comparison with their natural periods, vibrations of the system can be neglected. Therefore, Greszczuk (1982) employed a modified Hertzian law in his analysis of impact indentation on composite panels. The Hertzian force-deformation relationship was written in the form :

$$P = n\,\alpha^{3/2}$$

where P is the contact force,

α is a measure of indentation approach (depth), and

n is the contact stiffness parameter.

The contact stiffness parameter n reflects the material and geometrical properties of the plate and the impactor. For an elastic spherical impactor striking a transversely isotropic composite medium, the parameter n was derived by Conway (1956b) and Greszczuk (1982) in the form

$$n = \frac{4\sqrt{R_1}}{3\pi(K_1 + K_2)}$$

where

R_1 is the radius of a spherical impactor or indenter,

K_1 is the stiffness parameter of the impactor, and

K_2 is the stiffness parameter of the composite medium.

$$K_1 = \frac{1-\nu_1^2}{\pi E_1}$$

$$K_2 = \frac{\sqrt{A_{22}(\sqrt{A_{11}A_{22}}+G_{zr})^2-(A_{12}+G_{zr})^2}}{2\pi\sqrt{G_{zr}}(A_{11}A_{22}-A_{12}^2)}$$

$$A_{11} = E_z(1-\nu_r)\beta$$

$$A_{22} = E_r\beta(1-\nu_{zr}^2\delta)/(1+\nu_r)$$

$$A_{12} = E_r\nu_{zr}\beta$$

$$\beta = \frac{1}{(1-\nu_r-2\nu_{zr}^2\delta)}$$

$$\delta = \frac{E_r}{E_z}$$

The constants E_1 and ν_1 are the Young's modulus and Poisson's ratio of the impactor respectively. The constants E_r, E_z, G_r, G_z, and ν_r, ν_{zr} are the Young's moduli, the shear moduli, and the Poisson's ratios of the composite medium in r- (radial) and z- (transversal) directions, respectively.

By using this approach, the magnitude and distribution of surface pressure in the target caused by impact can be obtained, by analytically combining the dynamic solution to the problem of impact of solids to determine the peak contact force with the static solution for the pressure between two bodies in contact. This approach can be seen as a variation of the method described by Timoshenko (1934) for the impact of homogeneous isotropic spheres.

3.1.2 The Composite Shell Structures

Christoforou (1988) established a method for examining the response of simply-supported orthotropic cylindrical shells subject to impact loading. The approach which was originally proposed by Bert and Birman (1986). A closed-form solution obtained by linearising the contact force equations was used. The analysis focused on the transient response due to impact force to calculate deflections and strains. The impact force was assumed to be distributed over a small rectangular area.

Christoforou's approach represents a development of the classical method known as the Navier solution. It is based on the expansion of the load, displacements, and rotations in a double Fourier series which is chosen to satisfy the end boundary conditions of simple support. Each expansion is assumed to be separable into a function of time and a function of position. Furthermore, by neglecting the in-plane and rotary inertia effects, the problem becomes a second order ordinary differential equation in time for the Fourier coefficients of the radial deflection. The right hand side of the differential equation contains the Fourier coefficients of the loading function. Therefore, for a given loading impulse the solution can be found by invoking the convolution integral. The impact force is computed from the deceleration of the impactor mass, which appears in the equation of equilibrium between the impactor and the shell during contact. By further neglecting the local deformation, the resulting integral equation can be solved algebraically for the impact force by taking the Laplace transform. The expressions for the impact response and force as a function of time are obtained by using the inversion theorem for the Laplace transform in conjunction with the Cauchy residue theorem. In this analytical closed-form solution approach, the impactor is treated as non-deformable, and no damage mechanism is being considered. Further detail of the formulations of this analytical approach can be found in Christoforou's PhD thesis (1988).

The analytical method has been coded into two FORTRAN programs (ROOTFIND.f and IMPACT.f) by Christoforou in order to obtain results for low velocity impact on composite shells. ROOTFIND.f serves to find the response frequencies for a given impact situation. Once the frequencies are found, the impact response can be obtained

by using IMPACT.f. This routine computes the deflections, impact forces and strains under given load as a function of time, and spatial distributions of deflection and strain.

In the present study, results obtained from this analytical closed-form solution approach were used to validate the numerical solutions obtained by using the finite element (FE) approach. This can justify the use of the FE approach for investigating the impact behaviour of composite NGV pressure cylinder considered in the present study. One of the models analysed by Christoforou was chosen for validation (see Fig 3.1.1). The configurations and material properties for the model, and impact loading are given in Tables 3.1.1 and 3.1.2, and Fig 3.1.1.

Table 3.1.1 Configuration and Impact Loading

General Details

Items	Descriptions
Structural Shape	Cylindrical Shell (Half circular arc)
Lay-up	[90°/+-22°/90°/+-22°]
Material	IM7 / 55A Carbon / Epoxy

Geometric Dimensions and Impact Loading

	Analytical Method	**FE Method**
Inside Diameter	100 mm	100 mm
Length	420 mm	420 mm
Thickness	1.524 mm (0.245 mm/layer)	1.524 mm (0.254 mm / layer)
Initial Velocity	3.03 m/s	3.03 m/s
Contact Area for Load Distribution	0.0106 mm^2 20.936 mm^2 83.744 mm^2 251.232 mm^2	Point Loading [Point] 20.936 mm^2 (4 elements, 21 nodes) [A1] 83.744 mm^2 (16 elements, 65 nodes) [A2] 251.232 mm^2 (36 elements, 133 nodes) [A3]
Impactor Mass	0.0163 kg	[Point] 0.0163 kg [A1] 0.7762E-3 kg / node [A2] 0.251E-3 kg / node [A3] 0.1226E-3 kg / node
Mass Ratio **(impactor mass / shell mass)**	0.1	0.1

Table 3.1.2 Material properties

Material : IM7 / 55A Carbon / Epoxy

E_{11} = 169 GPa

E_{22} = 6.72 GPa = E_{33}

G_{12} = 5.26 GPa = G_{13}

ν_{12} = 0.26 = ν_{13}

ν_{21} = 0.11

ν_{23} = 0.3

ρ = 1650 kg / m^3

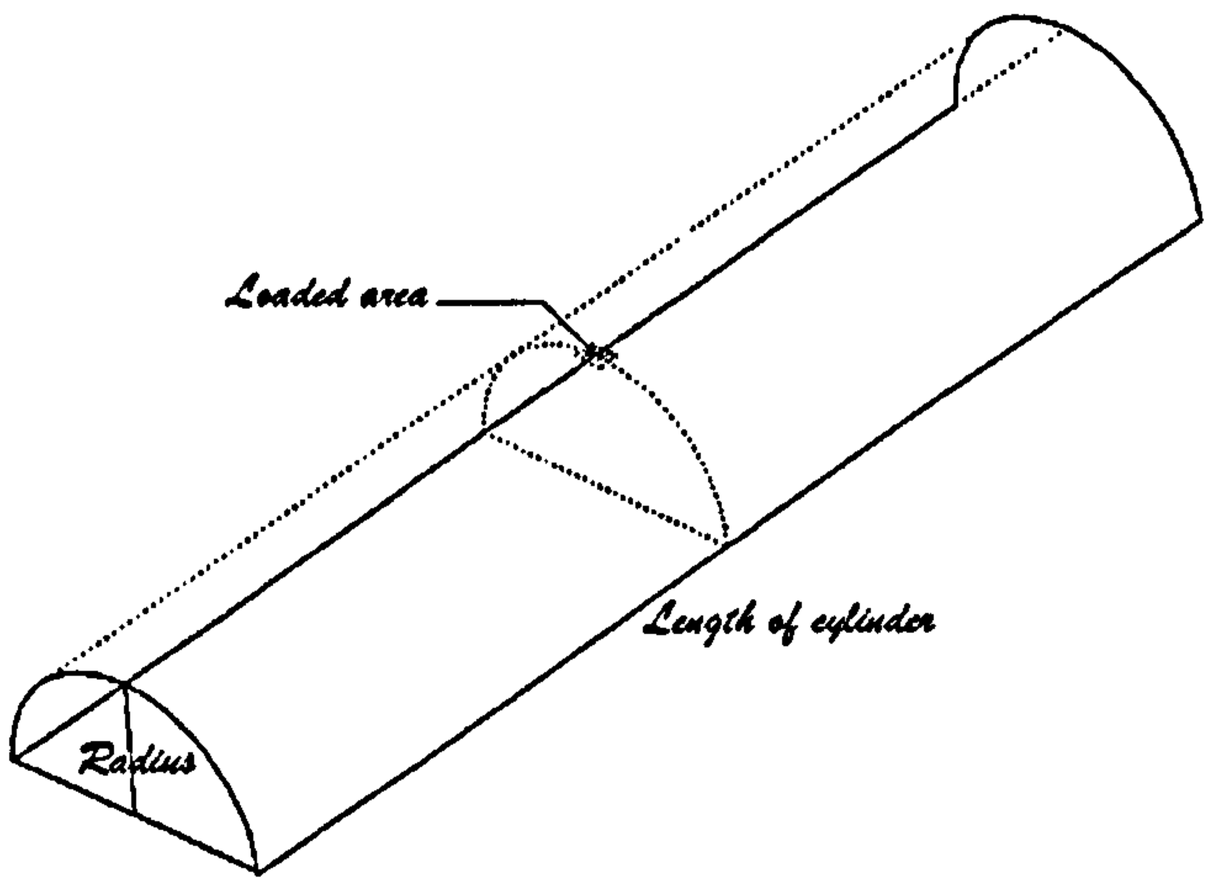

Fig 3.1.1 Geometry of an analytical model

3.1.3 The IFRM Theory

The task of complete evaluation of the stresses in a composite laminate subjected to impact loading is a complex problem of anisotropic elasticity. In addition to the complexity of orthotropy, this problem involves the variation of stress and strain fields in three dimensions.

In an attempt to reduce the degree of difficulty of such problems, a linear theory of ideal fibre reinforced materials (IFRM) was proposed by Spencer (1972) and Pipkin and Rogers (1971a).

The basic idea of this theory is to assume that the materials are completely inextensible in the fibre direction, and incompressible in volume. Due to these kinematical internal constraints the governing equations become simplified, so that even fully three dimensional problems can sometimes be solved in their entirely. Kurashige et al (1995) used IFRM in order to evaluate interlaminar shear stresses in a fibre reinforced laminate of [90°/0°/90°] under the action of a concentrated force.

They considered the problem of an infinitely extended laminate composed of three layers of [90°/0°/90°]. Both surface layers of this laminate have an infinitesimal thickness and inextensible in the fibre direction. With these conditions, the boundary value problem can be reduced to that only for the core layer. The laminate is subjected to a concentrated force normal to its upper surface.

The analytical solution was obtained by using a double Fourier transforms. The solution results in double infinite integral expressions for the interlaminar shear stresses at the lower interface. These can be reduced to single finite integrals by variable transformation, and be evaluated by numerical methods.

3.2 Finite Element Modelling

A general purpose finite element code PAFEC [1] Level 8.1 was used for analysing low velocity impact response. The finite element (FE) meshes for the discretised models were generated using PIGS [2] Level 8.1, a pre- and post-processor. One of the advantages of the FE approach to the analysis of impact behaviour is that it allows barely visible or invisible levels of damage to be assessed. It is also possible to account for the development of damage within the structure by degrading the material properties of failed elements, such as stiffness and strength.

Both dynamic and static analyses have been used in this investigation. For dynamic analysis, the Ahmad type eight-noded thick shell element with orthotropic material definition was used to generate the finite element mesh. This type of element is based upon a degenerate three dimensional analysis which incorporates the effects of transverse shear. The effects of direct stresses in the through-the-thickness direction are, however, neglected. Each node of the element has six degrees of freedom. Some degrees of freedom become redundant when the element is flat. Membrane and bending actions are included in the analysis, as well as the effects of shear deflections.

For static analysis, a twenty noded isoparametric three dimensional brick element with orthotropic material definition was used to generate the finite element mesh. This is a generally shaped three dimensional brick type element with six curvilinear faces and twelve edges. There are eight corner nodes and one mid-side node on each of the edges, giving twenty nodes in total.

The major difference of the dynamic analysis from its static counterpart is marked by the incorporation of the inertial effects. The effect is proportional to the acceleration of the structure, and its mass. Hence, the master degrees of freedom which represent the structural mass play a significant role in the dynamic analysis.

---

[1] Stands for Program for Automatic Finite Element Calculations.
[2] Stands for PAFEC Interactive Graphics System.

Data File Preparation for Analysis

A general outline of the preparation of a FE data file for analysis is given here to serve as a quick reference. A complete operation instruction can be found in PIGS User Manual Level 8.1, and PAFEC Data Preparation User Manual Level 8.1.

Similarly to the other commercial FE codes, PIGS provides complete mesh generation facilities. Automatic mesh generation or manually controlled element sub-division can be used to produce mesh refinement in the highly stressed regions. Various auxiliary axes can be defined in order to aid the user in generating sophisticated FE meshes. Once a FE mesh has been generated, PIGS can create a PAFEC data file with all the co-ordinations of nodes (in global Cartesian axes) and elements (with their topologies) of the generated FE mesh.

Once a data file containing the mesh description has been created, other data modules describing loading, constraints, material properties, local directions for degrees of freedom of nodes etc. can be added. A PAFEC data file must contain a control module, beginning with the instruction CONTROL and finishing with CONTROL.END. Unlike any other data module, it is not used to define properties of the FE mesh or any loading details. Instead this section acts as a qualifier to the mesh, or as a guide to a particular job execution, should the automatic sequence require to be modified in any way. It is an essential part of the data file, identifying specific functions that must be carried out, assigning certain type of response, and inserting modified sub-routines or auxiliary programs. Before any analysis is started, PAFEC locates and reads this control module.

PAFEC solution path is divided into ten phases forming a sequence. An outline of these ten phases is listed in Table 3.2.1 Once PAFEC has executed all of the specified phases, PIGS can be used again as a post-processor for analysing and displaying the results.

Table 3.2.1 An outline of operation at each PAFEC phase

Phase	Short Description	Description
1 ✓	Read	Data modules are read in; default values are inserted.
2	PAFBLOCKS	Any PAFBLOCK data are replaced by the full nodal co-ordinates and topological description of the complete mesh of elements.
3 *	IN.DRAW structure	The structure itself is drawn.
4 * ✓	Pre-solution housekeeping	The constraints of the problem are considered; a numbering system for the degrees of freedom is chosen.
5 *	IN.DRAW constraints	Constraints, degrees of freedom etc. are drawn.
6 ✓	Elements	Element stiffness matrices are calculated and stored.
7 ✓	**Solutions**	The primary system of equations is solved.
8 *	OUT.DRAW displacements	Displacements are drawn.
9 *	STRESS	The stresses are found.
10 *	OUT.DRAW	Stress contours, stress vector plots etc. are produced.

* Note that these PHASES may be requested even if the activities they refer to have not been mentioned in the modules. In such cases default modules are taken.

✓ These phases are compulsory.

3.2.1 Dynamic FEM Using Thick Shell Elements

3.2.1.1 Dynamic Analysis

In this investigation, transient impact loading applied to an initially stress-free structure is generated via the initial velocity technique. In this technique, the impactor is represented by adding lump masses to a number of nodes in the thick shell element, and ascribing an initial velocity to each of these nodes.

Further details of the technique used for applying impact loading to pre-stressed structures is given in Section 3.2.1.6.

The general form of the equation of motion for a discretised elastic system may be written as

$$[M]\{\ddot{x}\}+[C]\{\dot{x}\}+[K]\{x\}=\{F\} \qquad (3.1)$$

where

$[M]$ = *mass matrix*

$[C]$ = *damping matrix*

$[K]$ = *stiffness matrix*

$\{\ddot{x}\}$ = *acceleration vector* $\left(\frac{d^2x}{dt^2}\right)$

$\{\dot{x}\}$ = *velocity vector* $\left(\frac{dx}{dt}\right)$

$\{x\}$ = *displacement vector*

$\{F\}$ = *applied load vector*

Dynamic analysis is focused on the solution of these equations of motion. Although displacements are represented by discrete functions of space, they are thought of as continuous functions of time. In order to solve equation (3.1), it is necessary to integrate

it with respect to the time variable. The most widely used method for time integration in finite element analysis is the so-called direct integration method.

In this investigation, time-marching integration used for transient analysis is performed by using the Newmark β method. It is an implicit direct integration method which is accurate to the second order, and is unconditionally numerically stable for linear analysis of any choice of time step. With $\gamma = ½$ and $\beta = ¼$ [3], the method reduces to a trapezoidal rule in which no numerical damping is needed [Belytschko et al, 1975; Yener and Wolcott, 1989]. In other words, constant acceleration over each time step (or time interval) is used to obtain an unconditionally stable FE system of equations.

While the importance of stability cannot be disregarded, it represents only one aspect of the problem. The other aspects concern the accuracy of the solution. The accuracy generally deteriorates with increasing time step [Belytschko et al, 1975]. Figs 3.2.1 & 3.2.2 show the effect of displacement and velocity history on impact response obtained using various sizes of the time step (1, 4, 8 & 12 μs). It can be seen that the size of the time-step has only a minor influence on the response behaviour in this range of time-step sizes. Hence, the choice of time-step size in this range can be based on the consideration of the number of response solutions required during the impact process. It can be seen in Table 3.2.2 that the difference in total the computer time usage between tests with time-step sizes 1 μs and 12 μs was only 109 seconds. Type 2 analysis using the data module RESPONSE in PAFEC applies this method for the analysis of transient response without damping.

Since impact loading represents a case of transient loading, the impact duration can commonly be less than half of the period corresponding to the structure's fundamental response mode. For the purposes of impact response analysis, the failure of material is judged within this impact duration. It is widely accepted that the damping effect can be ignored in the calculation of impact response [Lin and Lee, 1990].

---

[3] γ and β are scalar parameters of Newmark expressions for displacement and velocity.

Master Degrees of Freedom

It is well known that dynamic analysis is inevitably computationally more expensive than static analysis since its solution involves multiple repetition of the computation used for static analysis. In the present investigation, every effort has been made to reduce the computational cost of analysis. Reduction techniques available in the literature aim to reduce the computational cost of the analysis by reducing the number of degrees of freedom used. One approach is based upon the assumption that it is low frequency modes of vibration that are important for obtaining a good approximation of the dynamic response, while the higher modes are progressively less important in the dynamic analysis [NAFEMS - A FE Dynamics Primer, 1992].

In PAFEC, a master degree of freedom (MDF) scheme is used for dynamic analysis to reduce both computer time and memory storage requirements. With this scheme, an eigenvalue solution of the structure is calculated based on the specially assigned number of *master* degrees of freedom, rather than the total number of degrees of freedom of the structure. This implies that the inertial effects of certain degrees of freedom are being neglected. Master degrees of freedom should be chosen judiciously to be those which are important in contributing to the total kinetic energy of the structure. PAFEC offers an automatic method for selecting these master degrees of freedom. The method involves the analysis of the ratio between the leading diagonal terms of the stiffness, K_{ii} and mass, M_{ii} matrices for degrees of freedom *i*. Master degrees of freedom are then chosen to correspond to those system equations where this ratio is the smallest, since these are likely to give rise to appreciable inertial effects. Further details on the method of selection of master degrees of freedom can be found in PAFEC Theory manual.

In general, the fewer master degrees of freedom used, the greater the incurred error will be. Hence, a sufficient number of MDF's must be chosen to achieve the required accuracy. One proposed approach suggests that the number of MDF's should lie somewhere between two and ten times the number of modes used in the model [NAFEMS - A FE Dynamics Primer, 1992]. Of course, this rule can be used only as a guideline. In fact, the number of modes required for achieving the same accuracy is quite

dependent on the design of the FE code. Moreover, even with a factor of ten, the consequence of the reduction scheme can still be very difficult to predict. However, a choice of too many MDF's can lead to a computational cost problem.

Table 3.2.3 shows the response results and computational time for the same structure with various number of automatically chosen MDF's under the same impact loading conditions. By choosing the transverse displacement for the model with 1000 MDF's as a reference value, it can be seen that the predicted transverse displacement for the model with 350 MDF's was only 4.15 % higher, while for the model with 630 MDF's was only 1.9 % higher. However, the computational time was reduced 4 and 1.6 times respectively.

Table 3.2.2 Time-step test -- CPU time for analysis

Model :320 shell elements in a single shell element layer (see Fig 3.2.5)

[a sub-model of Fig5.1.2]

Size of Time-Step	No. of Solutions Calculated	CPU Time
1 μs	450	1437.4 s
4 μs	113	1354.51 s
8 μs	57	1339.65 s
12 μs	38	1327.67 s

N.B. :

1. The total analysis duration was 450 μs for each test.
2. Material properties and loading can be found in Table 3.1.1.

Table 3.2.3 1080 elements model -- single shell element layer (see Fig 5.1.2)
(No. of usable frequencies are 63, calculated by PAFEC)

No. of Auto MDF's	Ratio of $\frac{\text{No. of Auto MDF's}}{\text{No. of usable freq}}$	Transverse Displacement Uz t = 100 μs (Nodes 1 & 6)	Stresses Node 1 element 18 (Top surface) t = 100 μs	CPU time (HP 730 workstation)
350	5.56	N1 -244.98 μm N6 -224.84 μm	σ_{11} -361MPa σ_{22} -17.8MPa	4 hours
630	10	N1 -239.72 μm N6 -220.01 μm	σ_{11} -333Mpa σ_{22} -17.9MPa	10 hours
1000	15.87	N1 -235.22 μm N6 -215.21 μm	σ_{11} -312MPa σ_{22} -18.0MPa	16 hours

Nb. : X-Y-Z co-ordinates for Node 1 were : x = 0 mm; y = 0 mm; z = 0.0 mm,
and for Node 6 were : x = -4 mm; y = 0 mm; z = 0.0 mm
(see Figs 5.1.3 & 5.1.4).

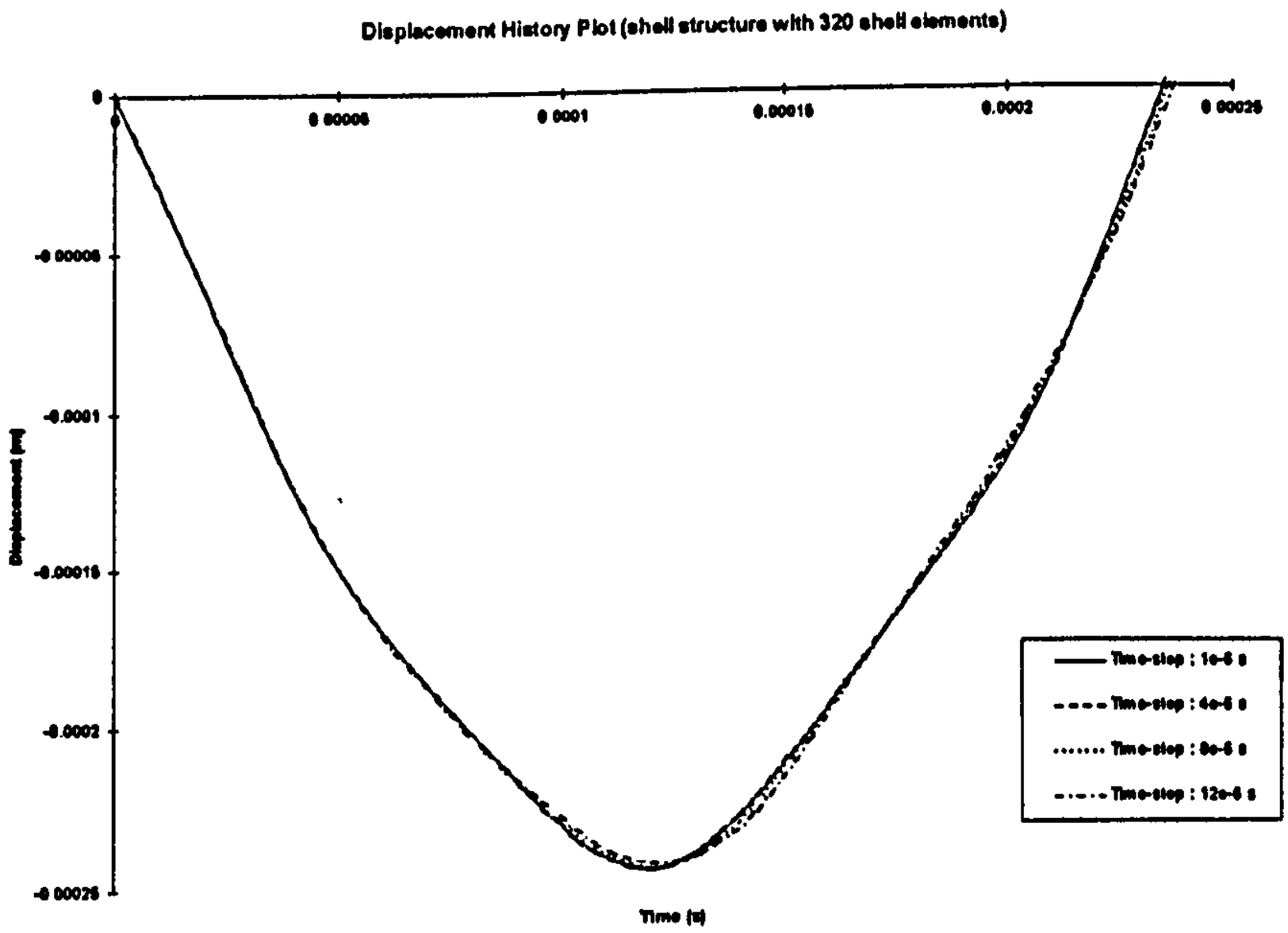

Fig 3.2.1 Time-step tests -- displacement history plot

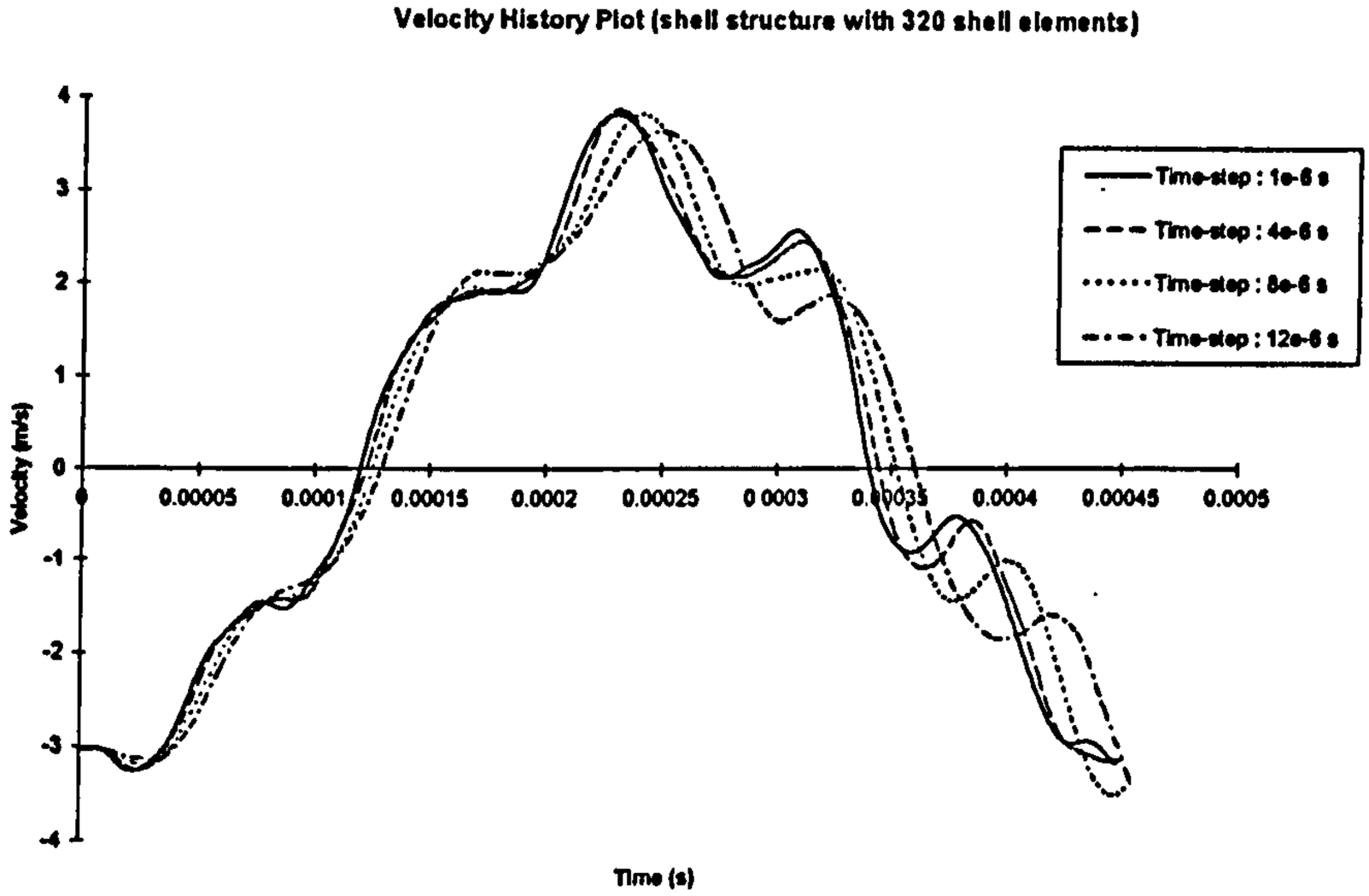

Fig 3.2.2 Time-step tests -- velocity history plot (initial velocity = 3.03 m/s)

3.2.1.2 The Ahmad Type Thick Shell Element

It is well known that shear deformation and rotational inertia should not be ignored in impact analysis, especially when deformation near the nodes experiencing direct impact is considered [Lin and Lee, 1990]. In this investigation, the Ahmad type curved thick shell element (type 46215 in PAFEC) is employed for finite element analysis in which the shear deformation is included. In this element type, eight nodes are used to define the middle neutral surface of the shell. This element type can be used to model both isotropic or orthotropic materials. The model is based upon a degenerate three dimensional analysis incorporating transverse shear effects. The effects of direct stresses in the through-the-thickness direction of the shell are, however, neglected. For this type of thick shell element, it is no longer required that after deformation the normals remain normal to the deformed middle surface. As a result of this change, the shell can experience 'shear deformation'. Therefore, membrane and bending actions are incorporated with the effects of this shear deformation [Ahmad et al, 1970]. Each node of the element has six degrees of freedom, i.e. three translational and three rotational.

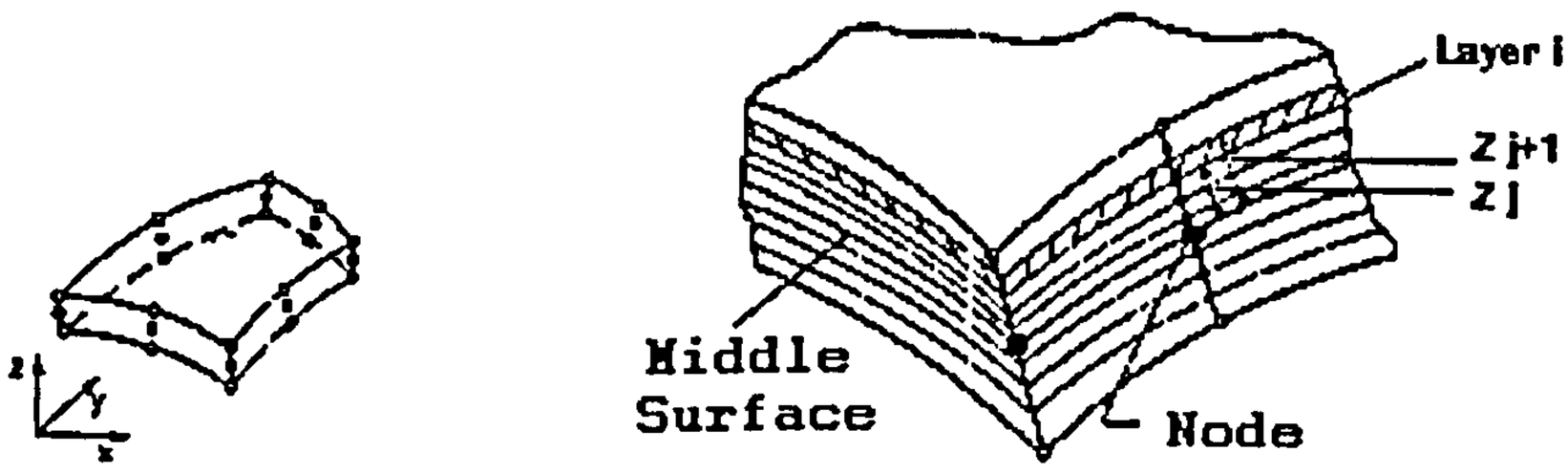

- Nodal points

o Upper and lower points

Fig 3.2.3 A schematic sketch of a thick shell element with n layers

In the case of orthotropic material definition, the thick shell element can consist of n layers of laminae (see Fig 3.2.3). Each layer in the thickness direction of the laminate is represented by a linear shell sub-element (or sub-layer). Shear deformation between sub-layers can be calculated with the removal of the requirement that after deformation the

normals remain normal to the deformed middle surface. Accordingly, the sub-elements of various layers can be represented by the same node in the middle surface. Lin and Lee (1990) reported that because both the in-plane and bending displacements are considered in the FE variational process, the numerical results are independent of the location of the nodal point, which can therefore be selected in the middle surface is for simplicity. Detailed formulation of this Ahmad type thick shell element can be found in Ahmad et al (1970) and Lin and Lee (1990).

3.2.1.3 Orthotropic Material Definition for Thick Shell Element

Composites may comprise thin layers having different principal material directions, in order to improve the composite stiffness and strength characteristics. The thick shell element can be used to define multi-layered composite structures, each layer having its own definition of material direction and layer thickness. In PAFEC, nine independent components of compliance are required to characterise a composite material with respect to symmetry axes. These are the three material compliances in the principal directions of the material (S11, S22 & S33), the three cross compliances (S12, S23 & S31), and the three shear compliances (SH12, SH23 & SH31). Moreover, the element axes and the material principal axes must be included to assist the definition of the material orientation. In PAFEC, a requirement that (S11*S22 - S12*S12) must be positive is imposed when defining the properties of an orthotropic material. The formulations for the values of these material compliances can be found in Table 3.2.4.

Table 3.2.4 Material compliances for orthotropic material in PAFEC data file

(1) Material compliances in the principal direction of the material S11, S22, S33

(2) Material cross compliances S12, S23, S31

(3) Material shear compliances SH12, SH23, SH31

(4) Elastic modulii E_{11}, E_{22}, E_{33}

(5) Shear modulii G_{12}, G_{23}, G_{31}

(6) Poisson's ratios ν_{12}, ν_{13}, ν_{23}, ν_{31}

$$S11=\frac{1}{E_{11}} \qquad S12=\frac{-\nu_{21}}{E_{22}}=\frac{-\nu_{12}}{E_{11}} \qquad SH12=\frac{1}{G_{12}}$$

$$S22=\frac{1}{E_{22}} \qquad S23=\frac{-\nu_{32}}{E_{33}}=\frac{-\nu_{23}}{E_{22}} \qquad SH23=\frac{1}{G_{23}}$$

$$S33=\frac{1}{E_{33}} \qquad S31=\frac{-\nu_{31}}{E_{33}}=\frac{-\nu_{13}}{E_{11}} \qquad SH31=\frac{1}{G_{31}}$$

The following formula can be used to calculate G_{23} : $G_{23}=\frac{E_{33}}{2(1+\nu_{23})}$, etc.

3.2.1.4 Stress Analysis

In a stressed composite material, the significant stresses are parallel and perpendicular to the principal fibre directions. In PAFEC, the stresses in a thick shell element are referred to the axes of material symmetry. This approach facilitates the application of failure criteria. However, the code does not provide a facility for detecting failure in a composite material. Therefore, the appropriate sub-routines (i.e. R96017.f, D70650.f and D70640.f) must be modified to include this function. For each node of an element, stresses within a sub-layer can be requested. Moreover, in each sub-layer, three integration points through the thickness are available for stresses, i.e. top, middle and bottom surfaces of each sub-layer. The default value of the shear correction factor [4] for this isoparametric thick shell element is 5/6, which was chosen based on the result by Mindlin [Mindlin, 1951; Ahmad et al, 1970].

---

[4] The purpose for this shear correction factor is to improve the shear displacement approximation. From the displacement definition it will be seen that the shear distribution is approximately constant through the thickness, whereas in reality the shear distribution is approximately parabolic.

3.2.1.5 Composite Cylinder with Two Layers of Thick Shell Element

The NGV pressure cylinder considered in the present investigation contains a thin liner. Hence, it is important to examine the details of the stresses and deflections at the interface. Although the Ahmad type thick shell element allows many sub-layers to be defined in the through-the-thickness direction, it uses the assumption of perfect bonding between the sub-layers. Within one thick shell element, no free surfaces exist between any two layers, and no relative movements take place. The bending stress distribution cannot be correctly predicted using this method if free surfaces exist at some interface. To overcome this difficulty, an alternative method must be used.

The alternative solution put forward here is to generate a FE model with two layers of thick shell elements stacked together in the through-the-thickness direction. By using two thick shell elements, an interface between the surfaces of two consecutive layers is created which can give correct bending stresses and displacements even if delamination took place at the interface. The validation of the selected method for simulating an interface will be given in Appendix A.

I. An Investigation into the Modelling of an Interface

Four approaches to modelling an interface that can be envisaged by combining control and data modules. These four approaches were tested in order to identify the most suitable method that can be used to model an interface.

PAFEC data modules such as SKIP.COLLAPSE, RIGID.LINKS and HINGES.AND.SLIDES were involved in modelling.

The function of the SKIP.COLLAPSE modulus is to impose a constraint on the analysis which requires that coincident nodes do not collapse. RIGID.LINKS can be used to establish a rigid link between two construction nodes. While a rigid link is defined, these two construction nodes are not allowed to have relative displacements in their alignment direction. However, a restriction is associated with this data module that the degree of

freedom in which the nodes are linked cannot be manually chosen to be a master d.o.f., nor can it correspond to a prescribed displacement. Because of this restriction, the impact loading nodes cannot have rigid links in the present model.

HINGES.AND.SLIDES module is used to connect two construction nodes so that all the translational and rotational degrees of freedom are identical (or repeated) except for those specified. It is the inverse of the REPEATED.FREEDOMS data module.

In order to test these four approaches, a FE model with two shell element layers, which has 320 elements in each layer was used. There were six laminae through-the-thickness, and the fibre direction of each lamina was orientated parallel to the element axis for ease of checking the bending stress distribution. Each shell element layer had three laminae. Another FE model of a single shell element layer with the same lay-up, thickness and FE mesh design under the same loading was used as a reference for verifying the response results obtained from these four approaches. An illustration of the FE mesh with two shell element layers is given in Fig 3.2.4. By off-setting the through-the-thickness reference point, the bottom surface of top layer and top surface of bottom layer can be made to coincide. In the LAMINATES data module, the thickness of a sub-layer in a thick shell element is defined by the positions of the boundaries of this layer (UPPER and LOWER) in the through-the-thickness direction. Creating many sub-layers within a thick shell element is possible by defining these UPPER and LOWER boundaries in consecutive order. The sub-layer definitions used in this test are shown in Table 3.2.6. The impact loading details are the same as the FE model used in Section 5.1.1.1.

Approach 1 - Two layers of shell elements bonded together (No SKIP.COLLAPSE)

In this test, SKIP.COLLAPSE control module was not used. Transverse displacement (Uz) is given in Table 3.3.7. Node 1 was located at the reference point of the structure in the top shell element layer, while Node 6691 was also at the reference point but in the bottom shell element layer. Through-the-thickness stresses are given in Tables 3.2.8 and 3.2.9. It can be seen that the transverse displacements and stress distributions obtained from this model are identical with those from a single shell element layer model. A typical compressive-tensile through-the-thickness bending stress variation obtained from

this model confirms that the top and bottom shell element layers are firmly secured together, and behave as continuous in the thickness direction, with no relative movements allowed at the interface. The deformed shape for this model is shown in Fig 3.2.5 which is identical with that for a single shell element layer model.

This method of stacking two shell element layers clearly cannot predict interface stresses and relative movement, and hence will not be considered further to be used in the present investigation.

Approach 2 - Two layers of shell elements (with SKIP.COLLAPSE)

In this test, the SKIP.COLLAPSE control module was used. From Tables 3.2.7 to 3.2.9 and Fig 3.2.6, it is clear that the top and bottom shell element layers deform independently. The internal forces developed in the top shell element layer are not transmitted to the bottom layer, so that only the top shell element layer deformed under loading.

Literally, this method cannot stack two shell element layers together. Hence, it was not considered further.

Approach 3 - Establish 'zero length' rigid links

In this test, the SKIP.COLLAPSE control module and the RIGID.LINKS data module were used. From displacement and stress value shown in Tables 3.2.7 to 3.2.9, it can be seen that the behaviour is similar to Approach 1 apart from the loaded area. Since no rigid links can be established with loading nodes, the elements in the loaded area become debonded and deform separately as seen in Fig 3.2.7. This approach of stacking two shell element layers together cannot give a faithful representation of the stresses at the interface, therefore, and will not used in modelling.

Approach 4 (a & b)- Establish 'zero length' hinges

In this test, the SKIP.COLLAPSE control module and the HINGES.AND.SLIDES data module were used. Two tests were undertaken. In the first test, Approach 4(a), only the thickness direction (i.e. z-direction) degrees of freedom of all coincident construction

node pairs were constrained. In the second test, Approach 4(b), all the degrees of freedom of all coincident construction node pairs were constrained. From the bending stress distribution shown in Tables 3.2.8 and 3.2.9, it can be seen that in the first test compressive-tensile bending stress pattern is developed in each layer. This suggests that free sliding conditions exist at the interface. Note 3 in Table 3.2.7 confirms that in-plane relative movement (sliding) occurs at the interface.

Given the advantages of this approach, it was chosen to be used in the present investigation. The validation of this approach has been given in Appendix A.

Table 3.2.5 An outline of the four approaches to modelling the interface

Approaches	CONTROL Module	DATA Module
1. Two layers of shell elements bonded together	No SKIP.COLLAPSE	--
2. Two layers of shell elements (SKIP.COLLAPSE)	SKIP.COLLAPSE	--
3. Establish 'zero length' rigid links	SKIP.COLLAPSE	RIGID.LINKS
4. Establish 'zero length' hinges	SKIP.COLLAPSE	HINGES.AND. SLIDES

Table 3.2.6 Thickness definition for the two shell element layers

	Sub-layer extremities	Co-ordinates in thickness direction
⇑	UPPER	0.762E-3
TOP	LOWER	0.508E-3
SHELL	UPPER	0.508E-3
LAYER	LOWER	0.254E-3
	UPPER	0.254E-3
⇓	LOWER	0.0
⇑	UPPER	0.0
BOTTOM	LOWER	-0.254E-3
SHELL	UPPER	-0.254E-3
LAYER	LOWER	-0.508E-3
	UPPER	-0.508E-3
⇓	LOWER	-0.762E-3

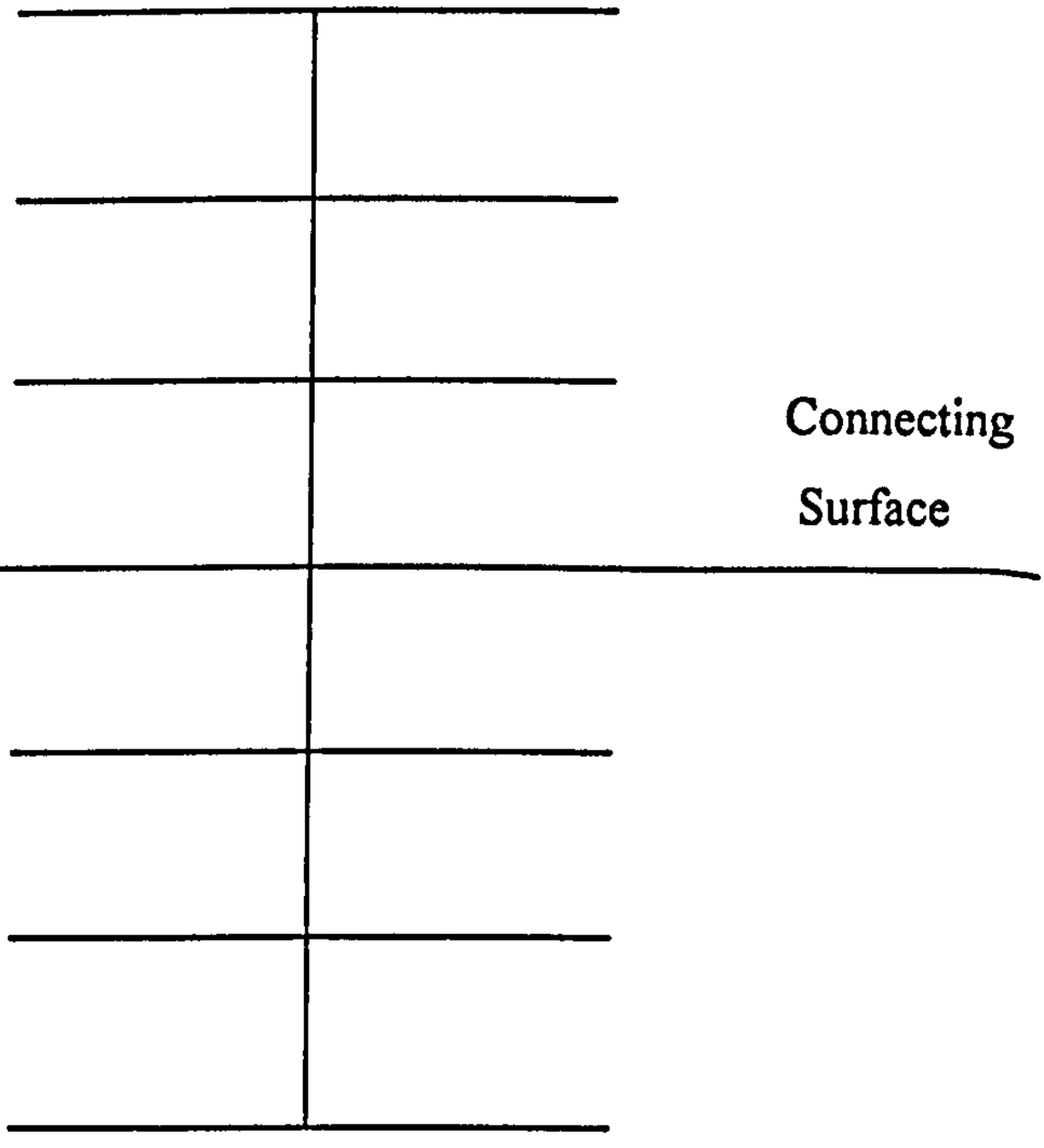

NB :

The connecting surface between these two shell element layers does not necessary lie at the middle of the total thickness.

Table 3.2.7 Transverse displacement at Nodes 1 & 6

Reference : Displacement U_z of a single shell element layer model at 100 μs :

node 1 = -280.24 μm ; node 6 = -260.86 μm

Approach	Displacement U_z Node 1 (Node 6691)	Displacement U_z Node 6 (Node 6681)
1	N1 -280.19 μm N6691 -280.19 μm	N6 -260.67 μm N6681 -260.67 μm
2	N1 -306.88 μm N6691 0.0 μm	N6 -289.24 μm N6681 0.0 μm
3	N1 -294.01 μm N6691 -272.07 μm	N6 -258.51 μm N6681 -258.51 μm
4(a)	N1 -306.77 μm N6691 -306.77 μm	N6 -284.96 μm N6681 -284.96 μm
4(b)	N1 -280.19 μm N6691 -280.19 μm	N6 -260.67 μm N6681 -260.67 μm

NB :

1. The lamination angle for each layer was set to zero, i.e. material principal axes were the same as element axes.
2. The distance between Node 1 in top shell element layer (Node 6691 of bottom shell layer) and Node 6 (Node 6681) was 4 mm in the longitudinal direction. Node 1 was located at the reference origin of the structure.
3. HINGES.AND.SLIDES were used in Approaches 4(a) and 4(b). For Approach 4(a), the in-plane relative displacements, U_x & U_y, were allowed between the surfaces connected by the construction node pair. Example data :

	Node 1	Node 6691	Relative displacement	Node 6	Node 6681	Relative displacement
U_x	0.028 μm	-0.032 μm	0.060 μm	-2.778 μm	3.11 μm	5.888 μm
U_y	-0.041 μm	-0.05 μm	0.009 μm	-0.106 μm	-0.062 μm	0.044 μm

Table 3.2.8 Through-thickness bending stresses distribution

Stresses in the fibre direction (σ_{11}) obtained at 100 μs

Node 1 (Element 18) - Upper shell element layer

Node 6691 (Element 2286) - Lower shell element layer

Sub Layer No.	Surface	Single shell (MPa)	Approach 1 (MPa)	Approach 2 (MPa)	Approach 3 (MPa)	Approach 4(a) (MPa)	Approach 4(b) (MPa)
1	T	-208	-207	-160	-266	-180	-207
	M	-175	-174	-110	-225	-115	-174
	B	-142	-141	-60.6	-184	-49.0	-141
2	T	-142	-141	-60.6	-184	-49.0	-141
	M	-109	-109	-11.1	-144	16.6	-109
	B	-76.2	-75.8	38.4	-103	82.3	-75.8
3	T	-76.2	-75.8	38.4	-103	82.3	-75.8
	M	-43.4	-43.0	87.9	-62.4	148	-43.0
	B	-10.5	-10.3	137	-21.8	214	-10.3
4	T	-10.5	-10.3	0	-15.4	-209	-10.3
	M	22.3	22.5	0	14.6	-144	22.5
	B	55.2	55.2	0	44.7	-78.0	55.2
5	T	55.2	55.2	0	44.7	-78.0	55.2
	M	88.0	88.0	0	74.8	-12.4	88.0
	B	121	121	0	105	53.2	121
6	T	121	121	0	105	53.2	121
	M	154	154	0	135	119	154
	B	187	186	0	165	184	186

N.B. :

1. T : Top surface; M : Middle surface; B : Bottom surface.
2. sub layers 1 - 3 belong to the top shell element layers, and sub layers 4 - 6 belong to the bottom shell element layer.
3. The bold line between sub layers 3 and 4 in the table indicates the interface between the joined surfaces.

Table 3.2.9 Through-thickness bending stresses distribution

Stresses in the fibre direction (σ_{11}) obtained at 100 μs

Node 6 (Element 17) - Upper shell element layer

Node 6681 (Element 2285) - Lower shell element layer

Layer No.	Surface	Single shell (MPa)	Approach 1 (MPa)	Approach 2 (MPa)	Approach 3 (MPa)	Approach 4(a) (MPa)	Approach 4(b) (MPa)
1	T	-134	-134	-92.7	-80.6	-80.6	-134
	M	-113	-113	-66.3	-72.5	-63.3	-113
	B	-92.6	-92.7	-39.9	-64.5	-46.0	-92.7
2	T	-92.6	-92.7	-39.9	-64.5	-46.0	-92.7
	M	-72.0	-72.1	-13.6	-56.5	-28.7	-72.1
	B	-51.5	-51.5	12.8	-48.4	-11.3	-51.5
3	T	-51.5	-51.5	12.8	-48.4	-11.3	-51.5
	M	-30.9	-31.0	39.2	-40.4	5.96	-31.0
	B	-10.3	-10.4	65.5	-32.4	23.3	-10.4
4	T	-10.3	-10.4	0	19.8	-63.2	-10.4
	M	10.3	10.2	0	34.7	-45.9	10.2
	B	30.8	30.8	0	49.6	-28.6	30.8
5	T	30.8	30.8	0	49.6	-28.6	30.8
	M	51.4	51.4	0	64.5	-11.3	51.4
	B	72.0	71.9	0	79.4	6.05	71.9
6	T	72.0	71.9	0	79.4	6.05	71.9
	M	92.6	92.5	0	94.3	23.4	92.5
	B	113	113	0	109	40.7	113

N.B. :

1. T : Top surface; M : Middle surface; B : Bottom surface.
2. sub layers 1 - 3 belong to the top shell element layer, and sub layers 4 - 6 belong to the bottom shell element layer.
3. The bold line between sub layers 3 and 4 in the table indicates the interface between the joined surfaces.

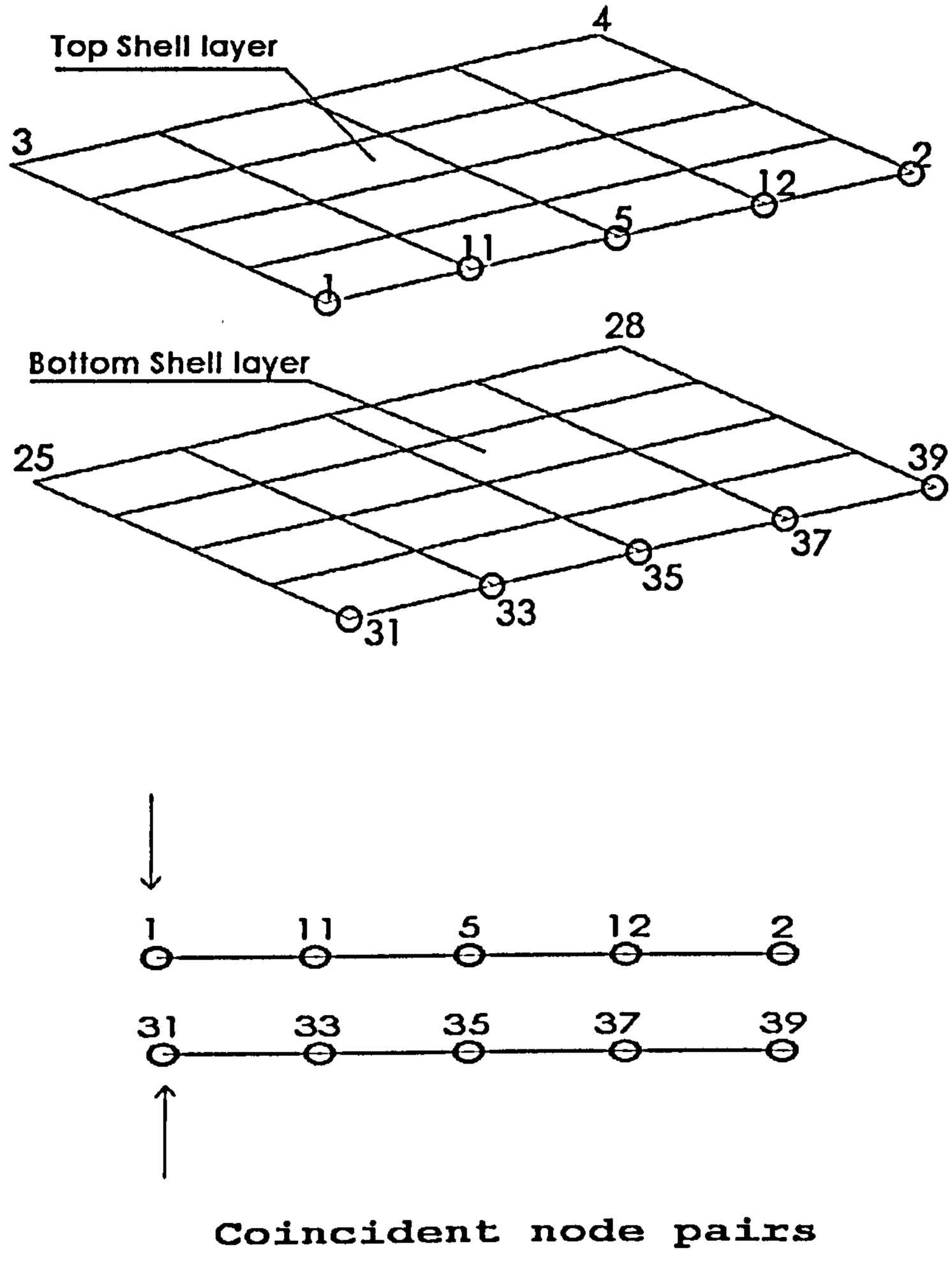

(E.g. Nodes 1 & 31 are coincident construction nodes)

Fig 3.2.4 An illustration of stacking of two shell element layers

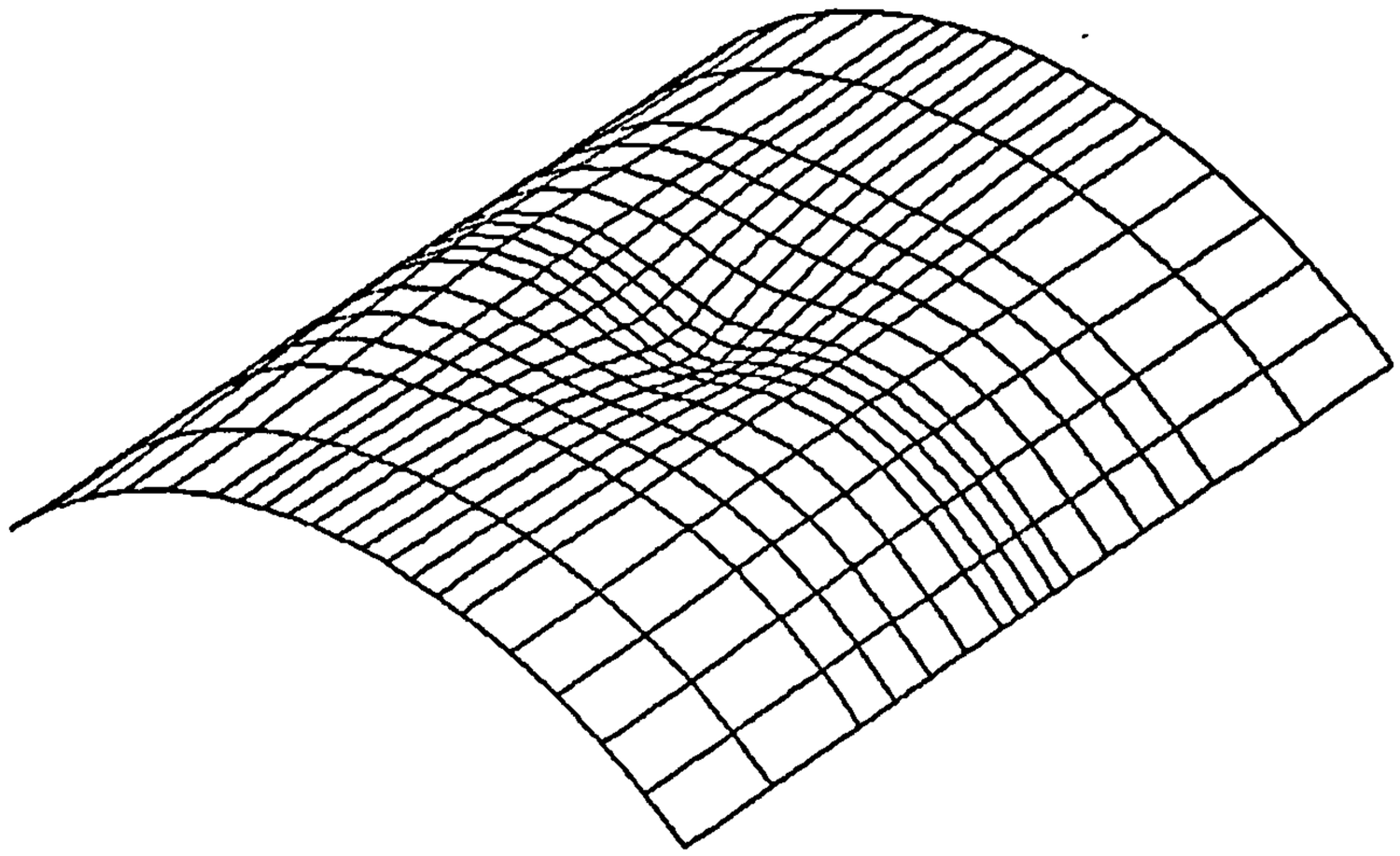

Fig 3.2.5 Deformed shape from a single shell element layer model
Approach 1 and Approach 4 (b)

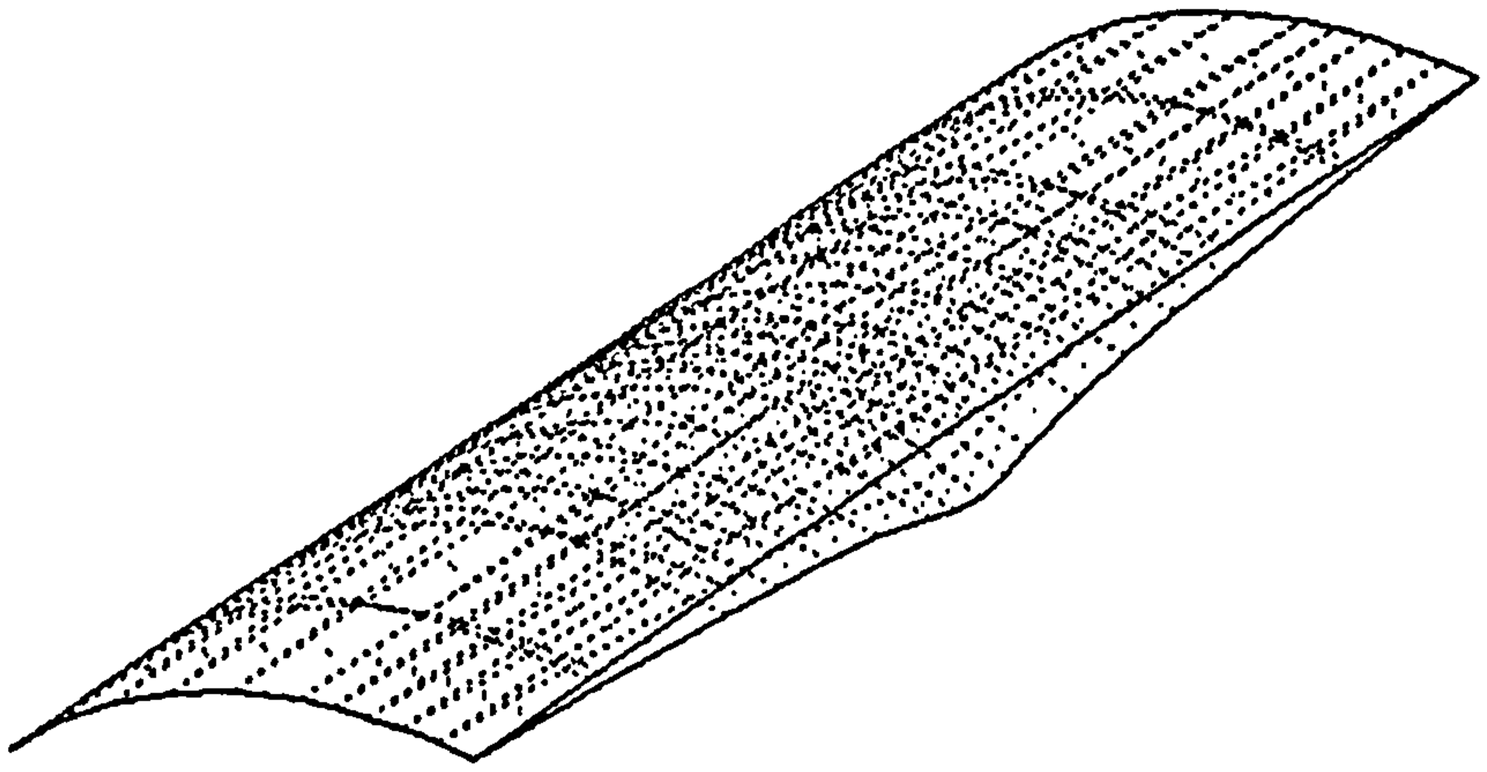

Fig 3.2.6 Deformed shape of Approach 2
(shell element layers become debonded)

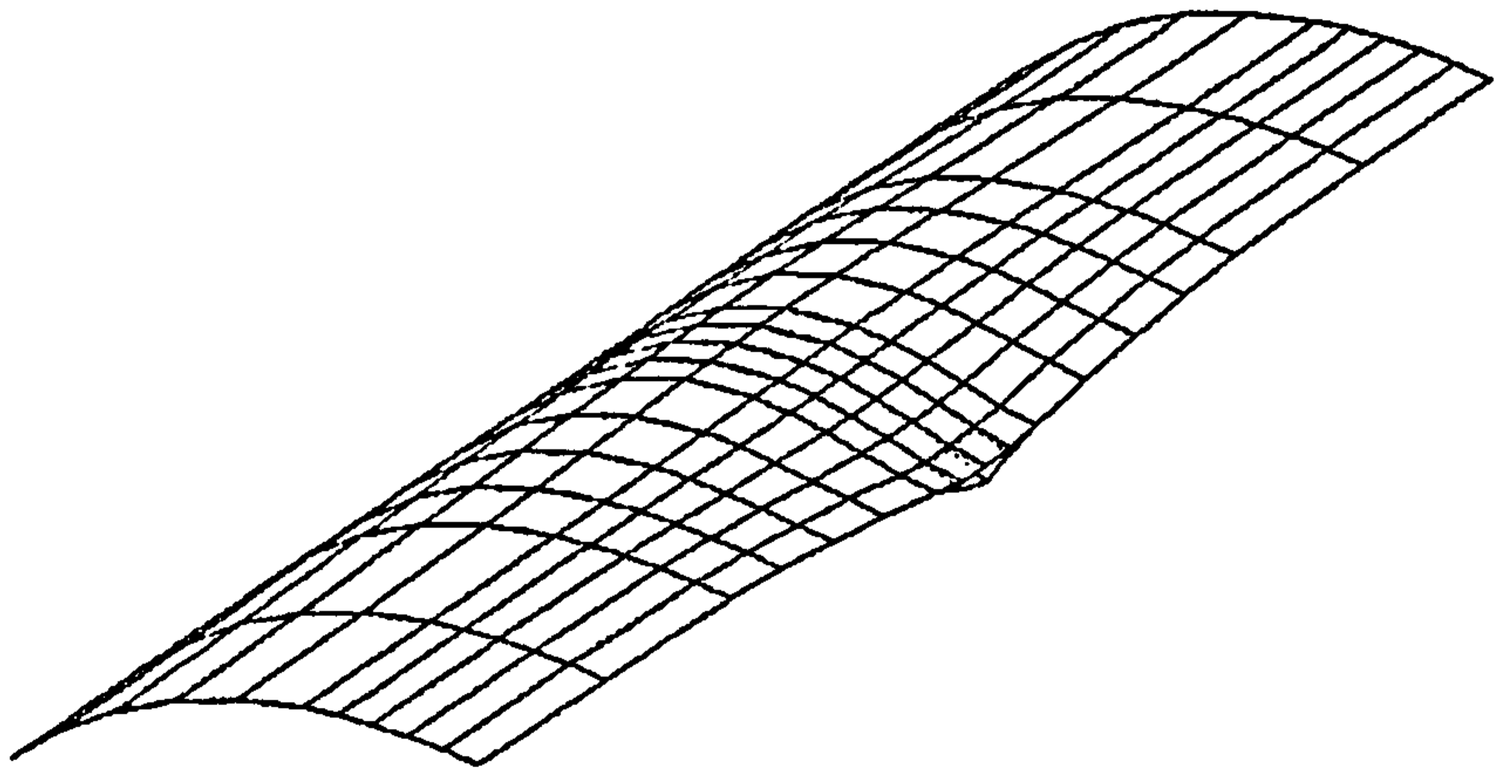

Fig 3.2.7 Deformed shape of Approach 3 (RIGID.LINKS)
(no rigid links allowed in the loaded area)

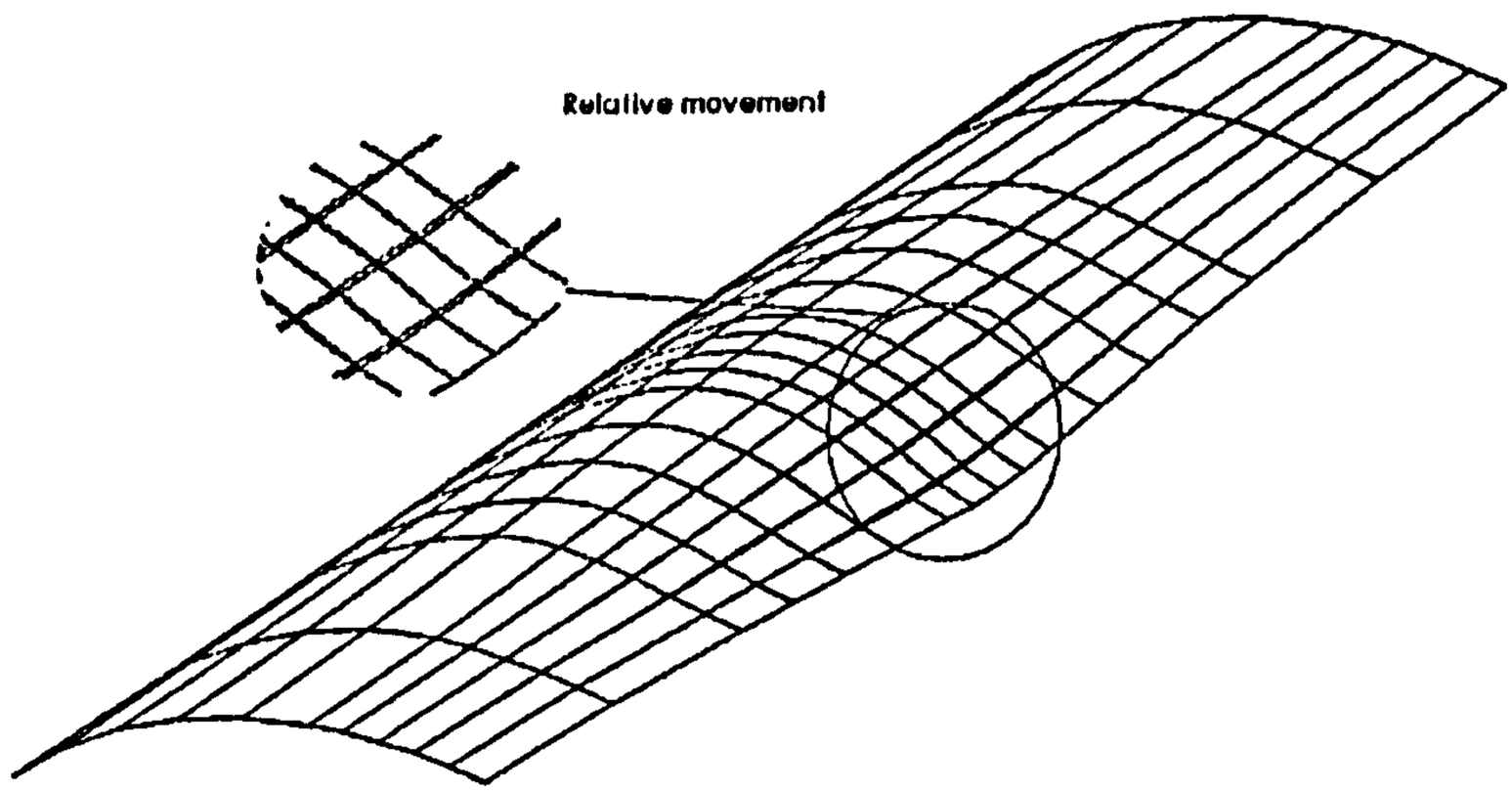

Fig 3.2.8 Deformed shape of Approach 4 (a)
(in-plane relative displacements between top and bottom layers are allowed to occur)

3.2.1.6 Modelling Impact Behaviour in Service

For a NGV composite cylinder, most of the exposure to the physical attack, such as impact by foreign objects, takes place at its service condition. Therefore, it appears necessary to consider the impact behaviour of the composite cylinder in a pre-pressurised condition.

The data module "VELOCITIES.PRESCRIBED" does not allow to generate a pressurised condition before impact loading is being applied, since the prescribed initial velocity value is imposed at the beginning of the dynamic analysis. An alternative method was proposed in order to be able to investigate the impact behaviour of the cylinder under service conditions. The method consists of two steps. The first step creates the pre-pressurise condition in the cylinder, while the second step applies the impact-loading to the pre-pressurised cylinder.

I. Pre-Pressurised Technique (PPT)

Applying pressure to the cylinder is easier to model by static analysis than by dynamic analysis. However, since dynamic loading must follow the pressurisation of the cylinder, dynamic application of pressure to the cylinder was undertaken. This technique makes use of the FORCING data module in PAFEC. The FORCING data module allows to specify the timing at which the forces are applied.

In dynamic analysis , any suddenly applied loading, such as step input, generates unstable oscillation in the system. Because of this instability, an artificial numerical damping must be applied to the system in order to reach a steady-state needed for the application of impact loading. However, this arbitrary artificial numerical damping can introduce unreasonable damping effects to the response. Accordingly, the nature and the magnitude of the deformation under impact loading may be distorted.

Taking the above considerations into accounts, a ramp input was used to pressurise the cylinder. Undamped single and multiple degree of freedom (d.o.f.) systems were used to

study the rise-time effect for this ramp input. For undamped single d.o.f. system, a mathematical model (Duhamel's Integral) and the present finite element model will be used to demonstrate the rise-time effect. Then, for an undamped multiple d.o.f. system, finite element results obtained by both static and dynamic analyses will be used to validate the techniques.

Undamped single d.o.f. system (mathematical model)

Duhamel's Integral

The response of an undamped single-d.o.f. system (Fig. 3.2.9) to an arbitrary excitation F(t) is represented by the integral

$$\int dx = \int \frac{1}{\sqrt{mk}} F_0 \sin \omega_n (t-\tau) d\tau$$

$$x = \frac{1}{\sqrt{mk}} \int_0^t F_0 \sin \omega_n (t-\tau) d\tau$$

Spring-mass System

Fig. 3.2.9

where :

m : mass of the spring-mass system

k : stiffness of spring

F_o : maximum force

τ : time at which the response is measured

t: time variable

$(t-\tau)$: elapsed time from the moment the impulse is imposed until the response is measured.

ω_n : natural frequency of the system

x : displacement

This is known as Duhamel's integral, or the convolution integral, or the superposition integral [Thomson, 1993]. In this integral, τ is the independent variable; accordingly, the integration is performed with respect to τ, with t being treated as a constant in this process. The response determined in this manner represents the complete motion for the initial conditions of zero displacement and zero velocity.

The response of an undamped system to the constant force without a rise time

The forcing condition is defined by $F = F_0 = \text{constant}$. Then,

$$x = \frac{1}{\sqrt{mk}} \int_0^t F_0 \sin \omega_n (t-\tau) d\tau$$

$$= \frac{F_0}{\sqrt{mk}} \left[\frac{\cos \omega_n (t-\tau)}{\omega_n} \right]_0^t$$

$$= \frac{F_0}{k} (1 - \cos \omega_n t)$$

The response to the step input is as shown in Fig 3.2.10. The response oscillates at a high amplitude , equal to the steady-state displacement, F_0/k. This sinusoidal motion does not decay or converge to a constant unless artificial numerical damping is to be applied in the analysis.

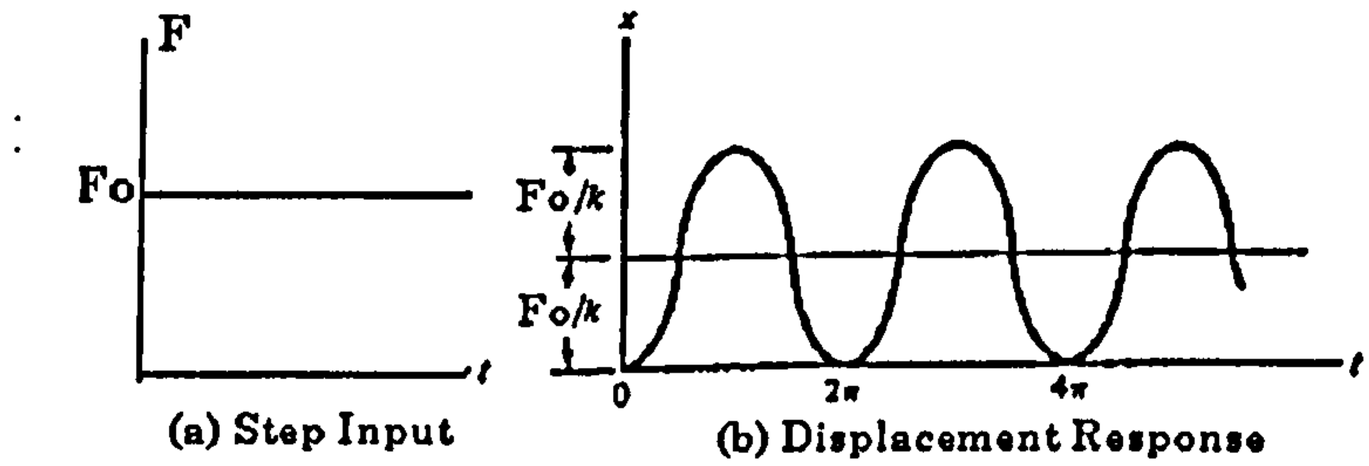

Fig. 3.2.10 Step input and its response

The response of an undamped system to a constant force with a rise time

The forcing condition is defined by $F = \beta\tau$, where $\beta = F_0/t_1$, for the rise time t1; after that the forcing condition is defined by F = Fo = constant. By considering the forcing input as two functions, the response becomes

for $t < t_1$

$$x = \frac{\omega_n}{k} \int_0^t F_0 \frac{\tau}{t_1} \sin \omega_n (t-\tau) d\tau$$

$$= \frac{F_0}{k} \left(\frac{t}{t_1} - \frac{\sin \omega_n t}{\omega_n t_1} \right)$$

and for $t > t_1$,

$$x = \frac{F_0}{k}\left[1 - \frac{\sin \omega_n t}{\omega_n t_1} + \frac{1}{\omega_n t_1}\sin \omega_n (t - t_1)\right]$$

The response is shown in Fig 3.2.11. When using the ramp input method, the response oscillate around the slope of $\beta/k\omega_n$ with a very small amplitude compared to step input. At the end of the ramp input when constant forcing starts, the oscillation of response remains at a low magnitude. Thus a smoother response is achieved without any artificial numerical damping. The amplitude of the oscillation is dependent on the gradient of the ramp input, i.e. related to the rise-time. The validation of this technique can be found in Appendix B.

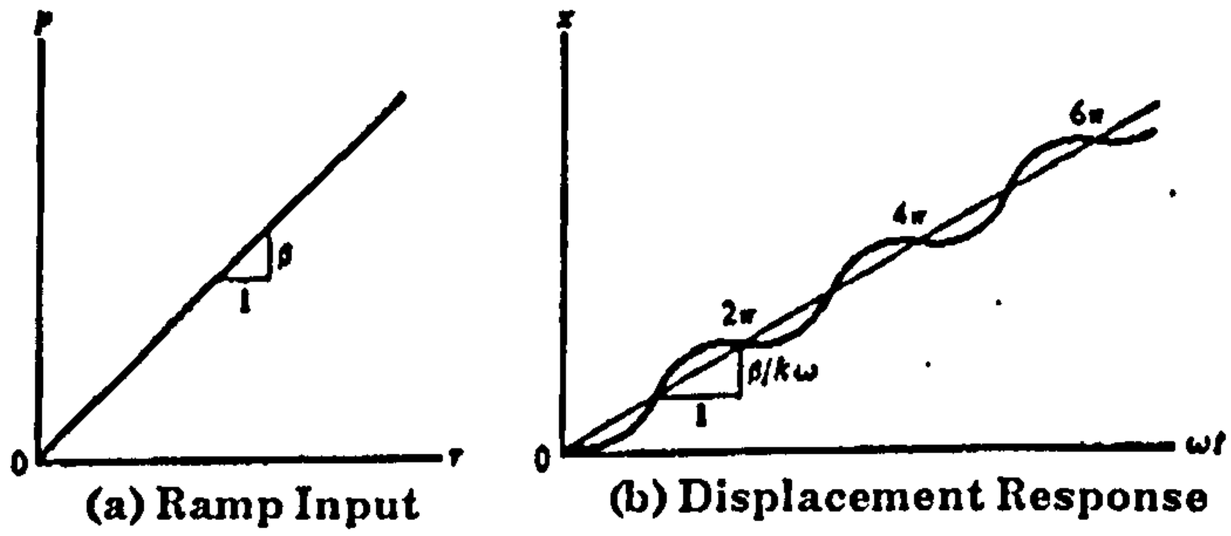

Fig 3.2.11 Ramp input and its response

II. Impulse Excitation Technique (IET)

The main purpose for this alternative technique is to create an initial condition for impact loading at pre-pressurised condition (or at any time during the analysis). This initial condition for an impact loading prescribes an initial velocity with an impactor mass in the loaded area.

This impulse excitation technique is based on the principle of conservation of momentum, which states that the total momentum of an isolated system is conserved. The relationship between the change of momentum and the impulsive force is $mv - mv_0 = F\Delta t.$ [*where* m = *mass of a particle;* v & v_o = *initial and final velocity;* F = *force acting on the particle;* Δt = *elapsed time*]

Consider an impulse applied over a short duration of time (shock impulse) to a stationary target. A transient response is generated, which can produce a substantial local velocity at the end of the duration of this impulse. At that particular time, the loaded area is displaced by a very small distance, while other parts of the structure remain un-disturbed. An impactor mass is then added to those loaded nodes, and dynamic analysis continues with these conditions. It is important to note that the duration of excitation impulse is chosen to be with many orders of magnitude less than the impact duration. The basic idea of this technique is illustrated in Fig 3.2.12. Finite element models of both undamped single d.o.f. and multiple d.o.f. systems were used to validate this technique. The validation of this technique can be found in Appendix C.

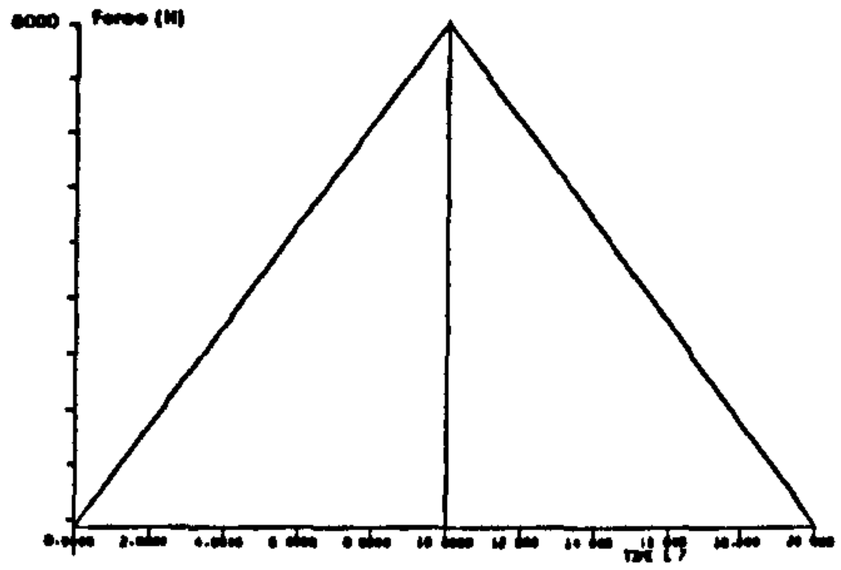

(a) Force Excitation Impulse
Duration of the Impulse : 2E-6 Sec

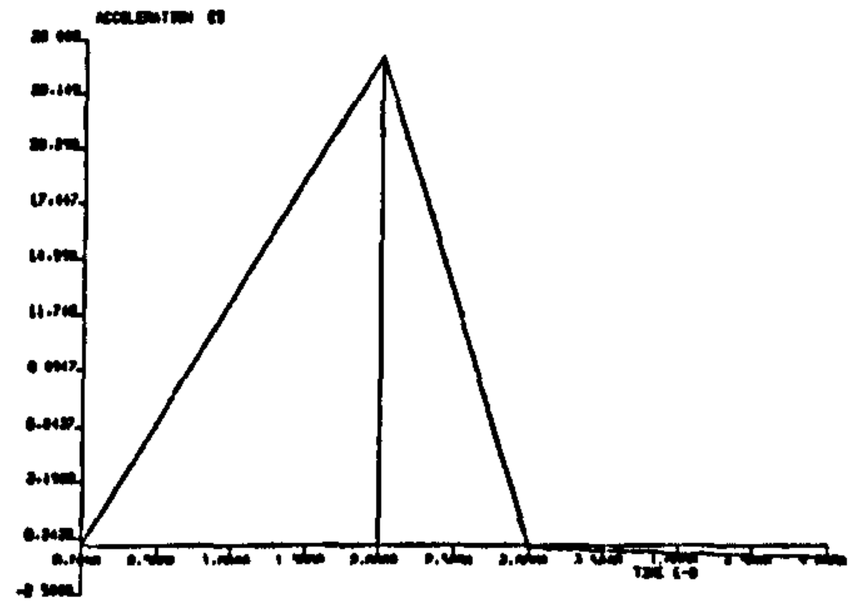

(b) Acceleration Response

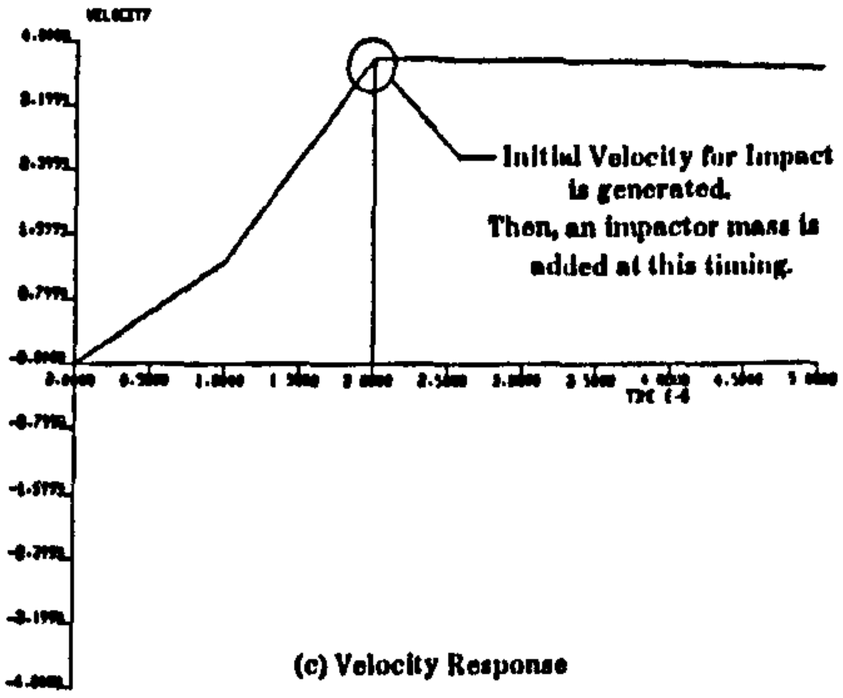

(c) Velocity Response

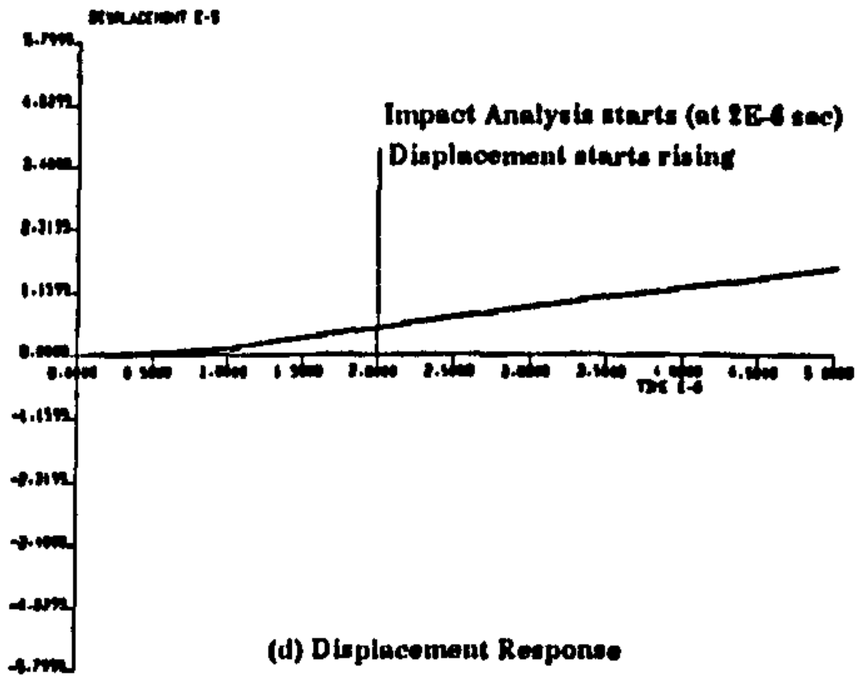

(d) Displacement Response

Fig 3.2.12 An illustration of the basic idea of IET

3.2.2 Static FEM Using 3D Brick Element

3.2.2.1 3D Brick Element

One of the cases where two dimensional models are not sufficient to describe the structural behaviour of composite structures in a satisfactory manner is where high transverse shear and normal stresses arise at the loading site. Since they are responsible for local deformation and damage such as delamination, it is important to use models which can faithfully represent the variation of stresses and displacements in the through-thickness direction.

In order to study the local damage and deformation, a twenty noded isoparametric three dimensional brick element was used to generate the finite element mesh for static analysis (see Fig 3.2.13). In general, isoparametric elements have curved sides (2D) or curved edges and faces (3D).

The basic idea of isoparametric elements is that, in order to derive stiffness and other elemental matrix terms, the elements are transformed into a very simple shape in the (ξ, η) or (ξ, η, ζ) domains. Schematic diagrams illustrating this idea can be seen in Fig 3.2.14, which shows an eight noded quadrilateral element. The four vertices can lie anywhere in the (X,Y) plane, and the mid-side nodes can also be placed arbitrarily. In practice, however, the eight nodes should form a shape that is a quadrilateral with mildly curved sides. Then, through isoparametric transformation, this quadrilateral shape can be mapped onto a square with sides of half-length unity in the (ξ,η) plane. In three dimensional analysis, a third curvilinear co-ordinate ζ would be included. The details of these isoparametric transformations can be found in the PAFEC Theory Manual (1984) and Zienkiewicz (1973).

The isoparametric three dimensional element employed in this analysis is a generally shaped three dimensional brick type element with six curvilinear faces and twelve edges. There are eight corner nodes and one mid-side node on each of the edges, giving twenty nodes in total. The element has three translatory degrees of freedom at each of its

twenty nodes. A reasonable distortion from the basic cubical shape is allowed for this type of element. However, PAFEC has a built-in allowable limit to govern the distortion of the element under loading. PAFEC warns if the element is too distorted and in extreme cases a failure is signalled.

The method of defining orthotropic material properties for the brick element is similar to that for the thick shell element described in Section 3.2.1.3. However, it only allows a single orthotropic layer to be defined within one element. That is to say, if n layers are needed through-the-thickness with various material axes orientations then at least n elements are required.

A composite structure is usually composed of many thin layers with various fibre orientations. Hence in order to model it in three dimensions, very small 3D elements is required. Moreover, allowable geometric aspect ratios must be maintained for all elements, otherwise PAFEC will signal an error message. As shown in Fig 3.2.15, a quarter of a composite ring with 7 layers already required 1932 elements and 9376 nodes. Additionally, PIGS allows a maximum of 10,000 nodes to be defined for a FE mesh. The static analysis of this FE model required three hours of total computer time to obtain the solution. Therefore, three dimensional elements of this type are expensive to use and should be employed only when full three dimensional stress analysis is required.

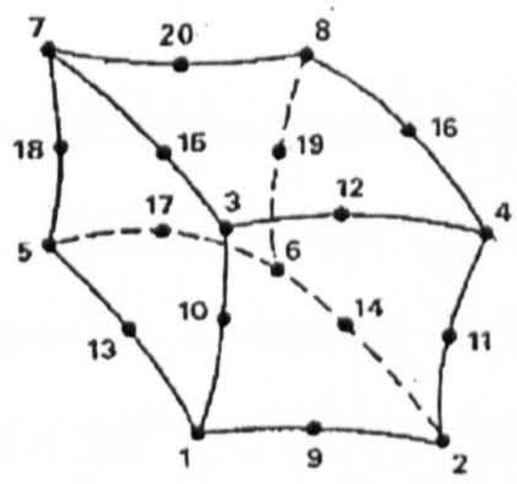

Fig 3.2.13 Twenty-noded 3D brick element (type 37115 in PAFEC)

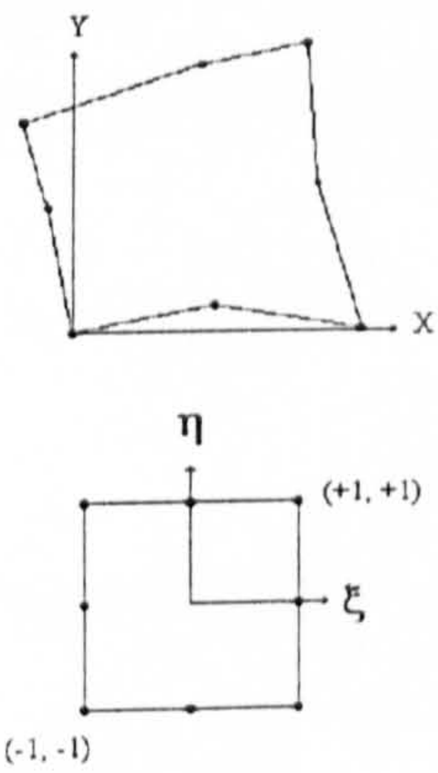

Fig 3.2.14 Schematic diagram of isoparametric mapping

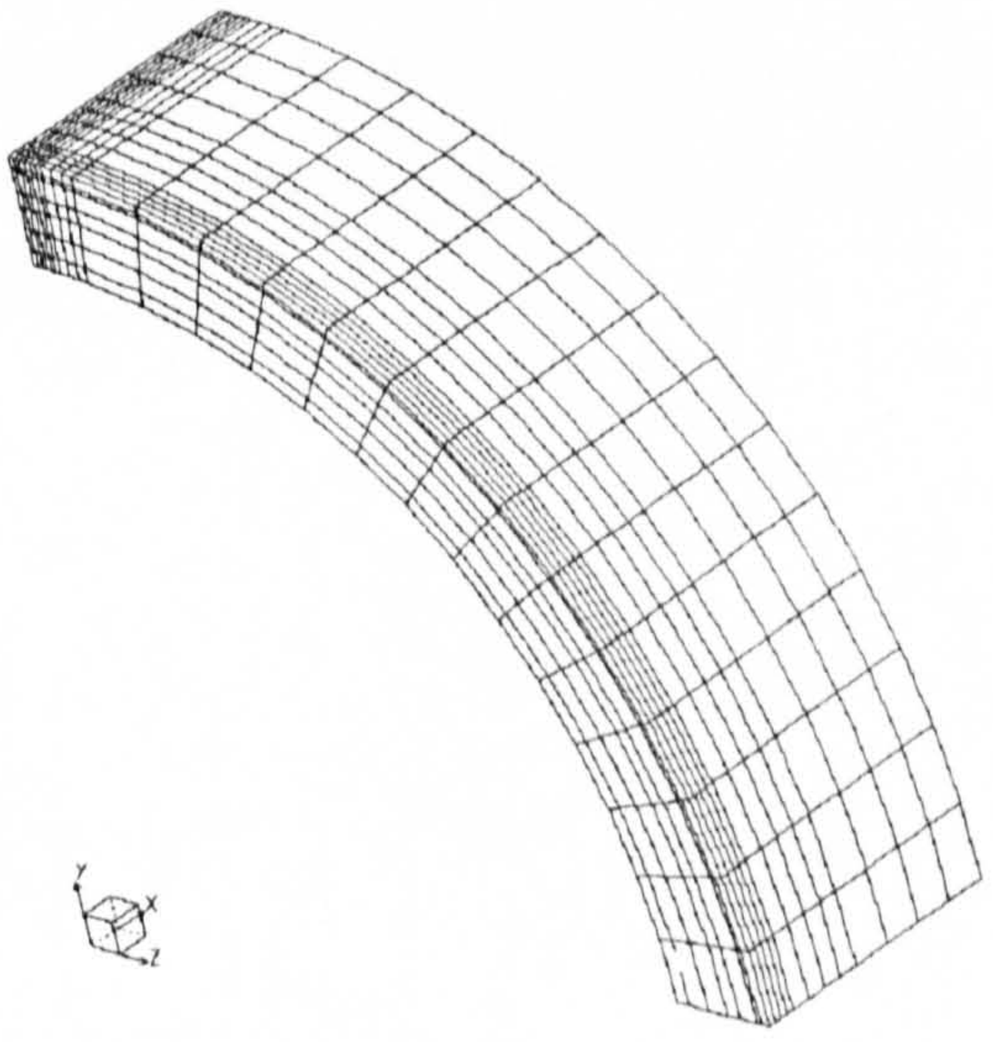

Fig 3.2.15 A 3D composite ring model (quarter symmetric)

3.2.2.2 Stress Analysis

When this type of twenty noded isoparametric brick element is used for three dimensional orthotropic analysis, stresses in the principal material directions are given. Since the FE code does not provide a facility for detecting failure for orthotropic material, the appropriate sub-routines (i.e. R87003.f and R87015.f) had to be modified to extract the stresses after the analysis. These stress data could then be examined with respect to the appropriate failure criteria.

In this static analysis, Hertzian pressure distribution was used for defining the pressure loading on the FE model. The pressure distribution has the following form :

$$q_{x,y} = q_o \sqrt{1 - \frac{x^2 + y^2}{a^2}}$$

where x and y are the in-plane coordinates, and a is the contact radius, and

$q_o = \frac{3P}{4\pi a^2}$; where P is the contact force.

Since linear static analysis is being used, the displacement field and stress field should be linear with respect to the applied loading, provided the contact area remains the same. One set of results under certain loading conditions can easily be transferred to another set by a linear proportional scaling.

3.2.3 Material Failure Criteria and Material Degradation Model

3.2.3.1 Material Failure Criteria

In this study, the composite structure is regarded as 'damaged' when its original designed load carrying capacity has been reduced by failure of its constituents, such as matrix cracking, delamination, and fibre breakage. In order to determine the conditions for the onset of damage, material failure criteria have to be incorporated. As BVID and repeated impact behaviour were studied in the present investigation, criteria that reflect strength and integrity of a material must be chosen. Therefore, stress based failure mode identification criteria proposed by Hashin (1980) were adopted. The use of these criteria allows the identifications of such types of material damage and failure modes as fibre breakage and matrix cracking. Choi and Chang (1992) believed that the initiation of delamination is likely to occur following the onset of matrix cracking. Delamination can be seen as a debonding process happening at the interface between two layers with different lay-up angles. It takes place when a critical combination of out-of-plane stresses (σ_{33}^{+}, τ_{13}, τ_{23}) is attained [Ainsworth, 1990, and Finn and Springer, 1993]. Therefore, in order to predict the initiation and growth of delamination, information about the stresses, especially the transverse shear stresses at the interface must be obtained [Choi and Chang, 1992]. It is important to note that the Ahmad type thick shell element gives through-the-thickness averaged transverse shear stresses, and thus cannot provide an accurate solutions for the transverse shear stress variation to make such a prediction.

Formulations for the failure mode identification criteria which adopted were implemented in a PAFEC subroutine (Phase 9 - R96017.f). The criteria assumed are given by the followings : (out-of plane direct stress, σ_{33}, is not included)

(1) Fibre breakage

Tensile failure of fibres (for $\sigma_{11} > 0$) :

$$\left[\frac{\sigma_{11}}{S_{1T}}\right]^2 + \left[\frac{\sigma_{12}}{S_{12}}\right]^2 + \left[\frac{\sigma_{13}}{S_{13}}\right]^2 = 1$$

Compressive failure of fibres (buckling or crushing, for $\sigma_{11} < 0$) :

$$\left[\frac{\sigma_{11}}{S_{1C}}\right]^2 = 1$$

(2) Matrix cracking

Tensile failure of matrix (for $\sigma_{22} > 0$) :

$$\left[\frac{\sigma_{22}}{S_{2T}}\right]^2 + \left[\frac{\sigma_{23}}{S_{23}}\right]^2 + \left[\frac{\sigma_{12}}{S_{12}}\right]^2 + \left[\frac{\sigma_{13}}{S_{13}}\right]^2 = 1$$

Compressive failure of matrix (for $\sigma_{22} < 0$) :

$$\frac{1}{S_{2C}}\left[\left(\frac{S_{2C}}{2S_{23}}\right)^2 - 1\right]\sigma_{22} + \left[\frac{\sigma_{22}}{2S_{23}}\right]^2 + \left[\frac{\sigma_{23}}{S_{23}}\right]^2 + \left[\frac{\sigma_{12}}{S_{12}}\right]^2 + \left[\frac{\sigma_{13}}{S_{13}}\right]^2 = 1$$

where :

σ_{11}, σ_{22}, σ_{33} : direct stresses

σ_{12}, σ_{13}, σ_{23} : shear stresses

S_{1T}, S_{2T} : direct tensile strength

S_{1C}, S_{2C} : direct compressive strength

S_{12}, S_{13}, S_{23} : shear strength

Failures of material with corresponding failure modes were assumed to have occurred once these criteria have been satisfied.

3.2.3.2 Material Degradation Model

In order to model the effect of repeated impact on a cylinder, the pre-existing flaws in the material induced by previous impact must be included. For this reason, a material degradation model was incorporated in the analysis. Once material failure had been detected by one or several of the failure mode identification criteria, the relevant material properties of the corresponding lamina were degraded accordingly. A material degradation model proposed by Wang (1989) postulates that (see Table 3.2.10) :

(1) For the occurrence of matrix cracking, and also for a delamination initiation, the transverse modulus E_{22}, and shear moduli G_{12}, G_{23} as well as Poisson's ratios ν_{21} and ν_{23} of the material in the region must be degraded to zero. This degradation model implies that the material in that failed region is no longer capable to carry load in the in-plane and out-of-plane transverse directions, but retains strength in the fibre direction.

(2) For fibre breakage, the nine material properties E_{11}, E_{22}, E_{33}, G_{12}, G_{23}, G_{31}, ν_{12}, ν_{23}, ν_{13}, in the failed region are degraded to zero. This degradation model implies that the material in that region can no longer carry any load in any direction.

Table 3.2.10 Material degradation model

Material failure mode	Material properties to degrade	Degraded value
Matrix cracking and initiation of delamination	E_{22}, G_{12} and G_{23} ν_{21} and ν_{23}	zero
Fibre breakage	E_{11}, E_{22}, E_{33}, G_{12}, G_{23}, G_{31}, ν_{12}, ν_{23}, ν_{31}	zero

3.2.4 Repeated Impact Modelling

In the real in-service situation, it is very likely that a composite cylinder is subjected to more than a single act of impact. It is, therefore, important to investigate the behaviour under repeated impact. Usually most of the accidental impact takes place during service. In this study, therefore, both empty and pressurised composite cylinders were considered. Moreover, repeated impact was assumed to take place at the same location. It was chosen to represent the worst situation, as maximum damage to the material accumulated from each impact.

The approach chosen to model this progressive impact damage was to up-date the structural stiffness in the FE model after each impact by degrading the material properties of appropriate elements according to the material degradation model applied to each element. Correspondingly, the structural stiffness was reduced after each instance of property degradation.

Chapter 4 Experimental

Two experimental investigations have been undertaken. The first one was used as a preliminary step aimed at the identification of some well known failure modes in composites under quasi-static indentation. It was carried out on composite pipes, and is reported in Section 4.1.

The second one was performed on a composite pressure cylinder which was the subject of analysis in the present study. The experimental findings were used to confirm some FE and analytical predictions. Experimental analysis of the dynamic inelastic response of anisotropic composite structures is notoriously difficult.

4.1 Quasi-Static Indentation on Composite Pipe

4.1.1 Test Procedures

An experimental investigation was carried out on composite curved panels cut off from cylindrical composite pipes. The panels were subjected to central transverse quasi-static indentation. All composite pipes were of the same material and geometric dimensions, made by filament-winding E-glass fibre with an epoxy matrix. The winding angles were +- 55°. Also, a very thin initial helical winding layer (~70° to the axial direction) was present at the inner surface. The outside pipe diameter was 210 mm, and the wall thickness was 5 mm. The section longitudinal width was 155 mm. These materials were chosen because the pipes were transparent, and hence the internal damage induced by indentation was easily visible. The panels were sectioned subsequently to the tests in order to inspect the internal damage geometry.

The composite curved panels were prepared in three different arc lengths, with sector angles 40°, 80° and 120° (Table 4.1). These three type of panels possess different structural stiffness under indentation.

Simply supported condition was used for these test specimens (see Fig 4.1) by placing them on a solid steel base. Three tests were also done on a curved panel placed on a top of a steel cylinder. The description of four types of test set-up can be found in Table 4.2, and the schematic diagrams can be seen in Fig 4.1.

A hemi-spherical steel indenter with a diameter of 22 mm was used to apply the loading. The load was gradually increased until visible damages could be seen. The trace of the indentation force against displacement of the indenter was recorded (Fig 4.3).

4.1.2 Damage Detection and Assessment

In Fig 4.2, it can be seen that, under the moderate loads applied, the damage due to quasi-static indentation was mainly matrix cracking and delamination. These were confined to a conical region with its base at the back surface. The complexity of the resulting matrix cracking and delamination network is clearly evident. The main source of this damage is likely to be the bending stresses [Sun and Jih, 1990]. This kind of damage phenomenon can be generalised in a schematic diagram as shown in Fig 4.7.

Since the loading was applied to the outer surface, the upper half of the region inside the cone has little matrix cracking. Compressive through thickness stresses dominate in this region.

Further damage could be found on both outer and inner surfaces. It can be seen that a pair of asymmetric cracks emanated from the loading site (see Fig 4.3), with surface fibre being cut by these cracks. Matrix splitting of the helical layer parallel to the fibre direction has also been found (see Fig 4.4).

It is believed that matrix splitting at the inner surface was caused by the high bending stresses. In contrast, the inter-fibre bending stress may be the main cause for the initiation and propagation of asymmetric cracks on the upper surface.

Clark (1989) proposed a basic impact damage model (see Fig 4.7 (A)) to explain the basic delamination mechanism for two plies with +- θ°. The basic idea was that the peel forces, due to deflection, acting at point A promote delamination, while the interlamina compression, due to ply curvature, at point B prevent delamination. Hence, the model suggests that delamination would be more likely to occur in the region away from the indentation.

In all these tested specimens, the delamination formed near the middle or in the lower half of the thickness, where maximum transverse shear stresses have been induced. Delamination had a fairly regular oval or rectangular shape, shown in Figs 4.5 and 4.6 in transmitted light. The damaged areas appear dark compared to the intact, more transparent material.

In the overall observation, specimens with larger sector angles (and longer arc length) possessed lower structural stiffness and showed a larger extent of damage under the same load.

4.1.3 Experimental Results

Typical load-deflection curves for each test can be seen in Fig 4.8. The different gradients of the curves show that the structural stiffnesses were different. The magnitudes of the loading applied in all tests were sufficient to produce some permanent deformation and / or damage in the tested panels. Therefore, none of the specimens showed complete elastic recovery, as evidenced by the different gradients for loading and unloading curves, and non-zero deflection persisting upon load removal. Specimen possessing a lower structural stiffness deflected more under the maximum load, making more extensive damage likely.

The load-displacement trace collected from Specimen (A) appears similar to those seen during loading on a solid material. A large permanent indentation has been produced in the loading region. No fibre breakage, matrix cracking or delamination could be seen in the specimen.

The load-deflection curve of Specimen C was no longer smooth, especially at higher loads. This reflects the discrete outward movement of the supporting edges under increased load. In view of this aspect, it is important to note that the residual displacements seen in these load-deflection curves (except for Specimen A (I)), cannot be taken totally as the permanent deformation produced by indentation. It partly contains the retained displacement due to the movement of the two supporting edges. It is also important to allow for the loading machine backlash.

The results obtained from these tests could not be used for the purpose of quantitative analysis. However, they serve as a good initial qualitative guideline on composite damage under quasi-static loading.

Table 4.1 Specimens dimensions

Test Specimens	Sector Angle	Arc Length
Specimen A	40°	75 mm
Specimen B	80°	150 mm
Specimen C	120°	220 mm

Table 4.2 Indentation tests

Tests	Descriptions
(a)	Specimen A on a steel ring
(b)	Specimen A on a steel base
(c)	Specimen B on a steel base
(d)	Specimen C on a steel base

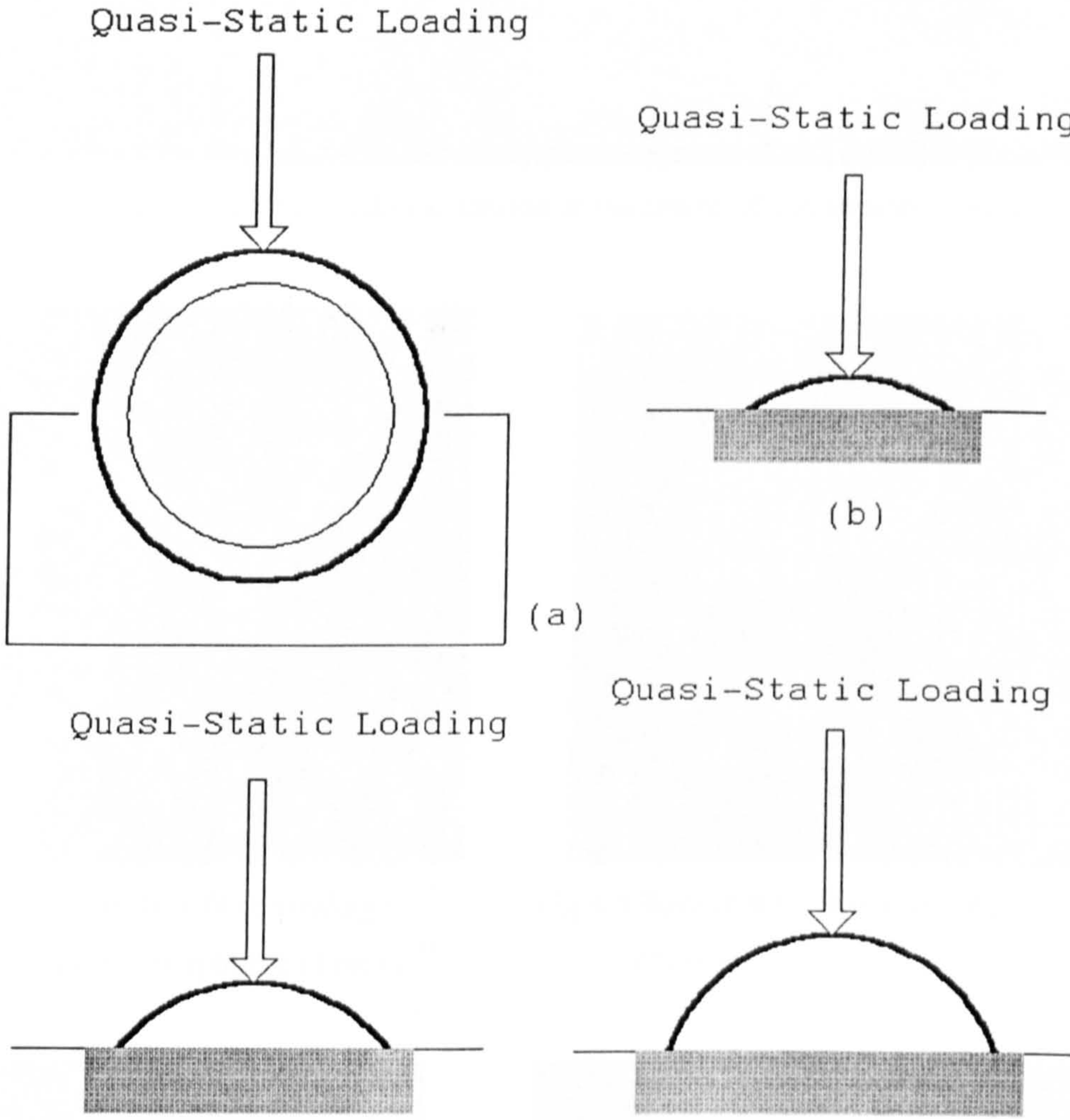

Fig 4.1 Schematic diagrams of quasi-static indentation tests on composite curved panels

(a) Specimen A on a steel ring; (b) Specimen A on a steel base;

(c) Specimen B on a steel base; (d) Specimen C on a steel base.

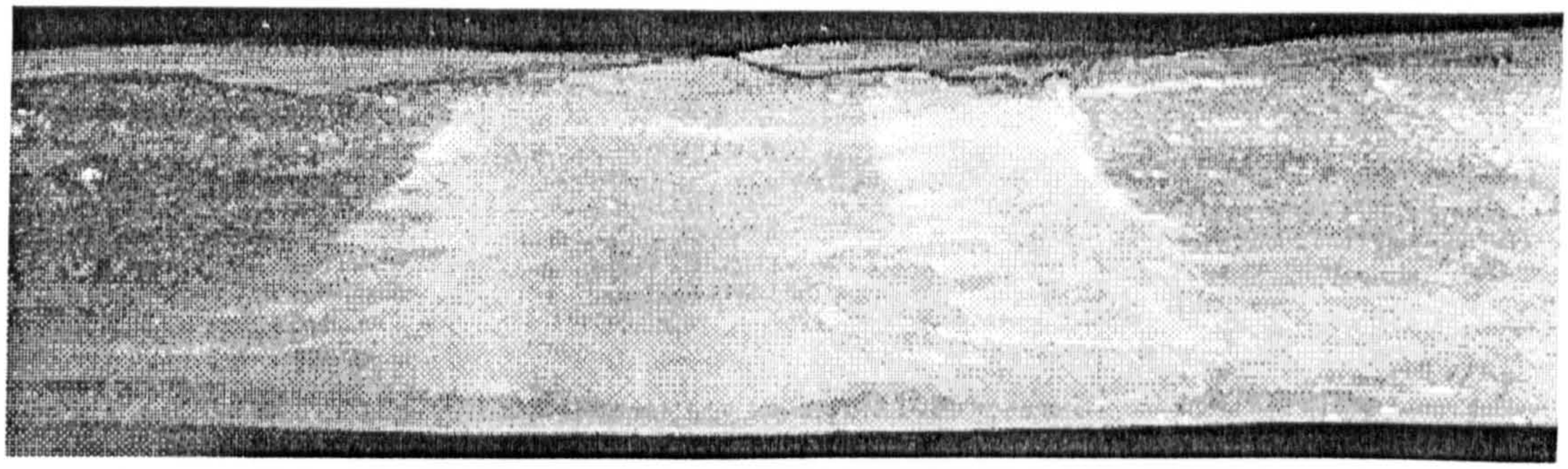

Fig 4.2 Through-the-thickness section at the centre of indentation (Test d)

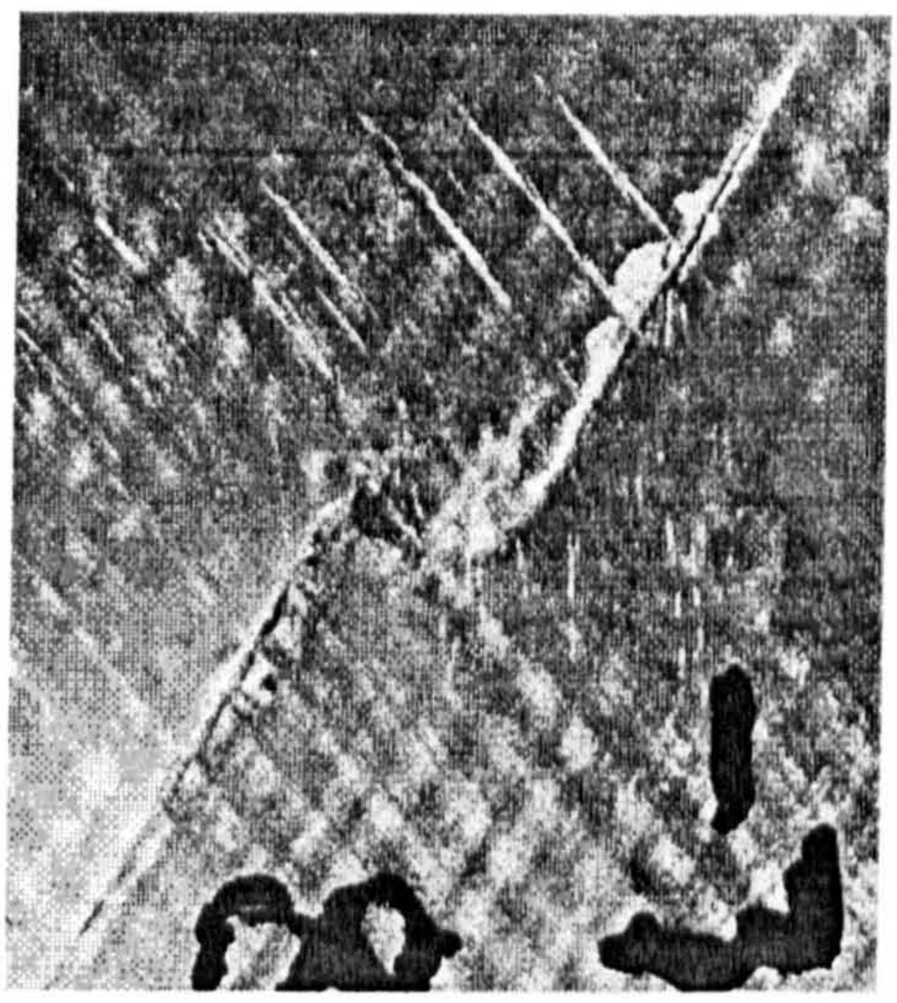

Fig 4.3 Top surface fibre breakage and matrix splitting (Test c)

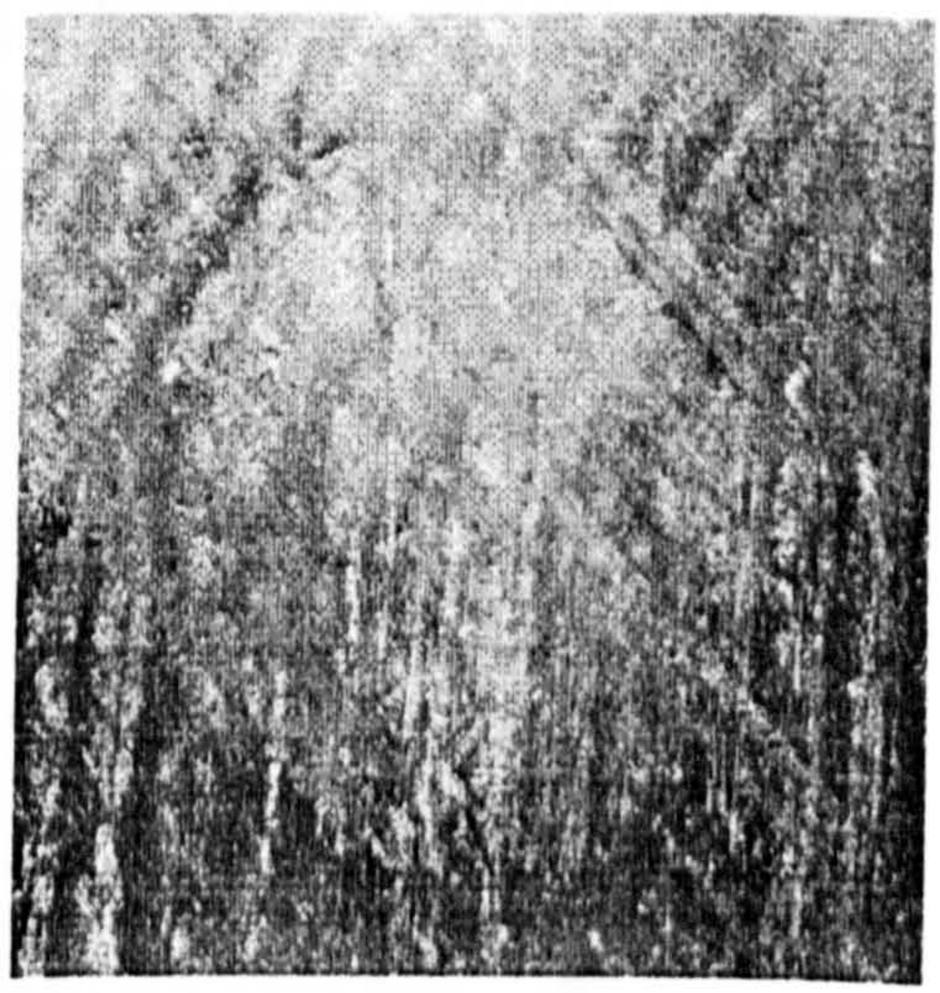

Fig 4.4 Bottom surface matrix splitting (Test c)

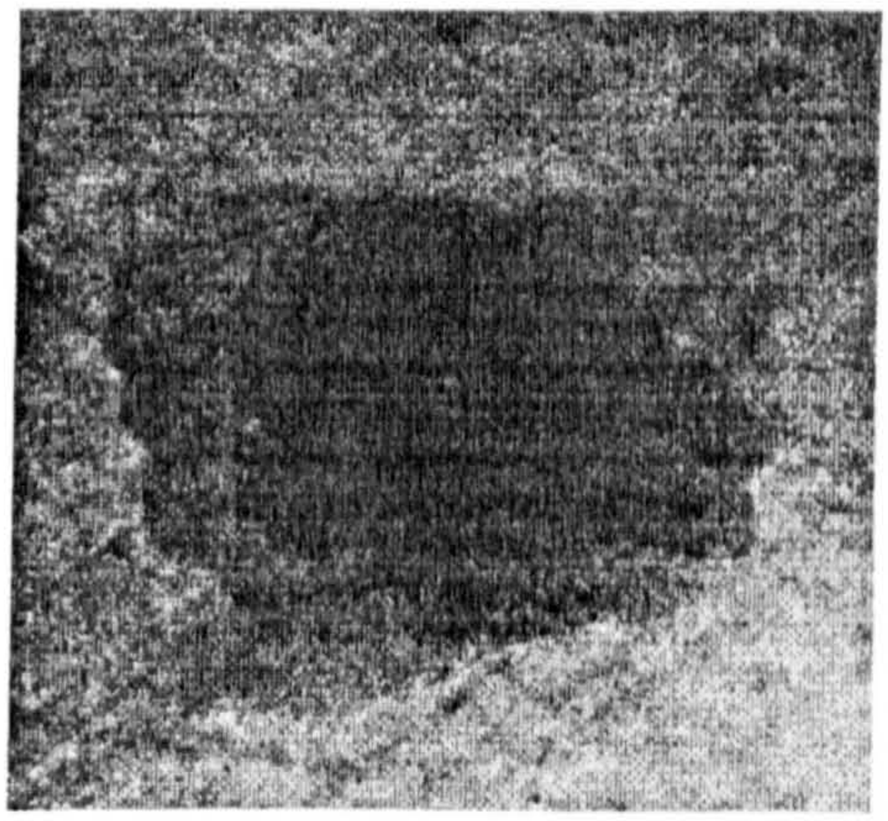

Fig 4.5 Delamination (Test b)

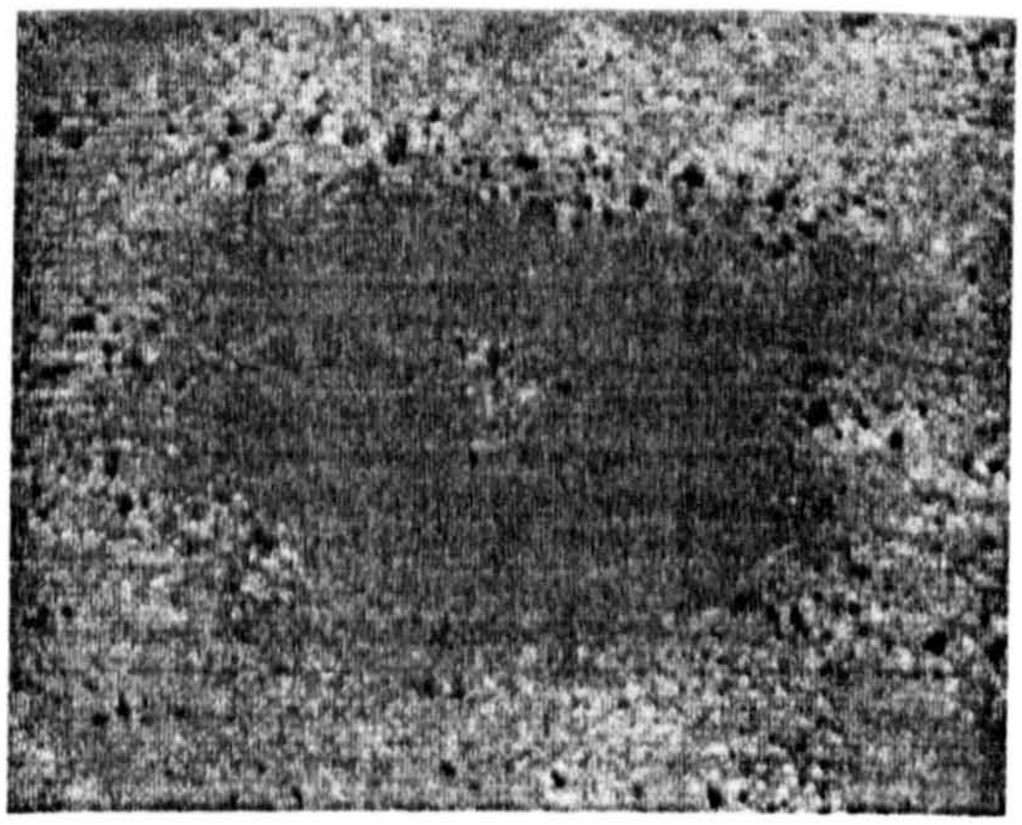

Fig 4.6 Delamination (Test c)

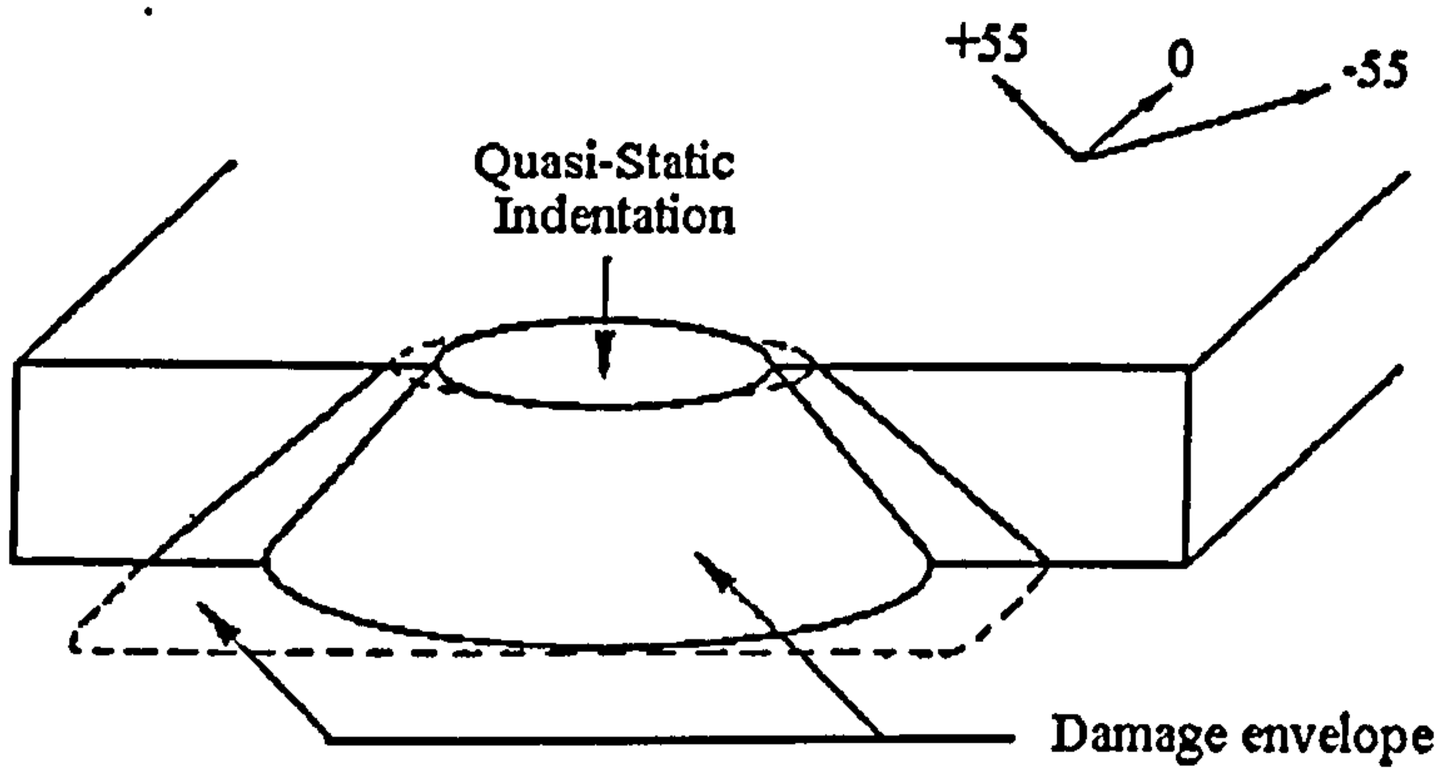

Fig 4.7 Schematic illustration of damage envelope

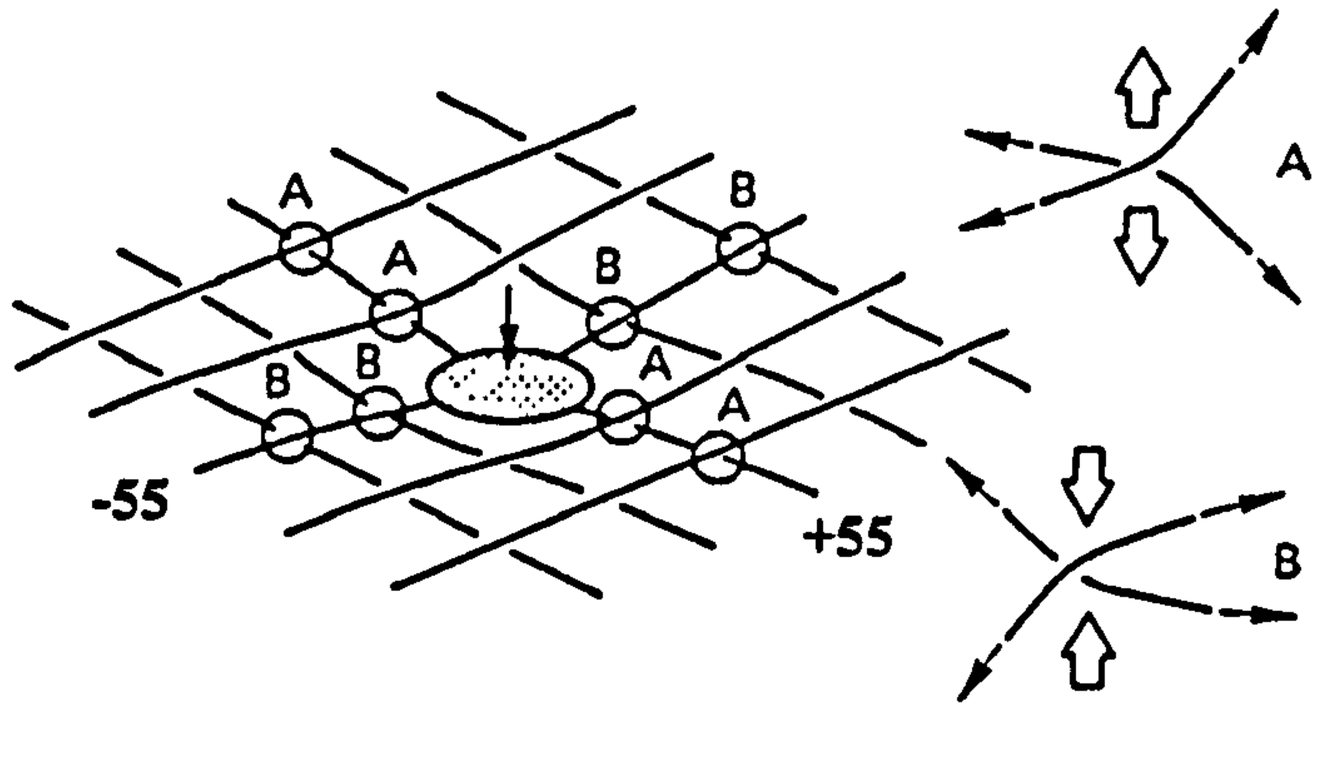

Fig 4.7(A) Basic model of delamination mechanism (Clark, 1989)

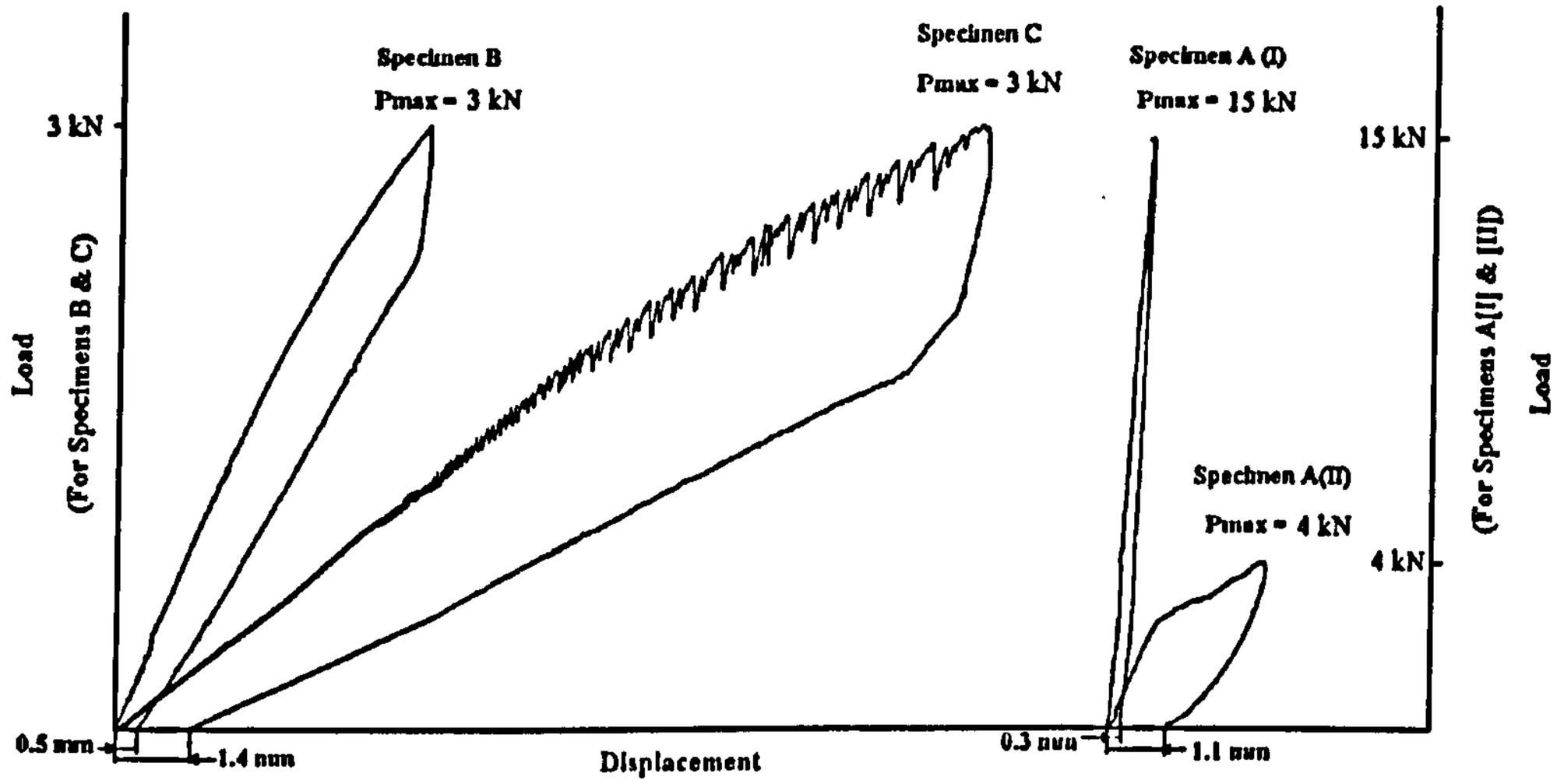

Fig 4.8 Load-deflection curves

Curves for specimens A(I) & (II) were in a same scale,

and B & C were in a same scale.

4.2 Quasi-Static Indentation on Composite Ring

4.2.1 Test Procedures

There were two parts in this second experimental investigation. In part 1, the loading and unloading processes to and from various maximum load (see Table 4.3) were undertaken at the same position of a composite ring, which was sectioned from the central portion of the NGV composite cylinder (see Fig 4.9). This type of cylinder was chosen for FE modelling in this study. The lay-up and material properties of this composite ring can be found in Tables 5.1.A and 5.1.B. The composite ring was placed on the steel base and held in position by two wooden wedges on each side during loading. The main purpose for this part of tests was, as an initial step, to find out the loading and unloading characteristic of the composite ring before further tests have been undertaken.

In part 2, ten tests were carried out at different azimuth positions of the composite ring (see Table 4.4). In these tests, the composite ring was placed on a wooden cradle, so as to impose some kind of constraints to avoid serious distortion of the composite ring at each test. Various load were applied in each test to record the load-deflection characteristic, and to investigate damage modes of this composite ring.

A hemi-spherical steel indenter with a diameter of 22 mm was chosen for the application of the loading. In each test, the load was gradually increased until the designated maximum was reached. It is understood that the size and shape of the indenter affects the load-displacement traces and the local damage modes or even global behaviour. However, the main purpose for this experimental investigation was to identify the major damage modes and behaviour of composite ring under quasi-static loading, and to complement and illustrate the results of the FE modelling. The size of the indenter was chosen so as to match approximately the total thickness of the composite ring, which was also 22 mm.

4.2.2 Damage Detection and Assessment

A sectioned composite ring is shown in Fig 4.10. It is worth noting that the aluminium liner detached itself and could be easily taken out after the first piece of composite layer was removed by sawing. Marks of adhesive were found at the interface between the composite layer and liner. These findings indicated that bonding between the two layers was not strong. After careful examination of the liner it was established that sites of permanent deflection had been created at positions loaded by higher contact forces (30, 32 and 35 kN). This suggests that some gaps may have been generated at the interface after indentation.

A diagram of the hoop section along a plane passing through the middle of the indentation site by a load of 35 kN is shown in Fig 4.11. A permanent indentation can be seen clearly. In the first 90° hoop layer, an array of radial cracks (or transverse shear cracks) was induced. Sun and Jih (1990) suggested that these transverse shear cracks arise due to high transverse shear stresses. This pattern of cracking extended to the second 90° layer. However, they split into two groups to each side of the load axis. When these transverse shear cracks arrive at the interface between the second 90° layer and +- 15° layer, they propagate outward to form an area of delamination. In the third 90° layer, vertical and horizontal cracks can be seen. Those interlaminar horizontal cracks mainly propagate outward. At least one delaminated crack was found which propagated inward to form a damaged patch in the middle of the third 90° layer. These cracks most likely arose were due to bending stresses in the lower half of the composite ring. A schematic diagram in Fig 4.12 demonstrates that the directions of loading forces were quite in line with those radial cracks in the top two 90° layers. A similar network of cracks could be seen in the longitudinal section, but less massive.

As the loading increased, the contact area also increased as can be seen by the load-contact radius relationship in Fig 4.15 (see also Table 4.5). It is obvious that the maximum contact radius is not only dependent on the loading, but also the diameter of the indenter. The permanent indentation produced by various levels of loading also increased in a similar manner as contact radius (see Fig 4.15).

4.2.3 Experimental Results

The load-deflection curves for part 1 loading and unloading tests were given in Fig 4.13. Six loading and unloading cycles were carried out at the same position.

The loading and unloading paths of the initial 5 kN load were virtually indistinguishable (curve 1). This indicated that there was a complete elastic recovery after loading. No damage was induced in the cylinder.

The cylinder was then reloaded to 15 kN (curve 2), and unloaded from that peak load. It can be seen that the loading and unloading paths were different. The area bounded by these two paths is related to the amount of energy dissipated to create damage in the system. A permanent indentation was created.

The cylinder was then reloaded to 10 kN (curve 3). Although the unloading path was different to the loading path, it returned to the same origin. It seems to indicate that some further portion of energy was dissipated, but no further indentation has been produced.

The cylinder was then reloaded to 20 kN (curve 4), and the large area bounded by the loading and unloading curves indicated that quite a large amount of energy was irreversibly consumed to create material damage. The unloading path returned back to the same position as for curve 2, which suggested that the magnitude of indentation has not changed significantly from that for curve 2.

The cylinder was reloaded to 15 kN (curve 5). Similarly to curve 3, a very small portion of energy was dissipated.

At the final step, it was reloaded to 25 kN (curve 6). A further significant amount of energy was dissipated into the system to create material damages. The unloading path returned back to the same position as for curves 2 and 4, indicating that an indentation of similar magnitude remained, and no further permanent impression was produced.

It is important to be careful in interpreting the energy dissipation taking place during the loading and unloading cycling process in terms of creating damage. Machine compliance is one of the factors that affect the load-deflection path, which means that the machine itself may have absorbed some portion of energy during the loading and unloading process. Another important factor is that the indenter may be loaded not in exactly the same position as previously simply because the deflection due to loading and unloading may have altered the position of the cylinder to some extent. However, the general features and characteristics of the indentation load-deflection relationship of the composite ring have been recorded with good accuracy. It may be worth noting that, in all these tests, a large proportion of the unrecoverable energy was used to create local indentation. Material immediately near the contact region suffered very high local strains due to the very high magnitude of contact stress. Sun and Jih (1990) found that the magnitude of the transverse shear stress is directly related to the magnitude of the contact force and the size of the contact area. More quantitative interpretation of Fig 4.13 is problematic, especially since the damage induced by each test on the same position was hard to estimate.

In Fig 4.14, the load-deflection curves for the three highest loads (30, 32 and 35 kN) applied in part 2 are given. A typical load-deflection curve was obtained for 30 kN (curve 1). A permanent indentation of about 1 mm was produced.

In the curve 2, it can be seen that when the loading increased to about 30 kN, the loading repeatedly dropped and resumed for three times before it arrived to a maximum loading of 32 kN. It indicates that extensive damage of material must have been taken place at 30 kN level. Also, a global deflection of the composite ring took place, which was reflected by a sudden drop in the structural stiffness after reaching the 30 kN load level. It finally produced a 1.4 mm indentation.

Curve 3, which is similar to curve 2, shows a drop of load which occurred at about 30 kN level. Again, a global deflection of the composite ring took place. It finally produced a 1.7 mm indentation. From the sectioned composite ring, it was found that

large areas of delamination were created under these high loading conditions, both locally and at some remote locations.

The results strongly suggest that there exists a critical loading level for this composite ring, and the chosen indenter radius, beyond which extensive damage develops, and also global behaviour has to be considered. From the observations in this investigation, it is natural to conclude that the 30 kN loading level represents the critical load boundary. However, before global behaviour was seriously affected, a local contact region must have already developed serious and extensive damage. This 30 kN critical level is likely to be significantly influenced by the diameter of the indenter. If a smaller indenter were used, it may have already penetrated into the composite material under a 30 kN loading. Then, different extents of damage and failure modes might have been introduced.

Table 4.3 Loading and unloading tests in part 1

Sequential Order	Maximum Loading (kN)
1	5
2	15
3	10
4	20
5	15
6	25

Table 4.4 Maximum loading for tests in part 2

Test Numbering	Maximum Loading (kN)
1	5
2	8
3	12
4	16
5	20
6	25
7	32
8	30
9	35
10	32

Table 4.5 Measured contact radius and calculated permanent indentation

Test Numbering	Maximum Load (kN)	Measured Contact Radius (mm)		Calculated Permanent Indentation * (mm)
		Longitudinal Direction	Hoop Direction	
2	8	3	3	0.42
3	12	3	3	0.42
5	20	4.75	4.5	0.96
6	25	5.4	5	1.2
8	30	6	5.5	1.47
9	35	8.4	6.5	2.13

* This calculated permanent indentation was based on the geometry relation between radii of indenter and contact radius. The shorter contact radius was used in calculation.

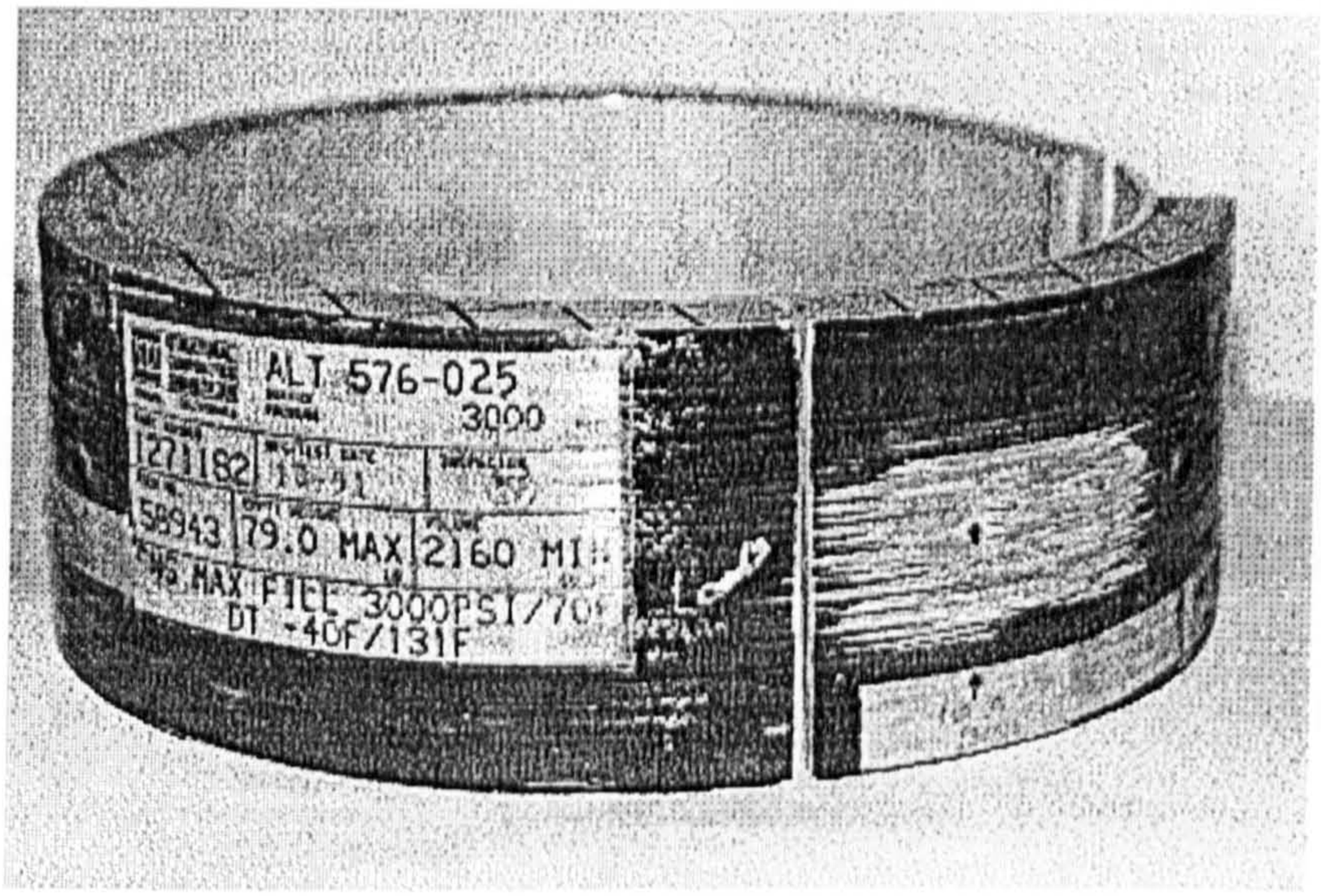

Fig 4.9 Composite ring cut from a composite pressure cylinder for NGV

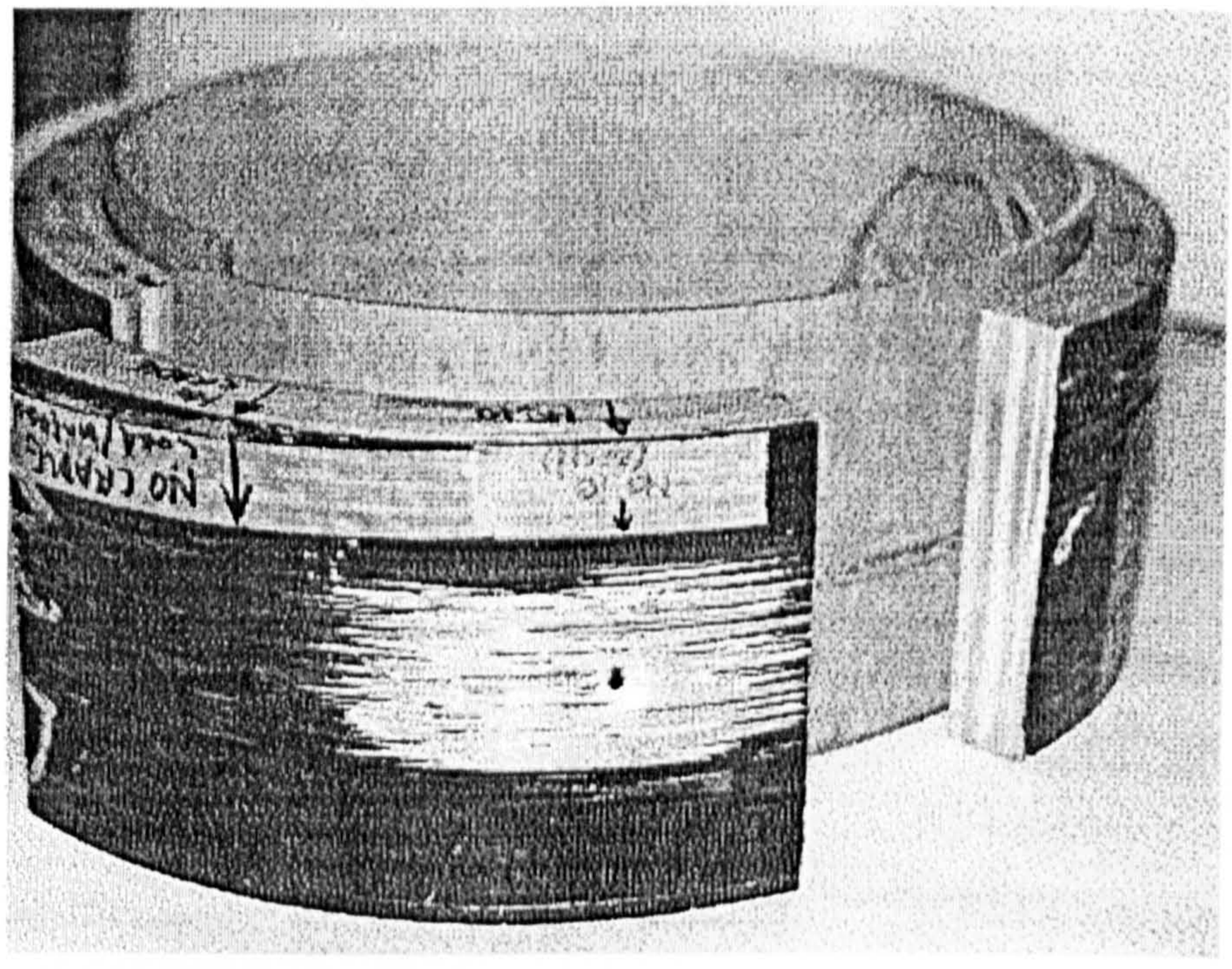

Fig 4.10 Sectioned composite ring after indentation tests

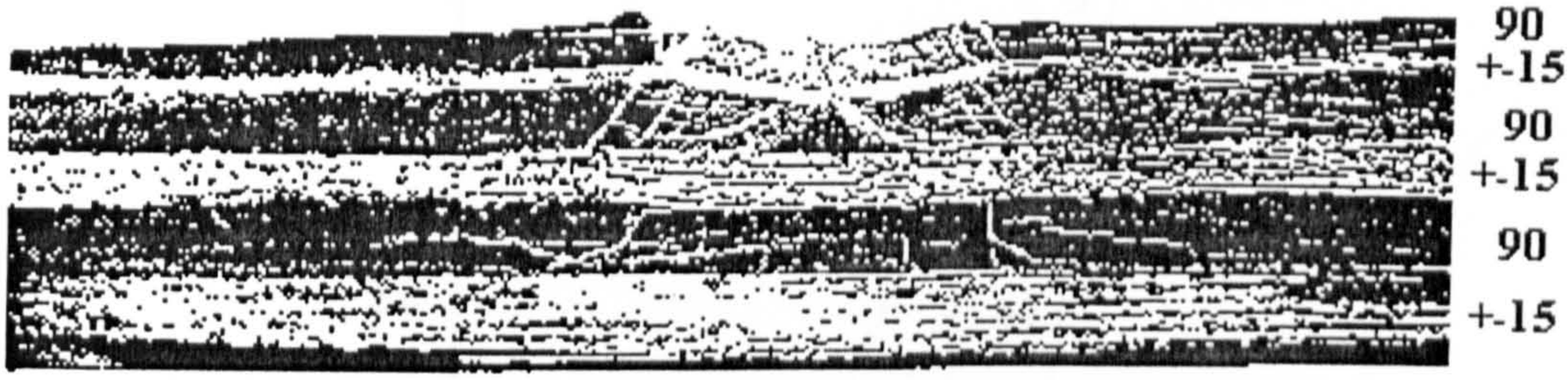

Fig 4.11 Damaged hoop section of the composite ring (Pmax = 35 kN)
(90° fibres were perpendicular to the paper)

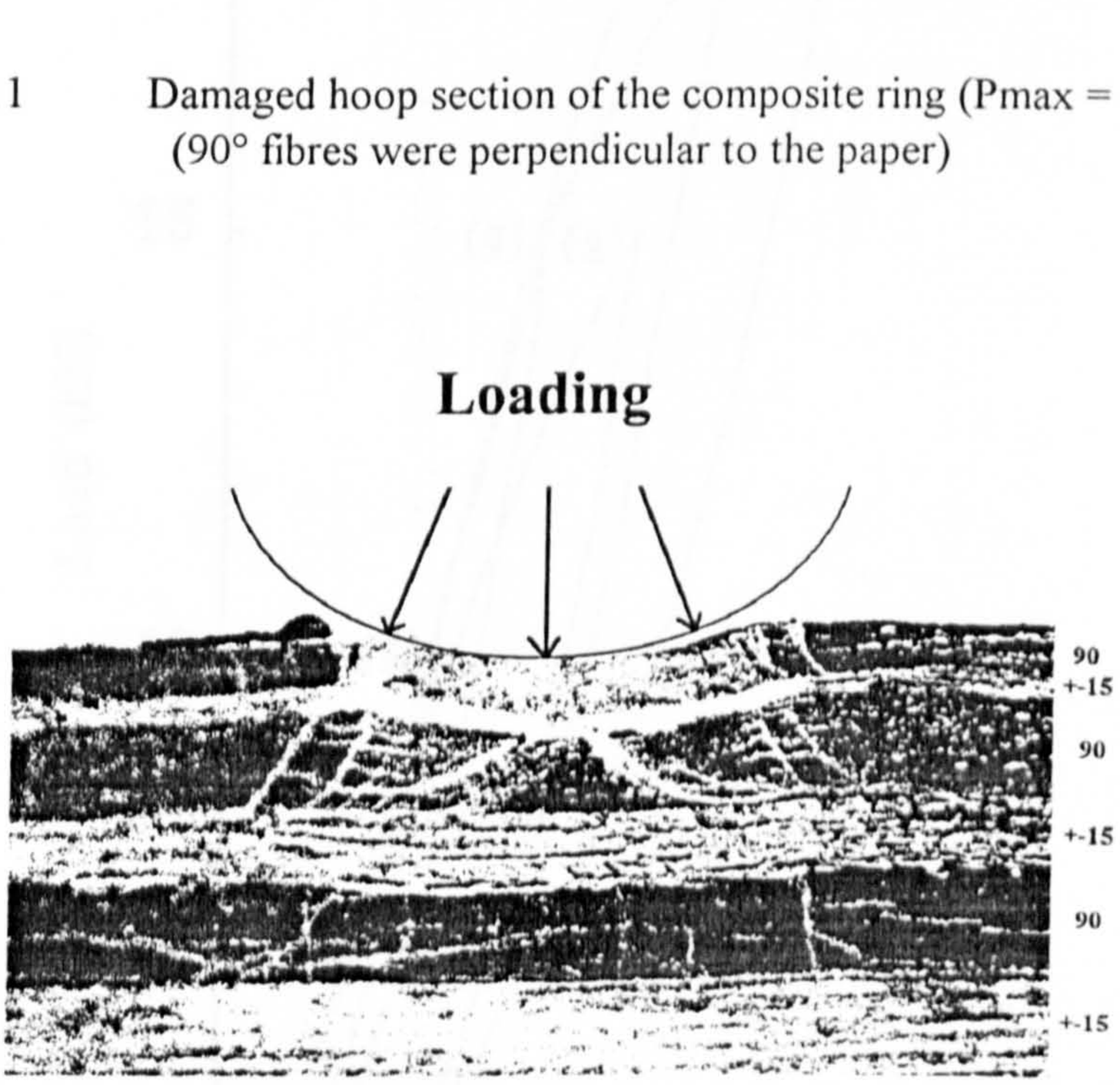

Fig 4.12 Schematic diagram of loading applied to cylinder
(90° fibres were perpendicular to the paper)

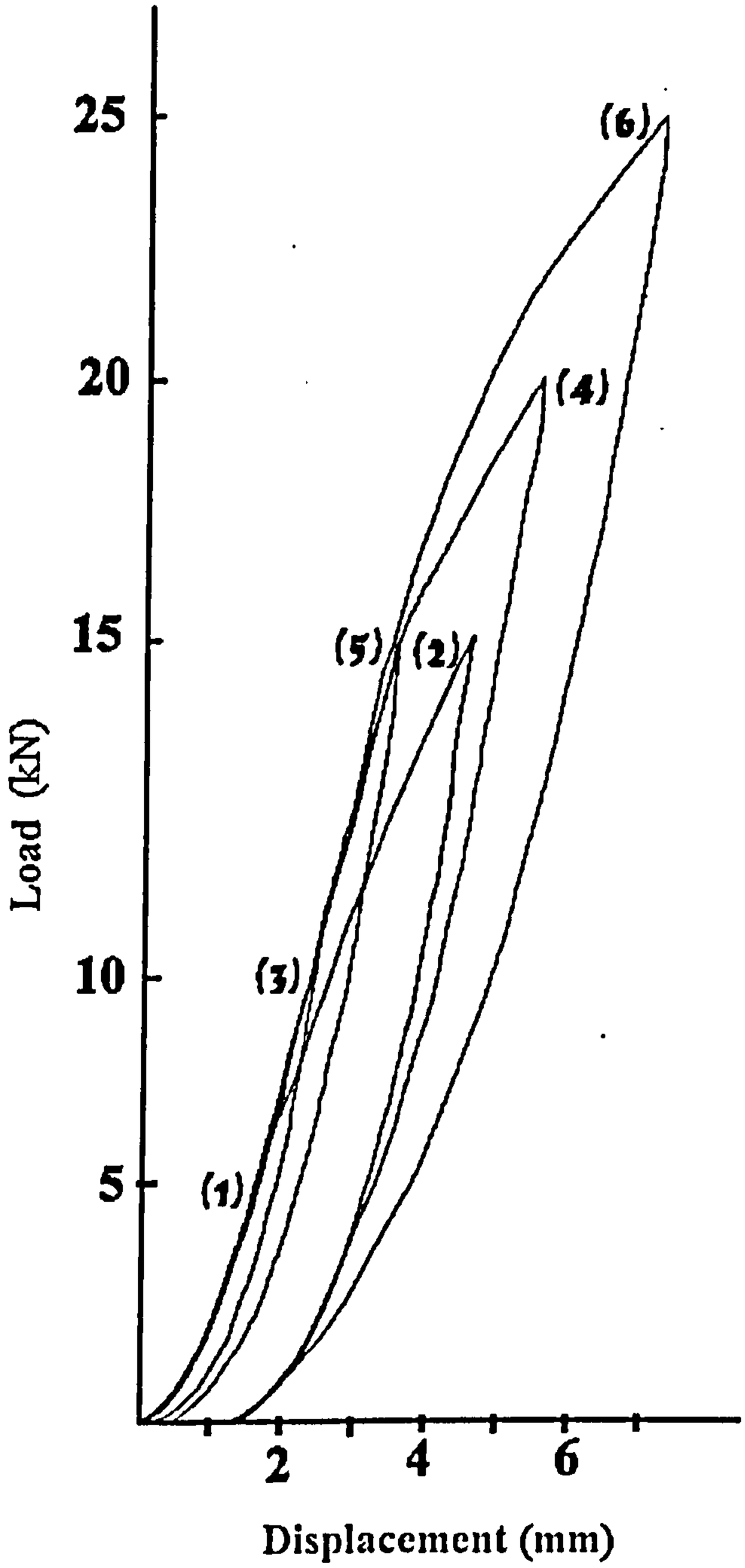

Fig 4.13 Loading and unloading tests

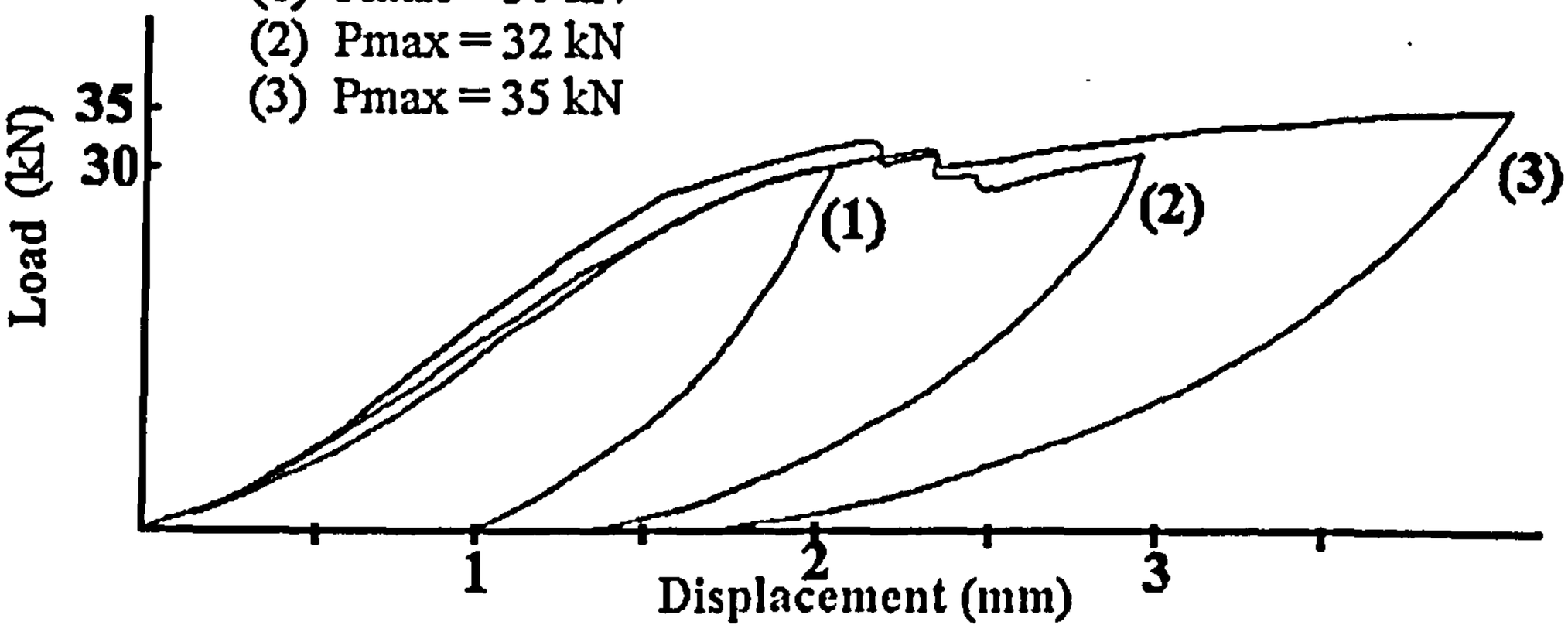

Fig 4.14 Load-deflection curves

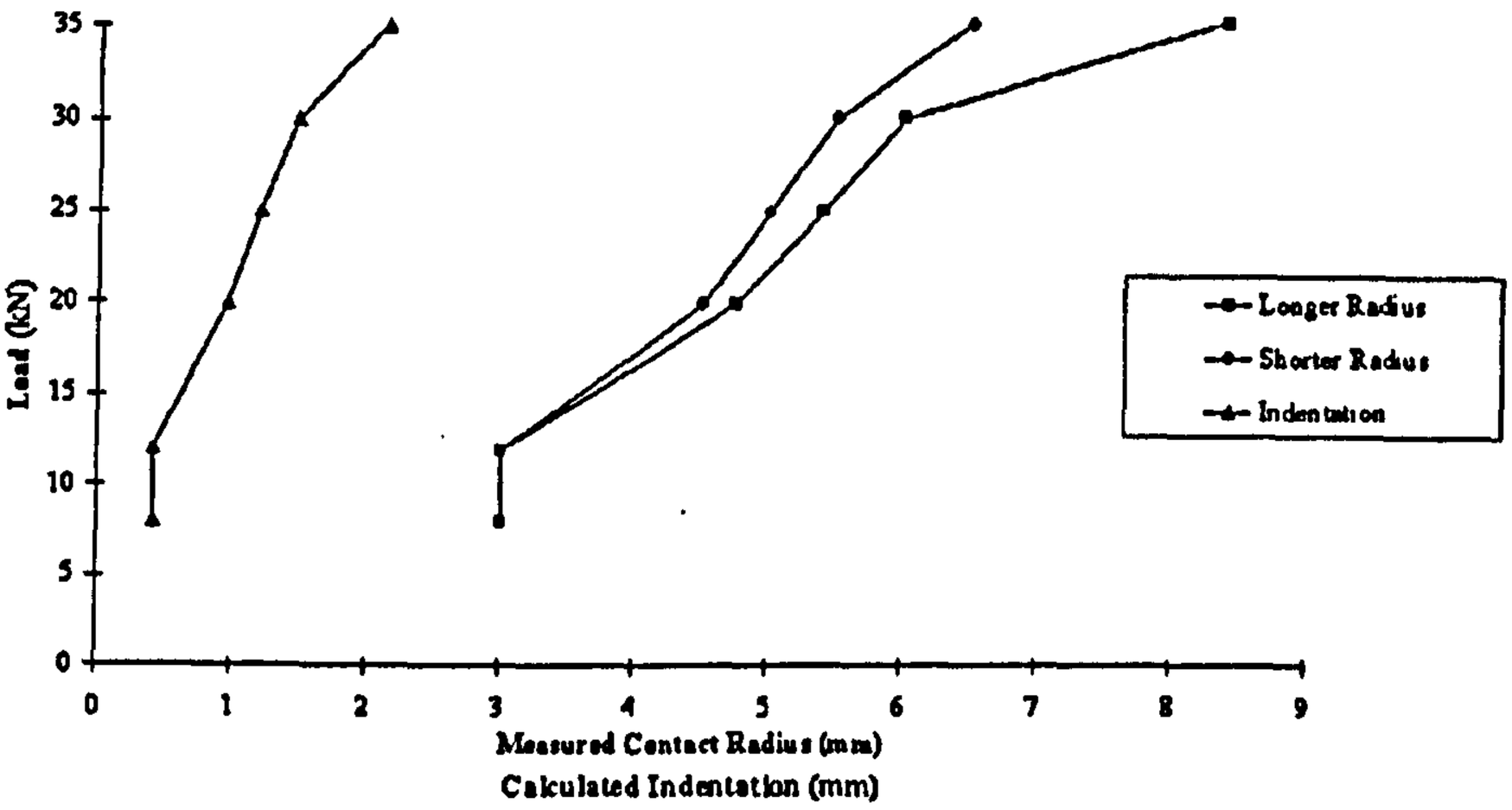

Fig 4.15 Load -contact radius relationship &
Load - indentation relationship

4.3 Concluding Remarks

Generally, the failure modes that could be identified in the experiments, albeit with varying degrees of success, were fibre breakage, matrix cracking, and delamination.

These were also predicted by FE analysis (see Chapter 5). Direct matching of FE modelling to experimental traces is problematic due to the following difficulties :

1) Experimental load-displacement curves are affected by inaccuracies in the measurement and systematic offsets associated with machine backlash;
2) Indentation response may be highly sensitive to the local surface conditions, overcoat thickness, etc.
3) Direct FE to experimental matching would require faithful modelling of the local "plastic" deformation under the indenter. This, in turn, requires substantial mesh and load increment refinement, and is largely impracticable.

The results of tests can be used instead to attempt to match the extent of damage observed under certain maximum load to that predicted by the model. Reliable matching of this type would still require a statistically significant number of specimens to be available, which was not the case in this project. However, the tests suggest that such approach would be feasible.

Christoforou (1988) has utilised the simple beam theory in conjunction with fracture meachanics analysis to develop an analytical 2D ring model which allowed him to calculate the extent of delamination in the cylindrical rings. The resulting equations can be used to calculate the critical load required to start delamination , which is in the form :

$$F_c = \frac{3}{4} h^2 \tau_c$$

where

F_c is the critical load,

τ_c is the maximum allowable interlaminar shear stress, and

h is the wall thickness of the cylinder.

This equation was used in the present study to calculate the critical load for the initiation of delamination in the composite ring being analysed. The calculated critical load is 34.5 kN. This value matches well with the experimental findings, where at the 30 kN load level, persistent delamination (and some others failure modes) were observed. This agreement with analytical calculation suggests that the repeated load drops observed at around the 32 kN level may indeed be associated with progressive delamination.

Chapter 5 Modelling : Application

5.1 FEM : Dynamic Response

5.1.1 Correlation with Analytical Closed-Form Solutions

Time dependent stresses are found from the dynamic response calculation. The considerations for FE mesh design must be applied. The element mesh density is usually chosen to be the highest around areas of stress concentration. As suggested by NAFEMS, the best choice for a dynamic mesh is the simplest one consisting of a uniformly dense mesh over the whole structure. These principles were taken into account when designing a suitable FE mesh for the present validation. However, if a uniformly fine mesh were used for the whole structure, a model with quite a large number of shell elements would result, which would require both a long computation time and a huge amount of memory. Moreover, the present version of PIGS only allows a maximum of 10,000 structural nodes to be generated for a FE mesh. In fact, an impact loading usually induces very localised displacement and stresses. Therefore, for the cylindrical structure such as the one considered in this study, a FE mesh with a gradual reduction of mesh density with the distance from the impact site may be sufficient. The coordination system for all the FE thick shell models is given in Fig 5.1.1. It can be seen in Figs 5.1.2, 5.1.3 and 5.1.4 that a fine mesh was used in the impact region. This FE mesh had 1080 eight-noded thick shell elements.

The size of the fine elements in the impact site cannot be chosen too small. Since elements in the region of lower element mesh density may have unacceptable high element aspect ratio. The size of the finest elements located at the central position of this model was 2 mm x 2.617 mm. The highest discontinuity of stresses at the common nodes was 4.3 % (in the fibre direction.), and 1.8 % (perpendicular to the fibre direction).

5.1.1.1 Impact Loading with a Small Loading Contact Area

Response solutions of FE model were compared with the predictions of a closed-form analytical model considered by Christoforou [1988] (see Table 3.1.1 for configuration and impact loading). The parameters used in the FE dynamic analysis are given in Table 5.1.1. The impact loading was distributed over a small area (20.936 mm^2). In the FE model this region was represented as bounded by four elements (numbered 18, 19, 468 & 472) with 21 nodes. The deformed shape of the cylinder (Fig 5.1.5) displayed localised deformation due to impact loading. It can be seen in Fig 5.1.6 that the transverse displacement history showed good agreement between the two models at the central point, with a difference of 15 μm at the maximum peaks (i.e. 5.5 %). The transverse displacement along the longitudinal direction (x-axis) of the cylinder was predicted to have a similar deformed shape according to both models, as shown in Fig 5.1.7.

The impact force history due to point loading was calculated for comparing with analytical impact force history, which is shown in Fig 5.1.8. It was found that FE prediction was only 14 N lower than the analytical solution at the maximum (i.e. a 4.2 % lower). Although the FE model predicted a higher longitudinal strain after 250 μs than its analytical counterpart (see Fig 5.1.9), in general the responses predicted by both models closely agreed with each other.

5.1.1.2 The Effect of Loading Contact Area

In order to compare the effect of loading contact area on the impact response, the results obtained using three different contact areas and a point load with the same impact loading are shown in Figs 5.1.10 to 5.1.14.

In general, the transverse displacements predicted by the FE analysis (Fig 5.1.10) have higher magnitudes than those predicted by the analytical approach (Fig 5.1.11). It can be seen that, as expected, a point load produces higher predicted deflections at the central position, Node 1. Generally, a larger contact area will give less displacement than a

smaller contact area under the same impact load. However, for FE analysis, apart from point loading, the responses for different contact areas were very close. Similar conclusion can also be made for the analytical model. From the variation of transverse displacements along the longitudinal direction, it can be seen that loading on a larger contact area predicted higher displacement away from the central region of the cylinder. The longitudinal strain history shown in Fig 5.1.14 once again confirms that a point load induces very highly localised stresses and displacements, however, which quickly decay away from the impact site.

In general, the impact response due to the three different contact areas compared to the point load is the variation of magnitude rather than the response behaviour. Since the FE predictions for the stresses and displacements using various contact areas were quite close to each other, it may be concluded that the choice of contact area does not significantly affect the impact response inducing mild variations in magnitude. In Fig 5.1.12, it can be seen that the global deflection of the cylinder loaded over a larger contact area tends to be larger.

Table 5.1.1 Details of FE dynamic analysis

Number of auto master d.o.f.	630
Number of manual master d.o.f.	1, 21, 65, 133
(for various contact areas)	
Time-step	1 μs

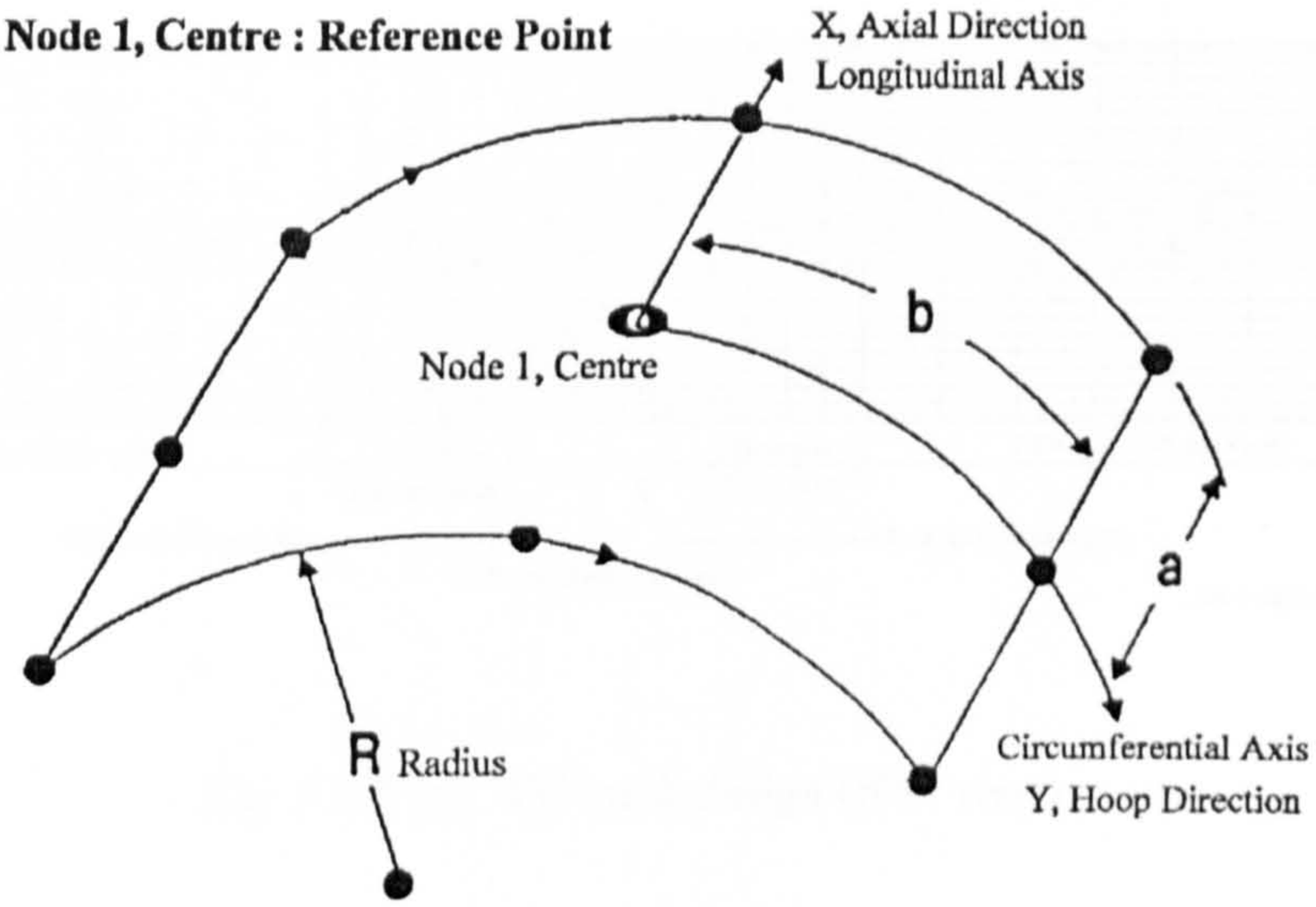

Fig 5.1.1 Coordination system for FE models

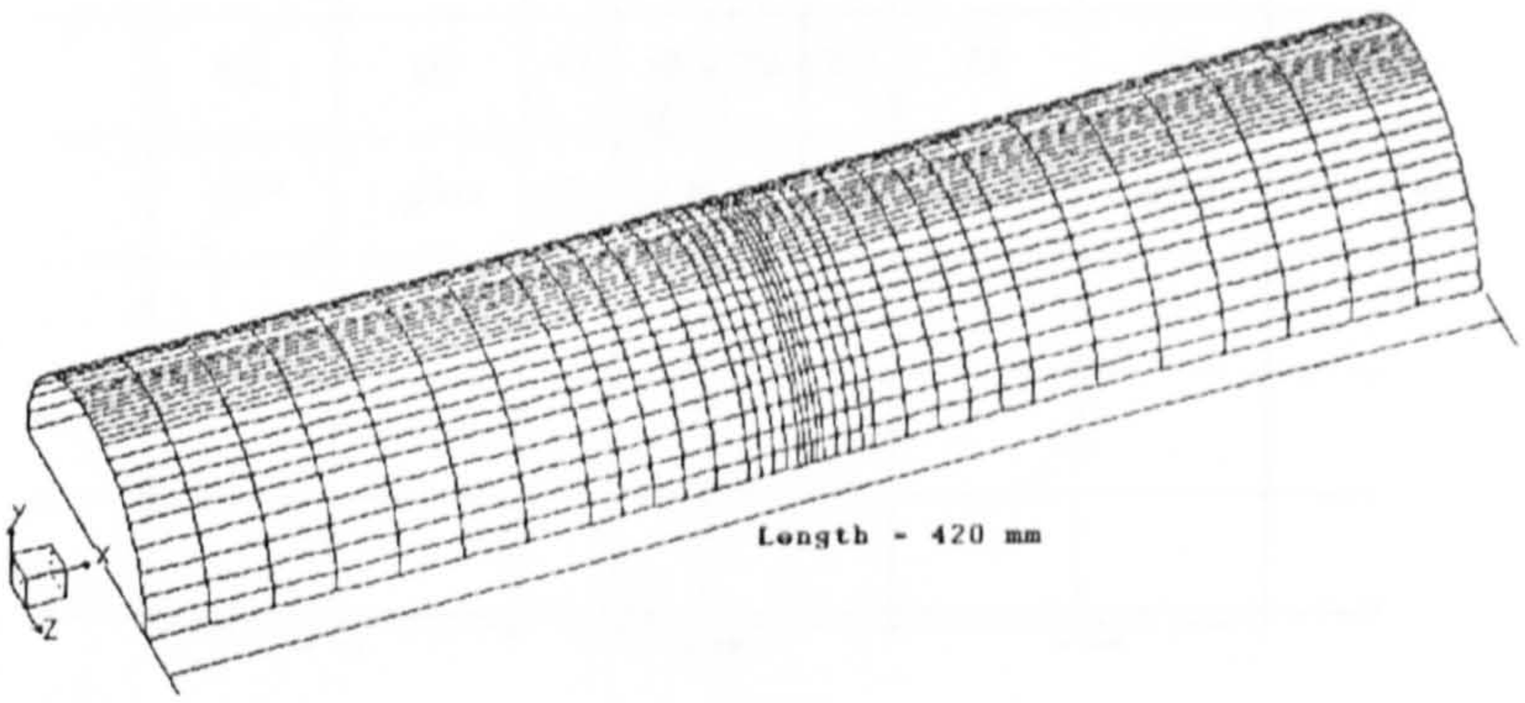

Fig 5.1.2 Geometry of the FE model

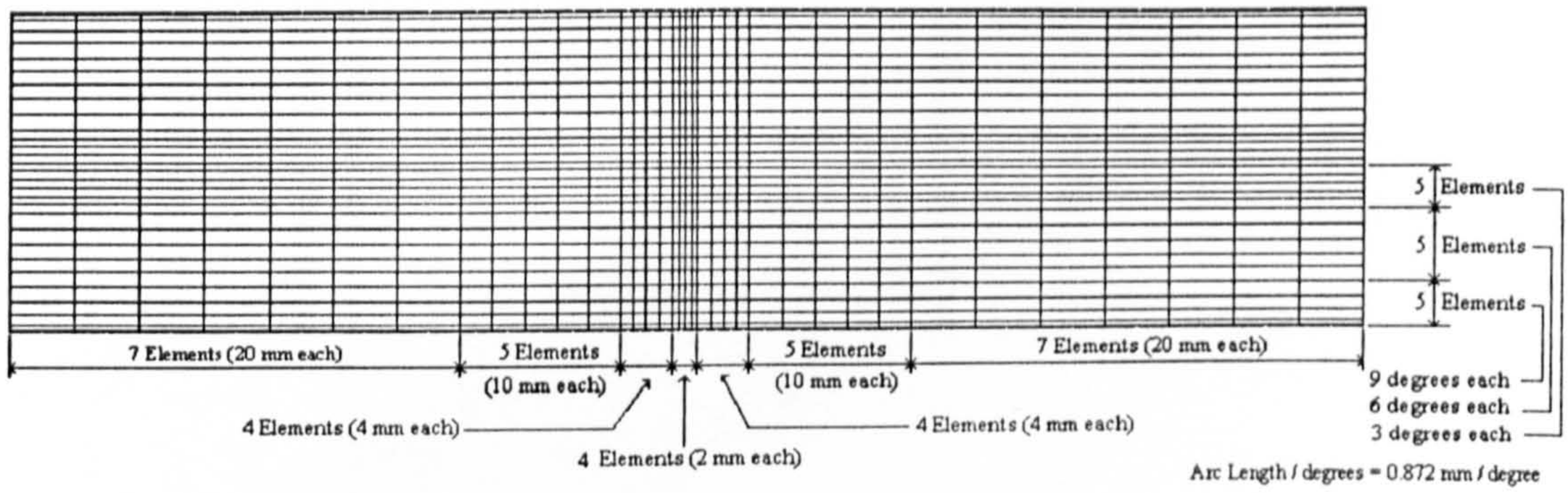

Fig 5.1.3 (a) FE mesh design (plan view)

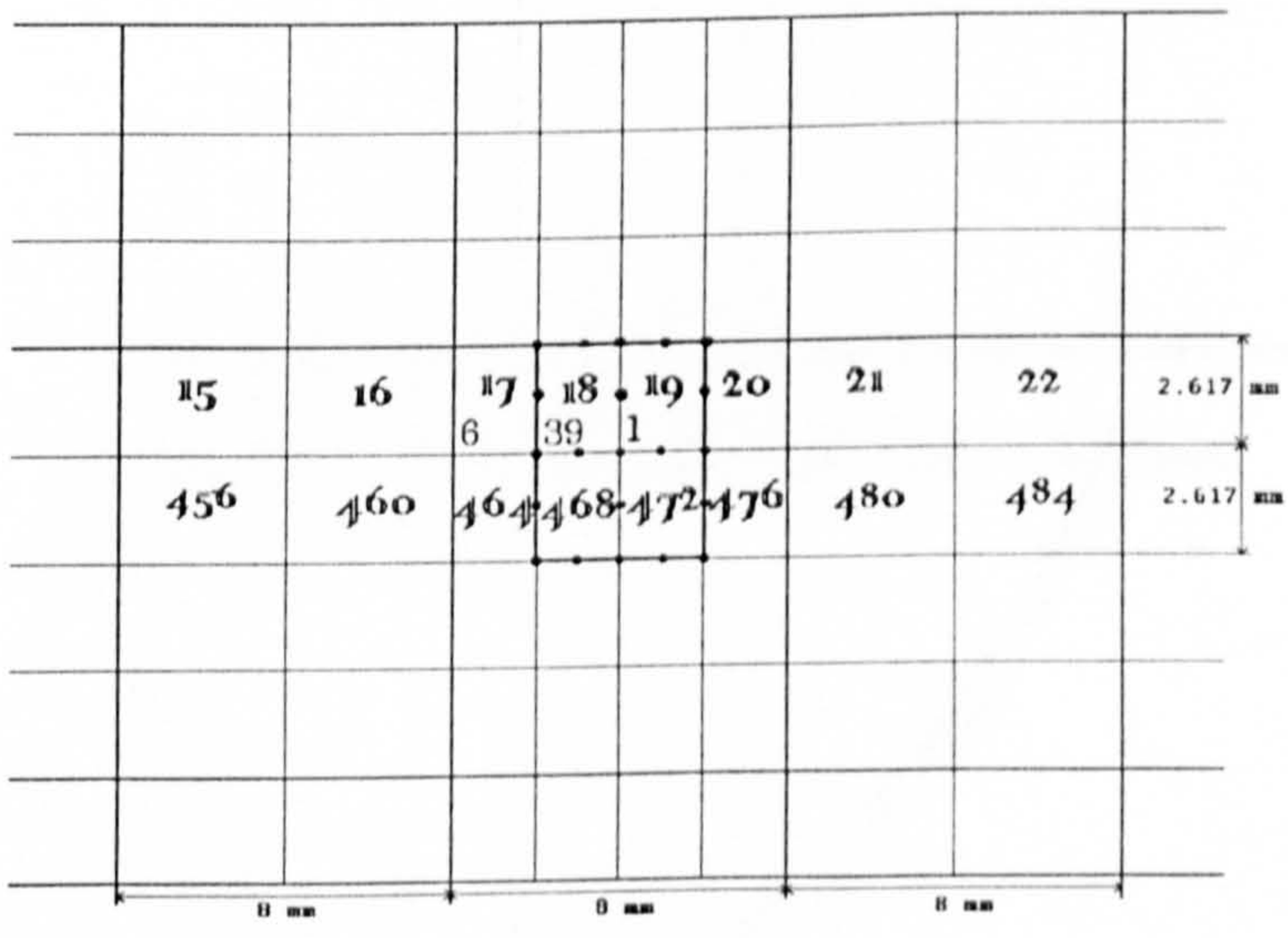

Fig 5.1.4 Element size of FE model at the impact region

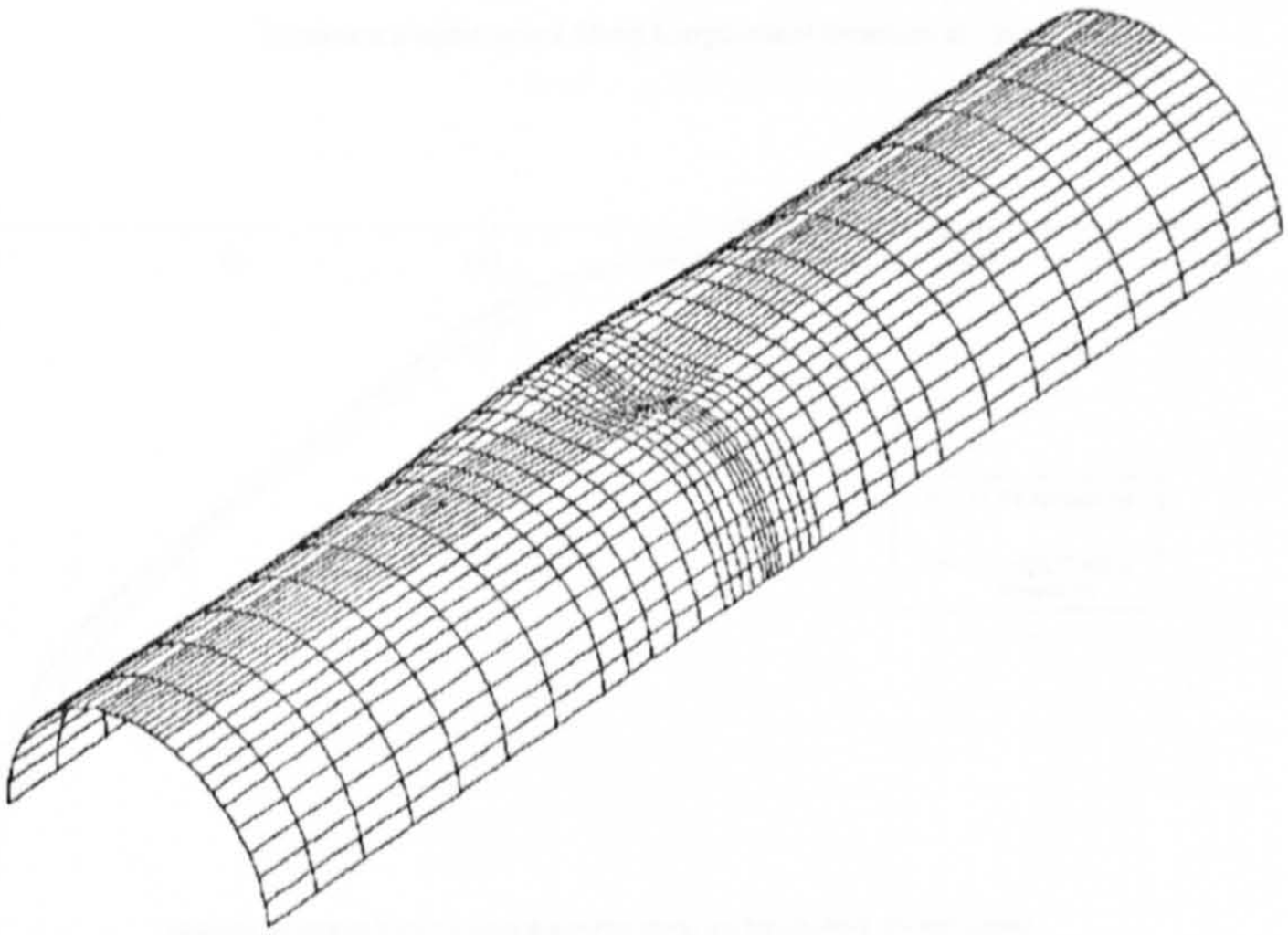

Fig 5.1.5 Deformed shape (at 150 μs)

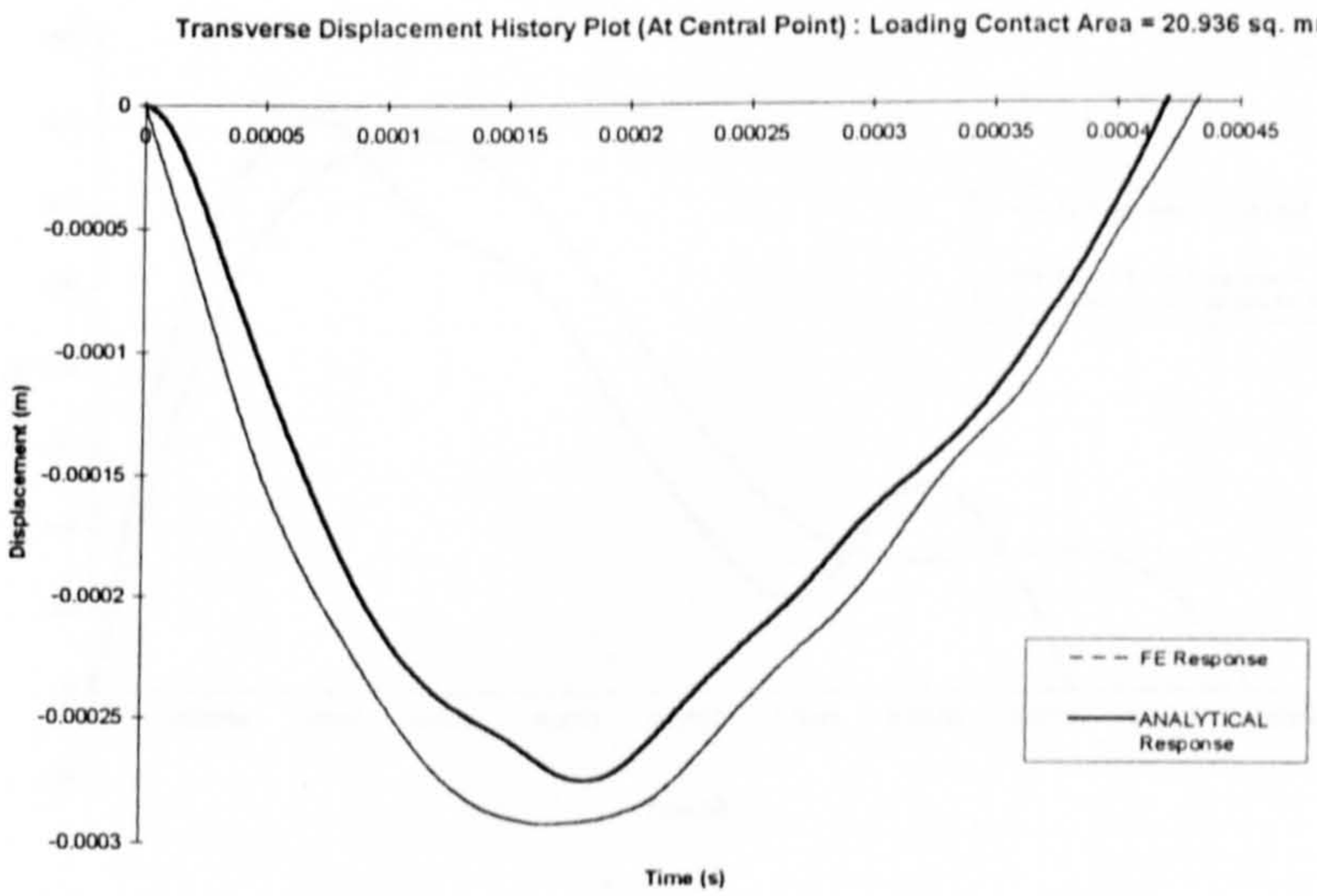

Fig 5.1.6 Transverse displacement history plot

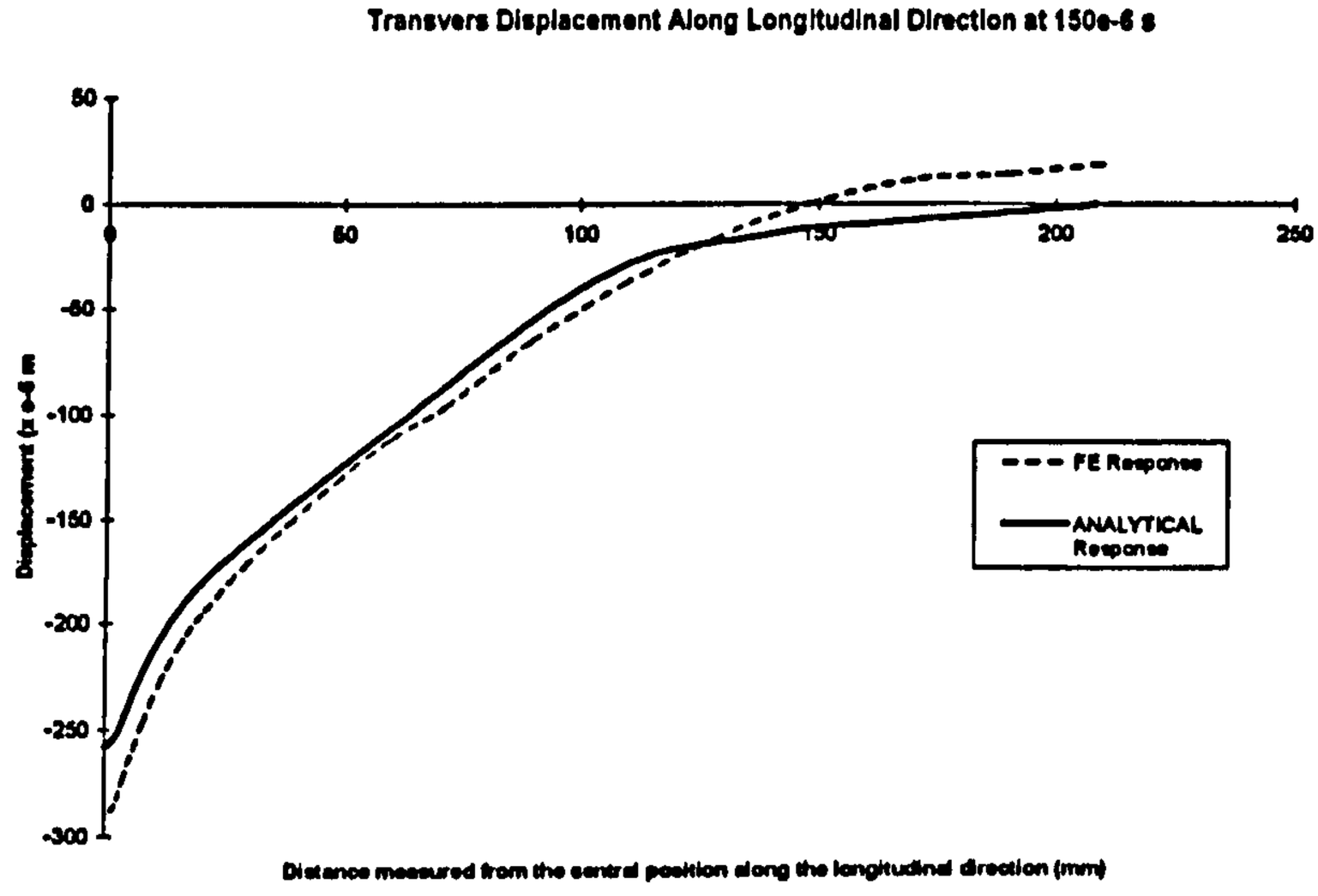

Fig 5.1.7 Transverse displacement in the longitudinal direction (at 150 μs)

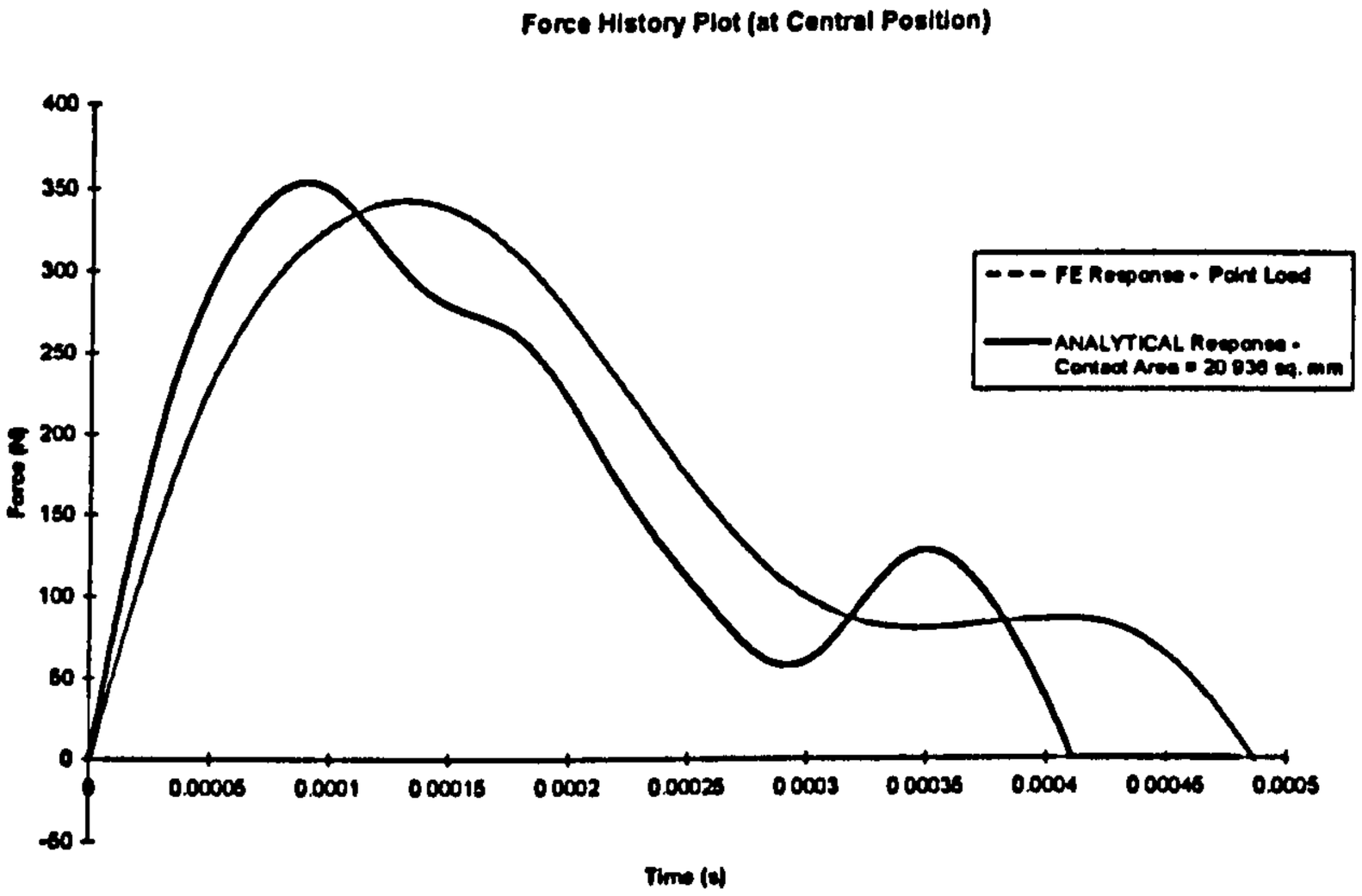

Fig 5.1.8 Force history plot

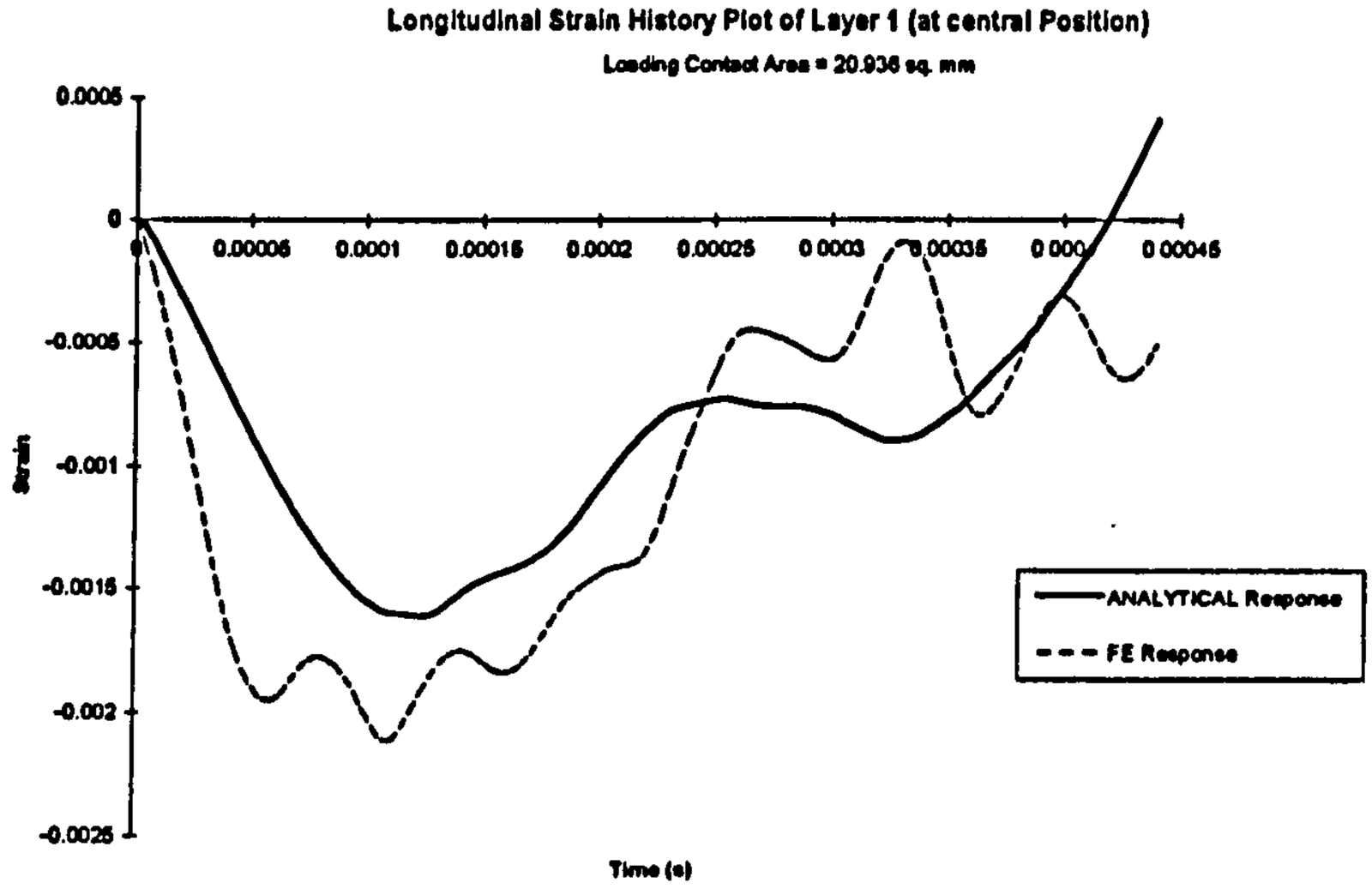

Fig 5.1.9 Strain history plot

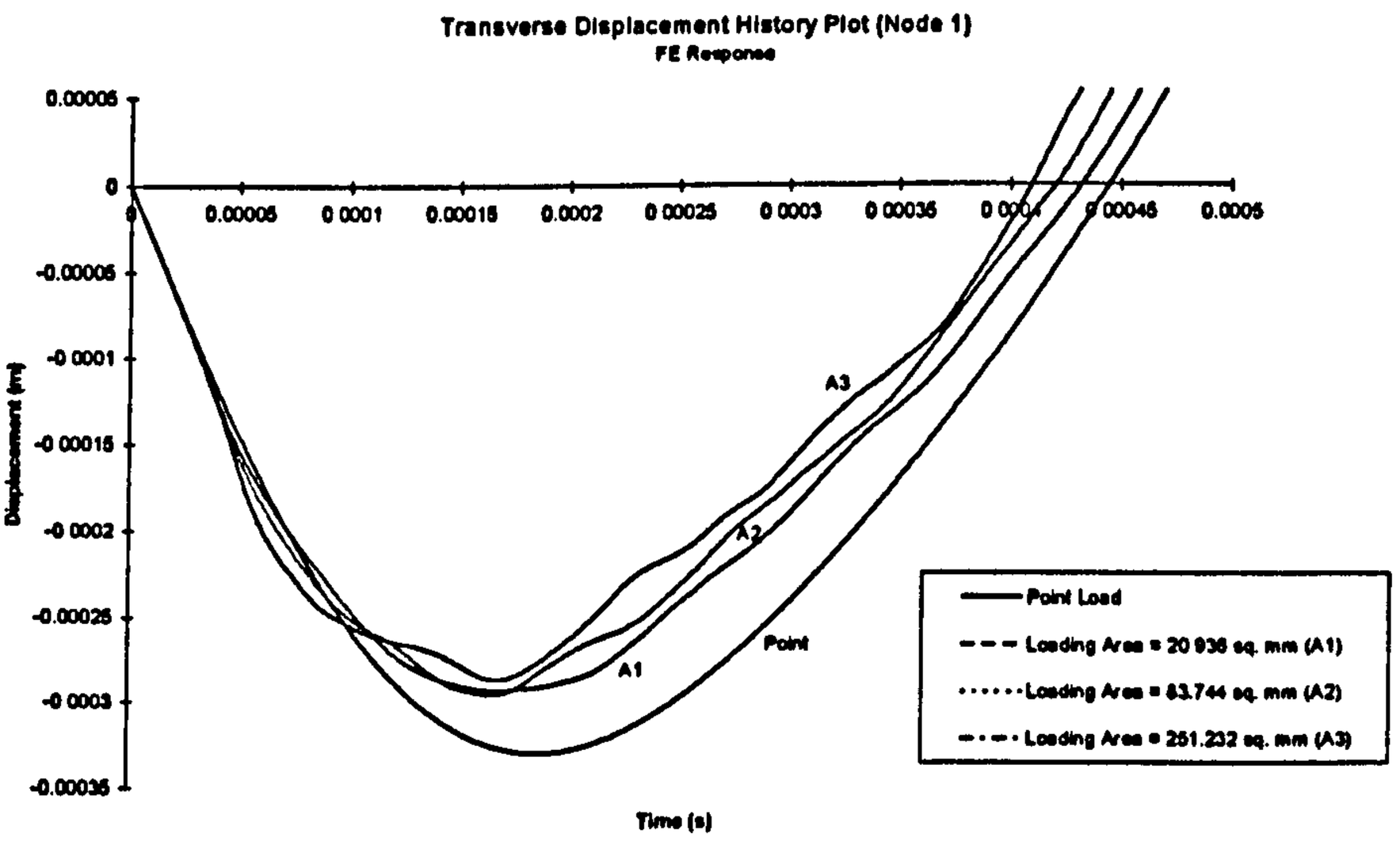

Fig 5.1.10 Transverse displacement history plot (FE response)

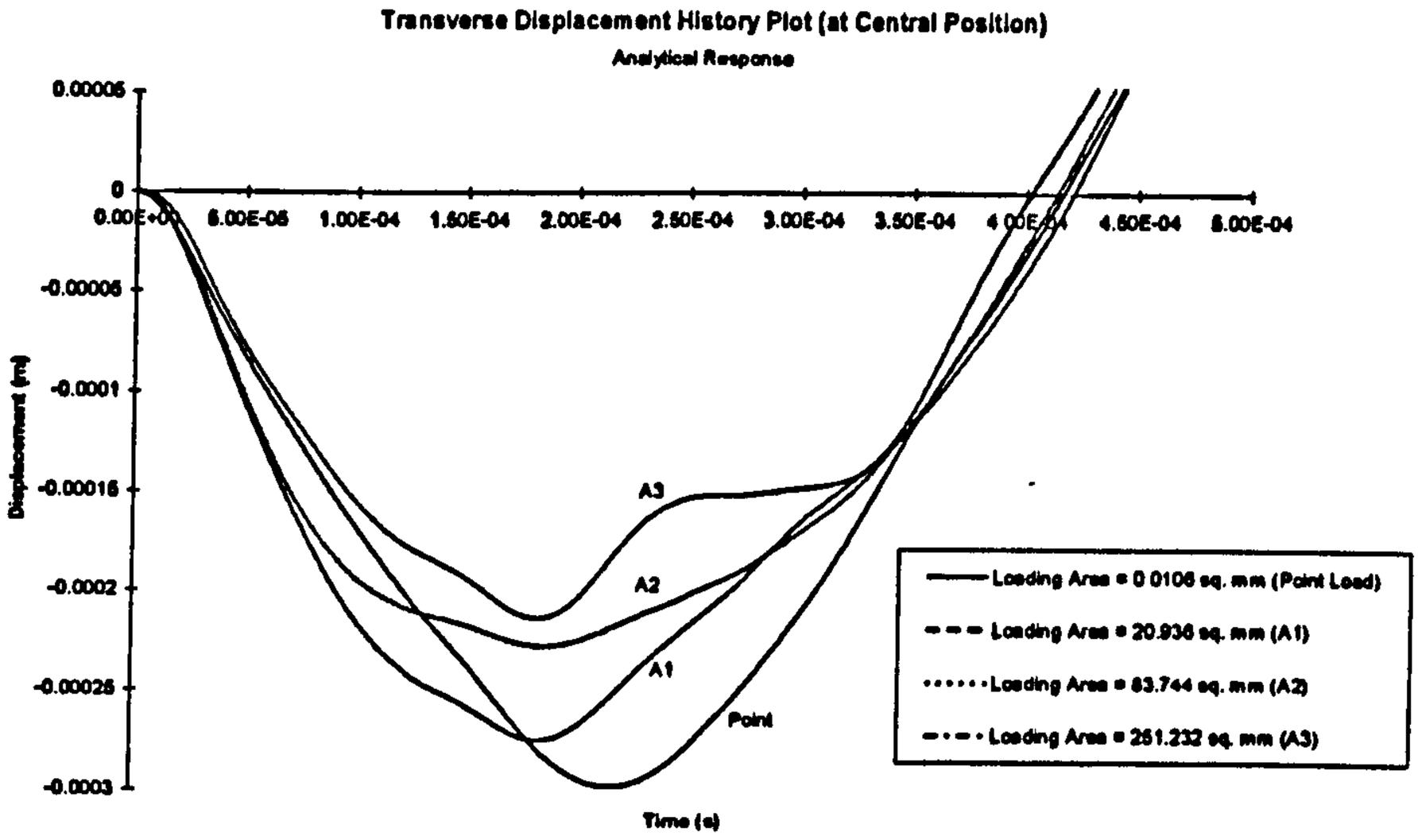

Fig 5.1.11 Transverse displacement history plot (analytical response)

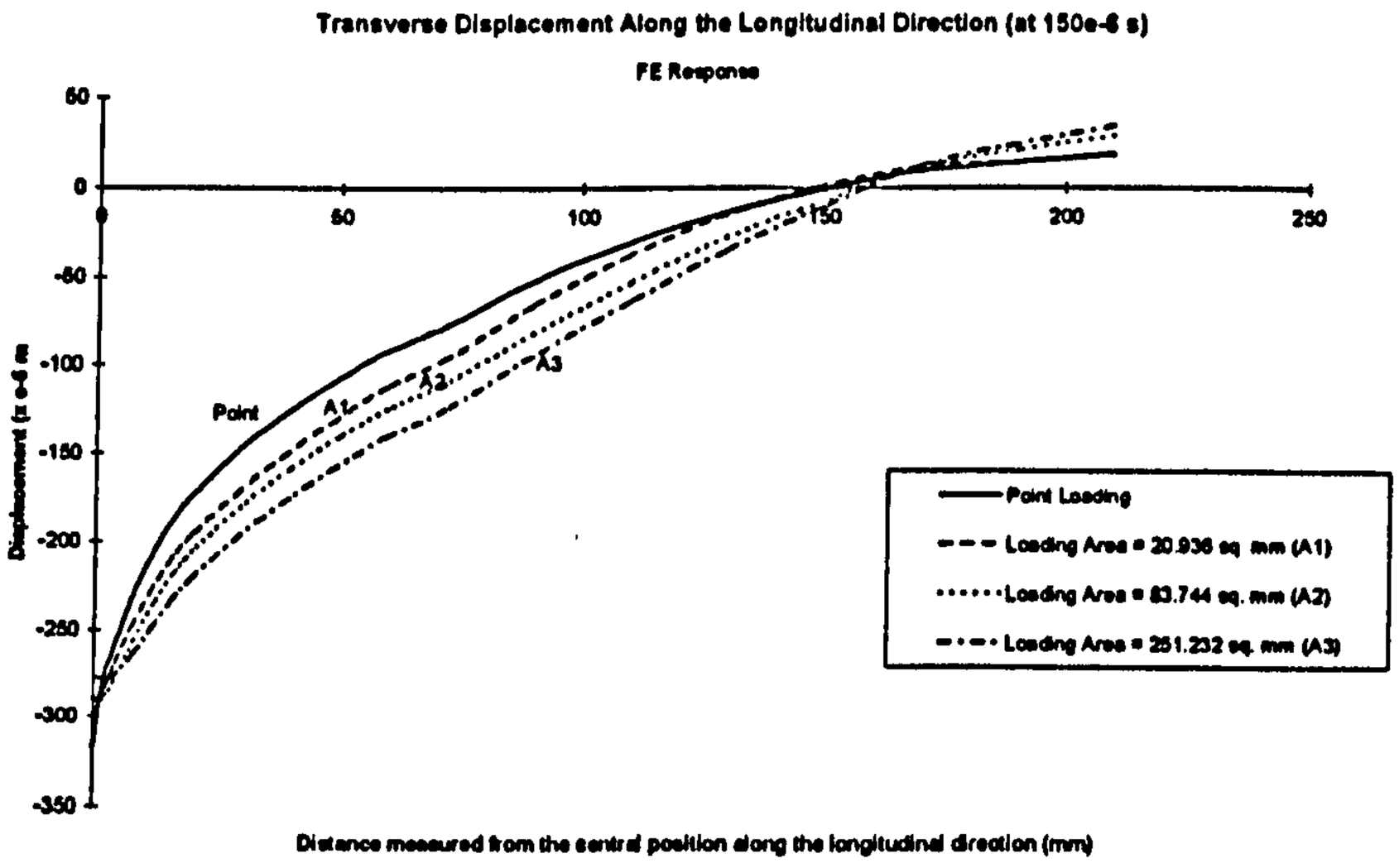

Fig 5.1.12 Transverse displacement along longitudinal direction (at 150 μs)

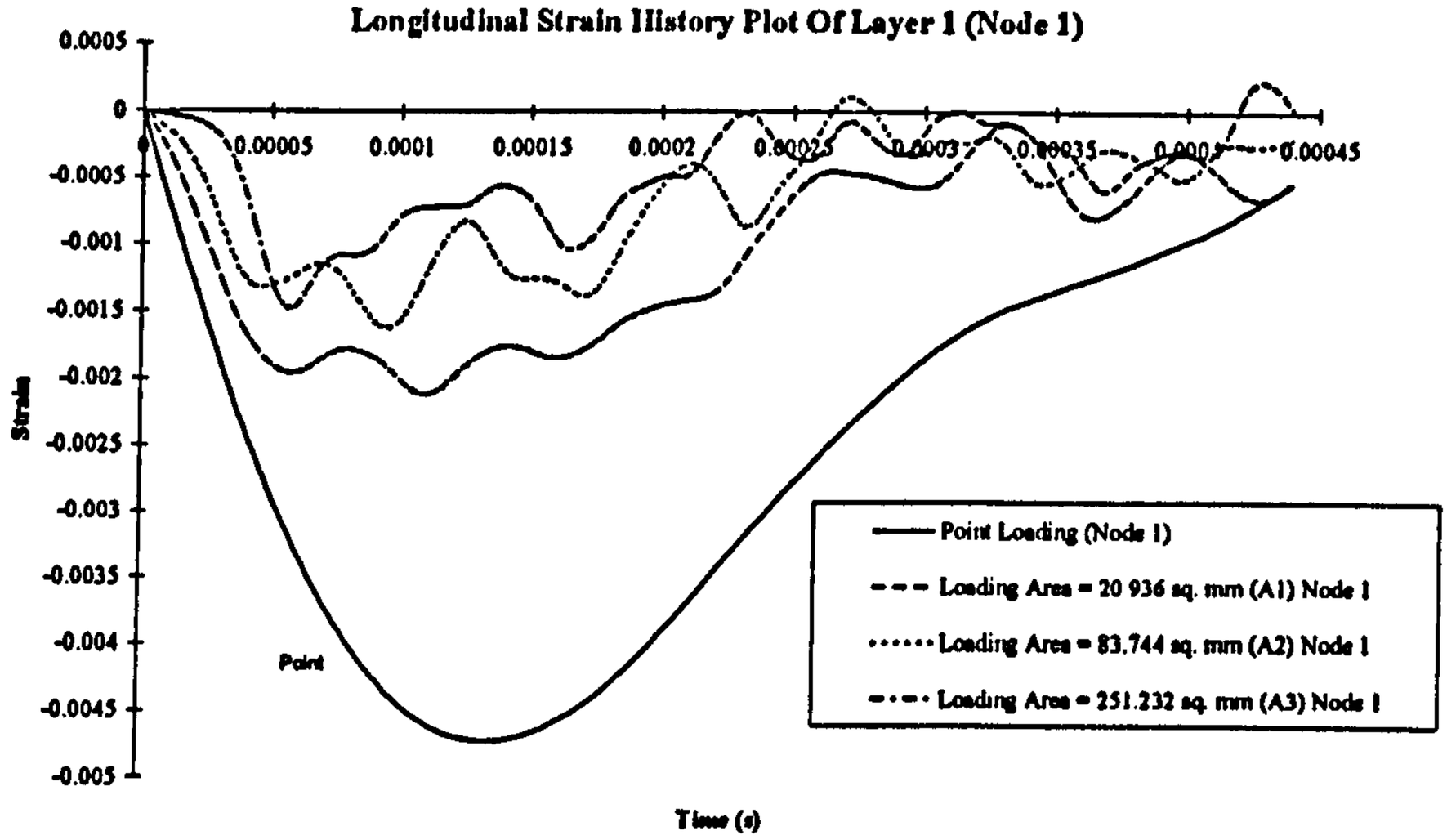

Fig 5.1.13 Longitudinal strain history plot (Node 1)

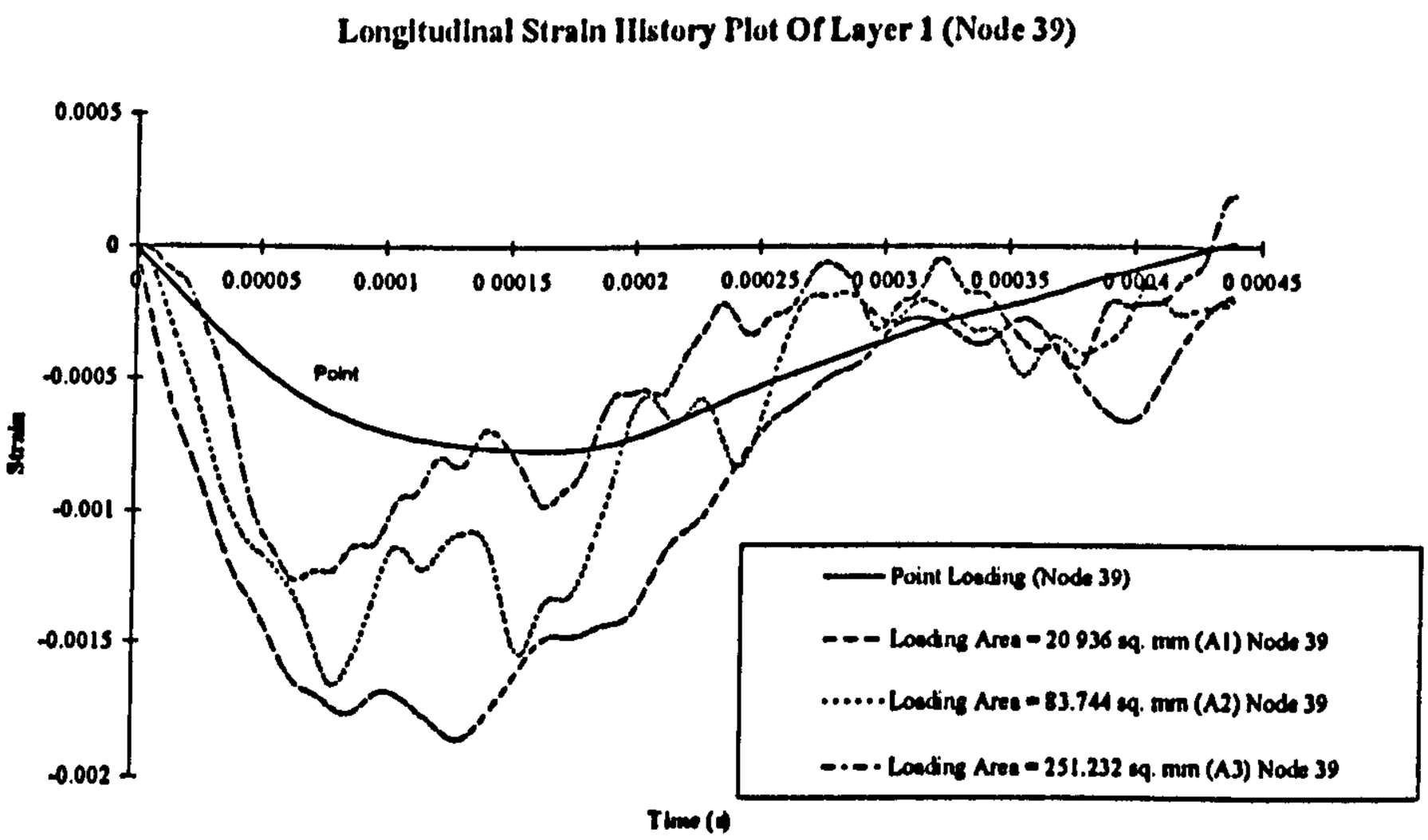

Fig 5.1.14 Longitudinal strain history plot (Node 39)
(2 mm from Node 1)

5.1.2 Modelling Impact Response

5.1.2.1 The Effect of Using a Sub-Model

The nature of an impact loading is such that the contact forces are applied to the target for a very short time on the scale of the fundamental period of the target structure. Very localised impact response is induced as a result. An impact loading that applied to the upper half of a pressure cylinder is not expected to produce any significant excitation in the lower half and both domes of the cylinder. A model with the upper half of the cylinder therefore seems sufficient for modelling impact response (Fig 5.1.15). However, this half cylinder model having two layers of shell elements (1564 thick shell elements in each shell element layer) cannot be handled by the computer capacity currently available. Since localised impact response was expected, a sub-model was chosen (Fig 5.1.19) consisting of a region cut from the central part of the half cylinder. This sub-model was used in the present investigation. For justifying the validity of such approach, it is important to know the effect of using a sub-model on the predicted impact response. To this end, a comparison of impact response prediction using these two models was undertaken. In this comparison a single layer of shell elements was used, and the initial velocity technique was used to simulate impact loading on the nodes of four loaded elements.

The FE mesh and the element sizes in the half cylinder are given in Figs 5.1.15 and 5.1.16. Finer mesh was used in the central region of the cylinder where the stresses are likely vary rapidly under impact loading. The size of the elements increases gradually away from the impact site. The dimensions of the finest elements at the central region are 2.3 mm by 2.269 mm. With this mesh design, good continuity of stresses between adjacent elements was achieved up to about four elements away from the loaded elements. The node and element numbering system of this FE mesh is shown in Fig 5.1.17. The NGV cylinder's dimensions, material properties and FE modelling data are given in Tables 5.1.A, 5.1.B and 5.1.C.

The boundary conditions used for this half cylinder model were such that the two curved edges were fully restrained in all degrees of freedom, since they represent the junction of

the cylindrical portion with the domes, which are very stiff due to the geometrical shape of the dome. The two straight edges were simply supported, allowing radial expansion. It should be noted that the curvature of the cylinder created a natural constraint to deformation under external loading, so that the boundary conditions at the edges do not have much influence on the impact response.

The sub-model, Fig 5.1.19 has 400 thick shell elements. The element dimensions for this sub-model are given in Fig 5.1.20. The node and numbering system is shown in Fig 5.1.21. This mesh design, gives a similarly good continuity of stresses between adjacent elements to about four elements away from the loaded elements. The boundary conditions for this sub-model is that all degrees of freedom of all edges have been restrained. This excessive constraint may increase the structural stiffness and predict lower transverse displacement than the half cylindrical model.

Transverse displacement history using both models at the centre (Node 1) are given in Fig 5.1.25. It can be seen that the displacement history from beginning to 33 μs for both models is the same, and shows linear time dependence. After this time, both models deviate from the linear displacement histories. Their predictions differ both in the magnitude and impact duration. However, their peak displacement occurred at the same time of 100 μs. This suggests that the impact response of both models is similar before recovery of the deflection begins. A 95 μm reduction (i.e. 17 %) in the transverse displacement was predicted by the sub-model at the peak. A shorter impact duration for the sub-model implicates that it possesses a higher structural stiffness. The deformed shapes for both models which are shown in Figs 5.1.18 and 5.1.23. In the local region of high deflection, the transverse displacement varies in the longitudinal direction in a similar manner for both models. Examination at the through-thickness stress distribution pattern, given in Figs 5.1.27 and 5.1.28 shows that the stress distribution patterns of both models were also similar.

In general, reduced sub-model seems to capture all the features of impact behaviour predicted by the cylinder model. The effect of using the sub-model is that a lower transverse displacement and deflection of the structure is predicted.

5.1.2.2 The Effect of In-Plane Sliding at the Interface between Composite and Aluminium Liner

The composite cylinder is formed by filament winding of resin-coated fibre on an aluminium liner. Discontinuity may exist between the liner and the reinforced fibre layer even though epoxy was applied to fill these voids during the winding process. The interface was further pressed together by the 'sizing' process, but it would be incorrect to consider these two layers as bonded firmly together into one piece without slipping or sliding. Relative in-plane movement and transverse opening of this interface may still be possible under external load. HINGES.AND.SLIDES data module was used to describe the contact condition between the surfaces of the two layers, so that in-plane sliding was allowed at this interface. Since the impact loading applied to the cylinder consists of the out-of-plane transverse displacement and traction acting in the direction normal to the plane of the shell element, it does not encourage in-plane sliding directly. However, in-place sliding may occur at this interface due to the effect of structural bending. Thus, sliding displacement is expected to be in magnitude and to be highly localised to the region of impact.

This section examines the effect of allowing in-plane sliding at the interface between the composite layer and the liner. Through-the-thickness stress distribution predicted by the two shell element layers model at the origin is shown in Fig 5.1.29. The bending stress in the liner shows a typical compressive-tensile gradient which implies that the liner is not firmly secured to the composite layer. Fig 5.1.28, for model with single shell element layer, shows the bending stress in the liner having a tensile-tensile pattern as a result of perfect bonding between the two layers at the interface. Fig 5.1.26 shows that a higher transverse displacement is predicted by the two shell element layer model in comparison with a single shell element layer model. A longer impact duration suggests that the two shell element layer model possesses a lower structural stiffness. The transverse displacement along the longitudinal direction of this two shell element layers model behaves in a similar manner to the single element layer (see Fig 5.1.31).

In general, allowing in-plane sliding at the interface between the liner and the composite layer affects the bending stress pattern in the liner and also causes re-distribution of bending stress in the composite layer. The structure appears slightly less stiff than one with perfect bonding at the interface.

Table 5.1.A Dimensions of NGV cylinder and lay-up

For the cylindrical part of the cylinder

Mean radius : 130 mm

Length : 760 mm

Total Thickness : 22 mm

Lay-up : [90/+-15/90/+-15/90/+-15] + liner

Lay-up (Winding Angle)	**Thickness**
90° (The Outer layer)	2 mm
+- 15°	1 mm
90°	4 mm
+- 15°	3 mm
90°	4.5 mm
+- 15°	4.5 mm
Liner	3 mm
Total Thickness →	22 mm

Table 5.1.B Material properties and strengths

(1) **S-glass epoxy Composite**

Material properties

In-plane longitudinal modules E_{11}*	35 GPa			
In-plane transverse modulus	E_{22}**	10 GPa		
Out-of-plane transverse modulus	E_{33}**	10 GPa		
In-plane shear modulus	G_{12}	3 GPa		
Out-of-plane shear modulus	G_{23}	3.55 GPa		
	G_{13}	3 GPa		
In-plane Poisson's ratio	ν_{12}	0.28;	ν_{21}	0.083
Out-of-plane Poisson's ratio	ν_{23}	0.41;	ν_{13}	0.28
Density	ρ	2000 kg / m^3		

Strength

Longitudinal Strength S_{11}	782 MPa (-500 MPa)
Transverse Strength S_{22}	68 MPa (-204 MPa)
Transverse Shear Strength S_{12}, S_{13}, S_{23}	95 MPa

NB : (1) * *in fibre direction;* ** *perpendicular to fibre direction*

(2) *Material properties were obtained from mechanical tests undertaken by British Gas plc Engineering Research Station on a small patch of specimen cut from the NGV composite cylinder. The fibre volume fraction was 60 %.*

(2) **Aluminium Liner**

Material property (6061-T6 Al alloy)

Young's modulus	E	70 GPa
Shear modulus	G	26.3 GPa
Poisson's ratio	ν	0.3
Density	ρ	2800 kg / m^3

Strength

Ultimate Strength	σ_u	348 MPa
Shear Strength	τ_u	220 MPa

NB : Material properties of 6061-T6 Al alloy was obtained from mechanical tests undertaken in BG's ERS.

Table 5.1.C Material properties data for PAFEC data file

(1) Material compliances in the principal direction of the material

$$S11 = \frac{1}{E_{11}} = 2.857E-11$$

$$S22 = \frac{1}{E_{22}} = 1.0E-10$$

$$S33 = \frac{1}{E_{33}} = 1.0E-10$$

(2) Material cross compliances

$$S12 = \frac{-\nu_{21}}{E_{22}} = \frac{-\nu_{12}}{E_{11}} = \frac{-0.28}{35G} = -8.0E-12$$

$$S23 = \frac{-\nu_{32}}{E_{33}} = \frac{-\nu_{23}}{E_{22}} = \frac{-0.41}{10G} = -4.1E-11$$

$$S31 = \frac{-\nu_{31}}{E_{33}} = \frac{-\nu_{13}}{E_{11}} = \frac{-0.28}{35G} = -8.0E-12$$

(3) Material shear compliances

$$SH12 = \frac{1}{G_{12}} = \frac{1}{3G} = 3.33E-10$$

$$SH23 = \frac{1}{G_{23}} = \frac{2(1+\upsilon 23)}{E_{33}} = 2.82E-10$$

$$SH31 = \frac{1}{G_{31}} = \frac{1}{3G} = 3.33E-10$$

(4) Material density

Ro = ρ = 2.0E+3

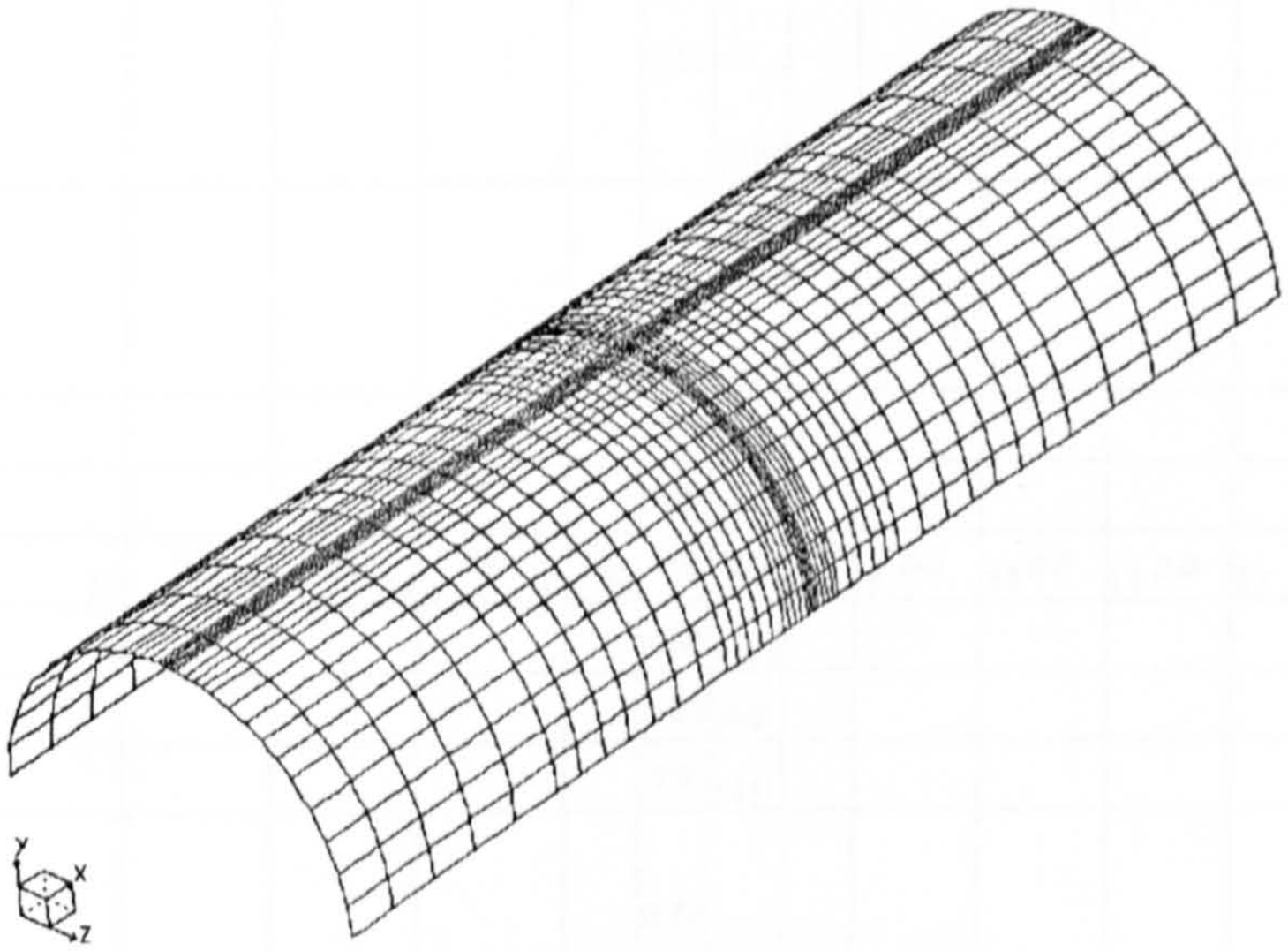

Fig 5.1.15 Half cylinder model

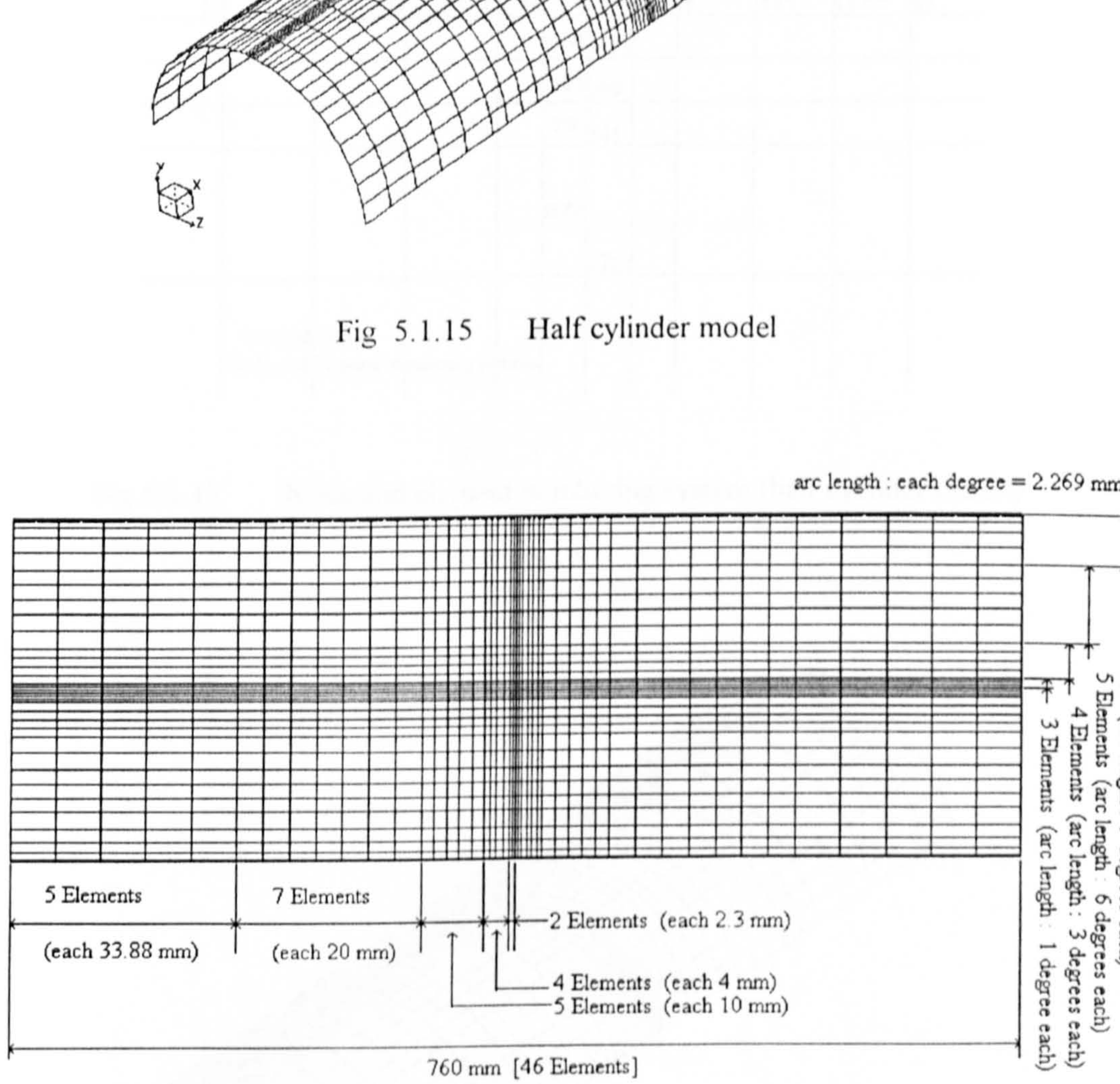

Total thick shell element = 46 x 34 = 1564

Fig 5.1.16 FE mesh design of half cylinder model (plan view)

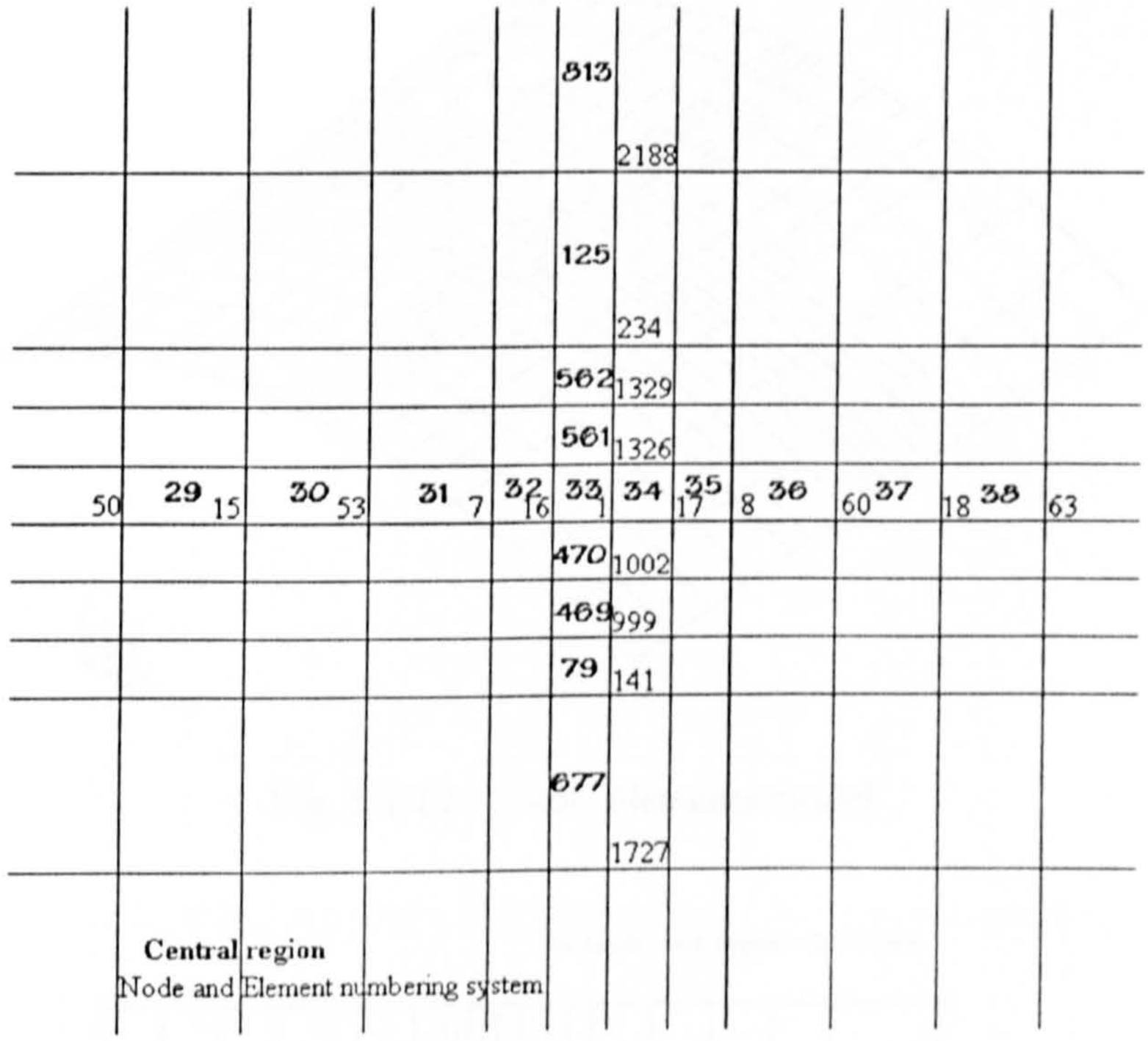

Fig 5.1.17 Node and element numbering system (half cylinder model)

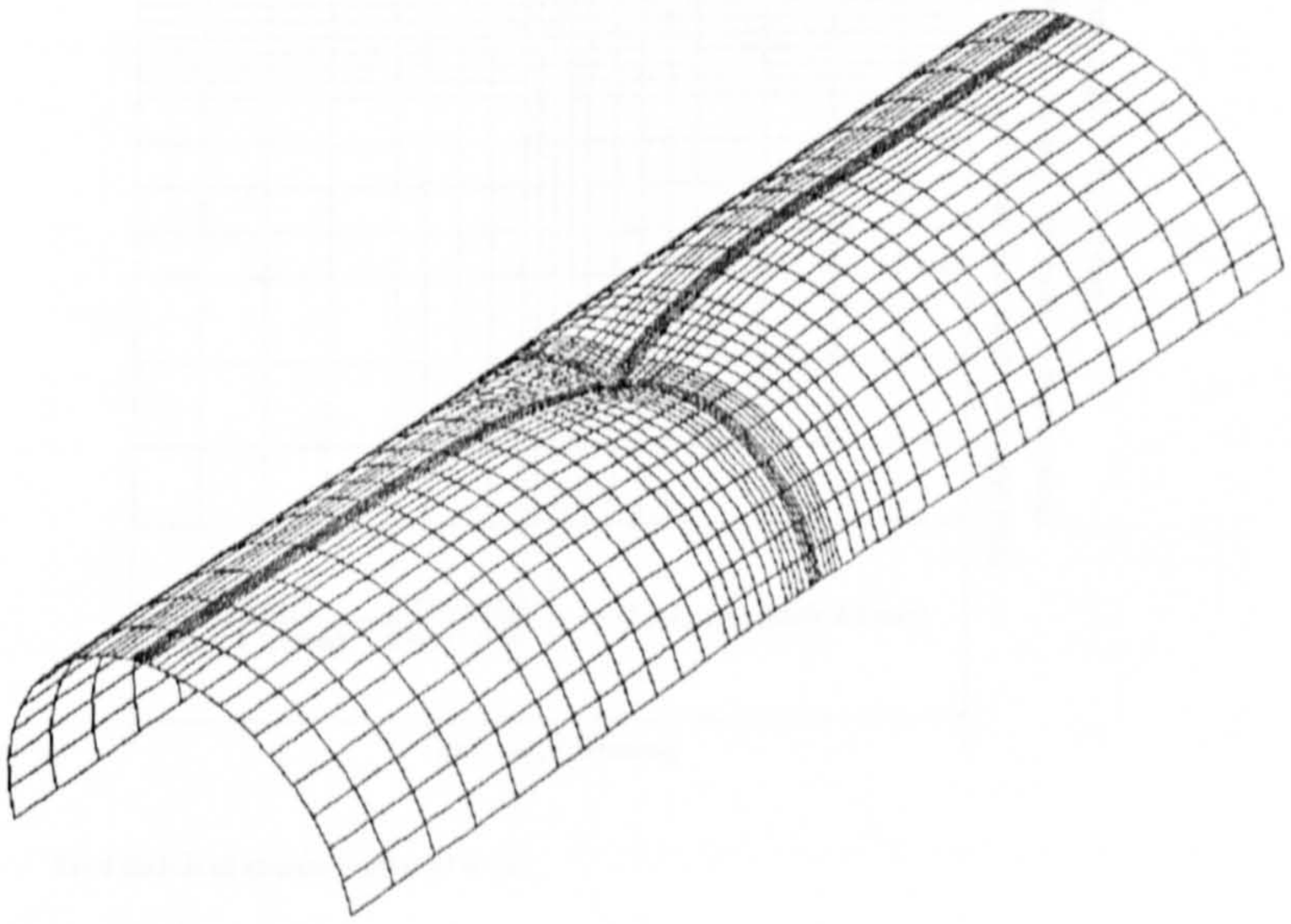

Fig 5.1.18 Deformed shape of half cylinder model (at 100 μs)

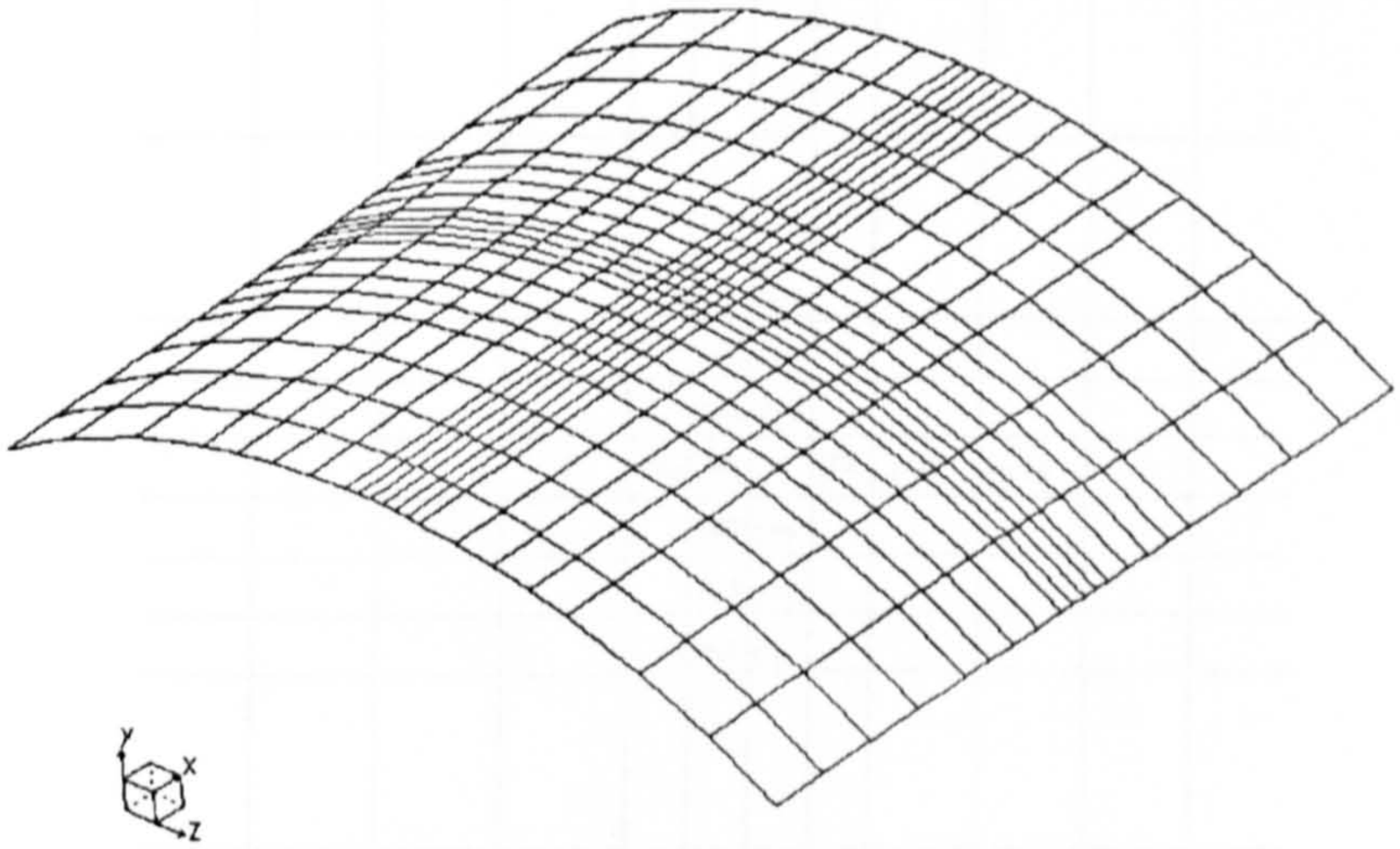

Fig 5.1.19 400 Elements model

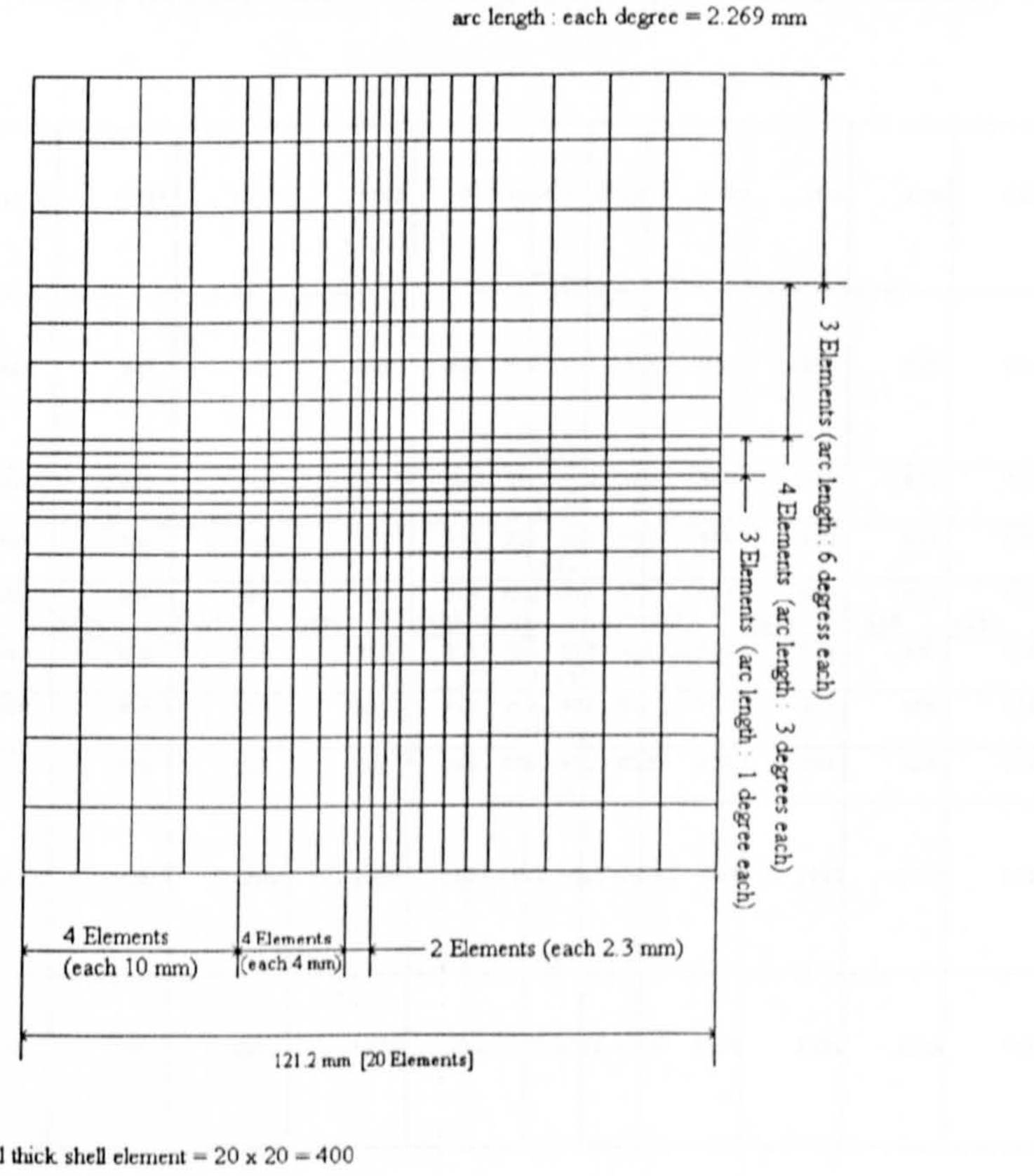

Fig 5.1.20 FE mesh design of 400 elements model (plan view)

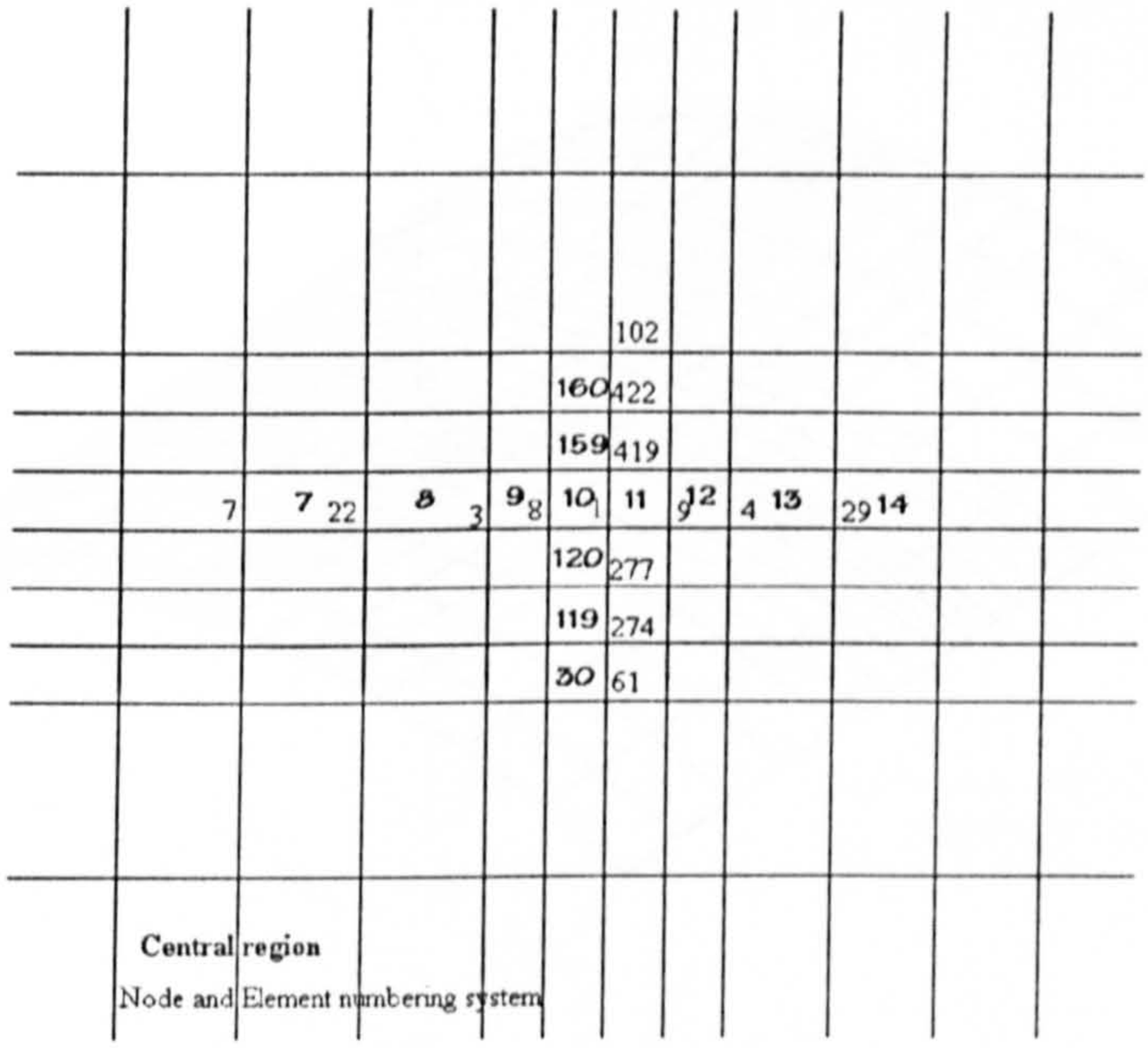

Fig 5.1.21 Node and element numbering system (400 elements model) top layer

1050	1053	1056	1059	1062	1065	1068	1071	1074	1077	1080	1083	1086	
						2820							
844	845	846	847	848	849	850	851	852	853	854	855	856	
						2819							
948	950	952	954	956	958	960	962	964	966	968	970	972	
						3202							
947	949	951	953	955	957	959	961	963	965	967	969	971	
						2614							
804	805	806	807	808	809	810	811	812	813	814	815	816	
	2583	2588	2593	2598	2603	2608	2613	2618	2623	2628	2633	2638	
908	910	912	914	916	918	920	922	924	926	928	930	932	
						3119							
907	909	911	913	915	917	919	921	923	925	927	929	931	
						2717							
824	825	826	827	828	829	830	831	832	833	834	835	836	
						2716							
992	995	998	1001	1004	1007	1010	1013	1016	1019	1022	1025	1028	
						3317							
991	994	997	1000	1003	1006	1009	1012	1015	1018	1021	1024	1027	

Fig 5.1.22 Node and element numbering system (400 elements model) bottom layer

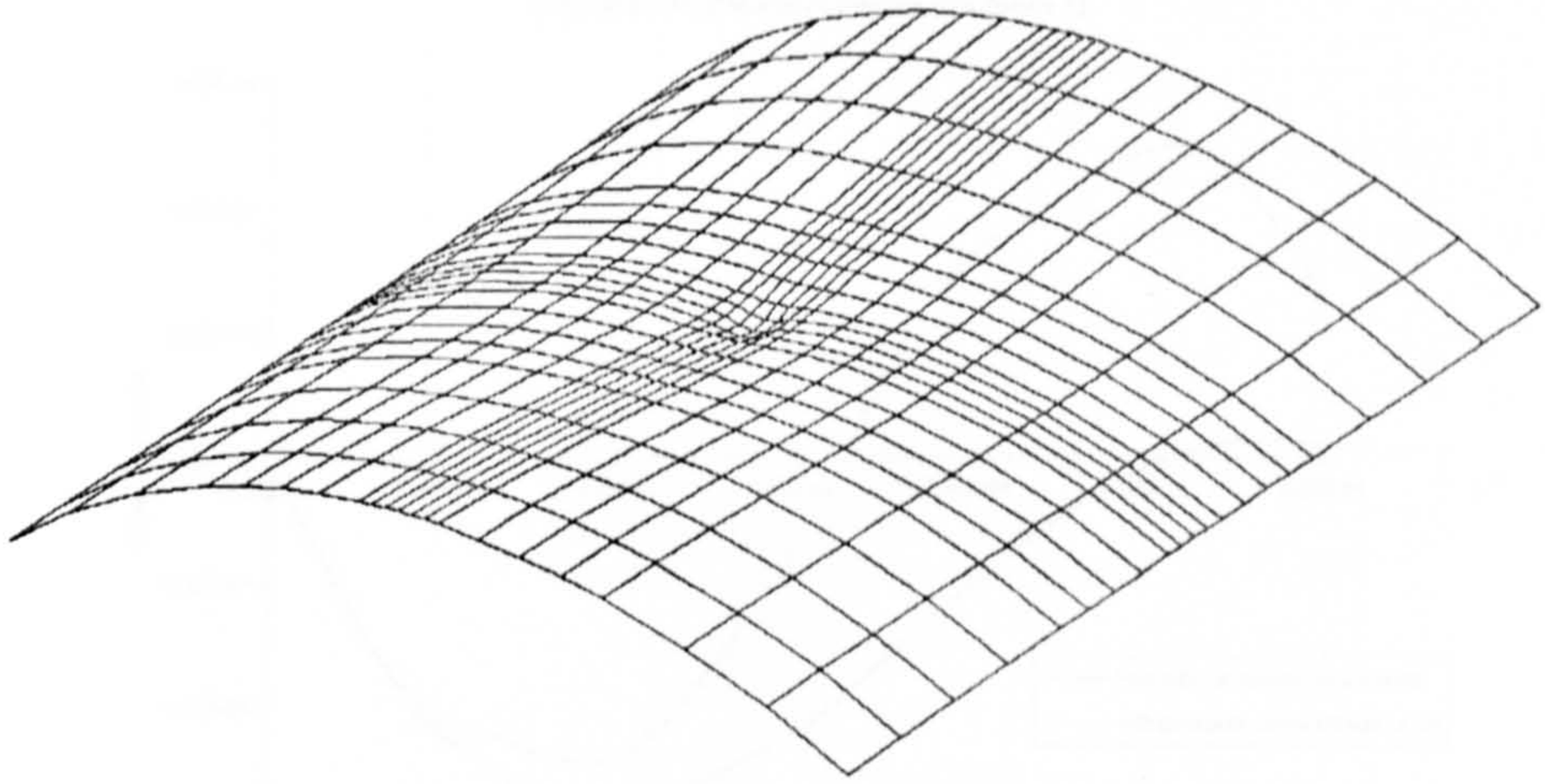

Fig 5.1.23 Deformed shape of 400 elements model (with a single layer)

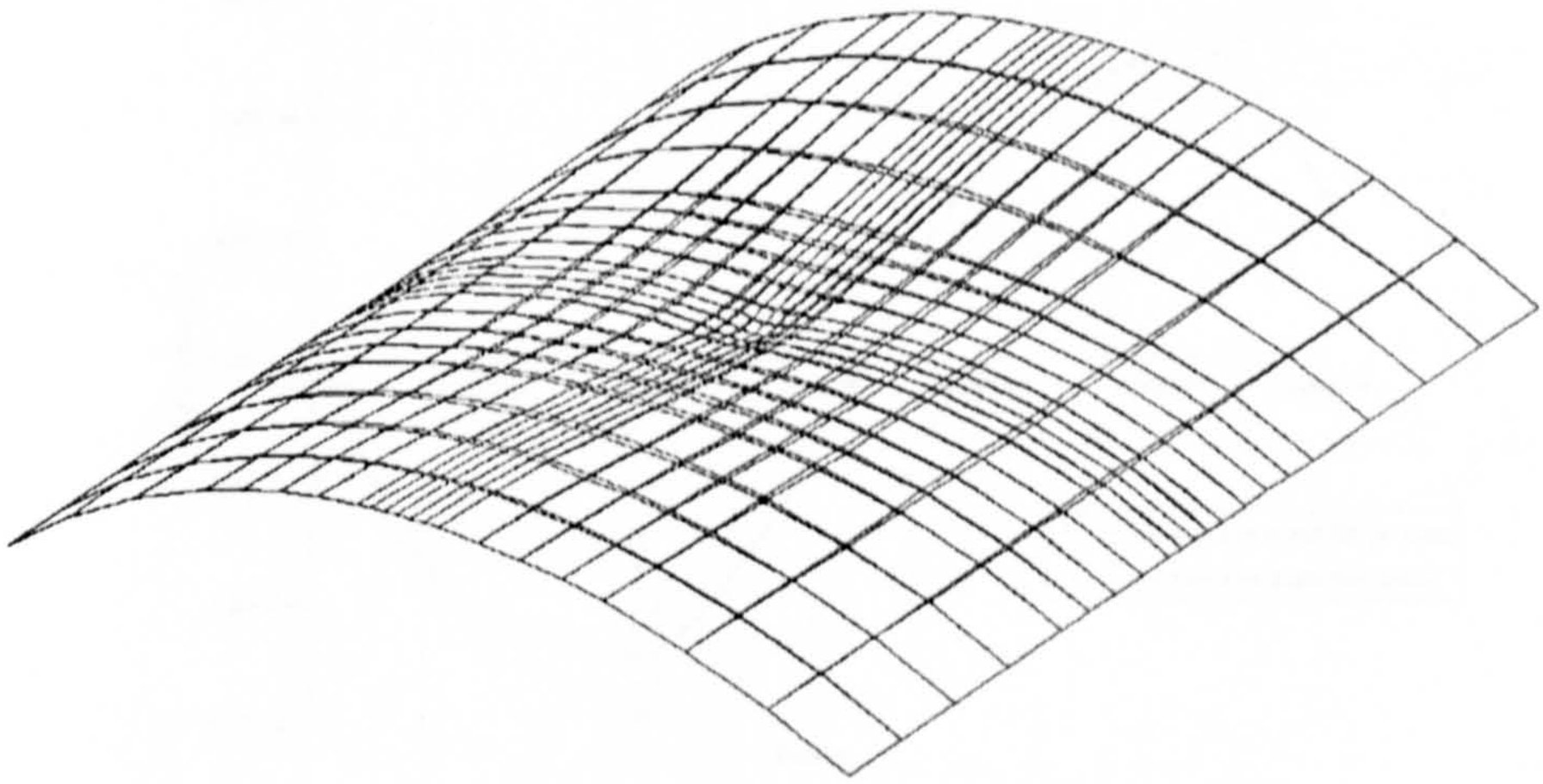

Fig 5.1.24 Deformed shape of 400 elements model (with two layers)

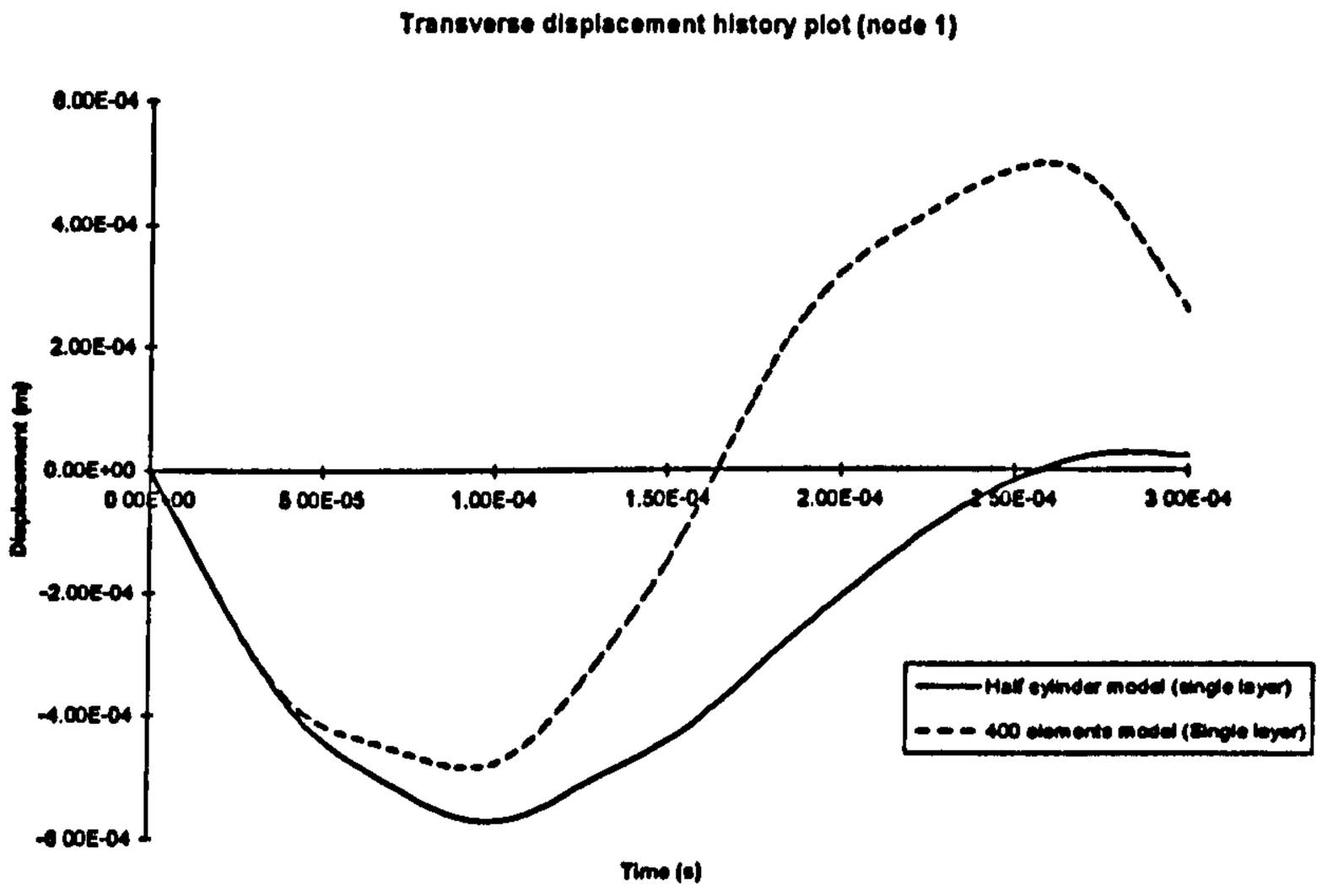

Fig 5.1.25 Displacement history of half cylinder and 400 elements models

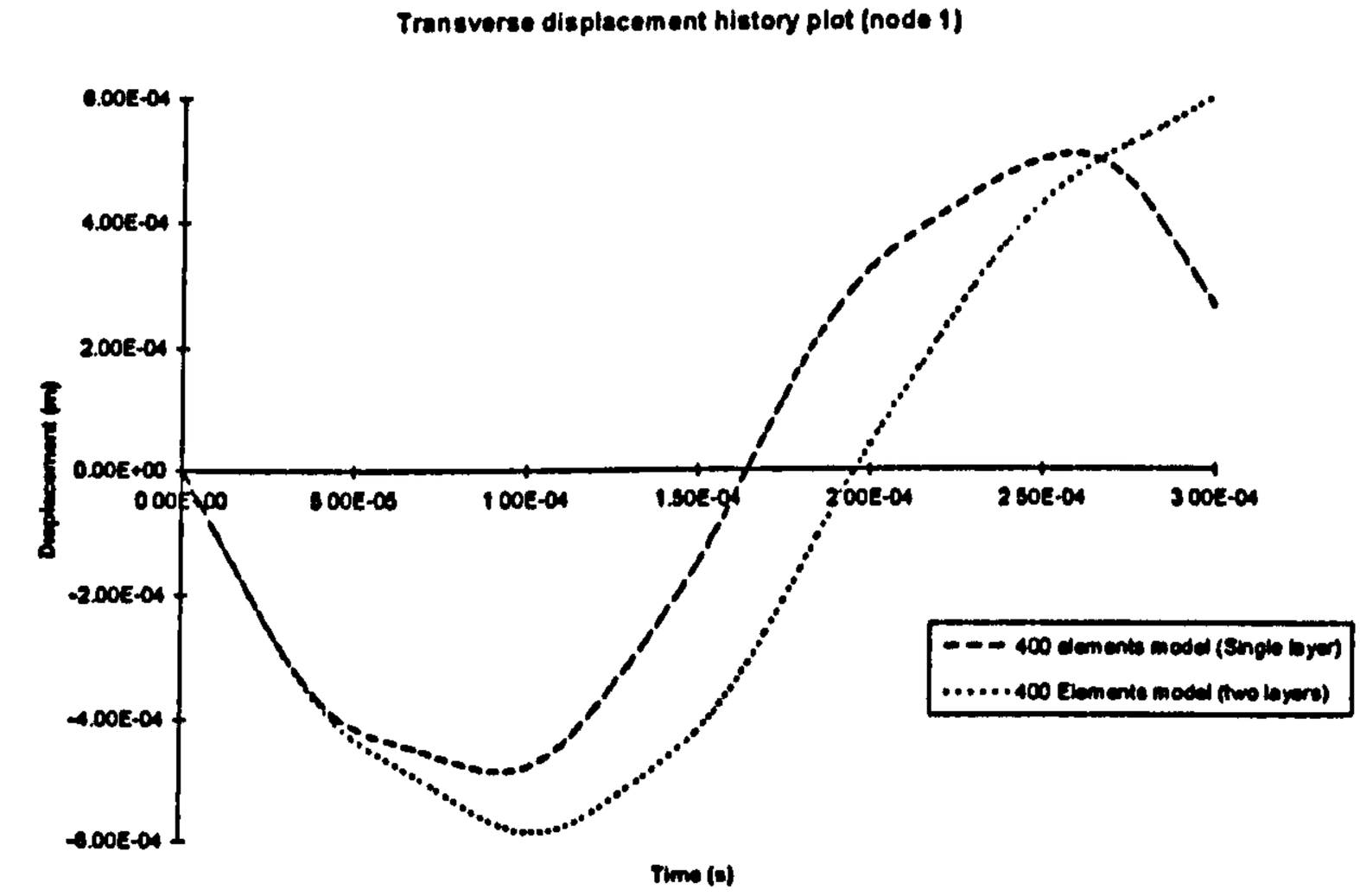

Fig 5.1.26 Displacement history of 400 elements models (with single and two layers)

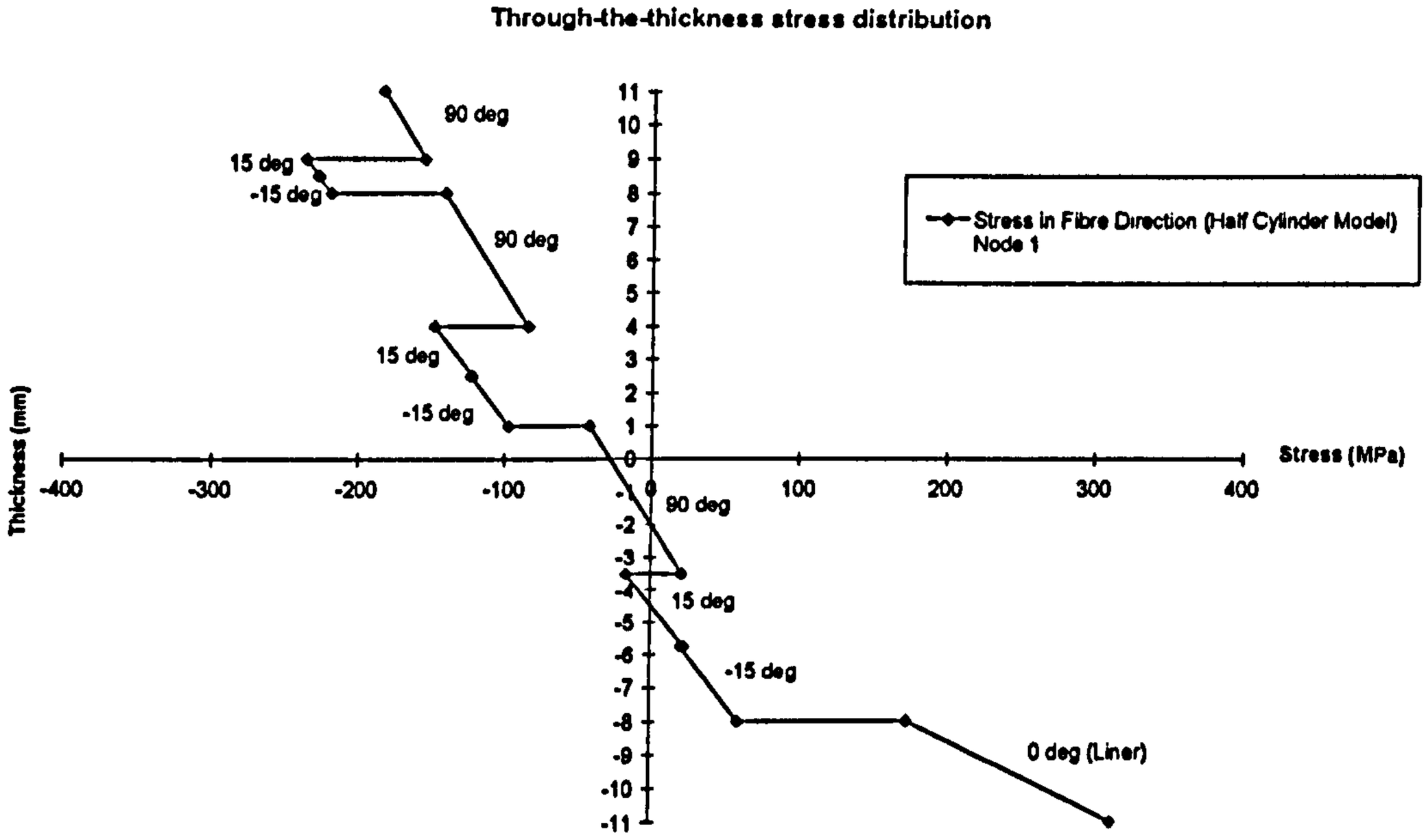

Fig 5.1.27 Through-the-thickness stress distribution (half cylinder model)

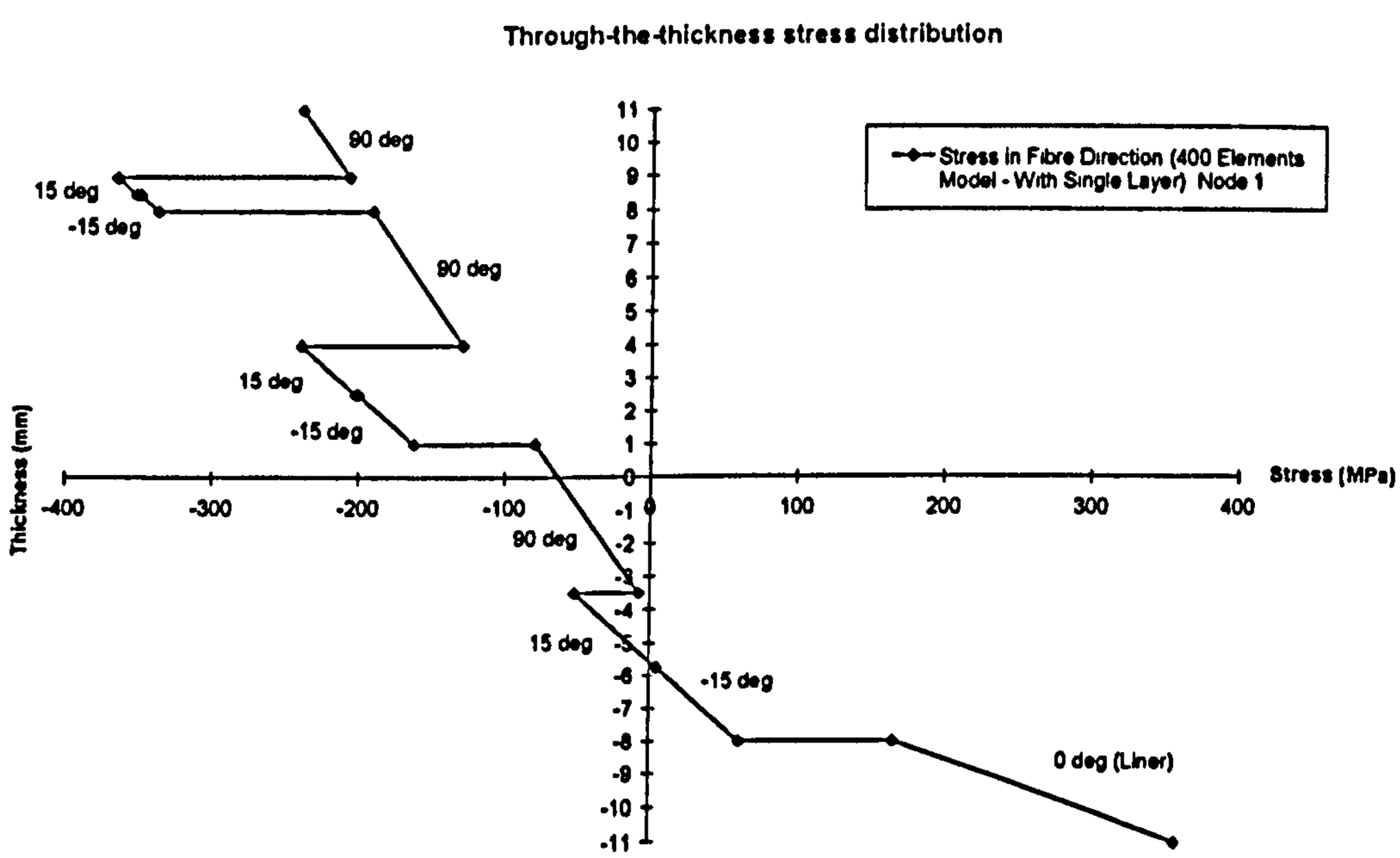

Fig 5.1.28 Through-the-thickness stress distribution
(400 elements model - with single layer)

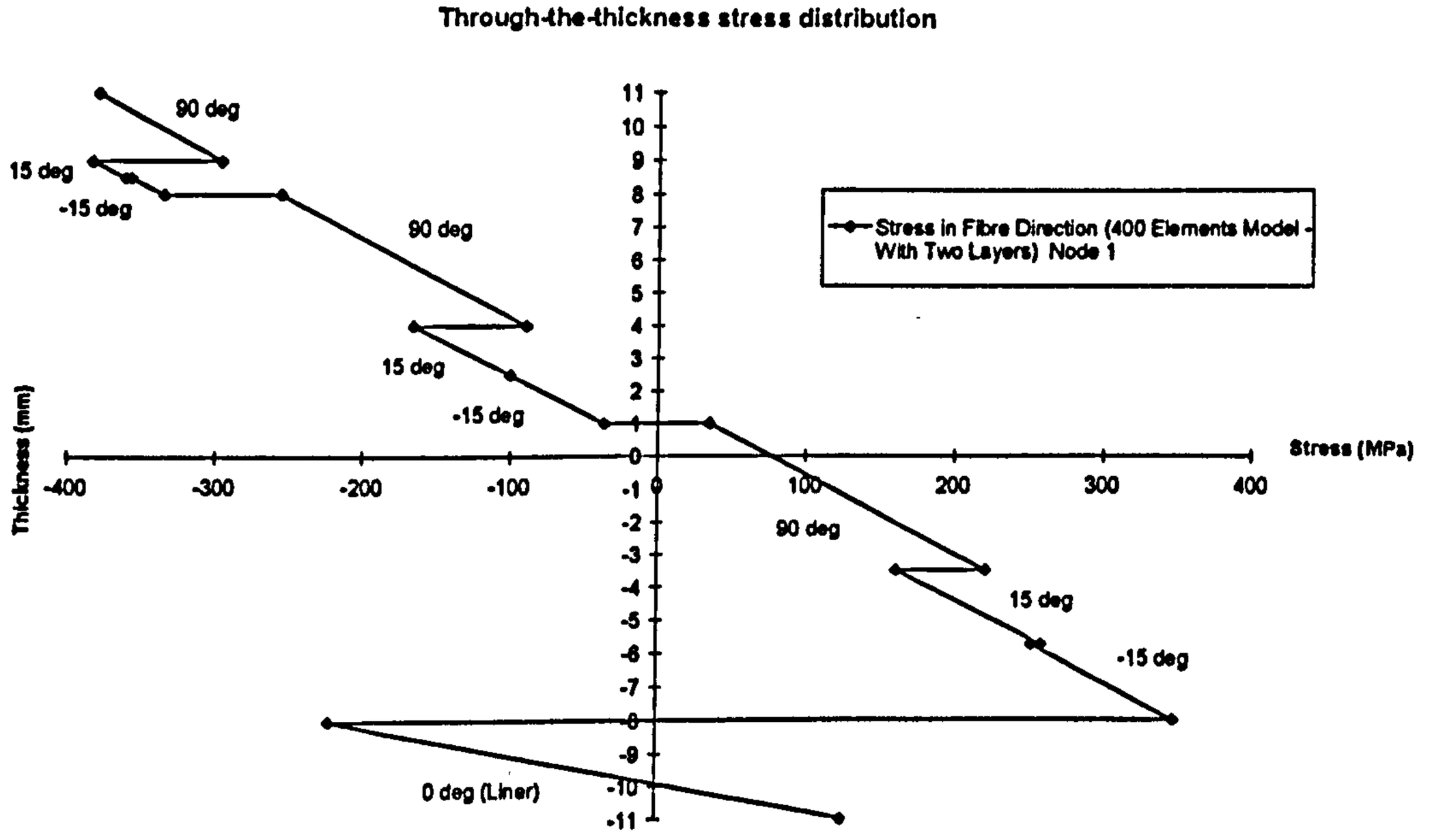

Fig 5.1.29 Through-the-thickness stress distribution
(400 elements model - with two layers)

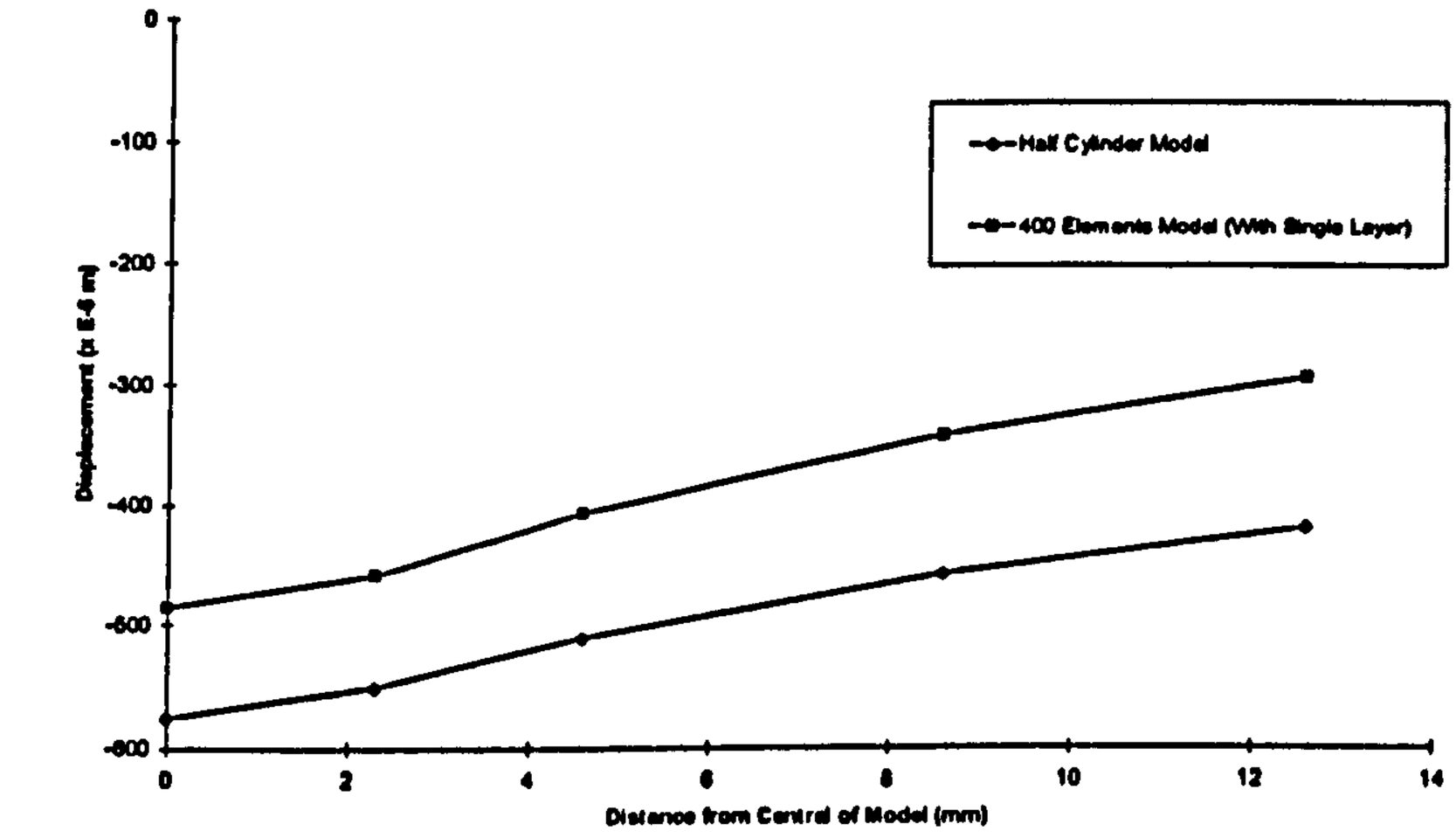

Fig 5.1.30 Transverse displacement along longitudinal direction

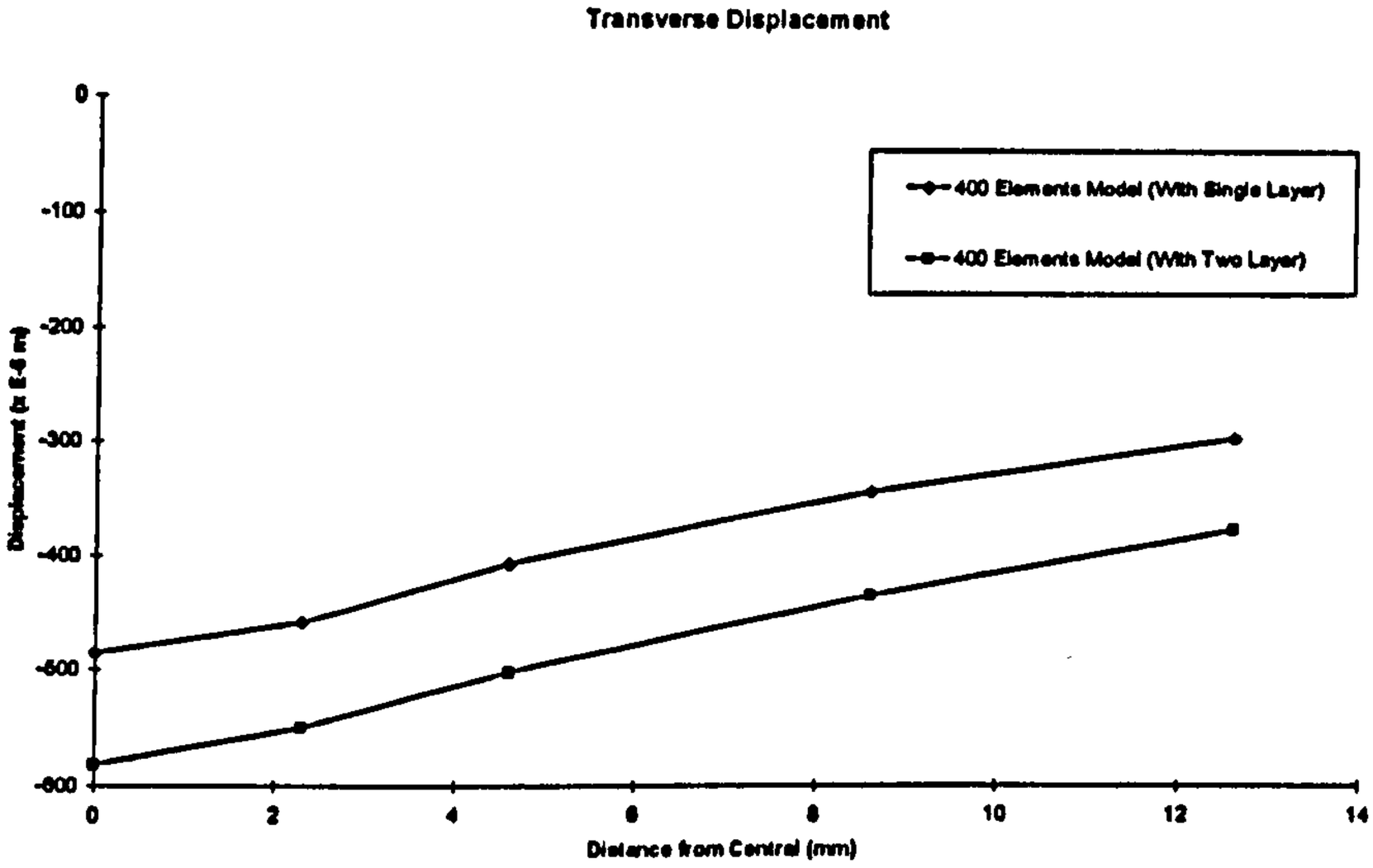

Fig 5.1.31 Transverse displacement along longitudinal direction

5.1.3 Parametric Study of Impact Response

A parametric study was undertaken in order to study the effect of impact parameters on impact response. Those parameters which were of most relevance to the present investigation were considered. These were the impact velocity, impactor mass, impact energy, and the initial pre-stress condition due to internal pressure. The impact forces were calculated from the deceleration of the loaded node combined with the impactor mass. A point load and a lumped mass at the loaded node were used for predicting the deceleration. It was established that this approach provided a more stable deceleration history. It is expected that the true dynamic response may be slightly different as could be that predicted by considering impact on a small area (four element) with impactor mass spread equally among the nodes. For the purposes of comparison, however, the impact force response should be representative enough, although it may predict a higher impact force and longer impact duration. The impact parameters for parametric study are listed in Table 5.1.2. The impact forces and peak transverse displacements for each tests are listed in Table 5.1.3. In this analysis, terms and quantities were used with specific sign convention shown in Fig 5.1.32.

5.1.3.1 The Effect of Impact Velocity

In order to study the effect of impact velocity on impact response, two impact tests (Test 1 and Test 2) by the same impactor mass, 0.36 kg, with different impact velocities, 10 m/s and 20 m/s, were considered.

Fig 5.1.33, shows the impact force histories obtained in each test. The maximum impact forces in these two tests were 46.54 kN for Test 1 and 93.08 kN for Test 2. They occurred at time of at 150 μs. The impact duration for both tests was the same, 215 μs.

As shown in Fig 5.1.34, the peak transverse displacements in these two tests were -461.79 μm for Test 1 and -923.59 μm for Test 2, and occurred at 85μs. It is interesting to note that the impact duration for both tests was the same, 200 μs, and their responses

were related to each other in a linear manner. The impact duration for transverse displacement was 15 μs shorter than for impact force.

The transverse displacement in the longitudinal direction is shown in Fig 5.1.35. Once again, the linear proportion between the two sets of impact responses is seen.

5.1.3.2 The Effect of Impactor Mass

In order to study the effect of the impactor mass on impact response, two impact tests (Test 3 and Test 4) by two different impactor masses, 0.36 kg and 1.0 kg, with the same impact velocity, 10 m/s, were considered.

Fig 5.1.36, shows the two impact force histories induced in each test. However, the maximum impact force occurred earlier (at first peak) in the test with the heavier impactor, and was nearly twice the impact force induced by a lighter impactor (maximum impact force of 89.41 kN for Test 4, and 46.54 kN for Test 3).

As shown in Fig 5.1.37, the peak transverse displacement for the impactor mass of 0.36 kg was 461.79 μm and occurred at 85 μs, and for impactor mass of 1 kg was 854.96 μm at 141 μs. The impact duration of tests was different. Impact with the heavier impactor mass produced a longer impact duration of 320 μs, while for the lighter impactor mass it was 200 μs. The displacement history plots for both tests show similar characteristics of the impact response behaviour, but are different in terms of the scale and timing. For the first 20 μs of their response, the displacements response of these two tests were indistinguishable.

The transverse displacement in these two tests at the time when their peak displacement occurred is shown in Fig 5.1.38.

5.1.3.3 The Effect of Impact Energy

In order to study the effect of impact energy on impact response, two impact tests (Test 5 and Test 6) with two different combinations of impactor mass and impact velocity were carried out. The impact energy was maintained the same.

The impact force history plots for these two tests are shown in Fig 5.1.39. A 14 kN difference is observed between their maximum impact force value, with the impact by a heavier impact inducing a larger maximum impact force which occurred later.

As shown in Fig 5.1.40, the impactor with a heavier impactor also produced a transverse displacement which was 102 μm higher at the maximum. The comparison with the impact with a lighter impactor, the impact duration is longer, and the maximum force and transverse displacement occur later in a test with a heavier impactor.

The variation of the transverse displacement in the longitudinal direction in these two tests is shown in Fig 5.1.41. The impact with a heavier impactor produced larger transverse displacements around the impact site. However, comparatively smaller transverse displacements were produced in the remote regions.

5.1.3.4 The Effect of Initial Pre-Stress Condition

In order to study the effect of the initial pre-stress due to internal pressure on impact response, two impact tests (Test 7 and Test 8) with the same combination of impactor mass and impact velocity were modelled, i.e. M_i = 0.36 kg & V_o = -20 m/s. One test considered impact on an empty cylinder, and the other impact on a pre-pressurised cylinder (200 bar).

Fig 5.1.42 shows an impact force history plot induced by impact on a pre-pressurised cylinder. The impact started at 3000μs (at the steady state of dynamically pressurising). The maximum impact force was 90.5 kN. In order to compare the impact force response in both tests, unit time was adjusted match these two response plots together. For

instance, for impact on a pre-pressurised cylinder, time 3000μs was used as time-step number zero, while for impact on an empty cylinder, time 0 μs was also used as time-step number zero (each unit time = 4 μs). These approximately scaled impact force history plots are given in Fig 5.1.43. It can be seen that they behave in a quite similar manner, with the exception of a 2.58 kN difference and a 6 μs delay between their maximum values.

The transverse displacement history plots for both tests are shown in Fig 5.1.44. For the impact on a pressurised cylinder, the transverse displacement due to impact started at +470.7 μm reflecting the initial displacement due to the internal pressure. As seen in Fig 5.1.45, these two response plots can be scaled to match by choosing a suitable unit of time (each unit time = 4 μs). It can be seen that the two plots display similar response behaviour. In order to examine closer the differences in magnitude, transverse displacement plot for impact on the pre-pressurised cylinder was shifted to zero, as shown in Fig 5.1.46. It can be seen that the increment of transverse displacement in the pre-pressurised cylinder was higher by 104 μm at the maximum.

The variation of the transverse displacement in the longitudinal direction in both tests are given in Fig 5.1.47. This plot serves two purposes, i.e. to show the distribution of transverse displacements as well as the deformed shape. It can be seen that the net transverse displacements due to impact on a pre-pressurised cylinder were somewhat higher.

5.1.3.5 Discussion

The study of the effect of impact velocity on impact response shows that the magnitude of impact velocity affects the response values for both the impact force and the transverse displacement. However, it does not appear to affect the characteristics of response behaviour in general. The same impact duration produced by the two impacts indicates that they excited a similar spectrum of response frequencies. It is worth of noting that the maximum displacement due to Test 2 (-923.59 μm) was only 4.2 % of the total wall thickness of the cylinder. Therefore, linear dynamic analysis used here is

sufficiently justified as an approach to predicting impact response [Lakshminarayana et al, 1994(a)]. Figs 5.1.33 to 5.1.35, show a linear proportion between the responses, with the maximum and transient values due to the higher impact velocity being twice those due to the lower impact velocity. In general, impact velocity tends to affect the magnitude of impact response rather than the time characteristics of impact behaviour. This dominant impact velocity effect is consistent with the findings of other researchers performing low velocity impact on composites [Robinson and Davies, 1992; Prasad et al, 1994]. Thus, impact response due to a different impact velocity with a same impactor mass can be predicted in direct proportion to the impact velocity, or the square root of the impact energy.

In the study of the effect of impactor mass on the impact response, it can be seen that the impact response behaviour from the two tests was not similar in general. The impact response by a heavier impactor seems to be mass-dominated, i.e. marked by a longer impact duration and by the higher maximum values of impact response quantities occurring at a later time [Prasad et al, 1994]. The impact response values due to a heavier impactor were nearly twice (1.8 times) greater than those due to a lighter impactor. This ratio of impact responses measured by the maximum values was similar to that in Test 1 and Test 2 (comparing the velocities). A heavier impactor also produces a more localised impact response compared to a lighter impactor which produces a more widespread effect.

In the study of impact at constant energy shown in Figs 5.1.39 and 5.1.40, it can be seen that a higher impact force and transverse displacement were induced by impact with a heavier impactor. Fig 5.1.41 shows that this higher transverse displacement was confined a smaller region around the impact site. This demonstrates that the impactor mass plays an important role in controlling the distribution of impact energy. This also further indicated the inadequacy of using the impact energy alone as a parameter to characterise impact response without specifying the impactor mass [Choi et al, 1992].

In general, the three impact parameters, i.e. impact velocity, impactor mass and impact energy, cannot be considered separately in studying their influence on impact response

behaviour. Impact velocity mainly affects the magnitude of the impact response. The impactor mass influences the impact response both in terms of impact duration and the distribution of impact energy. The impact energy, a combined term although inadequate to characterise the impact response fully, seems sufficient to predict the localised impact response quite well [Robinson and Davies, 1992].

In the study of the effect of internal pressure on the impact response illustrated in Figs 5.1.42 to 5.1.46, it can be seen that the impact force histories in both tests were quite similar. The maximum impact force induced by impact on a pre-pressurised cylinder was merely 2.58 kN less and occurred at 6 μs later. Moreover, it has to be noted that the excitation forces used for generating initial velocity for an empty and pre-pressurised cylinders were not the same, i.e. 4600 N/node for an empty cylinder and 3600 N/node for a pre-pressurised cylinder. A lower excitation force required for a pre-pressurised cylinder, and a slightly lower impact force and longer impact duration induced seem to implicate that the structural stiffness of this pre-pressurised cylinder may have been reduced. In view of this result, the cylinder became more flexible at pressurised condition. Fig 5.1.45 shows that a higher transverse displacement (103.26 μm higher at their peak) for an impact on a pre-pressurised cylinder has been seen. This finding is interesting because some researchers [Sankar and Sun, 1985; Chen and Sun, 1985; Bert and Birman, 1988] have done impact analysis on pre-stressed composite structures found that the pre-stressed structures became stiffer and resulted in less transverse displacement due to the same impact loading for un-prestressed structures. However, the analyses in these research works either in-plane sketching due to a pre-stress for composite plates, or no prescribed displacements for pre-stressed shell structures were considered. On the contrary, as a cylindrical structure is considering here, and prescribed displacements have been included in the analysis, the cylinder behaved differently. This reduced structural stiffness effect due to internal pressure demonstrates the influence of change of geometric shape of an impacting structure on impact behaviour. However, even more interesting is the similar magnitude of their transverse displacements at the beginning and ending of impact duration (see Fig 5.1.45). However, these unusual predicted results based on the sub-model should be further confirmed by experimental investigation.

Table 5.1.2 Impact tests

Impact tests	Test number	Impact loading	Impact energy
Constant impactor mass	Test 1	M_i = 0.36 kg V_o = 10 m/s	K.E. = 18 J
	Test 2	M_i = 0.36 kg V_o = 20 m/s	K.E. = 72 J
Constant impact velocity	Test 3	M_i = 0.36 kg V_o = 10 m/s	K.E. = 18 J
	Test 4	M_i = 1.0 kg V_o = 10 m/s	K.E. = 50 J
Constant impact energy	Test 5	M_i = 0.36 kg V_o = 20 m/s	K.E. = 72 J
	Test 6	M_i = 1.0 kg V_o = 12 m/s	K.E. = 72 J
The effect of internal pressure	Test 7	M_i = 0.36 kg V_o = 20 m/s (on empty cylinder)	K.E. = 72 J
	Test 8	M_i = 0.36 kg V_o = 20 m/s (on pre-pressurised cylinder)	K.E. = 72 J

Table 5.1.3 Impact force and peak transverse displacement

Impact on an empty cylinder

Impactor mass M_i (kg)	Impact velocity V_o (m/s)	Impact force (Node 1)	Peak transverse displacement & its timing (Node 1)
0.36	10	46.54 kN	-461.79μm @ 85μs
	20	93.08 kN	-923.59μm @ 85μs
1.0	10	89.41 kN	-854.96μm @ 141μs
	12	107 kN	-1026μm @ 141μs
	20	179 kN	-1710μm @ 141μs

Impact on a pre-pressurised cylinder

Impactor mass M_i (kg)	Impact velocity V_o (m/s)	Impact force (Node 1)	Peak transverse displacement & its timing (Node 1)
0.36	20	90.5 kN	-1027.3μm @ 3085μs (impact started at 3000μs)

N.B. : The "-ve" means direction towards the centre of a cylinder.

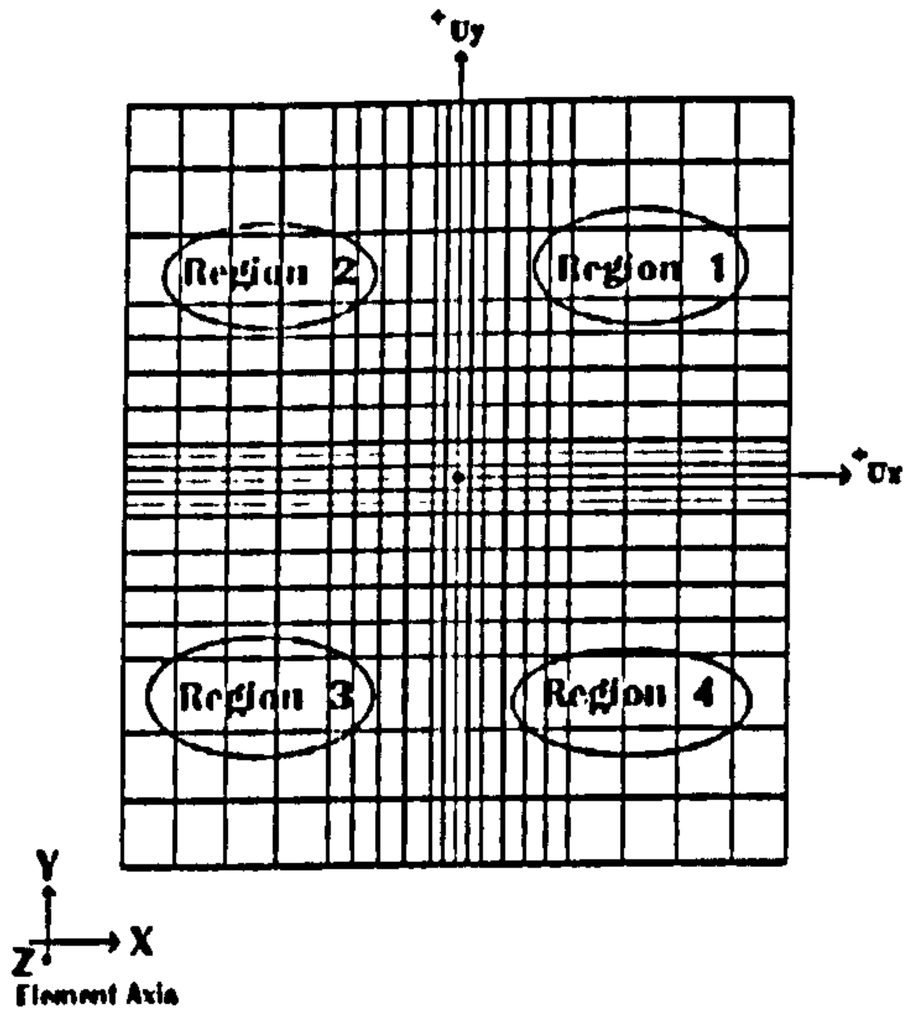

Fig 5.1.32 Schematic diagram for illustrating sign convention and regions

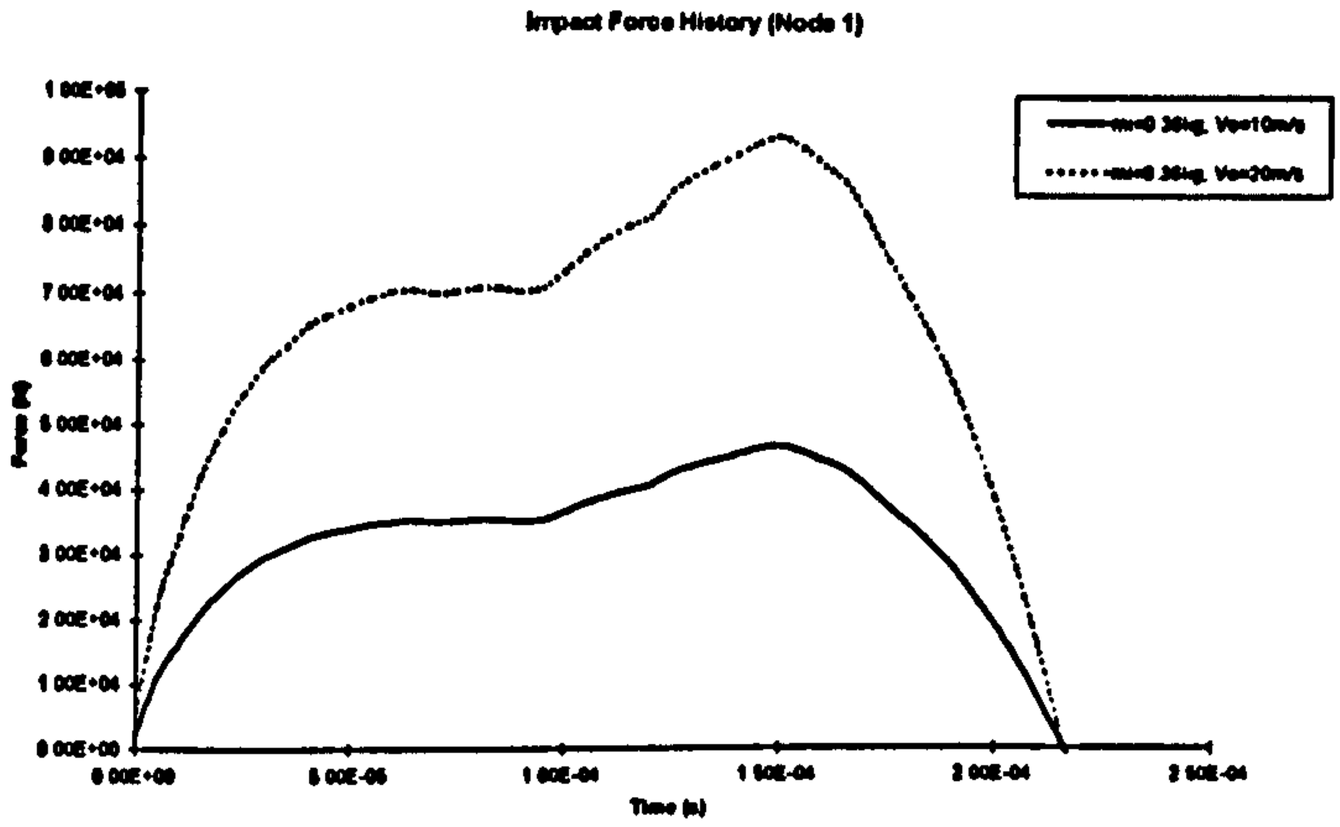

Fig 5.1.33 Impact force (constant impactor mass)

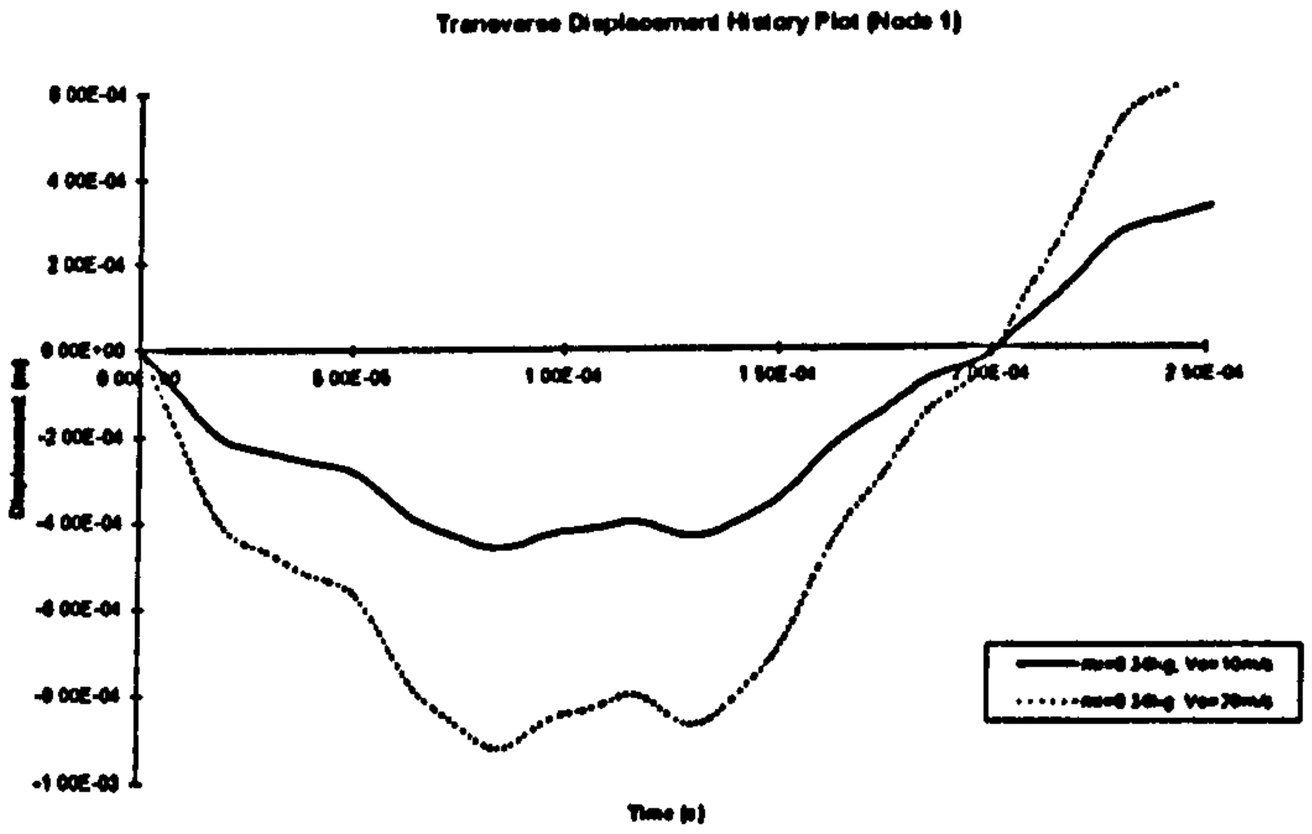

Fig 5.1.34 Transverse displacement (constant impactor mass)

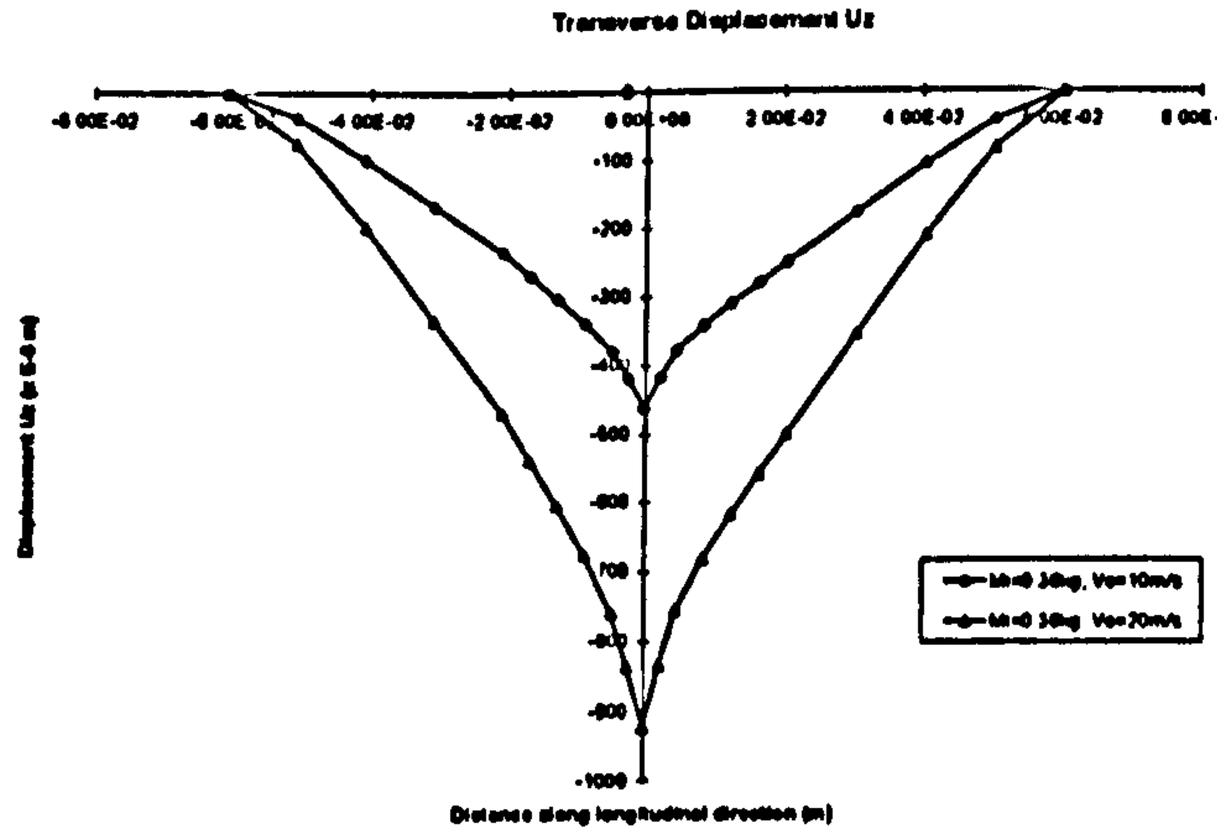

Fig 5.1.35 Transverse displacement along longitudinal direction (constant impactor mass)

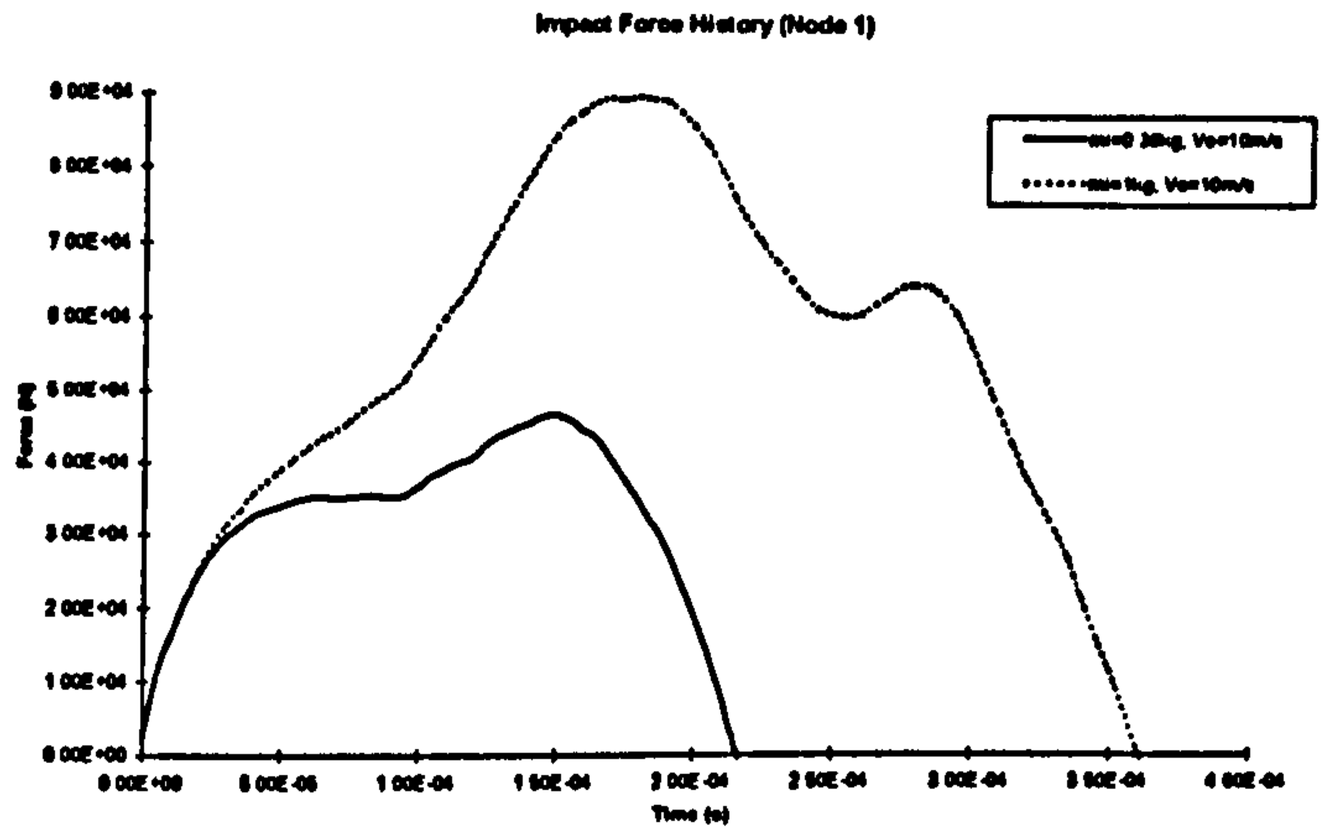

Fig 5.1.36 Impact force (constant impact velocity)

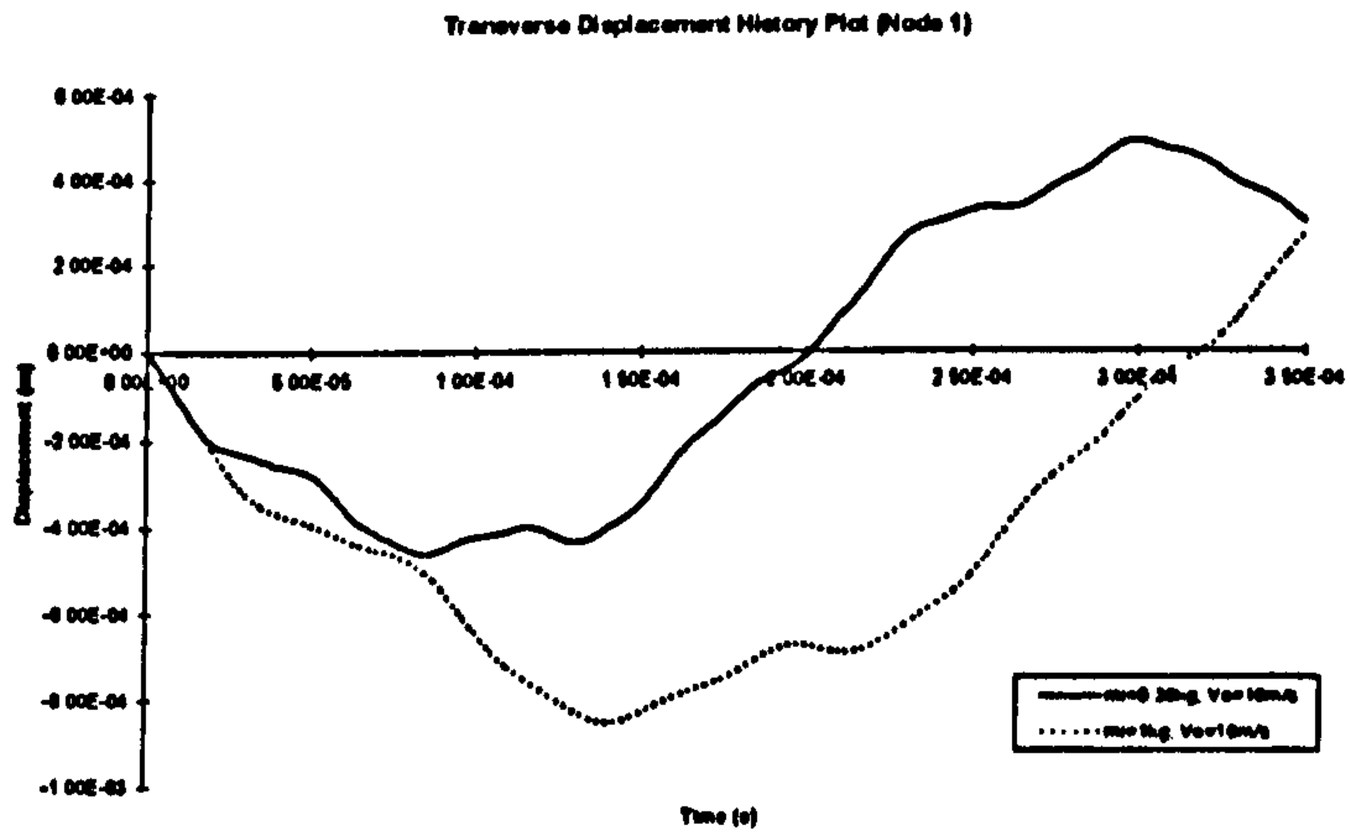

Fig 5.1.37 Transverse displacement (constant impact velocity)

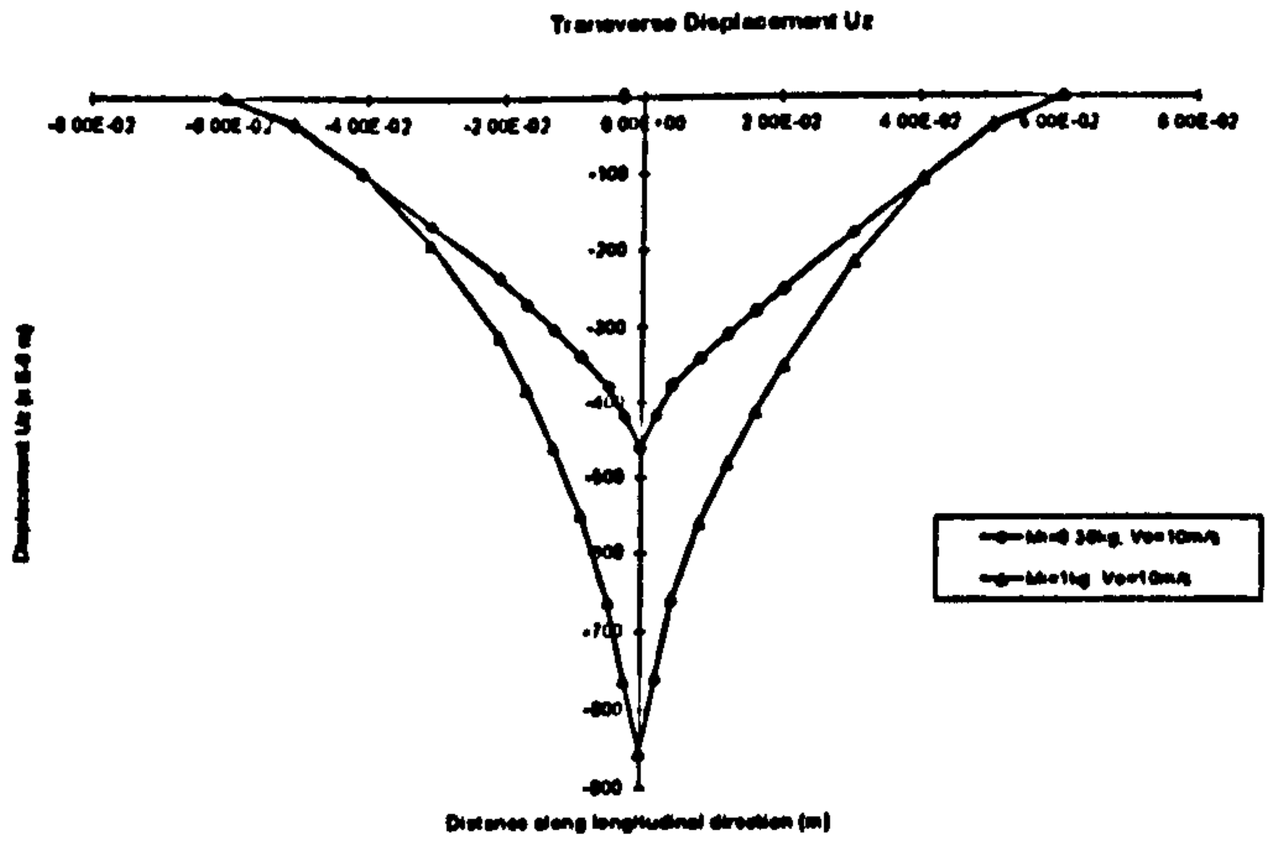

Fig 5.1.38 Transverse displacement along longitudinal direction (constant impact velocity)

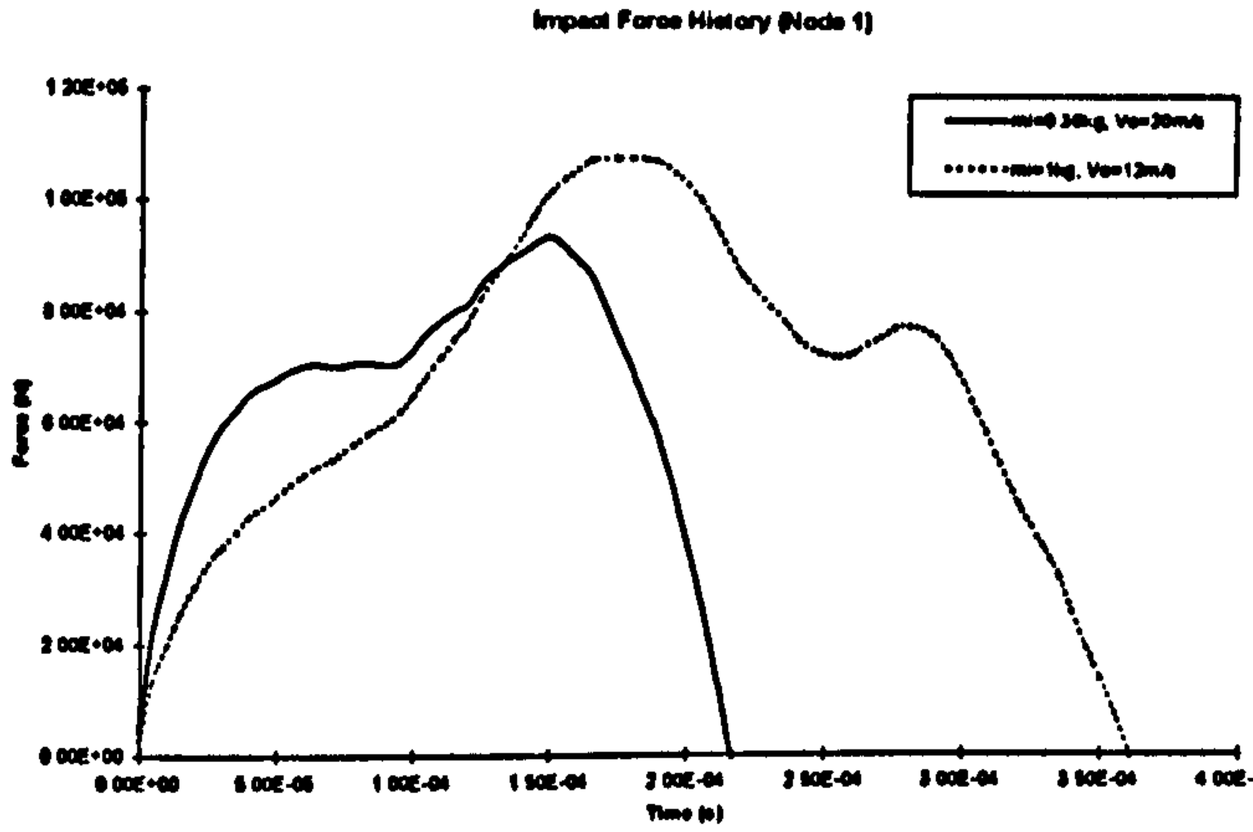

Fig 5.1.39 Impact force (constant impact energy)

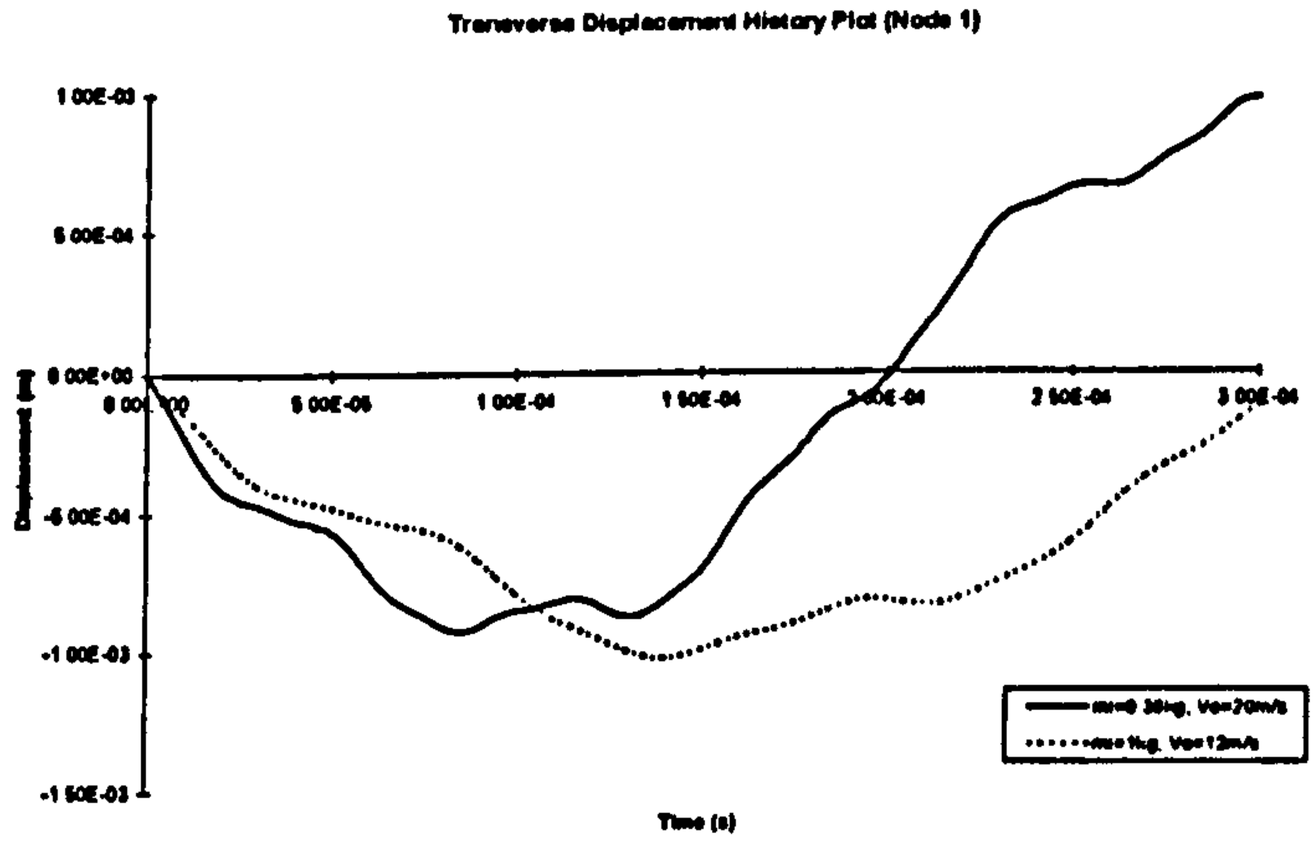

Fig 5.1.40 Transverse displacement (constant impact energy)

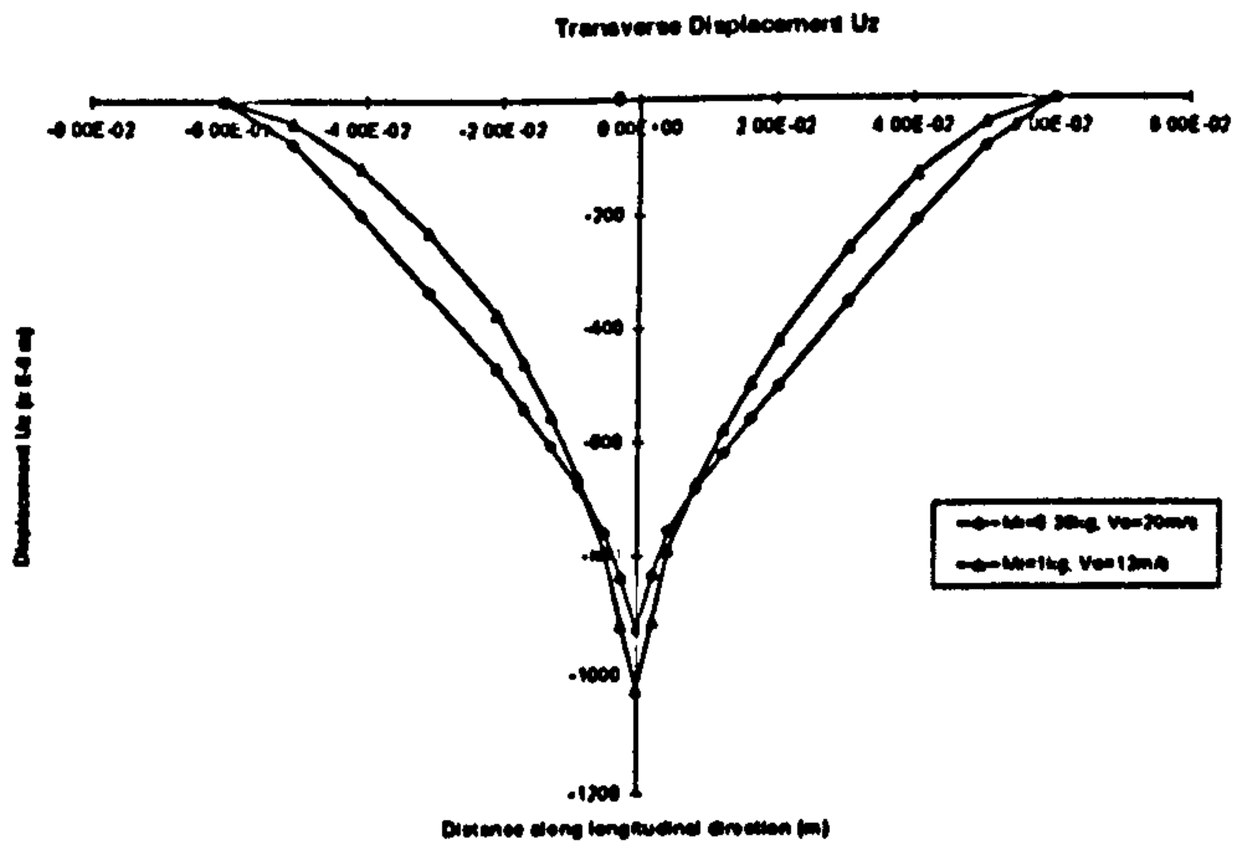

Fig 5.1.41 Transverse displacement along longitudinal direction (constant impact energy)

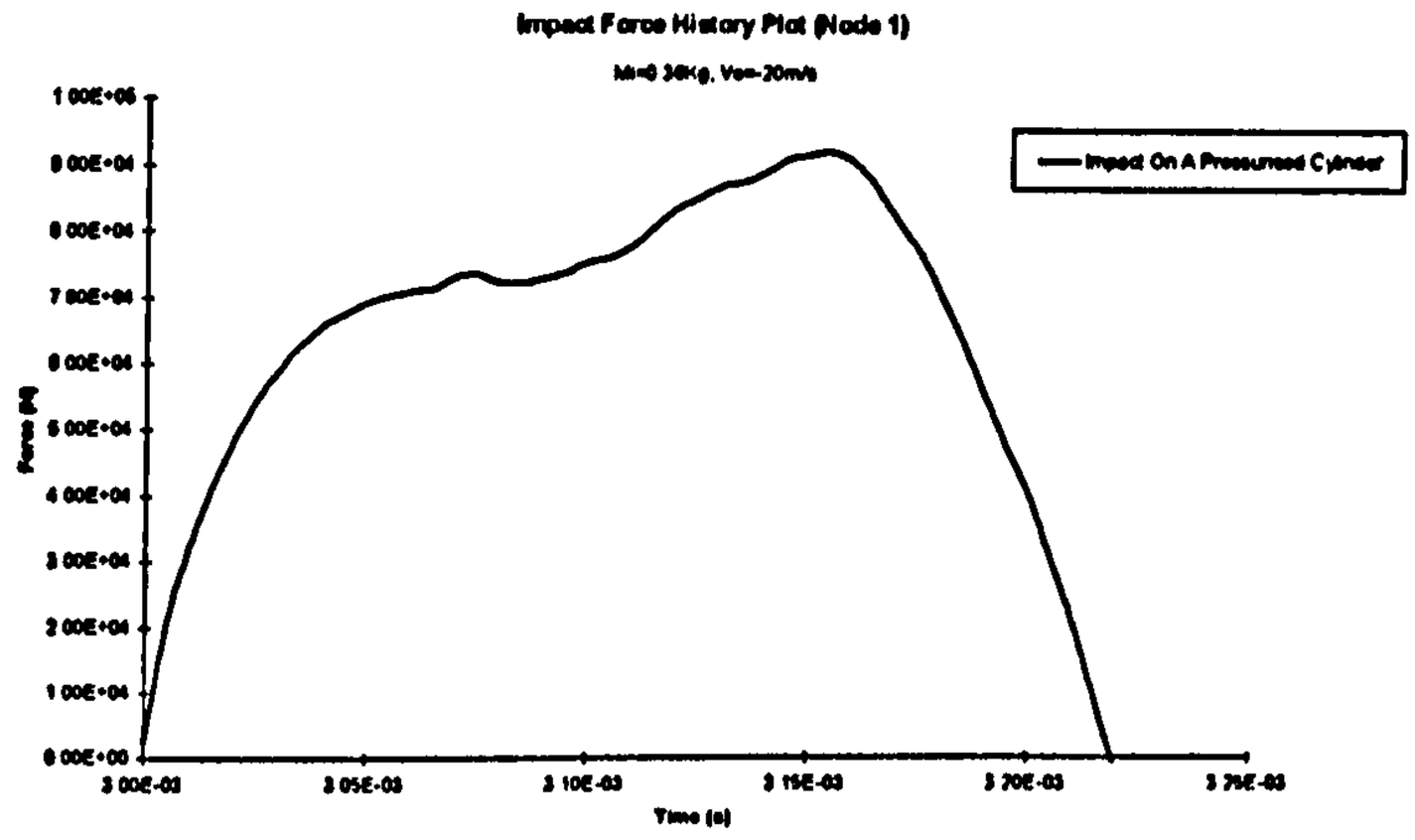

Fig 5.1.42 Impact force (impact on a pre-pressurised cylinder)

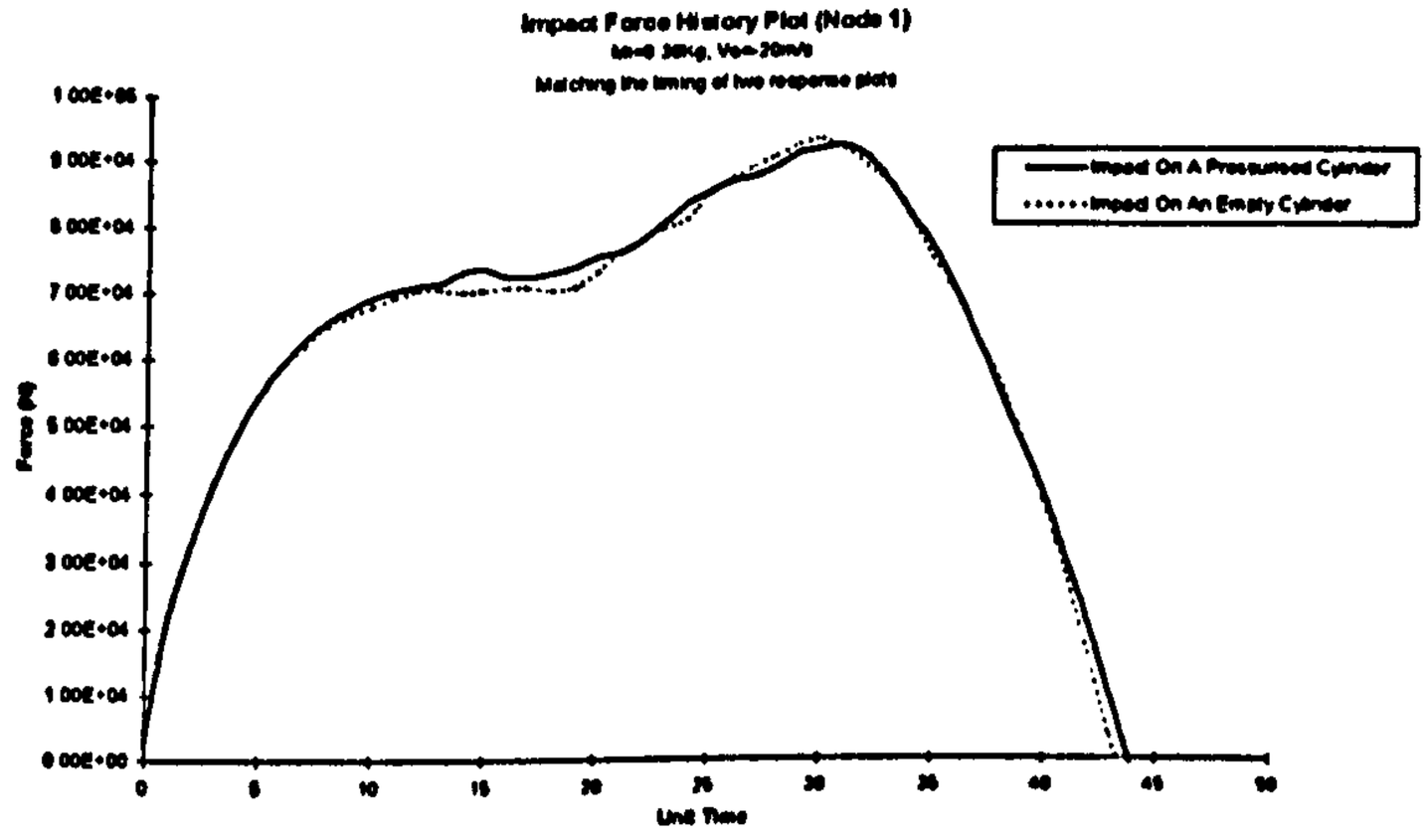

Fig 5.1.43 Impact force (impact on a cylinder with & without internal pressure)

(each unit time = 4 μs)

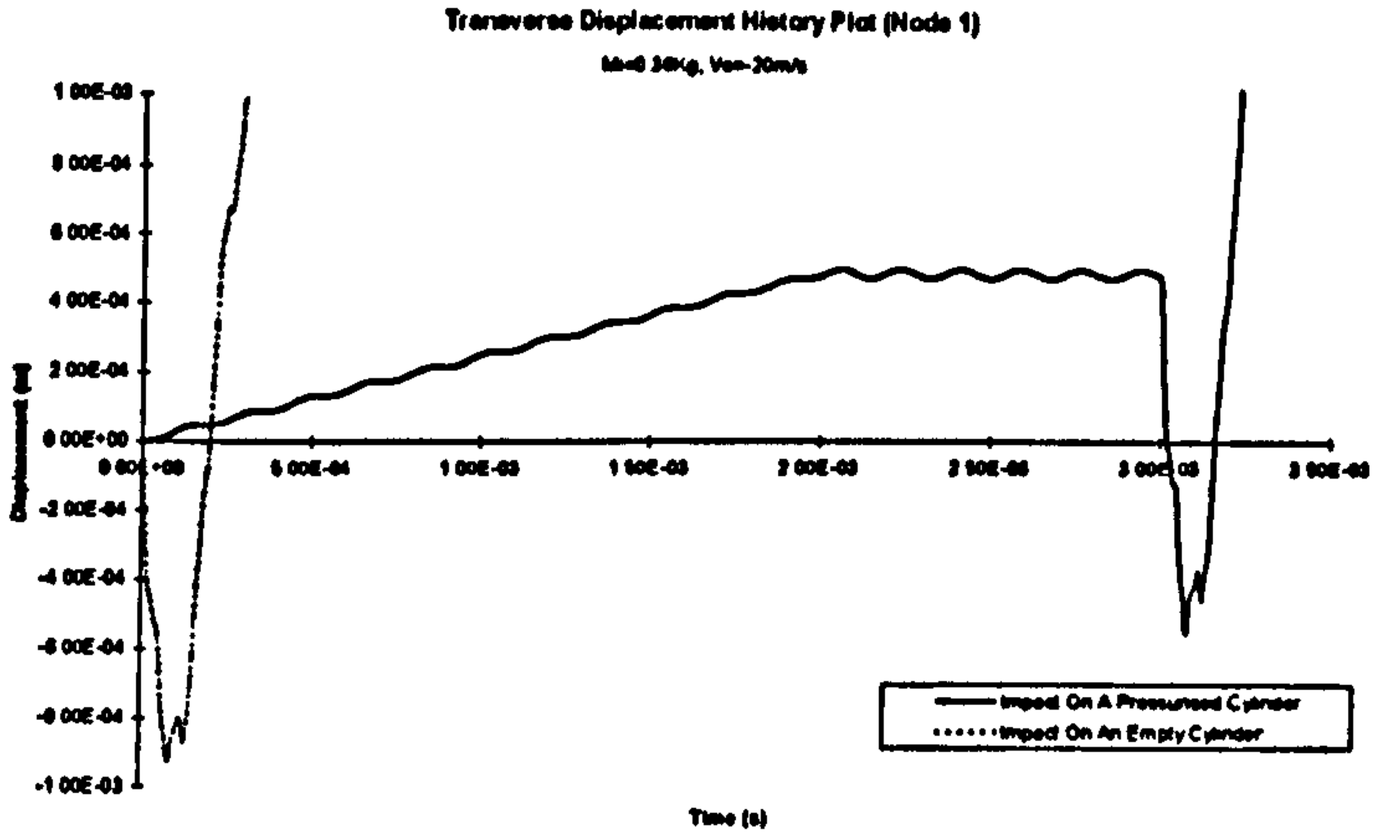

Fig 5.1.44 Transverse displacement

(impact on a cylinder with & without internal pressure)

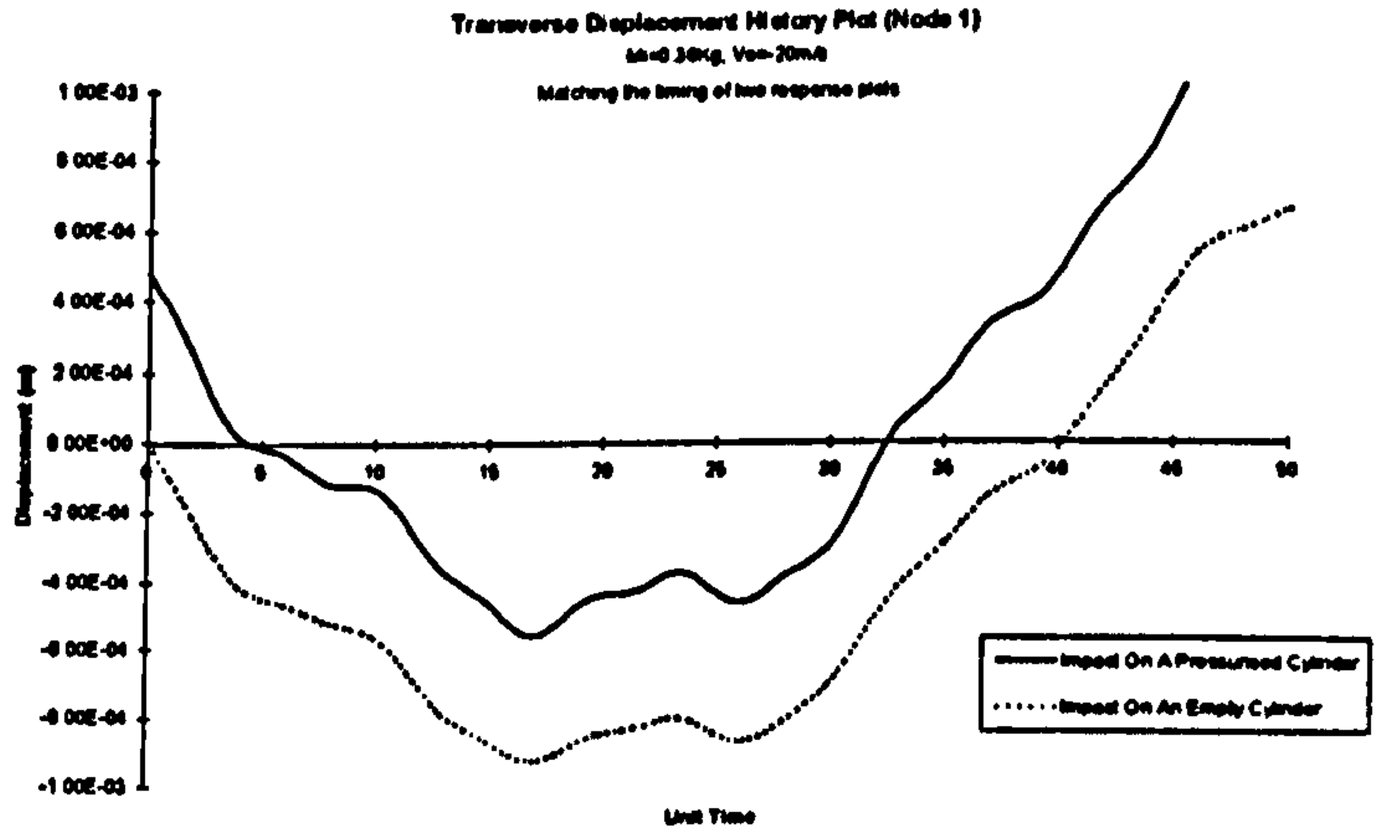

Fig 5.1.45 Transverse displacement

(impact on a cylinder with & without internal pressure)

(each unit time = 4 μs)

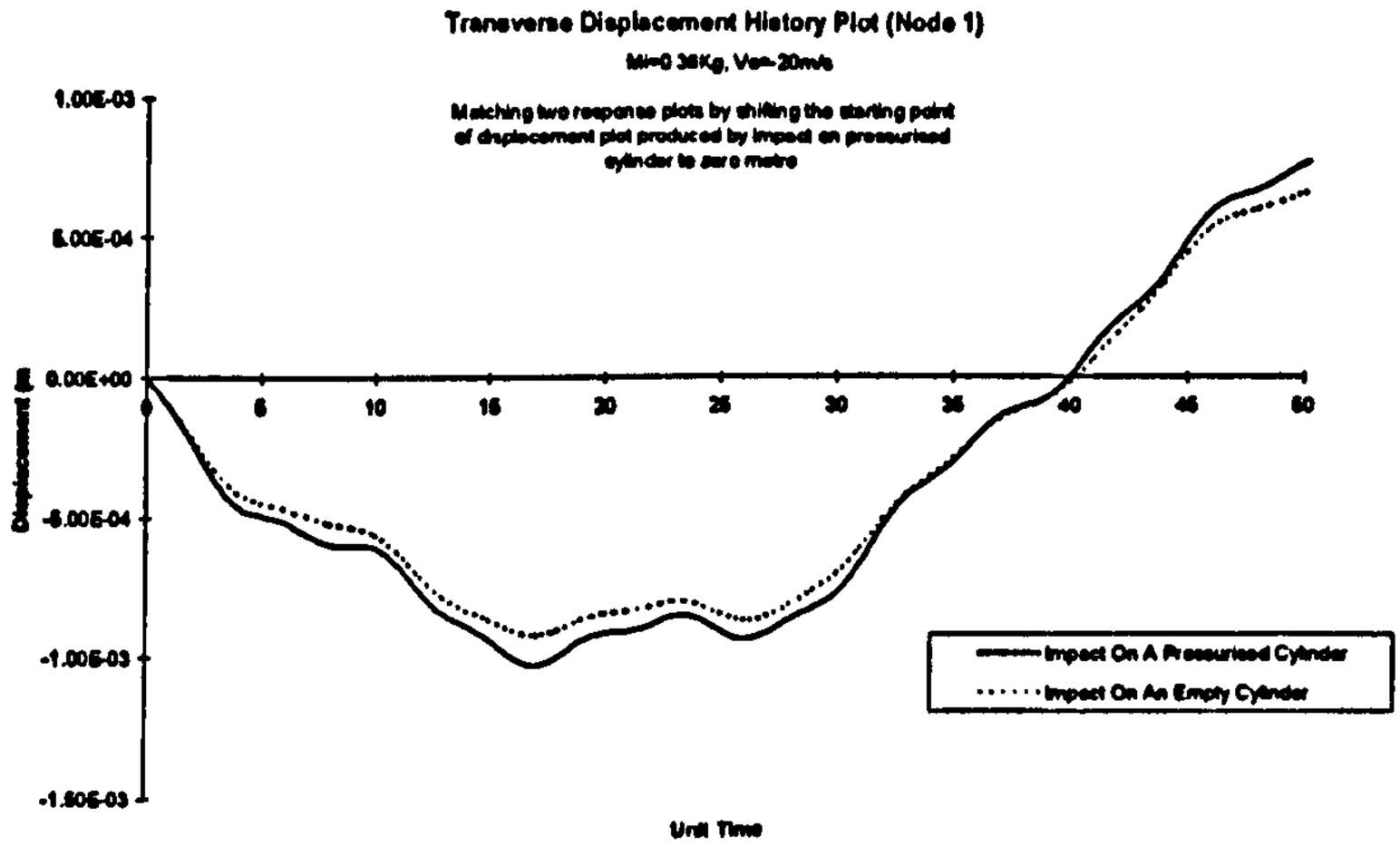

Fig 5.1.46 Transverse displacement

(impact on a cylinder with & without internal pressure)

(each unit time = 4 μs)

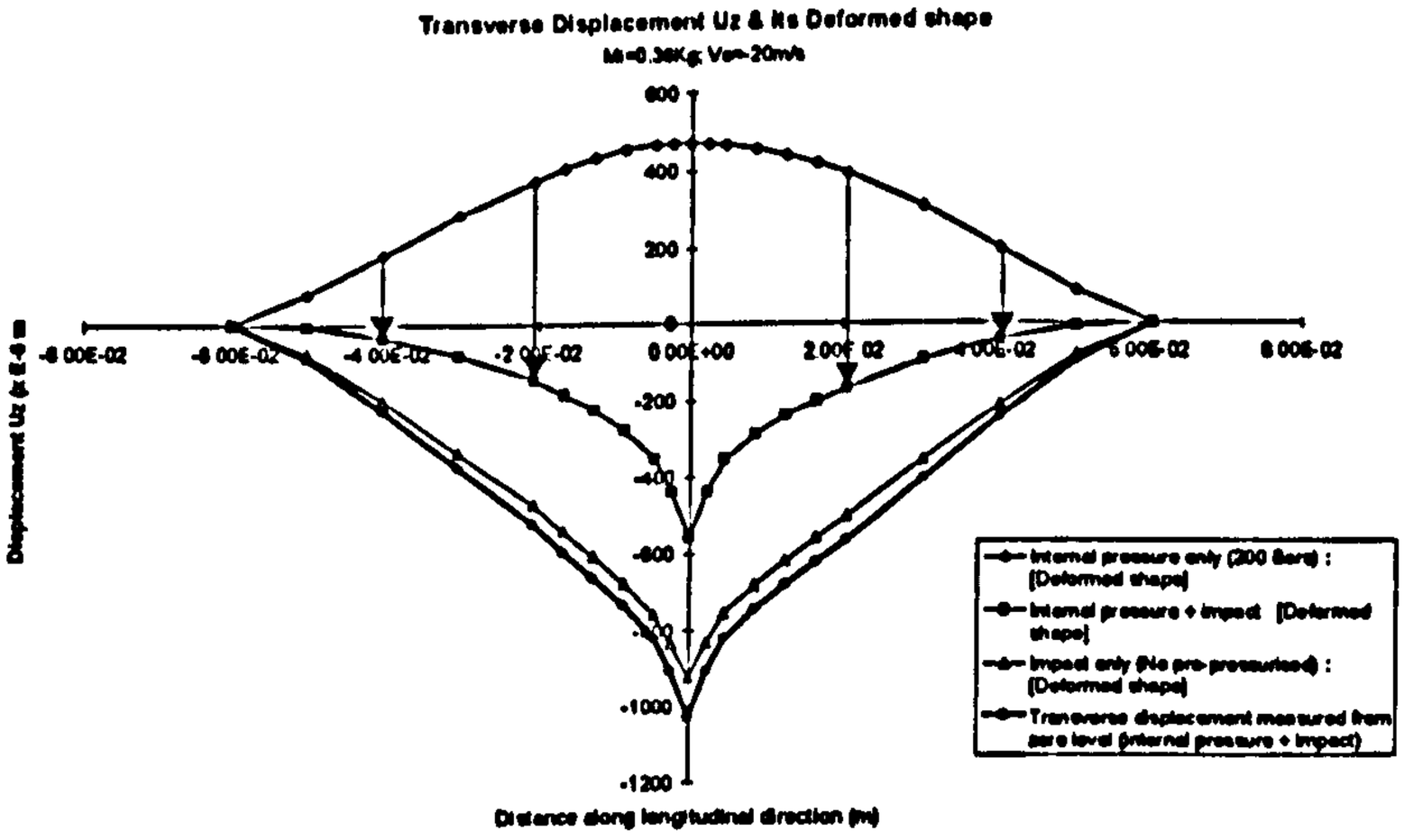

Fig 5.1.47 Transverse displacement

(impact on a cylinder with & without internal pressure)

5.1.4 Kinematic Response

A parametric study of the effect of impact parameters on impact response was given in the previous section. Impact energy seems to be a controlling factor in determining of localised impact response. In this section, the effect of internal pressure on the impact behaviour is investigated more thoroughly. The focus of analysis is mainly on comparing the structural response and material response of an empty and a pressurised cylinder. Impact loading with impact energy of 72 J was used in Test 7 and Test 8 (see Table 5.1.2), i.e. M_i=0.36 kg; V_o=-20 m/s. In the study of structural response, dynamic responses of the cylinder are examined. In the study of material response, the extent and the corresponding mechanisms of damage in a composite cylinder were investigated. All the FE predicted results for kinematic response analysis can be found in Appendix D.

Discussion

Kinematic response to impact on an empty cylinder is reflected by the in-plane and out-of-plane displacements, and twisting.

Both in-plane and out-of-plane twisting occur in the cylinder under impact loading [Finn and Springer, 1993]. The combination of these two kinds of twisting, results in a folding phenomenon (see Figs D12 and D17). The displacements appear on a comparatively small scale and may appear insignificant. However, the presence of these aspects in the FE modelling results demonstrates the ability of FE analysis to predict the material behaviour to a good level of detail.

Two main sources may be deemed responsible for the twisting. First, a balanced laminate appears orthotropic in its in-plane behaviour, but is not orthotropic in terms of its flexural behaviour. Tsai and Hahn (1980) demonstrated that in terms of the shear and twisting behaviour an unsymmetric laminate behaves exactly like a homogenous plate. In other word, the ply grouping and mid-plane symmetry have no effect on the shear and twisting properties. Impact is a highly concentrated load and can cause both localised and global bending of the structure, thus causing the twisting effect. Secondly, the wall

of the composite cylinder investigated here is neither a balanced nor a symmetric laminate. It is formed by three groups of [90°/+-15°] lay-ups of varying thickness and a 3 mm aluminium liner on one side. Thus, a high mismatch of bending stiffness occurs at the interface between the composite layer and the aluminium liner. Therefore, under impact loading, the composite layer and the liner attempt to assume different bending curvatures. This difference in the bending curvature causes the two layers to undergo relative in-plane displacements until stress equilibrium is obtained (see Figs D1, D2, D6 and D7). Liu (1988) proposed that the mismatch of bending stiffness between two adjacent layers can be used as an indicator of the likelihood of delamination in composite laminates subjects to subperforation impact. Out-of-plane separation of the two layers in the delaminated region may also become possible [Wu and Springer, 1988]. However, the present FE model does not allow out-of-plane displacement discontinuities between the two layers, so that the in-plane relative movements may have been overestimated as a consequence.

The occurrence of the folding phenomenon is mainly due to the pattern of twisting of the composite layer and liner (see Fig D14). The pattern of the twisting is greatly influenced by the geometry of the cylinder, the lay-up of the composite layer, and the comparatively thin liner.

The kinematic response to the impact on a pressurised cylinder is largely similar to the impact on an empty cylinder, in that the total relative in-plane movements due to impact for both cases were quite similar (see Fig D16).

Internal pressure alone produces twisting as well as in-plane relative displacements between the two layers of the cylinder, in the direction opposite to those due to impact. As illustrated in Fig D15, "hogging" of a cylinder wall is produced due to internal pressure, while "sagging" is caused by impact loading. This difference in the deformed shapes is likely to be one of the reasons responsible for the opposition sense of the effect.

As folding deformation of the cylinder is induced, buckling of the liner may become possible. Note that the magnitude of in-plane twisting were very small. However, as can

be seen in Figs D3, D4, D8 and D9, the liner displaced by a comparatively high amount (10.8 % of the transverse displacement at maximum) towards the centre of the cylinder. It may be suggested that the main cause of this out-of-plane twisting and folding phenomenon was the large deformation of the liner under either internal pressure or impact loading. As can be seen in Fig D13, the distance between the two peaks was about 80 mm, while the thickness of the liner was 3mm. Thus, buckling of the liner may take place. This folding phenomenon produces bending sites around the impact site, which may promote damage from pre-existing invisible flaws such as matrix cracks or delamination in the composite layer. However, experimental confirmations are required for these FE predictions.

5.1.5 Material Response

In this section, the material response of an empty and a pressurised cylinder under impact loading is studied. Impact loading used in this study was the same as in previous section, i.e. M_i = 0.36 kg; V_o = -20 m/s. Single impact at the central of the cylinder was considered. Material failure criteria were employed to identify failure modes such as matrix cracking and fibre fracture of composite material due to impact loading. Only the stress state at the time of peak transverse displacement were examined. The FE results for this material response analysis can be found in Appendix E.

Discussion

The impact behaviour of the empty and pressurised cylinders are, in general, quite similar. As seen in Figs E23 and E24, internal pressure induces initial tensile stresses in the cylinder.

The application of the failure criteria to examining stresses at the time of maximum transverse displacement, for the empty cylinder, fibre breakage occurs at the contact area (i.e. the impact site, four shell elements). Excessive matrix cracking takes place in the region surrounding the impact site in nearly all composite layers.

For the pre-pressurised cylinder, it was found that no fibre breakage occurs in the contact area, while the volume of matrix cracking was similar to the initially stress-free cylinder.

As fibre breakage is the major failure mode responsible for the degradation of performance of a composite pressure cylinder [Yener and Wolcot, 1989], the empty cylinder appears to be more vulnerable to impact damage than the pre-pressurised cylinder. Surface fibre breakage presents a potential threat to the cylinder, since its effective load bearing thickness is reduced.

Repeated impact of the empty cylinder was also modelled. The material degradation model was used to degrade the material properties of the elements where fibre breakage was induced during previous impact. It was found that, on top of the pre-existing fibre breakage, further breakage developed in layers 3, 4 & 8. Repeated application of material degradation to the failed layers was followed by subjecting the cylinder to in-service pressure. The transverse displacements due to repeated impact are given in Figs 5.1.48 and 5.1.49. It can be seen that a bulge is produced at the impact site, a weak spot was created due to fibre failure. The bending stress plots along the longitudinal and the hoop directions shown in Figs 5.1.49 and 5.1.53 indicate that, although additional bending is confined to a small area, the magnitudes of bending stresses were not small comparing with the overall stresses (nearly +- 50 %).

The bending created by the bulging effect may, in the long term, affect the fatigue life of the liner, and the service life of the composite pressure cylinder.

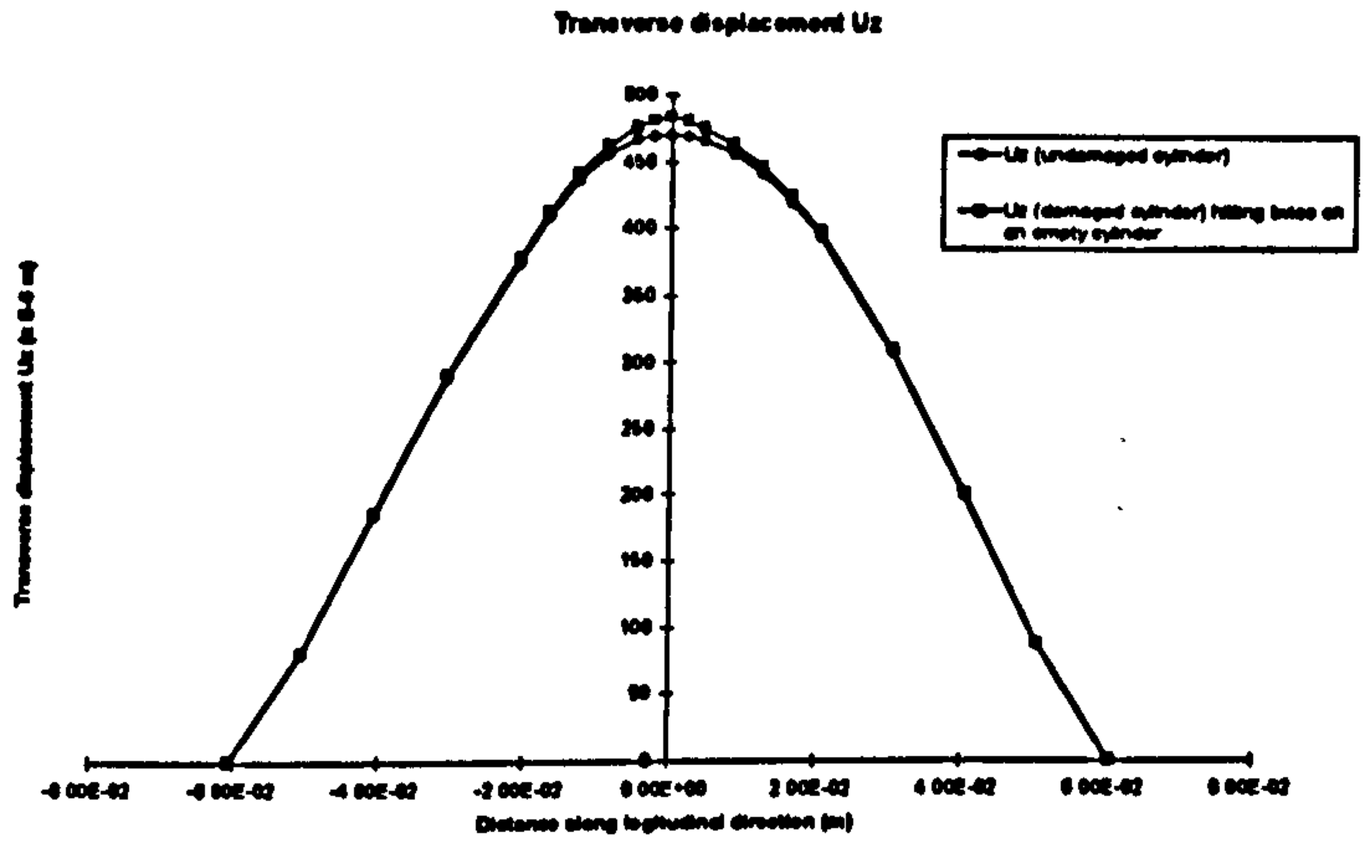

Fig 5.1.48 Transverse displacement due to repeated impact (along longitudinal direction)

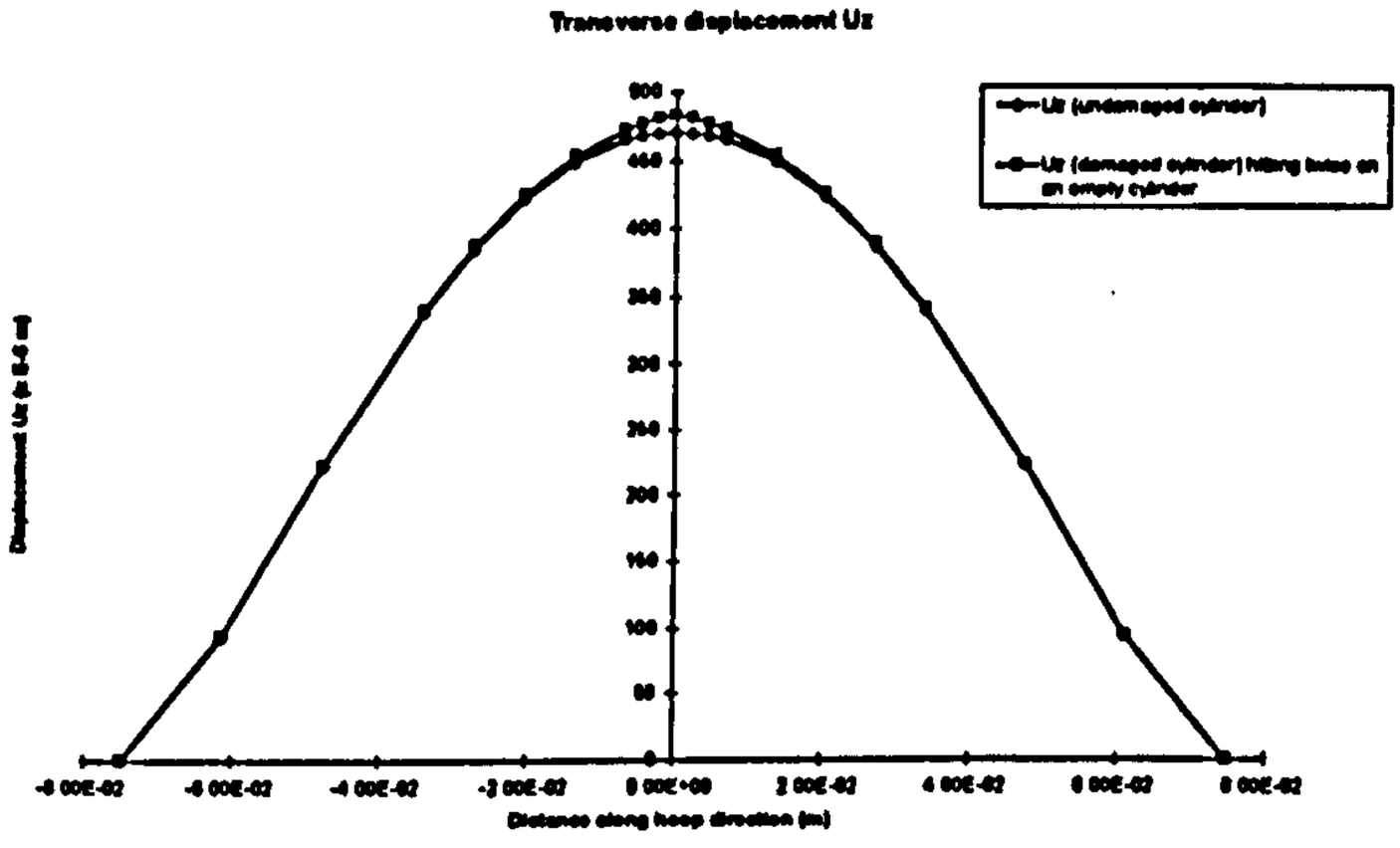

Fig 5.1.49 Transverse displacement due to repeated impact (along hoop direction)

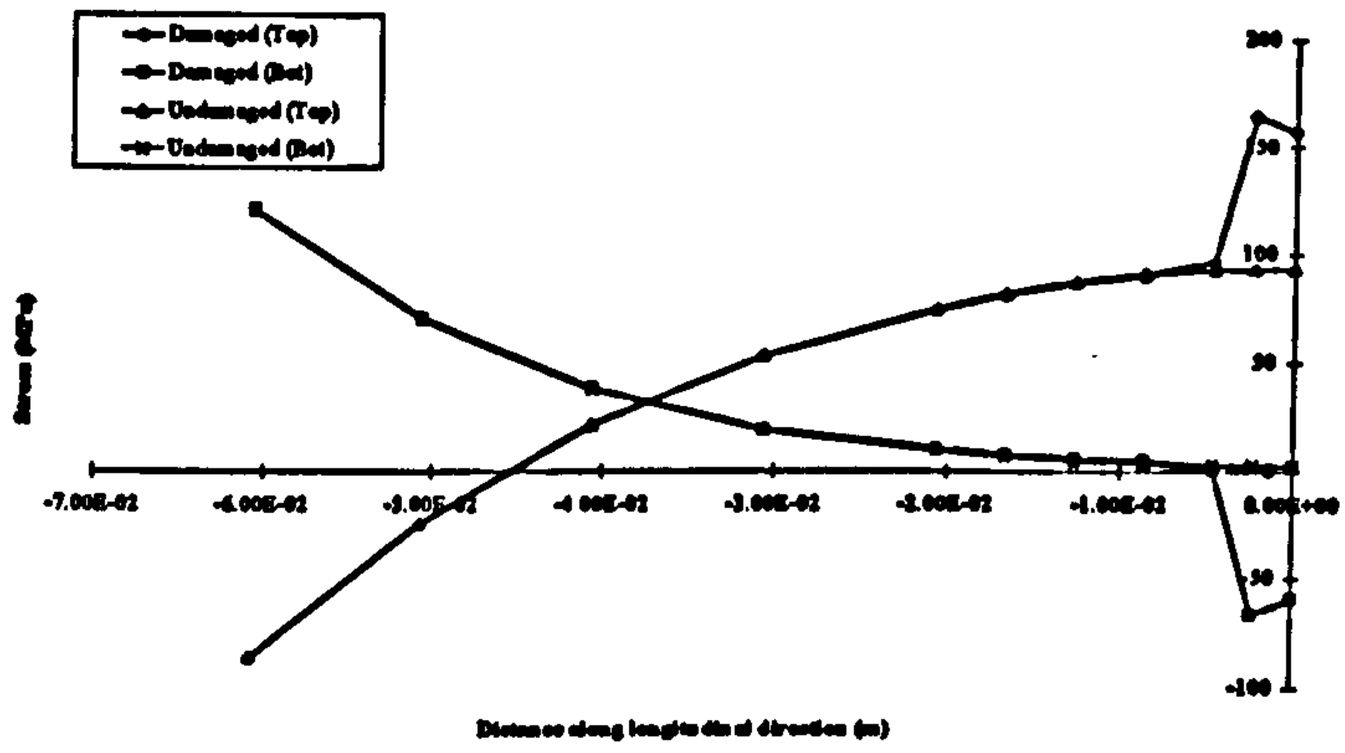

Fig 5.1.50 Bending stress in the liner (S11)
(along the longitudinal direction)

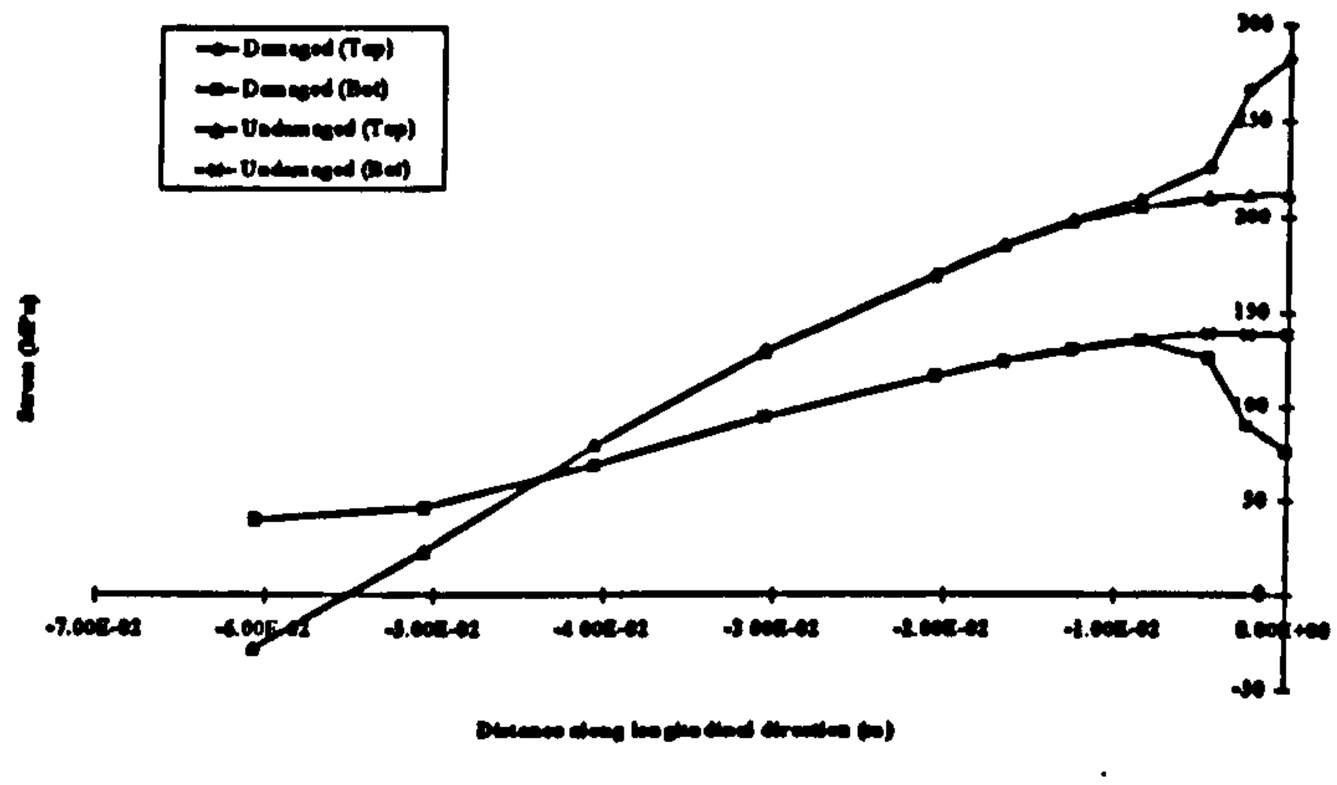

Fig 5.1.51 Bending stress in the liner (S22)
(along the longitudinal direction)

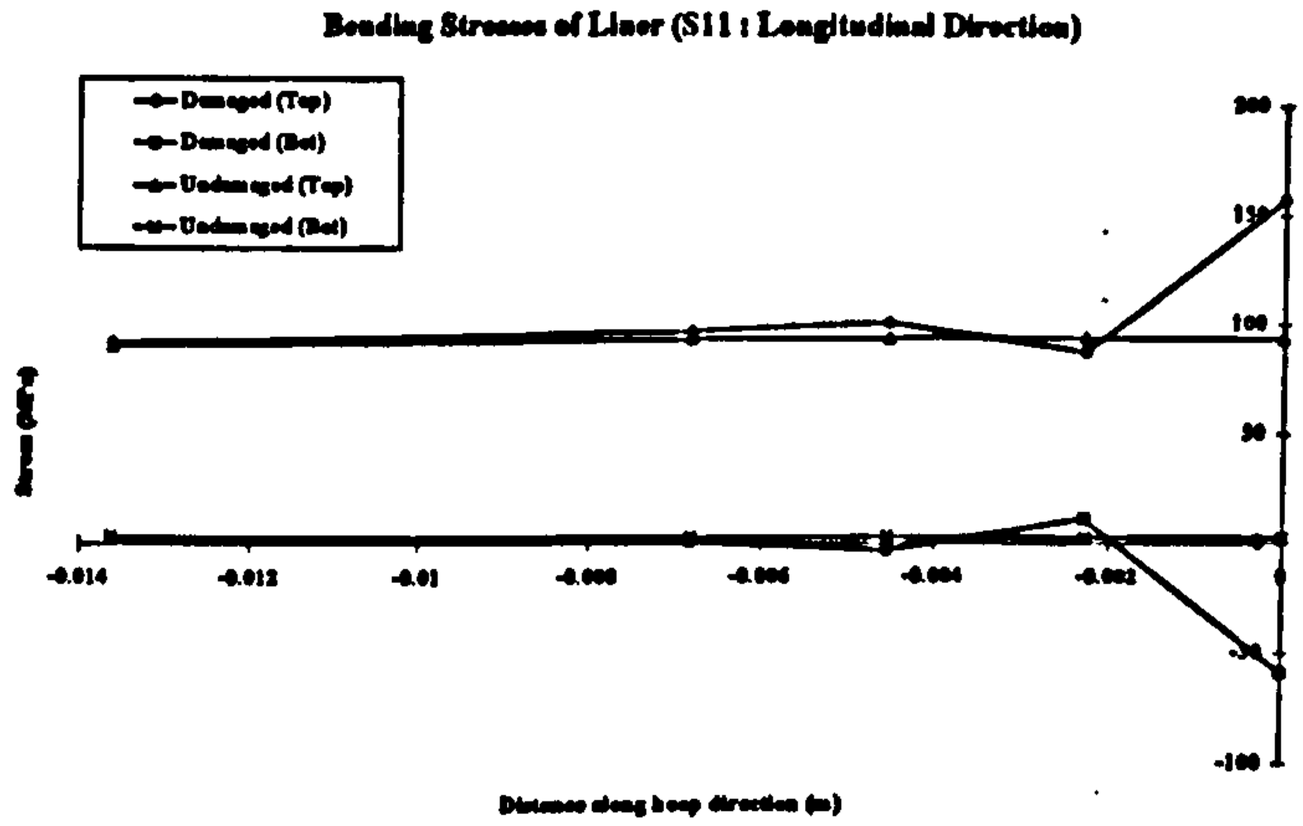

Fig 5.1.52 Bending stress in the liner (S11)
(along the hoop direction)

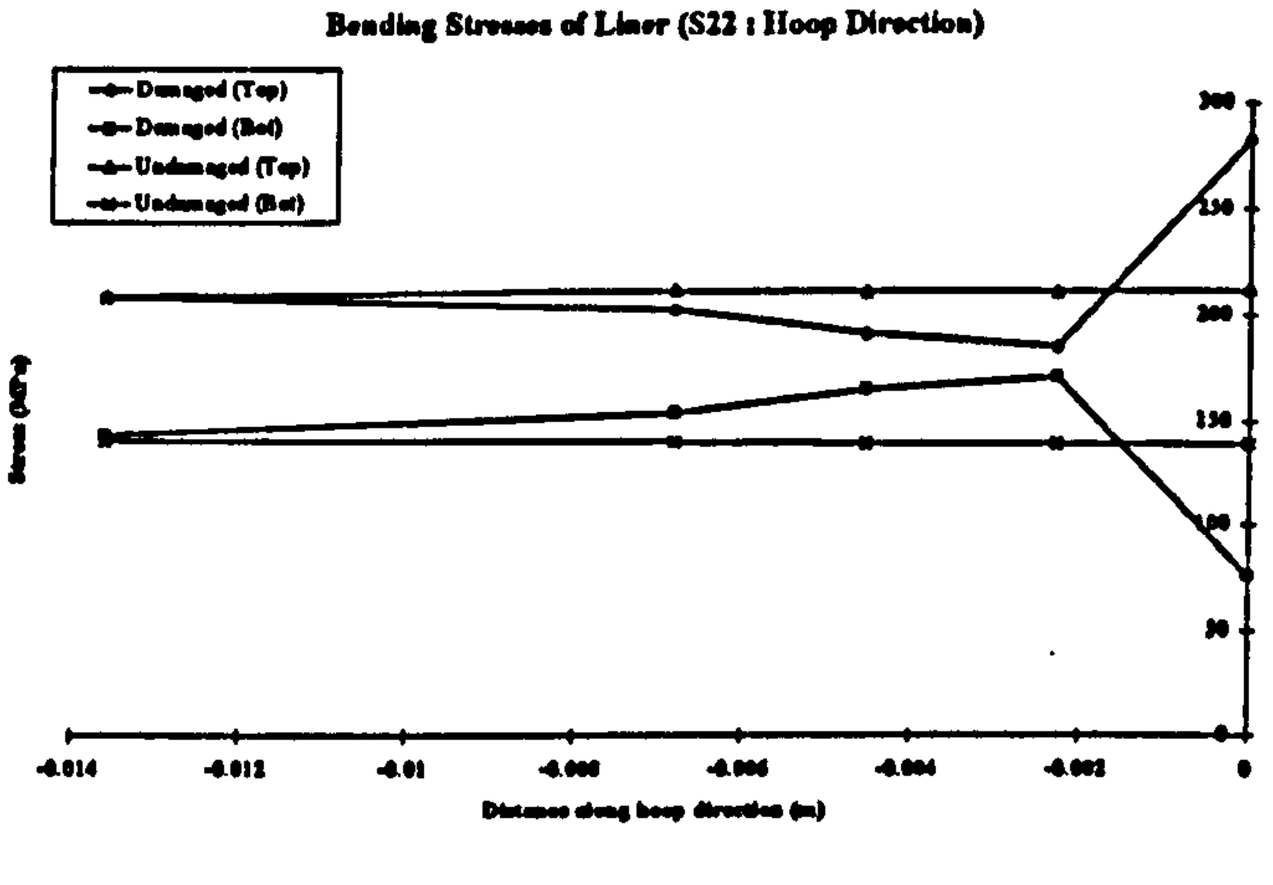

Fig 5.1.53 Bending stress in the liner (S22)
(along the hoop direction)

5.2 FEM : Static Response

5.2.1 Cylindrical Model

The composite ring considered in this section had similar structural dimensions, configuration, and material properties to the one used in the experimental investigation (see Fig 5.2.1). A static load with a Hertzian pressure distribution over a small contact area was applied along the central axis of the width of the composite ring. The applied load of 100 kN was approximated from the maximum force predicted in dynamic analysis for impact with energy of 72 J (i.e. M_i=0.36 kg, V_o=-20 m/s; see Fig 5.1.39).

5.2.1.1 FE Model

In order to reduce the total number of 3D brick elements and nodes for the FE mesh, a quarter of the composite ring was modelled. Therefore, mirror symmetry boundary conditions were applied on the appropriate planes. For simplicity, a cross-ply lay-up was used [$90°_{2mm}/0°_{1mm}/90°_{4mm}/0°_{3mm}/90°_{4.5mm}/0°_{4.5mm}$ + $Liner_{3mm}$]. Therefore, the thickness was divided into seven layers by seven elements. The FE mesh and modelling details are given in Table 5.2.1. In order to define the orthotropic material properties and fibre orientations, local axes have been assigned to every element. The contact radius due to loading was 6 mm. The contact radius of 6 mm was estimated based on the Hertzian approximation from the indenter diameter of 22 mm, and contact stiffness of the indenter and the composite ring. The reference directions and the region for FE results have been shown in Fig 5.2.2. Node 1 was chosen as the reference point, or centre. Globally, the axial direction (longitudinal coordinate line) and hoop direction (circumferential coordinate line) were used to describe the two reference axes passing through the centre. Locally, every node had its reference axes so that the through-thickness, or radial direction was always the Z-direction.

5.2.1.2 FE Results

The transverse displacement, Uz, along the hoop direction at both the top and bottom surfaces of the composite ring are given in Fig 5.2.4. The direct stresses at the top surface along both the hoop and axial directions are given in Figs 5.2.5 and 5.2.6.

Through-thickness direct and transverse shear stresses at different positions are shown in Figs 5.2.7 to 5.2.16. The stresses were calculated at three positions : at the reference point (x=0, y=0), 6 mm from the reference point along the axial direction, and 3° from the reference point along the hoop direction. The transverse shear stresses at the centre are given in Fig 5.2.7 and 5.2.8. The stresses along the line 6 mm from the centre in the axial direction are given in Fig 5.2.9, and those on the line 3° from the centre along the hoop direction are given in Fig 5.2.10. The direct stresses at the reference position are given in Figs 5.2.11 and 5.2.12, at 6 mm from the centre along the axial direction in Figs 5.2.13 and 5.2.14, and at 3° from the centre along the hoop direction in Figs 5.2.15 and 5.2.16.

In order to simply the diagram and make the stresses in each layer easier to identify, all through-thickness stresses shown were taken from the upper surface of each element except for layer 7, for which both upper and lower stresses are shown.

Stress contours of direct and transverse shear stresses at selected surfaces are given in Figs 5.2.17 to5.2.24. Stress contours for direct stresses on the upper surface of layer 1 are given in Figs 5.2.17 and 5.2.18. Stress contours for transverse shear stresses of layers 3, 4 and 6 are given in Figs 5.2.19 to 5.2.24. These stress contours were prepared by using MATLAB, a graphic presentation program.

5.2.1.3 Discussion

As can be seen in Fig 5.2.4, the transverse displacements at the top and bottom surfaces of the composite ring were considerably different in the loading region. The difference between these two displacements represents the compression of the material under contact loading. The bottom surface has mainly move due to global bending deflection, while the upper surface has been both compressed and deflected. A difference of 0.842 mm represents the maximum compression has been found at the centre of contact. This local compression of material under loading is illustrated in Fig 5.2.3.

As can be seen in Figs 5.2.5 and 5.2.6, very high direct stresses, S11 and S22, have been induced, at and near the loaded surface, which reflect the highly compressed state of material under the contact. These high contact stresses must be responsible for fibre breakage occurring at the contact site. However, these high contact stresses tend to decay quickly with the distance from the patch of contact.

Since high compression of material has occurred at the centre, no significant transverse shear stresses were induced immediately underneath the compression (see Figs 5.2.7 and 5.2.8). However, at a distance of one contact radius from the centre, high transverse shear stresses occur at the upper surface of the second layer (in Fig 5.2.9), and the upper surface of the third layer (in Fig 5.2.10). Parabolic stress distribution profiles are seen in both sets of through-thickness stress distributions.

The prediction of the location of high transverse shear stress by the FE model was quite close to the experimental findings, which suggested that a high density of transverse shear cracks occurred in the first three layers in the region close to contact area. Moreover, since no significant transverse shear stresses were predicted at the centre, this correlated well with the experimental finding that little matrix cracking occurred at the area immediately under the indentation. The combination of these effects explains the shape of the failure envelope shown in Fig 4.2 (pipe) and Figs 4.11 and 4.12 (cylinder).

From Figs 5.2.11 to 5.2.16, it can be seen that the top composite layer and the bottom aluminium liner have taken up a large portion of the bending stresses. High bending stress predicted in the liner may be a cause for concern. The bending stresses in the middle of the section were very low. This suggests that the probability of fibre breakage in the middle of the section is very low.

Figs 5.2.17 and 5.2.18 demonstrate that the high stress level for direct stresses at the upper surface of layer 1 are confined to the vicinity of the contact area.

Figs 5.2.19 and 5.2.20 show the transverse shear stresses at the upper surface of layer 3. The stress contours indicate that the locations of maximum lie at 5 mm in the hoop and axial direction from the centre of indentation. Figs 5.2.21 and 5.2.22 show the transverse shear stresses at the upper surface of layer 4. Similar pattern of stress contours can be seen, however, the locations of maximum stress have been shifted out to 6 mm. Figs 5.2.23 and 5.2.24 show the transverse shear stresses for the lower surface of layer 6, the interface with the liner. Once again, a similar pattern of stress contours can be seen. In this case, the locations of maximum of the stress contours have further shifted to 10 mm. Note also that the magnitude of the maximum shear stress diminishes with depth.

This shifting of the maximum of transverse shear stress further away from the centre of contact in the lower layers forms a conical region of high transverse shear stress with the base in the lower layer. This prediction is very close to the experimental finding that matrix cracking and delamination were confined in a conical envelope.

The predictions of this analysis further highlight the importance of considering the contact problem.

Table 5.2.1 FE mesh and modelling details

Configuration parameters

Total thickness = 22 mm

Radius of inner surface = 120 mm

Width = 107 mm

Lay-up : $[90°_{2mm}/0°_{1mm}/90°_{4mm}/0°_{3mm}/90°_{4.5mm}/0°_{4.5mm} + Liner_{3mm}]$

Modelling parameters

Total number of :

Element : 1932

Node : 9376

DoF : 26435

Boundary conditions :

mirror symmetry with respect to the global x-y, y-z and z-x planes.

Free surface for non-symmetry plane

Static loading = 100 kN (Hertzian pressure distribution was used)

Contact radius = 6 mm

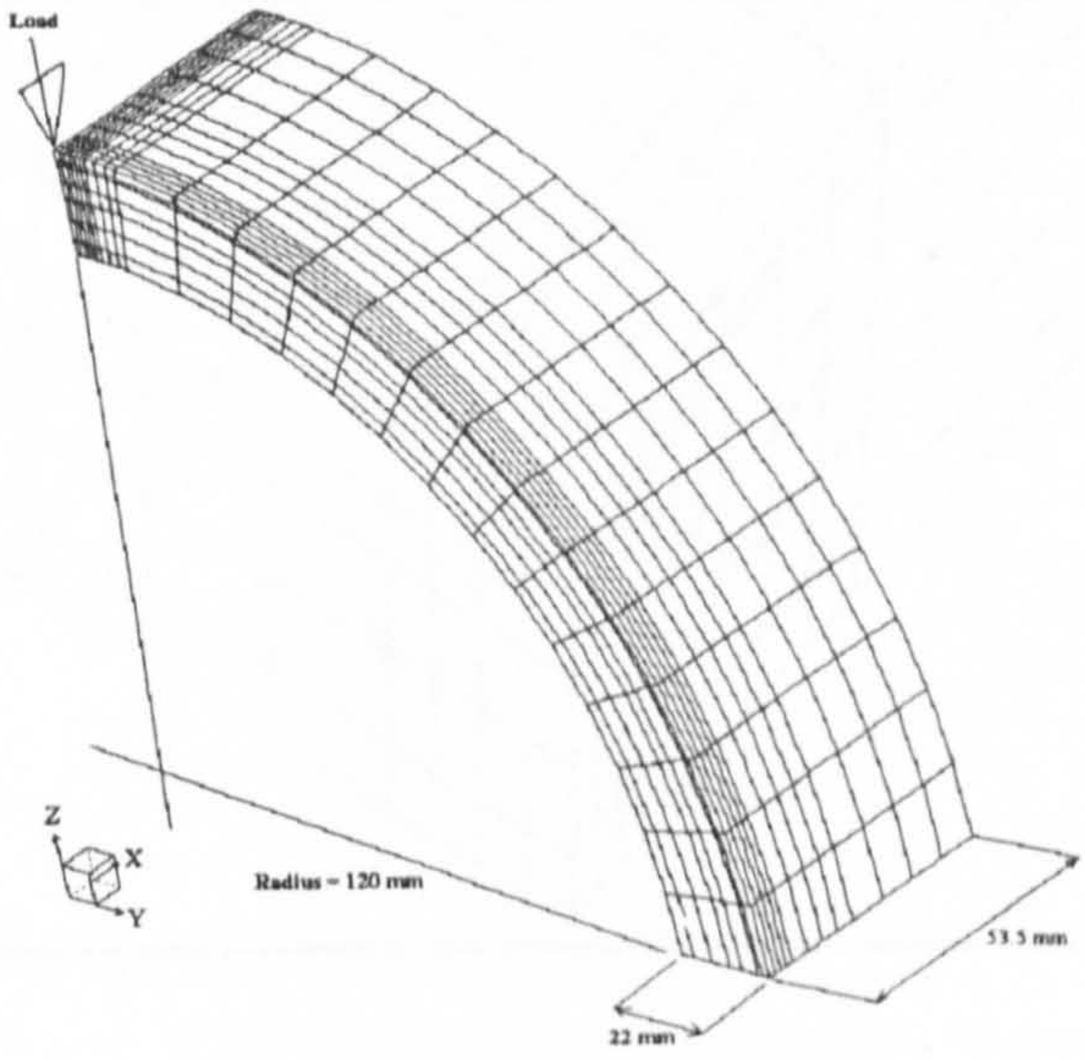

Fig 5.2.1 FE mesh of composite ring

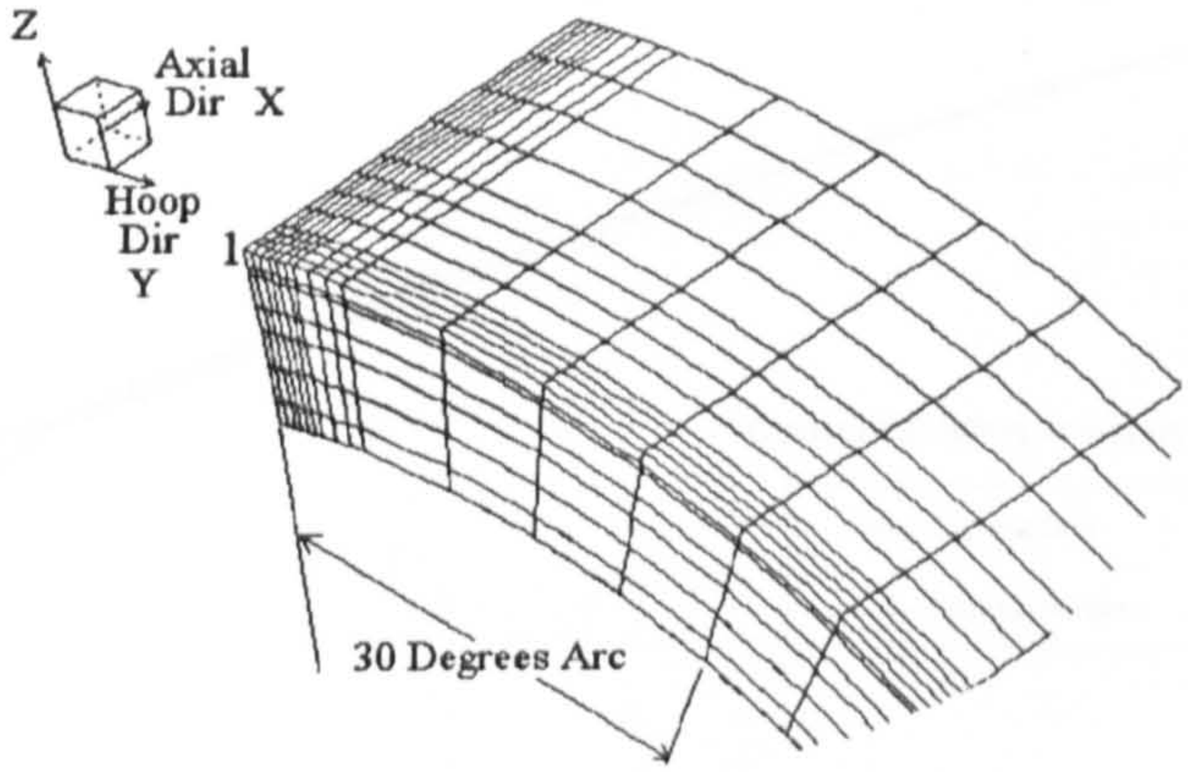

Fig 5.2.2 Reference directions and region for FE results
(Node 1 is the reference point)

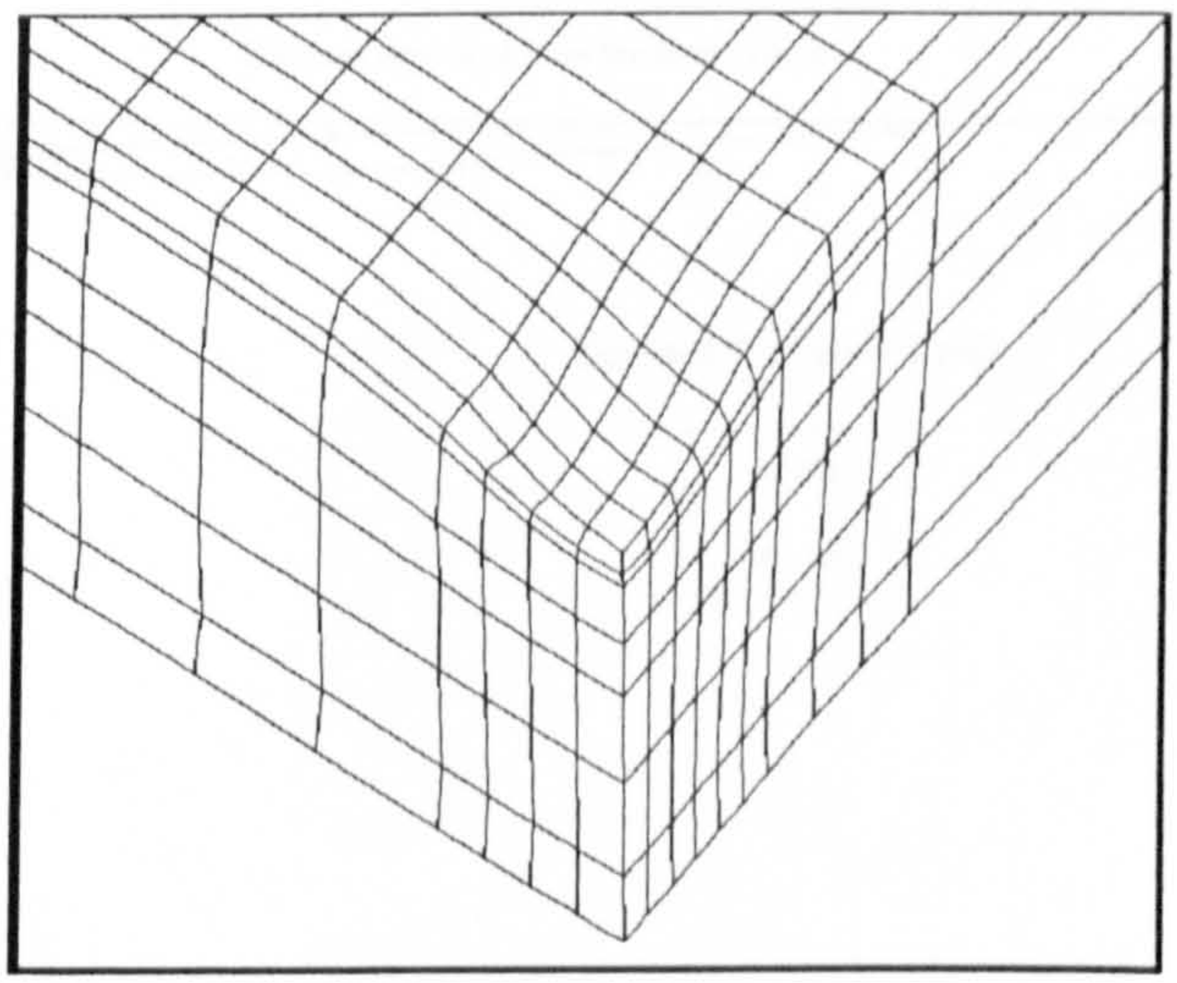

Fig 5.2.3 Deformed shape of composite ring under static loading

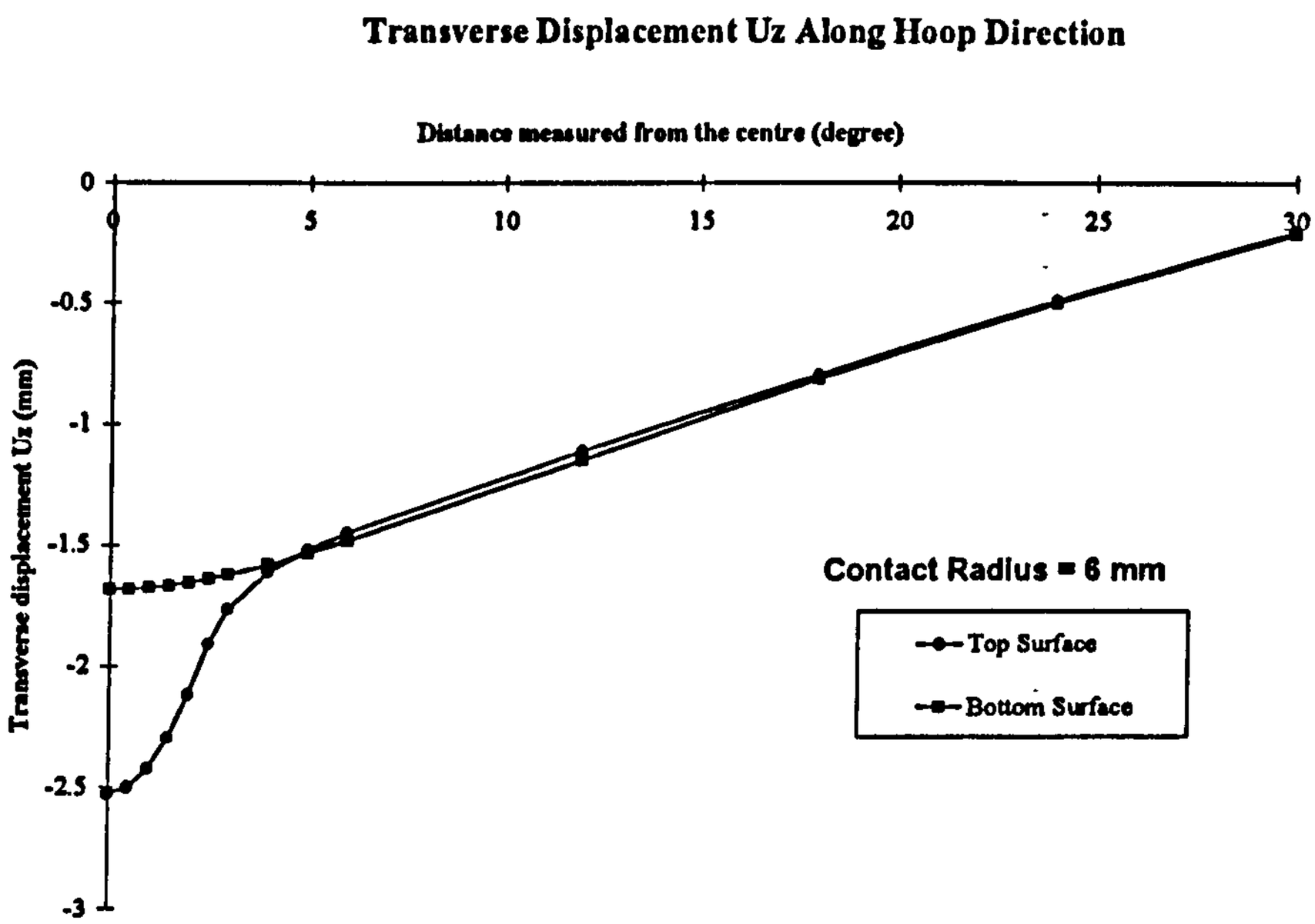

Fig 5.2.4 Transverse displacement along the hoop direction

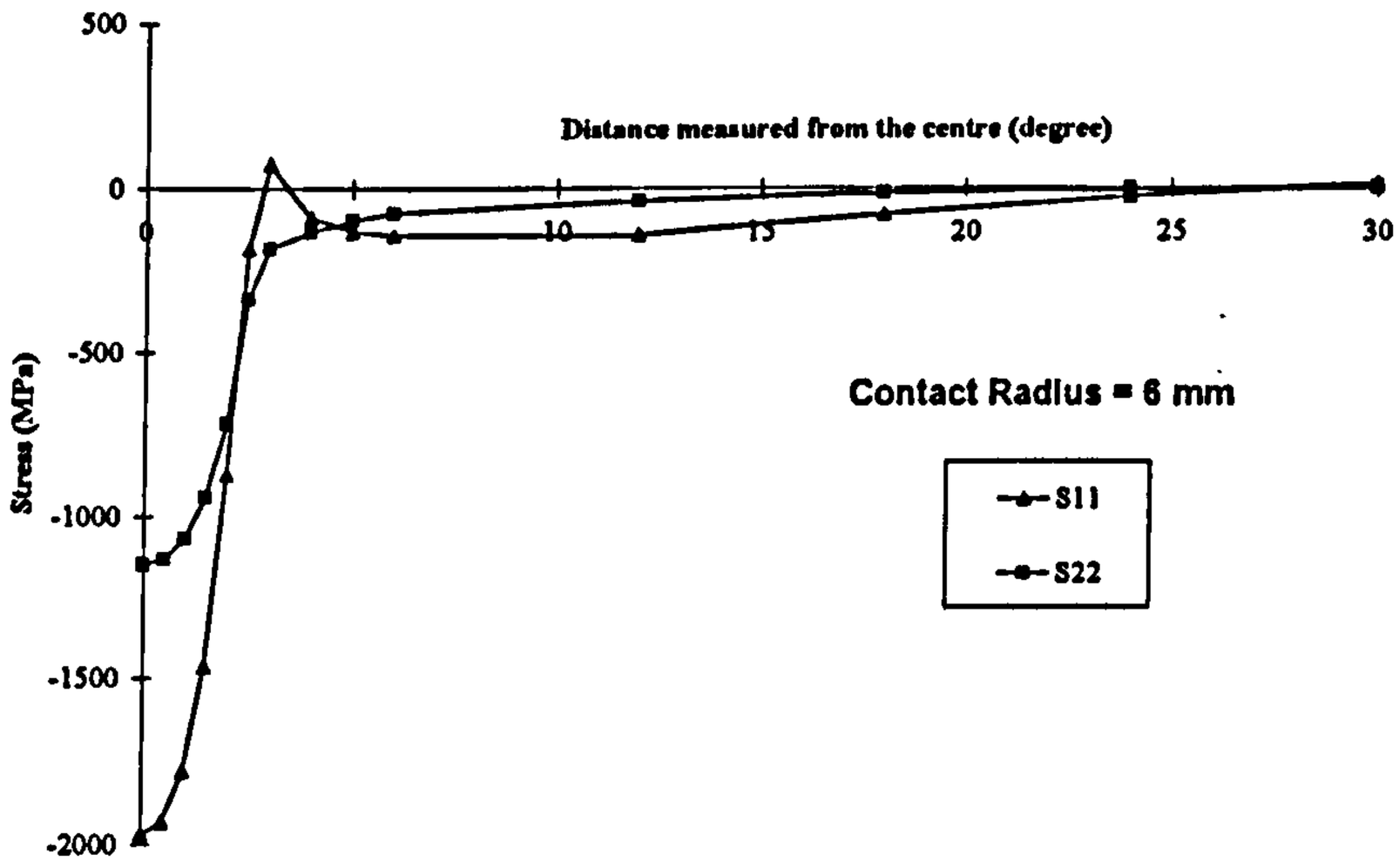

Fig 5.2.5 Stresses along the hoop direction (top surface)

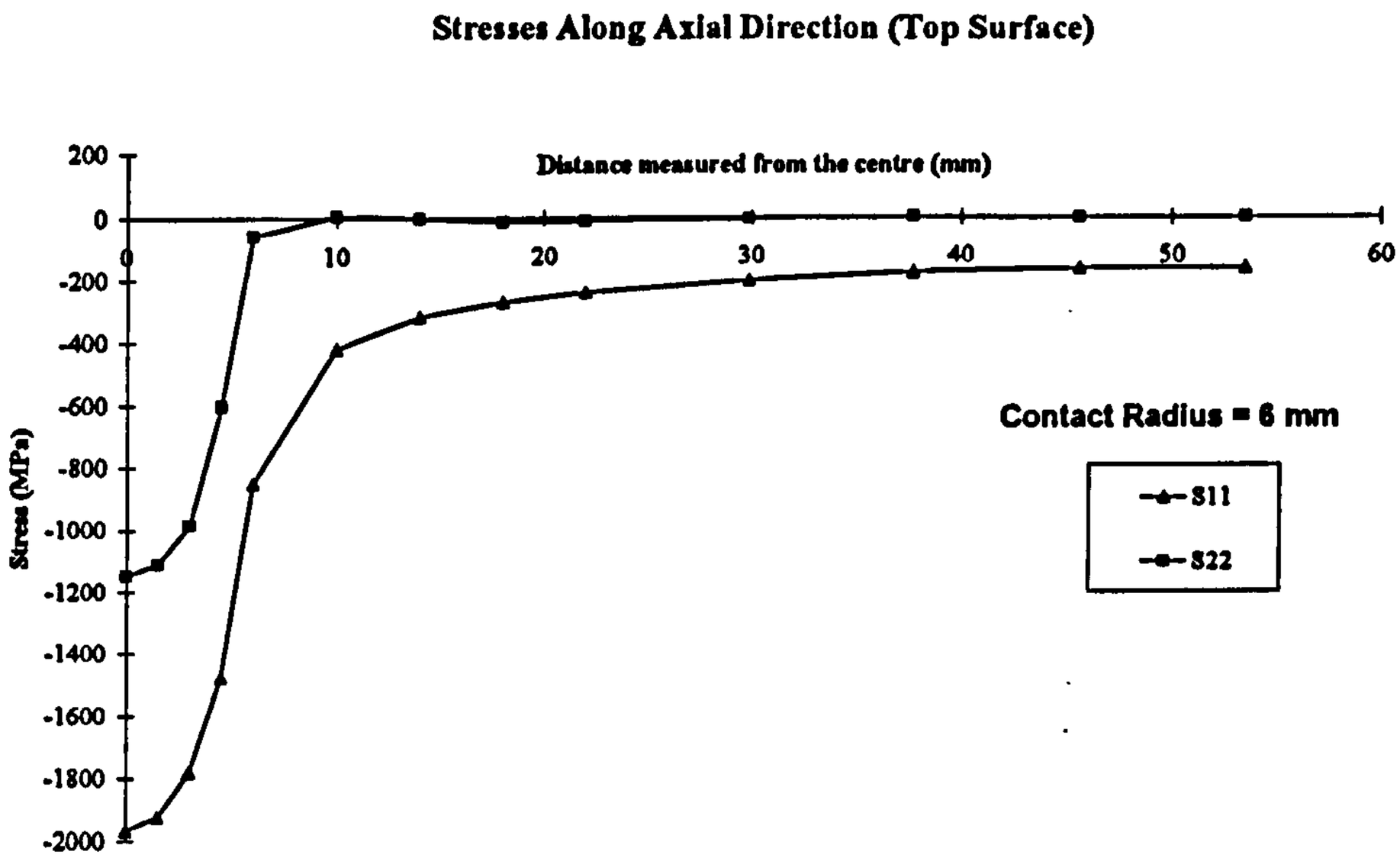

Fig 5.2.6 Stresses along the axial direction (top surface)

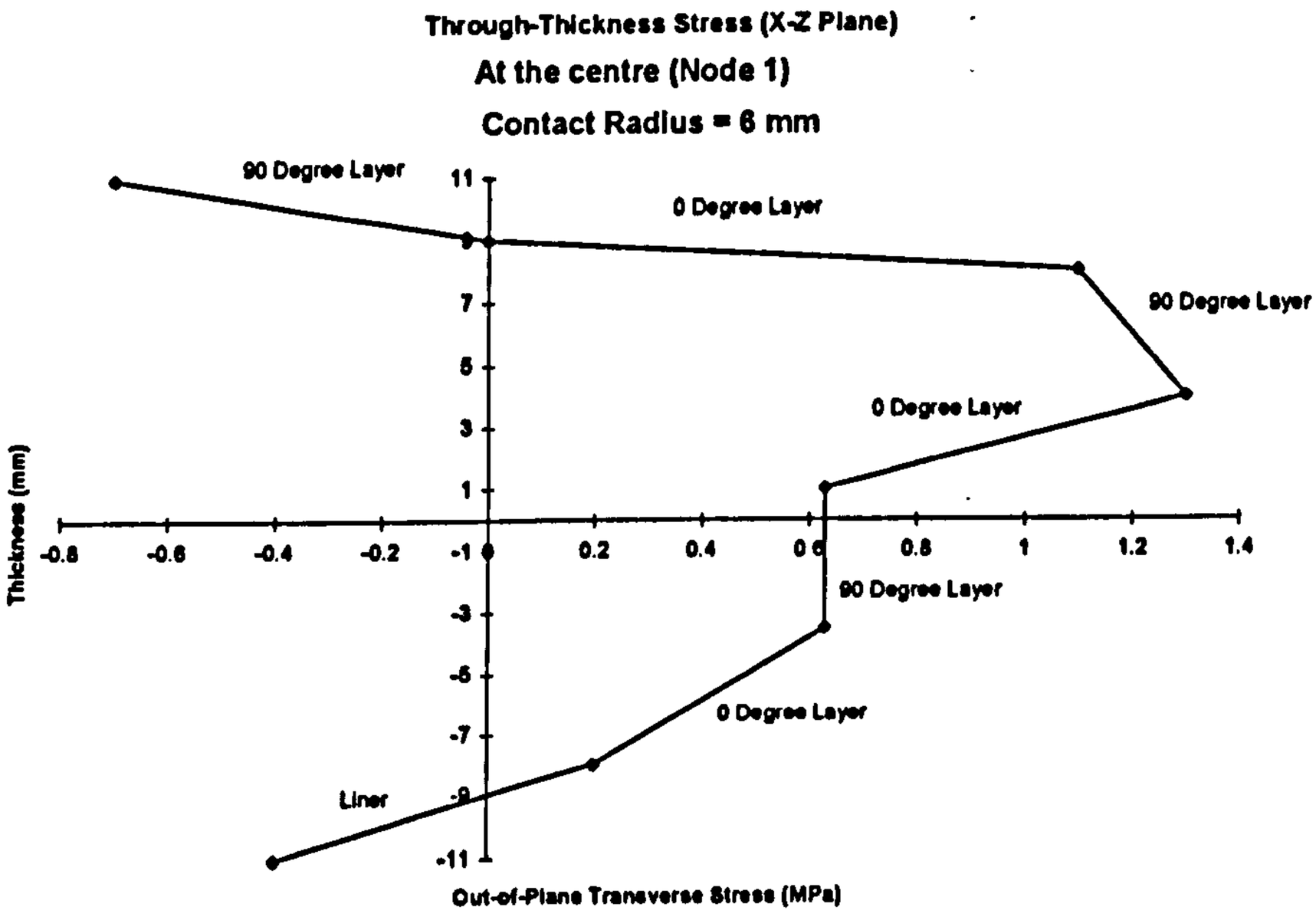

Fig 5.2.7 Through-thickness transverse shear stress on the X-Z plane at the reference point

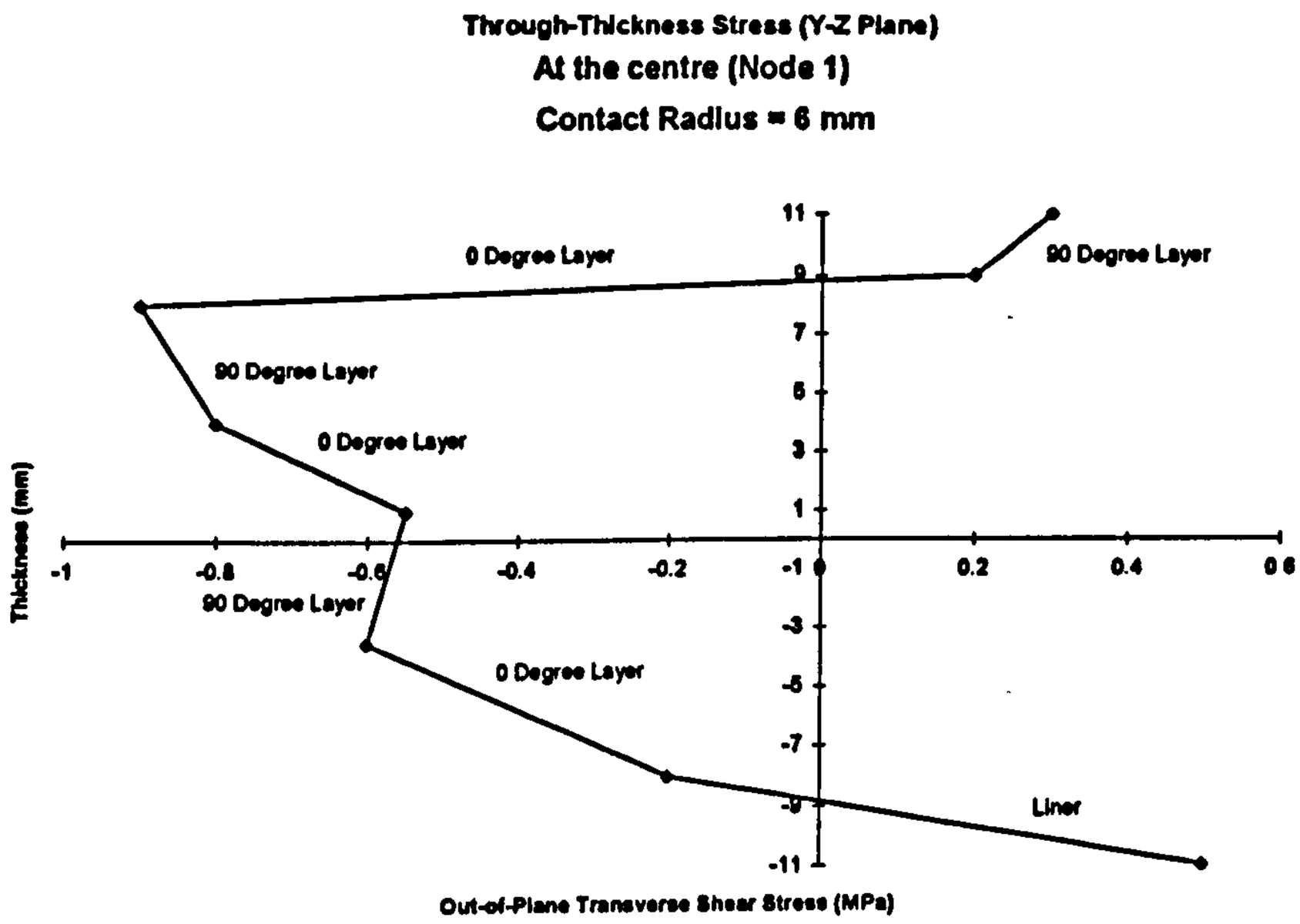

Fig 5.2.8 Through-thickness transverse shear stress on the Y-Z plane at the reference point

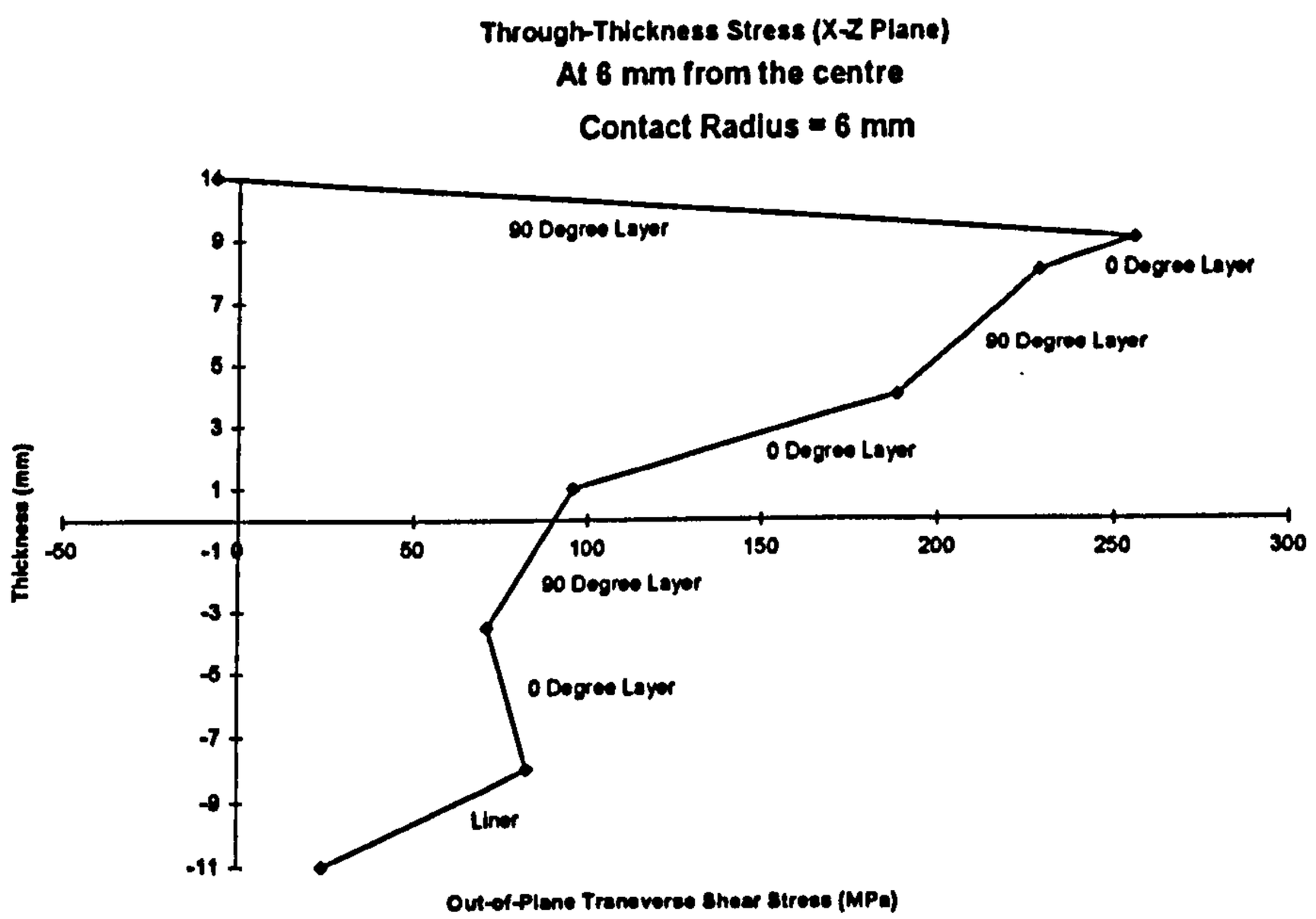

Fig 5.2.9 Through-thickness transverse shear stress on the X-Z plane at 6 mm from the reference point

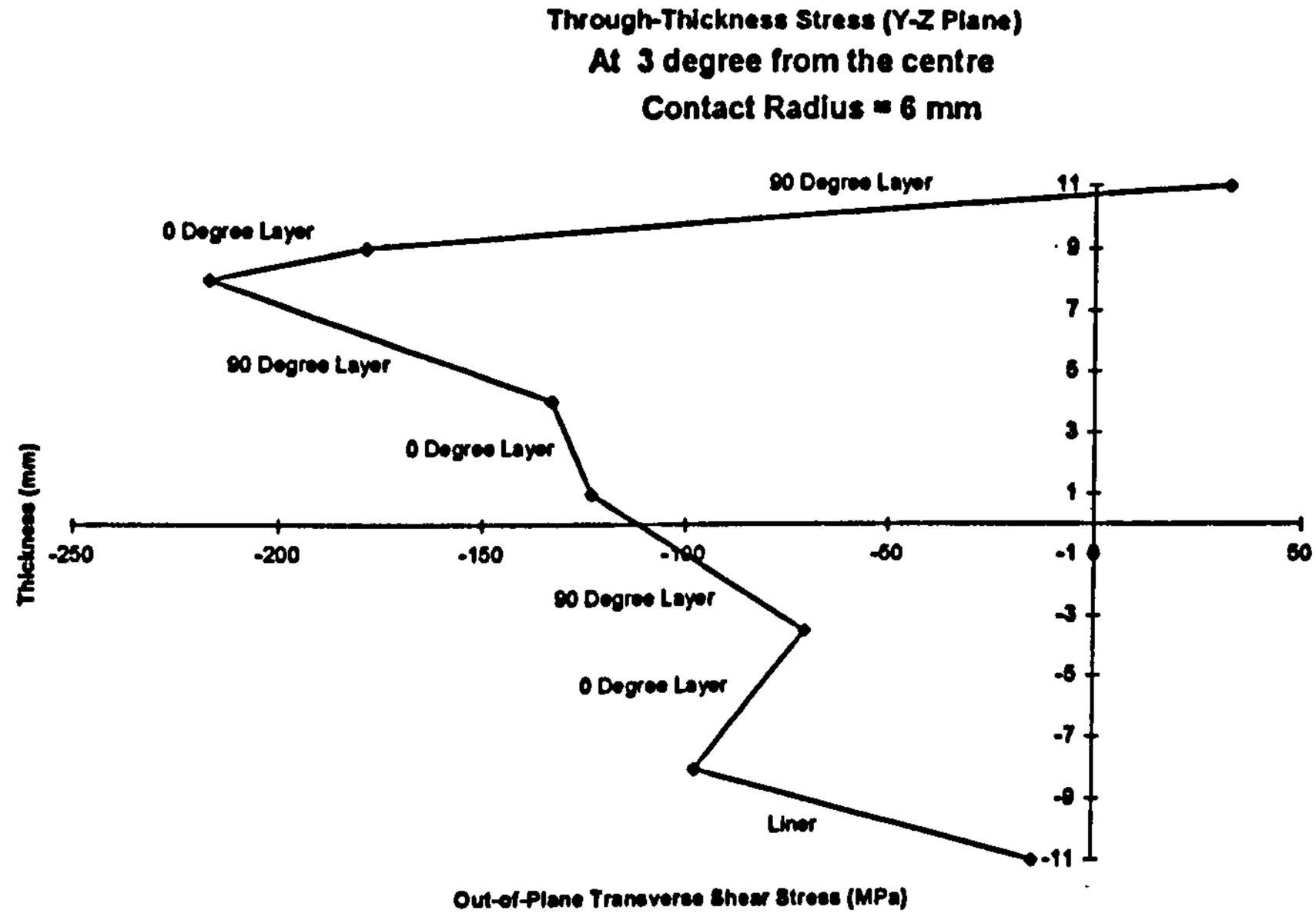

Fig 5.2.10 Through-thickness transverse shear stress on the Y-Z plane at 3° from the reference point

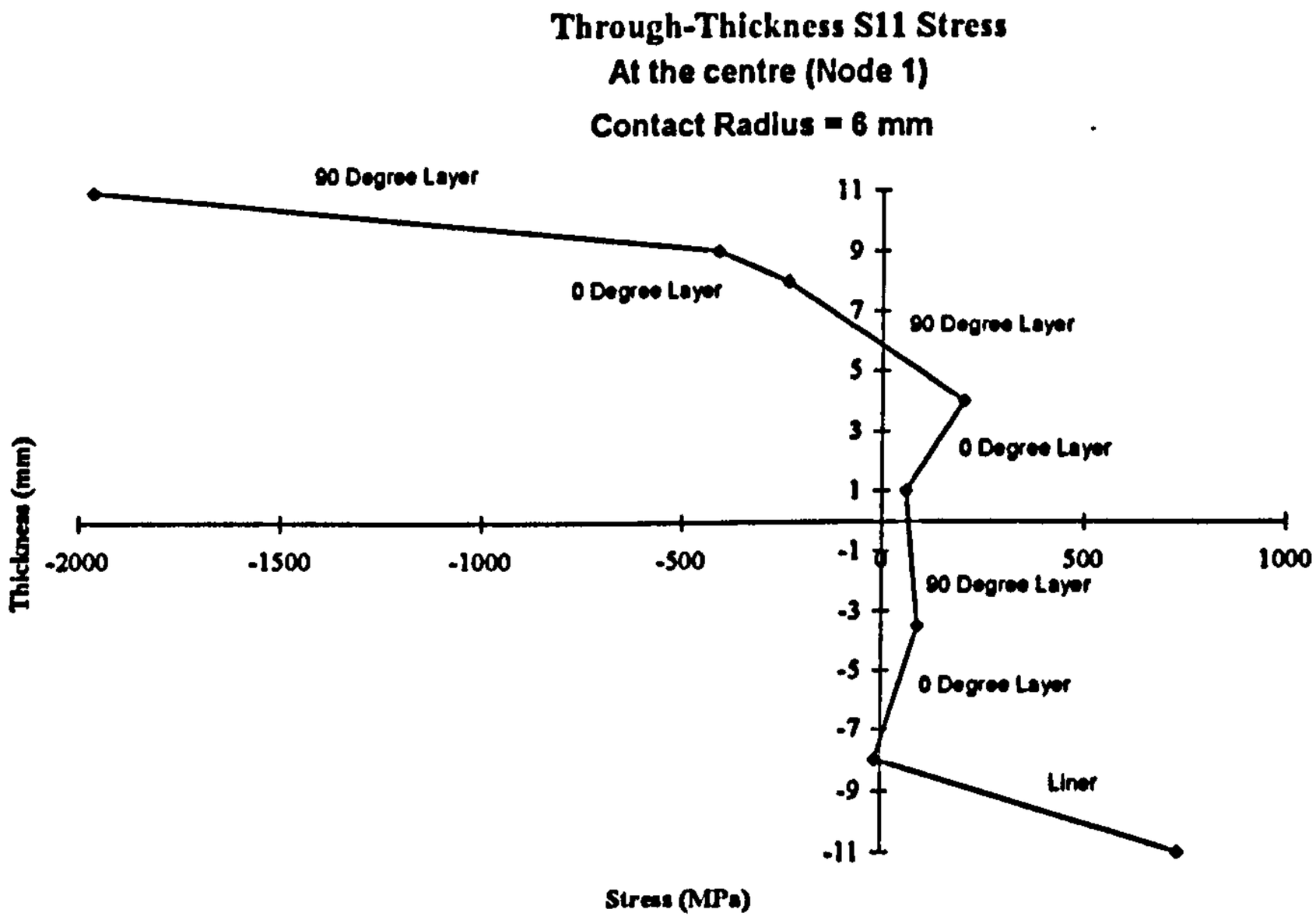

Fig 5.2.11 Through-thickness S11 stress at the reference point

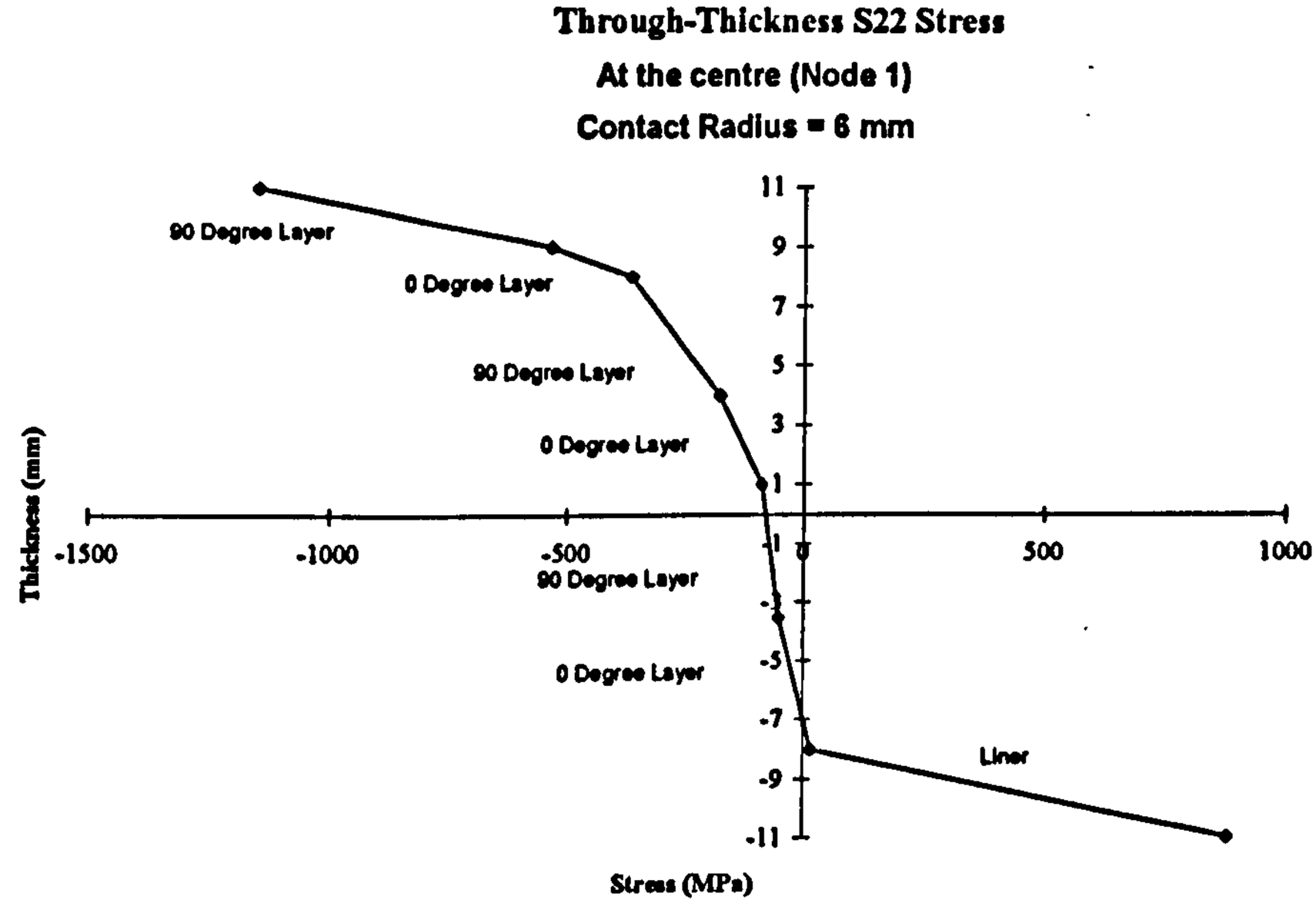

Fig 5.2.12 Through-thickness S22 stress at the reference point

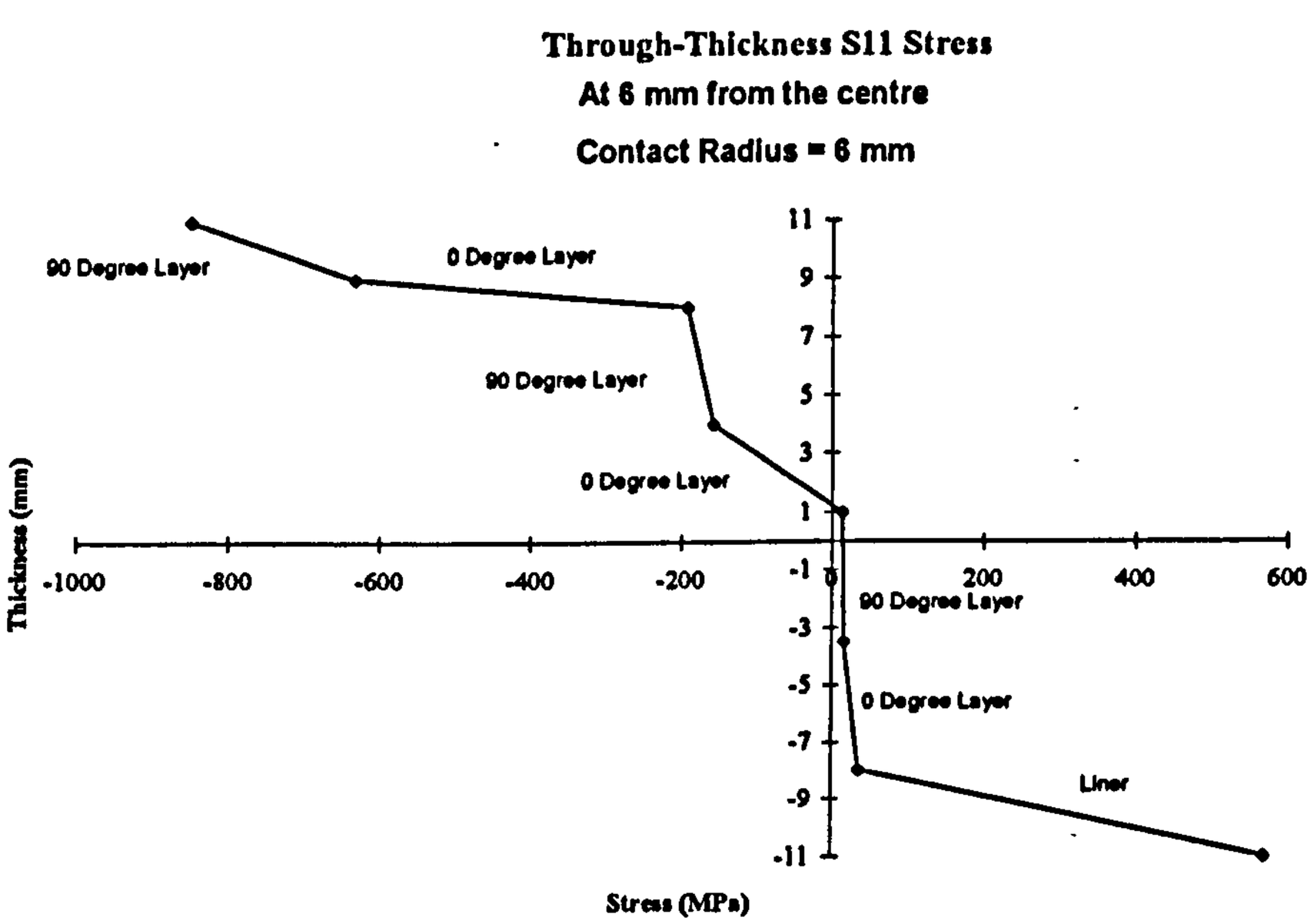

Fig 5.2.13 Through-thickness S11 stress at 6 mm from the reference point

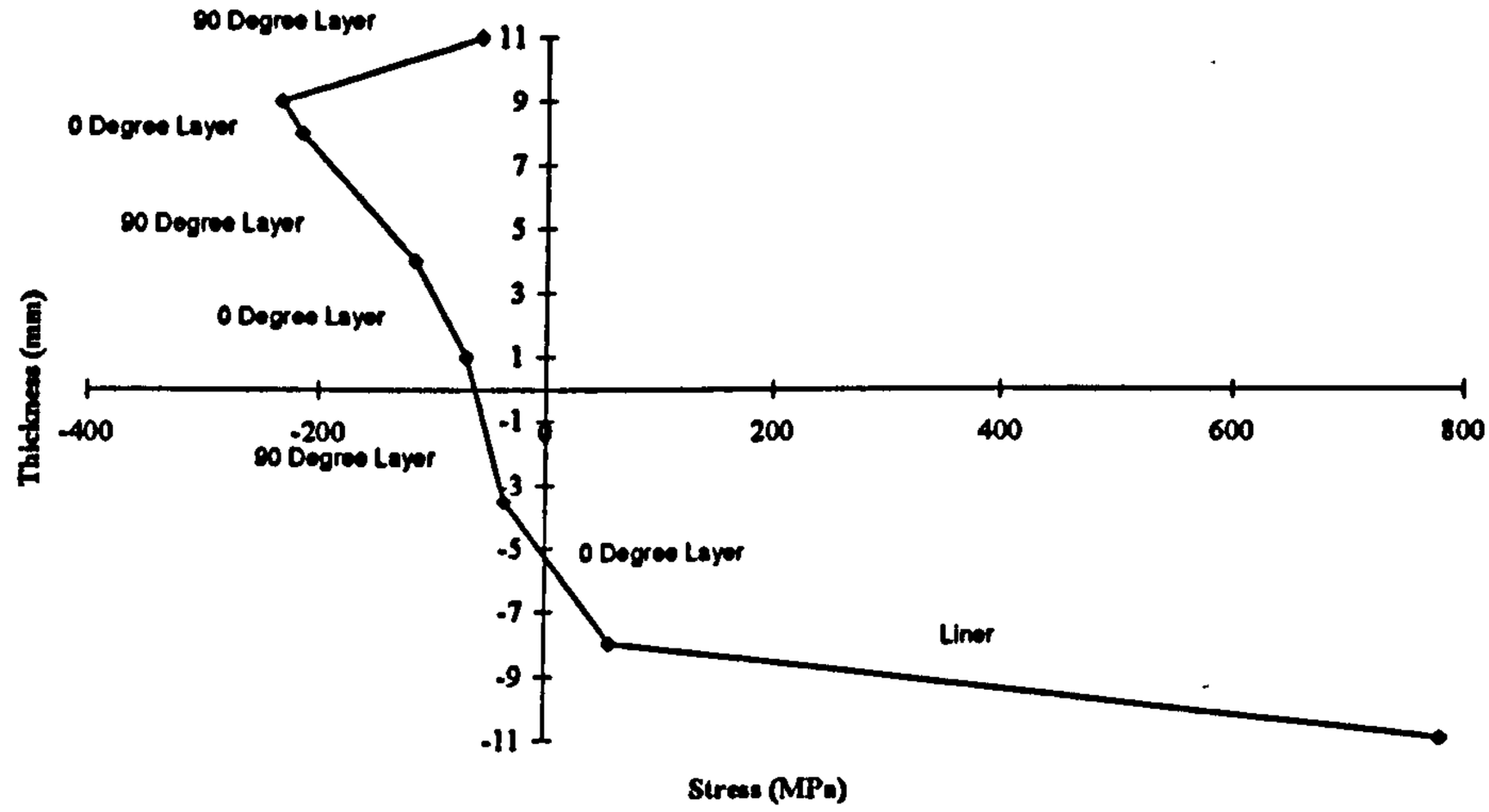

Fig 5.2.14 Through-thickness S22 stress at 6 mm from the reference point

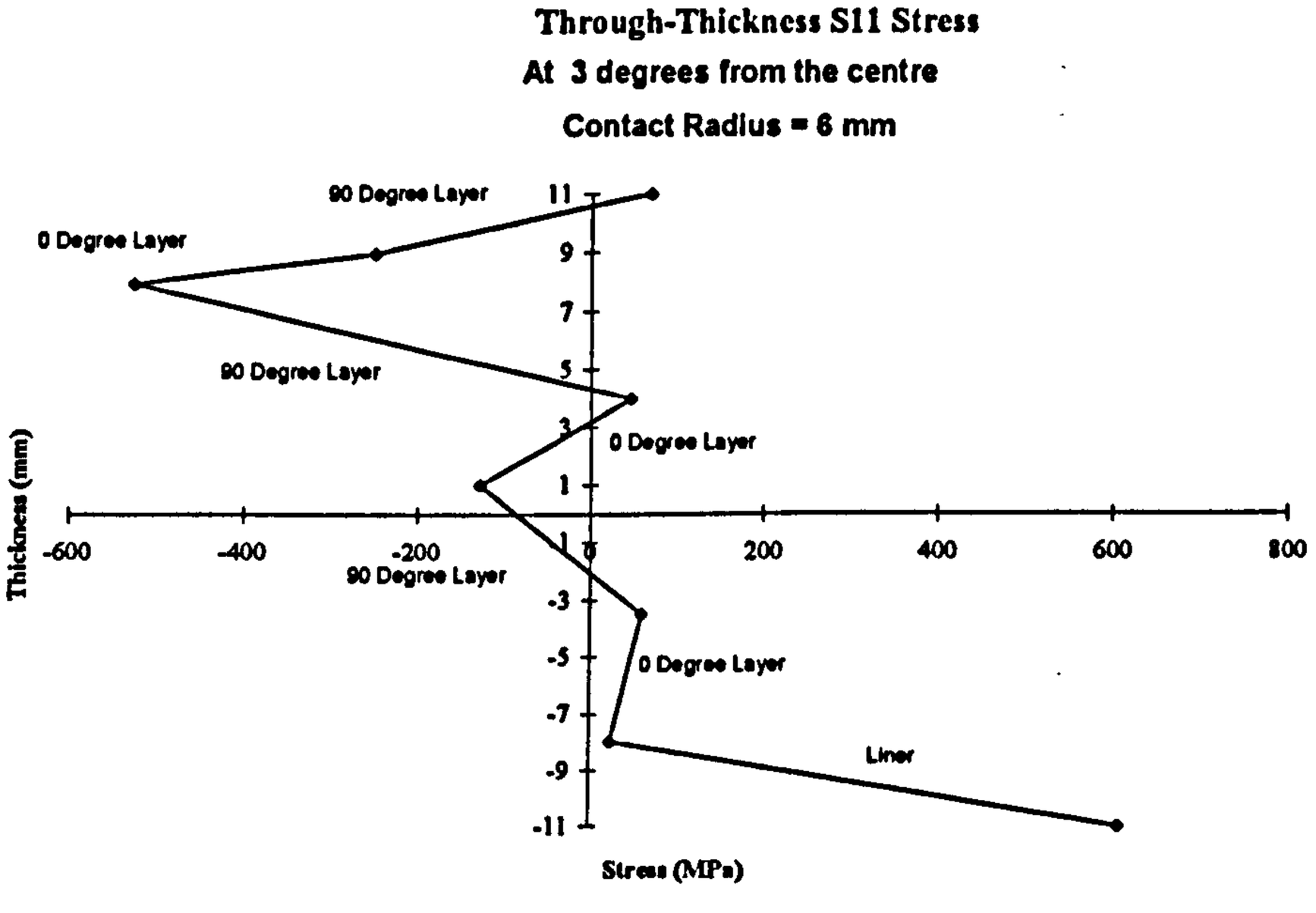

Fig 5.2.15 Through-thickness S11 stress at 3° from the reference point

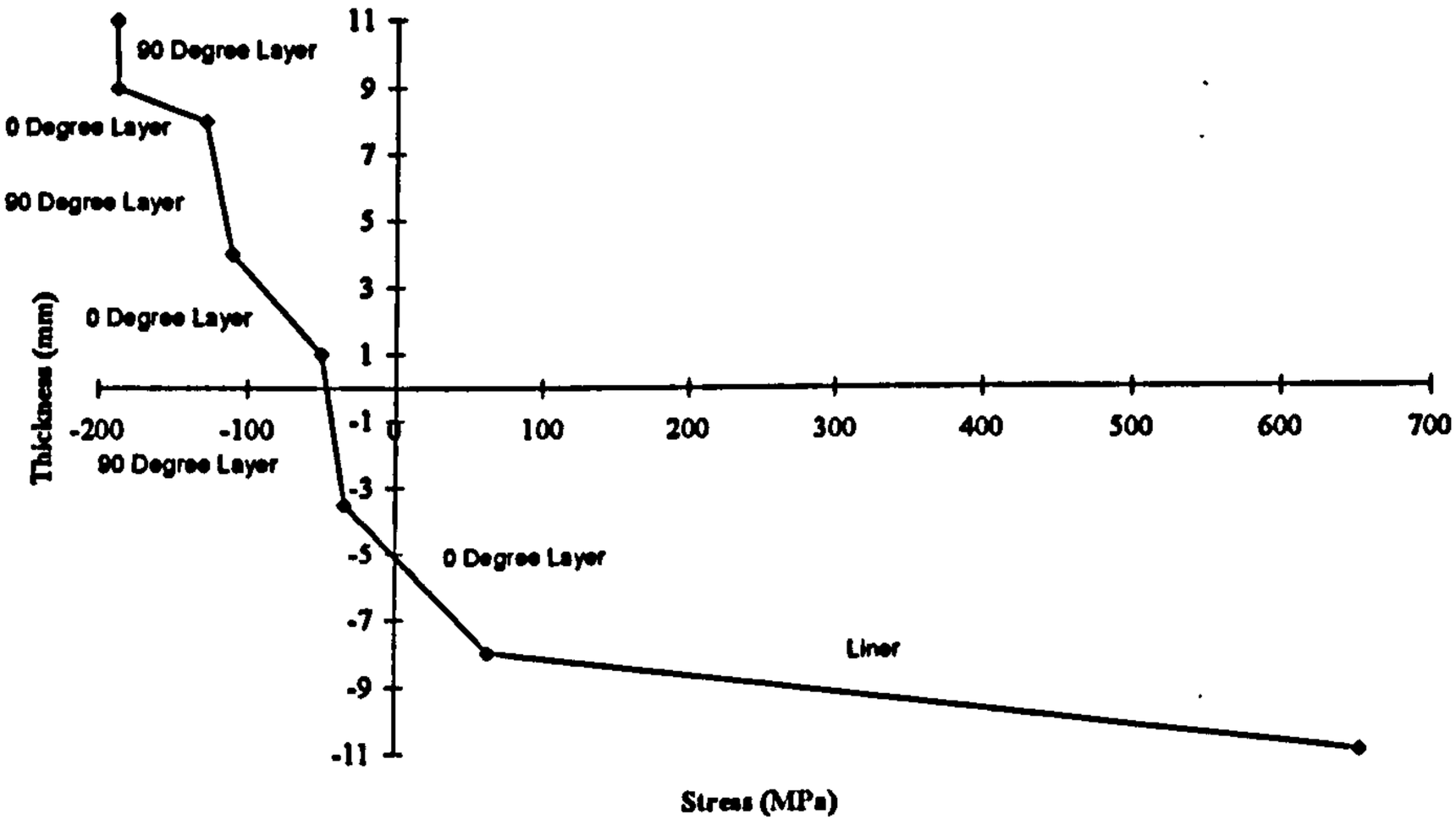

Fig 5.2.16 Through-thickness S22 stress at 3° from the reference point

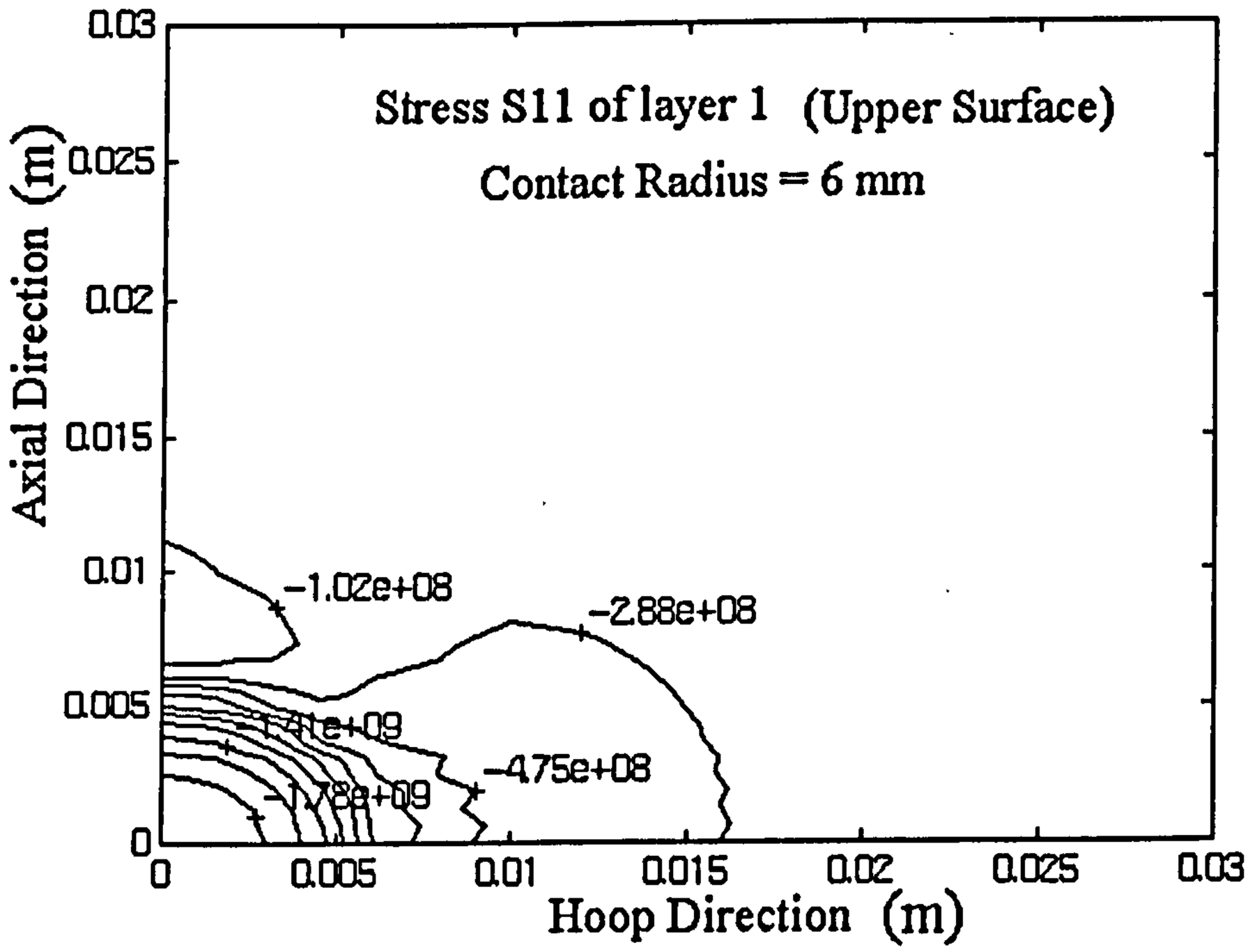

Fig 5.2.17 Stress contour plot of S11 of layer 1 (upper surface)

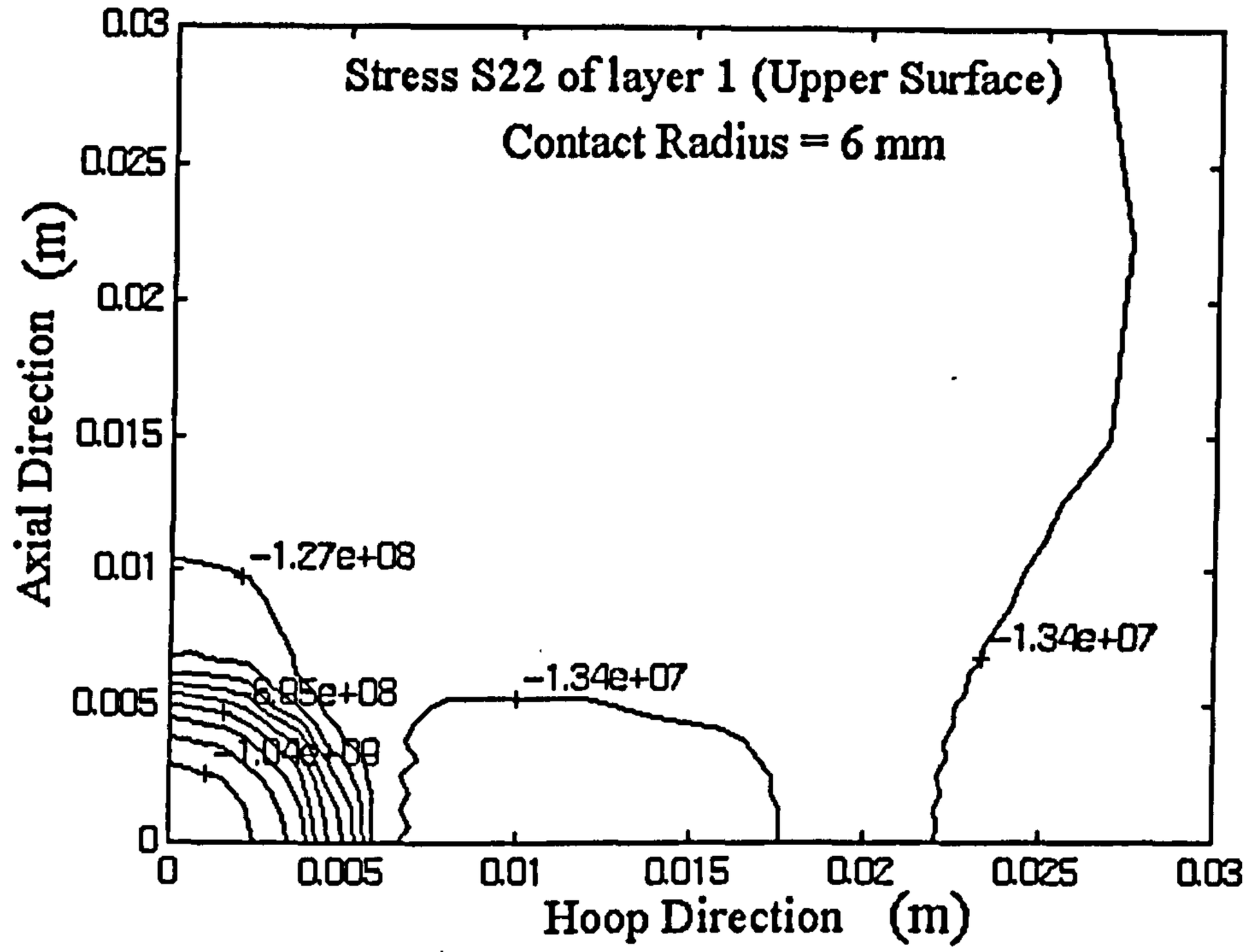

Fig 5.2.18 Stress contour plot of S22 of layer 1 (upper surface)

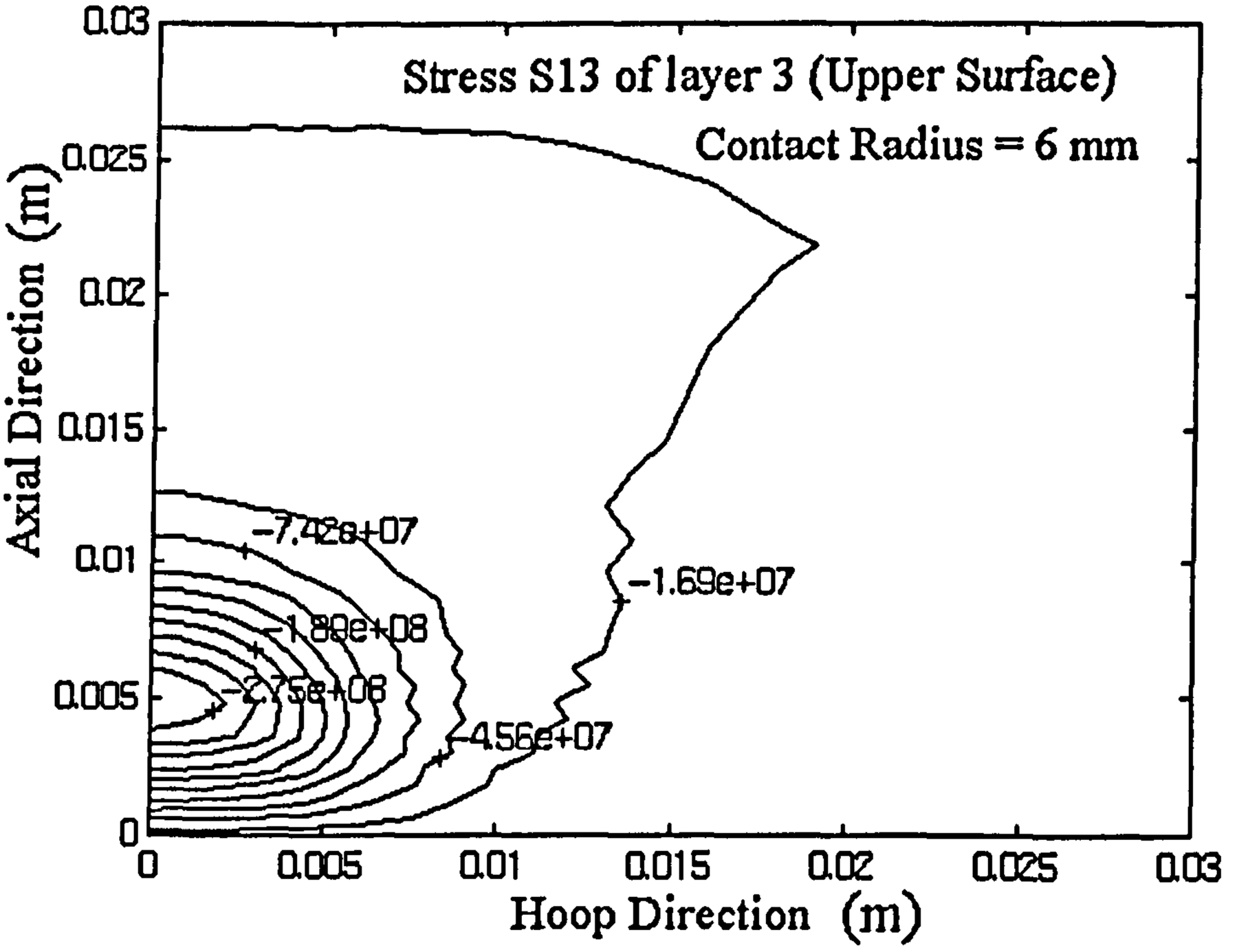

Fig 5.2.19 Stress contour plot of S13 of layer 3 (upper surface)

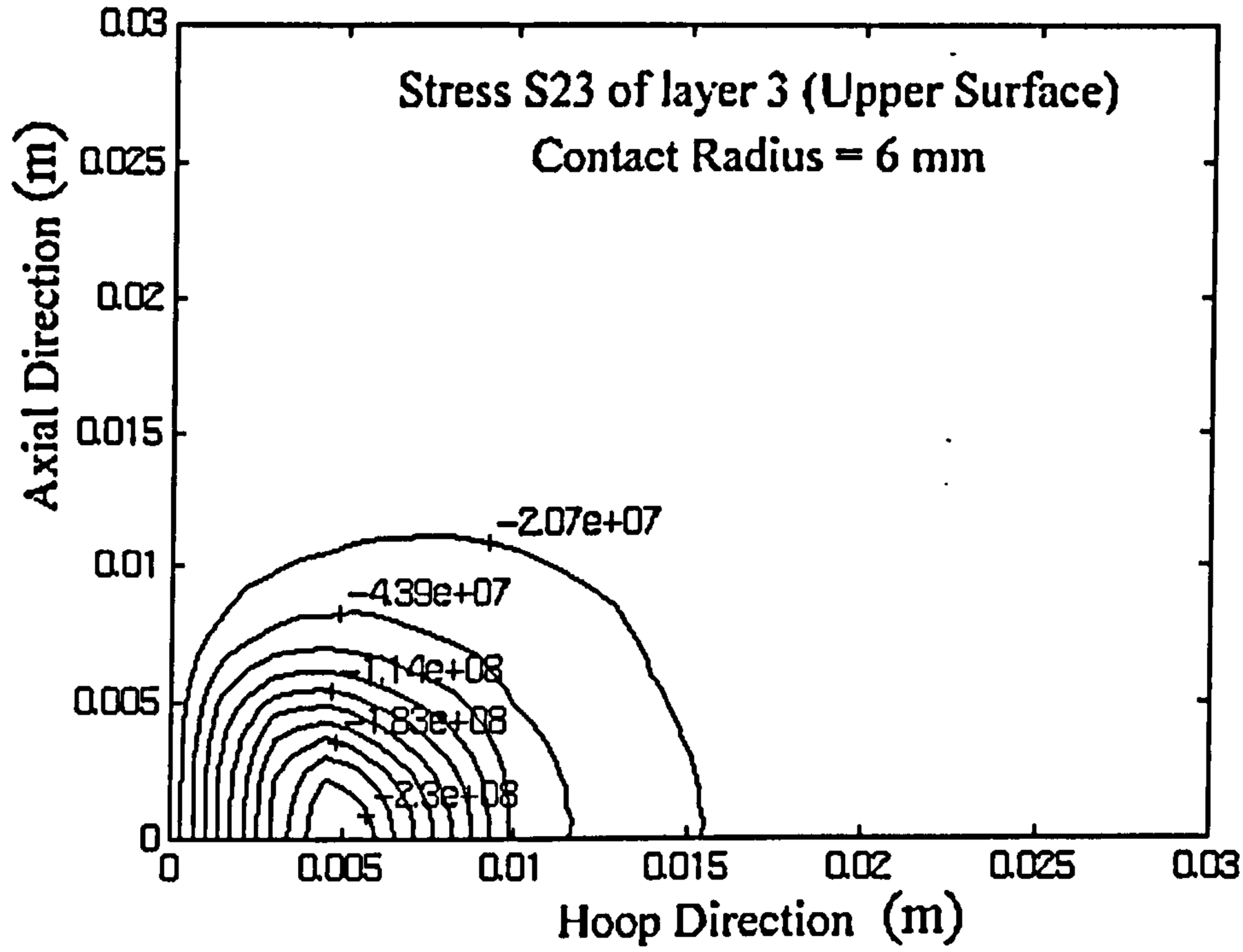

Fig 5.2.20 Stress contour plot of S23 of layer 3 (upper surface)

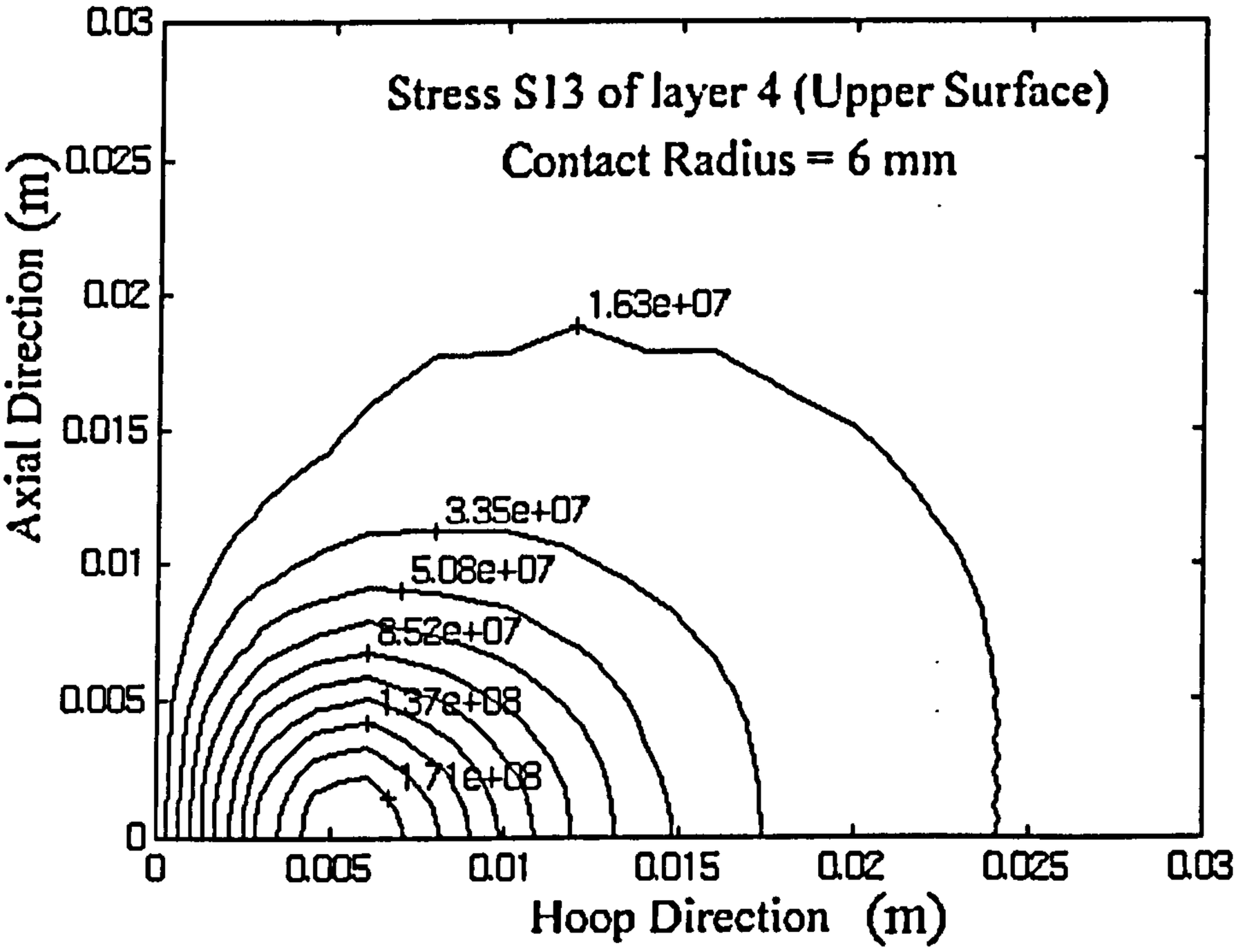

Fig 5.2.21 Stress contour plot of S13 of layer 4 (upper surface)

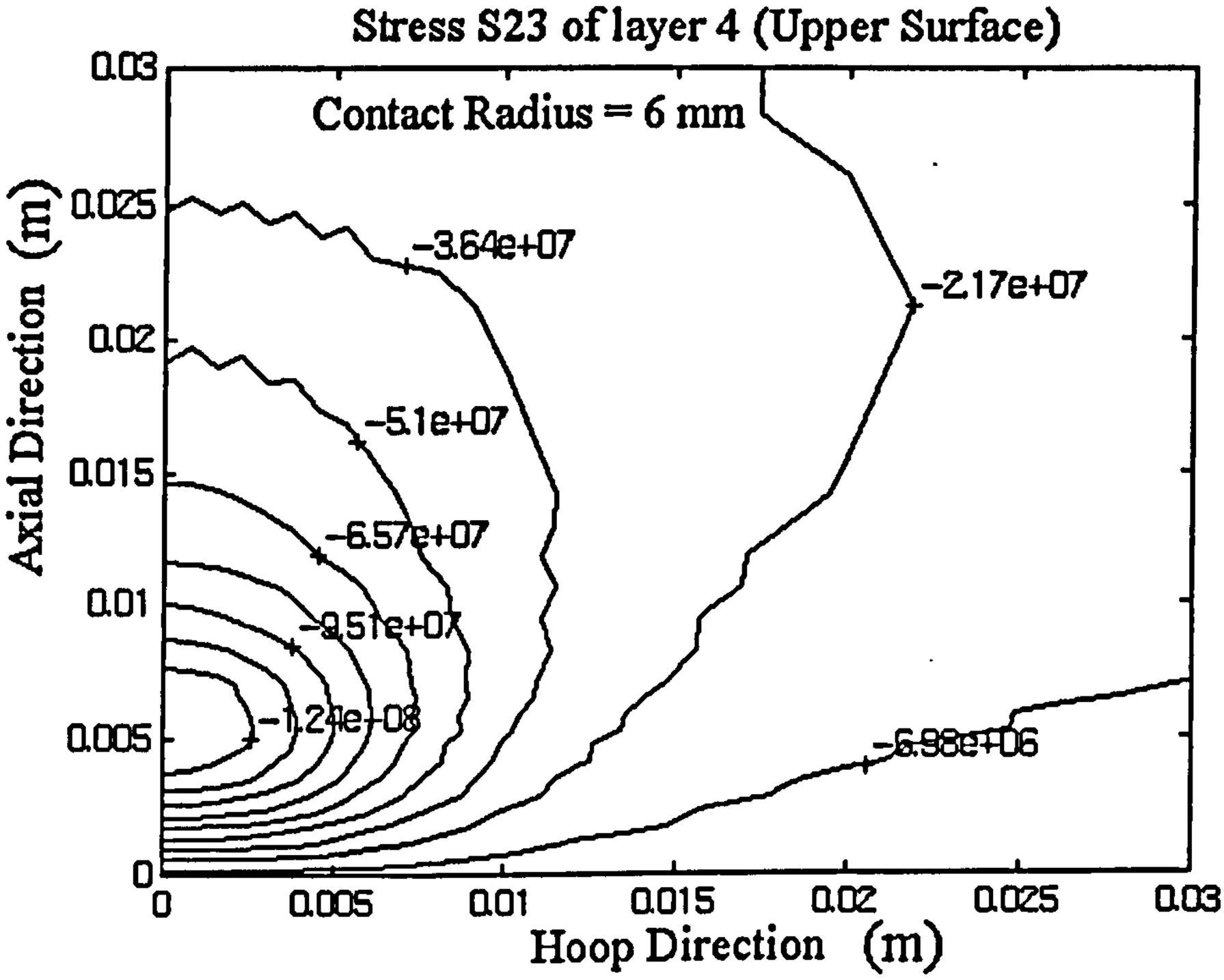

Fig 5.2.22 Stress contour plot of S23 of layer 4 (upper surface)

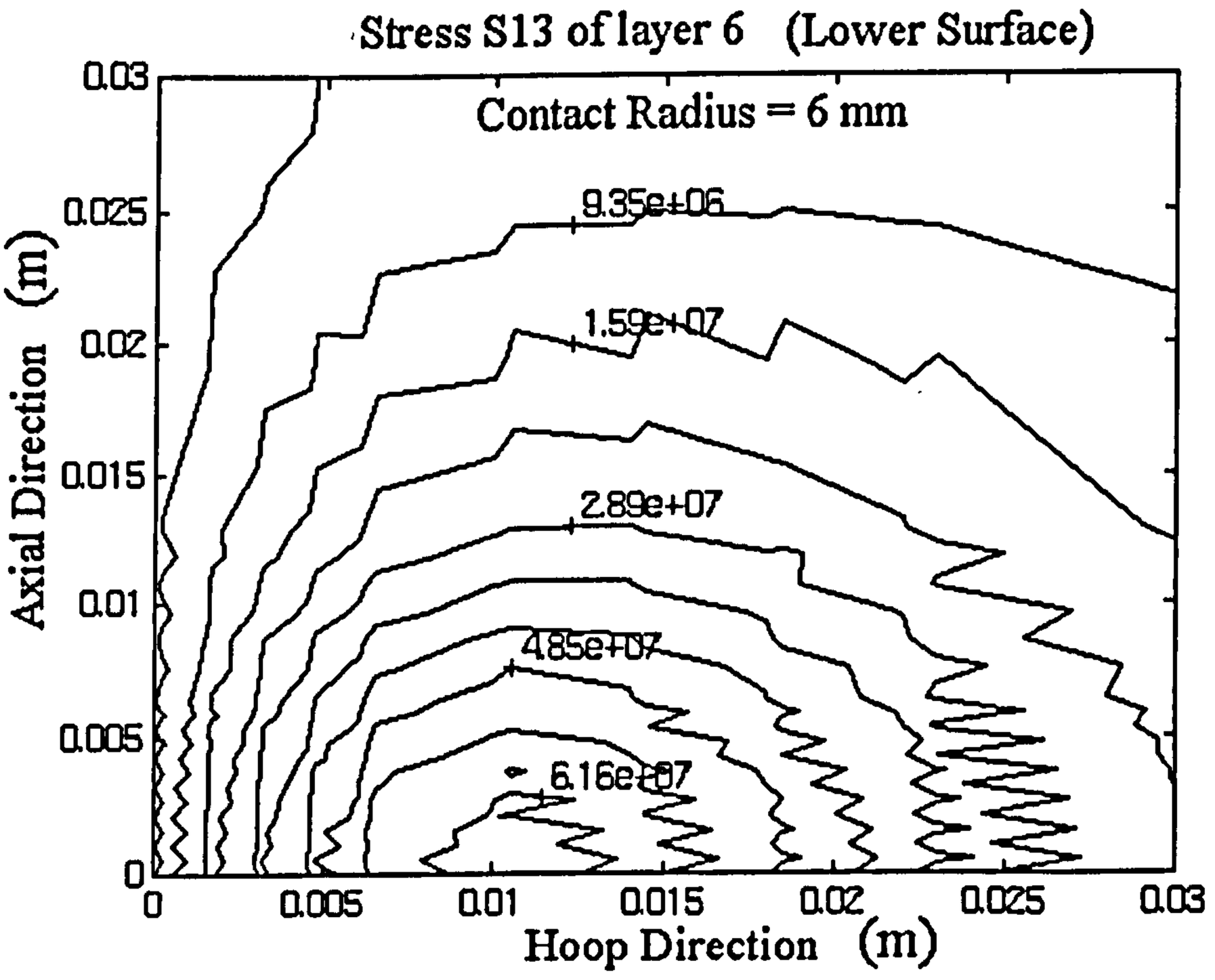

Fig 5.2.23 Stress contour plot of S13 of layer 6 (bottom surface)

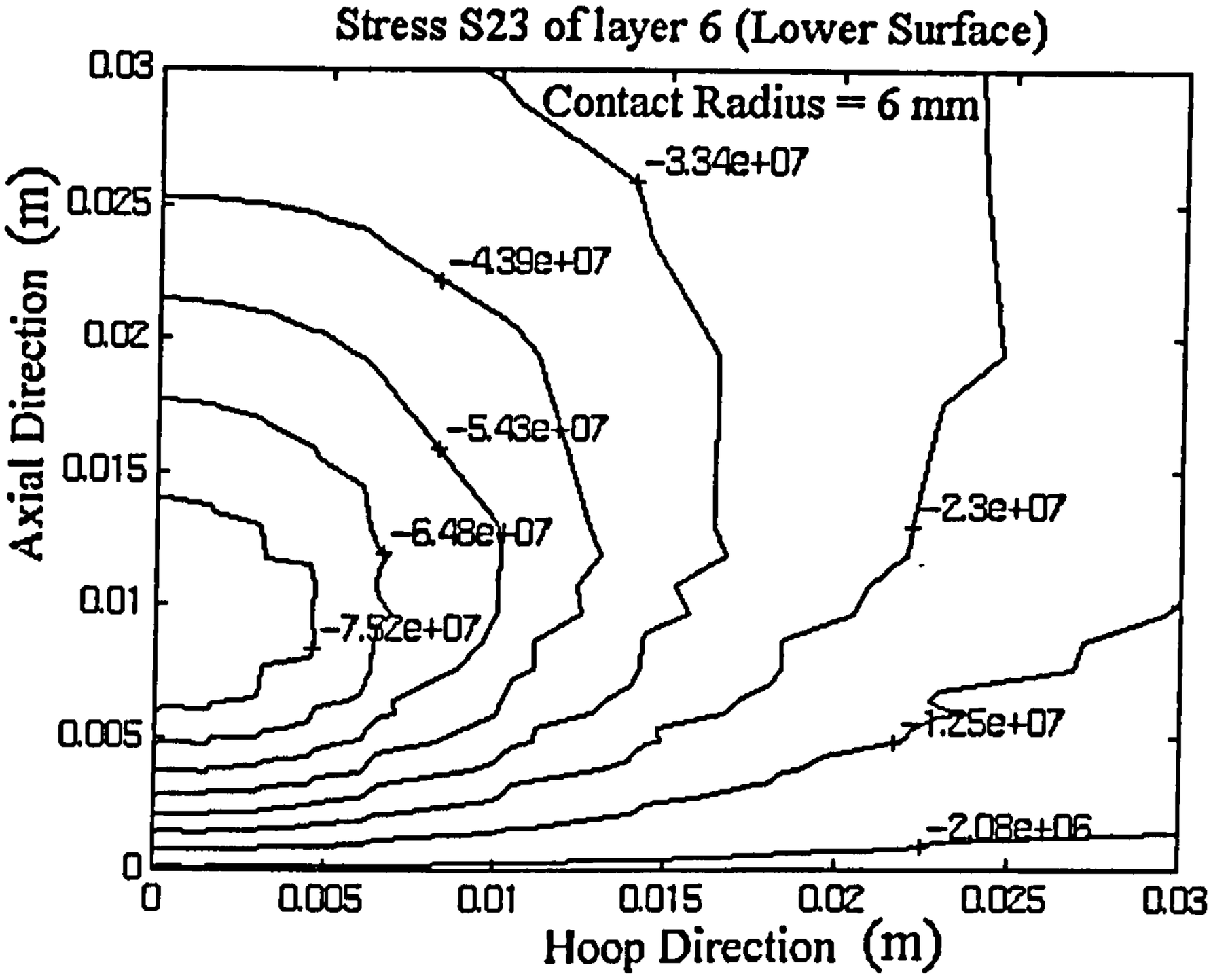

Fig 5.2.24 Stress contour plot of S23 of layer 6 (bottom surface)

5.2.2 The Effect of Contact Radius

Analytical theory of elastic contact (Hertz), as well as the experimental observation show that the contact area increases as the loading continues to increase. However, the present FE code does not have a facility to simulate this aspect of contact problem. In this section, a parametric study is undertaken in order to investigate the effect of contact radius on the structural response.

Three contact radii of 3 mm, 6 mm, and 12mm were used for pressure loading of the composite ring (see Section 5.2.1). A total force of 100 kN was used in all three cases. Thus, the pressure acting on the structure in each of these three cases was different. The modelling details are the same as given in Table 5.2.1.

The transverse displacements along the hoop direction are shown in Fig 5.2.25. The material is most severely compressed at the contact region in the case of loading over 3 mm contact radius. The behaviour is closest to that of a point indenter. For the case of 12 mm contact radius, global deflection of the composite ring was clearly the dominant response.

Contact stresses due to these three load cases are shown in Figs 5.2.26 and 5.2.29. For the case of the smallest contact radius, extremely high compressive stresses were induced at the contact site. Tensile surface stresses could be found at the distance of one contact radius. This effect is the origin of the so-called Hertzian contact cracking phenomenon, in which fracture initiates from the perimeter of the contact region.

Out-of-plane transverse shear stresses on the X-Z plane at a distance of 6 mm from the centre of contact are given in Fig 5.2.30. In general, the shear stress distribution profiles for these three cases are quite similar. However, the location of the peak stress is different. In the cases of both the largest and the smallest contact radii the predicted peak is located at the upper surface of the forth layer, while it lies at the upper surface of the second layer for the case of 6 mm contact radius.

In general, the contact radius used in the application of loading has a significant effect on the stress state induced by the contact. Penetration of material may be possible under contact loading over a small contact area. For the loading on a large contact area, global deflection of the composite ring becomes the dominant response. In view of these differences in response, it is important to be careful in selecting the appropriate contact radius in the analysis. Different failure modes may result under different conditions, so that experimental confirmation appears necessary.

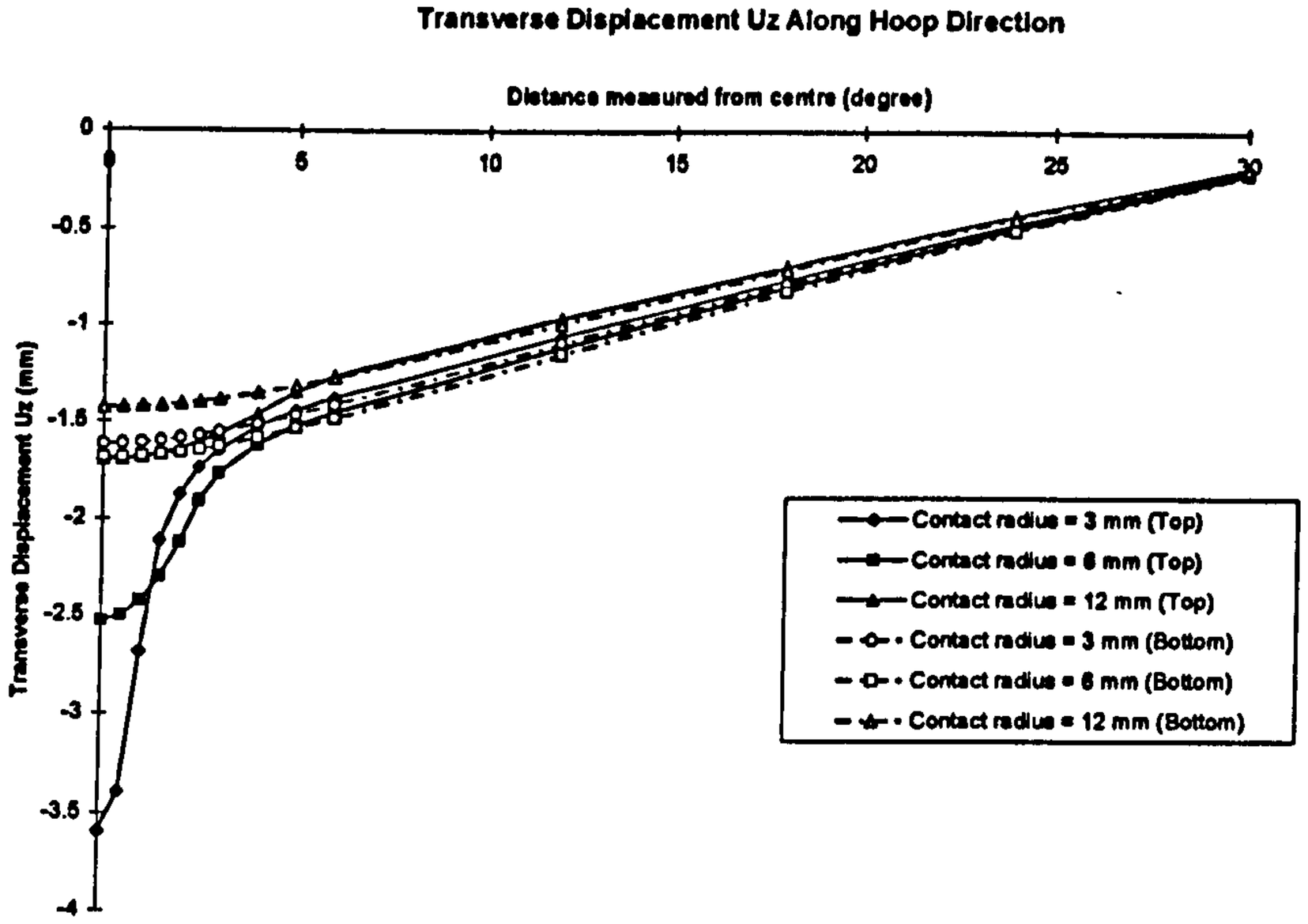

Fig 5.2.25 Transverse displacement along the hoop direction

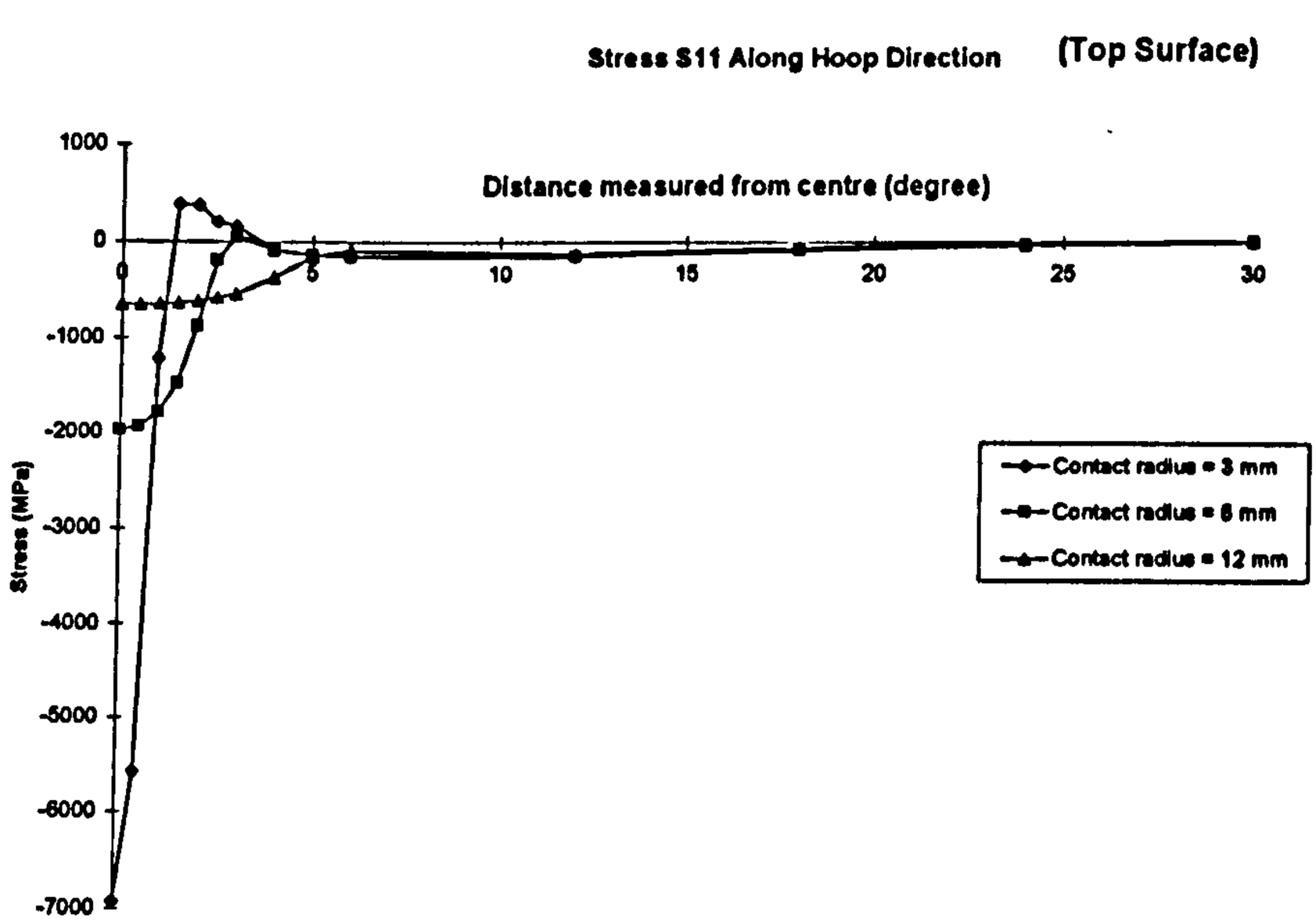

Fig 5.2.26 Stress S11 along the hoop direction (top surface)

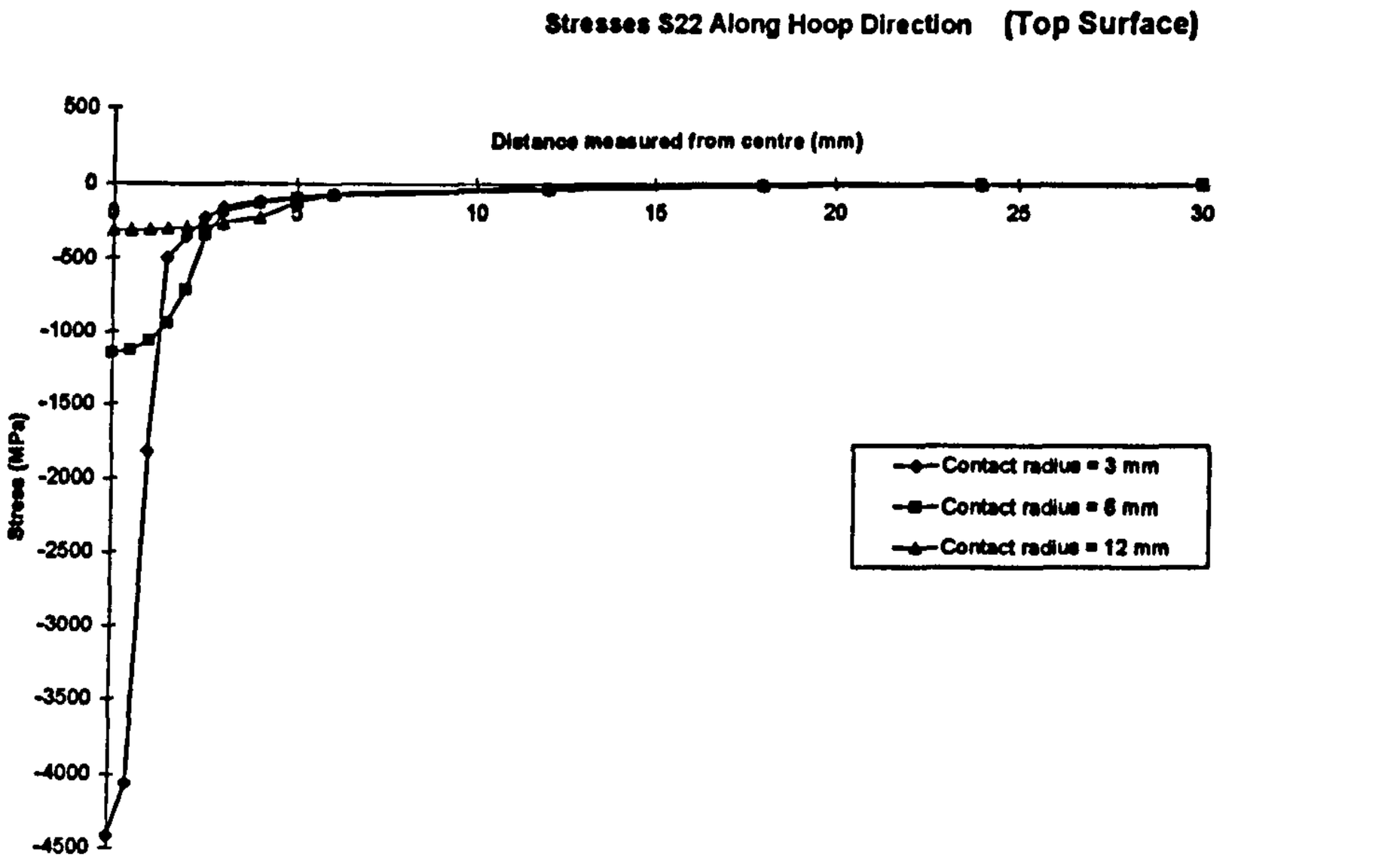

Fig 5.2.27 Stresses S22 along the hoop direction (top surface)

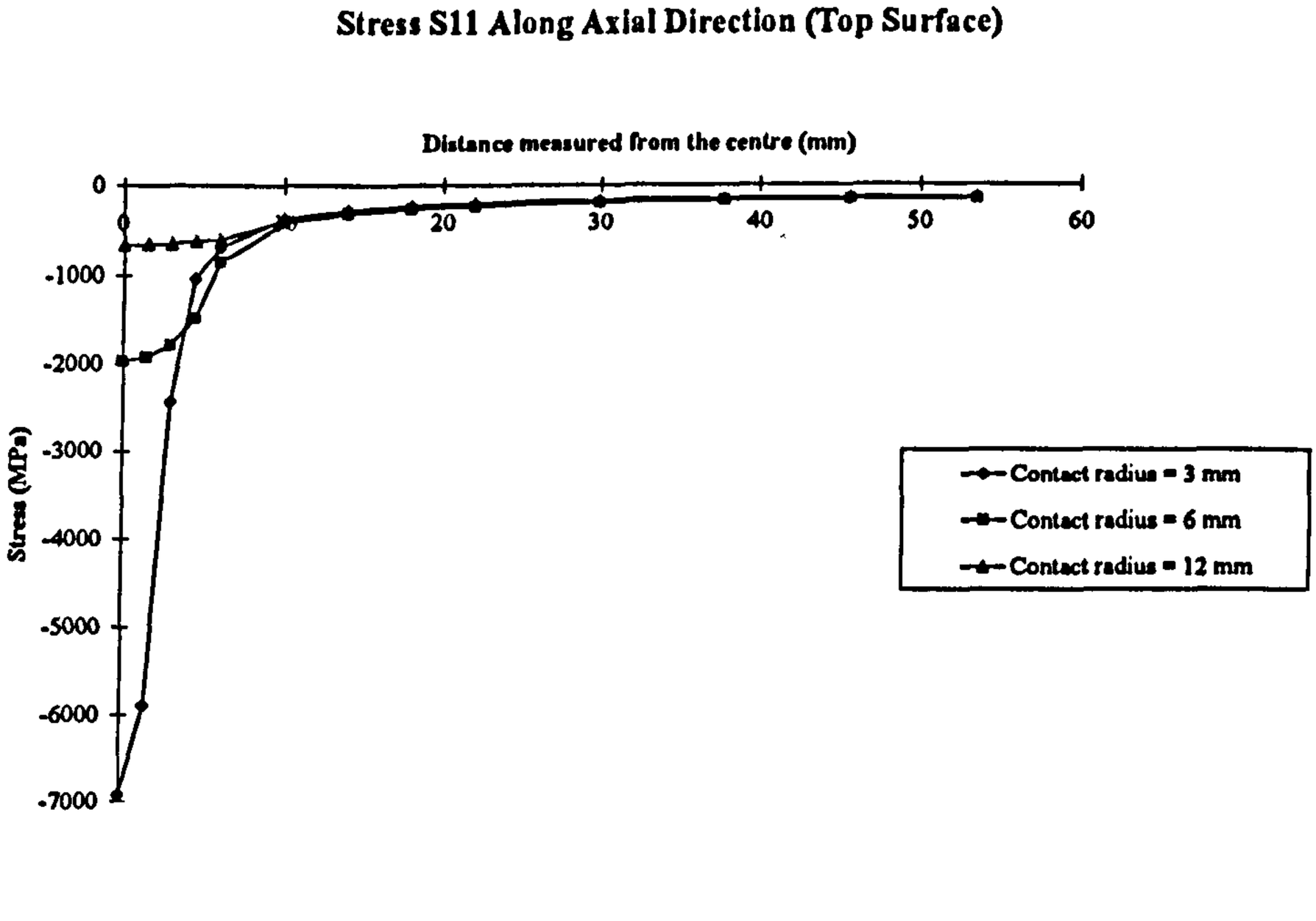

Fig 5.2.28 Stress S11 along axial direction (top surface)

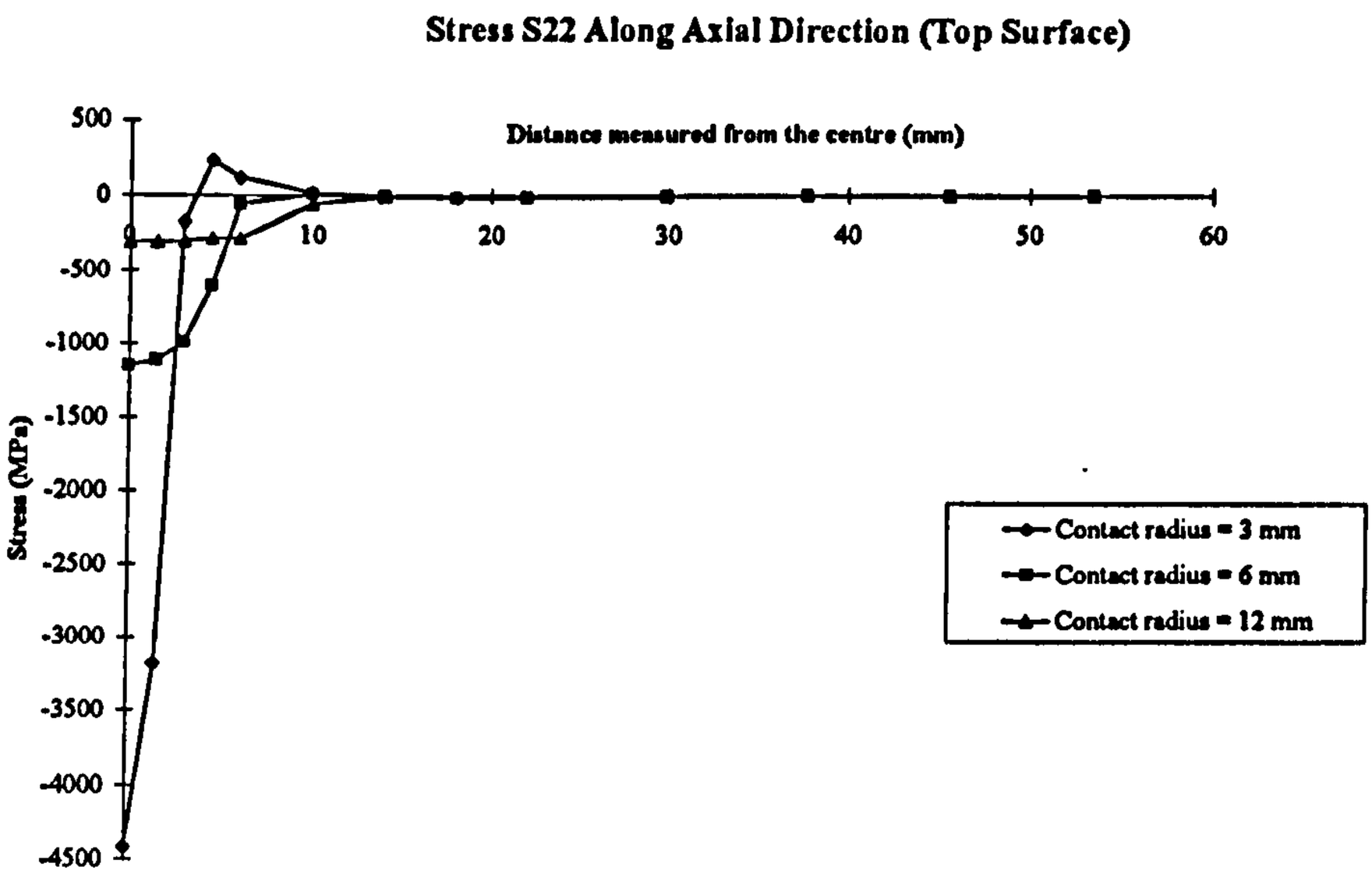

Fig 5.2.29 Stress S22 along axial direction (top surface)

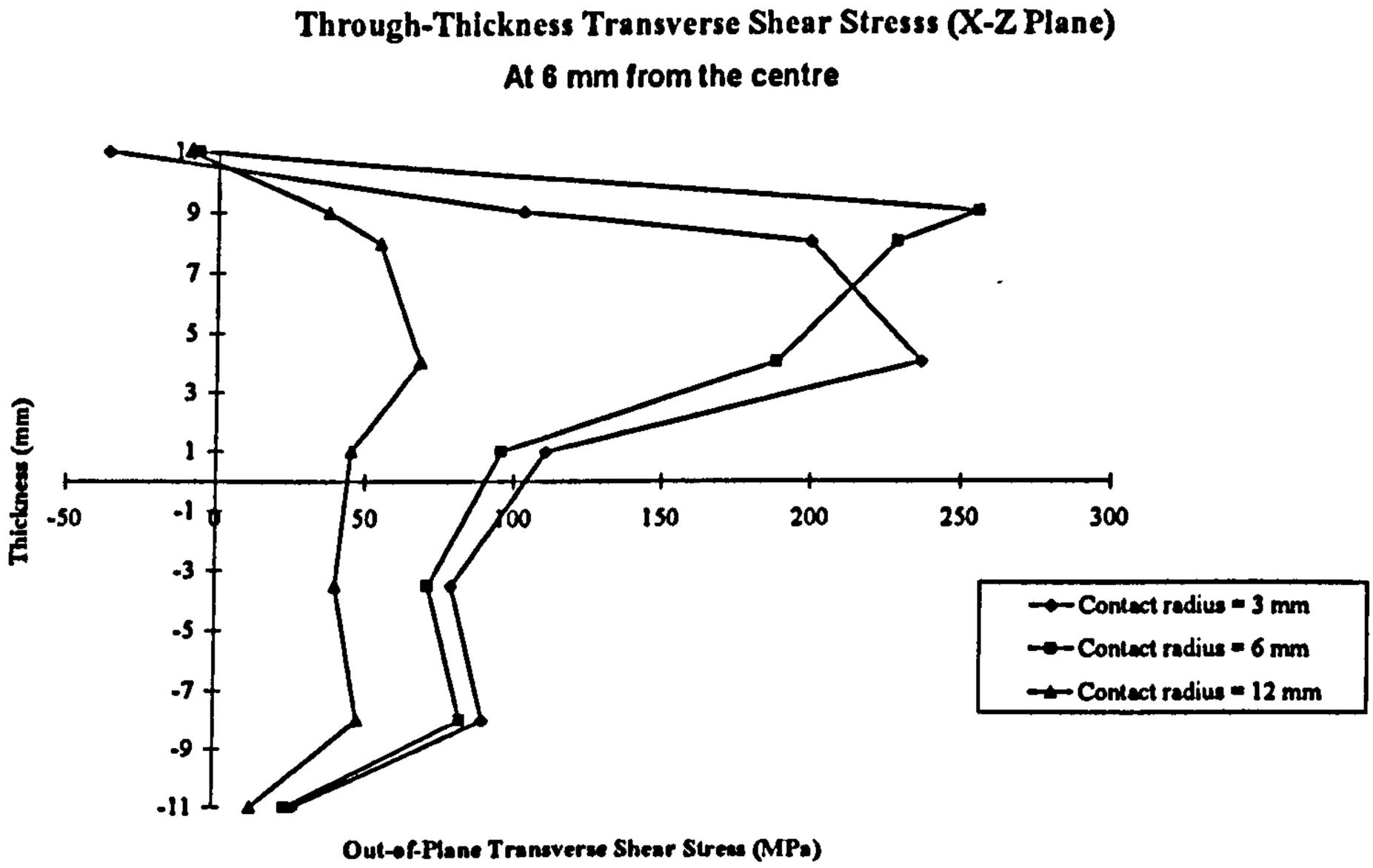

Fig 5.2.30 Through-thickness transverse shear stress on X-Z plane at 6 mm from the centre

Chapter 6 Strength Analysis

Deformation and stresses due to impact were investigated in the previous chapters. The stresses may result in failure zones which may continuously extend and multiply in the course of an impact event, or under repeated impact. They can, finally, occupy a significant fraction of the through-thickness section and lead to a reduction of a cylinder's load bearing capacity.

In this chapter, the main attention is paid to the methods and results of calculating the damage and initial failure of a composite cylinder under low velocity impact loading. Based on this evaluation of damage and the subsequent strength analysis, a general approach is established for a better understanding of the effect impact on the behaviour of a composite cylinder.

6.1 Solution Approaches

An analytical solution approach based on Fourier-series expansion of the cylinder equilibrium equations, coupled with the Laplace transform techniques to solve the dynamics problem has been described in Section 3.1.2. This approach, however, cannot yield full information about the through-thickness stress and strain distribution, which are required for strength analysis. The reason for this limitation is that it depends on averaging procedures for calculating the through-thickness stresses and strains. The method, however, allows one to evaluate the deflection and strain histories at any point in the shell structure. Criteria for strength analysis which can be employed in conjunction with this approach must be based on the maximum allowable strain or maximum stress theory, $f(\varepsilon)$ or $f(\sigma)$ = Constant.

The finite element approach using thick shell element which was used in dynamic analysis can overcome part of the limitation. However, this type of element only gives averaged out-of-plane shear stresses which are not sufficient for reliable prediction of

delamination. It can nevertheless be used to predict fibre breakage and matrix cracking in this study by using the failure criteria proposed by Hashin (1980) (see Table 6.1).

In order to obtain the solution of the complete set of equations of three dimensional elasticity, a suitable approach is the use of three dimensional finite element formulation. This approach was used for static analysis in this study. However, three dimensional finite element analyses are not well suited to laminate analysis, especially when the number of laminae is large, because of the need to have a sufficient number of elements in the through-thickness direction combined with the undesirability of using finite elements with high aspect ratios. These restrictions lead to the requirement of fine meshes consisting of many elements, and hence to computationally expensive solutions. The situation becomes even worse for dynamic analysis. However, when a full three dimensional state of stress is obtained, all of the three major failure modes (fibre breakage, matrix cracking and delamination) can be examined. The failure criteria used for predicting fibre breakage and matrix cracking are the same as for the thick shell element, in conjunction with the criterion for delamination proposed by Chang and Springer (1986) (see Table 6.1).

Table 6.1 Failure mode identification criteria proposed by Hashin (1980) and Chang and Springer (1986).

Fibre breakage:

Tensile failure of fibres (for $\sigma_{11} > 0$) :

$$\left[\frac{\sigma_{11}}{S_{1T}}\right]^2 + \left[\frac{\sigma_{12}}{S_{12}}\right]^2 + \left[\frac{\sigma_{13}}{S_{13}}\right]^2 = 1$$

Compressive failure of fibres (for $\sigma_{11} < 0$) :

$$\left[\frac{\sigma_{11}}{S_{1C}}\right]^2 = 1$$

Matrix cracking :

Tensile failure of matrix (for $\sigma_{22} > 0$) :

$$\left[\frac{\sigma_{22}}{S_{2T}}\right]^2 + \left[\frac{\sigma_{23}}{S_{23}}\right]^2 + \left[\frac{\sigma_{12}}{S_{12}}\right]^2 + \left[\frac{\sigma_{13}}{S_{13}}\right]^2 = 1$$

Compressive failure of matrix (for $\sigma_{22} < 0$) :

$$\frac{1}{S_{2C}}\left[\left(\frac{S_{2C}}{2S_{23}}\right)^2 - 1\right]\sigma_{22} + \left[\frac{\sigma_{22}}{2S_{23}}\right]^2 + \left[\frac{\sigma_{23}}{S_{23}}\right]^2 + \left[\frac{\sigma_{12}}{S_{12}}\right]^2 + \left[\frac{\sigma_{13}}{S_{13}}\right]^2 = 1$$

Delamination between layers ($\sigma_{33}>0$) :

$$\left(\frac{\sigma_{33}}{S_{2T}}\right)^2 + \left(\frac{\sigma_{13}^2 + \sigma_{23}^2}{S_{1F}^2}\right) = 1$$

where :

σ_{11}, σ_{22}, σ_{33} : *direct stresses*

σ_{12}, σ_{13}, σ_{23} : *shear stresses*

S_{1T}, S_{2T} : *direct tensile strength*

S_{1C}, S_{2C} : *direct compressive strength*

S_{12}, S_{13}, S_{23} : *shear strength*

S_{1F} : *interlaminar shear strength*

6.2 Failure Prediction

As discussed in Section 6.1, a three dimensional finite element model can predict all the three major failure modes. Therefore, stress results of the 3D model analysed in Section 5.2.1 were analysed with respect to the failure criteria listed in Table 6.1. Failure parameter contours were used to illustrate the distribution of failure on a surface. When the parameter is equal to 1, failure of a certain mode is likely to occur.

In Fig 6.1, it can be seen that fibre breakage was predicted at the loading surface (90° layer). The failure zone has an elliptical shape, with the major axis in the hoop direction, and the minor axis in the axial direction. From the pattern of distribution of the contour, fibre breakage is likely to spread along the hoop direction. At this loading surface, fibres are expected to have failed by excessive compressive stress in the contact area (contact radius was 6 mm).

Fig 6.5 displays the matrix failure contour at the surface. Similarly to fibre failure, the damage region was also elliptical in shape, but the orientation of major and minor axes were inverted.

In the experimental observation, it was found that the indentation area was also elliptical in shape, with the major axis in the axial (longitudinal) direction, and the minor axis in the hoop direction. Matrix splitting and fibre breakage were confirmed as the major failure modes at the contact surface. The prediction of matrix and fibre failure at the surface agrees very well with the experimental findings.

Fibre breakage was also found in all the subsequent layers until the fourth layer. However, as can be seen from Figs 6.2 to 6.4, the locations which they failed were not the same as at the cylinder surface. The fibres failed at a distance from the centre along the axis perpendicular to the fibre direction.

Matrix failure in the second layer (Fig 6.6) was in a quite regular circular shape, which had a larger diameter than the one at the cylinder surface. Matrix damage occurred in subsequent layers until the fifth layer.

Delamination was found at every interface. As seen from Figs 6.7 to 6.10, these delamination areas had quite regular circular shapes. A small region in the centre was not delaminated due to a high compressive direct stress in the thickness direction. In practice, this small region is likely to be also delaminated by the tensile force developed in thickness direction during unloading. It can be seen from these contour plots that the size of delamination was gradually increased from the first interface to the third interface, and then decreased. This was well correlated with the predicted transverse shear stress distribution.

Among the three major failure modes, delamination was the most effective energy absorbing mechanism. This conclusion is supported by the prediction of the occurrence of delamination in every interface.

In general, the failure prediction using 3D FE analysis was agreed well with the experimental findings. Both the apparent contact damage and the invisible damage was predicted with good accuracy.

6.3 Concluding Remarks

From the failure prediction of the composite ring under quasi-static loading, it can be seen that a variety of damage events happened underneath the loading surface. It further highlights the importance of studying barely visible impact damage.

Three dimensional FE analysis appears to be a suitable tool for obtaining a better understanding of BVID. In view of the stresses arising at the in-service condition of a composite pressure cylinder, delamination does not appear to be a performance-degrading damage mode. This is in contrast with fibre breakage, which leads to significant reductions in the burst pressure.

In view of this discussion it would appear logical to promote delamination as the most suitable energy absorption mechanism in the composite cylinder, and to aim to avoid fibre breakage. In doing so, the performance of the cylinder is not compromised significantly, while impact energy may be dissipated effectively.

However, if delamination happens too easily, fibre breakage will still take place. Large scale delamination affects structural parameters of a composite pressure cylinder. A calculation made by Christoforou (1988) predicts that a small patch of delamination at the mid-section of the wall of a thin composite ring (1.524 mm wall thickness) reduces the bending stiffness of the composite ring by four times, compared to the intact composite ring.

Best impact resistance can be achieved by fine tuning the properties of fibres and resin to the chosen impact conditions. In general, composites with low levels of fibre surface treatment can generate large areas of splitting and delamination under impact [Cantwell and Morton, 1991].

Impact resistance can also be improved through hybridisation with carbon fibre. The combination of low and high modulus fibres was found to promote delamination [Cantwell and Morton, 1991].

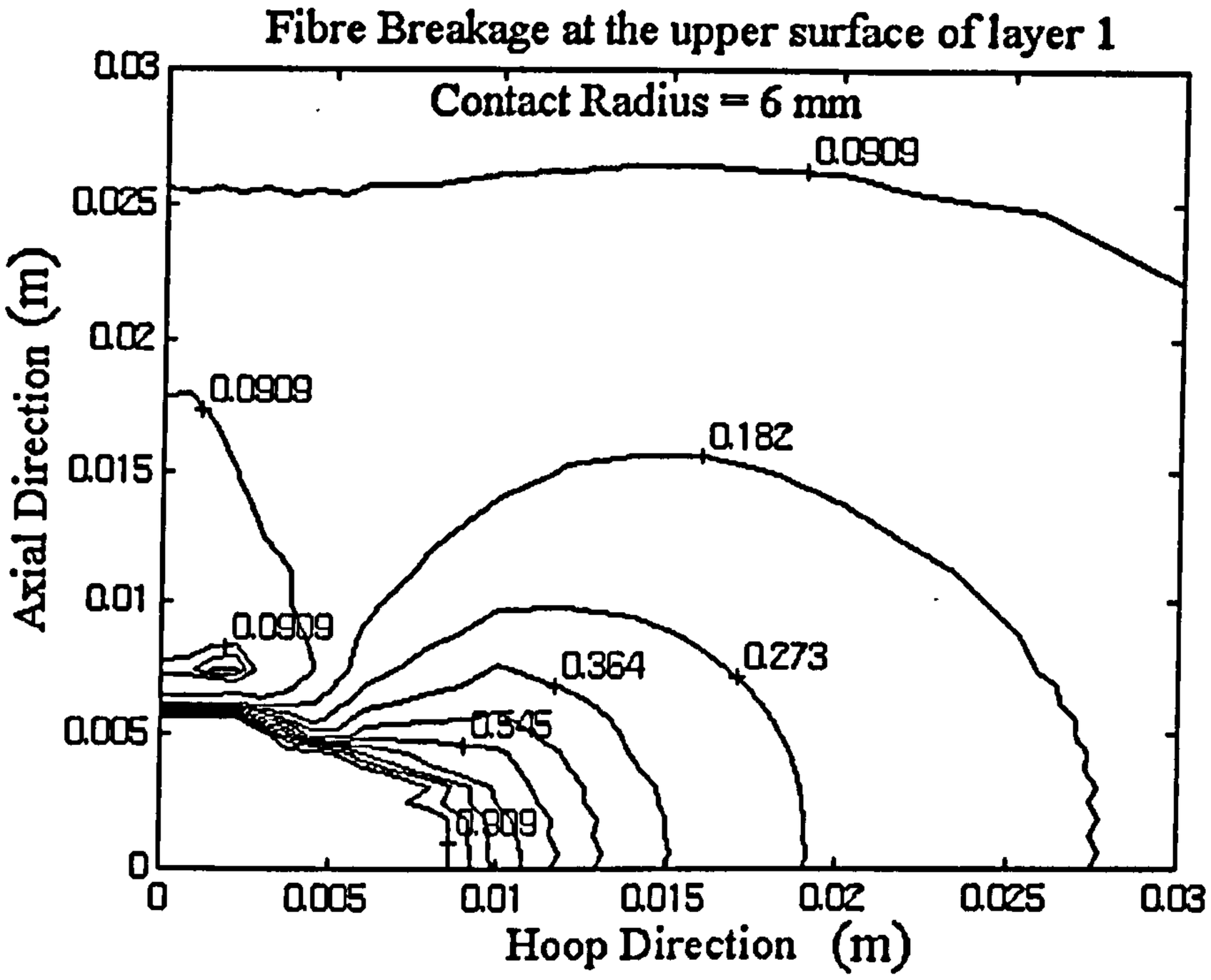

Fig 6.1 Fibre breakage at the upper surface of layer 1

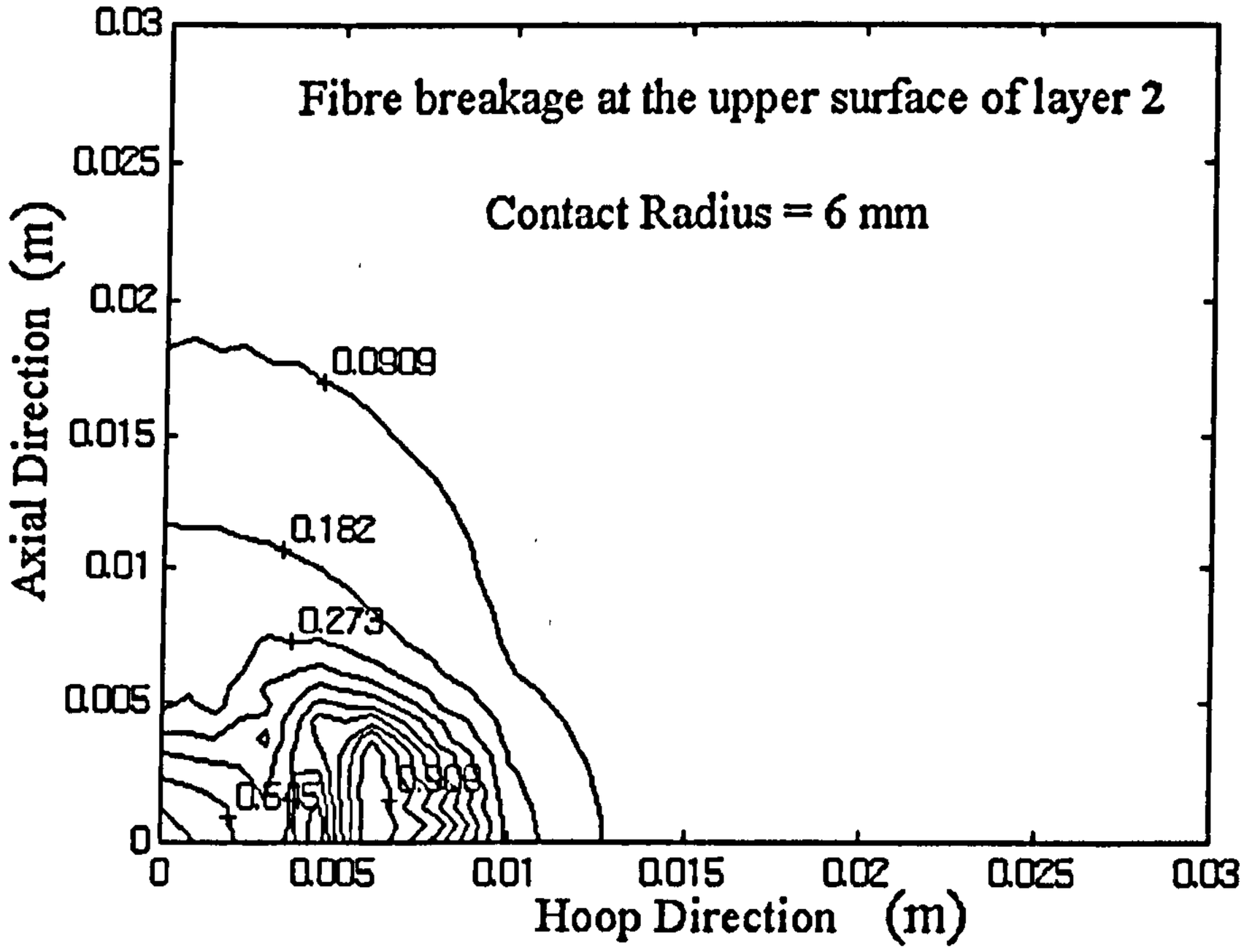

Fig 6.2 Fibre breakage at the upper surface of layer 2

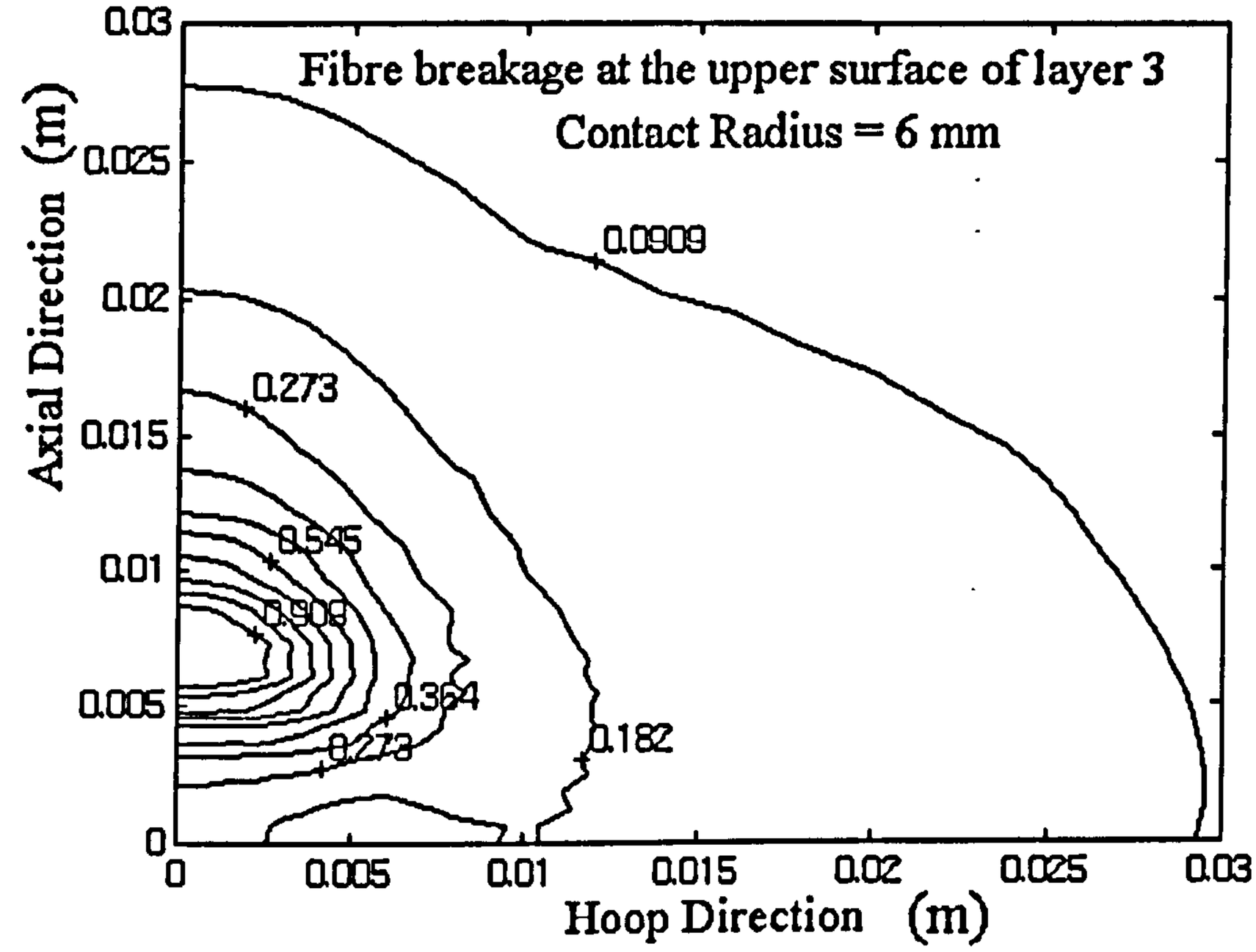

Fig 6.3 Fibre breakage at the upper surface of layer 3

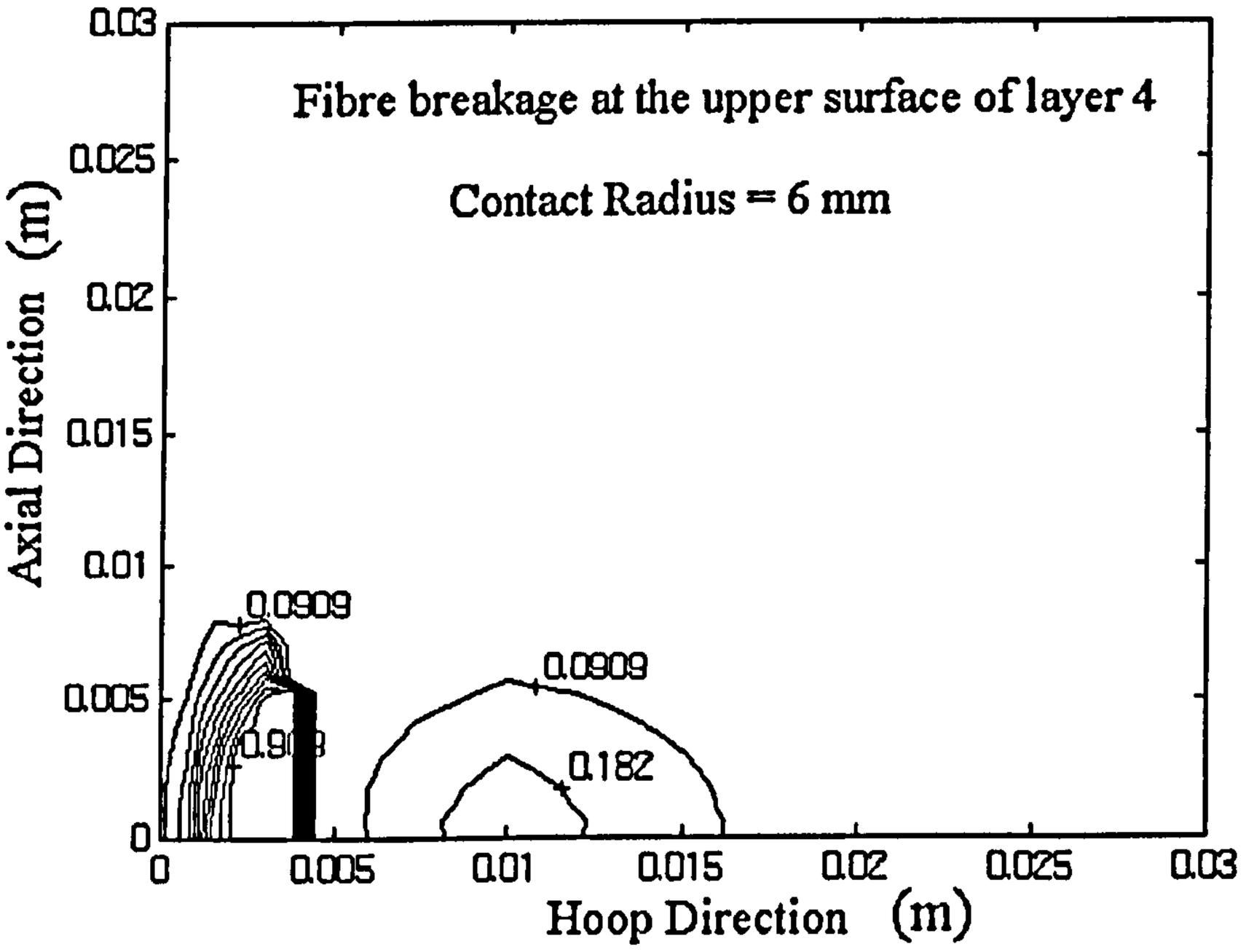

Fig 6.4 Fibre breakage at the upper surface of layer 4

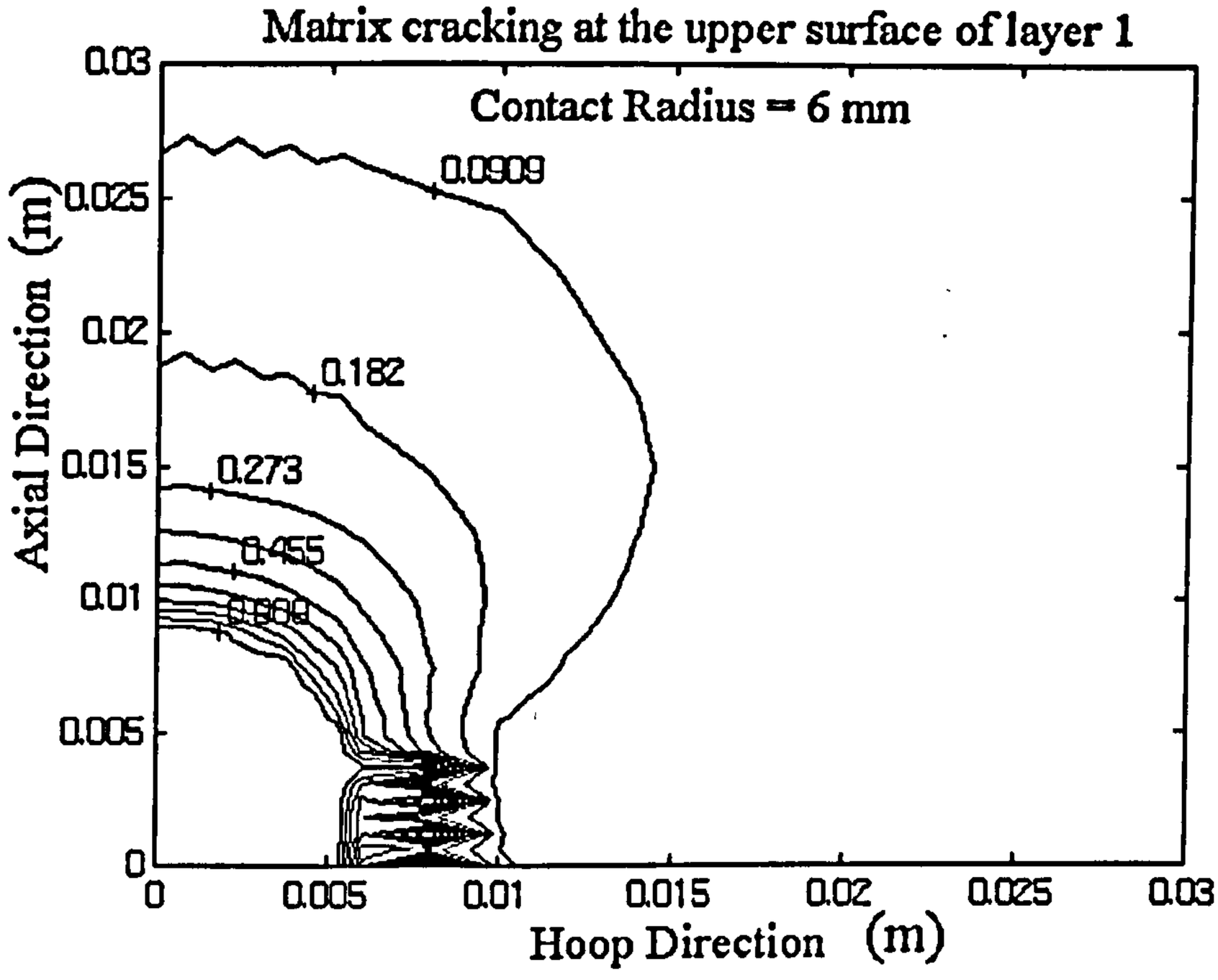

Fig 6.5 Matrix damage at the upper surface of layer 1

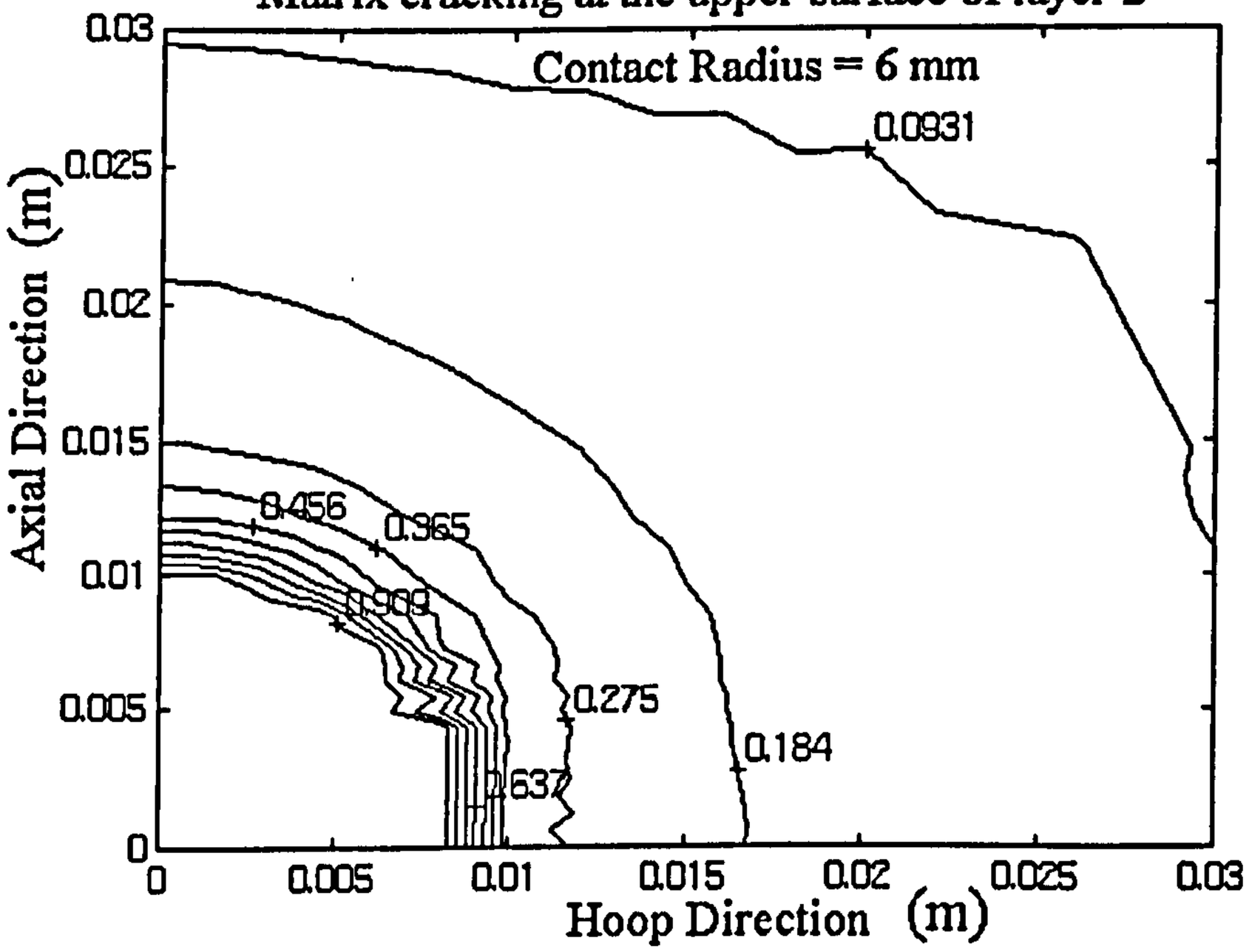

Fig 6.6 Matrix damage at the upper surface of layer 2

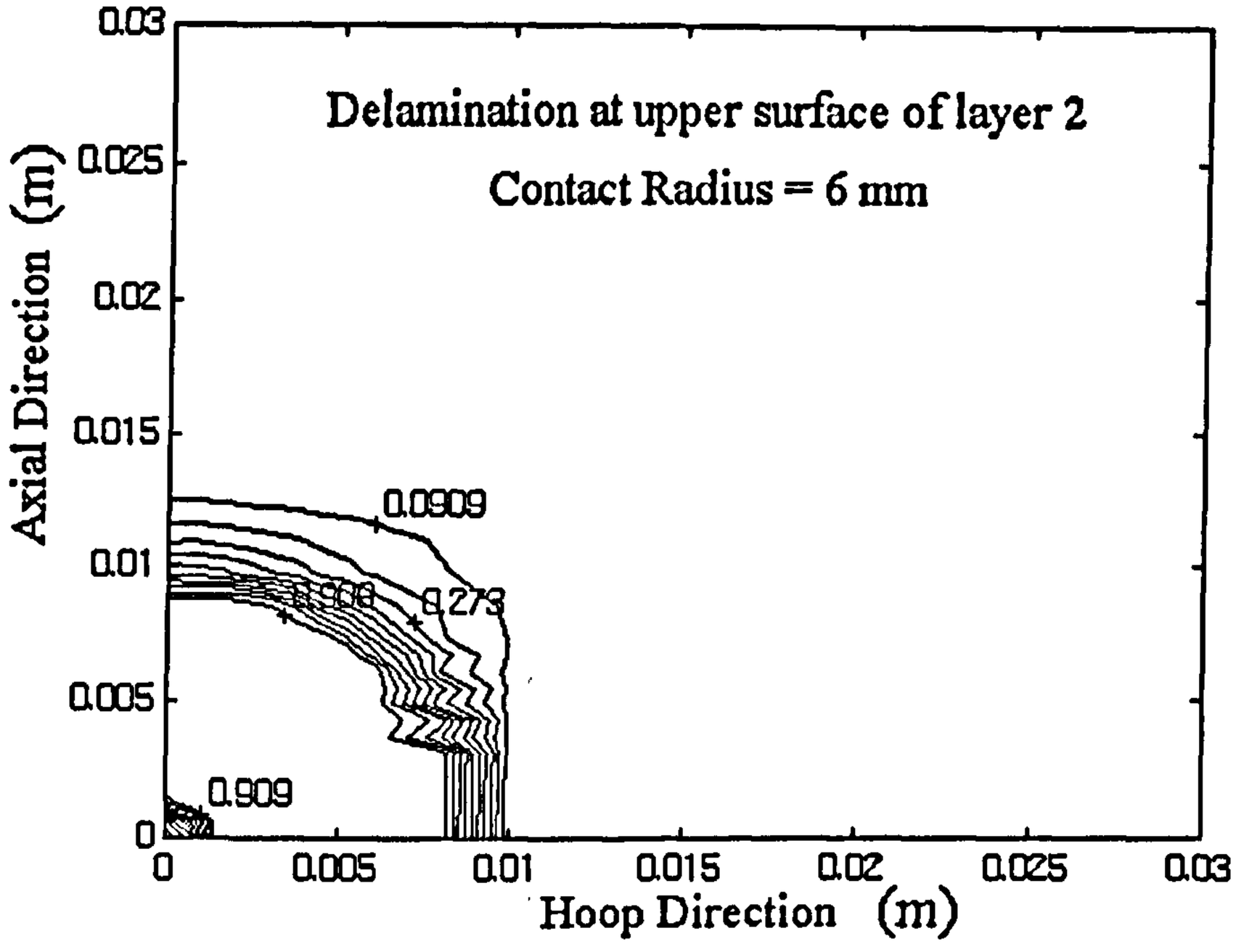

Fig 6.7 Delamination at the upper surface of layer 2

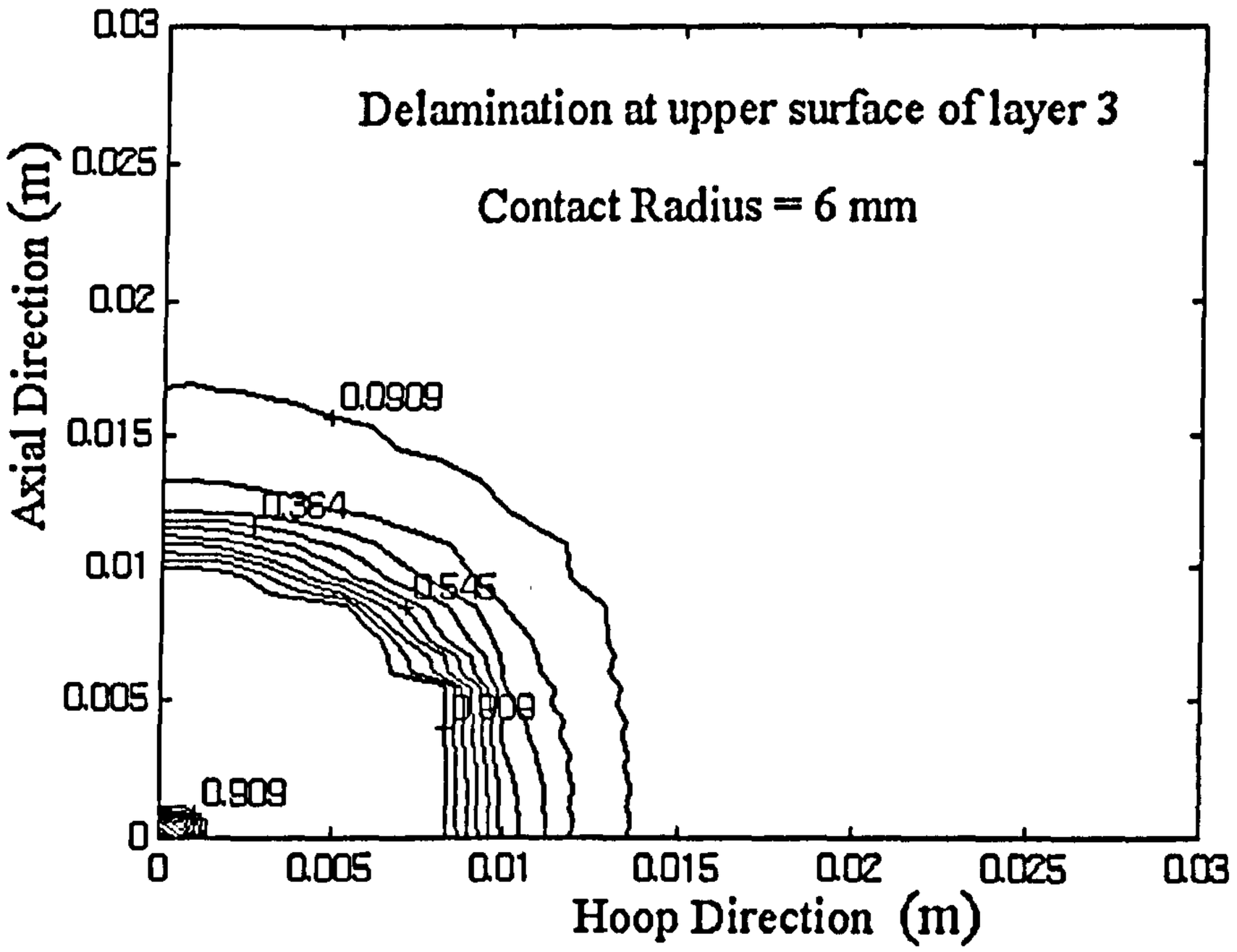

Fig 6.8 Delamination at the upper surface of layer 3

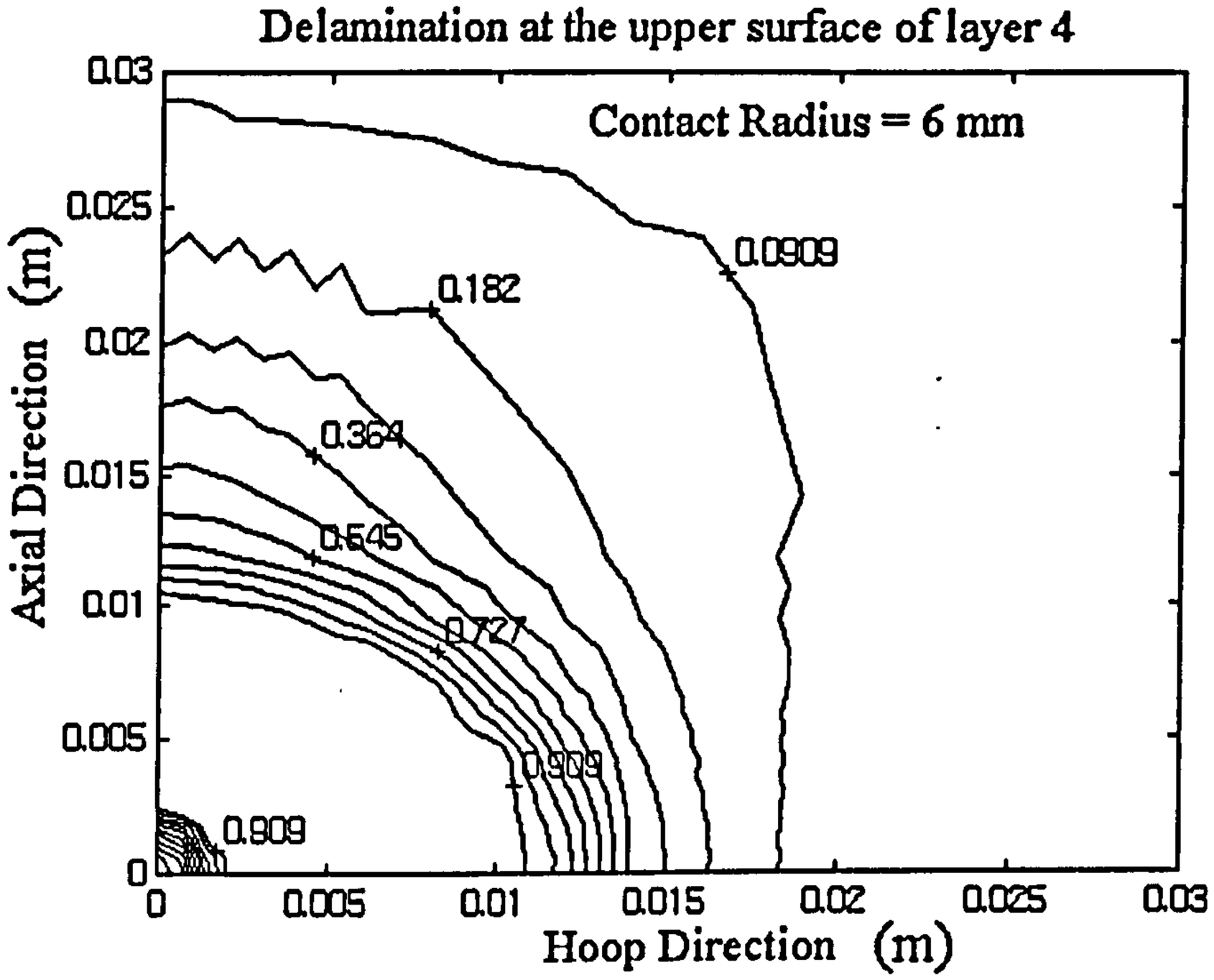

Fig 6.9 Delamination at the upper surface of layer 4

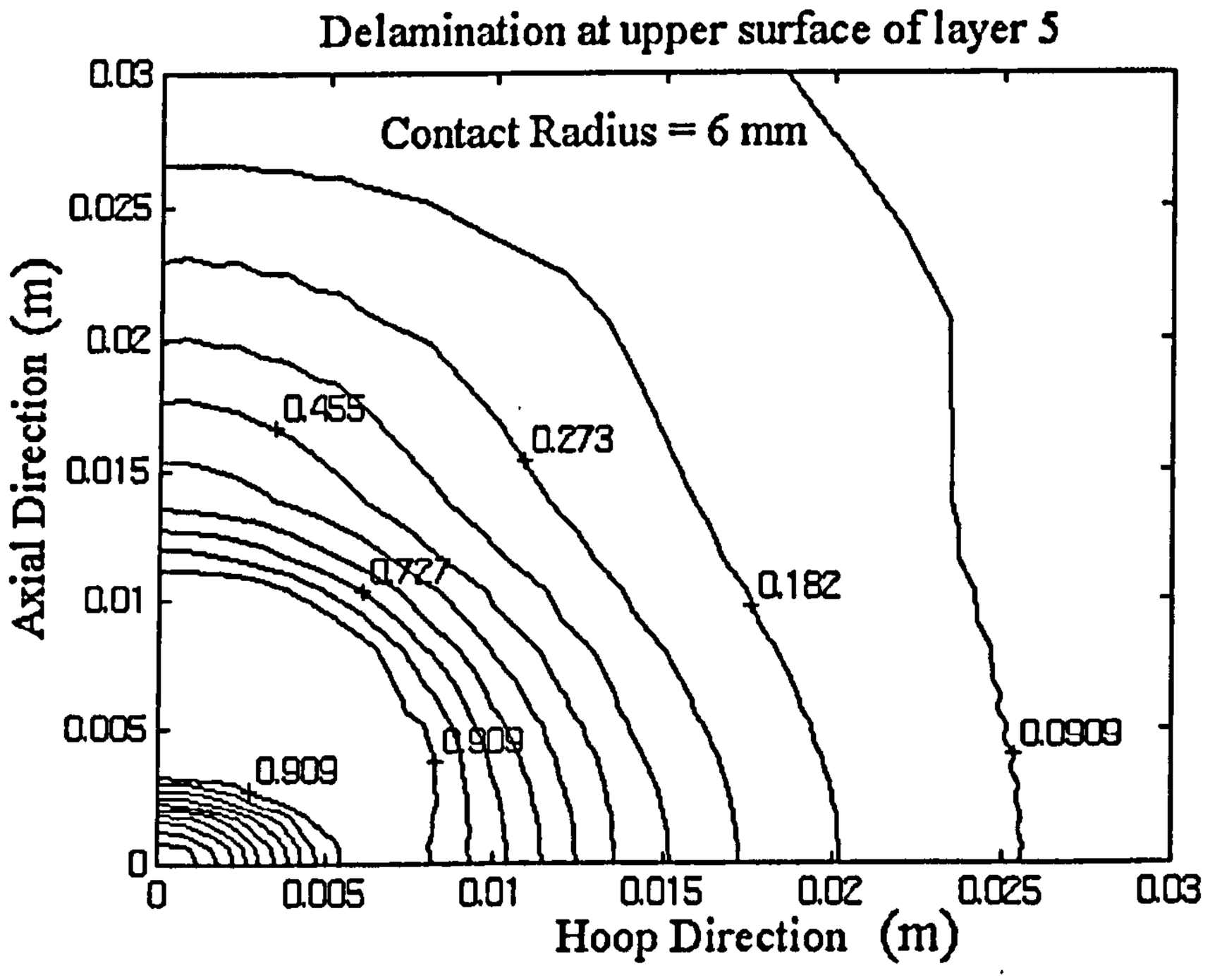

Fig 6.10 Delamination at the upper surface of layer 5

Chapter 7 Conclusions and Suggestions for Future Work

An approach which combined experimental techniques and finite element modelling was used to investigate and evaluate the behaviour of a fibre reinforced natural gas powered vehicle (NGV) pressure cylinder subjected to low energy impact, such as roadway stone hitting.

In FE modelling, it has been established that the approach that establishes "zero length" hinges between two thick shell element layers by using SKIP.COLLAPSE control module and the HINGES.AND.SLIDES data module can generate free in-plane sliding conditions at the interface. Based on this approach, a FE model for dynamic analysis has been developed in order to examine the stresses and deflections at the interface of the composite layer and the thin metallic liner. With the use of this FE model and the pre-pressurised technique and impulse excitation technique developed for this investigation, relative movement at the interface between the liner and the composite was predicted, which resulted from the twisting and folding of the liner. Although the magnitude of the twisting and folding were very small, they indicated a potential threat to the load-bearing capacity of the cylinder. Moreover, it was proposed that bulging of liner is possible under repeated impact as a weak spot was created due to fibre breakage.

A parametric study by FE dynamic analysis was undertaken in order to investigate the effect of impact parameters on impact response. It was concluded that the impact velocity, impactor mass, and impact energy cannot be considered separately in studying their influence on impact behaviour. However, the impact energy, with a specified impactor mass, seem sufficient to predict the localised impact response quite well. On the other hand, it was established that the composite pressure cylinder under roadway stone hitting behaves quasi-statically, i.e. the impact phenomenon predominately excites low frequency response.

For a pre-pressurised cylinder under impact loading, a higher transverse displacement, slightly lower impact force, and longer impact duration than for the empty cylinder were predicted by FE thick shell element model. In view of these predicted results, it

appeared that cylinder in the pressurised condition became less stiff. Twisting and folding of the cylinder due to internal pressure can produce an irregular shape change of the cylinder and may partly contribute to the flexibility of the cylinder.

Based on the three dimensional FE failure prediction of the composite ring under quasi-static loading, it was confirmed that a variety of damage events happened underneath the loading surface, which further highlighted the importance of studying BVID. It was concluded that three dimensional FE analysis is a suitable tool for obtaining better understanding of BVID. However, details analysis requires a large number of three dimensional elements, and hence leads to computationally expensive solutions.

Experimental investigations were carried out to identify the major failure modes under quasi-static indentation. The major failure modes were identified as fibre breakage, matrix cracking, and delamination. It was established that these failure modes have various strength and energy characteristics. In particular, fibre breakage requires fairly high tensile or compressive stress, while matrix cracking may happen both in shear and tensile rupture modes under moderate stresses. The cracking in matrix, however, acted as a precursor to delamination initiation.

A critical load level corresponding to a given indenter radius has been observed for the composite ring. At this critical load level, the phenomenon of repeatedly dropped and resumed of loading indicated that extensive damage of material must have been taken place. From the sectioned composite ring, large areas of delamination were found locally and at some remote locations suggested that delamination is an effective energy absorbing mechanism.

The energy absorbed in matrix cracking and delamination may be significant, due to the large area involved. Both the FE model and the experimental investigation show that delamination is the dominant failure mode. It is evidenced by the sudden drop of load on the composite ring around the 32 kN level, in which progressive delamination took place. However, delamination must be particularly favoured as the energy absorbing mechanism in composite pressure cylinders, since it does not affect the burst limit in any significant way.

There are five major areas open for future development of this research project.

Firstly, the sequence of failure modes under quasi-static and impact loading should be fully investigated and compared experimentally. The knowledge of the sequential order of failure modes is importance for re-tuning the failure modes of a cylinder at certain set of loading conditions. Moreover, it can be used to complement the development of FE modelling. Acoustic emission measurement can be utilised to detect failure associated with fibre breakage, matrix cracking and delamination, and their locations during quasi-static loading. Further, various matrix systems, such as Kevlar 29 (soft epoxy) and Kevlar 49 (rigid epoxy), can be used to investigate their influence on impact resistance.

Secondly, as has been discussed in this study, the indenter diameter has great influence on failure modes, hence, it is valuable to conduct a parametric study on various sizes and shapes of indenter / impactor under quasi-static and impact loading. A generalised model may then be established to obtain more understanding of the failure mechanisms and their occurrence sequences.

Thirdly, specimen for experimental tests should be extended from a composite ring to a fully charged cylinder to investigate the influence of pre-stress condition on impact behaviour. Moreover, performance subsequently to repeated impact can be assessed by burst testing of the damaged cylinder.

Fourthly, as was concluded in this study, three dimensional FE modelling is effective in predicting composite behaviour under static loading. Further development of three dimensional FE modelling to dynamic analysis should be carried on. An experimental study proposed for identifying the sequence, initiation and propagation of damage under both quasi-static and impact loading can be used to implement into the FE code to improve damage prediction, especially delamination at interface of two layers. This three dimensional FE dynamic analysis can then be further extended to establish a FE model with the implementation of progressive failure procedure to accurately predict the impact behaviour. However, the potential future usefulness of this FE model should be examined by comparing with experimental observations so as to put forward for the optimal design of composite structure.

Finally, as delamination is the major impact energy absorbing mechanism, therefore, the exact delaminated area under impact should be accurately predicted in order to assess the impact resistance and post-impact behaviour of the cylinder. In view of this, the IFRM theory may be further considered and developed to evaluate the shape and the size of delamination under static and impact loading.

REFERENCES

Abrate S., 1991, "Impact on Laminated Composite materials", Appl Mech Rev, vol. 44, No. 4, April 1991,pp155-190, ASME.

Agarwal B.D. and Broutman L.J., 1990, "Analysis and Performance of Fibre Composites", John Wiley and Sons Inc, ISBN 0-471-51152-8, CIP.

Ahmad S., Irons B. and Zienkiewicz O.C., 1970, "Analysis of Thick and Thin Shell Structures by Curved Finite Elements", Int. J. for Numerical Methods in Engineering Vol. 2, 1970, 419-451.

Ainsworth K.L., 1990, "Low Velocity Transverse Impact of Filament Wound E-Glass / Epoxy Resin Pipes," PhD Thesis, University of Liverpool, 1990.

Ainsworth K.L. and Evans K.E., 1990, "The measurement and Modelling of Filament Wound Pipes Undergoing Transverse Impacts", Proceedings of the Institution of Mechanical Engineers, Fourth Int. Conference FRC'90, C400/048, 143-148.

Ambur D.R., Starnes J.H. Jr. and Prasad C.B., 1993, "Influence of Transverse-Shear and large-Deformation Effects on the Low-Speed Impact Response of Laminated Composite Plates", NASA Technical Memorandum 107753, April 1993.

Anastasiadis J.S. and Simitses G.J., 1993, "Buckling of Pressure-Loaded, Long, shear deformable, Cylindrical laminated Shells", Composite Structures 23 (1993), pp221-231, ESP Ltd, 0263-8334/93.

Assam B.S., Muhammad M.A., Mokhtar M.O.A. and Kolkailah F.A., 1995, "A Theoretical and Design Analysis of the Filament-Wound Composite Pressure Vessels", Science and Engineering of Composite Materials, 1995, Vol. 4, No. 2, pp73-87.

Babel H.W., Vickers B.D. and Thomas D.A., 1989, "Sustained Load Behaviour of Graphite/Epoxy Metal-Lined Pressure Vessels for Long-Life Space Applications", AIAA 25th Joint Propulsion Conf, AIAA-89-2644, 1989.

Bachrach W.E. and Hansen R.S., 1989, "Mixed Finite-Element Method for Composite Cylinder Subjected to Impact", AIAA Journal, vol. 27, No.5, 1989, pp632-638, U.S.A.

Banks W.M., Tooth A.S. and Wilson P.M., 1989, "Design of Composite Cylindrical Vessels for Fluid Loading", Journal of Pressure Vessel Technology Vol.111, May 1989, 102-108.

Bartkus E.K. and Humphrey W.D., 1991, "Determination of Fibre-Reinforced Composite Material Properties Using Internal Pressurization of Filament Wound Cylinders", 36th International SAMPE Symposium, April 1991, Book 1, pp827-839.

Beaumont P.W.R., 1989, "The Failure of Fibre Composites: An Overview", J. Strain Analysis Vol 24 No 4, 1989, IMechE 1989, 0309-3247/89/10000-0189, 189-205.

Belytschko T. and Schoeberle D.F., 1975, "On the Unconditional Stability of an Implicit Algorithm for Nonlinear Structural Dynamics", Journal of Applied Mechanics, Transactions of the ASME, December 1975, pp865-869.

Bert C.W. and Birman V., 1988, "Response of Prestressed Cylindrically Curved Composite Structures Subjected to Low-Velocity Impact", Proc. 4th Japan-us conf Comp Mat. 1988, Washington, pp43-52.

Bhuyan G.S., 1992, "Effect of Composite Damage on the Fatigue Behaviour of the Metal-Lined Hoop-Wrapped Cylinders", Transactions of the ASME, Journal of Pressure Vessel Technology, February 1992, Vol. 114, pp120-123.

Bhuyan G.S. and Brezden W.J., 1989, "Influence of Environmental Variables and Intermittent Overloadings on Fatigue Crack Growth in On-Board NGV Cylinder Steel", Int. J. Pres. Ves. and Piping, 40 (1989), 139-149.

Bishop S.M. and Morton J., 1984, "Fatigue of Notched (0, +- 45) CFRP with Woven and Non-Woven (+- 45) Layers", Advances in Fracture Research, Valluri S.R. et al (Eds.), Pergamon Press Oxford, vol 4, 1984.

Bibo G.A. and Hogg P.J., 1996, "Review : The Role of Reinforcement Architecture on Impact Damage Mechanisms and Post-Impact Compression Behaviour", Journal of Materials Science, Vol. 31 (1996), pp1115-1137.

Boukhili R., Bojji C. and Gauvin R., 1994, "Fatigue Mechanisms Under Low Energy Repeated Impact of Composite laminates", Journal of Reinforced Plastics and Composites, Vol. 13, October 1994, pp856-870.

Boussouf D.M., 1992, "Membrane Analysis of Composite Reinforced Composite Spherical Shells", Transactions of the ASME, Journal of Pressure Vessel Technology, February 1992, Vol. 114, pp101-104.

Bowles K.J., 1988, "The Correlation of Low-Velocity Impact Resistance of Graphite-Fibre-Reinforced Composites with Matrix Properties", Composite Materials: Testing and Design (Eighth Conference), ASTM STP 972, 1988, 124-142.

Brosey W.D., Calfee M.T., Whittaker J.W., Henneke E.G., Post D., Reifsnider K.L. and Blake R.A., 1990, "Nondestructive Evaluation Performance in Predicting Failure Strength of Spherical Composite Specimens with Implanted Flaws", Materials Evaluation Vol 48, September 1990, The American Society for Nondestructive Testing, 1090-1095.

Burtin C. and Hamelin P., 1986, "Effect of Viscoelastic Characteristics of Polymers for a Composite behaviour Under Dynamic and Impact Loading", European Colloquium 214 Mechanical Behaviour of Composites and Laminates (1986: Yugoslavia), 1986, 32-44.

Butcher B.R. and Fernback P.J., 1981, "Impact Resistance of Unidirectional CFRP Under Tensile Stress : Further Experimental Variables", Fibre Science and Technology, Vol. 14 (1981), pp41-58.

Butcher B.R, 1979, "The Impact Resistance of Unidirectional CFRP Under Tensile Stress", Fibre Science and Technology, 1979, pp295-326.

Cairns D.S. and Lagace P.A., 1992, "A Consistent Engineering Methodology for the Treatment of Impact in Composite Materials", Journal of Reinforced Plastics and Composites, Vol. 11, April 1992, pp395-412.

Cantwell W.J., Curtis P.T. and Morton J., 1983, "Post-Impact Fatigue Performance of Carbon Fibre Laminates with Non-Woven and Mixed-Woven Layer", Composites, vol 14 (1983), pp301-305.

Cantwell W.J., 1986, "Impact Damage in Carbon Fibre Composites", PhD Thesis, Imperial College, London University, 1986.

Cantwell W.J. and Morton J., 1984, "LowVelocity Impact Damage in Carbon Fibre Reinforced Plastic Laminates", Proc Vth Int Comp Exp Mech, Montreal, June 1984, pp314-319.

Cantwell W.J. and Morton J., 1991, "The Impact Resistance of Composite Materials -- a Review", Composites, Volume 22, Number 5, Sept 1991, Butterworth-Heinemann Ltd, 0010-4361/91/050347-16.

Cantwell W.J. and Morton J., 1992, "The Significance of Damage and Defects and Their Detection in Composite Materials : A Review", Journal of Strain Analysis, Vol.27, No.1, 29-42.

Caprino G., Visconti I.C. and Di Ilio A., 1984, "Composite materials Response Under Low-Velocity Impact", Composite Structures, Vol. 2 (1984), pp261-271.

Carvalho A. and Soares C.G., 1996, "Dynamic Response of Rectangular plates of Composite Materials Subjected to Impact Loads", Composite Structures, Vol. 34 (1996), pp55-63.

CGA C-6.2, 1988, "Guidelines for Visual Inspection and Requalification of Fiber Reinforced High Pressure Cylinders", 2nd ed., Compressed Gas Associations, Inc., 1235 Jefferson Davis Highway, Suite 501, Arlington, VA 22202, U.S.A.

Chandler H.W., Devlin B.J. and Gibson A.G., 1992, "Mechanics of the Impregnation of Unidirectional Fibre Tows", 5th International Conference on Fibre Reinforced Composites, The Plastics and Rubber Institute, 24-26 March 1992, 10/1-10/15.

Chang F.K. and Springer G.S., 1986, "The Strengths of Fibre Reinforced Composite Bends", J Composite Materials, v20, pp30-45, 1986.

Chao W.C. and Reddy J.N., 1984, "Analysis of Laminated Composite Shells Using a Degenerated 3-D Element", International Journal for Numerical Methods in Engineering, Vol 20, 1984, 0029-5981/84/1119991-17, pp 1991-2007.

Chen J.K. and Sun C.T., 1985, "On the Impact of Initially Stressed Composite Laminates", J. Composite Materials, v19 (November), pp490-504.

Chen C.H. and Wu R.Y., 1986, " The Impact Properties of Carbon Fiber/Epoxy Composite Material with Various Ply Arrangements by Instrumented Falling Weight Impact Test", 31st International Sample Symposium, April 7-10 1986, 1549-1555.

Choi H.Y., Downs R.J. and Chang F.K., 1991, "A New Approach Towards Understanding Damage Mechanisms and Mechanics of Laminated Composites Due to Low-Velocity Impact : Part I - Experiments" Journal of Composite Materials, Vol. 25, August 1991, pp992-1011.

Choi H.Y., Wu H.Y. and Chang F.K., 1991, "A New Approach Towards Understanding Damage Mechanisms and Mechanics of Laminated Composites Due to Low-Velocity Impact : Part II - Analysis" Journal of Composite Materials, Vol. 25, August 1991, pp1012-1038.

Choi H.Y. and Chang F.K., 1992, "A Model for Predicting Damage in Graphite / Epoxy Laminated Composites Resulting from Low-velocity Point Impact", Journal of Composite Materials, Vol. 26, No. 14 (1992), pp2134- 2169.

Choi H.Y., Wang H.S. and Chang F.K., 1992, "Effect of Laminate Configuration and Impactor's Mass on the Initial Impact Damage of Graphite / Epoxy Composite Plates Due to Line-Loading Impact", Journal of Composite Materials, Vol. 26, No. 6 (1992), pp804- 827.

Chow T.S., 1971, "On the Propagation of Flexural Waves in an Orthotropic laminated Plate and Its Response to an Impulsive Load", J. Composite Materials, Vol. 5 (July 1971), pp306-319.

Christoforou A.P., 1988, "Investigation of Impact in Advance Composite", PhD Thesis, The University of Utah, U.S.A., 1988.

Christoforou A.P. and Swanson S.R., 1988, 'Strength loss in Composite Cylinders Under Impact", J. of Engineering Materials and Technology, Vol.110, April 1988, pp180-184, Transactions of the ASME.

Christoforou A.P., Swanson S.R., Ventrello S.C., and Beckwith S.W., 1987, "Impact Damage in Carbon/Epoxy Composite Cylinders", 32nd International SAMP Symposium, 6-9 April, 1987, 964-973.

Clark G., 1989, "Modelling of Impact Damage in Composite laminates", Composites, vol. 20, No. 3, May 1989, pp209-214, Butterworth and Co (Publishers) Ltd.

Collombet F., Bonini J. and Lataillade J.L., 1996, "A Three-Dimensional Modelling of Low Velocity Impact damage in Composite Laminates", International Journal for Numerical Methods in Engineering, Vol. 39, pp1491-1516 (1996).

Connolly and Hudak, 1994, "Fracture Mechanics Analysis of NGV Fuel Cylinders Part II : Metal Cylinder Liners", Topic Report SWRI Project No. 06-1566, GRI, Canada, 1994.

Conway H.D., 1955, "The Indentation of an Orthotropic Half Plane", J Appl Math Phys (ZAMP) 6, pp402-405, 1955.

Cristescu N., Malvern L.E. and Sierakowski R.L., 1975, "Failure Mechanisms in Composite Plates Impacted by Blunt-Ended Penetrators", Foreign Object Impact Damage to Composites, ASTM STP 568, ASTM, 1975, pp159-172.

Curtis P.T., 1989, "The Fatigue Behaviour of Fibrous Composite Materials", J. Strain Analysis Vol.24 No.4, 1989, IMechE 1989, 235-244.

Darms F.J., 1991, "Space Age Pressure Vessels", 36th International SAMPE Symposium, April 1991, Book 1, pp818-826.

Datoo M.H., 1991, "Mechanics of Fibrous Composites", Elsevier Science Publishing, ISBN 1-85166-600-1, 1991.

Doh Y.D. and Hong C.S., 1995, "Progressive Failure Analysis for Filament Wound Pressure Vessel", Journal of Reinforced Plastics and Composites, Vol. 14, December, 1995, pp1278-1306.

Dorey G., Sidey G.R. and Hutchings J., 1978, "Impact Properties of Carbon Fibre / Kevlar Hybrid Composites", Composites, vol 9, pp25-32.

Dorey G., 1987, "Impact Damage in Composites - Development, Consequences and Prevention", ICCM6 / ECCM 2, 1987, Vol. 3, pp3.1-3.26.

Dorey G., 1989, "An Overview of Impact Damage in Composites", Int. Conf. Mech. Prop. Materials at High Rates of Strain, Oxford, 1989, (Inst. Phys. Conf. Ser. No 102 : Session 8), 395-402.

Eason T.G. and Ochoa O.O., 1996, "Modeling Progressive damage in Composites : A Shear Deformable Element for ABAQUS", Composite Structures, Vol. 34 (1996), pp119-128.

Ecord G.M., 1977, "Composite Pressure Vessels for the Space Shuttle Orbiter", Proc ASME Energy Technology Conf 1977, PVP-PB-021, ASME, U.S.A., pp129-140.

Egerton M.W., Tanikella M.S. and Koury J.L., 1989, "Advanced Graphite/Polyimide Composites for High Temperature Filament Wound Structures", 34th International SAMPE Symposium, May 1989.

Faupel J.H., 1971, "The Design of Vessels for High Pressure", Pressure vessel Engineering Technology, Chapter 6, edited by R.W. Nichols, 1971, pp402-473, Applied Science Publishers Ltd, London.

Feng Z., Rowlands R.E. and Sanford R.J., 1991, "Stress Intensity Determination by an Experimental-Numerical Hybrid technique", Journal of Strain Analysis Vol. 26 No. 4, 1991, 243-251.

Finn S.R. and Springer G.S., 1993, "Delaminations in Composite Plates Under Transverse Static or Impact Loads - A Model", Composite Structures 23 (1993), pp177-190, Elsevier Science Publishers Ltd, England.

Foral R.F., 1979, "Composite Spherical Pressure Vessels with Hardening Metal Liners", Transactions of the ASME, Journal of Pressure Vessel Technology, August 1979, Vol. 101, pp200-206.

Frame C.S., 1989, "Introduction to Composite Materials", Proceedings of the IMechE Conference, Design in Composite Materials, C387/017 IMechE 1989, 1-12.

Gau S.J., Scavuzzo R.J. and Lam P.C., 1994, "Dynamic Behaviour of Elastic-Plastic Simply Supported Pipes", Journal of Pressure Vessel Technology, Transactions of the ASME, Vol. 116, August 1994, pp306-311.

Godwin E.W. and Davies G.A.O., 1988, "Impact Behaviour of Thermoplastic composites", CAD in Composite Material Tech., 1988, pp371-382, edited by C.A. Brebbia, W.P. de Wilde and W.R. Blain, ISBN 0-905451-97-X.

Goldsmith W, 1960, "Impact : The Theory and Physical behaviour of Colliding Solids", Edward Arnold, London, 1960.

Goldsmith W., 1963, "Impact : The Collision of Solids", Applied Mechanics Reviews, vol 16 (11), pp855-866, 1963.

Goldsmith W. and Sackman J.L., 1992, "An Experimental Study of Energy Absorption in Impact on Sandwich plates", Int. J. Impact Engng, Vol. 12, No. 2, pp241-262, 1992.

Gong S.W., Shim V.P.W. and Toh S.L., 1996, "Central and Noncentral Normal Impact on Orthotropic Composite Cylindrical Shells", AIAA Journal, Vol. 34, No. 8, August 1996, pp1619-1626.

Gordon R., 1981, "Composite Cylinders for CNG", Proc. 36th Annual Conference, Reinforced Plastics/Composites Institute, The Society of the Plastics Industry, Inc. February 16-20, 1981.

Graves M.J. and Lagace P.A., 1983, "Damage Tolerance of Composite Cylinders", SAE Technical paper Series, No. 830766.

Green W.A. and Micunovic M., (Eds), 1986, "Mechanical Behaviour of Composites and Laminates", European Colloquium 214, Elsevier Science Publishing, 1986, ISBN 1-85166-144-1.

Greenfield and Allen D.H., 1987, "The Effect of Surface Finish on the High Cycle Fatigue Strength of Materials", Gec Journal of Research Vol.5 No.3, 1987, 129-140.

Greszczuk L.B., 1982, "Impact Dynamics: Chapter 3, Damage in Composite Materials Due to Low Velocity Impact", Zukas J.A. et al Editors, John Wiley and Sons, 82/05494, 1982, 55-94.

Guild F.J., Ogin S.L. and Smith P.A., 1991, "Finite Element Modelling of Transverse Cracking in Composite Laminates", 1st International Conference on Deformation and Fracture of Composites, Mon.-Wed. 25-27 March 1991, 6/1-6/6.

Guynn E.G. and O'Brien T.K., 1985, "The Influence of Lay-Up and Thickness on Composite Impact Damage and Compression Strength", 26th AIAA Struct Struct Dyn Mat Conf 1985, USA AIAA, pp187-196.

Haanes H., Stokke R. and Thon H., 1991, "Performance of Glass Fibre Reinforced Plastics (GRP) Pipes under Impact Loading" OMAE, 1991, Vol. III-B, Materials Engineering ASME - 1991, 596-576.

Hardy S.J. and Malik N.H., 1990, "Optimum Design of Composite-Reinforced Pressure Vessels", Applied Stress Analysis, edited by T.H. Hyde and E. Ollerton, pp429-438, 1990, ISBN 1-85166-536-6 ESP Ltd.

Hart-Smith L.J., 1992, "A Scientific Approach to Composite Laminate Strength Prediction", Composite Materials: Testing and Design (Tenth Volume), ASTM STP 1120, 1992, 142-169.

Hashin Z., 1980, "Failure Criteria for Unidirectional Fibre Composites", Journal of Applied Mechanics, June 1980, Vol. 47, pp329-334.

Herakovich C.T., 1989, "Edge Effects and Delamination Failures", J. Strain Analysis Vol.24 No.4, 1989, IMechE 1989, 245-252.

Hertz H, 1881, J Reine Ang. Math., vol 92, p156.

Hill E.K., 1991, "Burst Pressure Prediction in 45.7 CM (18 INCH) Diameter Graphite/Epoxy Pressure Vessels Using Acoustic Emission Data", 36th International SAMPE Symposium, April 1991, Book 1, pp272-283.

Hill P.S., 1992, "Failure Mechanisms in Composite Materials", ERS R4783, British Gas.

Hill R, 1948, "A Theory of the Yielding and Plastic Flow of Anisotropic Metals", Proc Royal Society of London, A193, pp282-287, 1948.

Hoa S.V., 1985, "Laminate Theory and Fatigue Criteria for Fibre Reinforced Plastic Pressure Vessel Design", Proc Plastic Symposium - St. Louis, October 1985, pp130-139.

Hogg P.J., Ahmadnia A. and Kay M., 1992, "The Mechanical Properties of Non-Crimped Fabric Composites with Integral Through-Thickness Stitching", unpublished.

Hong S., and Liu D., 1989, "On the Relationship Between Impact Energy and Delamination Area", Proceedings of the Society for Experimental Mechanics, SEM,1989, Vol 46, 115-120.

Hoppel C.P.R., Bogetti T.A. and Gillespie J.W. Jr., 1995, "Literature review - Effects of Hydrostatic Pressure on the Mechanical Behaviour of Composite Materials", Journal of Thermoplastic Composite Materials, Vol. 8, October 1995, pp375-409.

Hsu P., Song H.C. and Chang Z.H., 1988, "On the Impact Properties of Fibre Composites and Their Hybrid Materials", CAD in Composite Material Tech., 1988, pp395-401, edited by C.A. Brebbia, W.P. de Wilde and W.R. Blain, ISBN 0-905451-97-X.

Iyer S.L. and Haugan M.D., 1986, "Cyclic Loading and Stress Concentration on Composites", 31st Int. SAMPE Symposium April 1986, 1780-1795.

Jegley D.C., 1992, "Effect of Low-Speed Impact Damage and Damage Location on Behaviour of Composite Panels", NASA Technical Paper 3196, 1992, USA.

Jenkins, 1920, "Materials of Construction Used in Aircraft and Aircraft Engines", Report to the Great Britain Aeronautical Research Committee.

Jenq S.T. and Goldsmith W., 1989, "Shear and Bending Phenomena in Normal Projectile Impact on Thin Targets", Computational Techniques for Contact, Impact, Penetration and Perforation of Solids", AMD-Vol.103, Dec 1989, pp223-233.

Johansen B.S. and Nielsen F.E., 1991, "The Geometry of Filament Winding and Computer Aided Design", ICAC 91, Netherlands.

Johnson W., 1972, "Impact Strength of Materials", Edward Arnold (Publishers) Ltd., ISBN 0-7131-3266-3, 1972.

Johnson R.F., 1967, "The Measurement of Yield Stress", Strong Tough Structural Steels, Proceedings of the Joint Conference Organized by the British Iron and Steel Research Association and the Iron and Steel Institute at the Royal Hotel Scarborough, 4-6 April 1967, 51-60.

Johnson K.L., 1982, "One Hundred Years of Hertz Contact", Proceedings IMechE 1982 Vol. 196, No.39, 363-378.

Jones B.H., 1977, "Design and Analysis of Circumferentially Reinforced Prestressed Pressure Vessels", Proc ASME Energy Technology Conf 1977, PVP-PB-021, ASME, U.S.A., pp51-68.

Jones D.T., Jones I.A. and Middleton V., 1996, "Improving Composite Lay-Up for Non-Spherical Filament-Wound Pressure vessels", Composites : Part A 27A (1996) pp311-317.

Johnston N.J., Editor, 1985, "Toughened Composites", Symposium on Toughened Composites, ASTM Special Technical Publication 937, 1985.

Jones N., 1976, "Dynamic Behaviour of Ideal Fibre-Reinforced Rigid-Plastic Beams", Transactions of the ASME, Journal of Applied Mechanics, June 1976, 319-324.

Jones N., 1979, "The Influence of Rotatory Interia and Transverse Shear on the Dynamic Plastic Behavior of Beams", Journal of Applied Mechanics, June 1979, Vol. 46, 303-311.

Jun E.J. and Kim T.W., 1986, "Development of Filament Wound S-2 Glass/Epoxy Pressure Vessel", Proc. Int. Symposium on Composite materials and structures, 1986 June, pp261-266.

Kant T. and Datye D., 1990, "Finite Elements Available for the Analysis of Curved Thin-walled Structures", Finite Element Applications to Thin-walled Structures, Chapter 1, edited by J.W. Bull, pp1-40, ESP Ltd, ISBN 1-85166-373-8.

Kapania R.K., 1989, "A Review on the Analysis of Laminated Shells", Journal of Pressure Vessel Technology, May 1989, Vol 111, Transactions of the ASME, 88-96.

Karandikar H. and Mistree F., 1992, "Designing a Composite Material Pressure Vessel for Manufacture: A Case Study in Concurrent Engineering", Engineering Opt. Vol.18, 1992, 235-262.

Kardos G., 1986, "Stress Concentrations in Composites ?", 31st International Sample Symposium, April 7-10, 1986, 396-409.

Kim S.J. and Goo N.S., 1997, "Dynamic Contact Responses of Laminated Composite Plates According to the Impactor's Shapes", Computers and Structures, Vol. 65, No.1, pp83-90, 1997.

Kim J.K. and Mai Y.W., 1991, "High Strength, High Fracture Toughness Fibre Composites with Interface Control - A Review", Composites Science and Technology Vol 41, 1991, 0266-3538/91, 333-278.

Kubo J.T. and Nelson R.B., 1975, "Analysis of Impact Stresses in Composite Plates", Foreign Object Impact Damage to Composites, ASTM STP 568, ASTM, 1975, pp228-244.

Kurashige M., Watanabe K., Kuriyama T., 1995, "An Application of the IFRM Theory to Evaluation of Interlaminar Shear Stress in a Fibre-Reinforced Laminate", in D.F. Parker and A.H. England (eds), IUTAM Symp. On Anisotropic, Inhomogeneity and Nonlinearity in Solid Mechanics, pp 359 - 370, Kluwer.

Labossiere P. and Neale K.W., 1991, "A Parametric Failure Criterion for Paperboard Material", J. Strain Analysis Vol 26 No 4, 1991, IMechE 1991,0309-3247/91/1000-0209, 209-314.

Lagace P.A., 1986, "Delamination in Composites: Is Toughness the Key?", 31st International Sample Symposium, April 7-10, 1986, 739-749.

Lakshminarayana H.V., Boukhili R. and Gauvin R., 1994(a), "Impact Response of Laminated Composite Plates : Prediction and Verification", Composite Structures 28 (1994), pp61-72, Elsevier Science Limited, U.K..

Lakshminarayana H.V., Boukhili R. and Gauvin R., 1994(b), "Finite Element Simulation of Impact Tests of Laminated Composite Plates", Composite Structures 28 (1994), pp47-59, Elsevier Science Limited, U.K..

Lakshminarayana H.V. and Murthy M.V.V., 1990, "Finite Element Analysis of Shell Structures with Cutouts and Cracks", Finite Element Applications to Thin-walled Structures, Chapter 3, edited by J.W. Bull, pp63-87, ESP Ltd, ISBN 1-85166-373-8.

Langlie S. and Cheng W., 1989, "Numerical Simulation of High Velocity Impact of Fiber-Reinforced Composites", ASME Pressure Vessels and Piping Division, 1989, Vol. 159, 51-64, ISBN/ISSN : 0277-027X.

Lark R.F., 1977, "Recent Advances in Lightweight, Filament-Wound Composite Pressure Vessel Technology", Proc ASME Energy Technology Conf 1977, PVP-PB-021, U.S.A., pp17-49.

Lesser A.J. and Filippov A.G., 1991, "Kinetics of Damage Mechanisms in Laminated Composites", 36th International SAMPE Symposium, April 1991, Book1, pp886-900.

Lee J.D., 1980, "Three Dimensional Finite Element Analysis of Layered Fibre-Reinforced Composite Materials", Computers and Structures, vol. 12, pp319-339, Pergamon Press Ltd., 1980, U.K.

Lee J.D., 1982, "Three Dimensional Finite Element Analysis of Damage Accumulation in Composite Laminate", Computers and Structures, vol. 15, No. 3, pp335-350, Pergamon Press Ltd., 1982, U.K.

Lee J.D., Du,S and Liebowitz, H., 1984, "Three Dimensional Finite Element and Dynamic Analysis of Composite Laminate Subjected to Impact", Computers and Structures, vol. 19, 5/6, pp807-813, Pergamon Press Ltd., 1984, U.S.A.

Lee S.M., 1988, "Failure Mechanism of Delamination Fracture", Composite Materials : Testing and Design (8th Conference), ASTM STP 972, J.D. Whitcomb, Ed., ASTM, Philadelphia, 1988, pp 356-365.

Lee S.W.R., 1992, "Investigation and Modelling of Penetration Process for Composite Laminates Impacted by a Blunt-Ended Projectile", PhD Thesis, Purdue University, U.S.A., 1992.

Li Y., Ruiz C. and Harding J., 1989, "Modelling of the Impact Response of Fibre-Reinforced Composites", University of Oxford Sixth Progress Report, Report No. OUEL 1784/89.

Lifshitz J.M. and Dayan H., 1995, "Filament-Wound Pressure Vessel with Thick Metal Liner", Composite Structures, Vol. 32 (1995), pp313-323.

Lin H.J. and Lee Y.J., 1990, "On the Inelastic Impact of Composite Laminated Plate and Shell Structures", Composite Structures, Vol. 14 (1990), pp89-111.

Lin H.L. and Lee Y.L., 1990, "Impact-Induced Fracture in Laminated Pates and Shells", Journal of Composite Materials, Vol. 24 - November 1990, pp1179-1199.

Liu J. and Jones N., 1987, "Experimental Investigation of Clamped Beams Struck Transversely by a Mass", Int. J. Impact Engng, Vol. 6, No.4, 303-335.

Liu J.H. and Jones N., 1988, "Dynamic Response of a Rigid Plastic Clamped Beam Struck by a Mass at Any Point on the Span", Int. J. Solids Structures, Vol.24, No.3, 251-270.

Liu D., 1988, "Impact-Induced Delamination - A View of Bending Stiffness Mismatching", J. Composite Materials Vol.22, July 1988, 674-692.

Liu S., Kutlu Z. and Chang F.K., 1991, "Matrix Cracking and Delamination in Laminated Polymeric Composites Resulting from Transversely Concentrated Loadings", 1st International Conference on Deformation and Fracture of Composites, Mon.-Wed. 25-27 March 1991, 30/1-30/6.

Liu S., Kutlu Z. and Chang F.K., 1991, "Matrix Cracking and Delamination in Laminated Polymeric Composites Resulting From Transversely Concentrated Loadings", 1st International Conference on Deformation and Fracture of Composites, Mon.-Wed. 25-27 March 1991, 30/1-30/6.

Lloyd B.A. and Knight G.K., 1986, "Impact damage Sensitivity of Filament-wound Composite Pressure vessels", JANNF Propulsion Meeting, Vol. 1, CPIA Publication 455 Vol. 1, August 1986, pp 7-15.

Lu T.J., Ji X. and Gu X.R., 1989, The Effect of Resin Properties on the Strength of Filamentary Structures", Journal of Strain Analysis Vol.24 No.2, 1989, IMechE 1989, 107-113.

Lubin G. (Editor), 1969, "Handbook of Fibreglass and Advanced Plastics Composites", SPE Polymer Technology Series, Van Nostrand Reinhold Company, 1969.

Macaulay M.A., 1987, "Introduction to Impact Engineering", Routledge Chapman and Hall, New York, 1987.

Maiti D.K. and Sinha P.K., 1996, "Impact Response of Doubly Curved Laminated Composite Shells Using Higher-Order Shear deformation Theories", Journal of Reinforced Plastics and Composites, Vol. 15, June 1996, pp575-601.

Makins R.K. and Adali S., 1991, "Bending of Cross-Ply Laminated Plates With Matrix Cracks", Journal of Strain Analysis Vol 26 No. 4, 1991, IMechE 1991, 253-257.

Manders P.W., Bader M.G., Hinton M.J. and Flower P.Q., 1979, "Mechanisms of Impact Damage in Filament-Wound Glass-Fibre/Epoxy-Resin Tubes", Proc. of the Int Conf Mechanical Behaviour of Materials, Vol.3, ICM 3, Cambridge, England, August 1979.

Martin R.H., 1992, "Delamination Failure in a Unidirectional Curved Composite Laminate", Composite Materials: Testing and Design (Tenth Volume), ASTM STP 1120, 1992, 365-383.

McGrath G.C. and Clegg D.W., 1991, "Fracture Toughness of Reclaimed Continuous Fibre APC-2", 1st International Conference on Deformation and Fracture of Composites, Mon.-Wed. 25-27 March 1991, 46/1-46/5.

Mindlin R.D., 1951, "Influence of Rotary Inertia and Shear on Flexural Motions of Isotropic Elastic Plates", ASME J Applied Mechanics, vol 18, pp31-38.

Mines R.A.W., Worrall C.M. and Gibson A.G., 1990, "The Response of GRP Sandwich Panels to Dropped Object Impact Loading", Proceedings of the Institution of Mechanical Engineers, Fourth Int. Conference FRC'90, C400/038, 149-155.

Montague Peter, 1985, "Composite, Double-skin Sandwich Pressure Vessels", Shell structures - Stability and Strength, Chapter 4, pp97-136, edited by R. Narayanan, Elsevier Applied Science Publishers, 1985, ISBN 0-85334-343-8.

Mori T., Hirase Y., Ishihara T., Kawahara M., Katoh A., Yu Q., and Shirtori M., 1991, "Strength Estimation of Metal-FRP Bonded Joints and Its Application to a Filament Wound Product", 36th International SAMPE Symposium, April 1991, pp806-817.

Morris E.E., Patterson W.P., Landes R.E. and Gordon R., 1977, "Composite Pressure Vessels for Aerospace and Commerical Applications", PVP-PB-021, Composites in Pressure vessels and Piping, The Energy Technology Conference, Houston, Texas, September 18-23, 1977, pp89-128, ASME, The pressure vessels and piping divison.

Morris Edgar E., 1981, "Commercial Filament Wound Pressure vessels for Military and Aerospace Applications", SAE Transactions, Technical Paper Series, No. 811093, 1981.

Mortimer R.W., Rose J.L. and Blum A., 1972, "Longitudinal Impact of Cylindrical Shells with Discontinuous Cross-Sectional Area", Journal of Applied Mechanics, Transactions of the ASME, December 1972, 1005-1010.

Murthy P.L.N. and Chamis C.C., 1988, "Composite Interlaminar Fracture Toughness: Three-Dimensional Finite-Element Modelling for Mixed Mode I, II, and Fracture", Composite Materials: Testing and Design (English Conference), ASTM STP 972, J.D.Whitcomb, Ed.,American Society for Testing and Materials, Philadephia, 1988, 23-40.

Murty A.V.K., 1988, "Finite Element Estimation of Interlaminar Stresses in Laminated composites", CAD in Composite Material Tech., 1988, edited by C.A. Brebbia, W.P. de Wilde and W.R. Blain, ISBN 0-905451-97-X.

National Agency for Finite Element Methods and Stardards, 1992, "A Finite Element Dynamics Primer", Department of Trade and Industry, National Engineering Laboratory, Publisher, 1992, ISBN 1-874376-05-0.

National Agency for Finite Element Methods and Stardards, 1986, "A Finite Element Primer", Department of Trade and Industry, National Engineering Laboratory, Publisher, 1986, ISBN 0-903640-17-1.

O'Brien T.K., 1990, "Towards a Damage Tolerance Philosophy for Composite Materials and Structures", Composite Materials: Testing and Design (Ninth Volume), ASTM STP 1059, S.P. Garbo, Ed., ASTM, Philadelphia, 1990, 7-33.

Ophir, Z., Buchman, A., Flashner, F., Liran, I. And Simons, H., 1995, "Modified Epoxy Formulation for Improving the Fracture Resistance of Filament Wound Pressure Vessels", J. Adhesion Sci. Technol., Vol. 9, No. 2, pp159-175 (1995).

Osweiller F., 1992, "Basis of the Tubesheet Heat Exchanger design Rules Used in the French Pressure Vessel Code", Transactions of the ASME, Journal of Pressure Vessel Technology, February 1992, Vol. 114, pp124-131.

"PAFEC Theory Manual", 1984, published by PAFEC Ltd.

"PAFEC Data Preparation User Manual - Level 8.1", published by PAFEC Ltd.

"PIGS User Manual - Level 8.1", published by PAFEC Ltd.

Palazotto A. and Perry R., 1992, "Impact Response of Graphite / Epoxy Cylindrical panels", AIAA Journal, Vol. 30, No. 7, July 1992, pp1827-1832.

Paul R.J., Tay T.E. and Williams J.F., 1988, "Assessment of the Effect of Impact Damage in Composites : Some Problems and Answers", Composite Structures, Vol. 10 (1988), pp51-73.

Pawlik P.S. and Reismann H., 1973, "Forced Plane Strain Motion of Cylindrical Shells - A Comparison of Shell Theory with Elasticity Theory", Transactions of the ASME, Journal of Applied Mechanics, Sept. 1973, 725-730.

Perl M. and Arone R., 1988, "Stress Intensity Factors for a Radially Multicracked Partially Autofrettaged Pressurized Thick-Walled Cylinder", Journal of Pressure Vessel Technology Vol.110, May 1988, Transactions of the ASME, 147-154.

Perry R., Palazotto A. and Sandhu R., 1992, "The Analysis Related to the Impact", Proc 3rd Int. Conf. Eng Constr Oper Space Space 92, Vol. 1, pp1286-1296.

Peterson D.A. and Hart-Smith L.J., 1990, "A Rational Development of Lamina-to-Laminate Analysis Methods for Fibrous Composites", Composite Materials: Testing and Design (Ninth Volume), ASTM STP 1059, S.P. Garbo, Ed., ASTM, Philadelphia, 1990, 121-164.

Phillips L.N. (Editor), 1989, "Design with Advanced Composite Materials", The Design Council, London, Springer-Verlag, ISBN 0-85072-238-1, 1989.

Pipkin and Rogers, 1971a, J. Applied Mech. V38, pp634.

Poe Jr. C.C., "Simulated Impact Damage in a thick Graphite /Epoxy Laminate Using Spherical Indenters", Journal of Reinforced Plastic and Composites Vol.10, May 1991, 293-307.

Pohto H.A., 1979, "Energy Release From Rupturing High-Pressure Vessels: A Possible Code Consideration", Transactions of the ASME, Journal of Pressure Vessel Technology, May 1979, Vol. 101, pp165-170.

Prasad C.B., Ambur D.R. and Starnes J.H. Jr., 1994, "Response of Laminated Composite Plates to Low-Speed Impact by Different Impactors", AIAA Journal, Vol. 32, No. 6, June 1994.

Prevorsek D.C., Chin H.B. and Bhatnagar A., 1993, "Damage Tolerance : Design for Structural Integrity and Penetration", Composite Structures 23 (1993), pp137-148.

Price M.R. and Vandiver T., 1989, "JANNAF Interim Mechanical Test Standards for Filament Wound Composites", 34th International SAMPE Symposium, May 1989, pp1079-1093.

Prucz J.C., D'Acquisto J. and Smith J.E., 1988, "Dynamic Response of Composite Pressure Vessels To Inertia Loads", PVP Vol. 146, 1988, ASME Pressure Vessels and Piping Conf., June 1988, 55-62.

Qian Y. and Swanson S.R., 1990, "A Comparison of Solution Techniques for Impact Response of Composite Plates", Composite Structures, 14, 1990, pp177-192.

Radhamohan S.K. and Galletly G.D., 1979, "Plastic Collapse of Thin Internally Pressurized Torispherical Shells", Transactions of the ASME, Journal of Pressure Vessel Technology, November 1979, Vol. 101, pp311-320.

Rajendran A.M., 1994, "Modelling the Impact Behaviour of AD85 Ceramic Under Multiaxial Loading", Int. J. Impact Engng, Vol.15, No.6, pp749-768, 1994, Elsevier Science Ltd, England.

Ramesh T.C. and Ganesan N., 1995, "Vibration and Damping Analysis of Cylindrical Shells With Constrained Damping Treatment - A Comparison of Three Theories", Journal of Vibration and Acoustics, Transactions of the ASME, April 1995, Vol. 117, pp213-219.

Ray G.S., Sinha B.K. and Majumdar S., 1989, "Optimum Design of Radial-Flow Impellers", Proc Instn Mech Engrs Vol 203, 229-232.

Lord Rayleigh, 1906, Phil. Mag., vol 11, p283.

Reedy E.D. Jr., Mello F.J. and Guess T.R., 1997, "Modeling the Initiation and Growth of Delaminations in Composite Structures", Journal of Composite Materials, Vol. 31, No. 8, 1997, pp812-831.

Reddy J.N., 1982, "Impact on Laminated Composite Plates : A Review of Recent Computational Developments", Proc of the Army Research Office Workshop on Computational Aspects of Penetration Mechanics held at the ballistic Research Laboratory at Aberdeen Proving Ground, Maryland, 27-29 April, 1982.

Rehfield L.W. and Murthy P.L.N., 1982, "Toward a New Engineering Theory of Bending: Fundamentals", AIAA Journal Vol.20 No.5, May 1982, 693-699.

Reid S.R., Al-Hassani S.T.S. and Corbett G.G., 1991, "Project CP 05 Failure of Composite Pipes under Local Loading", The Cost Effective Use of Fibre Reinforced Composites Offshore - Phase I, Final Report - Volume Three, Pipe Elements, June 1991, Marinetech North West, 1-30.

Richards and Daniels M., 1987, "Enhancing Finite Element Surface Stress Predictions: A Semi-Analytic Technique for Axisymmetric Solids", Journal of Strain Analysis Vol.22 No.2, 1987, 75-85.

Robinson P. and Davies G.A.O., 1992, "Impactor Mass and Specimen Geometry Effects in Low Velocity Impact of Laminated Composites", Int.J. Impact Engng, Vol. 12, No.2, 189-207.

Rogers C.A. and Knight C.E., Jr, 1988, "An Axisymmetric Liner / High-Order Finite Element for Filament-Wound Composites - I. Formulation and Algorithm", Computers and Structures, Vol. 29, No. 2, pp265-271, 1988.

Rogers C.A. and Knight C.E., Jr, 1988, "An Axisymmetric Liner / High-Order Finite Element for Filament-Wound Composites - II. Evaluation on Filament-Wound Cylinders", Computers and Structures, Vol. 29, No. 2, pp273-281, 1988.

Rohwer K., 1992, "On Various Computational Models for Laminated Composites", Invited Lecture Special Technological Session NME3: Numerical Modelling of Composite Structures at the ECCOMAS Conference, Brussels, 7-11 Sept. 1992.

Rosenberg Z., Mironi J., Cohen A. and Levy P., 1994, "On the Catastrophic Failure of High-Pressure Vessels by Projectile Impact", Int. J. Impact Engng, Vol.15, No.6, pp827-831, 1994, Elsevier Science Ltd, England.

Rotem A, 1988, "Residual Flexural Strength of FRP Composite Specimens Subjected to Transverse Impact Loading", SAMPE J, 24 (2), pp19-25, 1988.

Roy A.K., 1987, "Study of Design Parameters of Cylindrical Composite Pressure Vessels", 32nd International SAMPE Symposium, April 1987, pp517-528.

Roy A.K. and Tsai S.W., 1988, "Design of Thick Composite Cylinders", Journal of Pressure Vessel Technology Vol.110, Transactions of ASME, August 1988, 255-262.

Ryan R.S., 1992, "Practices in Adequate Structural Design", Transactions of the ASME, Journal of Pressure Vessel Technology, August 1992, Vol. 114, pp300-307.

Saha N.K., Wang H.C. and El-Achkar R., 1992, "Frontal Offset Pole Impact Simulation of Automotive Vehicles", Computers in Engineering Vol 2, Finite Element Techniques, Robotics and Controls, Computers in Education, ASME 1992, pp203-207.

Sankar B.V. and Sun C.T., 1985, "Low Velocity Impact Response of Laminated Beams Subjected to Initial Stresses", AIAA J., vol 23(12), pp1962-1969.

Sang Z.F. and Widera G.E.O., 1988, "Stress and Strength Analysis of Concentric Reducers Consisting of Plates", Journal of Pressure Vessel Technology Vol.110, May 1988, Technical Briefs, 217-224.

SANZ NZS 5454, 1989, "Requirements for Lightweight Steel Automotive Compressed Natural Gas Cylinders for Use in New Zealand", Standards Association of New Zealand.

Saravanos D.A., 1994, "Integrated Damping mechanics for Thick Composite Laminates and Plates", Joural of Applied Mechanics, Transactions of the ASME, June 1994, Vol. 61, pp375-383.

Saravanos D.A. and Pereira J.M., 1995, "Dynamic Characteristics of Specialty Composite Structures with Embedded Damping layers", Journal of Vibration and Acoustics, Transactions of the ASME, January 1995, Vol. 117, pp62-69.

Sato N., Kurauchi T. and Kamigaito O., 1986, "Thermo-Acoustic Emission from Damaged Composite", 31st International SAMPE Symposium, April 7-10, 1986, 343-351.

SCI, "Advanced Composite Structures" (Catalogue to composite cylinders)

Scott E.G., 1991, "Characterizing the Failure of Composite Structures", Mechanical Engineering, Feb. 1991, 57-60.

Segletes S.B. and Zukas J.A., 1987, "The Effect of Material Interfaces on Calculations of Plate Penetration", Recent Advances in Impact Dynamics of Engineering Structures 1989, AMD-Vol.105, AD-Vol.17, pp39-45.

Seshadri R. and Fernando C.P.D., 1992, "Limit Loads of Mechanical Components and Structures Using the GLOSS R-Node Method", Transactions of the ASME, Journal of Pressure Vessel Technology, May 1992, Vol. 114, pp201-208.

Sharma A.V., 1981, "Low-Velocity Impact Tests on Fibrous Composite Sandwich Structures", Test Methods and Design Allowables for Fibrous Composites, ASTM STP 734, 1981, pp54-70.

Shaw K.J., 1992, "Impact Testing of Glass Reinforced Plastic (GRP) pipes", Nov 1992, British Gas Plc Internal Report.

Shim V.P.W., Toh, S.L. and Gong, S.W., 1996, "The Elastic Impact Response of Glass / Epoxy Laminated Ogival Shells", Int. J. Impact Engng, Vol. 18, No. 6, pp633-655, 1996.

Shivakumar K.N., Elber W. and Illg W, 1985, "Prediction of Impact Force and Duration Due to Low-Velocity Impact on Circular Composite Laminates", J. Applied Mechanics, Transactions of the ASME, Vol. 52, Sept 1985, pp674-680.

Simonen F.A., Henderson N.C., Winegardner R.D. and Specht K., 1975, "Analysis of Strength and Residual Stresses in Filament Reinforced Aluminum Cylinders", J. of Pressure Vessel Technology, August 1975, Transactions of the ASME, pp192-198.

Sjoblom P.O., Hartness J.T. and Cordell, T.M., 1987, "On Low-Velocity Impact Testing of Composite Materials", Journal of Composite Materials, Vol. 22, January 1988, pp30-52.

Soldatos K.P., 1992, "Nonlinear Analysis of Transverse Shear Deformable Laminated Composite Cylindrical Shells - Part II: Buckling of Axially Compressed Cross-Ply Circular and Oval Cylinders", Transactions of the ASME, Journal of Pressure Vessel Technology, February 1992, Vol. 114, pp110-114.

Soreide T.H. and Kavlie D., 1985, "Collision Damage and Residual Strength of Tubular Members in Steel Offshore Structures", Shell structures - Stability and Strength, Chapter 6, pp185-220, edited by R. Narayanan, Elsevier Applied Science Publishers, 1985, ISBN 0-85334-343-8.

Spencer A.J.M., 1972, "Deformations of Fibre-Reinforced Materials", Clarendon Press, Oxford, 1972.

Srinivasa L., Iyer L. and Haugan D., 1986, "Cyclic Loading and Stress Concentration on Composites", 31st International Sample Symposium, April 7-10, 1986, 1780-1795.

Staab G.H. and Gilat A., 1991, "A Direct-tension Split Hopkinson Bar for High Strain-rate Testing", Proceedings of the Society for Experimental Mechanics, SEM, 1991, Vol 48, 232-235.

Stephenson (Editor), 1991, "Hurrell M. : Like an Old Fuel", Green Magazine, Feb. 1991, pp16-19.

Strait L.H., Karasek M.L. and Amateau M.F., 1992, "Effects of Stacking Sequence on the Impact Resistance of Carbon Fiber reinforced Thermoplastic Toughened Epoxy Laminates", Journal of Composite Materials, Vol. 26, No. 12, 1992, pp1725-1740.

Summerscales J. "NDT of Advanced Composites - An Overview of the Possibilities", British Journal of NDT, Nov.1990, Vol. 32, No.11, 568-577.

Sun C.T. and Chattopadhyay S., 1975, "Dynamic Response of Anisotropic laminated Plates Under Initial Stress to Impact of a Mass", Journal of Applied Mechanics, Transactions of the ASME, September 1975, pp693-698.

Sun C.T. and Jih C.J., 1990, "Mechanics of Delamination in Composite Laminates Subjected to Low Velocity Impact", Impact Response and Elastodynamics of Composites, AMD-Vol.116, ASME, Nov. 25-30 1990, pp1-10.

Sun C.T. and Rechak S., 1988, "Effect of Adhesive Layers on Impact Damage in Composite Laminates", Composite Materials: Testing and Design (Eighth Conference), ASTM STP 972, 1988, 97-123.

Sun C.T. and Wang T., 1986, "Impact Wave Response and Failure in Composite Laminates", European Colloquium 214 Mechanical Behaviour of Composites and Laminates (1986: Yugoslavia), 1986, 19-31.

Swanson S.R., 1993, "Scaling of Impact damage in Fibre composites from Laboratory specimens to Structures", Composite Structures 25 (1993), pp 249-255. ESP Ltd. U.K.

Swanson S.R. and Qian Y., 1991, "Analytical and Experimental Strain Response in Impact of Composite Cylinders", Composite Structures 18, 1991, pp95-108, ESP Ltd., U.K.

Swaddiwudhipong S. and Liu Z.S., 1997, "Response of Laminated Composite Plates and Shells", Composite Structures, Vol. 37, No. 1, pp21-32, 1997.

Takeda N., Sierakowski R.L., and Malvern L.E., 1980, "Wave Propagation Experiments On Ballistically Impacted Composite Laminates", J. Composite Materials, Vol. 15, March 1981, 157-174.

Takeda T., 1991, "The Application of an Anisotropic Yield Function of the Sixth Degree to Orthotropic Material", Journal of Strain Analysis Vol 26 No. 3, 1991, IMechE 0309-3247/91/ 0700-0201, 201-207.

Talreja R., 1989, "Damage Development in Composites: Mechanisms and Modelling", J. Strain Analysis Vol 24 No 4, 1989, IMechE 1989, 0309-3247/89/10000-0215, 215-222.

Tan T.M. and Sun C.T., 1985, "Use of Statical Indentation Laws in the Impact Analysis of Laminated Composite Plates", J. of Applied Mechanics, Vol.52, March 1985, pp6-12, Transactions of the ASME.

Teply J.L. and Herbem W.C., 1985, "Failure Modes for Filament Wound Aluminium Natural Gas Cylinders", Proc Fracture Mechanism Program and related papers presented at the Int. Conf and Expo on Fatigue, Corrosion Cracking, Fracture Mechanics and Failure Analysis, December 1985, Utah, U.S.A.

Thomas D.A., 1992, "Long-Life Assessment of Graphite / Epoxy Materials for Space Station Freedom Pressure Vessels", J. Propulsion, Vol. 8. No. 1, Jan.-Feb. 1992.

Thomson W.T., 1993, "Theory of Vibration with Applications", 4th Edition.

Thomson R.G., Carden H.D. and Hayduk R.J., 1984, "Research at NASA on Crash Dynamics", Structural Impact and Crashworthiness Vol 1 Keynote Lectures, Edited by G.A.O. Davies, 1984. pp 1-43.

Tiller D.B., Newhouse N.L. and Veys R.B., 1990, "Design and Qualification of an 'All-Composite' Natural Gas Vehicle Fuel Cylinder", Brunswick Corporation, Lincoln, Nebraska, 1-9.

Timoshenko S., 1934, "Theory of Elasticity", McGraw-Hill, New York.

Tin W.P., Gott J. and Breckell T.H., 1988, "Residual Static Strength Prediction of Impacted Composite Laminates", CAD in Composite Material Tech., 1988, pp337-351, edited by C.A. Brebbia, W.P. de Wilde and W.R. Blain, ISBN 0-905451-97-X.

Tsai S.W. and Wu E.M., 1971, "A General Theory of Strength for Anisotropic Materials", J Composite Materials, vol 5, pp58-80, 1971.

Tsai S.W. and Hahn H.J., 1980, "Introduction to Composite Materials", Technomic Publishing Company Inc., U.S.A., ISBN 0-87762-288-4.

Ucmaklioglu M. and Dawe D.J., 1985, "Experimental and FEM Study of a Cylindrical Panel Loaded Through a Pad", Journal of Strain Analysis Vol. 20 No. 2, 1985, 111-119.

Ujihashi S., Sakanoue K., Adachi T. and Matsumoto H., 1990, "Experimental Measurement of the Mechanical Properties of Fibre-Reinforced Plastics Under Impact Loading", Proceedings of the Institution of Mechanical Engineers, Fourth Int. Conference FRC'90, C400/052, 157-162.

Valisetty R.R. and Rehfield L.W., 1985, "A Theory for Stress Analysis of Composite Laminates", AIAA Journal Vol.23 No.7, July 1985, 1111-1117.

Vaziri R., Quan X. and Olson M.D., 1996, "Impact Analysis of Laminated Composite Plates and Shells by Super Finite Elements", Int. J. Impact Engng, Vol. 18, Nos 7-8, pp765-782, 1996.

Vlot A., 1996, "Impact Loading on Fibre Metal Laminates", Int. J. Impact Engng, Vol. 18, No. 3, pp291-307, 1996.

Wang C.Y., 1989, "A Study of Impact Damage in Composite Laminates", PhD Thesis, The University of Texas Austin, U.S.A.

Waltz T.L. and Vinson J.R., 1976, "Interlaminar Stresses in Laminated Cylindrical Shells of Composite Materials", AIAA Journal Vol.14, No.9, September 1976, 1213-1218.

Wardle M.W. and Zahr G.E., 1987, "Instrumented Impacted Testing of Aramid-Reinforced Composite Materials", Instrumented Impact Testing of Plastics and Composite Materials, ASTM STP 936, 1987, pp219-235.

Wardle B.L. and Lagace P.A., 1997, "Importance of Instability in Impact Response and Damage Resistance of Composite Shells", AIAA Journal, Vol. 35, No. 2, February 1997.

Wekezer J.W., Oskard M.S., Logan R.W. and Zywicz E., 1993, "Vehicle Impact Simulation", J. Transport Engineering, Vol. 119, No. 4, July/Aug., 1993. pp598-617. ASCE, ISSN 0733-947X/93/0004-0598.

Whitcomb J.D., 1990, "Mechanics of Instability-Related Delamination Growth", Composite Materials: Testing and Design (Ninth Volume), ASTM STP 1059, S.P. Garbo, Ed., ASTM, Philadelphia, 1990, 215-230.

Widera G.E.O. and Logan D.L., 1979, "Layered Cylindrical Pressure Vessels", Transactions of the ASME, Journal of Pressure Vessel Technology, February 1979, Vol. 101, pp80-86.

Williams J.G. and Rhodes M.D., 1982, "Effects of Resin on Impact Damage Tolerance of Graphite / Epoxy laminate", ASTM STP 787, pp450-480, 1982.

Williams J.G., 1990, "Fracture Mechanics of Composites Failure", 26th John Player Lecture, Pro. Instn Mech Engrs, Vol. 204, 209-218.

Wu Y.S., Longmuir A.J. Chandler H.W. and Gibson A.G., 1992, "Through-Thickness Tensile Stresses in Curved Composite Shells", The Plastics and Rubber Institute, Fifth Int. Conference on Fibre Reinforced Composite FRC'92, 27.1-27.15.

Wu H.Y.T. and Springer G.S., 1988, "Impact Induced Stresses, Strains, and Delaminations in Composite Plates", J. Composite materials, Vol. 22, June 1988, pp533-560.

Wu C.L. and Sun, C.T., 1996, "Low velocity Impact Damage in Composite sandwich beams", Composite Structures, Vol. 34 (1996), pp21-27.

Wurzel D.P., 1989, "Torsional Impact of Filament Wound Tubes", 34th International SAMPE Symposium, May 1989, pp1099-1107.

Yasuda E. et al, 1991, "The Effect of Bridging on the Strength of a Unidirectional Carbon/Carbon Composite in Off-axis Tests", Composite Science and Technology Vol 41, 1991, 0266-3538/91, 55-61.

Yener M. and Wolcott E., 1989, "Damage Assessment Analysis of Pressure Vessels Subjected to Random Impact Loading", Transactions of the ASME, Journal of Pressure Vessel Technology, May 1989, Vol.111, 124-129.

Young K.S., 1992, "Advanced Composite Storage Containment for Hydrogen", Int. J. Hydrogen Energy, Vol. 17, No.7, pp505-507, 1992.

Yu J. and Jones N., 1991, "Further Experimental Investigations on the Failure of Clamped Beams under Impact Loads", Int. J. Solids Structures, Vol.27, No.9, 1113-1137.

Zhang W. and Evans K.E., 1988, "Computer Simulation of Failure Envelopes for Composites", CAD in Composite Material Tech., 1988, edited by C.A. Brebbia, W.P. de Wilde and W.R. Blain, ISBN 0-905451-97-X.

Zhu L, 1996, "Stress and Strain Analysis of Plates Subjected to Transverse Wedge Impact", Journal of Strain Analysis, Vol. 31, No. 1 (1996), pp1-7.

Zibdeh H.S., 1991, "Failure Probability Analysis for a Cylinder Subjected to General Loading Conditions" Transactions of the ASME, Journal of Pressure Vessel Technology, November 1991, Vol. 113, pp532-537.

Zienkiewicz O.C., 1972, "Introduction Lectures on the Finite Element Method", McGraw Hill Book Company (UK) Ltd.

Zienkiewicz O.C., 1977, "The time Dimension; Finite Element Approximation to Initial Value - Transient Problems", The Finite Element Method, Chapter 21, 3rd edition, McGraw-Hill book Co. (UK) Ltd.

Zukas J.A., 1982, "Numerical Simulation of Impact Phenomena", Impact Dynamics, Chapter 10, Zukas J.A. et al Editors, John Wiley and Sons, 82/05494, 1982, pp367-417.

Appendix A Validation of Approach 4

Approach 4 relying on the HINGES.AND.SLIDES data module was used in a further investigation to test its validity for modelling an interface with the consideration of various geometric shapes and overall dimensions. The test involved the comparison of impact response of the two shell element layer model with that of a single shell element layer model. The two models being compared are referred to as the "model pair" in each case considered below.

Three cases characterised by different geometric shapes, overall dimensions and element meshes were analysed (see Table A1 and Figs A1 to A4). Models with smaller overall dimensions were extracted from the largest master model so that the FE mesh design used in these cases was the same. The loading details are described in Table A2. The impact loading was applied to a small area bounded by four elements, 21 nodes, near the reference origin of the shell structure. The four elements are numbered 18, 19, 468 & 472 in the top shell element layer. Each thick shell element layer has three sub-layers, as shown in Table 3.2.6. VELOCITIES.PRESCRIBED data module was used to simulate impact loading.

For the models with two shell element layers, all d.o.f. of coincident construction nodes fully constrained. For each model, the number of master d.o.f. was assigned according to the number of the usable natural frequencies calculated by PAFEC. With reference to the guidelines given by NAFEMS, the number of master freedoms used was ten times the number of usable natural frequencies.

For dynamic analysis, only the master degrees of freedom are involved in the calculation of eigenvalues (response frequencies). Moreover, the FE system of equations used for calculating response solutions involves structural stiffnesses, masses, and the natural frequencies.. A close agreement of the natural frequencies generated by each "model pair" can serve as a preliminary indication of the validity of the model with two shell elements layers connected by HINGES.AND.SLIDES. Transverse displacements and stresses were also examined.

The first twelve natural frequencies of each model are listed in Table A5. It is believed that they are sufficient for validation purpose. It can be seen that the model pairs with 660 elements and 320 elements have excellent agreement in the first twelve natural frequencies. The model pair with 1080 elements only show a 0.3 % difference in the ninth natural frequency.

Transverse displacement response at three locations and stresses at two locations are listed in Tables A3 and A4. It can be seen that the model pairs with 660 elements and 320 elements give excellent agreement with a maximum difference of only 0.2 %. However, the model pair with 1080 elements shows a maximum disagreement of 1.7 % different. In order to find out whether this difference can be reduced, a further test was carried out by using 1000 automatic master degrees of freedom, i.e. 15.87 times the number of usable natural frequencies. From Table A6, it can be seen that the displacement difference has been significantly reduced to a maximum of 0.3 %. Figs A5 and A6 show the displacement and velocity history plots for each model pair. It can be seen that the response histories of each model pair are consistent.

After examining the natural frequencies, displacement and stress responses of all these models, the close agreement of all these responses suggests that this method of stacking two shell element layers together to form the wall of a shell structure with interface at the connecting surfaces is an effective method even for a highly curved structure. This validation further justifies the use of ten times of the number usable natural frequencies as the number of automatic master degree of freedom used in the analysis.

Table A1 Models

Number of thick shell element per layer (Length x Arc)	Cross-section	Dimensions [mm] (Length x Arc)	Restraints	Total D.O.F.	No. of usable frequencies (Auto masters used)
1080 (36 x 30)	Half-circle (arc = 180°)	420 x 157.08	Two straight edges fixed	16135	63 (630)
660 (22 x 30)	Half-circle (arc = 180°)	140 x 157.08	Two straight edges fixed	9975	50 (500)
320 (16 x 20)	Quarter-circle (arc = 90°)	80 x 78.54	All edges fixed	4445	33 (330)

NB : The radius of the cylinder was 50 mm.

Table A2 Impact loading and technique

Impact Loading	
Total impactor mass	0.0163 kg (ie 0.0007762 kg / node)
Impact velocity	-3.03 m/s
Loading area	20.936 mm^2 (ie four elements, 21 nodes)
Location	Central of the cylinder
Number of Manual Master d.o.f.	21 (Loading nodes)
Time-step	1 μs
Loading Technique	
Initial velocity technique (by using VELOCITIES.PRESCRIBED and MASSES data module)	

Table A3 Displacement response

Transverse displacement response at 100 μs [μm]

	1080 element Model			660 element Model			320 element Model		
Node No.	Single Layer	Two Layers	Error %	Single Layer	Two Layers	Error %	Single Layer	Two Layers	Error %
1	- 239.72	- 236.59	1.3	- 234.09	- 234.12	0.01	- 230.26	- 230.13	0.06
39	- 233.19	- 229.21	1.7	- 227.21	- 227.07	0.06	- 217.57	- 217.41	0.07
6	- 220.01	- 216.38	1.65	- 215.75	- 215.30	0.2	- 191.19	- 191.06	0.07

Table A4 Stress response

Stress response at 100 μs [MPa] : top surface, laminate sub-layer 1 (90°)

		1080 element Model			660 element Model			320 element Model		
Elem (Node)	Stress	Single Layer	Two Layers	Error %	Single Layer	Two Layers	Error %	Single Layer	Two Layers	Error %
18(1)	σ_{11}	-333	-336	0.9	-296	-297	0.34	-591	-590	0.17
	σ_{22}	-17.9	-18.1	1.1	-17.1	-17.3	1.2	-32.3	-32.3	0.0
17(39)	σ_{11}	-316	-323	2.2	-291	-290	0.34	-560	-561	0.18
	σ_{22}	-13.6	-13.7	0.74	-12.6	-12.7	0.8	-23.2	-23.1	0.43

Stress response at 100 μs [MPa] : bottom surface, laminate sub-layer 6 (-22°)

		1080 element Model			660 element Model			320 element Model		
Elem (Node)	Stress	Single Layer	Two Layers	Error %	Single Layer	Two Layers	Error %	Single Layer	Two Layers	Error %
18(1)	σ_{11}	152	154	1.32	148	145	2.0	309	309	0.0
2286 (6691)	σ_{22}	15.7	15.5	1.3	15.1	15.1	0.0	26.9	27.2	1.1
17(39)	σ_{11}	115	98.6	14.3	83.8	85.4	1.9	232	232	0.0
2285 (6686)	σ_{22}	14.7	14.4	2.0	13.8	13.9	0.72	24.3	24.4	0.41

NB :Elements 18 & 17 are in the top layer of the two shell element layer model or of the single shell element layer model. Elements 2286 & 2285 are in the bottom layer of the two shell element layer model.

Table A5 Natural frequencies [Hz]

	1080 element model			660 element model			320 element model		
Mode No.	Single Layer	Two Layers	Error %	Single Layer	Two Layers	Error %	Single Layer	Two Layers	Error %
1	663.0	663.0	0.0	600.9	600.9	0.0	2120.1	2120.1	0.0
2	1162.0	1161.7	0.0	1015.5	1015.5	0.0	4894.0	4893.9	0.0
3	1523.0	1522.5	0.0	1446.9	1446.8	0.0	7668.9	7667.8	0.0
4	1788.8	1788.0	0.0	2452.7	2452.5	0.0	8177.2	8177.1	0.0
5	1793.5	1793.0	0.0	2775.5	2775.2	0.0	11151	11150	0.0
6	2367.8	2367.0	0.0	2811.4	2811.1	0.0	12034	12033	0.0
7	2804.7	2802.7	0.0	4231.1	4229.6	0.0	12252	12252	0.0
8	2821.2	2819.3	0.0	4451.5	4451.2	0.0	12954	12953	0.0
9	3023.6	3031.8	0.3	4523.2	4522.4	0.0	13259	13258	0.0
10	3089.1	3085.3	0.12	5259.6	5256.7	0.0	13646	13646	0.0
11	3114.3	3114.3	0.0	5840.1	5838.0	0.0	14721	14720	0.0
12	3647.6	3644.5	0.1	6285.4	6282.9	0.0	15612	15606	0.0

Table A6 Displacement response

Transverse displacement response at 100 μs [μm]

	1080 element model (630 auto MDF's)			1080 element model (1000 auto MDF's)		
Node No.	Single Layer	Two Layers	Error %	Single Layer	Two Layers	Error %
1	- 239.72	- 236.59	1.3	- 235.22	- 234.70	0.22
39	- 233.19	- 229.21	1.7	- 227.87	- 227.40	0.2
6	- 220.01	- 216.38	1.65	- 215.21	- 214.59	0.29

Table A7 Stress response

Stress response at 100 μs [MPa] : top surface, laminate sub-layer 1 (90°)

		1080 element model (630 auto MDF's)			660 element model (1000 auto MDF's)		
Elem (Node)	Stress	Single Layer	Two Layers	Error %	Single Layer	Two Layers	Error %
18(1)	σ_{11}	-333	-336	0.9	-312	-315	0.96
	σ_{22}	-17.9	-18.1	1.1	-18.0	-18.1	0.56
17(39)	σ_{11}	-316	-323	2.2	-305	-307	0.66
	σ_{22}	-13.6	-13.7	0.74	-13.4	-13.6	1.5

Table A8 PAFEC data modules used for FE analysis

Type	Data Module	Control Module
Mesh Description	ELEMENTS NODES RESTRAINTS LOCAL.DIRECTIONS AXES MASSES	SKIP.COLLAPSE
Material Properties	LAMINATES ORTHOTRPIC.MATERIAL	
Dynamic Analysis	RESPONSE MODES.AND.FREQUENCIES MASTERS FULL.DYNAMIC.OUTPUT VELOCITIES.PRESCRIBED STRESS.ELEMENT HINGES.AND.SLIDES	

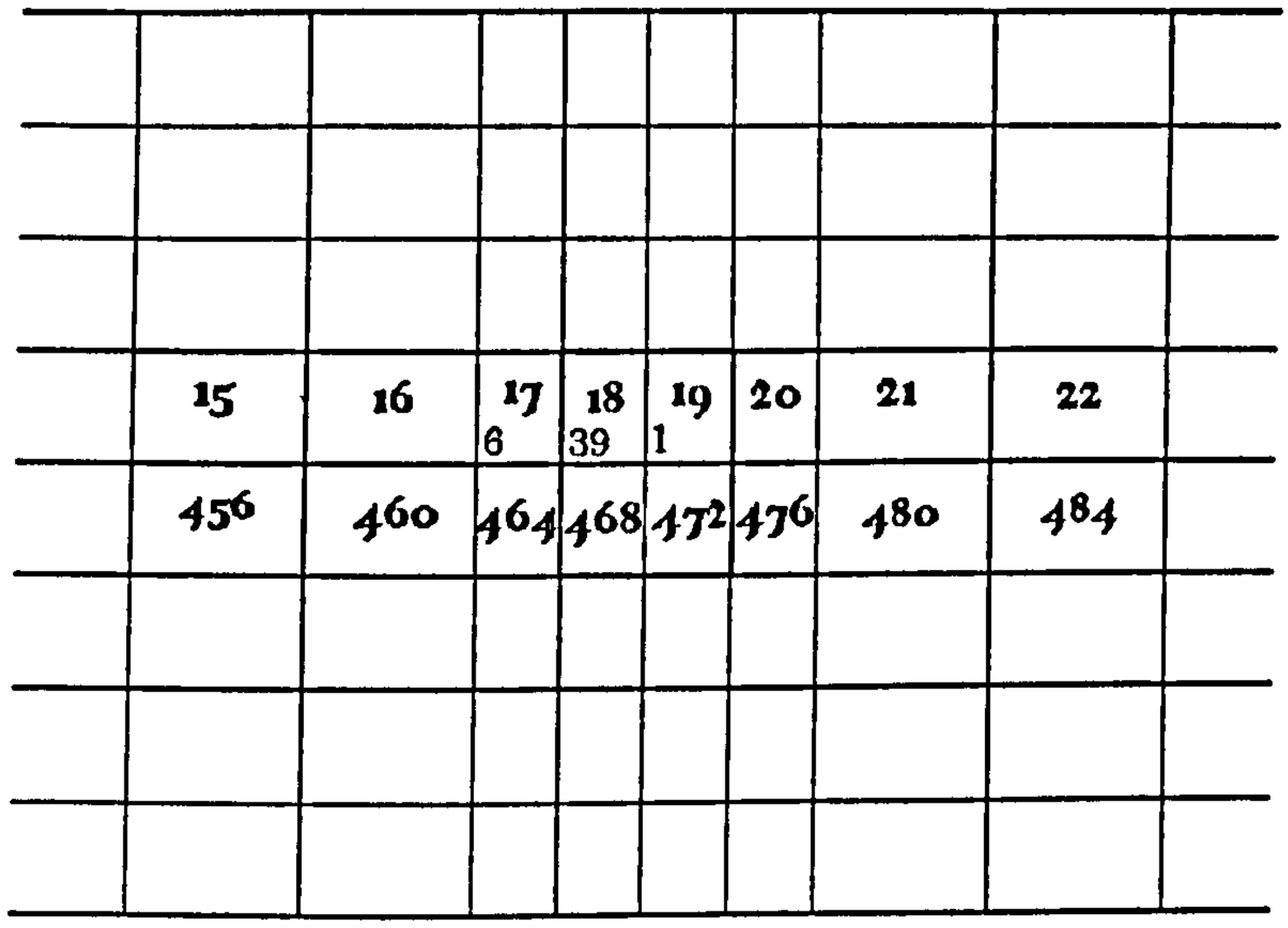

(a) Top shell element layer

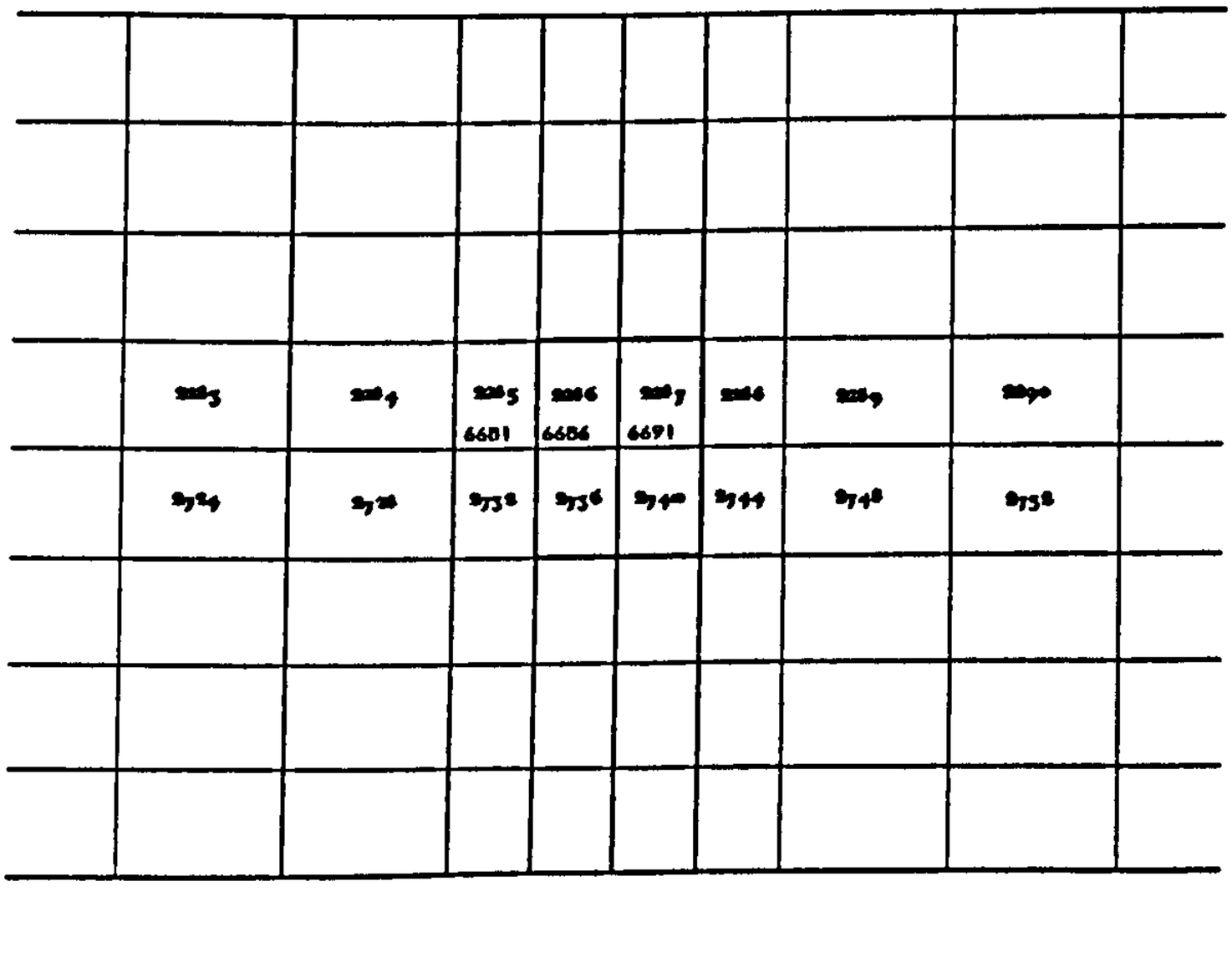

(b) Bottom shell element layer

Fig A1 Node and element numbers

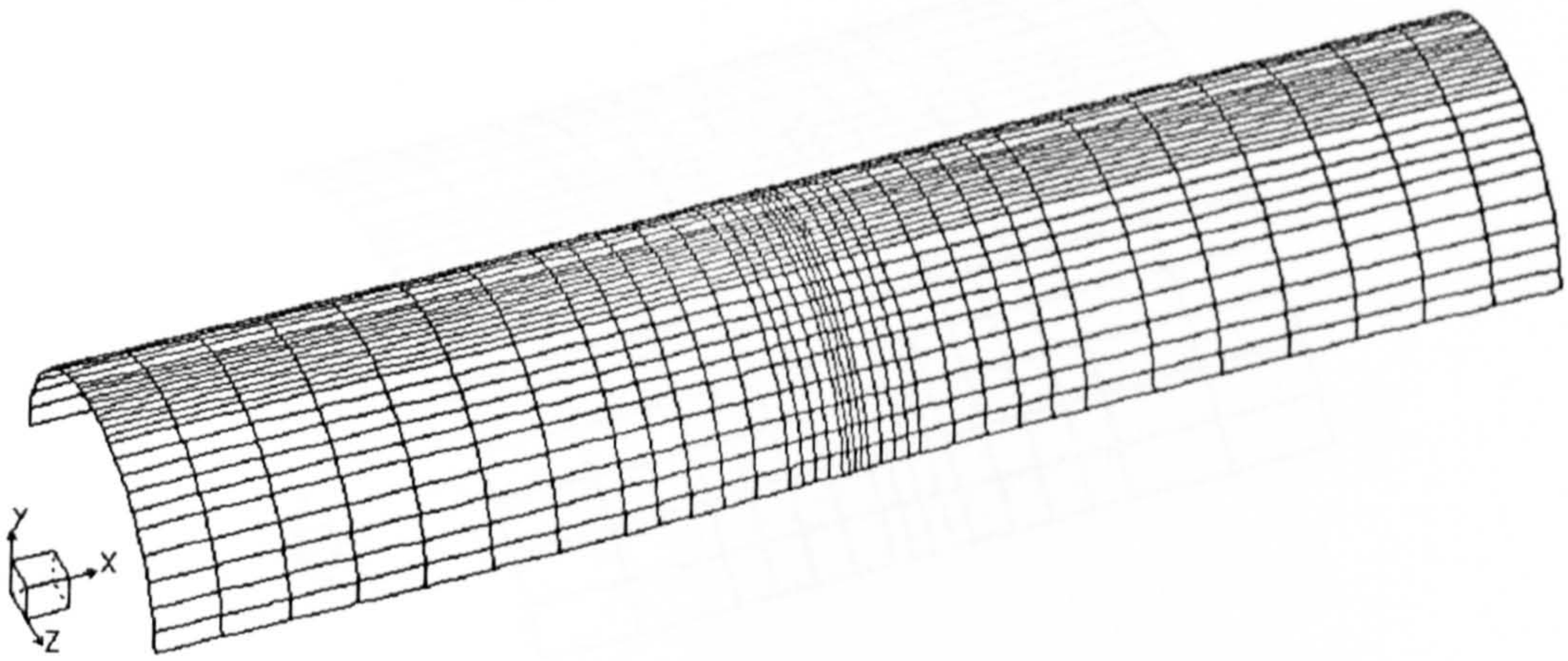

Fig A2 1080 shell element per layer model

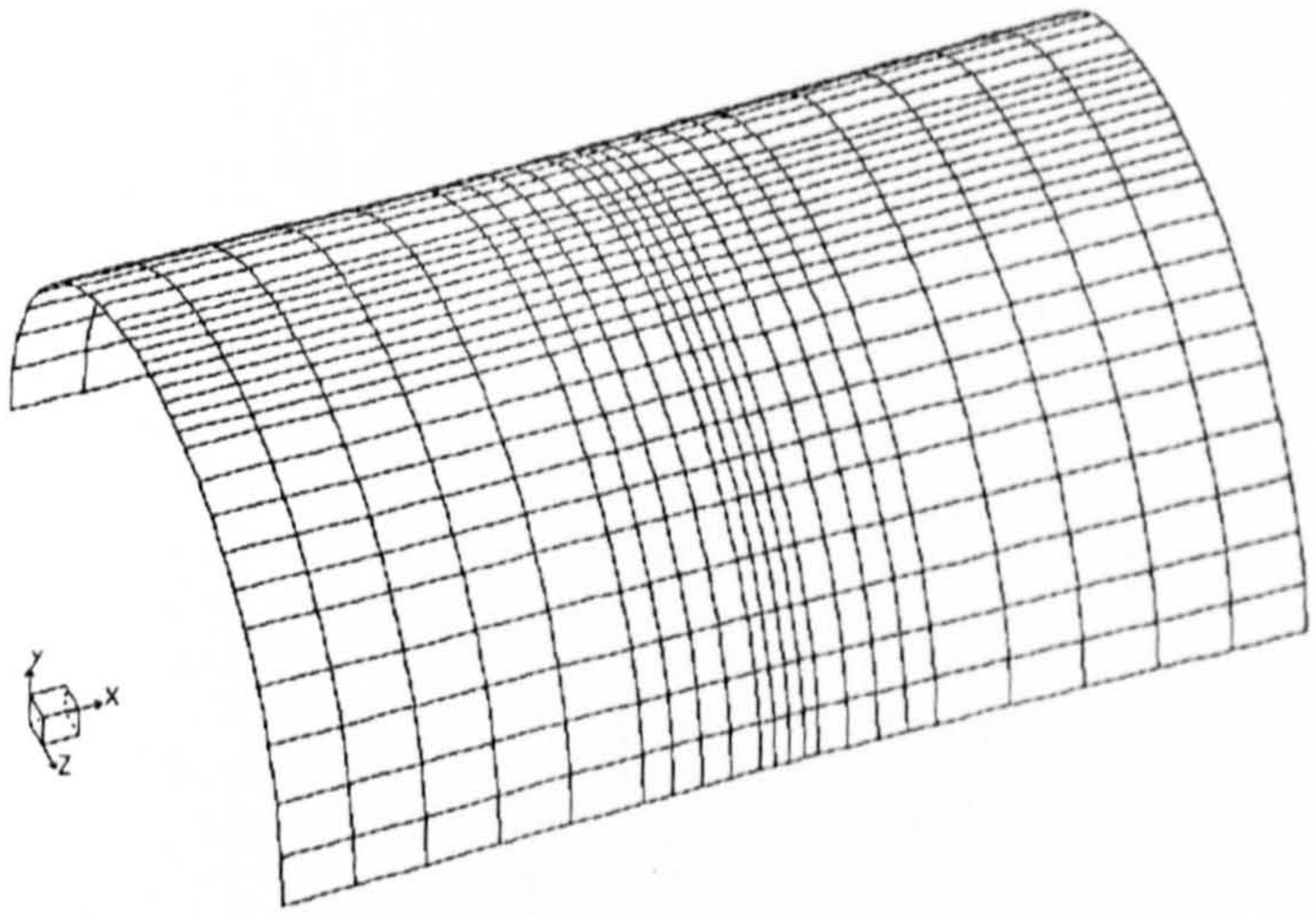

Fig A3 660 shell element per layer model

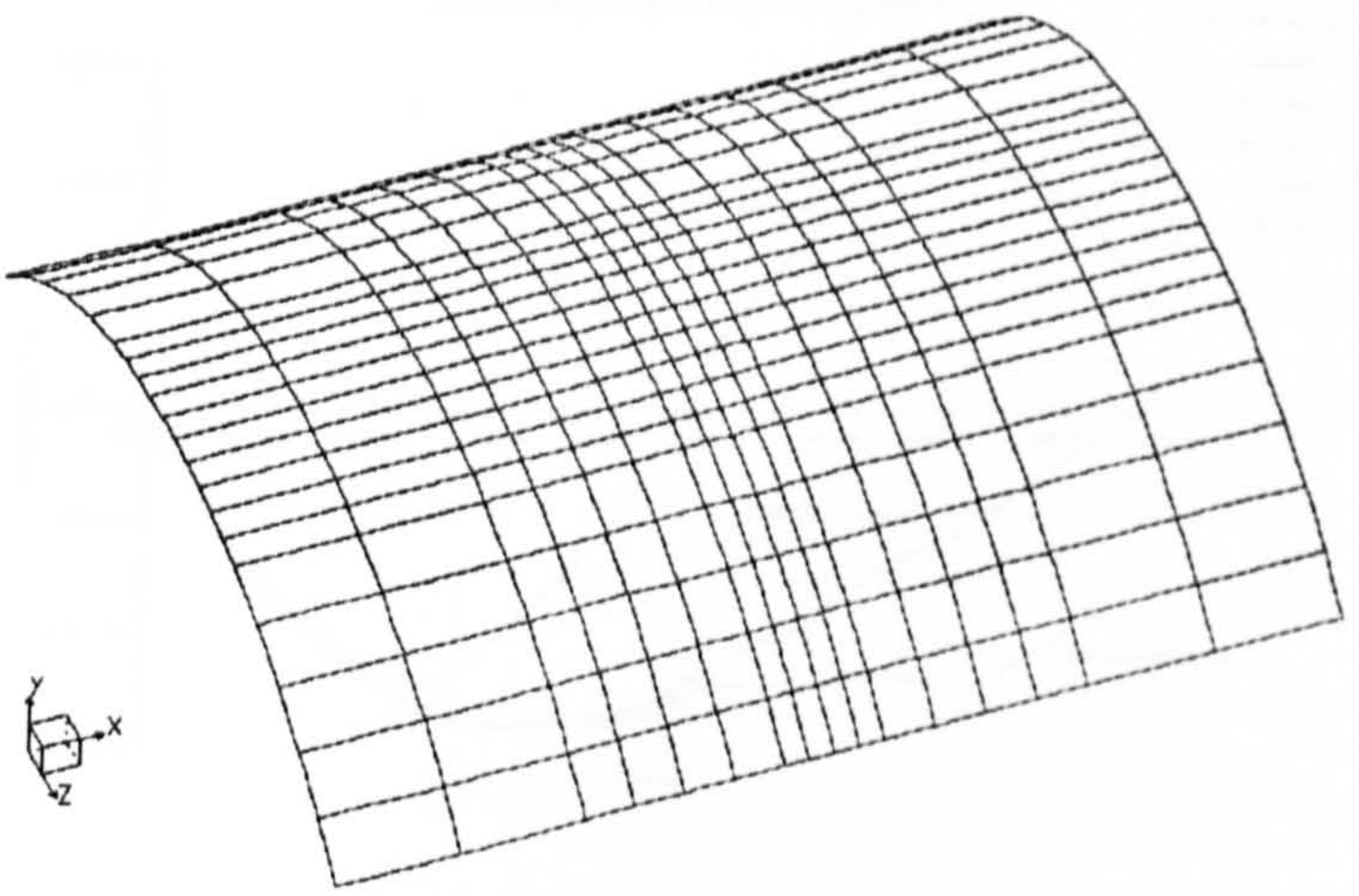

Fig A4 320 shell element per layer model

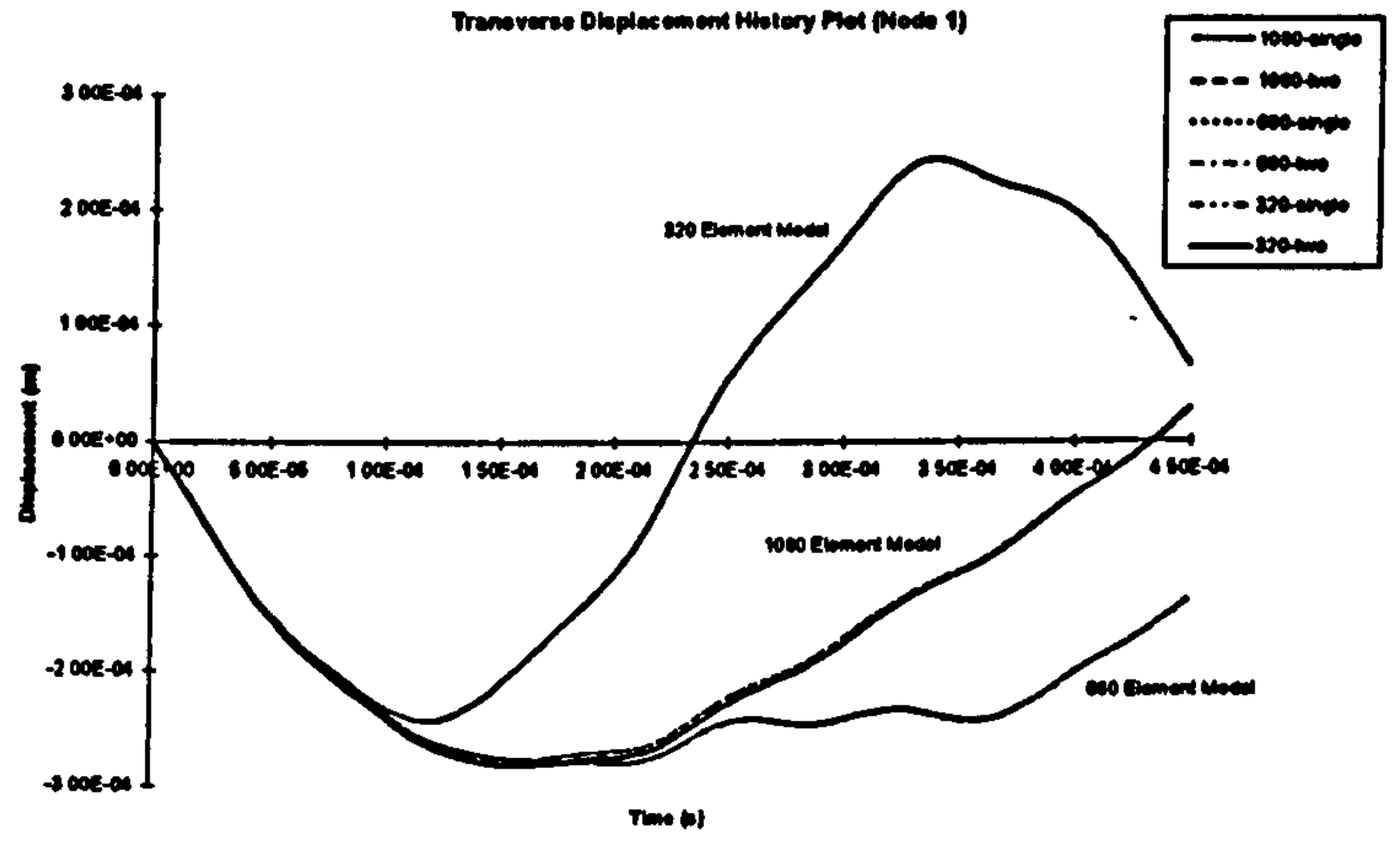

Fig A5 Displacement history plot

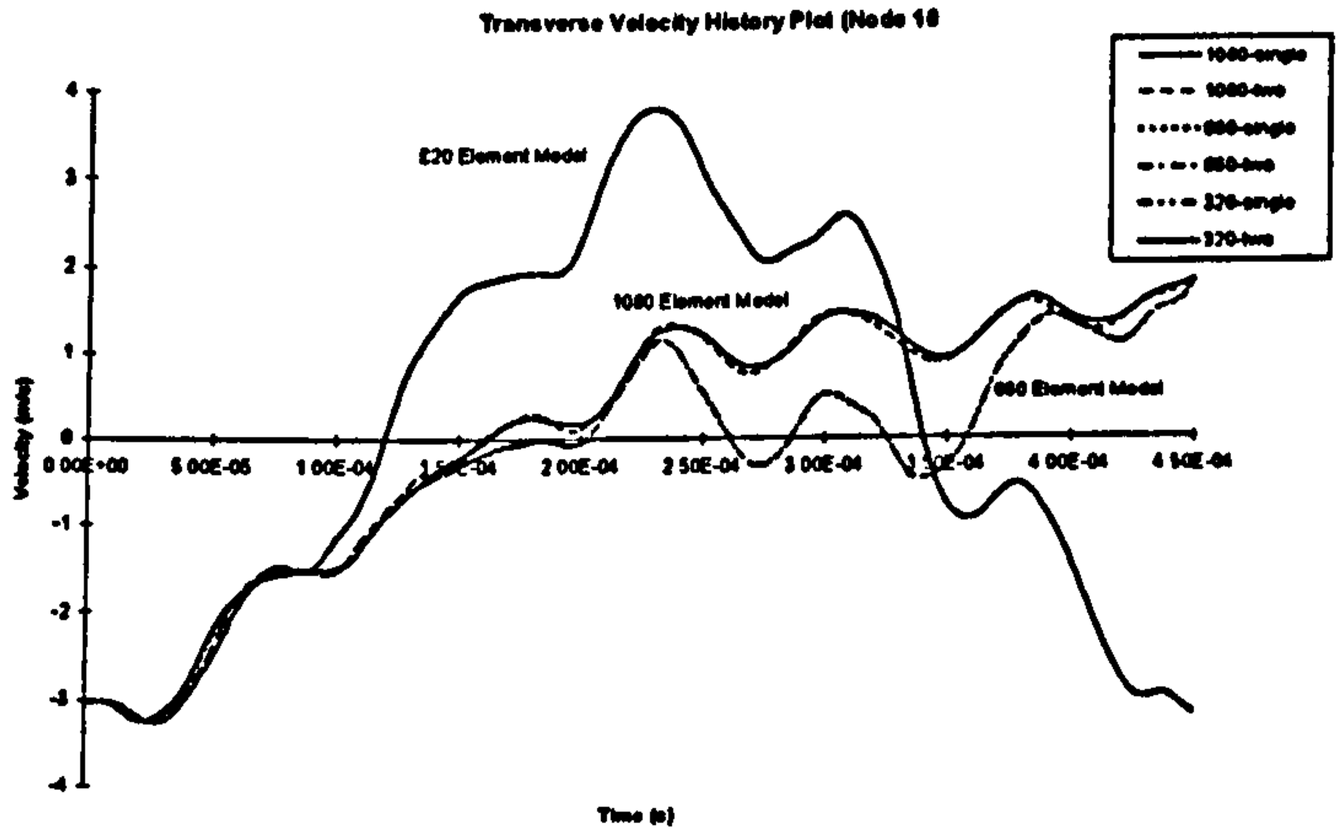

Fig A6 Velocity history plot

Appendix B Validation of Pre-Pressurised Technique (PPT)

Undamped single and multiple degree of freedom (d.o.f.) systems represented by the mathematical model and the FE model were used to validate the pre-pressurised technique. The parameters of the single d.o.f. system (Table B1) were adjusted to match those of the multiple d.o.f. system (Table B2), so that the dynamic responses from both systems could be compared. It can be seen in Figs B1 & B2 that, for the single d.o.f. system, the dynamic responses of both mathematical and FE models were similar to each other. It is also clear that the length of the rise-time is an essential parameter that can affect the oscillation amplitude after the rise-time. From the parametric study of rise-time shown in Figs B1 & B2, it is clear that a longer rise-time results in a lower oscillation amplitude. This is confirmed by the data in Tables B3 & B4. A conclusion drawn from this analysis is that it is possible to obtain an approximately steady-state response without applying arbitrary damping. In comparison, a step input (represented here by a very short rise-time, 10μs) is unsuitable for introducing a pre-pressurised condition to an undamped system, since it excites oscillations of large amplitude. The multiple d.o.f. system (Fig B3) behaves similarly to a single d.o.f. system, although the responses were not as smooth as for a single d.o.f. system.

Static analysis for pressurising the shell structure predicts a transverse displacement of 200.76 μm at the central. It shows agreement with the response obtained from dynamic analysis (200.66 μm by the single d.o.f. model, and 200 μm by the multiple d.o.f. system model).

The ratios of equivalent nodal forces for modelling a uniform pressure applied to a thick shell element can be found in Fig B5, which are as recommended by the PAFEC code.

Table B1 Single d.o.f. system (spring-mass system)

Model details for both mathematical and FE models

Parameter	**value**	**Description**
Spring stiffness (k)	141 MN/m	obtained from (F_o / displacement) the shell model
Mass of the system (M)	0.0158 kg	total mass of the shell model
Natural Frequency (W_n)	15028 Hz (94427 rad/s)	calculated by PAFEC
Input Force (F_o)	28284 N	equivalent to 50 bars pressure applied onto the shell model

NB : The shell model means that the multiple d.o.f. system was used.

Table B2 Multiple d.o.f. system (shell structure)

Model details for FE model

Parameter	**value**
Dimension	70.7 mm x 80 mm
Thickness (& layer No.)	1.524 mm (6 layers)
Mass of structure	0.0158 kg
D.O.F.	4445
Restraints	all edges clamped
Internal Pressure	50 bar (50E5 N/m^2)

NB : It is a shell structure constructed by 320 thick shell elements.

Table B3 Single d.o.f. system

The oscillation amplitude and the deviation percentage.

(The steady-state displacement is 200.66 μm)

Model	**Rise-time (t) = 10μs**	**Rise-time (t) = 100μs**	**Rise-time (t) = 200μs**	**Rise-time (t) = 400μs**
Mathematical	410 μm (> ±100 %)	72.04 μm (±17.96 %)	0.579 μm (±0.144 %)	0.579 μm (±0.144 %)
FE	400 μm (> ±100 %)	83.3 μm (±20.76 %)	< 0.1 μm (< ±0.1 %)	< 0.1 μm (< ±0.1 %)

Table B4 Multiple d.o.f. system

The oscillation amplitude and the deviation percentage.

(The steady-state displacement is 200 μm)

Model	**Rise-time (t) = 10μs**	**Rise-time (t) = 100μs**	**Rise-time (t) = 200μs**	**Rise-time (t) = 400μs**
FE	450 μm (> ±100 %)	62.5 μm (± 15.6%)	50 μm (± 12.5 %)	25 μm (± 6.25 %)

Table B5 PAFEC data module used for FE dynamic analysis

Type	Module	Description
Mesh Description	ELEMENTS	
	NODES	
	RESTRAINTS	
	LOCAL.DIRECTIONS	
	AXES	
	SPRINGS	(for single d.o.f. only)
	MASSES	(for single d.o.f. only)
Material Properties	LAMINATES	(for single d.o.f. only)
	ORTHOTRPIC.MATERIAL	(for single d.o.f. only)
Dynamic Analysis	RESPONSE	
	MODES.AND.FREQUENCIES	
	MASTERS	
	FORCING	
	FULL.DYNAMIC.OUTPUT	
	STRESS.ELEMENT	

Response during rise-time

Response after rise-time

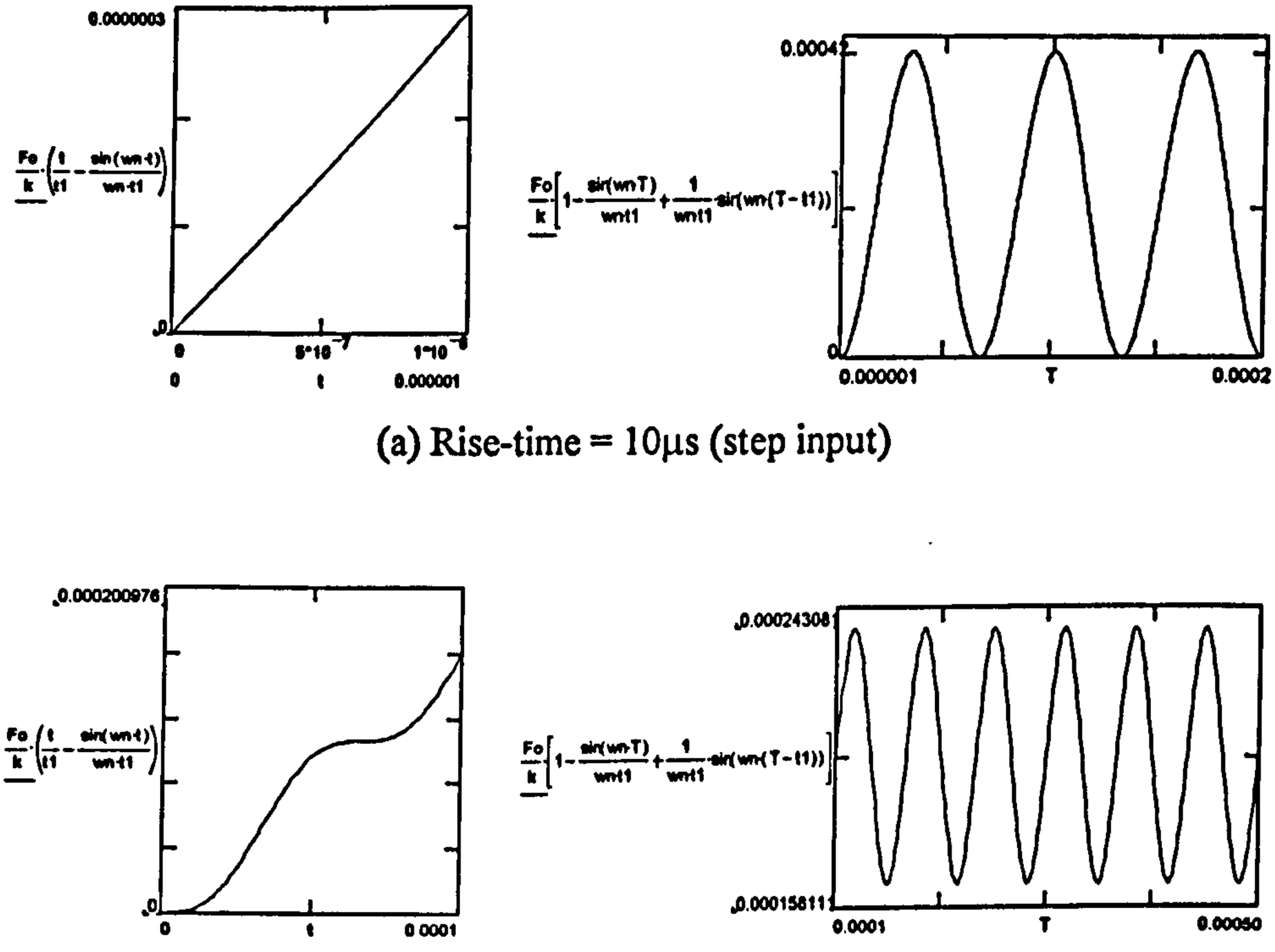

(a) Rise-time = 10μs (step input)

(b) Rise-time = 100μs

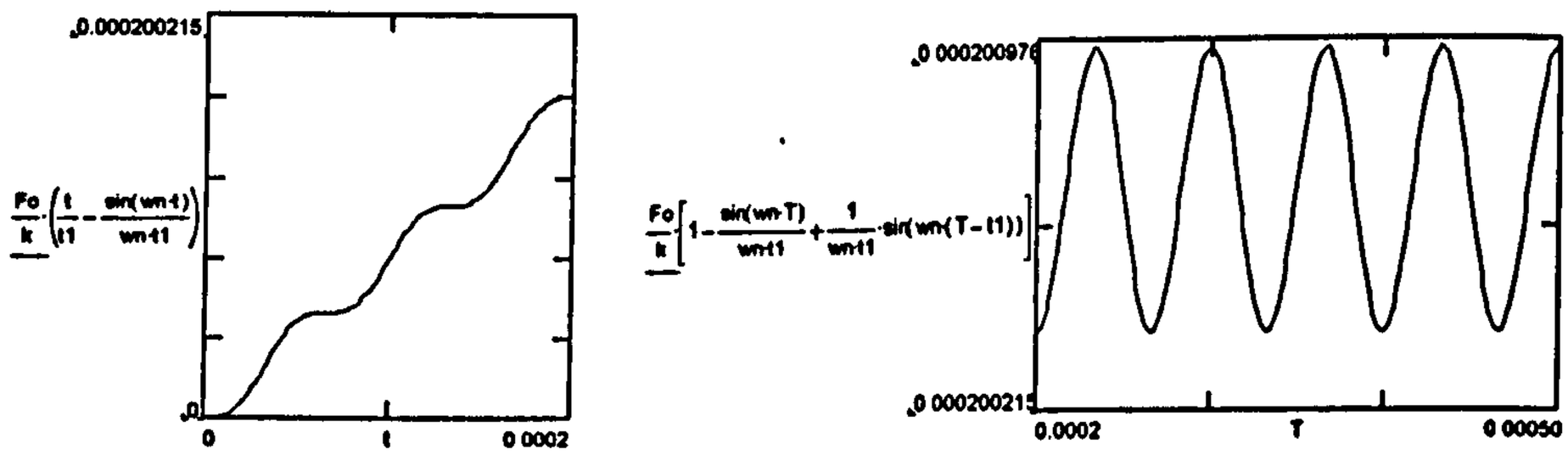

(c) Rise-time = 200μs

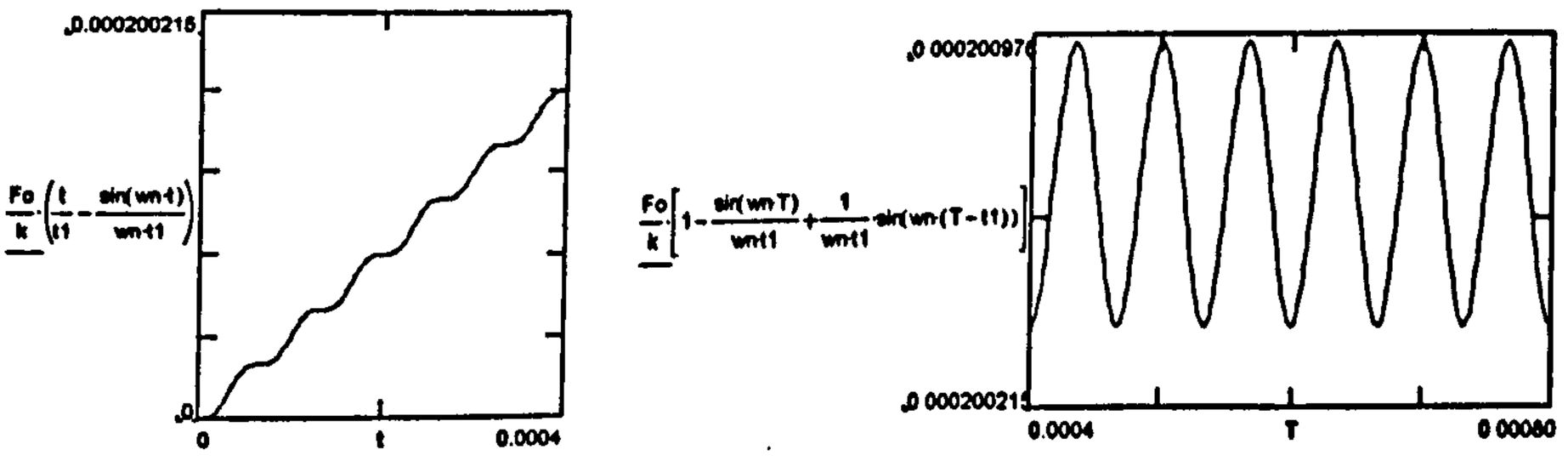

(d) Rise-time = 400μs

Fig B1 Mathematical model (single d.o.f. system)

[displacement response]

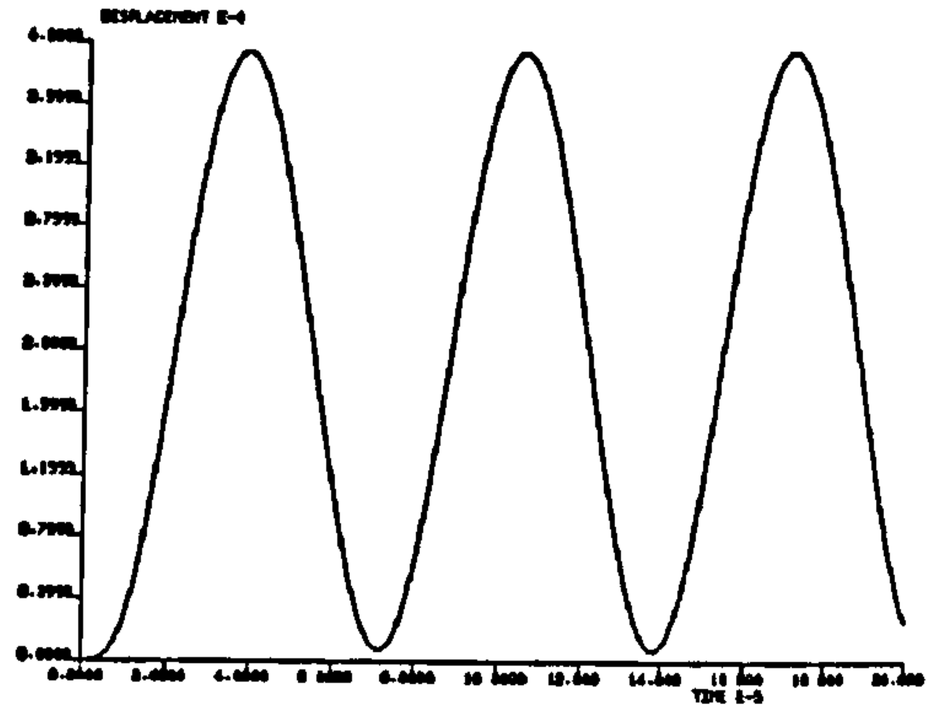

(a) Rise-time = 10 μs (step input)

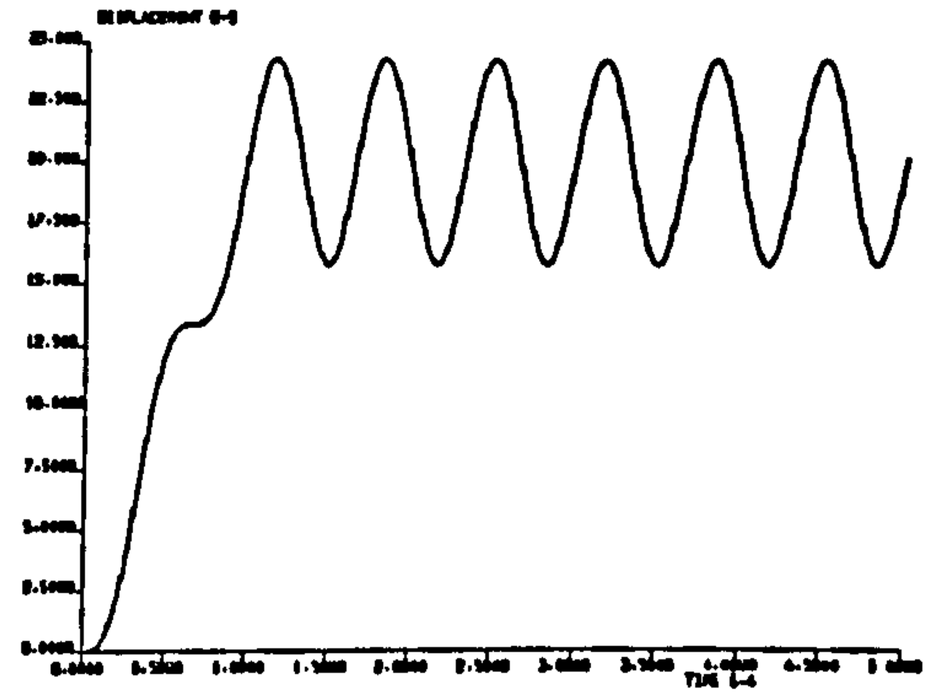

(b) Rise-time = 100 μs

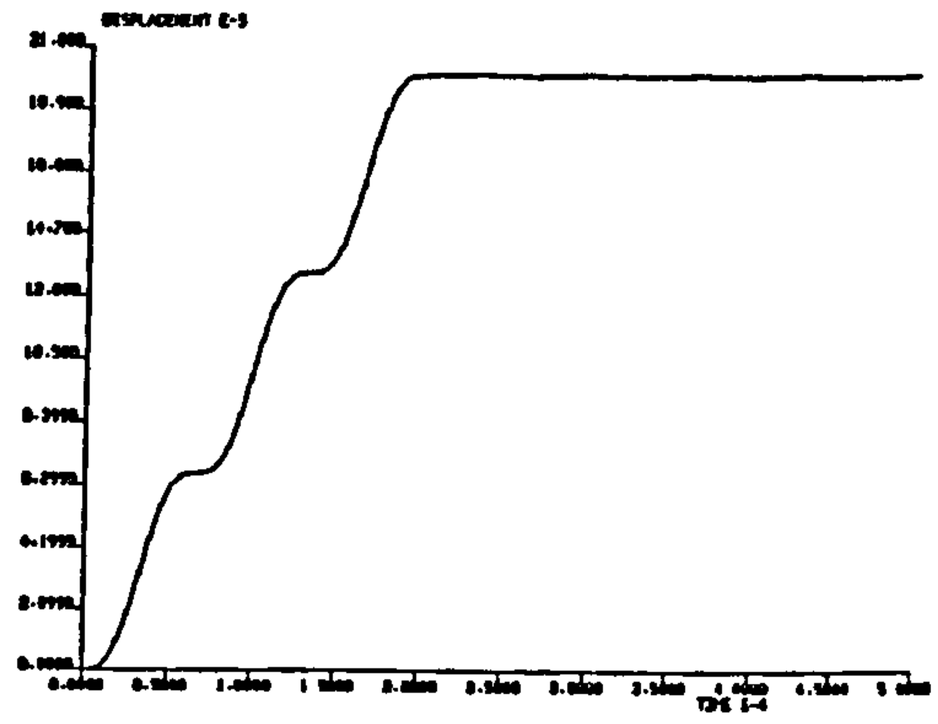

(c) Rise-time = 200 μs

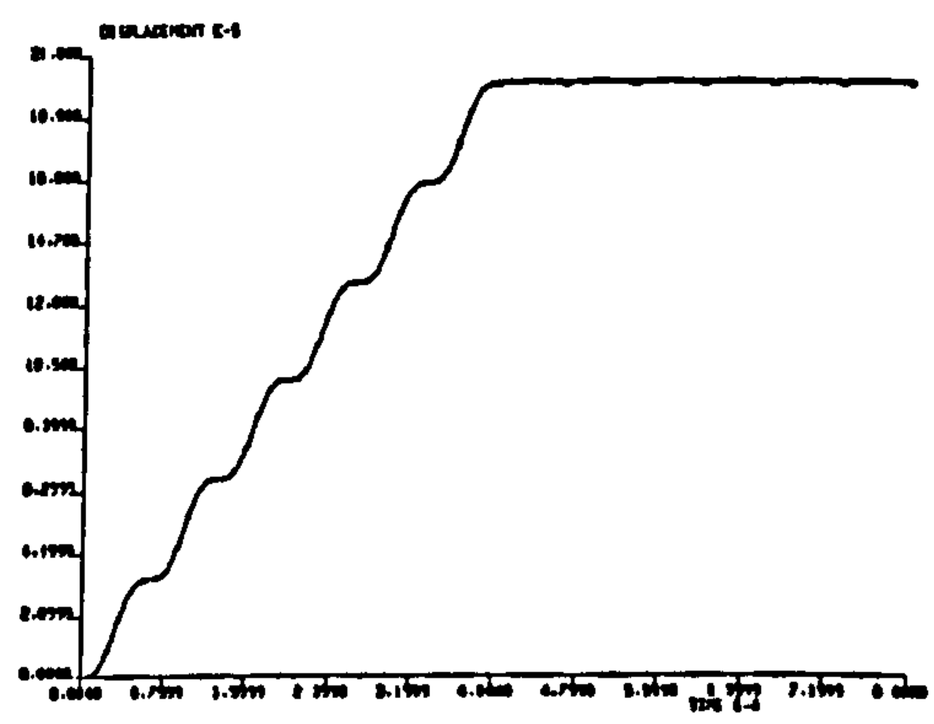

(d) Rise-time = 400 μs

Fig B2 FE model (single d.o.f. system)

[displacement response]

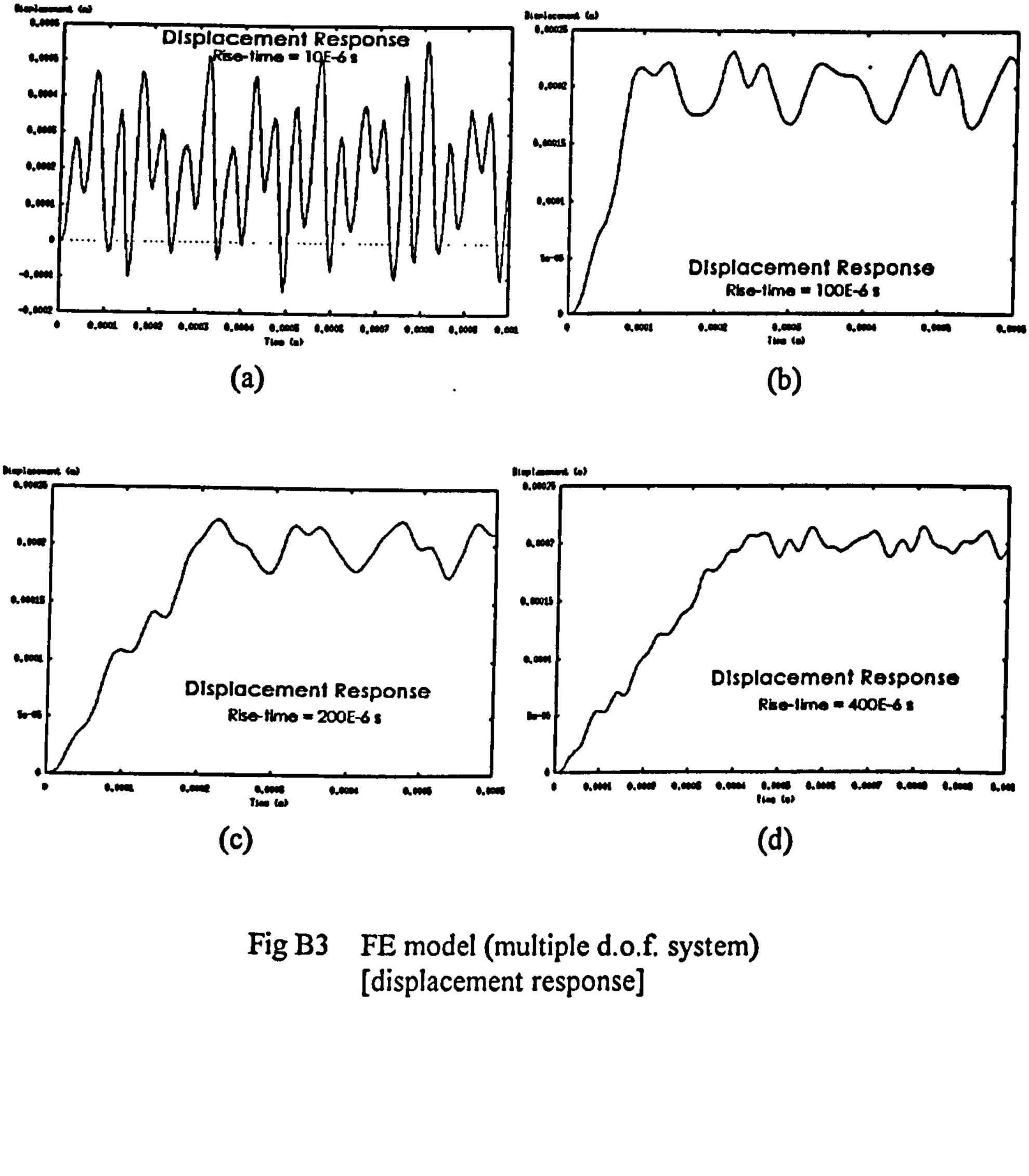

Fig B3 FE model (multiple d.o.f. system)
[displacement response]

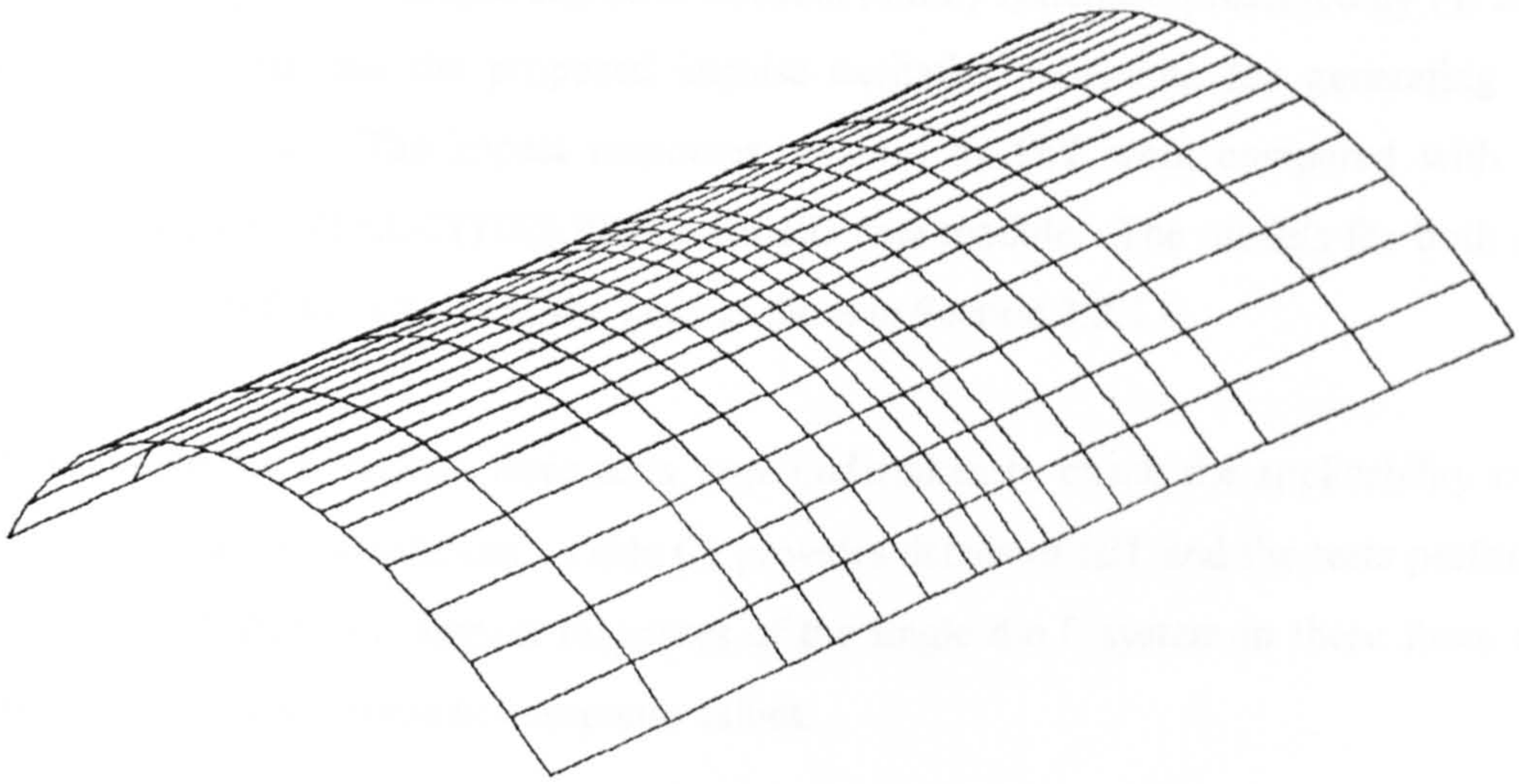

Fig B4 FE shell structure for multiple d.o.f. system

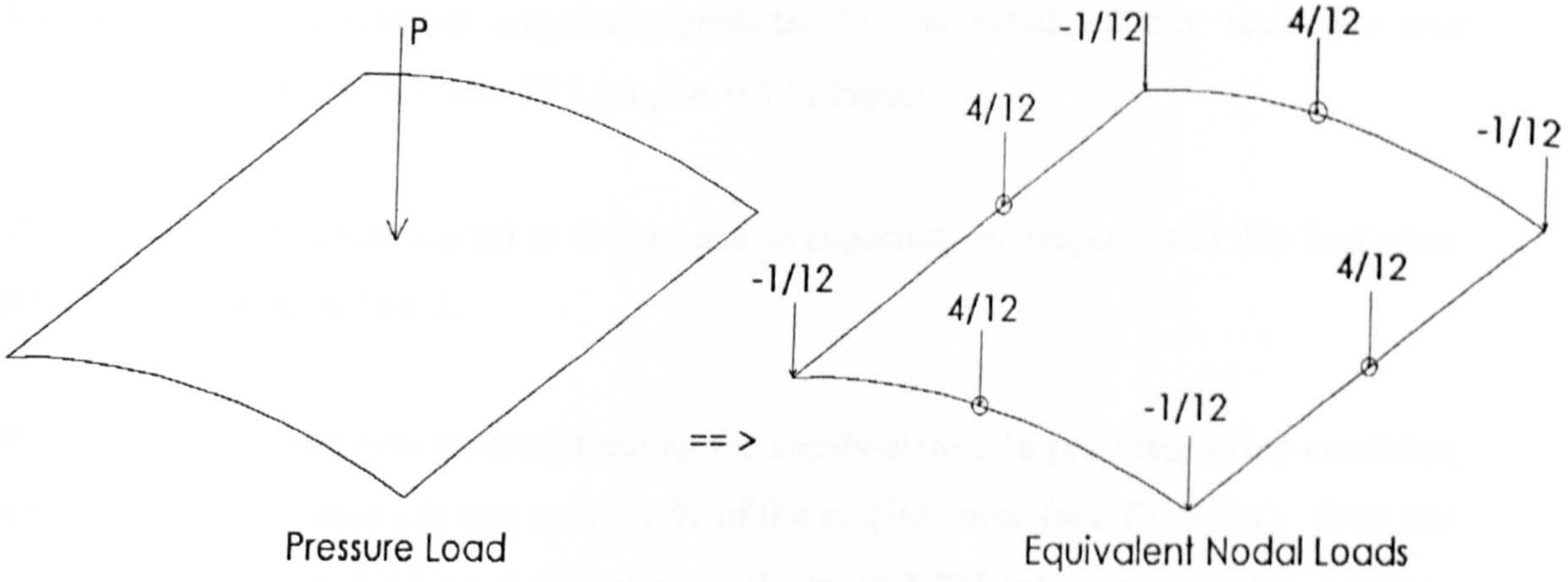

Fig B5 Equivalent nodal loads for pressure load

Appendix C Validation of Impulse Excitation Technique (IET)

Undamped single and multiple degree of freedom (d.o.f.) systems represented by FE models were used to validate the proposed impulse excitation technique for generating initial velocity of impact. The impact responses obtained by IET were compared with those obtained by using VELOCITIES.PRESCRIBED data module. The models for both single and multiple d.o.f. systems were the same as those in Section 3.2.1.6.

For the single d.o.f. system, three tests were undertaken to check the applicability of this technique to various conditions. Table C1 provides details of IET and the tests performed. Figs C1 to C4 show the impact responses of the single d.o.f. system in these three tests. Table C2 summarises some key response values.

In the first test, the excitation impulse generated a velocity of 3.78 m/s at the end of the shock impulse. Another dynamic job was then run using the initial velocity technique (the VELOCITIES.PRESCRIBED data module), in which 3.78 m/s was used as the initial velocity. From Figs C1 and C2, it can been seen that the responses in the two cases agreed well with each other, with the timing of the maximum displacement being the same (24 μs). The maximum displacement magnitude predicted by the initial velocity technique was 57.015 μm, and by the IET was 57.2 μm, i.e. 0.3 % higher.

The impact in Test 2 was started at 100 μs, and as expected, the responses in this Test were exactly the same as in Test 1.

In Test 3a, the impact was generated during the steady-state of a pre-pressurised condition with an oscillation amplitude less than 0.1 % of the median value (see Table B3). With the same excitation force (80kN) and time-step, a velocity of 3.775 m/s was generated, which is only 0.08 % lower than those in Test 1 and Test 2. The maximum displacement due to impact (57.38 μm) at 524 μs was 0.3 % higher.

In Test 3b, with the same excitation force (80kN) and time-step, a velocity of 3.782 m/s was generated, which is 0.1 % higher than in Test 1 and Test 2, and 0.2 % higher than in

Test 3a. The maximum displacement due to impact (57 μm) at 524 μs was 0.6 % lower than in Test 3a.

It is obvious that the difference in the velocity and maximum displacement is due to the effect of oscillation amplitude. As shown in Table C2, the pre-displacements at the time of applying impulse were not the same (0.47 μm different).

For multiple d.o.f. system, two tests by IET were undertaken. One was loaded at a point and the other one was loaded on a small area (4 elements). Another two tests by initial velocity technique were undertaken as references. Tables C3 and C4 provided details of these tests. Figs C5 to C8 show the impact responses of this multiple d.o.f. system. Table C7 lists the maximum displacements in these tests.

For the case of loading at a point, the displacement response due to IET agreed well with that by the initial velocity technique, with only 0.2 % difference at maximum displacement. However, for the case of loading on a small area, the velocity and displacement responses predicted by the two techniques were quite different in manner and magnitude. The velocity response by IET showed a more oscillate behaviour, and the displacement response predicted lower magnitude than that by initial velocity technique.

Table C1 Impulse excitation and tests (for single d.o.f. system)

IET details

Time-step used in analysis	1 μs
Excitation Force (in 2 time-step)	80 kN
Impulsive Force	0.08 N.s
Excited velocity	3.778 m/s
Mass of spring	0.0158 kg
Mass of impactor	0.0163 kg
Impact energy	0.11633 J

Tests for Analysis

Test 1 Impulse excitation applied at time = 0.0 s (Fig C1)

Test 2 Impulse excitation applied at time = 100 μs (Fig C3)

Test 3 a. Impulse excitation applied at time = 500 μs (Fig C4)

b. Impulse excitation applied at time = 800 μs

- at the steady-state of pre-pressurised condition
- the system was pressurised by a force (28284 N) equivalent to 50 bars
- rise-time was 200 μs

Table C2 Test results (for single d.o.f. system)

	Excited velocity (m/s)	**Transverse Displacement (μm)**			
Test 1	3.778 @2 μs	1.2 @1 μs	5 @2 μs	57.2 @24 μs	
Test 2	3.778 @102 μs	1.2 @101 μs	5 @102 μs	57.2 @124 μs	
Test 3 a (@500)	-3.7754 @502 μs	199.74 @501 μs	195.96 @502 μs	143.62 @524 μs	201.0 @500 μs (steady-state)
Test 3 b (@800)	-3.782 @802 μs	199.27 @801 μs	195.47 @802 μs	143.51 @824 μs	200.53@800 μs (steady-state)

NB : For all three tests, the impact duration were the same, i.e. 24 μs.

Table C3 Impulse excitation and tests (for multiple d.o.f. system)

IET details		
Time-step used in analysis	1 μs	
Excited velocity (same for the two tests)	-2.7594 m/s	
Mass of the structure	0.0158 kg	
Mass of impactor	0.0163 kg	
Impact energy	0.0621 J	
	Test 1(point load)	Test 2 (on a small area)
Excitation Force (in 2 time-step)	-100 N	-21.38 N/node (totally 21 nodes)
Impulsive Force	0.0001 N.s	21.38 E-6 N.s /node

Tests for Analysis

Test 1	Impulse excitation applied at a point (node 1)	(Fig C5)
Test 2	Impulse excitation applied on a small area (4 elements)	(Fig C7)

Table C4 Initial velocity technique and tests (for multiple d.o.f. system)

Input Details	
Time-step used in analysis	1 μs
Initial velocity (same for the two tests)	-2.7594 m/s
Mass of the structure	0.0158 kg
Mass of impactor	0.0163 kg
Impact energy	0.0621 J

Tests for Analysis

Test 1V	Initial velocity applied at a point (node 1)	(Fig C6)
Test 2V	Initial velocity applied on a small area (4 elements)	(Fig C8)

NB : Initial velocity Technique by using VELOCITIES.PRESCRIBED data module

Table C5 Maximum transverse displacements of tests and their differences

Tests	Max. Displacement	Difference
Test 1	239.65 μm @138 μs	
Test 1V	240.21 μm @138 μs	0.56 μm (0.233 %)
Test 2	169.37 μm @112 μs	
Test 2V	223.24 μm @118 μs	53.87 μm (24.13 %)

NB : The percentages are calculated by taking displacements by initial velocity technique as base values.

Table C6 PAFEC data module used for FE dynamic analysis

Type	Module	Description
Mesh Description	ELEMENTS	
	NODES	
	RESTRAINTS	
	LOCAL.DIRECTIONS	
	AXES	
	SPRINGS	(for single d.o.f. only)
	MASSES	(for single d.o.f. only)
Material Properties	LAMINATES	(for single d.o.f. only)
	ORTHOTRPIC.MATERIAL	(for single d.o.f. only)
Dynamic Analysis	RESPONSE	
	MODES.AND.FREQUENCIES	
	MASTERS	
	FORCING	
	FULL.DYNAMIC.OUTPUT	
	STRESS.ELEMENT	
	CHANGE.OF.MASS	
	VELOCITIES.PRESCRIBED	

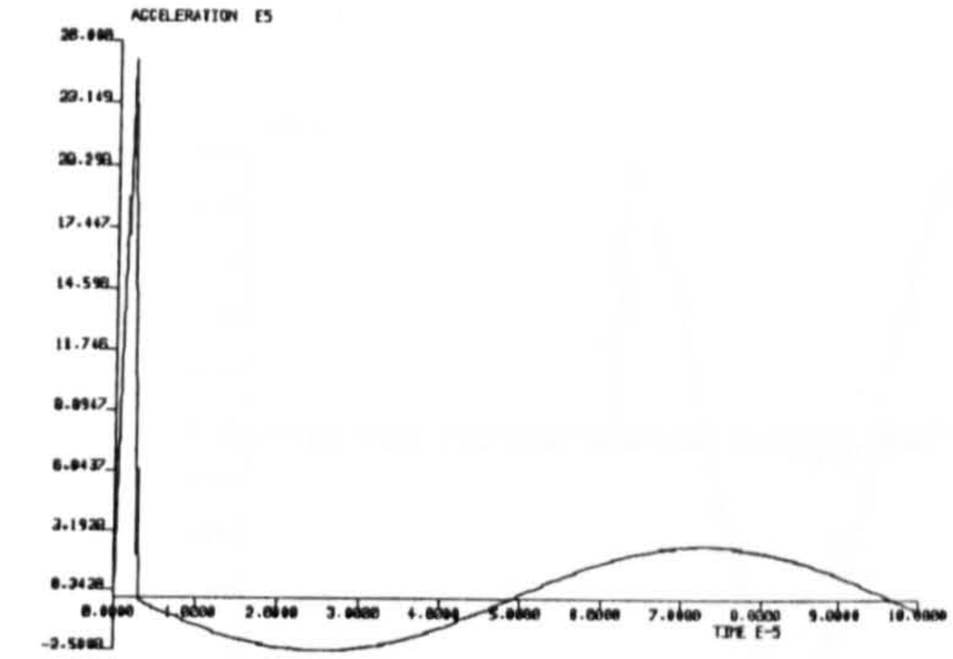

(a) Acceleration Response (IET)

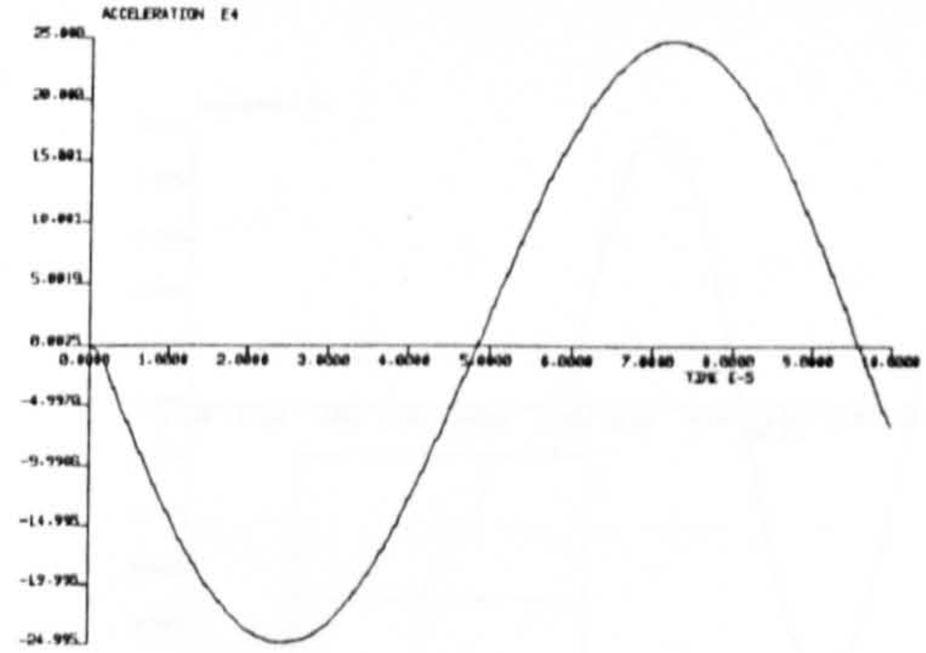

(a) Acceleration Response (VELO.PRE)

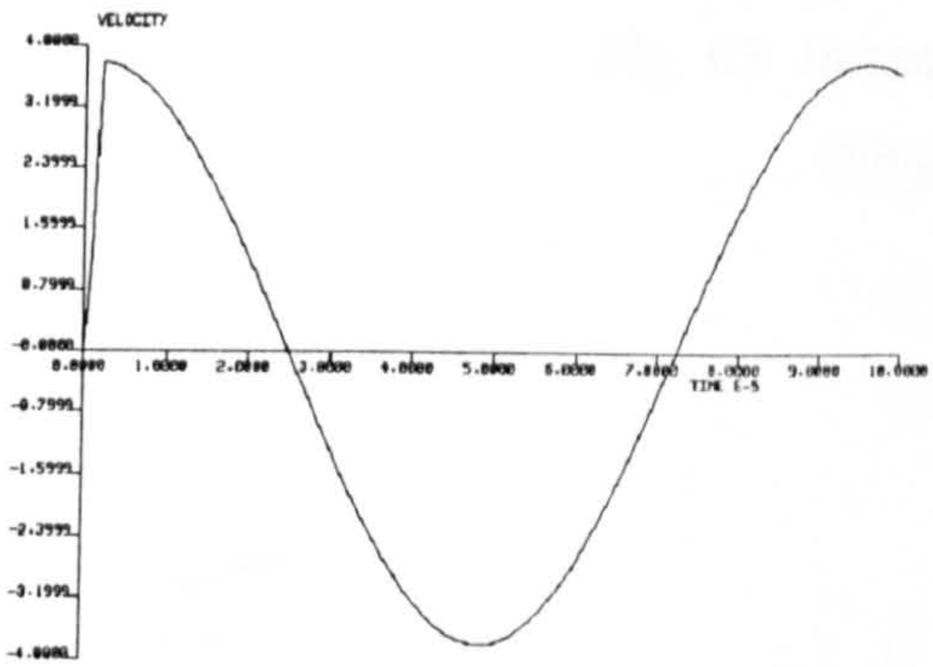

(b) Velocity Response (IET)

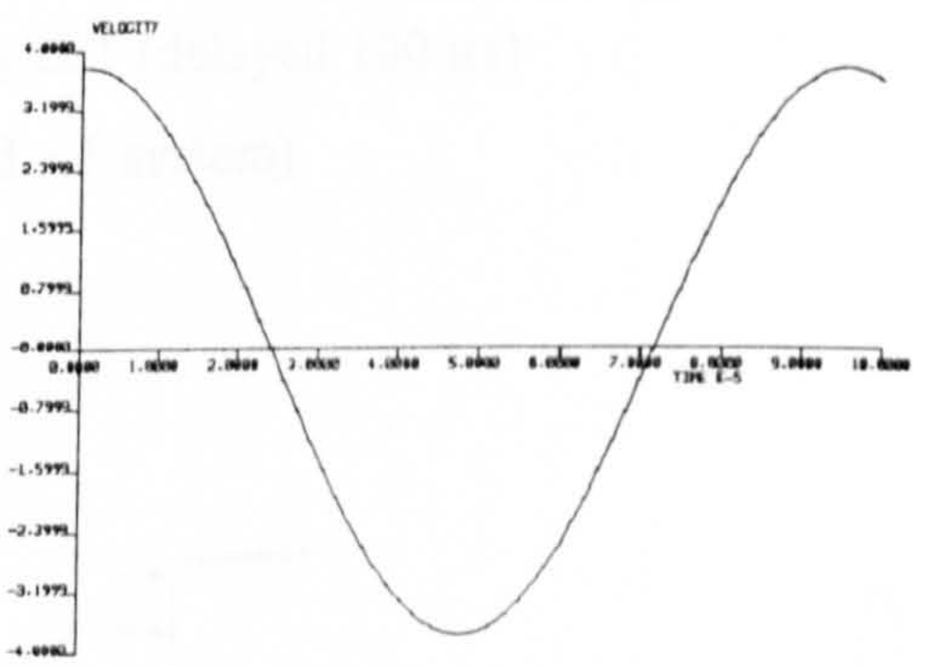

(b) Velocity Response (VELO.PRE)

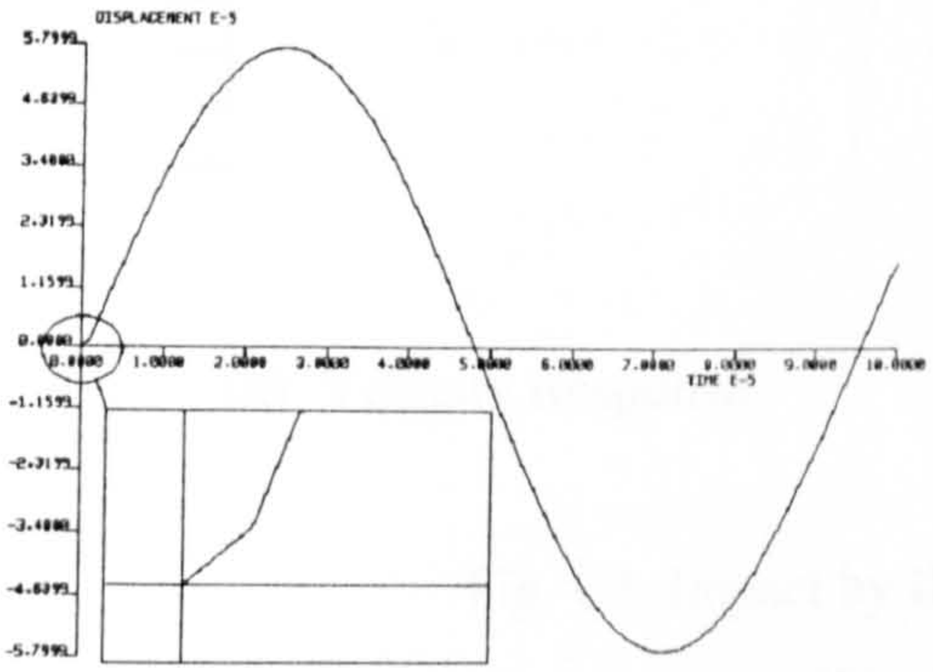

(c) Displacement Response (IET)

Fig C1 By IET

(single d.o.f. system)

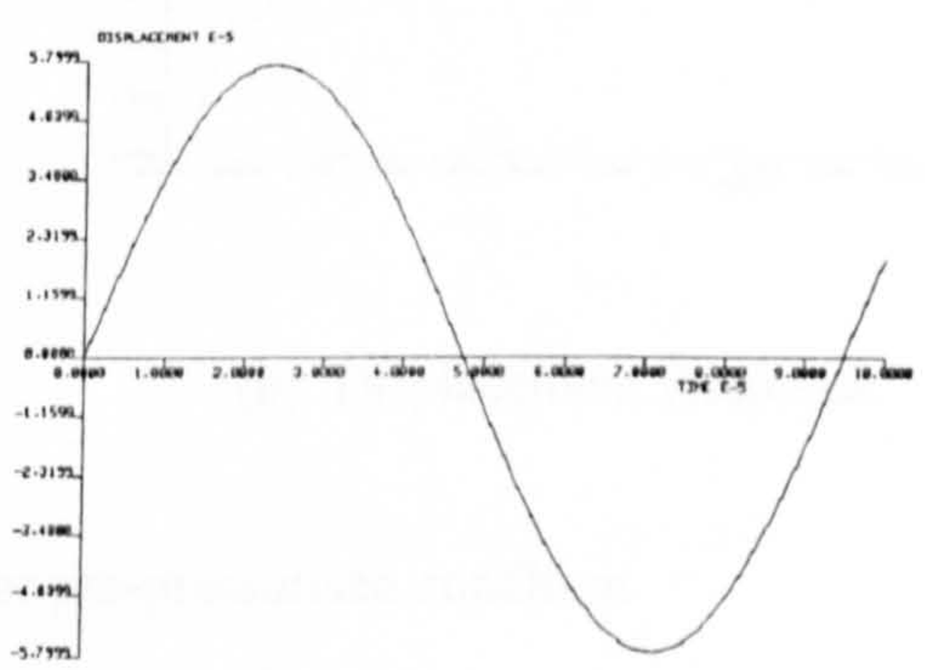

(c) Displacement Response (**VELO.PRE**)

Fig C2 By VELOCITIES.PRES module

(single d.o.f. system)

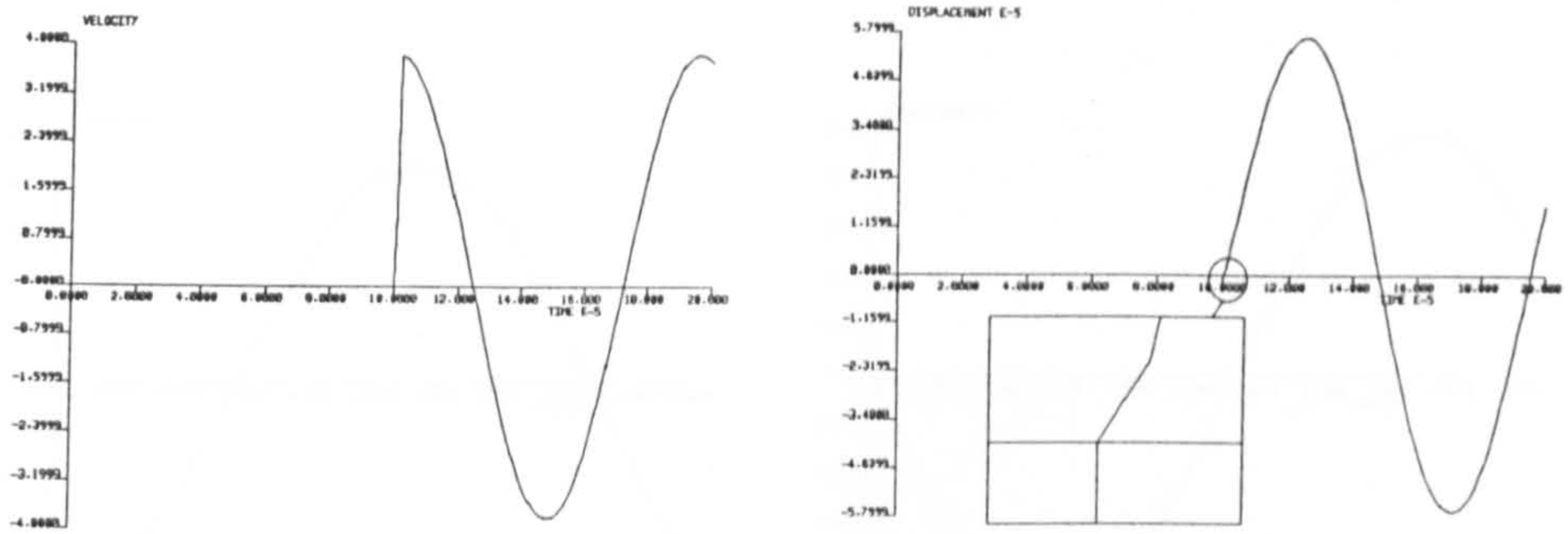

(a) Velocity Response (b) Displacement Response

Fig C3 Impact by IET (delayed 100 μs)

(Single d.o.f. system)

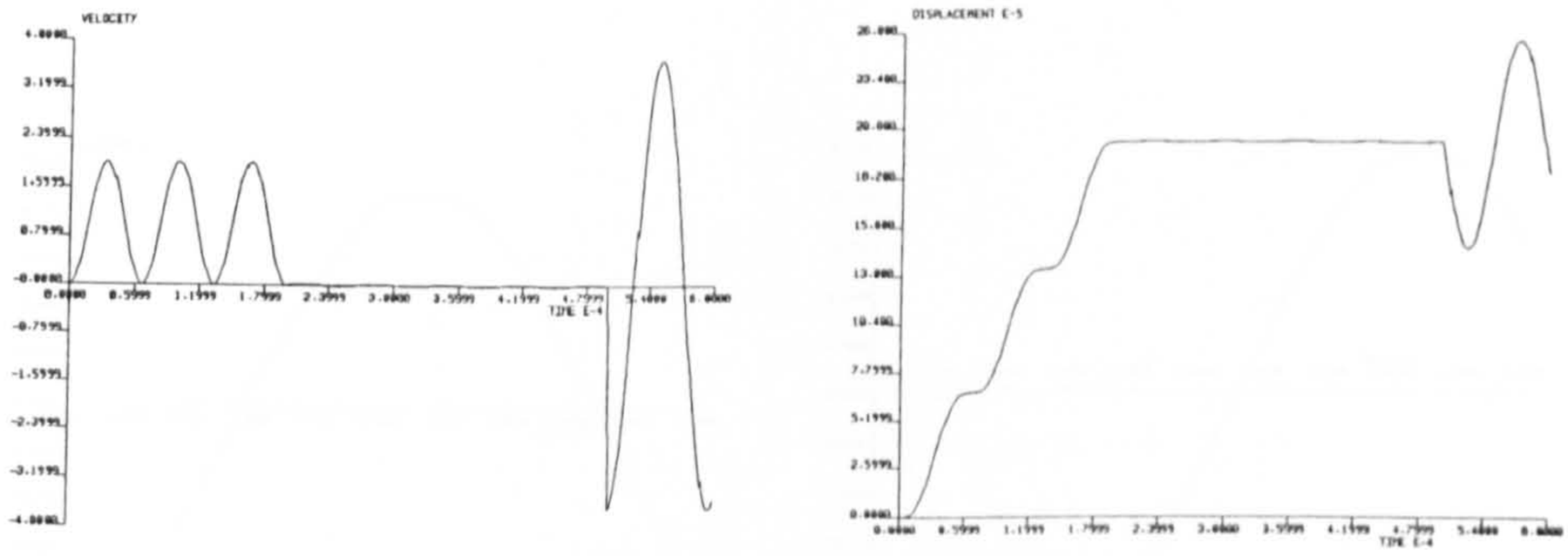

(a) Velocity Response (b) Displacement Response

Fig C4 Impact by IET at pre-pressurised condition

(Single d.o.f. system)

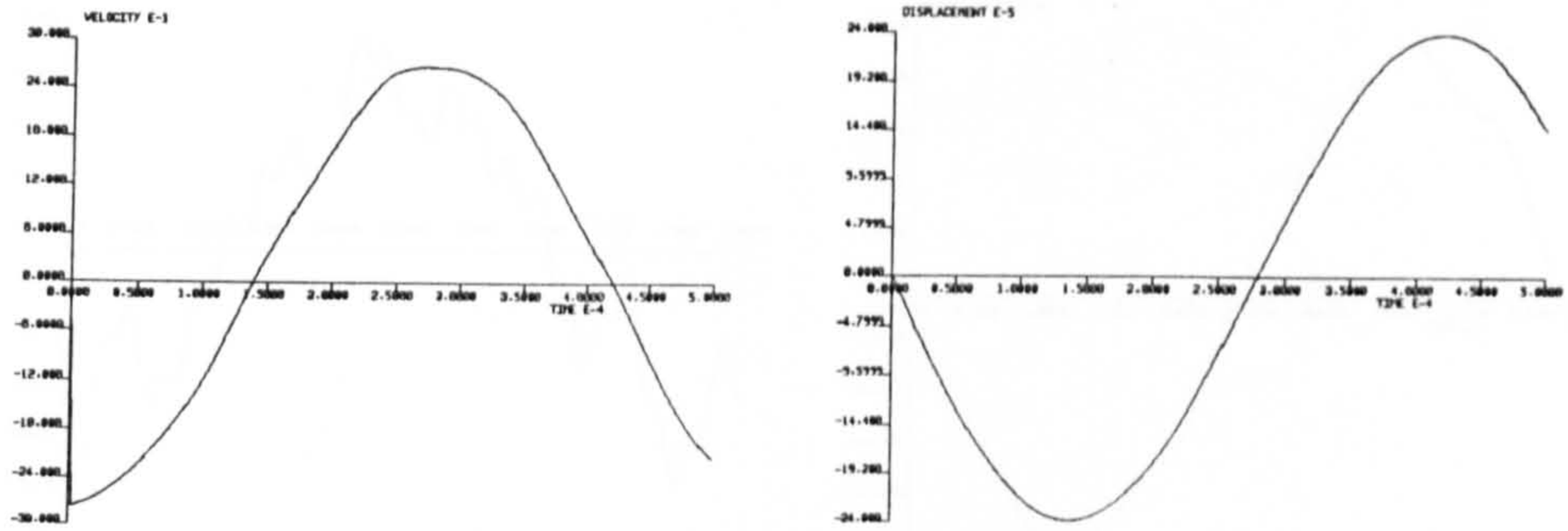

(a) Velocity response (b) Displacement response

Fig C5 Impact by IET (point Load)
multiple d.o.f. system

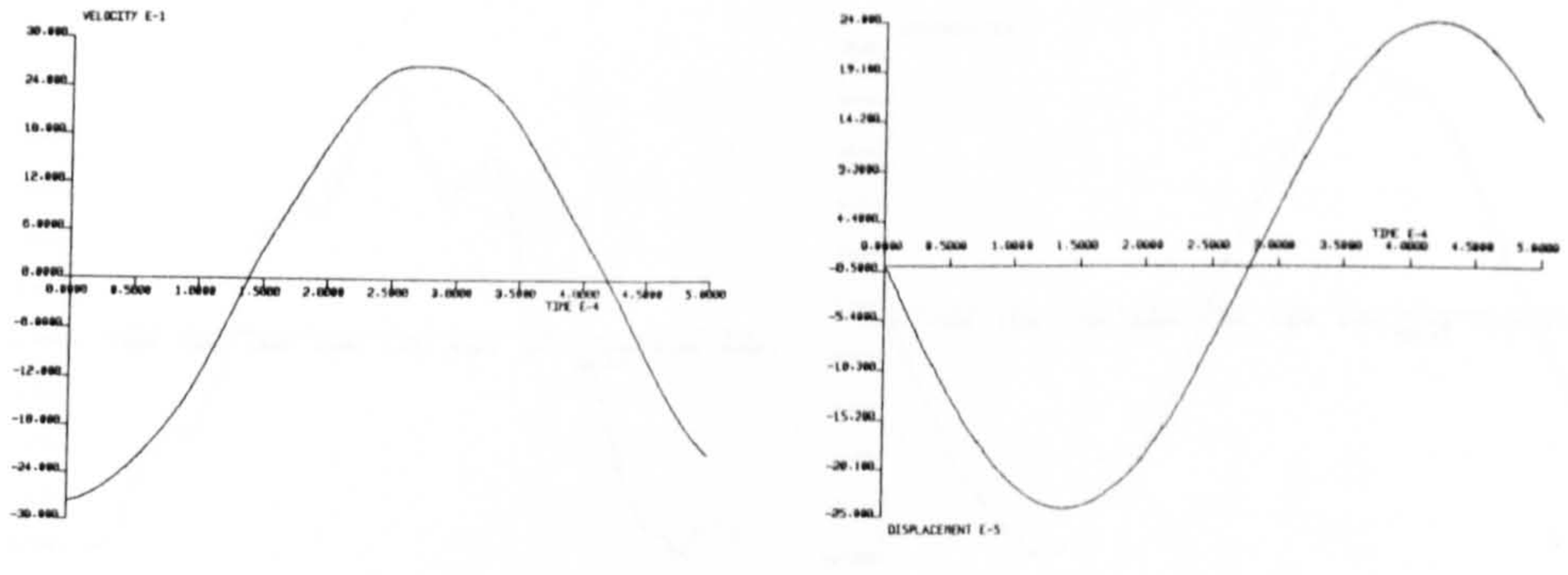

(a) Velocity response (b) Displacement response

Fig C6 Impact by initial velocity technique (point load)
multiple d.o.f. system

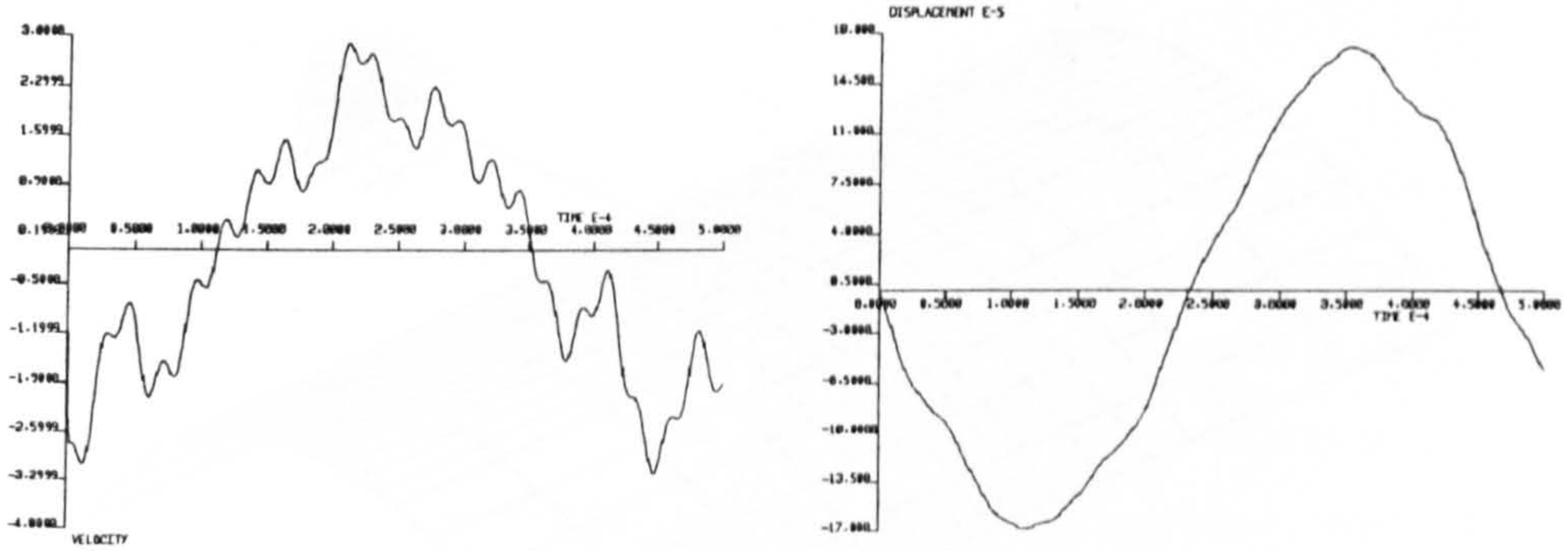

(a) Velocity response (b) Displacement response

Fig C7 Impact by IET (loaded on a small area)
multiple d.o.f. system

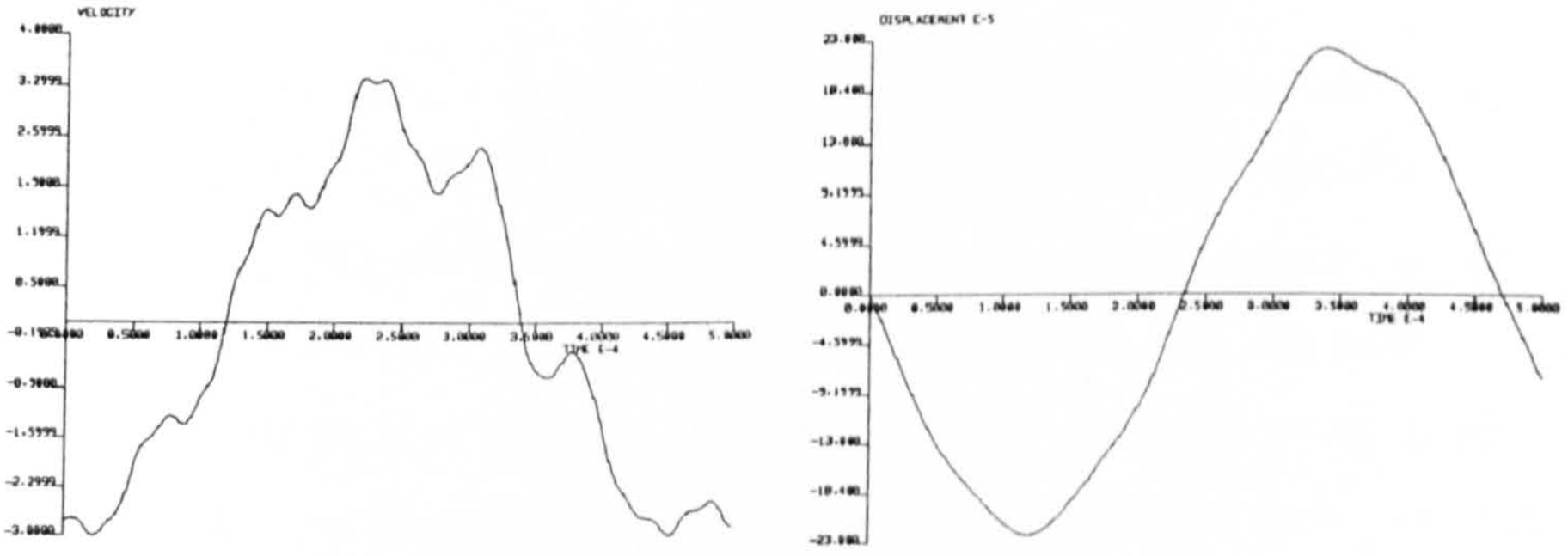

(a) Velocity response (b) Displacement response

Fig C8 Impact by initial velocity technique (loaded on a small area)
multiple d.o.f. system

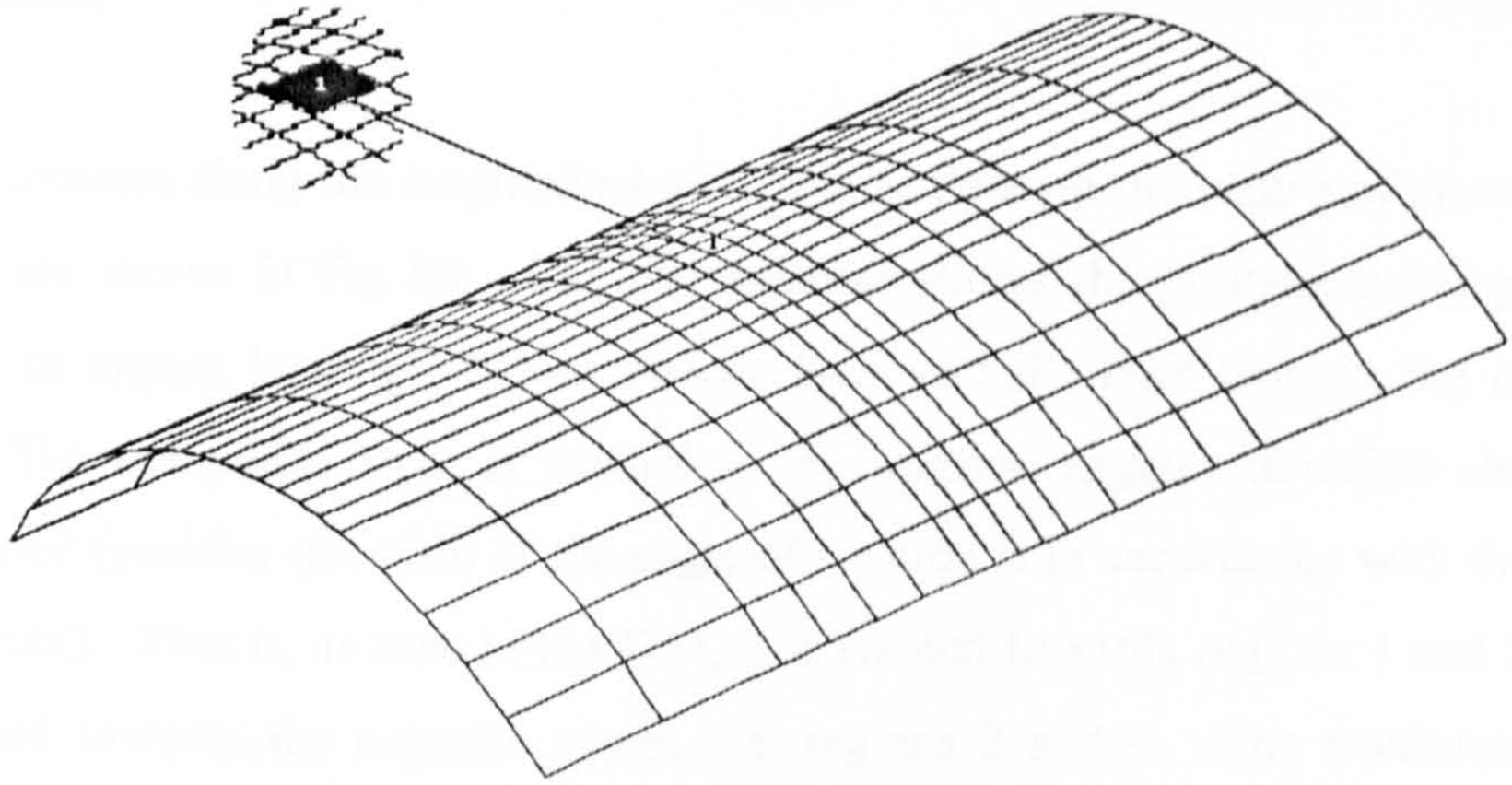

Fig C9 Location of impact loading

Appendix D Kinematic Response - FE Results

Empty Cylinder

Hoop displacements along the longitudinal axis passing through the centre of symmetry of the cylinder are shown in Fig D1. The displacement shows the in-plane twisting of the cylinder due to impact loading. The composite layer and the liner twist in the opposite directions. The composite layer is twisted in the positive angular direction about the thickness vector (positive direction of the angle of rotation is in accordance with the right-hand-screw rule). That is, as seen in Fig D14, it is twisted towards regions 1 and 3. The liner is twisted towards the negative angles, i.e. regions 2 and 4. The maximum hoop displacement for the composite layer and liner were 5 μm and 2 μm respectively. The twisting of these two layers was not symmetric. Moreover, very small hoop displacements were observed at the centre of the cylinder. The opposite twisting of the composite layer and the liner suggests that there may arise some relative movement between the contacting surfaces of these two layers. However, the in-plane displacement was minimal compared with transverse displacement of -923.59 μm.

Longitudinal displacement on the hoop circle passing though the centre of the cylinder are shown in Fig D2. Similar to Fig D1, this diagram shows in-plane twisting of the cylinder due to impact loading. The composite layer and the liner once again twist in the opposite directions. The composite layer twists towards region 1 and 3. On the hand, the liner twists by a positive angle, i.e. towards regions 2 and 4. The maximum longitudinal displacements for composite layer and liner were 2 μm and 4 μm respectively. The twisting of these two layers was once again not symmetric. The liner displacement was much higher than that of the composite layer, once again suggesting the possibility of relative movement between the contacting surfaces of the two layers.

Fig D3 shows the longitudinal displacements on the longitudinal axis passing through the origin, and illustrates the deformation of the composite layer and liner. The liner is seem to move towards the centre by a comparatively large displacement (110 μm maximum). It suggests that the liner gets highly contracted in the longitudinal direction. On the other

hand, although the composite layer also moves towards the centre, its displacements are very small compared with those in the liner. Small relative movement is also present at the contacting surfaces of the two layers, which is mainly due to the movement of the liner.

The relative movement of the contacting surfaces of the two layers along the hoop circle can be seen in Fig D4. The composite layer and the liner move in the opposite directions with quite similar magnitude. The composite layer move away from the centre, while the liner towards it. The maximum displacements of the composite layer and the liner were 90 μm and 50 μm respectively.

The distribution of transverse displacement along the longitudinal and hoop direction are shown in Fig D5. The purpose for this diagram was mainly to illustrate further the twisting phenomenon due to impact loading. The displacement on two sides of the vertical axis were not symmetric. This slightly unsymmetric displacement distribution suggests that out-of-plane twisting of the cylinder takes plane.

Pressurised Cylinder

Hoop direction displacement on the longitudinal axis passing through the centre of the cylinder are shown in Fig D6. This diagram shows in-plane twisting of the cylinder due to internal pressure as well as due to impact loading. The directions and pattern of twisting of the two layers are quite different (cf. Fig D1). The way in which the two layers are twisted by internal pressure is in the opposite sense to that by impact loading. No hoop displacement was found at the centre of the cylinder for these two layers.

Longitudinal displacements along the hoop axis passing through the centre of the cylinder are shown in Fig D7. Twisting mode deformation similar to that for the empty cylinder under impact loading can be seen (cf. Fig D2).

Fig D8 represents the plot of axial displacements along the longitudinal axis of the cylinder. Fig D9 shows the hoop displacements along the hoop axis.

The distribution of transverse displacement along the longitudinal axis passing through the centre is shown in Fig D10. The distribution of transverse displacement along the hoop axis passing through the centre is shown in Fig D11. The diagram of transverse displacement along the circular hoop line on the cylinder does not reflect the deformed shape due to the internal pressure and / or due to impact on a pressurised cylinder. The two diagrams show that the displacements on the two sides of the vertical axis are not symmetric. This slightly asymmetrical displacement distribution suggests that some out-of-plane twisting of the cylinder occurs.

In order to illustrate further this out-of-plane twisting, the transverse displacement distribution along the longitudinal axis at a plane 34 mm from the centre are given in Fig D12. The purpose of this diagram was mainly to show the deformed shapes due to the internal pressure and due to impact on a pressurised cylinder. The displacement distribution due to impact loading suggests that folding-like deformation is taken place. The transverse displacement along the hoop axis at a hoop plane 20.6 mm from the centre is shown in Fig D13. In this diagram, an asymmetrical distribution of displacement is seen once again.

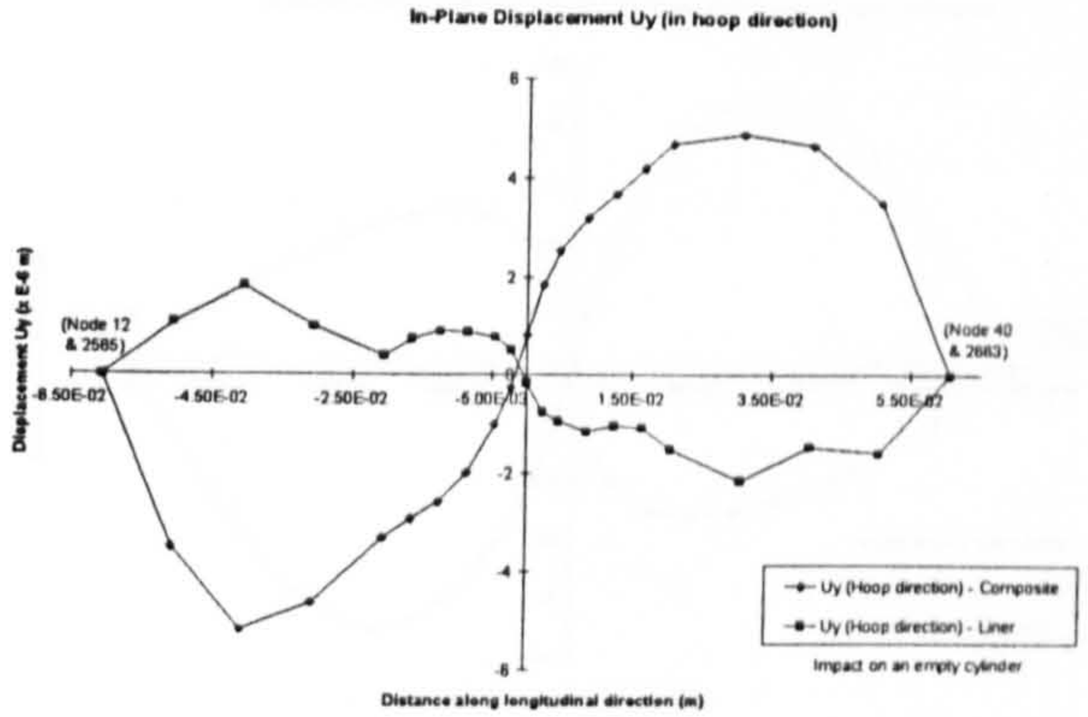

Fig D1 Distribution of Uy along the longitudinal direction

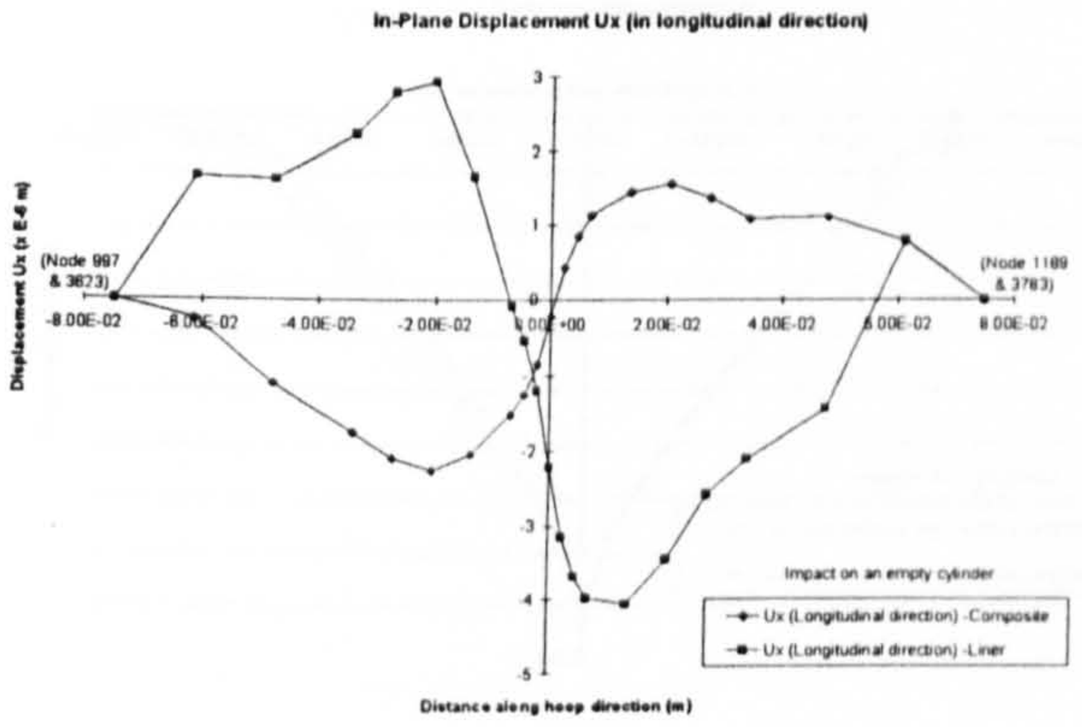

Fig D2 Distribution of Ux along the hoop direction

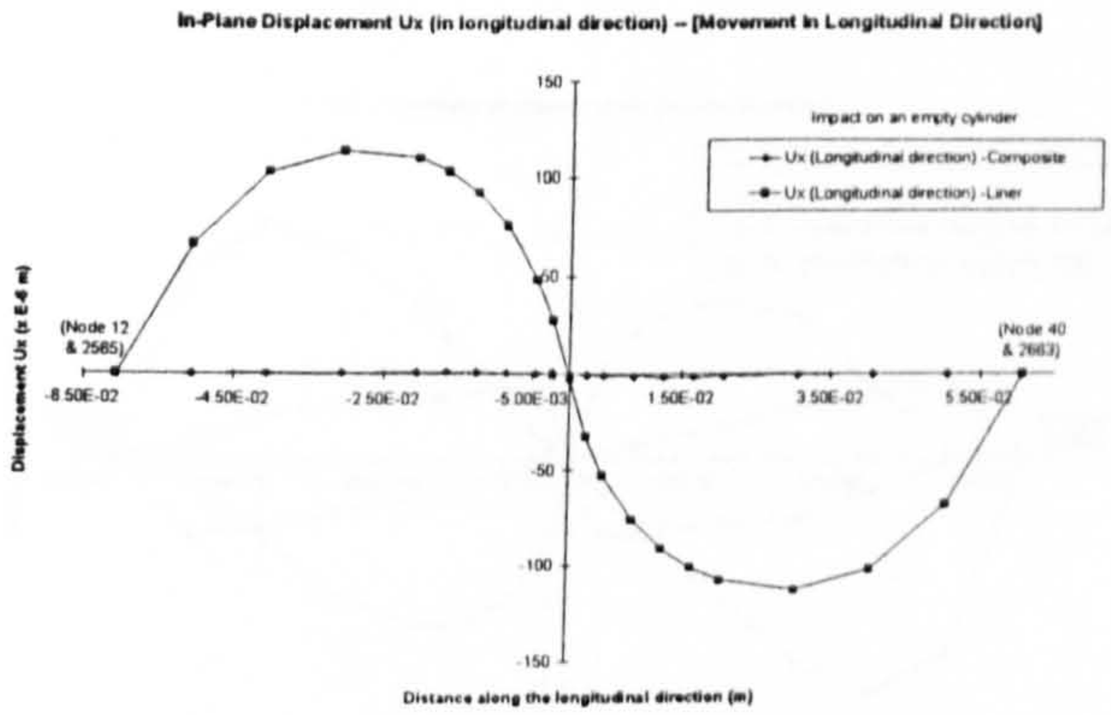

Fig D3 Distribution of Ux along the longitudinal direction

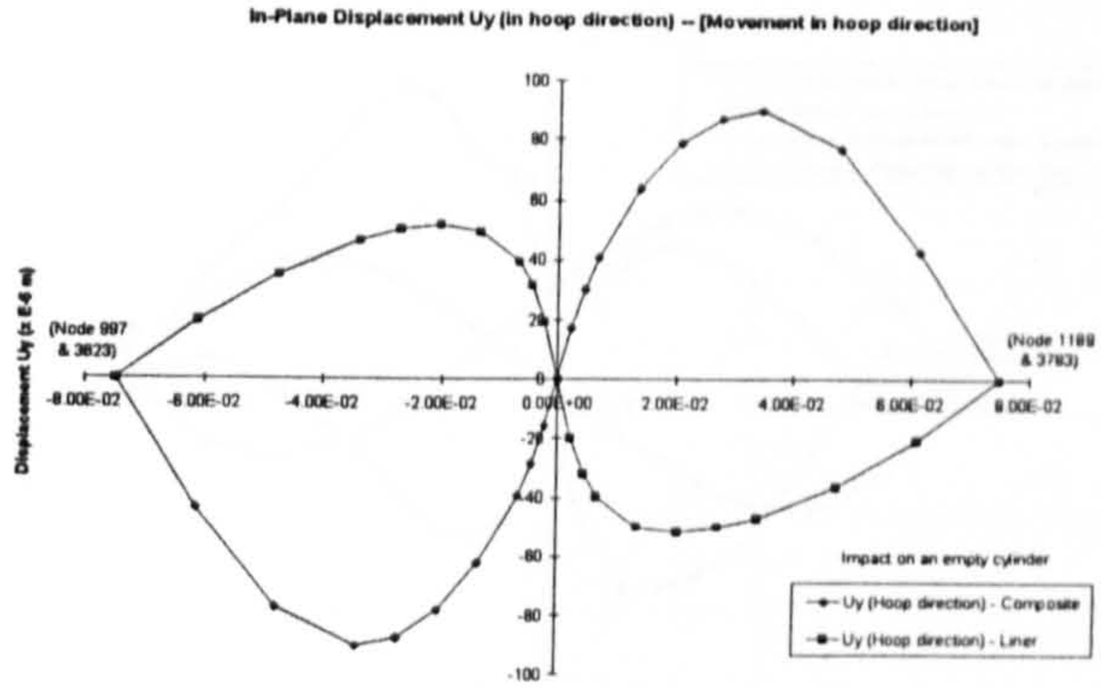

Fig D4 Distribution of Uy along the hoop direction

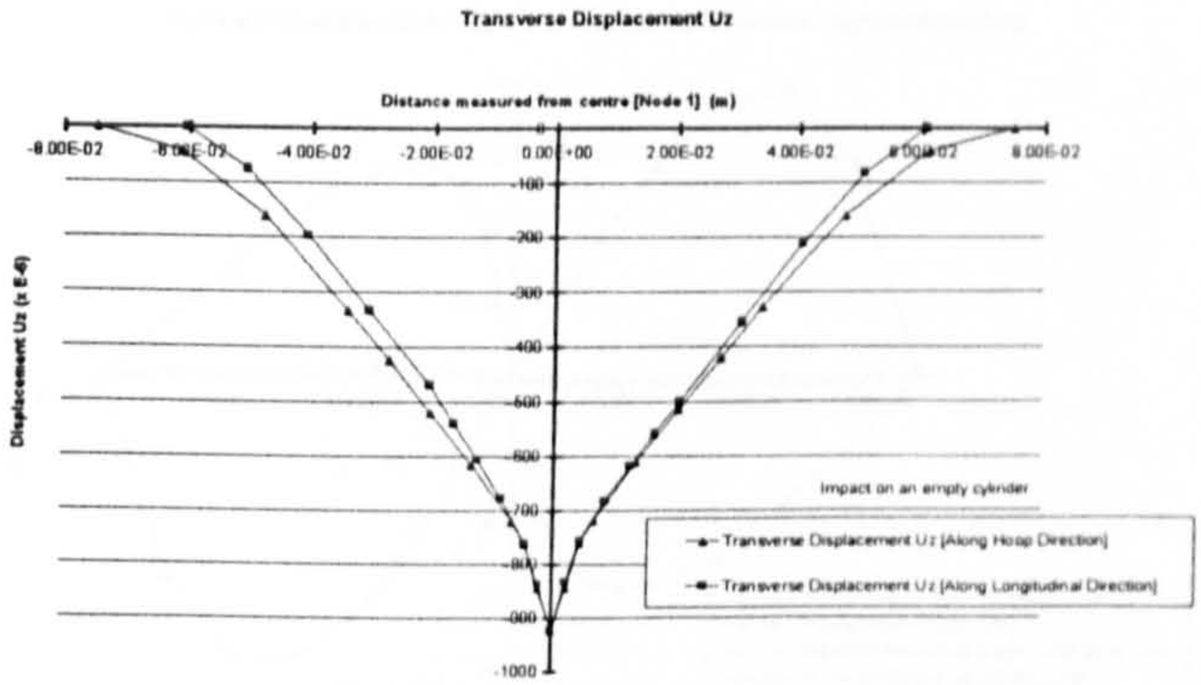

Fig D5 Distribution of the transverse displacement Uz

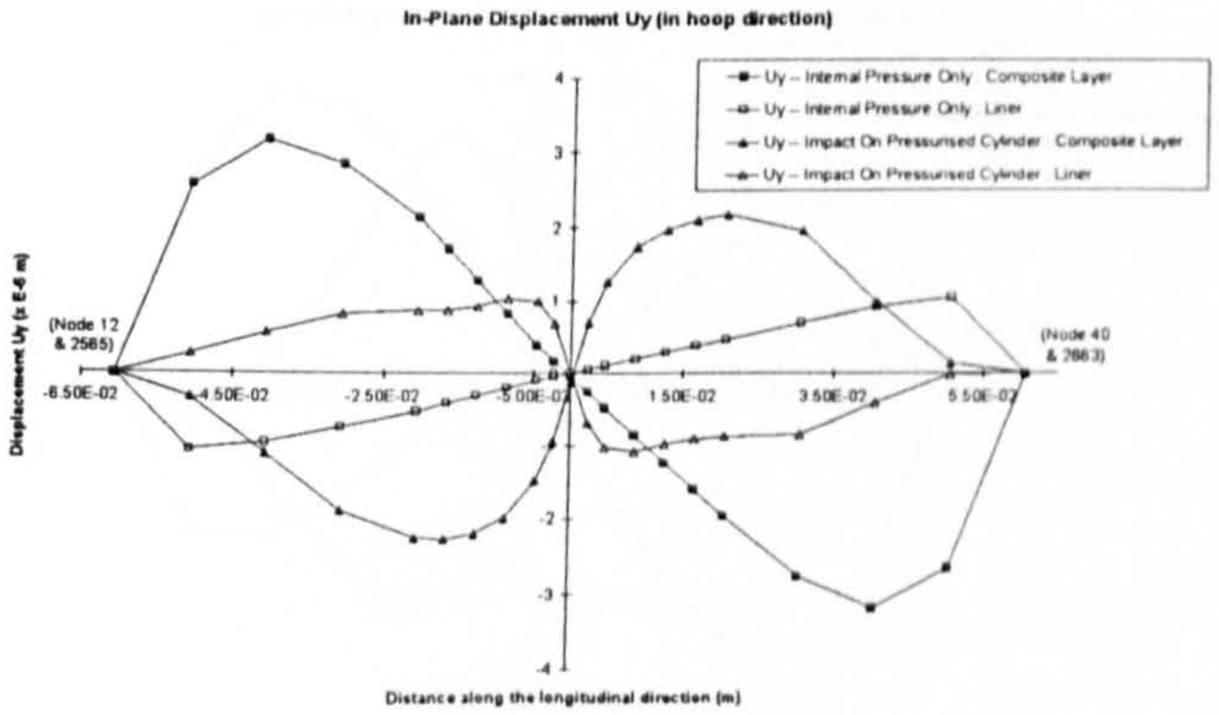

Fig D6 Distribution of Uy along the longitudinal direction

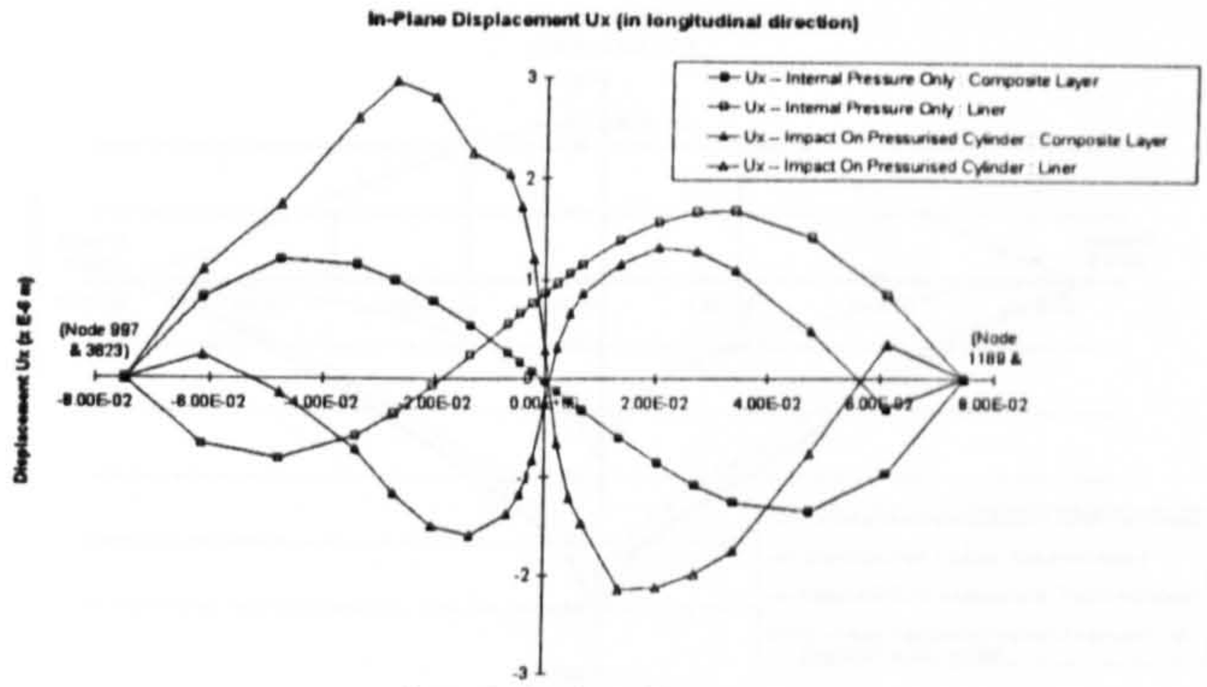

Fig D7 Distribution of Ux along the hoop direction

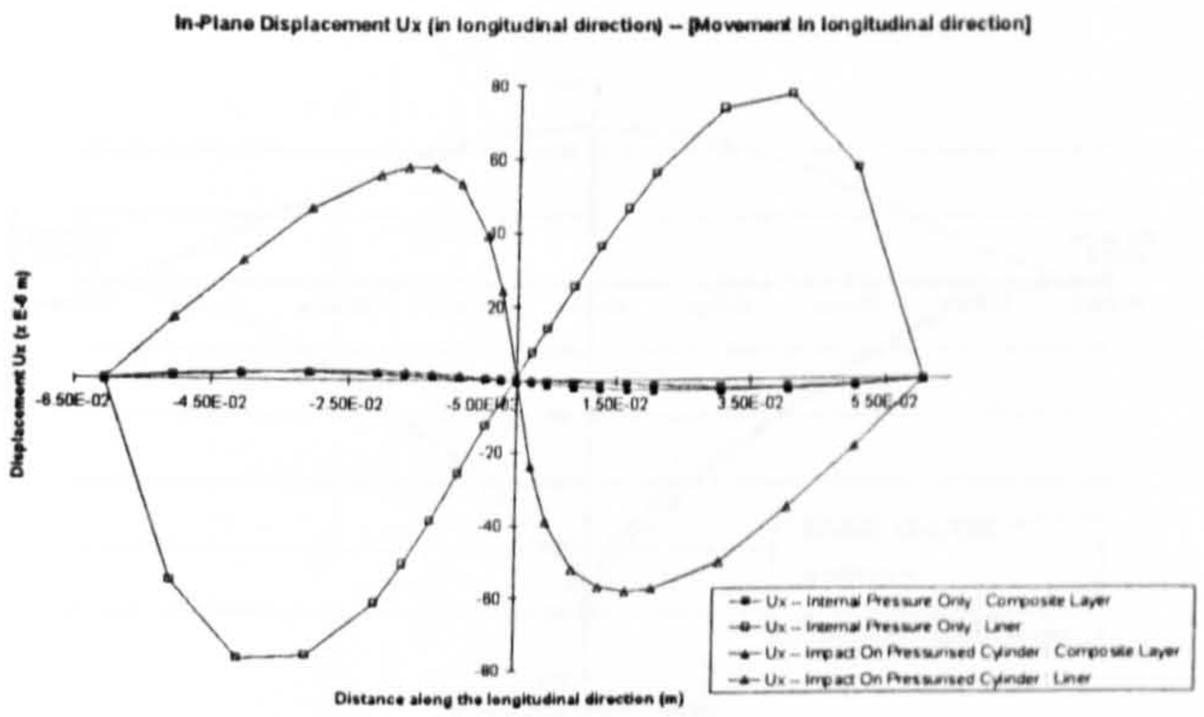

Fig D8 Distribution of Ux along the longitudinal direction

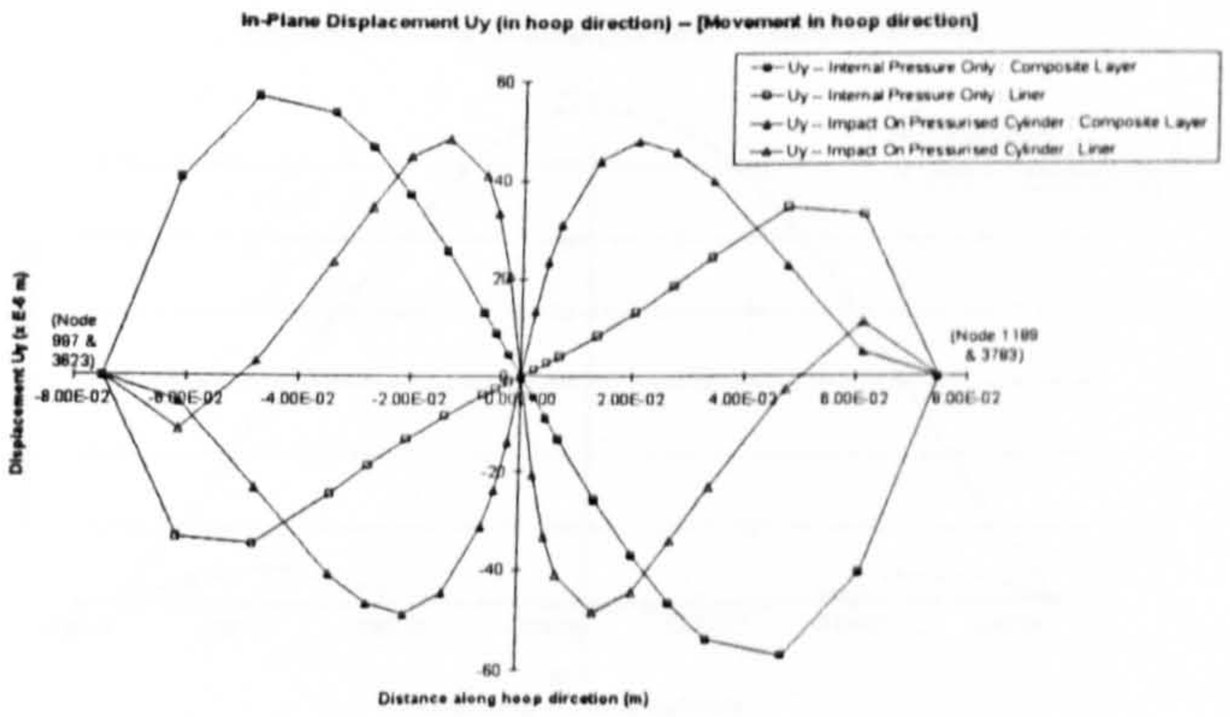

Fig D9 Distribution of Uy along the hoop direction

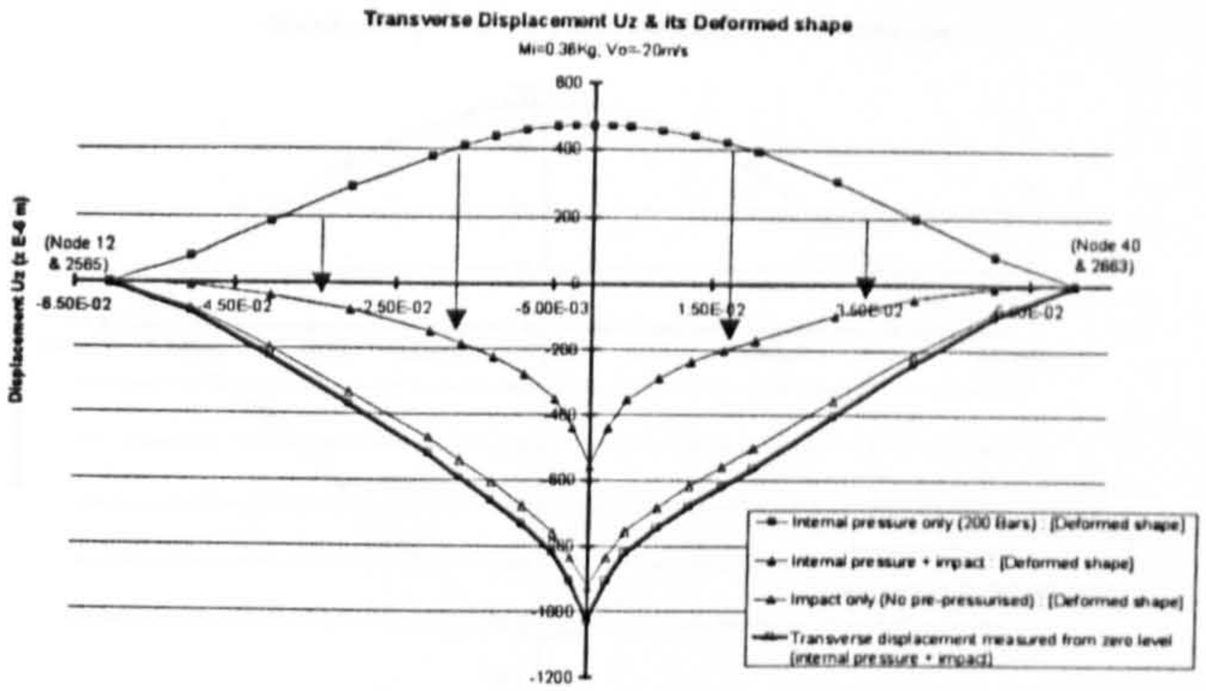

Fig D10 Distribution of the transverse displacement Uz

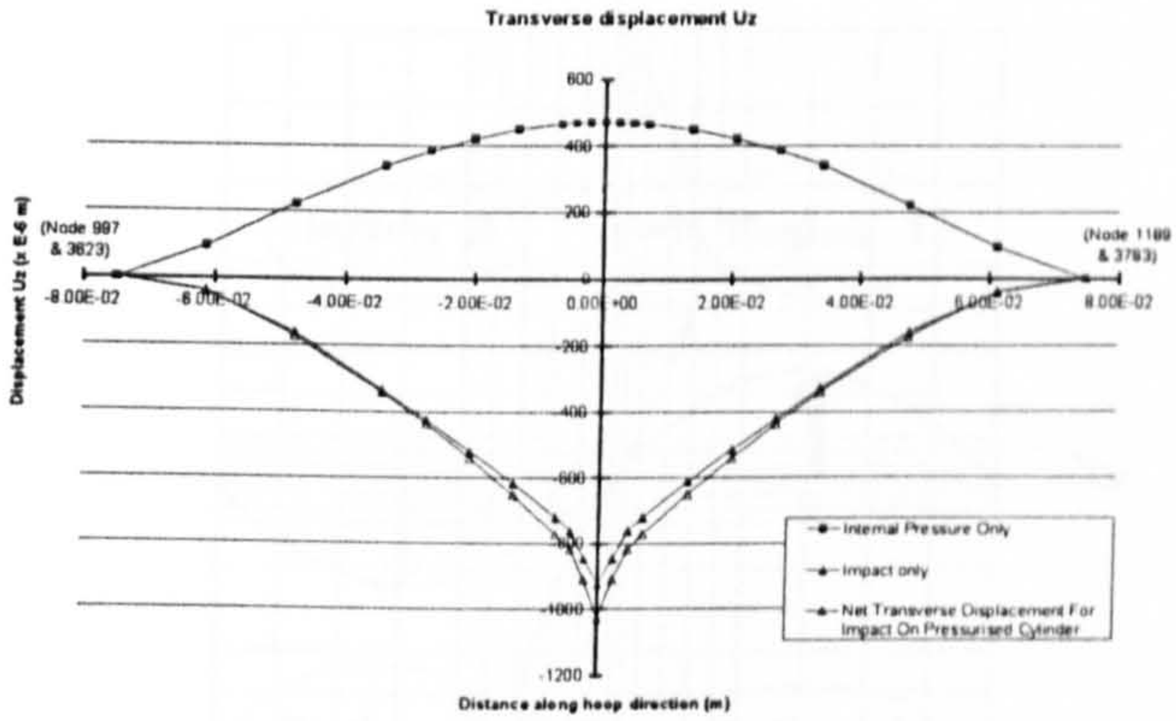

Fig D11 Distribution of the transverse displacement Uz

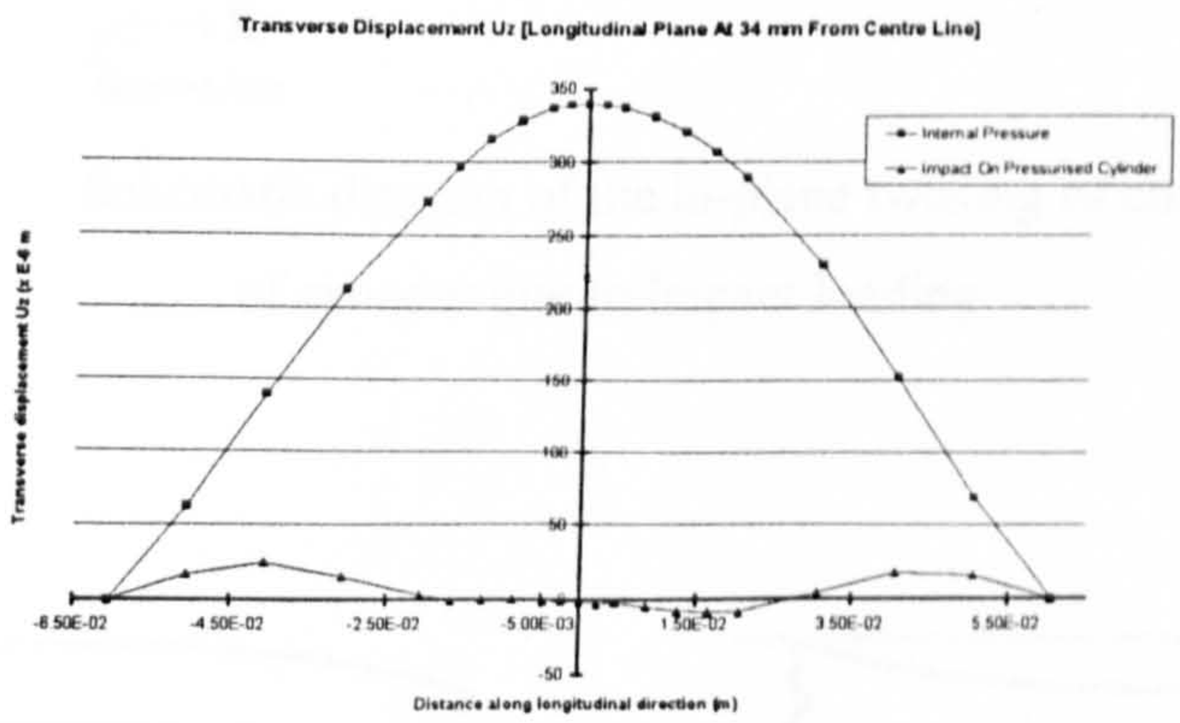

Fig D12 Distribution of the transverse displacement Uz

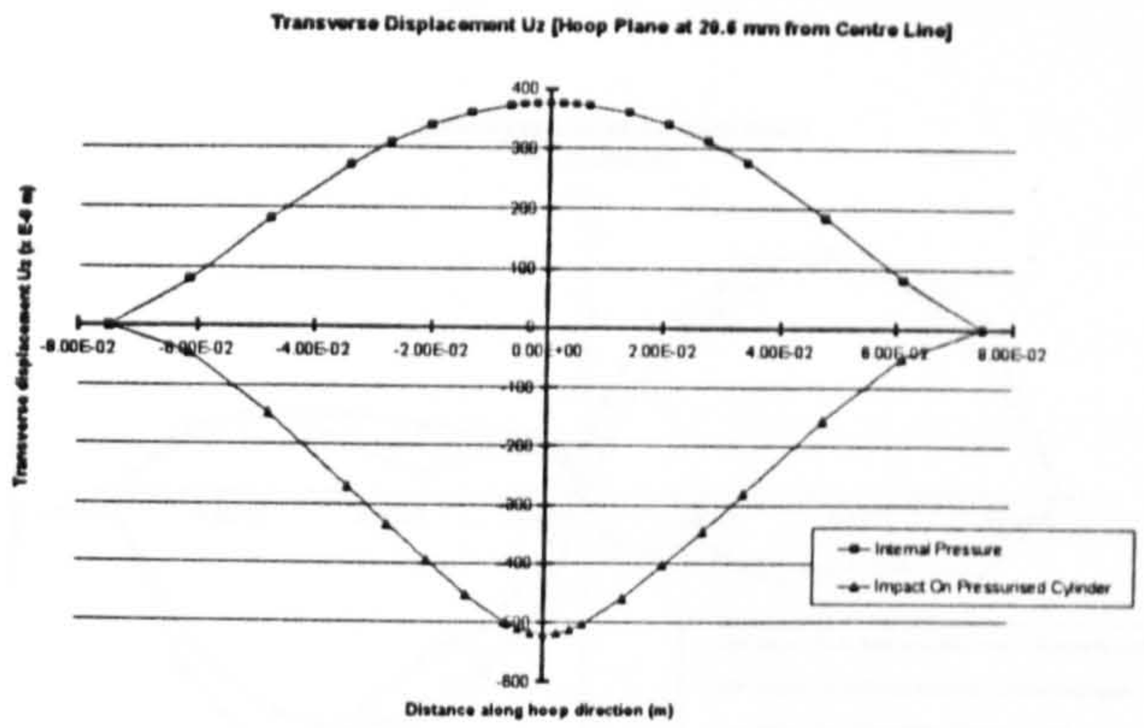

Fig D13 Distribution of the transverse displacement Uz

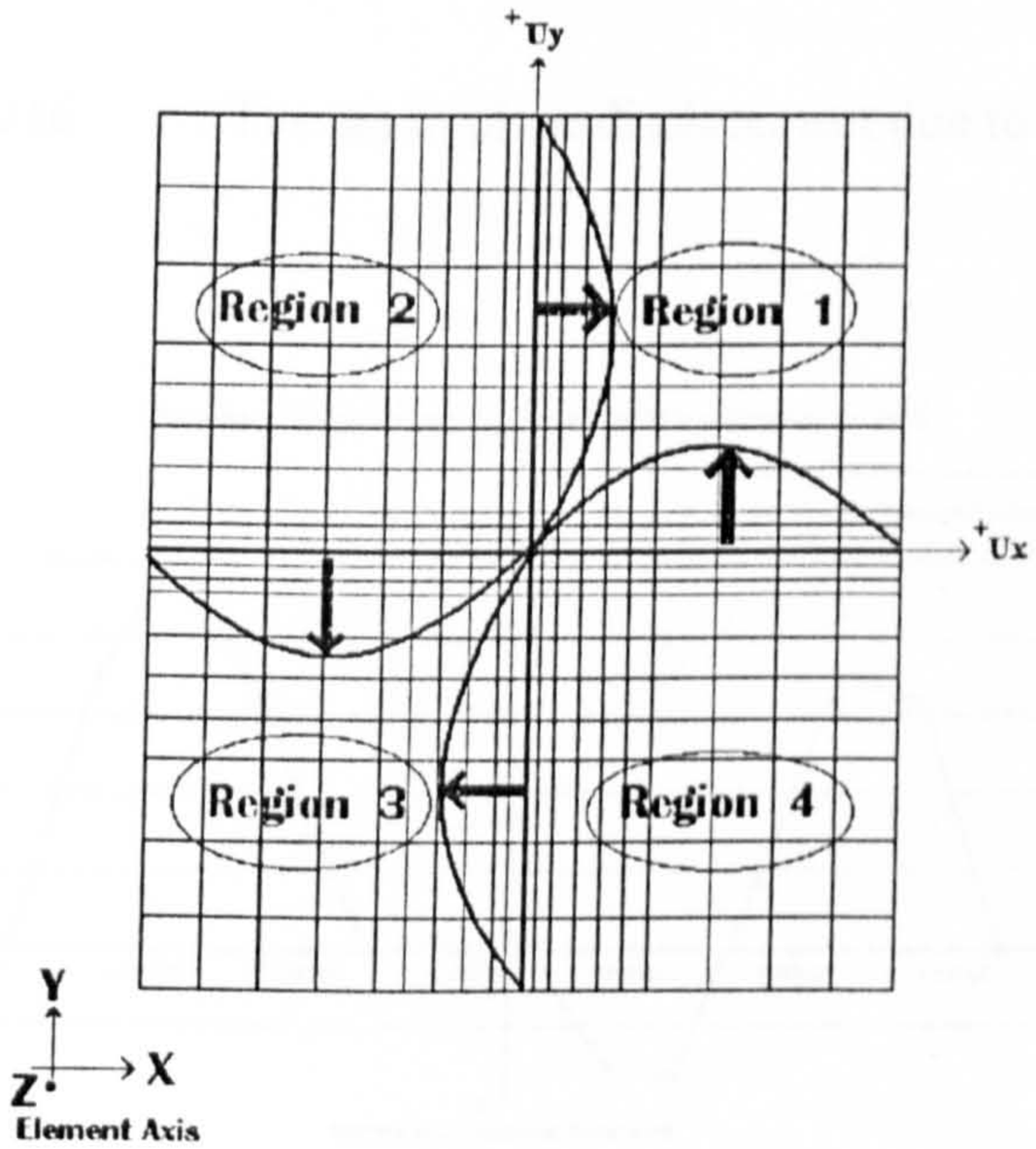

Fig D14 Schematic diagram of the in-plane twisting of composite layer of cylinder due to impact loading

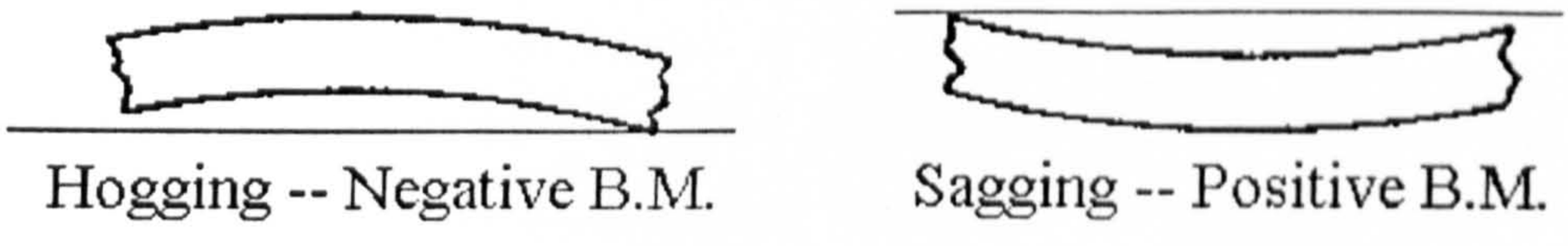

Fig D15 Bending shapes of cylinder wall due to (1) internal pressure – hogging; (2) impact – sagging

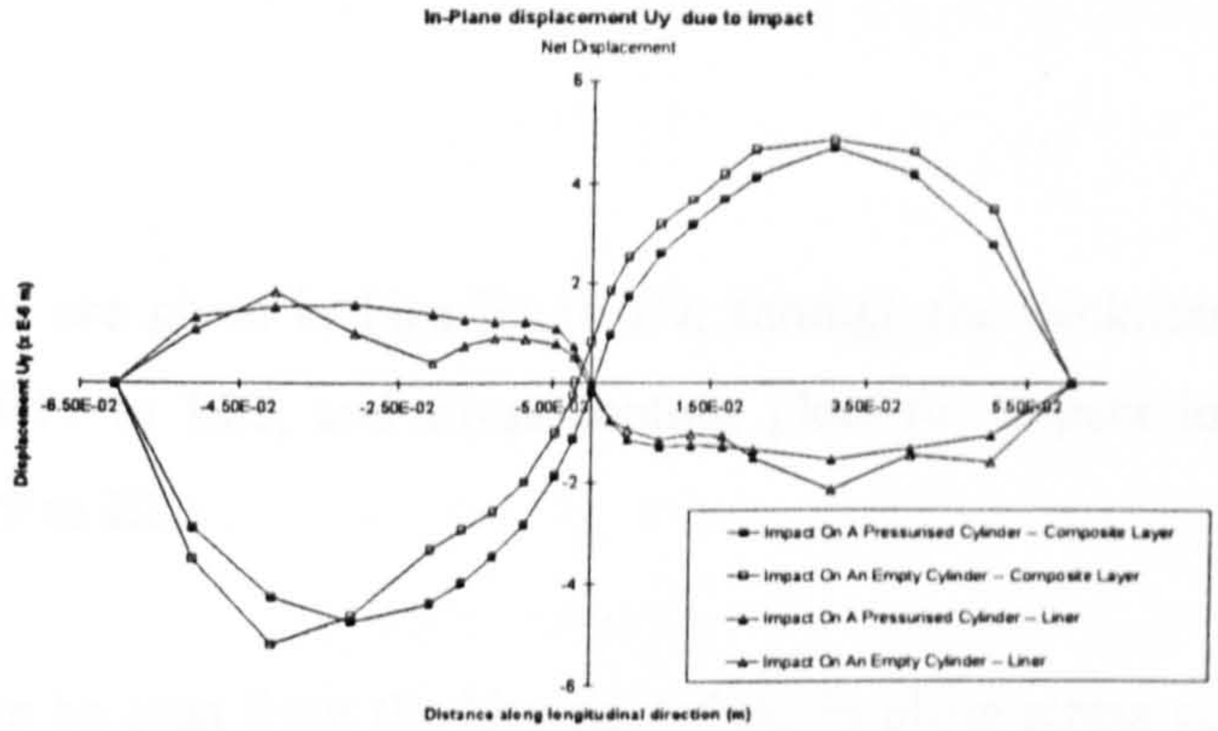

Fig D16 The net in-plane displacement due to impact

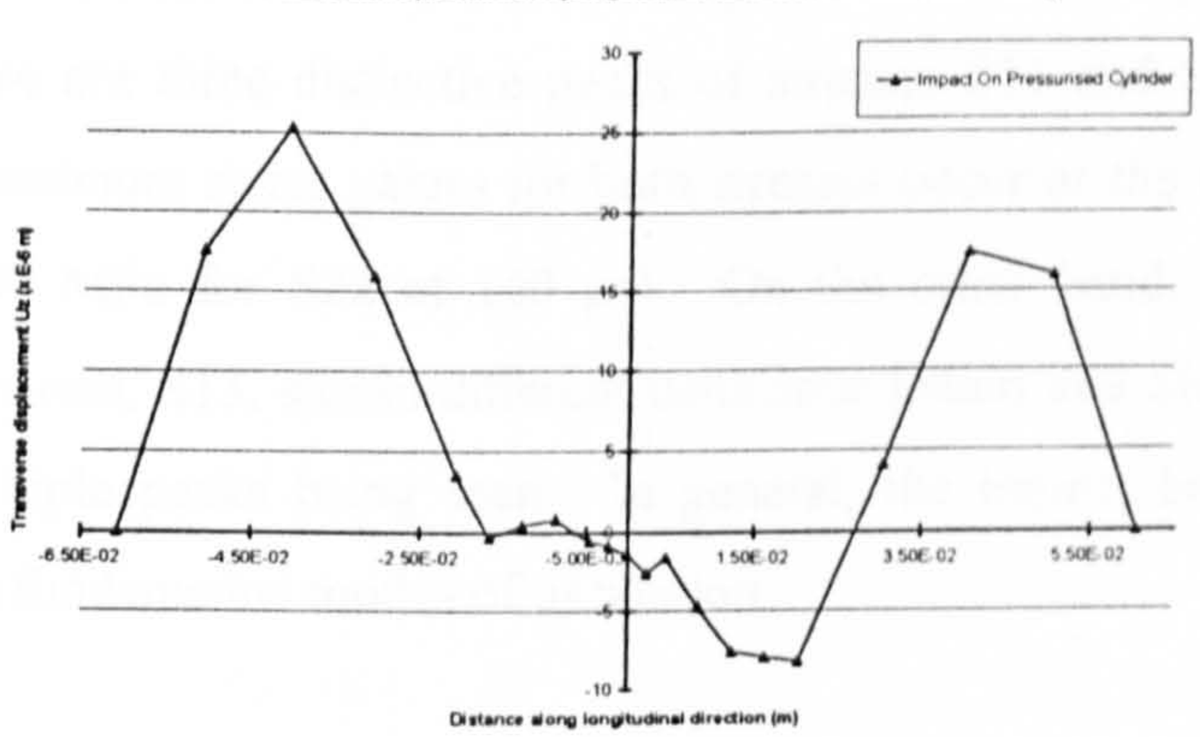

Fig D17 The transverse displacement along longitudinal plane at 34 mm from centre

Appendix E Material Response - FE Results

Empty Cylinder

Stress history plots are given in Figs E1 to E9, through-the-thickness stress distribution diagrams in Figs E19 to E22, and stress contour plots for impact loading of an empty cylinder in Figs E29 to E30.

From Fig E1, it can be seen from the histories of the in-plane stress components S11 and S22 at the top surface of layer 2 at Node 1 that initially the impact phenomenon is a localised event, but gradually the whole structure is involved in the deformation, and the structural stiffness plays an important role in controlling the response of the structure [Maiti and Sinha, 1996]. The time at which the maximum stress is attained (at 140 μs) does not coincide with the time for the maximum out-of-plane transverse displacement. It can also be seen that there are three distinctive peaks of stresses S11 and S22 within the impact duration. The maximum stress values for both stresses occur at the third peak (-760 MPa for S11 and -280 MPa for S22 at 140 μs). On the other hand, the behaviour of the transverse shear stress, S13, shows different behaviour [Maiti and Sinhu, 1996] during the impact, with multiple peaks being seen. In general, the impact behaviour seems to be dominated by the fundamental modes of oscillation.

In Fig E2, the stress histories of the stresses S11 and S22 at the bottom surface of the composite layer 9 are given. Similar qualitative observations as for Fig E1 can be made, with the stresses being of the opposite sign and different magnitude. In comparing with the response in Fig E1, the maximum stress values are lower, with the maximum of the stress being 620 MPa, and for the stress S22 being 275 MPa.

Stress histories for the top surface of the liner can be found in Fig E3. For the first 10 μs, both the longitudinal stress, S11, and the hoop stress, S22, behave similarly with nearly the same magnitudes. The difference between these two stress components gradually increases with time, until their maximum values occur at 75 μs.

Stress histories at the bottom surface of the liner are given in Fig E4. Some feathers of the stress histories are similar to those in Fig E3, in which the three distinctive peaks occur at similar time.

Figs E5 to E9 present stress histories for the liner and the composite layer depicted at 8.6 mm (three shell elements) passing through the central point in longitudinal axis. The main purpose of these plots was to observe the effect of impact away from the source of disturbance. In general, the corresponding stress values are much lower than that at the point of impact. The response histories are dominated by the fundamental modes.

The through-thickness distribution of the stress components S11 and S22 at the central point and 8.6 mm from the central point at the time of peak displacement (i.e. 85 μs) are given in Figs E19 to E22. In general, the stress distribution in the composite layers shows a typical compressive-tensile bending stress pattern. The liner mainly experiences compressive through-the-thickness stress. For the top surface of composite layer 1, the stress magnitude ratio of S11 to S22 is 2.6 at the central point, and 4.3 at a distance of 8.6 mm from the central point. For the liner, the hoop stress (S22) is higher than the longitudinal stress (S11). For the top surface the ratio was 1.6 at the central point, and 2 at a distance of 8.6 mm from the central point.

Figs E29 and E30 show the stress distribution (S11 and S22) over the top surface of composite layer 1 of the entire FE model at the time of peak transverse displacement, 85 μs. It can be seen that the iso-stress contours have a rectangular shape expanding from the central point. Since the composite layer 1 was hoop-wound at 90 degree, the longer side of the rectangular oval shape for stress S11 was in the longitudinal direction (perpendicular to the fibre direction), while for stress S22 was in the hoop direction.

Pressurised Cylinder

The stress history plots are given in Figs E10 to E18, through-the-thickness stress distribution diagrams in Figs E23 to E28, and stress contour plots for the cylinder in Figs E31 to E34.

In Fig E10, shows that the impact loading started at 3000 μs and ended at 3200 μs, in which there were pre-stresses present in the cylinder due to internal pressure. Generally speaking, the response behaviour of S11 and S22 were quite similar to those from an empty cylinder, except the stresses magnitudes were slightly lower (-700 MPa for S11 and -250 MPa for S22 at 3140 μs, the third peak). In the same way, stress history of the bottom surface of composite layer 9 behaved similarly with those from an empty cylinder (Fig E2).

The stress histories for the liner are given in Figs E12 and E13. It behaved quite different to the liner of an empty cylinder. The hoop and longitudinal stresses at the middle of stress history were nearly the same. It indicates that the pre-stress effect due to internal pressure was effectively increased the hoop stress of the liner at impact loading.

Figs E14 to E18 are stress history for liner and composite layers depicted at 8.6 mm (three shell elements) passed through the central point in longitudinal axis. In general, from the response of these stress histories, the effect of internal pressure was to reduce compressive stresses at the outer surface (at impacting surface), however, it increased the hoop stress at the bottom surface of the liner. On the other hand, the transverse shear stress, S13, of the liner (Fig E18) was increased by 10 % comparing with that of empty cylinder (Fig E19). It reflected the net transverse displacement due to impact on this pressurised cylinder has also been increased by 11.2 %.

The through-the-thickness stress distribution of S11 and S22 at the central point and 8.6 mm from the central point at peak transverse displacement are given in Figs E23 to E24. In Figs E23 and E24, show that , subjected to internal pressure, hoop stresses of liner were nearly double the longitudinal stresses. With these pre-stresses, the through-the-thickness stress distributions under impact loading were more compressive-tensile pattern for the liner.

The stress contour plots of impact on a pressurised cylinder (Figs E33 and E28) were quite similar to those of the empty cylinder (Figs E29 and E33), except that the compressive region were smaller due to pre-tensile stresses were present (Figs E31 and E32).

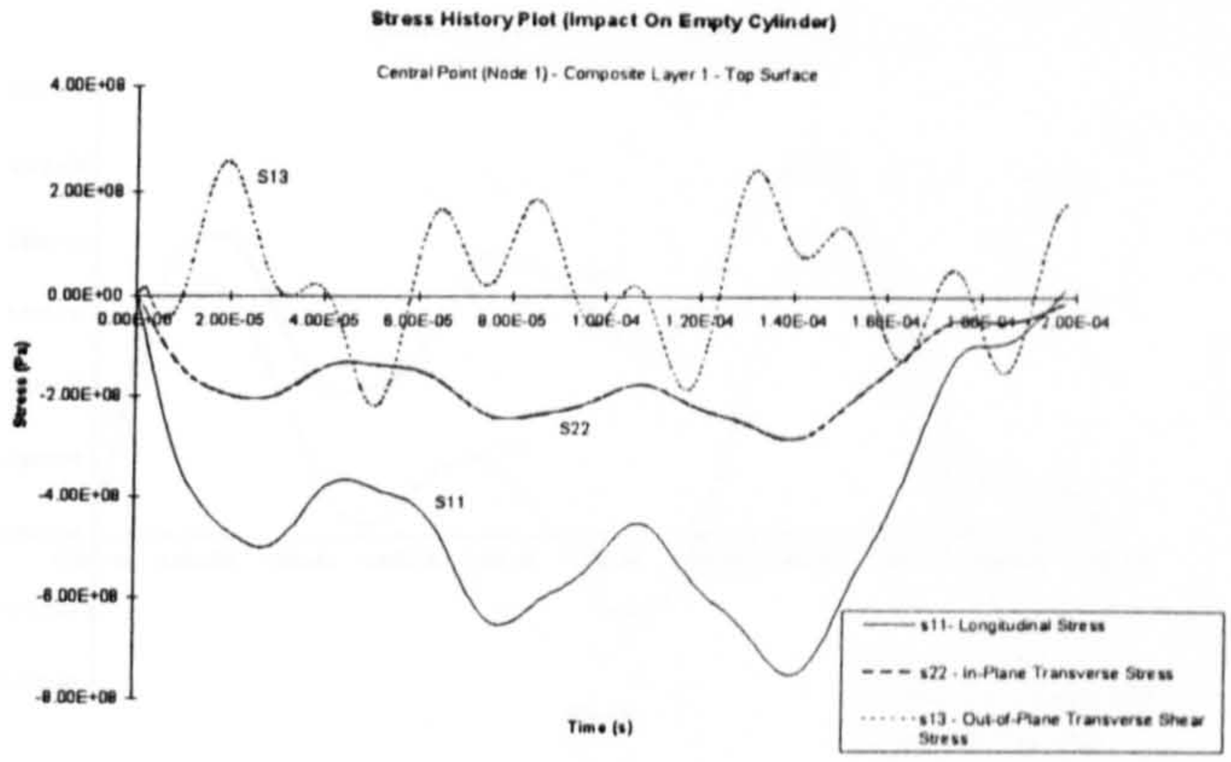

Fig E1 Stress history plot (Node 1) - Composite layer 1 (Top surface)

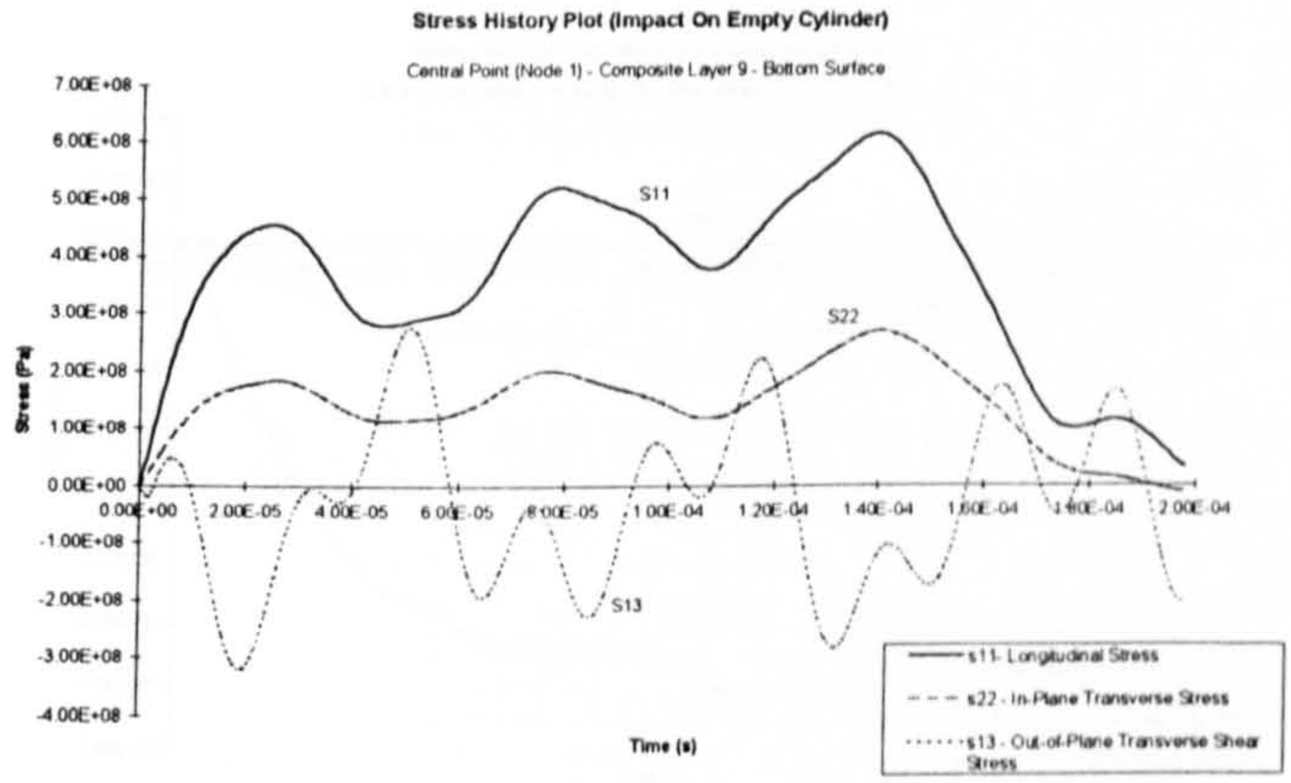

Fig E2 Stress history plot (Node 1) - Composite layer 9 (Bottom surface)

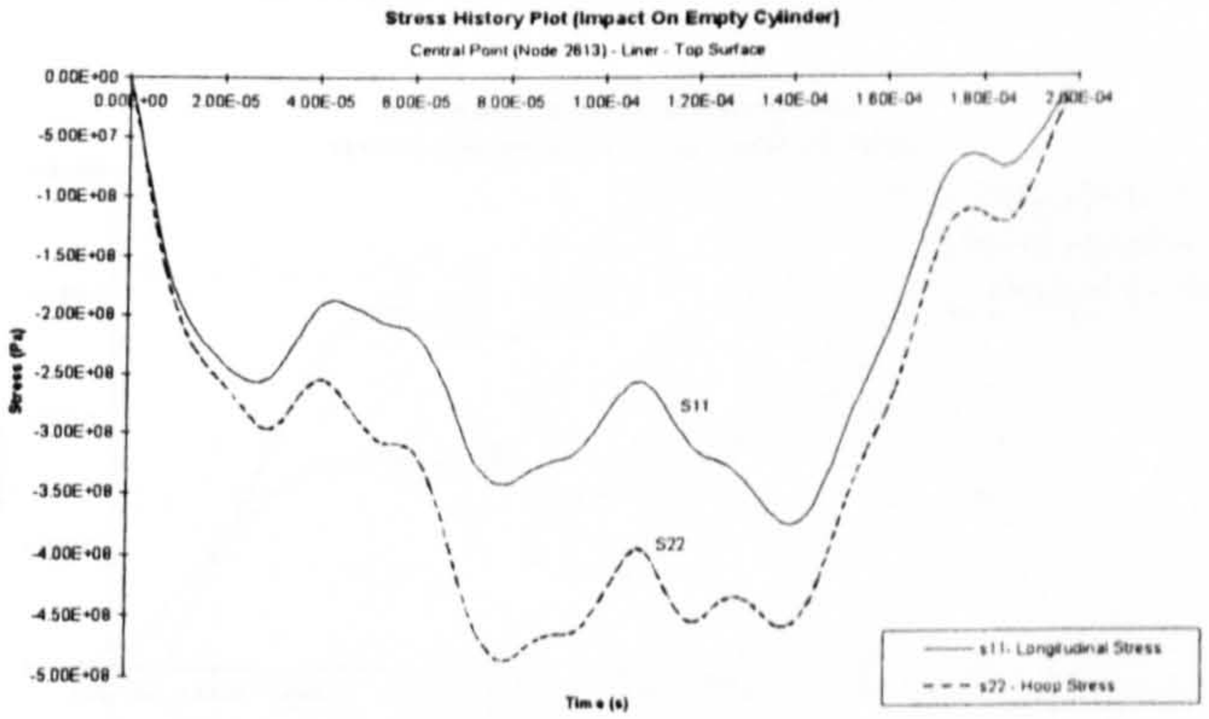

Fig E3 Stress history plot (Node 2613) - Liner 1 (Top surface)

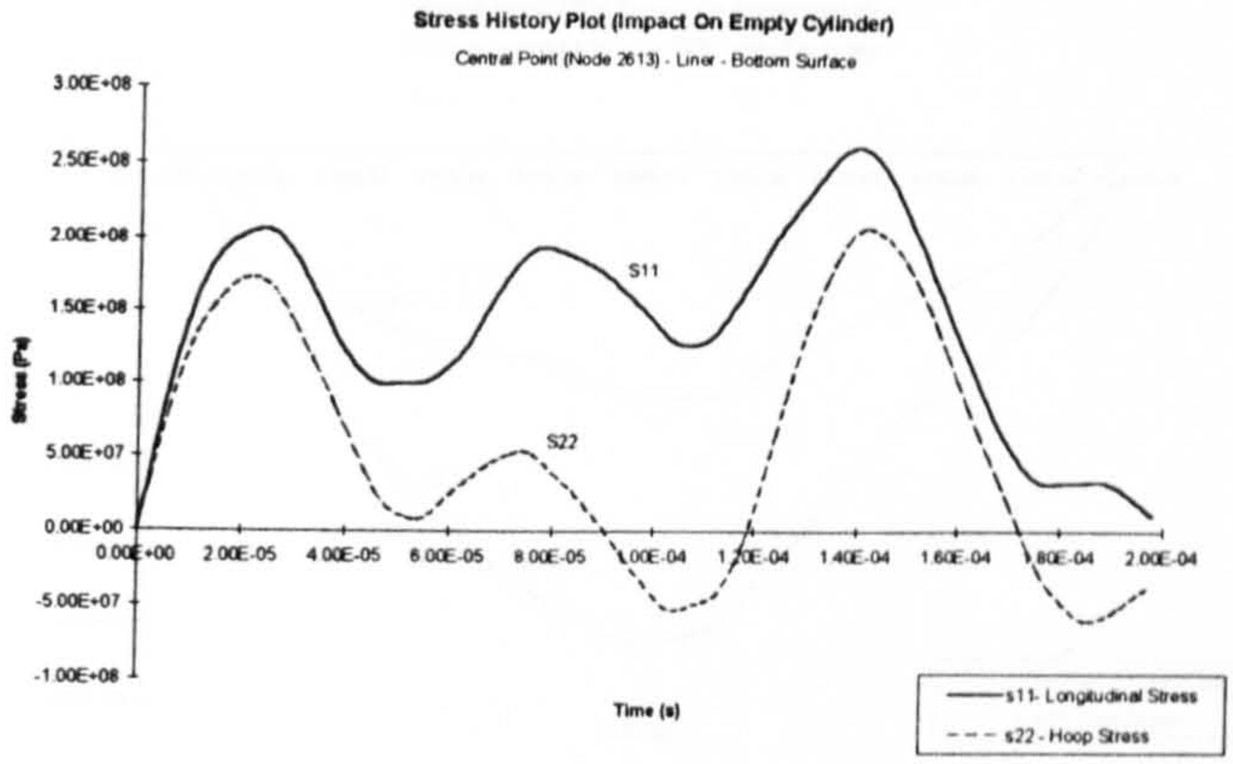

Fig E4 Stress history plot (Node 2613) - Liner (bottom surface)

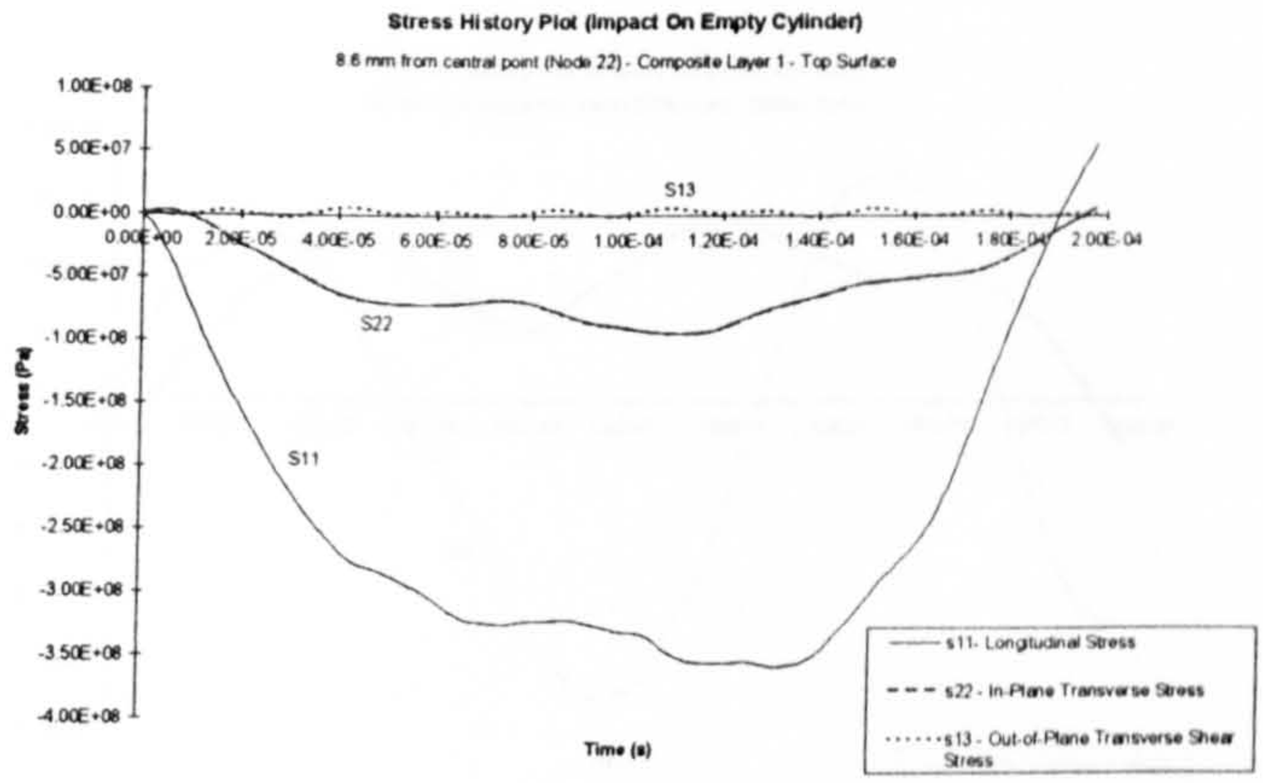

Fig E5 Stress history plot (8.6 mm from central point in longitudinal axis) Composite layer 1 (top surface)

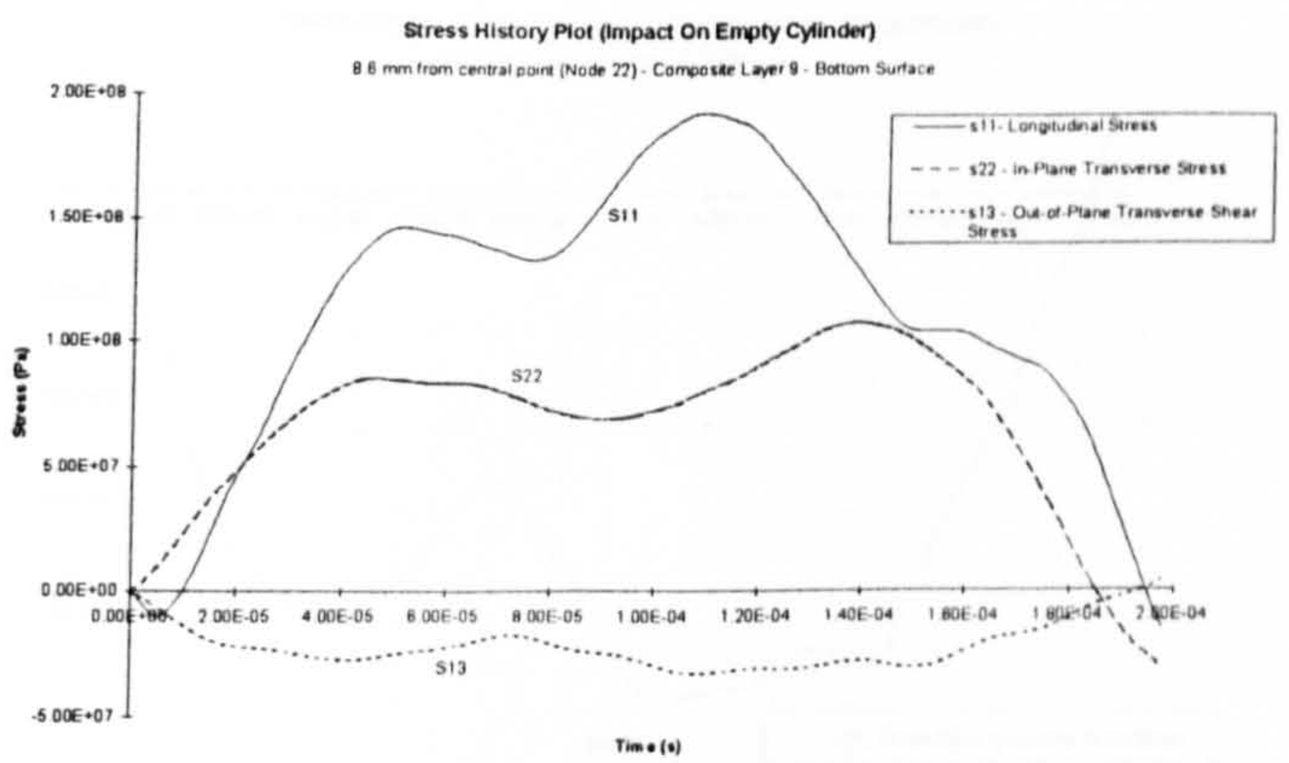

Fig E6 Stress history plot (8.6 mm from central point in longitudinal axis) Composite layer 9 (bottom surface)

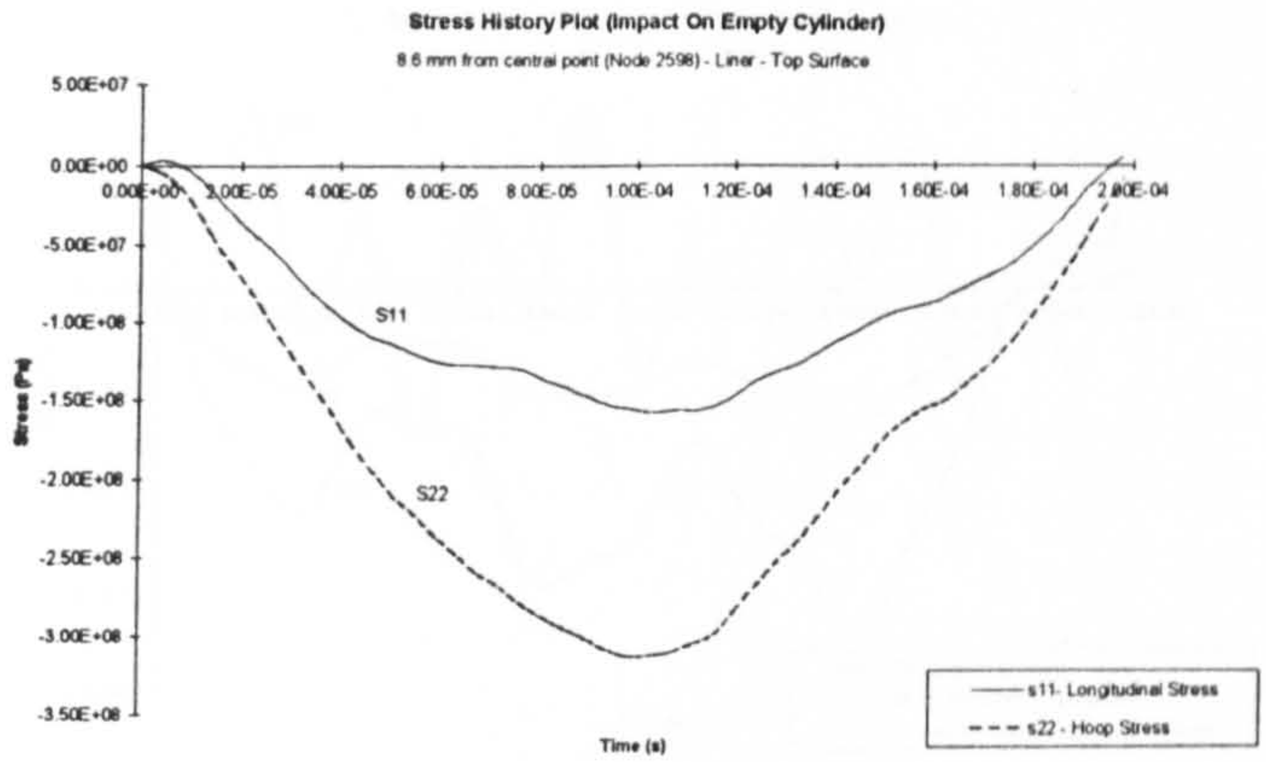

Fig E7 Stress history plot (8.6 mm from central point in longitudinal axis) Liner (top surface)

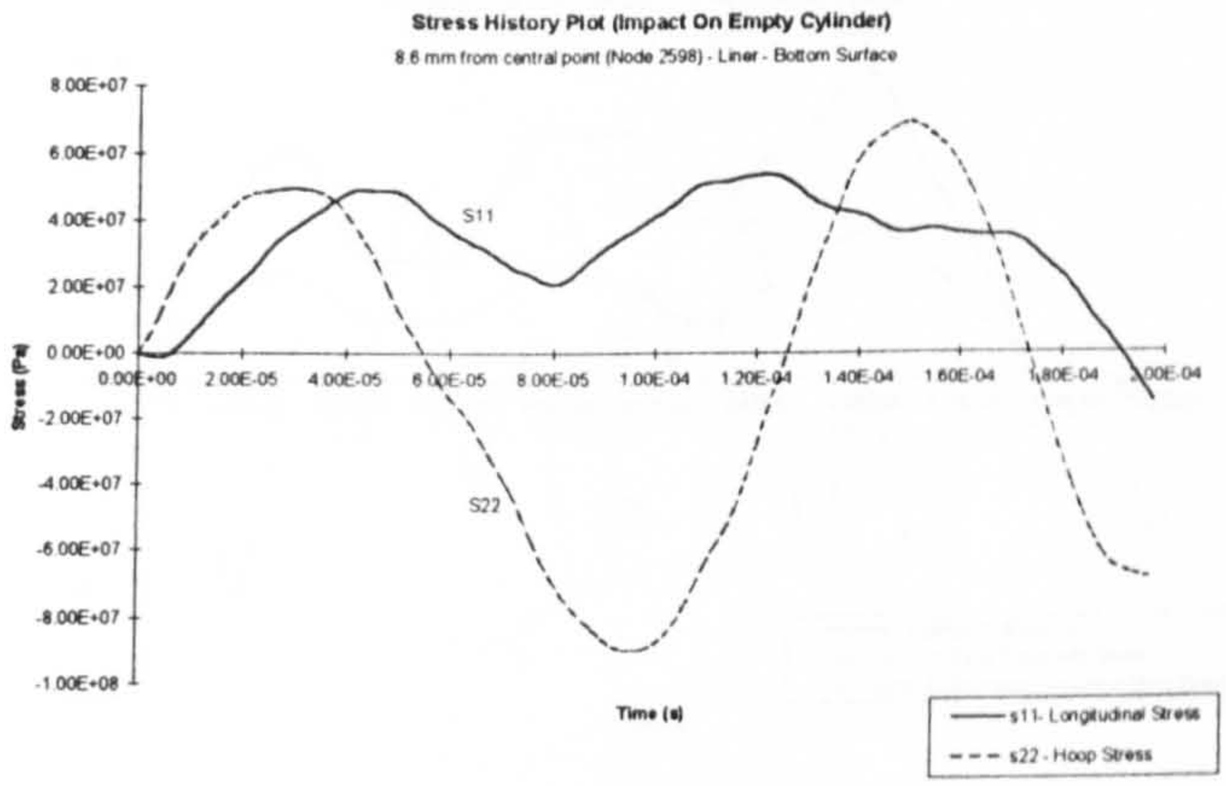

Fig E8 Stress history plot (8.6 mm from central point in longitudinal axis) Liner (bottom surface)

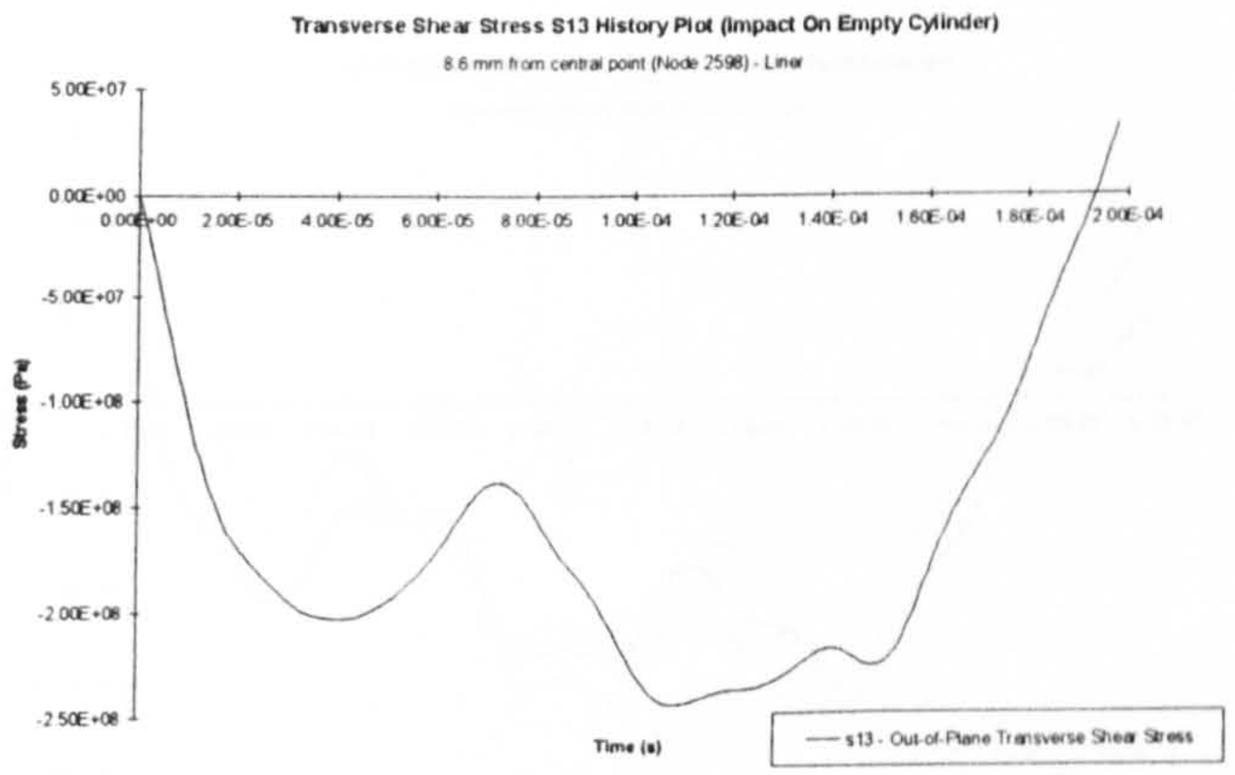

Fig E9 Transverse shear stress history plot (8.6 mm from central point in longitudinal axis) - Liner

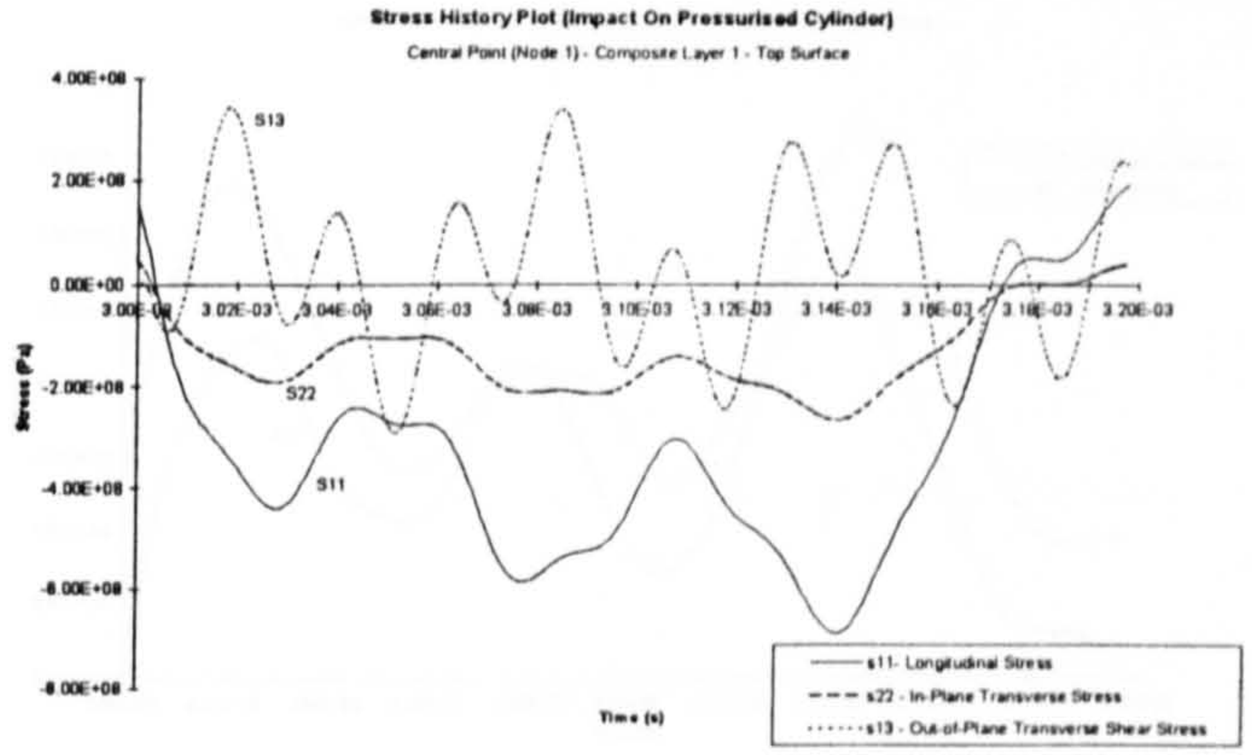

Fig E10 Stress history plot (Node 1) - Composite layer 1 (top surface)

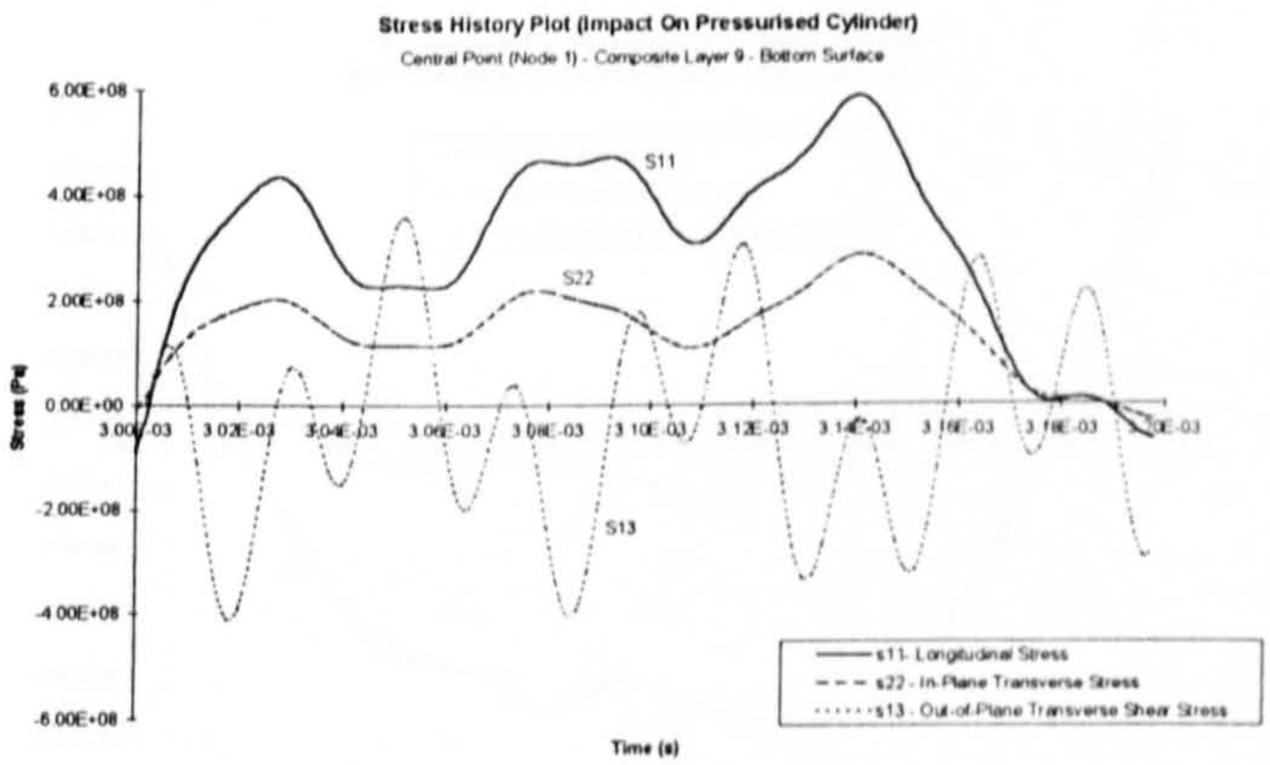

Fig E11 Stress history plot (Node 1) - Composite layer 9 (bottom surface)

Fig E12 Stress history plot (Node 1) - Liner (top surface)

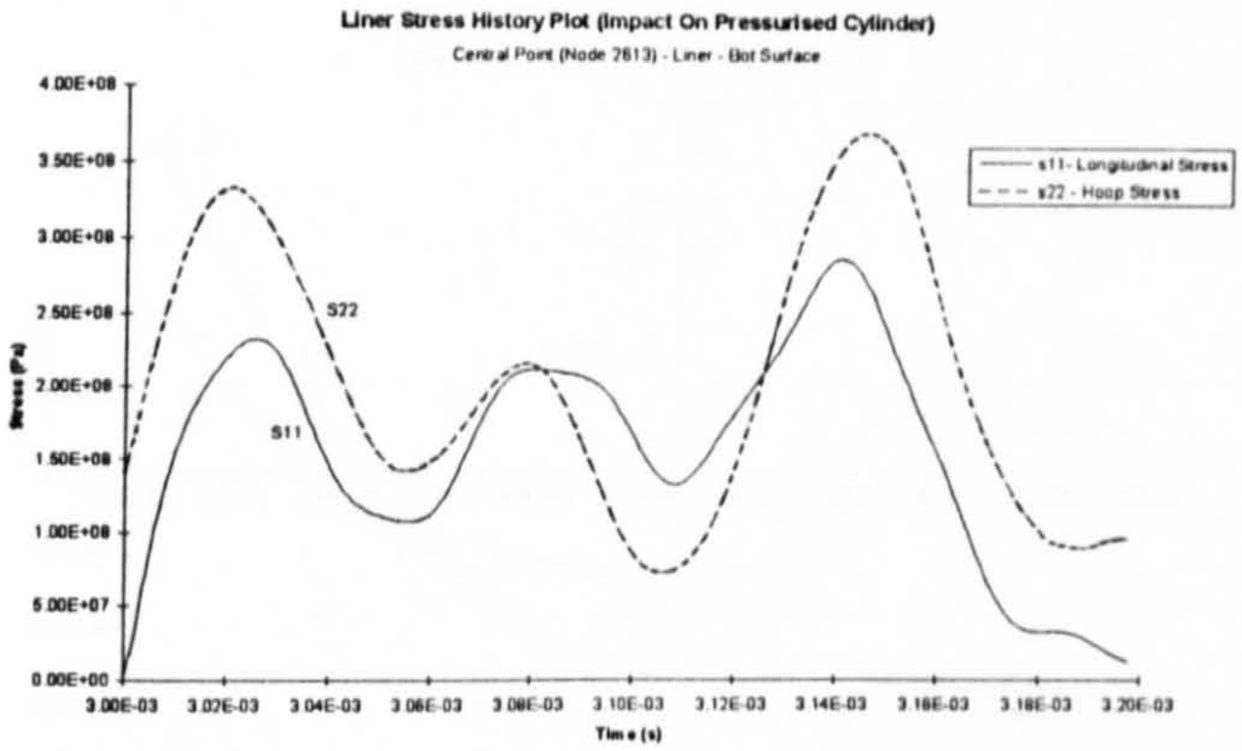

Fig E13 Stress history plot (Node 1) - Liner (bottom surface)

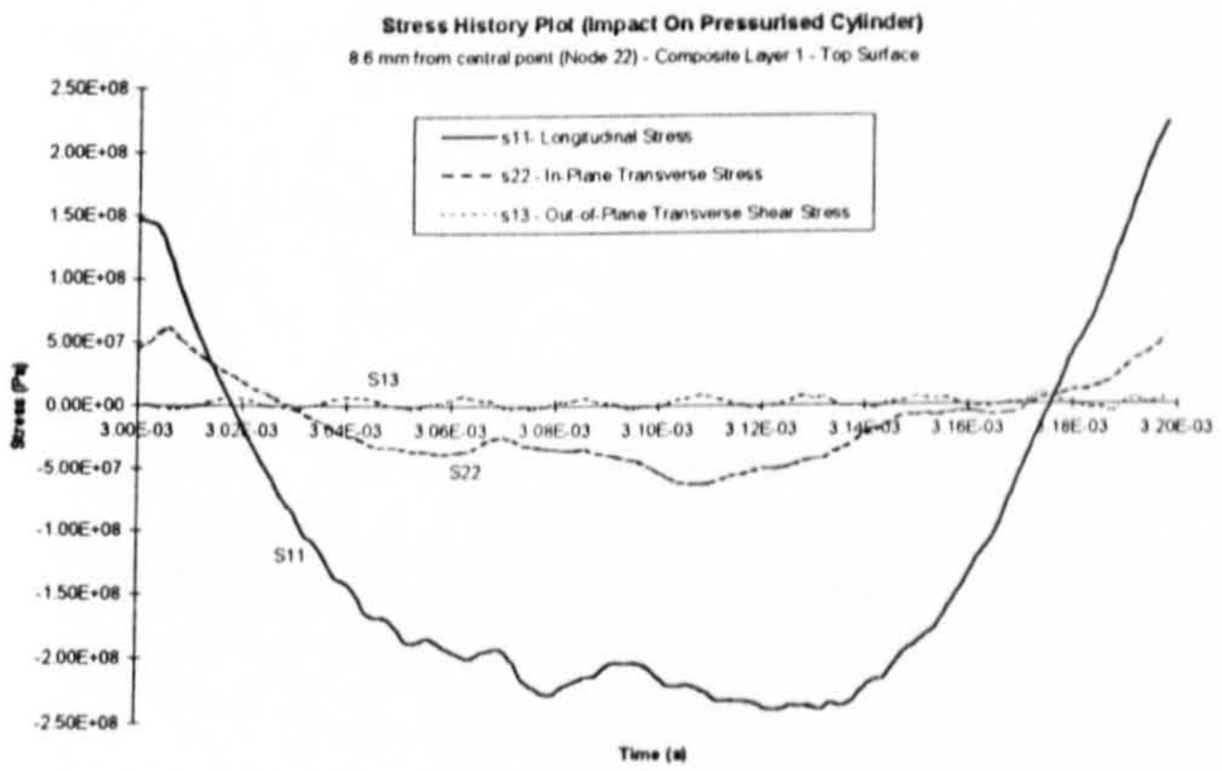

Fig E14 Stress history plot (8.6 mm from central point in longitudinal axis) Composite layer 1 (top surface)

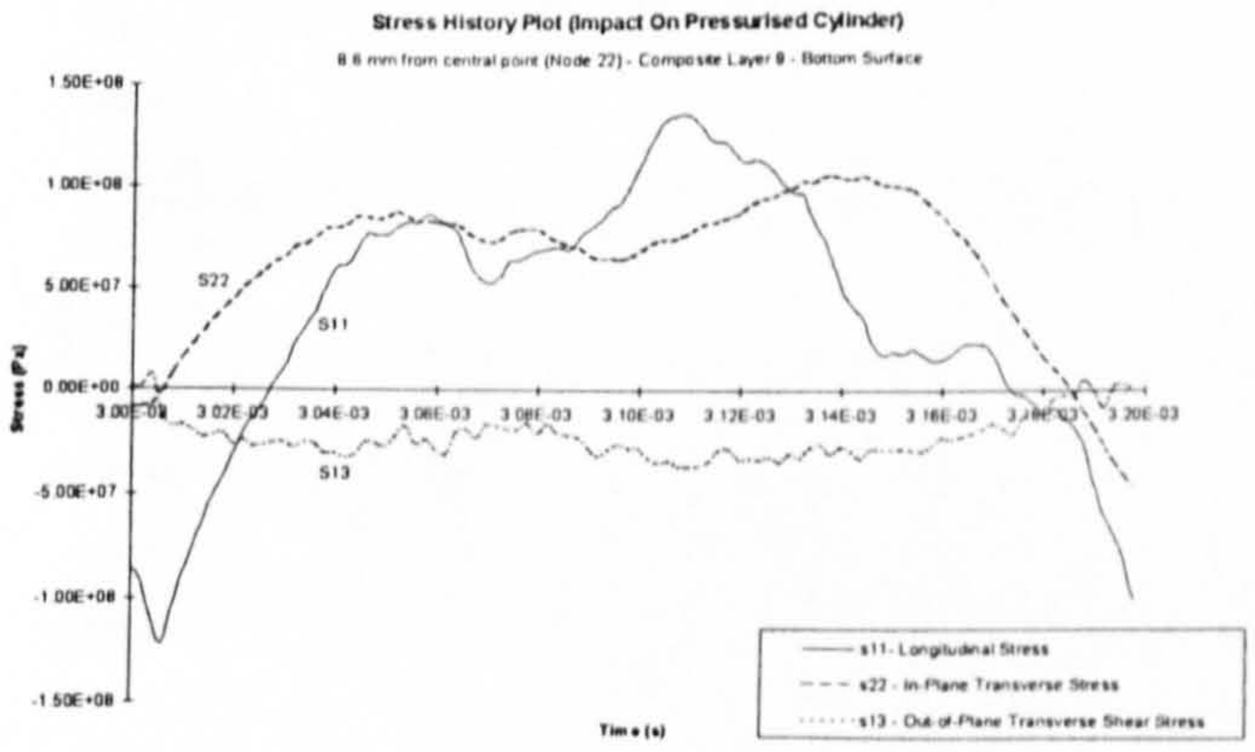

Fig E15 Stress history plot (8.6 mm from central point in longitudinal axis) Composite layer 9 (bottom surface)

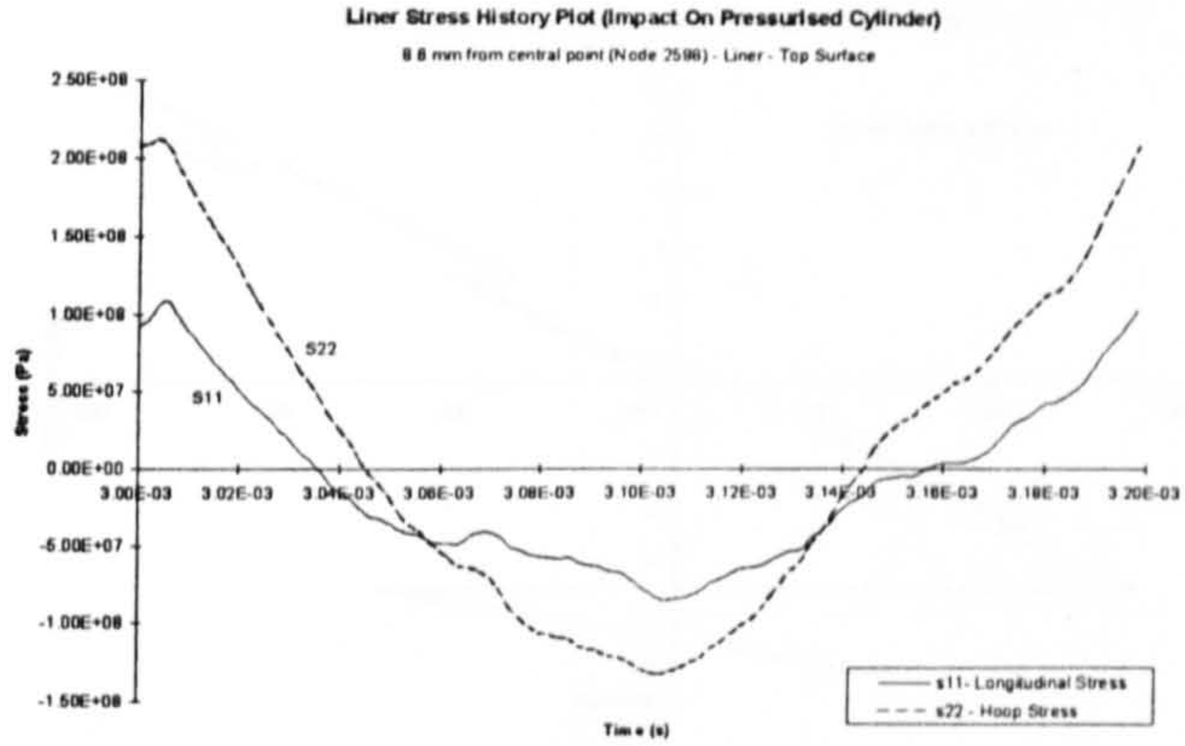

Fig E16 Stress history plot (8.6 mm from central point in longitudinal axis) Liner (top surface)

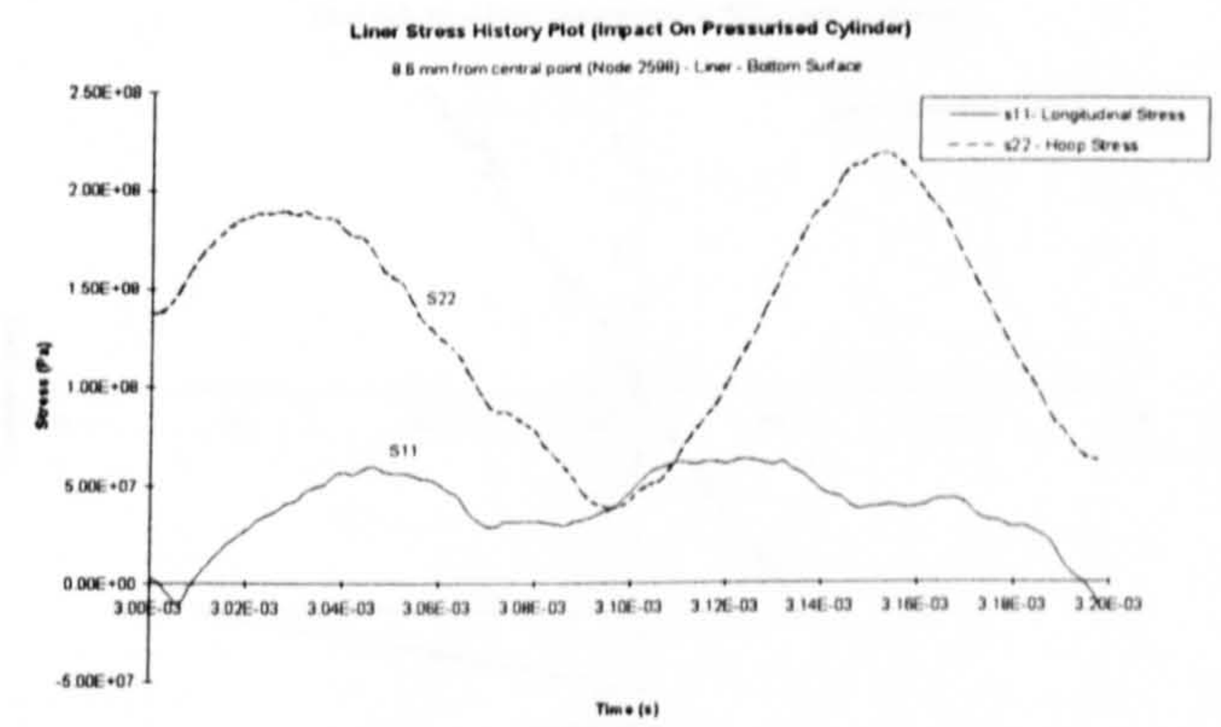

Fig E17 Stress history plot (8.6 mm from central point in longitudinal axis) Liner (bottom surface)

Fig E18 Transverse shear stress history plot (8.6 mm from central point in longitudinal axis) - Liner

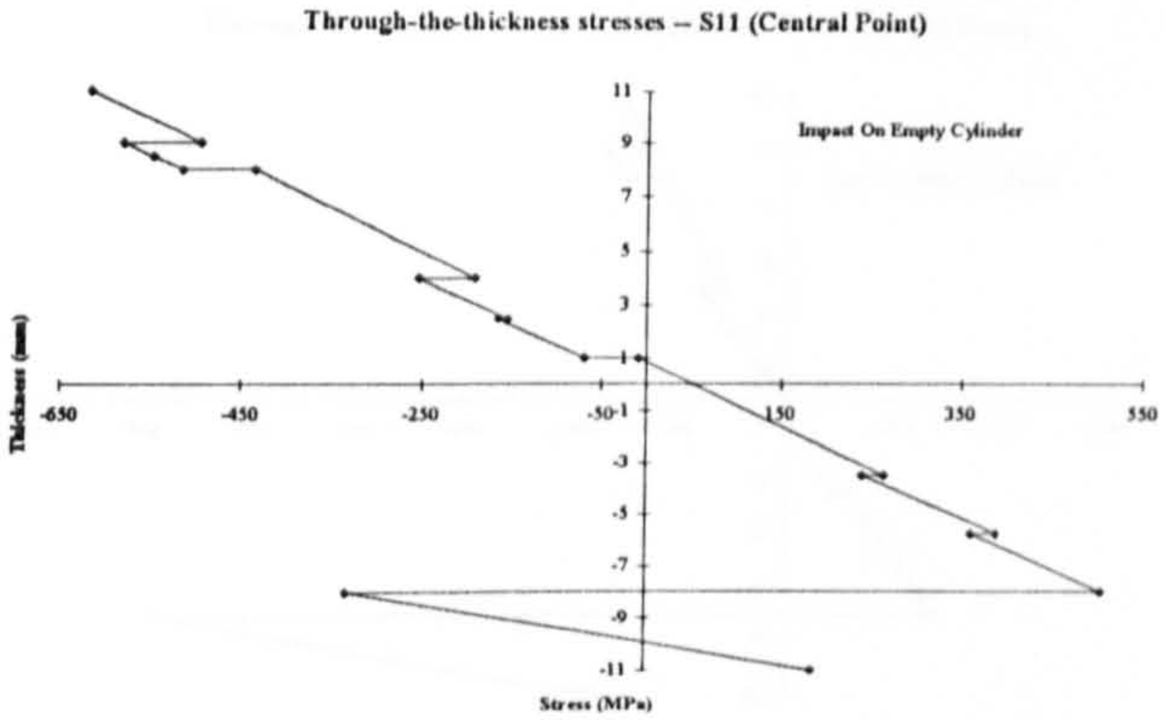

Fig E19 Longitudinal through-the-thickness stress (S11) of central point (including the liner)

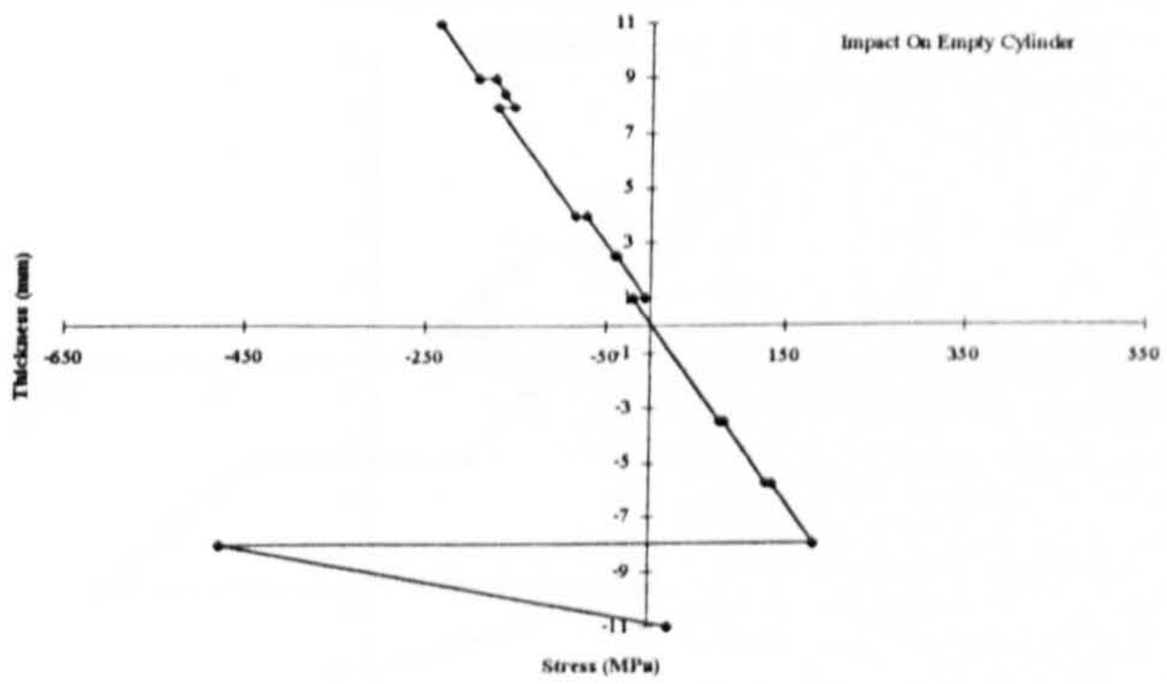

Fig E20 Transverse through-the-thickness stress (S22) of central point (including the liner)

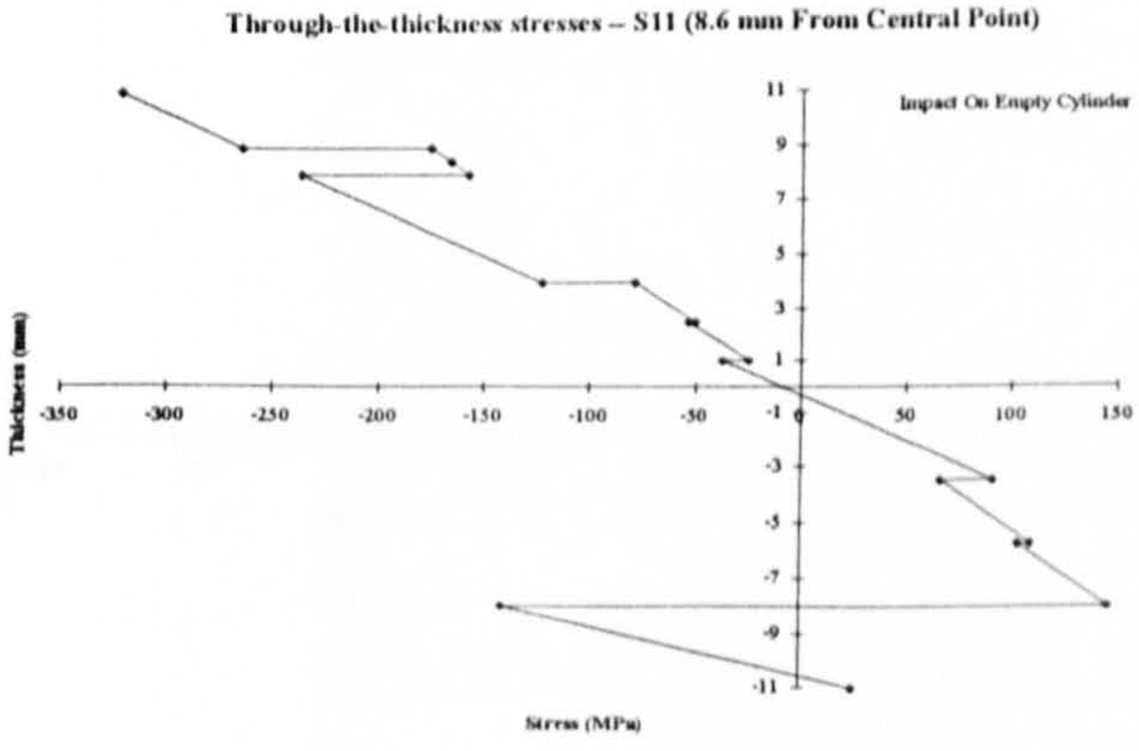

Fig E21 Longitudinal through-the-thickness stress (S11) - [including the liner] 8.6 mm from central point in longitudinal direction

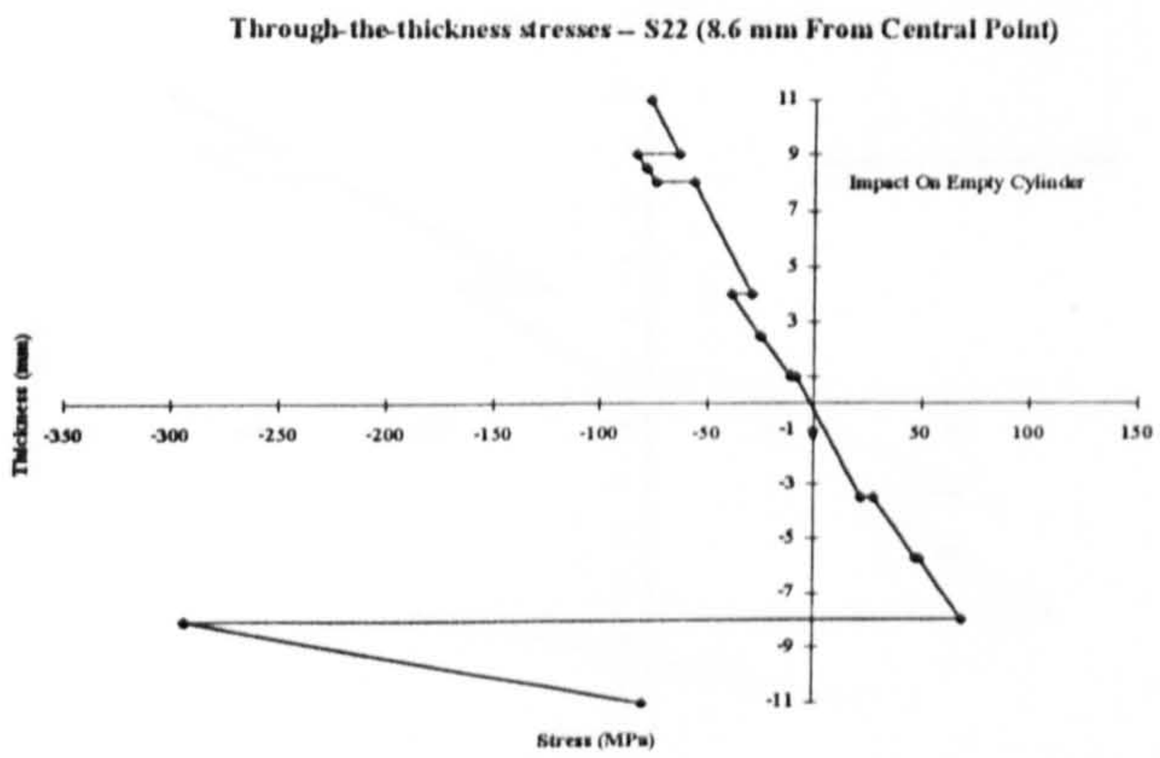

Fig E22 Transverse through-the-thickness stress (S22) - [including the liner] 8.6 mm from central point in longitudinal direction

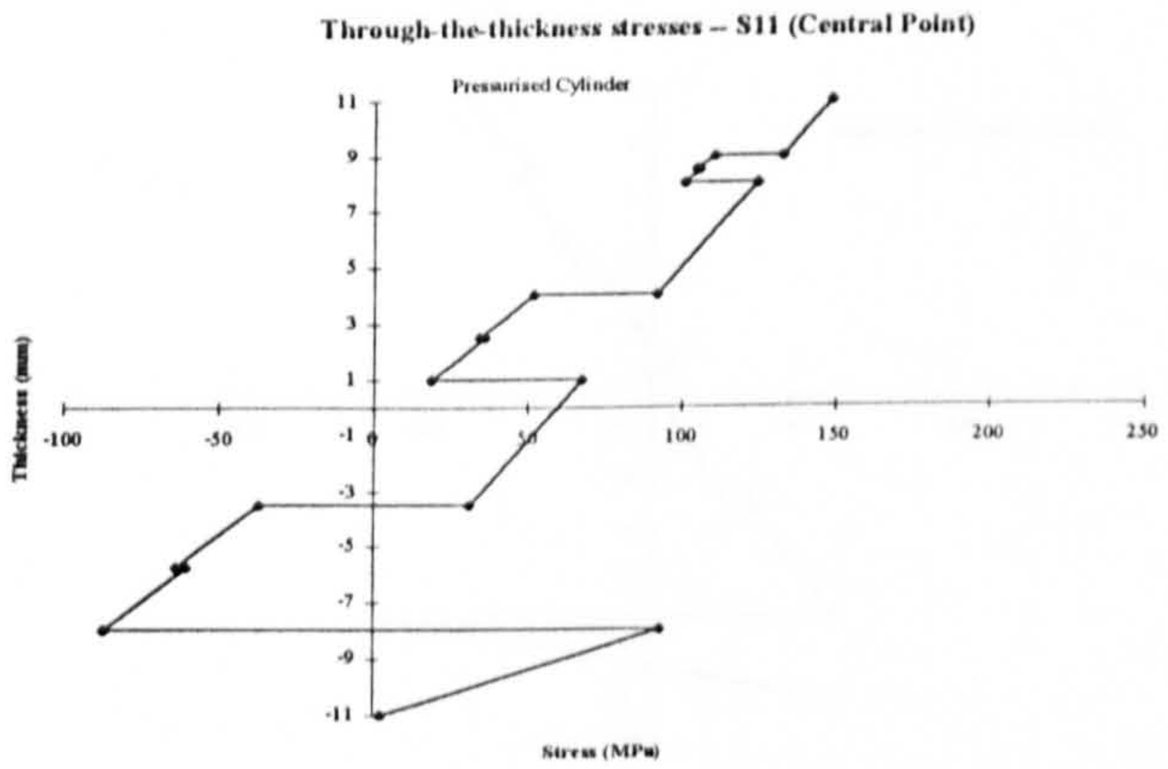

Fig E23 Longitudinal through-the-thickness stress (S11) of central point (including the liner)

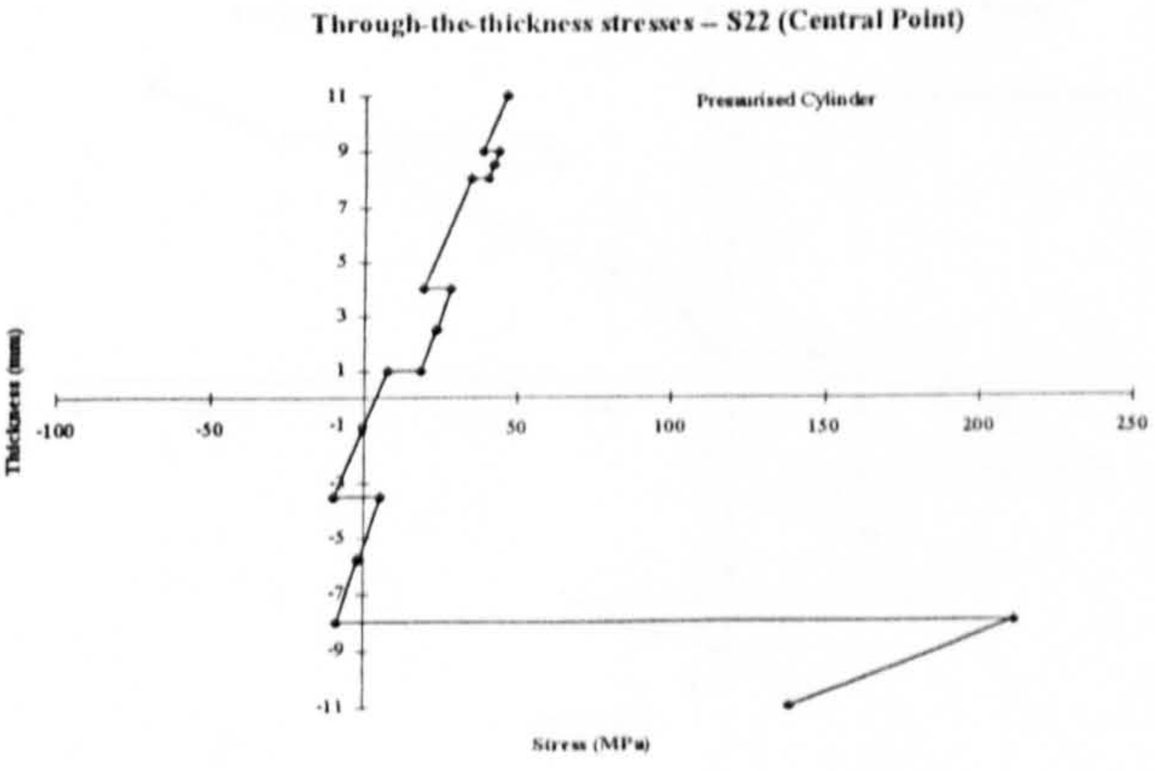

Fig E24 Transverse through-the-thickness stress (S22) of central point (including the liner)

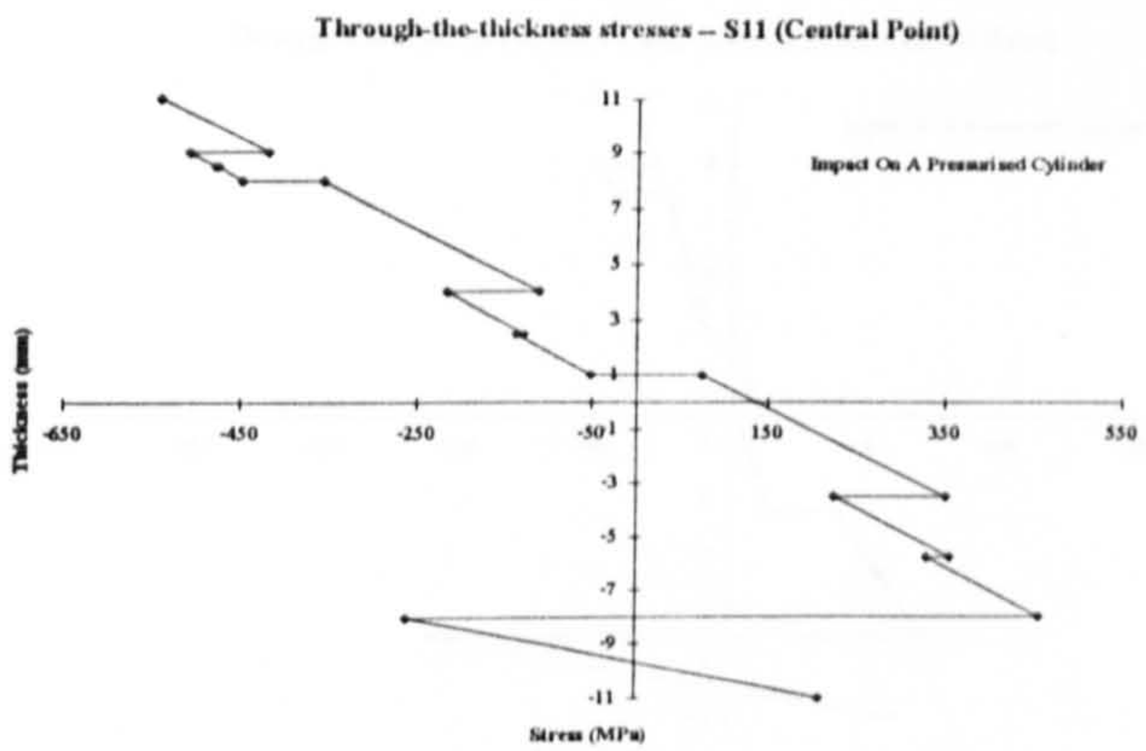

Fig E25 Longitudinal through-the-thickness stress (S11) of central point (including the liner)

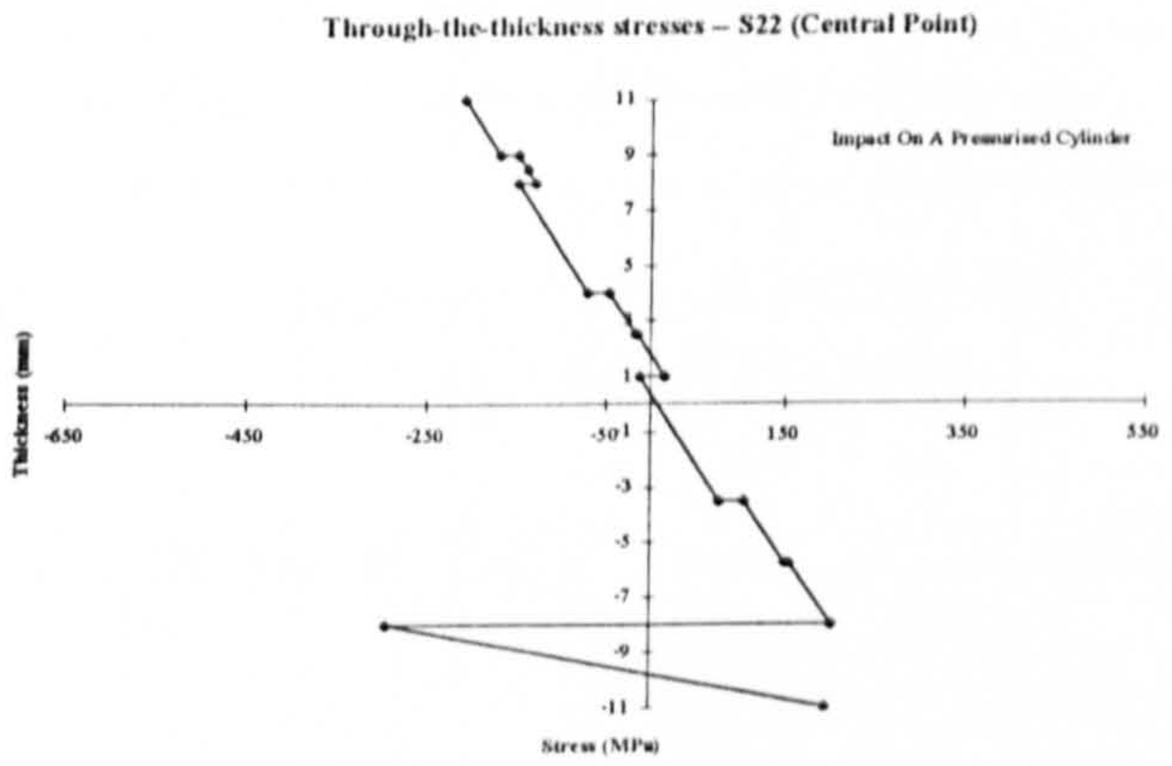

Fig E26 Transverse through-the-thickness stress (S22) of central point (including the liner)

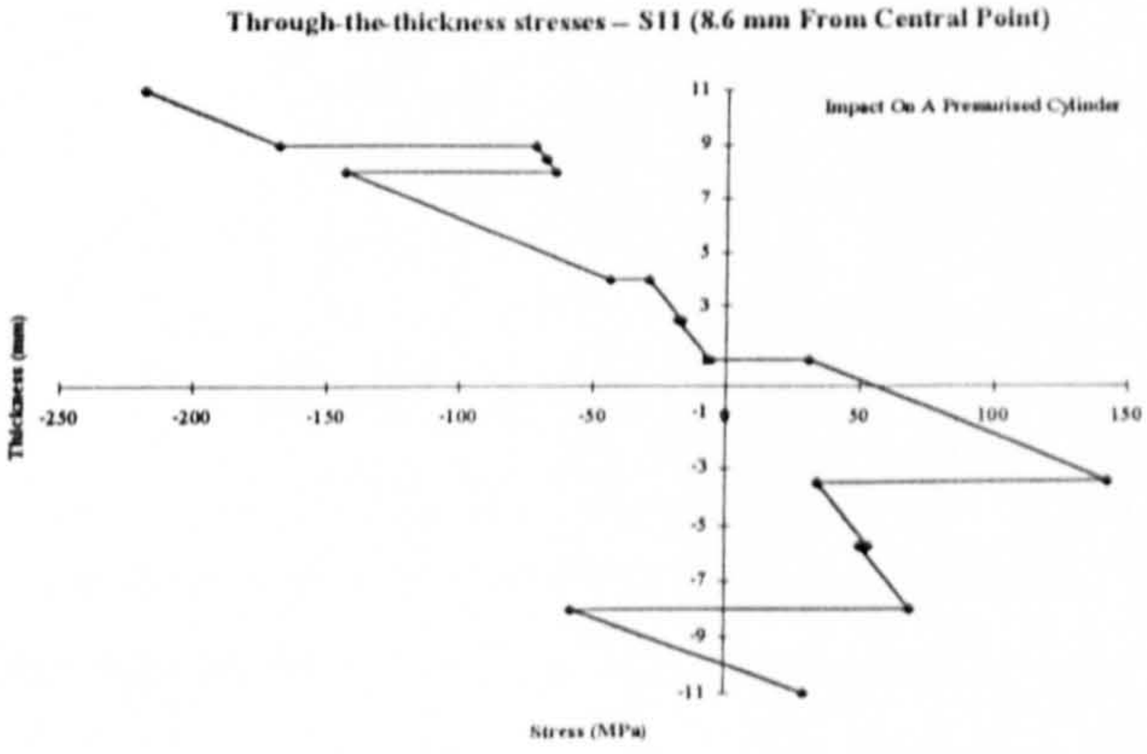

Fig E27 Longitudinal through-the-thickness stress (S11) - [including the liner] 8.6 mm from central point in longitudinal direction

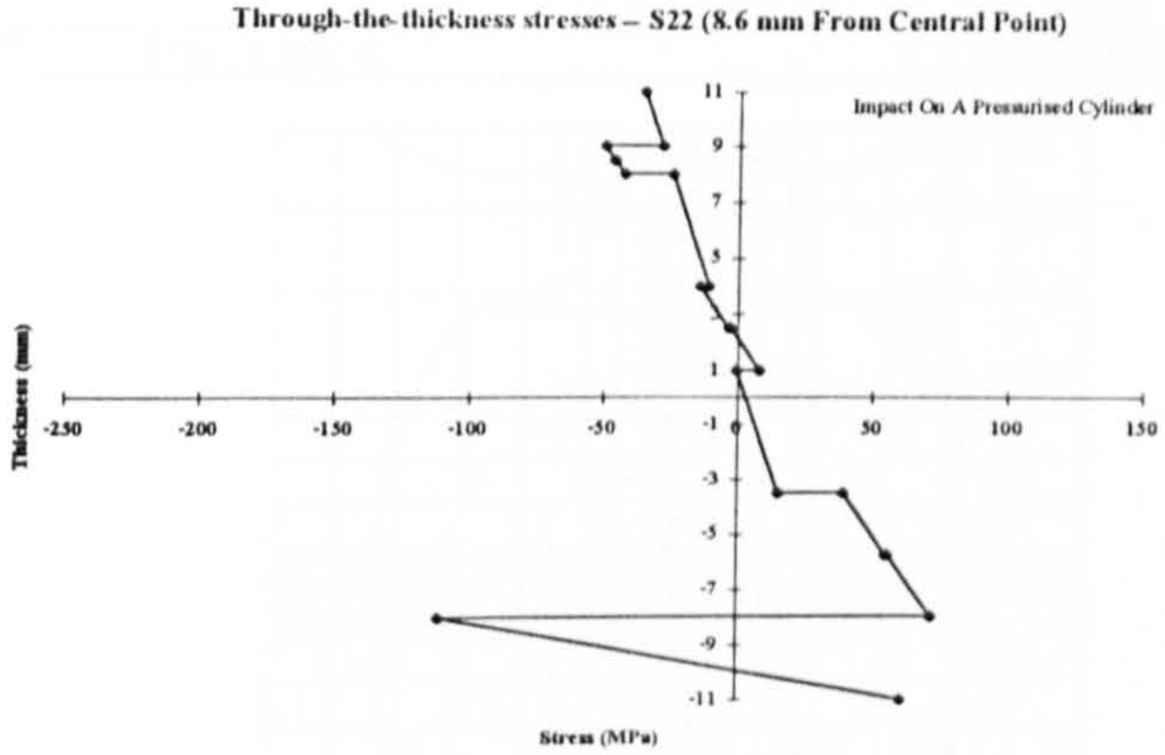

Fig E28 Transverse through-the-thickness stress (S22) - [including the liner] 8.6 mm from central point in longitudinal direction

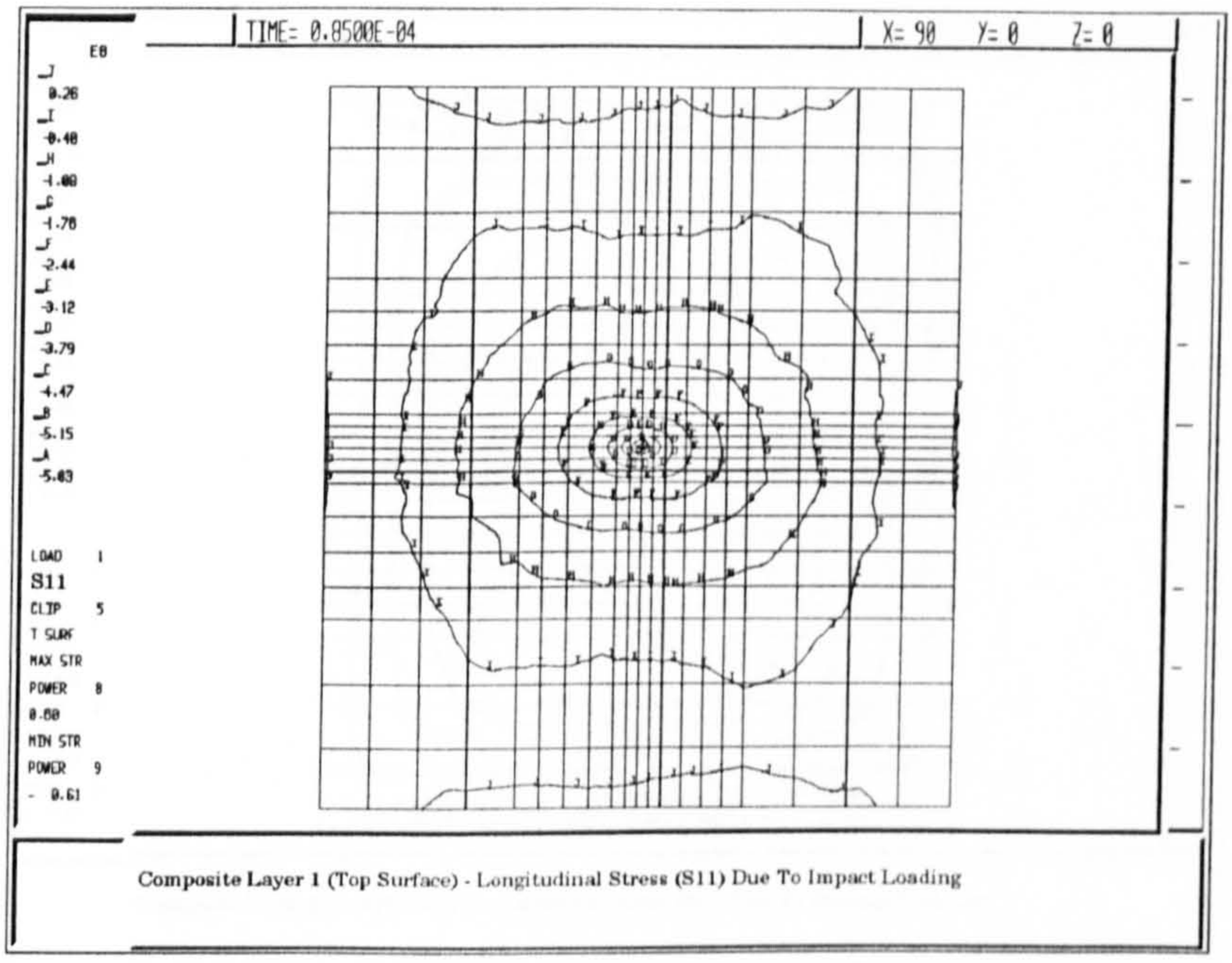

Fig E29 Longitudinal stress contour (S11) due to impact loading
Composite layer 1 (top surface)

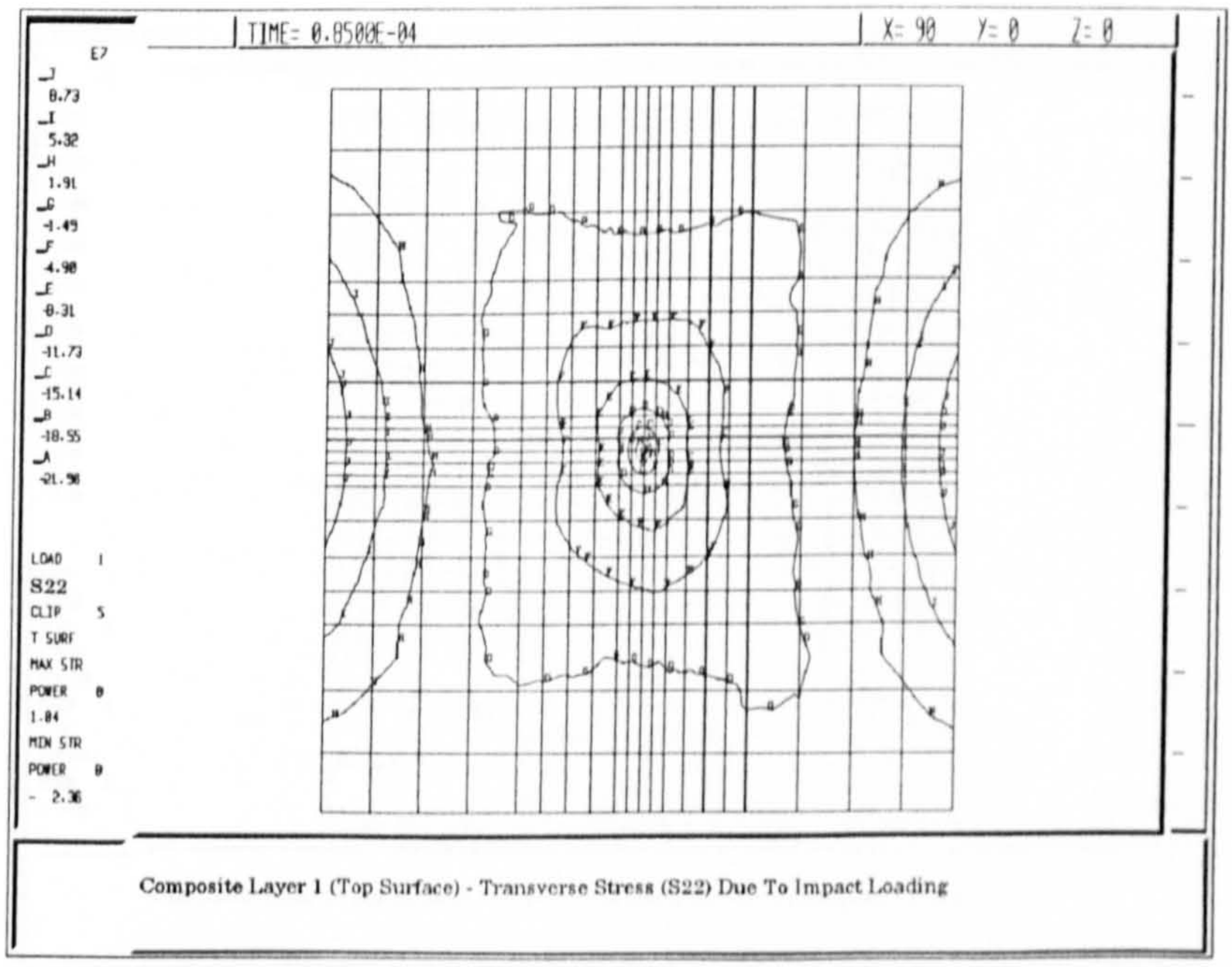

Fig E30 Transverse stress contour (S22) due to impact loading
Composite layer 1 (top surface)

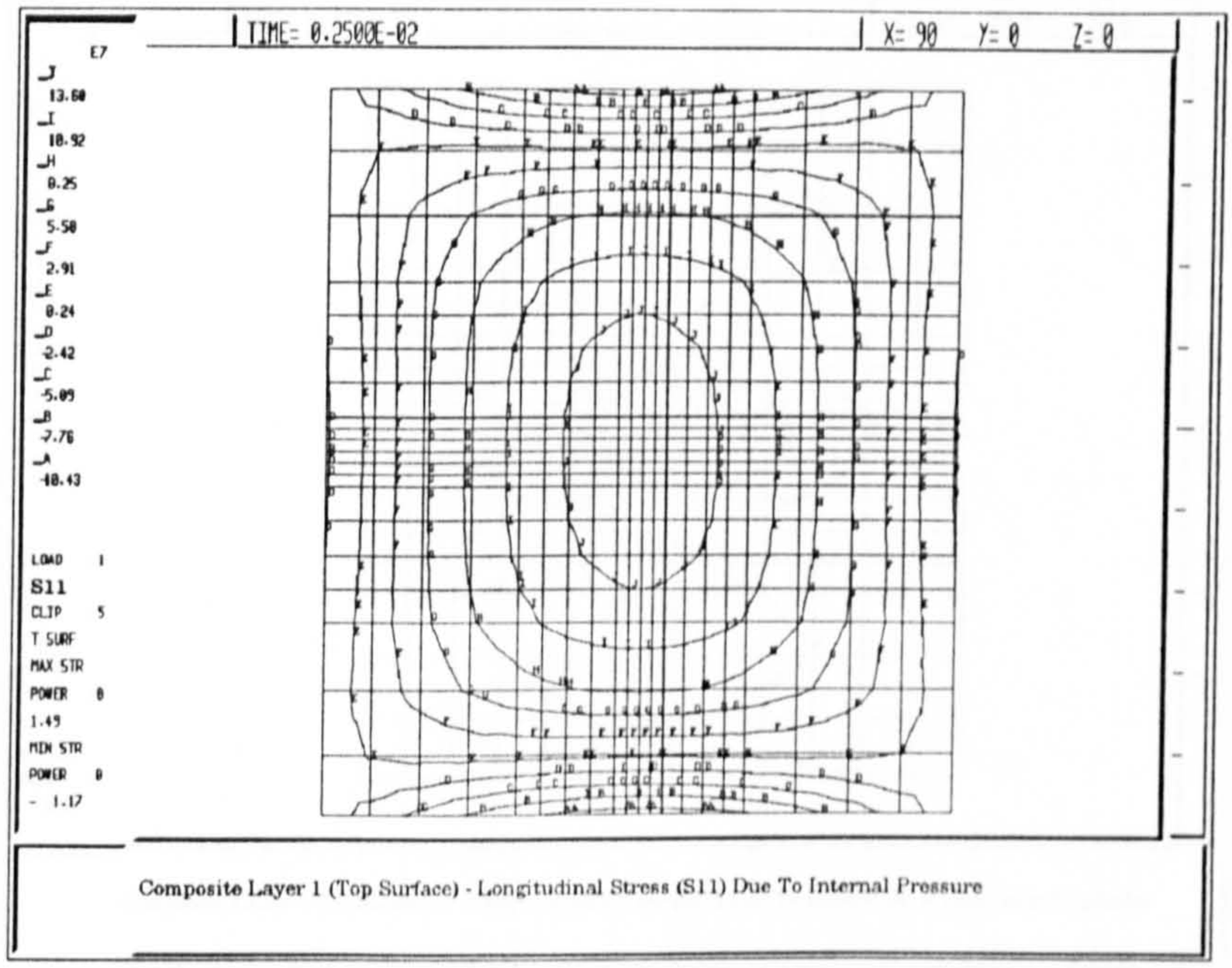

Fig E31 Longitudinal stress contour (S11) due to internal pressure Composite layer 1 (top surface)

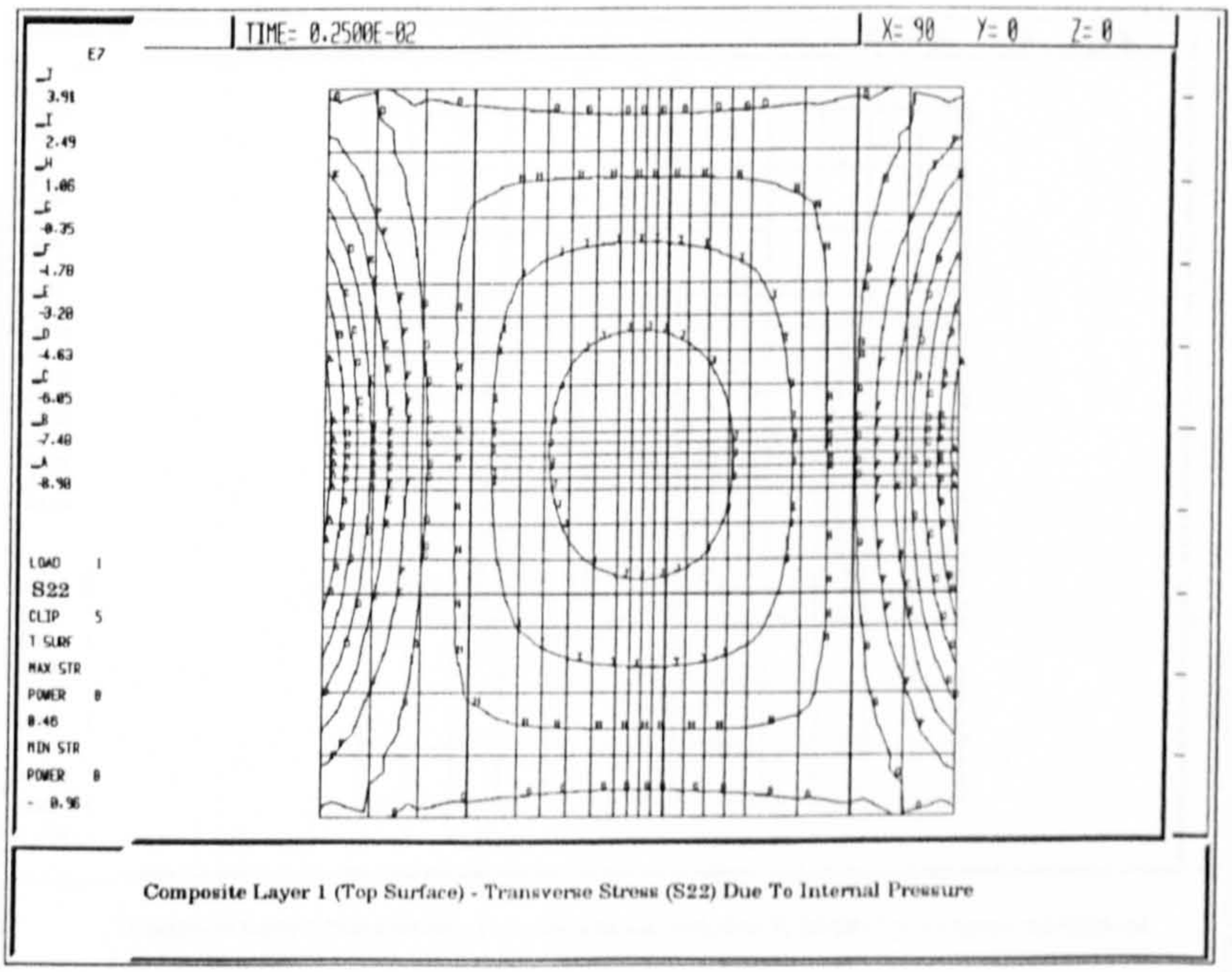

Fig E32 Transverse stress contour (S22) due to internal pressure Composite layer 1 (top surface)

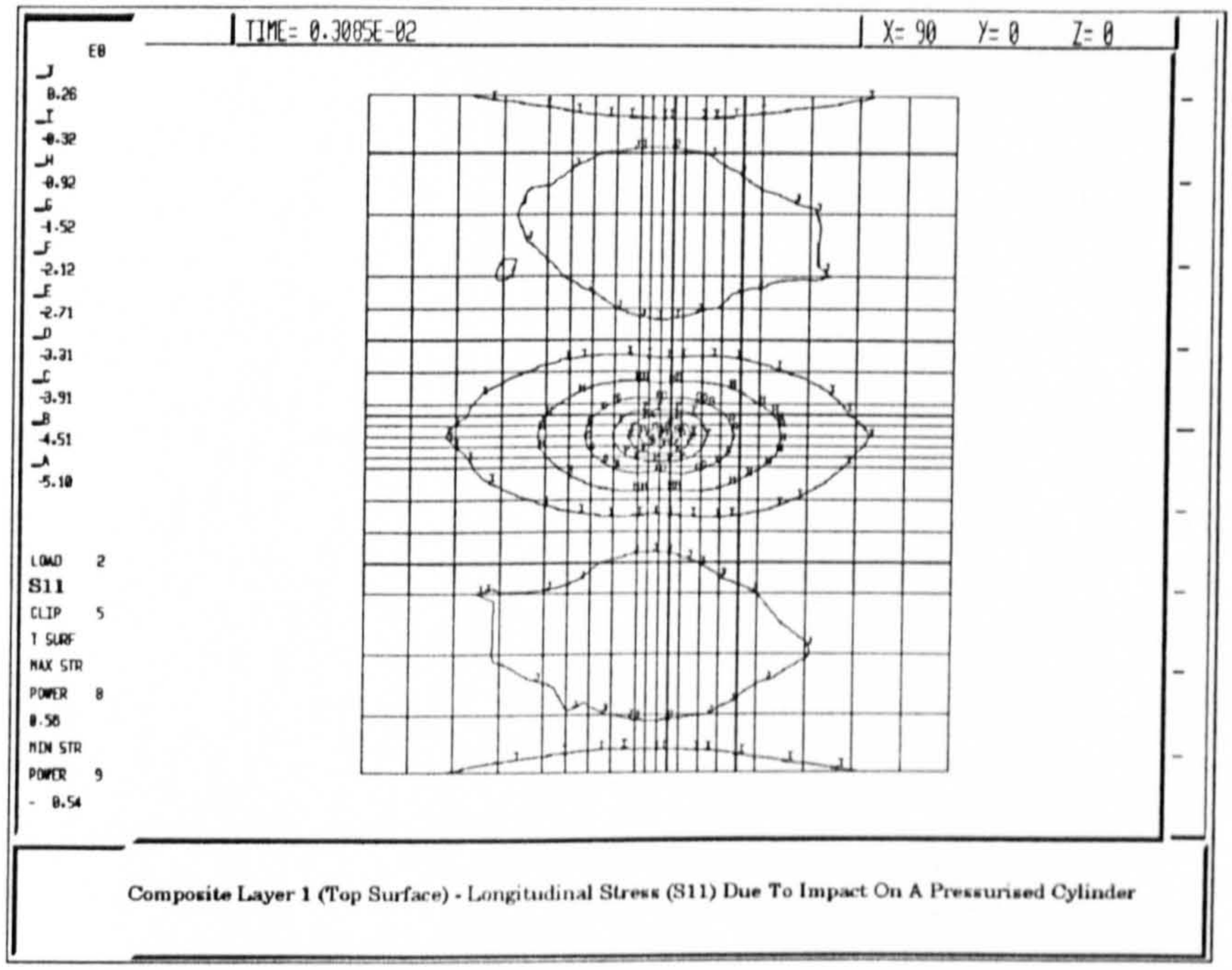

Fig E33 Longitudinal stress contour (S11) due to impact on a pressurised cylinder Composite layer 1 (top surface)

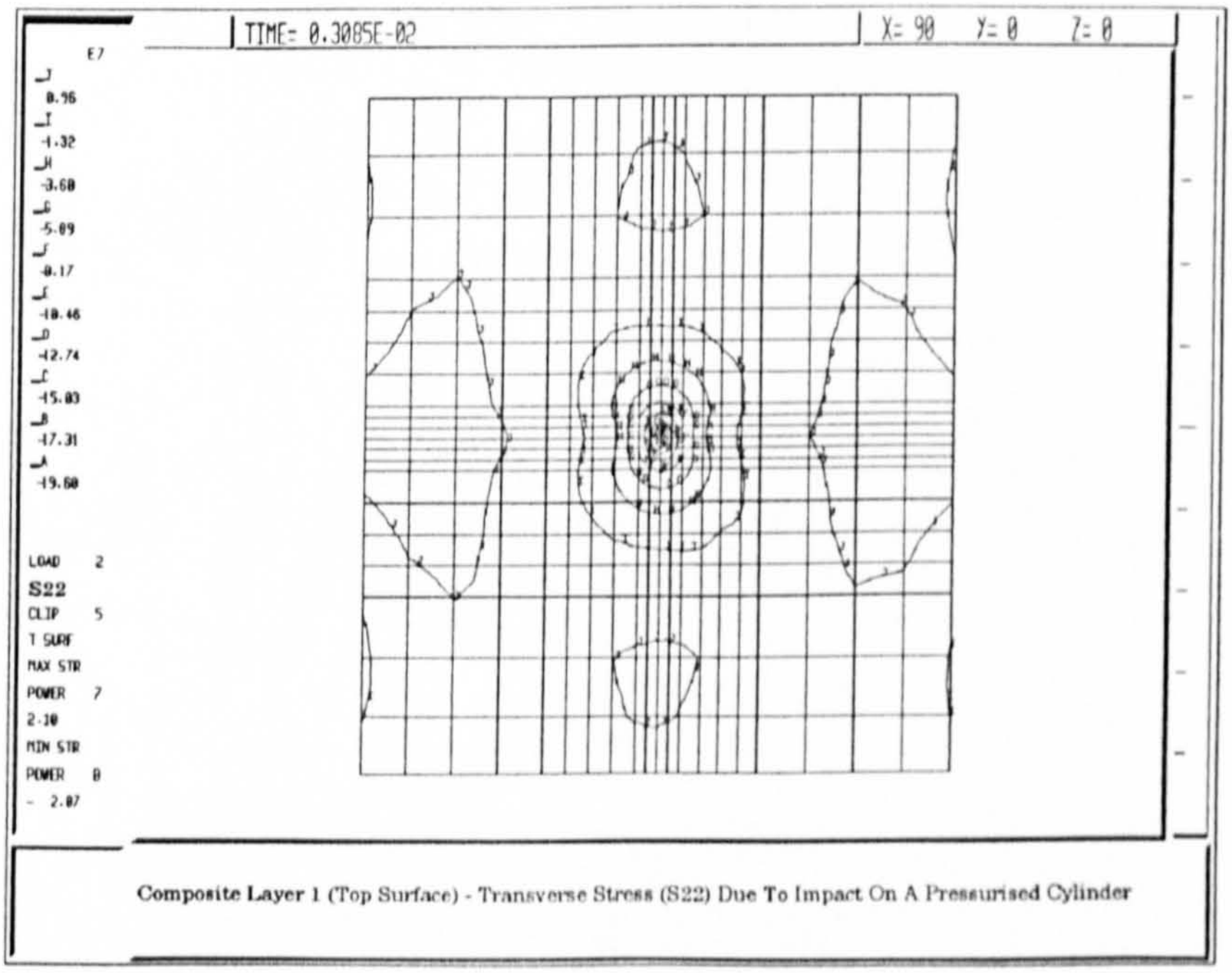

Fig E34 Transverse stress contour (S22) due to impact on a pressurised cylinder Composite layer 1 (top surface)